

AD-A284 698



AFIT/DS/ENC/94-1

11

DTIC
ELECTE
SEP 22 1994
S G D

A NUMERICAL ANALYSIS OF SMOOTHED
PARTICLE HYDRODYNAMICS

DISSERTATION
David Allen Fulk
Captain, USAF

AFIT/DS/ENC/94-1

~~94-30533~~ 94-30533
3528



Microfilm Edition 3

Approved for public release; distribution unlimited

94 9 22 0 6 0

A NUMERICAL ANALYSIS OF SMOOTHED PARTICLE
HYDRODYNAMICS

DISSERTATION

Presented to the Faculty of the School of Engineering
of the Air Force Institute of Technology

Air University

In Partial Fulfillment of the
Requirements for the Degree of

Doctor of Philosophy

David Allen Fulk, B.S., M.B.A., M.A.

Captain, USAF

September, 1994

Accession For	
NTIS CRA&I	<input checked="checked" type="checkbox"/>
DTIC TAB	<input type="checkbox"/>
Unannounced	<input type="checkbox"/>
Justification	
By	
Distribution /	
Availability Codes	
Dist	Avail and/or Special
A-1	

A NUMERICAL ANALYSIS OF SMOOTHED PARTICLE
HYDRODYNAMICS

David Allen Fulk, B.S., M.B.A., M.A.

Captain, USAF

Approved:

Dennis W Quinn 7 Sept 94

Dr. Dennis W. Quinn, Research Advisor

Kirk A Mathews 7 SEPT 94

Dr. Kirk A. Mathews

Michael G Stoecker 31 Aug 94

Dr. Michael G. Stoecker

Firooz A. Allahdadi 6 Sept 94

Dr. Firooz A. Allahdadi

D L Coulliette 1 Sep 94

Dr. David L. Coulliette

J S Przemieniecki 7 Sep 94

J. S. Przemieniecki

Senior Dean

Preface

Several years ago while at the Phillips Laboratory, I was introduced to a numerical technique known as Smoothed Particle Hydrodynamics (SPH). I was intrigued by its simplicity and yet apparent accuracy. Unfortunately, my duties at the time kept me from thoroughly exploring the algorithm. So when it was suggested to me that SPH might make an interesting topic for research, I quickly agreed. Thus, the topic of analyzing SPH from a mathematical point of view became the basic theme for my dissertation.

I wish to thank committee member Dr. Kirk Mathews for his tough questions and pointed advice. His input greatly improved the quality of this dissertation. Thanks also to committee member Mike Stoecker for our many discussions and his numerous edits. Without his help I would have gotten lost at times. To Dr Firooz Allahdadi, I appreciate the advice and friendship given to me both before and during this work. He convinced me that I was capable of succeeding. I am indebted to my faculty advisor, Dr Dennis Quinn. His calm, non-intrusive ways eased the trouble spots, kept me focused, helped me to find the answers, and allowed me to grow on my own. Quite simply, through my work with him, I learned how to perform research and write in a professional manner.

Finally, I wish to thank my wife, Donna, and son, Ben, for their understanding and support during those periods when I could not be with them due to this project. I dedicate this work to my father, who died shortly before this work started; his analytical mind and strong will helped form and prepare me for this work.

David Allen Fulk

Table of Contents

	Page
Preface	iii
List of Figures	x
List of Tables	xiv
Abstract	xvi
 I. INTRODUCTION	 1-1
1.1 Advantages of SPH	1-1
1.2 Analysis of SPH	1-2
1.3 Contributions	1-3
 II. BACKGROUND	 2-1
2.1 The Equations	2-1
2.1.1 Introduction to Hypervelocity Impact	2-1
2.1.2 HVI Equations	2-2
2.1.3 Conservation Laws	2-5
2.1.4 Additional Equations and Models	2-8
2.2 Standard Numerical Techniques	2-10
2.3 Smoothed Particle Hydrodynamics	2-14
2.3.1 Introduction	2-14
2.3.2 Kernel Approximation	2-15
2.3.3 Particle Approximation	2-16
2.3.4 Procedure	2-18
2.3.5 Density	2-22

	Page
2.3.6 Momentum Equation	2-24
2.3.7 Energy Equation	2-26
2.3.8 Conservation	2-27
2.3.9 Particle Placement	2-28
2.3.10 Neighbor Searches	2-29
2.3.11 Artificial Viscosity	2-30
2.3.12 Artificial Heat Conduction	2-31
2.3.13 Penetration Avoidance	2-32
2.3.14 Equations of State	2-32
2.3.15 Strength Models	2-34
2.4 Summary	2-36
III. CONSISTENCY	3-1
3.1 Kernel Approximation	3-2
3.2 Particle Approximation/Rectangle Rule	3-5
3.3 Volume Element Calculation	3-8
3.4 Consistency Result	3-10
3.5 Applying SPH/Linearizing	3-14
3.6 Non-Smooth Functions	3-17
3.6.1 Scalar Equations	3-17
3.6.2 Euler Equations	3-22
3.7 Higher Dimensions	3-25
3.8 Artificial Viscosity/Wall Heating	3-30
3.9 Summary	3-33
IV. STABILITY	4-1
4.1 Linear Stability Analysis	4-2
4.1.1 Analysis Details	4-2

	Page
4.1.2 Smooth Data Analysis	4-7
4.1.3 Reconciliation with Other Analyses	4-10
4.1.4 Other Equations	4-12
4.1.5 Artificial Viscosity/Wall Heating	4-13
4.2 Techniques for Obtaining Linear Stability	4-22
4.2.1 Technique 1 - Concave Up/Down Kernels . . .	4-22
4.2.2 Technique 2 - Add a Constant to the Pressure	4-24
4.2.3 Technique 2a - Add a Constant to the Pressure	4-26
4.2.4 Technique 3 - A Pressure Difference Form . .	4-28
4.2.5 Technique 3a - A Pressure Difference Form . .	4-30
4.2.6 Technique 4 - Particle Motion Correction . . .	4-33
4.2.7 Some Computational Results	4-36
4.3 Total Variation Analysis	4-42
4.3.1 Lax-Friedrichs	4-43
4.3.2 General Monotone SPH Scheme	4-46
4.3.3 Kernels Ratio	4-47
4.4 Summary	4-48
V. CONVERGENCE	5-1
5.1 Finite Difference Approach	5-1
5.2 SPH Extensions	5-5
5.3 Summary	5-16
VI. KERNELS	6-1
6.1 Kernel Properties	6-1
6.1.1 Kernel Requirements	6-2
6.1.2 Higher Order Kernels	6-3
6.1.3 Smoothing Length	6-4

	Page
6.2 Kernel Comparisons	6-8
6.2.1 Accuracy From Consistency Analysis	6-9
6.2.2 Uniform Space, Smooth Data Analysis	6-11
6.2.3 Test 1: Plots of Results	6-13
6.2.4 Test 2: Error Norms	6-14
6.2.5 Test 3: Test Functions	6-16
6.2.6 Higher Order Kernel Comparisons	6-19
6.2.7 Non-Smooth Data	6-22
6.2.8 One-Sided Kernels	6-26
6.2.9 Riemann Shock Tube Problem	6-32
6.3 Conclusions	6-39
 VII. TIME SCHEMES	 7-1
7.1 Lax-Wendroff	7-3
7.1.1 First Order Wave Equation	7-3
7.1.2 Euler Equations	7-4
7.2 Central Time	7-9
7.2.1 General Conservation Equation	7-9
7.2.2 Euler Equations	7-9
7.3 Shu	7-11
7.3.1 General Conservation Equation	7-12
7.3.2 Euler Equations	7-13
7.4 Lower Order Methods	7-14
7.4.1 Lax-Friedrichs	7-14
7.4.2 Upwind	7-18
7.5 Summary	7-22

	Page
VIII. HYBRID METHODS	8-1
8.1 Introduction	8-1
8.2 Consistency Approach	8-3
8.3 Two Method Approach	8-4
8.3.1 Method 2	8-7
8.3.2 Methods 4, 6, and 8	8-8
8.3.3 Method 12	8-8
8.3.4 Method 20	8-9
8.3.5 Methods that Failed to Converge	8-9
8.4 Sample Calculations	8-10
8.4.1 Baseline	8-12
8.4.2 Method 2	8-17
8.4.3 Methods 4, 6, and 8	8-17
8.4.4 Method 12	8-18
8.4.5 Method 20	8-19
8.5 Method Comparisons	8-19
8.6 Summary	8-20
IX. SUMMARY/CONTRIBUTIONS	9-1
9.1 Numerical Properties	9-1
9.2 The Kernel	9-3
9.3 The Implementation	9-3
9.4 Future Direction	9-4
Appendix A. ADDITIONAL CONSISTENCY NOTES	A-1
A.1 Non-Smooth Functions	A-1
A.2 Artificial Viscosity/Wall Heating	A-13

	Page
Appendix B. ADDITIONAL STABILITY NOTES	B-1
B.1 Stability for Several Equations	B-1
B.2 Considerations on Two Equations of State	B-11
B.2.1 Ideal Gas Law	B-11
B.2.2 Mie - Grüneisen	B-12
Appendix C. ADDITIONAL KERNEL NOTES	C-1
C.1 Kernels Analyzed	C-1
C.2 Kernel Test 1 Plots	C-7
C.3 Higher Order Kernel Results	C-16
C.4 Kernel Test 3 Results	C-20
C.5 Shock Tube Results for Kernels	C-26
Appendix D. HYBRID CALCULATIONS	D-1
D.1 Introduction	D-1
D.2 Baseline	D-1
D.3 Method 2	D-6
D.4 Methods 4, 6, and 8	D-13
D.5 Method 12	D-27
D.6 Method 20	D-32
Appendix E. SOFTWARE	E-1
Bibliography	BIB-1
Vita	VITA-1

List of Figures

Figure	Page
2.1. Equations of State Phenomena (2:77)	2-9
2.2. Lagrangian Example (72:602)	2-12
2.3. Eulerian Example (72:603)	2-13
3.1. Partition for Rectangle Rule	3-6
3.2. Non-Smooth Data Consistency part 1	3-18
3.3. Non-Smooth Data Consistency part 2	3-19
3.4. 2-D Particle Triangulation	3-28
3.5. 2-D Particle Convex Polygon	3-29
4.1. Baseline Stability Results	4-38
4.2. Technique 3a Stability Results	4-39
4.3. Technique 4 Stability Results	4-40
4.4. Velocity Stability Comparisons	4-41
6.1. Test 3: Test Functions	6-17
6.2. Bar Chart for Test 3, l_1 , Smooth Data	6-18
6.3. Bar Chart for Test3, l_2 , Smooth Data	6-19
6.4. Bar Chart for Test 3, l_1 , Smooth Data, Higher Order	6-21
6.5. Bar Chart for Test3, l_2 , Smooth Data, Higher Order	6-22
6.6. Non-Smooth Data Example	6-22
6.7. Bar Chart for Test 3, l_1 , Non-Smooth Data	6-25
6.8. Bar Chart for Test3, l_2 , Non-Smooth Data	6-26
6.9. Bar Chart for Truncated 1-Sided Kernels, l_1 , Non-Smooth Data	6-29
6.10. Bar Chart for Truncated 1-Sided Kernels, l_2 , Non-Smooth Data	6-30
6.11. Bar Chart for Condensed 1-Sided Kernels, l_1 , Non-Smooth Data	6-31

Figure	Page
6.12. Bar Chart for Condensed 1-Sided Kernels, l_2 , Non-Smooth Data	6-32
6.13. Shock Tube Results, Selected Kernel	6-35
6.14. Shock Tube Results, Selected Kernel	6-36
6.15. Shock Tube Results, Density Comparisons	6-37
6.16. Shock Tube Results, Velocity and Energy Comparisons	6-38
6.17. Shock Tube Results, Pressure Comparisons	6-39
8.1. Baseline Shock Tube Results	8-13
8.2. Baseline Shock Tube Results	8-14
8.3. Baseline Shock Tube Results - Extra Particles	8-15
8.4. Baseline Shock Tube Results - Extra Particles	8-16
8.5. Shock Tube Results - 600 particles	8-20
8.6. Shock Tube Results - 816 particles	8-21
A.1. Non-Smooth Data Consistency part 1	A-1
A.2. Non-Smooth Data Consistency part 2	A-10
C.1. Bell Shaped Kernels	C-2
C.2. Derivatives of Bell Shaped Kernels	C-2
C.3. Hyperbolic Shaped Kernels	C-3
C.4. Derivatives of Hyperbolic Shaped Kernels	C-3
C.5. Parabolic Shaped Kernels	C-4
C.6. Derivatives of Parabolic Shaped Kernels	C-4
C.7. Additional Bell Shaped Kernels	C-5
C.8. Derivatives of Additional Bell Shaped Kernels	C-5
C.9. Additional Bell Shaped Kernels	C-6
C.10. Derivatives of Additional Bell Shaped Kernels	C-6
C.11. Gaussian Kernel (1) Test 1, $R = \Delta x/h$	C-7
C.12. W4 B-Spline Kernel (2) Test 1, $R = \Delta x/h$	C-7

Figure	Page
C.13. Cosine Kernel (3) Test 1, $R = \Delta x/h$	C-8
C.14. Exponential Kernel (4) Test 1, $R = \Delta x/h$	C-8
C.15. k-2 Exponential Kernel (5) Test 1, $R = \Delta x/h$	C-9
C.16. $1/X$, $U_0=2$ Kernel (6) Test 1, $R = \Delta x/h$	C-9
C.17. $1/X$, $U_0=4$ Kernel (7) Test 1, $R = \Delta x/h$	C-10
C.18. $1/X$, $U_0=10$ Kernel (8) Test 1, $R = \Delta x/h$	C-10
C.19. Kernel (9) Test 1, $R = \Delta x/h$	C-11
C.20. Kernel (10) Test 1, $R = \Delta x/h$	C-11
C.21. Kernel (11) Test 1, $R = \Delta x/h$	C-12
C.22. Kernel (12) Test 1, $R = \Delta x/h$	C-12
C.23. k-2 Gaussian Kernel (13) Test 1, $R = \Delta x/h$	C-13
C.24. L Gaussian Kernel (14) Test 1, $R = \Delta x/h$	C-13
C.25. Q Gaussian Kernel (15) Test 1, $R = \Delta x/h$	C-14
C.26. T Gaussian Kernel (16) Test 1, $R = \Delta x/h$	C-14
C.27. Quartic-1 Kernel (17) Test 1, $R = \Delta x/h$	C-15
C.28. Quartic-2 Kernel (18) Test 1, $R = \Delta x/h$	C-15
C.29. Higher Order Kernels	C-17
C.30. Derivatives of Higher Order Kernels	C-17
C.31. Super-Gaussian Kernel Test 1, $R = \Delta x/h$	C-18
C.32. Enhanced B-Spline Kernel Test 1, $R = \Delta x/h$	C-18
C.33. Super-Gaussian 2 Kernel Test 2, $R = \Delta x/h$	C-19
D.1. Baseline Shock Tube Results	D-2
D.2. Baseline Shock Tube Results	D-3
D.3. Baseline Shock Tube Results - Extra Particles	D-4
D.4. Baseline Shock Tube Results - Extra Particles	D-5
D.5. Shock Tube Results - Method 2	D-7
D.6. Shock Tube Results - Method 2	D-8

Figure	Page
D.7. Shock Tube Results - Method 2 - Extra Particles	D-9
D.8. Shock Tube Results - Method 2 - Extra Particles	D-10
D.9. Shock Tube Results - Method 2 - Variable h	D-11
D.10. Shock Tube Results - Method 2 - Variable h	D-12
D.11. Shock Tube Results - Method 4	D-15
D.12. Shock Tube Results - Method 4	D-16
D.13. Shock Tube Results - Method 4 - Always Average	D-17
D.14. Shock Tube Results - Method 4 - Always Average	D-18
D.15. Shock Tube Results - Method 4 - Extra Particles	D-19
D.16. Shock Tube Results - Method 4 - Extra Particles	D-20
D.17. Shock Tube Results - Method 6	D-21
D.18. Shock Tube Results - Method 6	D-22
D.19. Shock Tube Results - Method 8	D-23
D.20. Shock Tube Results - Method 8	D-24
D.21. Shock Tube Results - Method 8 - Extra Particles	D-25
D.22. Shock Tube Results - Method 8 - Extra Particles	D-26
D.23. Shock Tube Results - Method 12	D-28
D.24. Shock Tube Results - Method 12	D-29
D.25. Shock Tube Results - Method 12 - Extra Particles	D-30
D.26. Shock Tube Results - Method 12 - Extra Particles	D-31
D.27. Shock Tube Results - Method 20	D-33
D.28. Shock Tube Results - Method 20	D-34
D.29. Shock Tube Results - Method 20 - Extra Particles	D-35
D.30. Shock Tube Results - Method 20 - Extra Particles	D-36
E.1. Mathematica Code for Kernels Chapter, part 1	E-2
E.2. Mathematica Code for Kernels Chapter, part 2	E-3

List of Tables

Table	Page
4.1. Examples of Kernels Ratio	4-48
6.1. One-Dimensional Higher Order kernels	6-4
6.2. One Dimensional Kernels Analyzed	6-9
6.3. Kernel Integral Analysis	6-10
6.4. Relative Error Norms for Kernel Test 2	6-15
6.5. Rel Error Norms for Higher Order Kernel Test 2	6-20
6.6. Kernel Value at 0	6-24
6.7. Initial Particle Spacing for Shock Tube	6-34
B.1. Mie-Gruneisen Tension Results	B-15
B.2. Mie-Gruneisen Compression Results	B-15
C.1. Kernels Analyzed	C-1
C.2. One-Dimensional Higher Order kernels	C-16
C.3. Avg l_1 Rel Error Norms for Higher Order Kernel Test 3	C-19
C.4. Avg l_2 Rel Error Norms for Higher Order Kernel Test 3	C-19
C.5. Avg l_1 Relative Error Norms for Kernel Test 3	C-20
C.6. Avg l_2 Relative Error Norms for Kernel Test 3	C-21
C.7. Avg l_1 Error Norms for Test 3, Step Function, Truncated Kernels	C-22
C.8. Avg l_2 Error Norms for Test 3, Step Function, Truncated Kernels	C-23
C.9. Avg l_1 Error Norms for Test 3, Step Function, Condensed Kernels	C-24
C.10. Avg l_2 Error Norms for Test 3, Step Function, Condensed Kernels	C-25
C.11. Relative Error Norms for Selected Kernels	C-26
D.1. Relative Error Norms for Baseline	D-1

Table	Page
D.2. Relative Error Norms for Method 2	D-6
D.3. Relative Error Norms for Method 4	D-13
D.4. Relative Error Norms for Method 6	D-13
D.5. Relative Error Norms for Method 8	D-14
D.6. Relative Error Norms for Method 12	D-27
D.7. Relative Error Norms for Method 20	D-32

Abstract

This dissertation studies the numerical technique known as Smoothed Particle Hydrodynamics (SPH) from a mathematical point of view. As a framework for the research, problems from the Hypervelocity Impact (HVI) community were chosen. The gridless Lagrangian method, SPH, can handle the complicated geometries, high deformation rates, and material tracking features of HVI problems quite well. The research starts with a detailed consistency analysis of the method. Higher dimensions and non-smooth functions are considered in addition to the more standard smooth one-dimensional case. A stability analysis is then performed. Using a linearizing technique, an instability is found. Four solutions are proposed to resolve the instability. Also an initial Total Variation Stability analysis is performed on a simplified form of SPH. The concepts of consistency and stability are then brought together in a convergence proof. This proof uses three lemmas derived from the Lax-Wendroff Theorem in finite differences. The detailed study of the method itself is concluded with an analysis of the SPH Kernel function, the key element in SPH. Techniques to compare and evaluate different kernels are proposed. Bell-shaped kernels are shown to be superior over other shaped kernels and many new kernels are introduced. To provide a full discretization of the problem, three different time schemes are then applied to SPH. The Lax-Wendroff and Shu methods are used for the first time with SPH, while problems with implementations of the central time scheme are noted. In addition, an SPH Lax-Friedrichs type form is developed. This method is used in proposing the use of and developing flux-limited hybrid methods in SPH to control shocks. This idea allows the SPH continuity equation to be used for the first time when solving the classic Riemann shock tube problem.

A NUMERICAL ANALYSIS OF SMOOTHED PARTICLE HYDRODYNAMICS

I. INTRODUCTION

This dissertation addresses a numerical technique known as Smoothed Particle Hydrodynamics (SPH) for solving a class of partial differential equations. In order to limit the scope of the work, SPH will be studied as it applies to problems of deformative failure modes of material under high strain rate loading due primarily to hypervelocity impact (HVI). Although the exact nature of the problem is not required to perform most of the analysis detailed in this dissertation, it forms a framework in which the method may be understood, a set of equations to evaluate, and a user community interested in the applications.

Numerous techniques are available to solve partial differential equations and in particular the Euler equations. Finite difference and finite element techniques are two of the more popular general categories of methods because they are well-grounded in numerical theory and usage. Each has its own advantages and disadvantages when applied to problems of the type found in HVI, but SPH by its design has some other advantages over these other techniques. Since SPH is a rather new technique, it has not received as much theoretical attention as the older methods.

1.1 Advantages of SPH

HVI and related problems are characterized by extremely high deformation rates. When using a finite element method, these deformations will often cause the elements to become so elongated that time stepping goes to zero and can even cause elements to get turned inside out. Standard Eulerian finite difference techniques can handle the deformation rates much better, but do not have the material tracking

and interface accuracy desired for complicated geometries. However, the gridless Lagrangian method, SPH, can handle these sorts of problems quite easily.

1.2 Analysis of SPH

The results of this dissertation are split between two major categories: numerical properties of SPH and the implementation of SPH. The numerical properties are more fundamental and mathematical in nature, while, as the name suggests, the implementation work is more applied. These two categories overlap and rely on each other providing a continuity to the study of SPH in this work. Each of these areas is discussed below.

The numerical properties of any technique form the mathematical foundation upon which the method is built. Without these, a technique is simply an empirical method, approximating a differential equation under certain test conditions. For most techniques numerically solving differential equations, the properties of interest are consistency, stability, and convergence. Also in this category is any other property which is fundamental to the method itself. In SPH, the kernel function has fundamental influence on the properties above as well as accuracy. Therefore, in this dissertation, a chapter is devoted to each of these four topics.

The implementation of a technique is a mixture of engineering, physics, computer science, and mathematics to convert the fundamental properties into a usable tool. Therefore, discussing this category would vary from technique to technique and problem to problem as to what to include. For the SPH method, the kernel function is a good starting point. Although it was also listed as a numerical property, it is a primary element in implementing the technique and is easily changed from problem to problem. Two items that also fit in the category of implementation issues (and also closely relate to the HVI problem) are the areas of time stepping and shock handling. These two items each have a chapter devoted to them.

1.3 Contributions

Chapter II (Background) discusses relevant background material on the equations of interest, other numerical techniques, and SPH itself. This is essentially a review of material from the literature. This chapter is quite useful, in that it is one of the few instances that all of this background material appears in one place with details.

Chapter III (Consistency) discusses the mathematical concept of consistency with regards to SPH. The general idea of consistency is related to how well the numerical equations model the physical equations. The analysis of the consistency of SPH is formalized in this chapter. As usual, consistency is studied under the assumptions of sufficiently smooth data. Although this seems restrictive, since information on a numerical function is generally unavailable on a sub-grid basis, the numerical function can usually be assumed to be smooth without loss of generality. In addition, for those few times when a smooth function assumption is not acceptable, a second approach to analyzing consistency is taken. In this, a version of SPH is developed that is consistent even if the function has a discontinuity in it. Most of the work in this chapter is performed in one space dimension, but is later shown to apply in higher dimensions as well. A key assumption in the consistency analysis performed here is that volume elements based on the particle spacing are equivalent (in a sense defined later) to volume elements based on the mass and density of particles.

Chapter IV (Stability) discusses the mathematical concept of stability with regards to SPH. The basic concept of stability is the analysis of error propagation. As is common, this is first accomplished by performing a linear stability analysis. In this, SPH is applied to the Euler equations, with the field variables represented by perturbations around equilibrium points. This sort of analysis yields an amplification matrix that can be analyzed to determine the stability of the system. An instability is found in the system and four corrections are proposed. Next, an alternative method

for studying stability based on the total variation of the function is introduced. This is a more powerful technique, but more difficult to obtain results.

Chapter V (Convergence) relates the consistency and stability of the method to the mathematical concept of convergence in SPH. Convergence is the most important concept since it implies that the numerical solution is close to the actual solution. Direct proofs of convergence are often difficult to perform, but theorems relating convergence with consistency and stability are easier to prove. This is the approach taken here. A convergence theorem, obtained from the study of finite difference methods, is extended to SPH through the statement and proof of three new lemmas. Although there are several assumptions made in the theorem and lemmas that restrict its use, this is a fundamental mathematical result, providing a cornerstone upon which SPH can build a theoretical foundation.

Chapter VI (Kernels) bridges the gap between the numerical properties and implementation of SPH by discussing the kernel function. The kernel has primary roles in the consistency and stability of the method (and therefore indirectly the convergence). The kernel also directly influences the accuracy of the method. Kernel functions are relatively easy to develop and implement, but they do affect the computational cost. Hence, a choice of kernel for a particular problem will influence accuracy, stability, and practical costs; so the choice should be made wisely. Although kernel requirements, higher order kernels, and the smoothing length are all discussed in this chapter, the significant contribution is in the development of measures of merit for SPH kernels. These measures of merit are developed for both smooth and non-smooth data and then tested using eighteen kernels (many of which are first proposed here). The results lend some insight into the kernel under given assumptions while the measures of merit are general enough so that they can be used under many different assumptions.

Chapter VII (Time Schemes) discusses temporal discretizations that can be applied with the SPH spatial discretization for the complete implementation of the

method. This chapter gathers work performed in Chapters III, IV, and VI to fully discuss three alternative, second order time schemes. In addition two first-order time schemes are introduced. These are used with the hybrid schemes in Chapter VIII.

Chapter VIII (Hybrid Methods) introduces a flux-limited hybrid scheme to SPH as a way to handle shocks. This scheme is much newer than the more traditional artificial viscosity notion in finite differences, but in some cases seems to perform better. The scheme weight averages lower and higher order methods with the lower order method having more weight near a shock and the higher order method more weight away from a shock. A shock sensing algorithm is developed and incorporated into the flux-limiter (weight function). Six hybrid schemes are proposed and tested against a baseline case. Under basic assumptions (no-frills implementation) they perform roughly the same as the baseline. This concept has a long way to go before it appears in production SPH codes, but the basic foundation for the work is laid here.

In summary, through six chapters of new work, this dissertation leads the reader from the basic mathematical foundation through some important implementation concerns. This provides a solid theoretical basis to the relatively new SPH method and establishes a foundation for future development of the method.

II. BACKGROUND

The material in this chapter summarizes a combination of articles found in the published literature, informal papers, and books. The background is split into three sections: the equations, standard methods, and SPH. In the section on the equations of interest, the hypervelocity impact problem and related equations are discussed. The next section is devoted to a discussion of the finite difference and finite element techniques including some advantages and disadvantages relevant to the equations and problem. In the section on SPH, the smoothed particle hydrodynamics (SPH) method is introduced.

2.1 *The Equations*

This section addresses the fundamental properties of the equations which are to be solved. It starts with a review of the application, hypervelocity impact problems, which is governed by the Euler equations, conservation laws, and constitutive models. The emphasis of this dissertation is the analysis of the SPH methodology; however, a scenario in which the method is applied assists in fully understanding the methodology. Also, this scenario creates a framework that ties into the sponsor's needs and provides a set of equations to evaluate.

2.1.1 Introduction to Hypervelocity Impact. The basic problem is to evaluate the effects of projectiles impacting upon space assets (satellites, space stations, shuttles, etc.). These projectiles can be micrometeoroids, pieces of space debris, or anti-satellite weapons. The source does not matter as long as the projectiles are small in relation to the overall size of the satellite. In addition, many similar effects result even when the projectile and target are of similar sizes. Since the speeds of the orbiting space assets and projectiles can each be over 8 km/sec, most impacts occur at very high speeds. Although the minimum speed for an impact to be considered a hypervelocity impact is not firmly fixed, these collisions definitely fall into the HVI

category following any definition as will be seen. Zukas characterizes HVI by "impact velocities in excess of the local sound speeds ($v_s \gg c$) and usually the complete pulverization of the projectile and target material in the impact region." (71, 72). The second part of this characterization can imply that very soft, dense materials are considered HVI at much lower velocities than very strong, low-density materials. However, since Zukas states that even the strong materials collide at "hypervelocities" when speeds are in the 8-10 km/sec range, the initial impacts are considered to all be HVI regardless of materials involved.

Although opinions on this vary, Zukas summarizes the effects at hypervelocity rather succinctly: "shock waves propagate through the colliding bodies which, for all practical purposes, behave as fluids. Analytically, the equations of motion and a high pressure equation of state are the key descriptors of material behavior. Material strength is significant only for the late stages of this energy driven problem and may often be treated with a simple incremental elastic, perfectly plastic model with an appropriate value of flow stress obtained from dynamic (wave propagation) experiments. Spallation is a frequently encountered failure mechanism. Because of the short time scale of the material response, simple time-independent failure criteria for spall often give satisfactory results." (72:594)

Some key sources for information on HVI are: Zukas, et al. (71, 72) for impact dynamics and the two Hypervelocity Impact Symposia (23, 24), especially Anderson (1) and Asay and Kerley (2) for HVI effects.

2.1.2 HVI Equations. As in classical mechanics, the starting equations are almost always the conservation equations. Conservation of mass, momentum, and energy are all required to be satisfied. Some general information on conservation laws is presented later. For now, the most basic forms (steady state) of these are

seen in equations (2.1):

$$\begin{aligned}
\text{Conservation of Mass: } \int_V \rho dV &= \text{const} \\
\text{Conservation of Momentum: } \sum_{i=1}^N m_i \vec{v}_i &= \text{const} \\
\text{Conservation of Energy: } \sum_{i=1}^N m_i E_i &= \sum_{i=1}^N \left(m_i e_i + \frac{1}{2} m_i v_i^2 \right) = \text{const},
\end{aligned} \tag{2.1}$$

where ρ is the mass density, m is the mass, V is the volume, \vec{v} is the velocity, E is the total energy, and e is the internal energy. These basic equations are not sufficient to capture variation in time, but are useful in verifying that a numerical method used for spatial derivatives conserves the mass, momentum, and energy.

To capture the time variation, partial differential equations of motion are needed. For this problem we use the Euler equations of gas dynamics. These can be written in what is referred to as Eulerian or Lagrangian forms. Since the primary numerical method studied in this dissertation is a Lagrangian formulation, those forms of the equations are given (ref Anderson (1:33)) below

$$\frac{D\rho}{Dt} = -\rho (\nabla \cdot \vec{v}) \tag{2.2}$$

$$\frac{D\vec{v}}{Dt} = \vec{F} - \frac{1}{\rho} (\nabla \cdot \boldsymbol{\sigma}) \tag{2.3}$$

$$\frac{DE}{Dt} = \vec{F} \cdot \vec{v} - \frac{1}{\rho} \nabla \cdot (\boldsymbol{\sigma} \cdot \vec{v}), \tag{2.4}$$

where $\boldsymbol{\sigma}$ is the stress tensor and F are external body forces. The $\frac{D}{Dt}$ derivatives are the Lagrangian or Stokesian derivatives and are defined as

$$\frac{D}{Dt} = \frac{\partial}{\partial t} + \vec{v} \cdot \frac{\partial}{\partial \vec{r}}.$$

Although the forms of the Euler equations found in equations (2.2)–(2.4) could be used as is, it is common in SPH to make some simplifications. The first simplification

is to just solve for internal energy (e) instead of solving for total energy (E), where total energy equals kinetic plus internal. Nothing is lost in this change because total energy can be recovered from the momentum and internal energy equations. Further, because most of the common forms of the equation of state use internal energy, this is a useful change. To make this change, do the following

$$\begin{aligned}\frac{DE}{Dt} &= \frac{D}{Dt} \left(e + \frac{1}{2}v^2 \right) = \frac{De}{Dt} + \vec{v} \cdot \frac{D\vec{v}}{Dt} = \vec{F} \cdot \vec{v} - \frac{1}{\rho} \nabla \cdot (\boldsymbol{\sigma} \cdot \vec{v}) \\ \frac{De}{Dt} &= \vec{F} \cdot \vec{v} - \frac{1}{\rho} \nabla \cdot (\boldsymbol{\sigma} \cdot \vec{v}) - \vec{v} \cdot \frac{D\vec{v}}{Dt} \\ &= -\frac{1}{\rho} \nabla \cdot (\boldsymbol{\sigma} \cdot \vec{v}) + \frac{\vec{v}}{\rho} \cdot (\nabla \cdot \boldsymbol{\sigma}) = -\left(\frac{\boldsymbol{\sigma}}{\rho} \cdot \nabla \right) \cdot \vec{v} .\end{aligned}$$

The second simplification is to assume there are no external body forces (that is, $\vec{F} = 0$). For most HVI problems, boundaries are essentially at infinity, where the field variables are zero. So nothing is lost in this simplification. The third simplification is to deal with strictly hydrodynamic problems. This implies the deviatoric stress tensor is zero and the stress tensor given in the equations above can be replaced with just the pressure, P . This last assumption makes the analysis much simpler and is frequently done. However, for many impact problems material strength is important and this assumption cannot be made in those cases. Material models are briefly discussed later in this section. Using these three simplifications, the form of the Euler equations as used throughout most of this dissertation is

$$\text{Continuity Equation:} \quad \frac{D\rho}{Dt} = -\rho (\nabla \cdot \vec{v}) \quad (2.5)$$

$$\text{Momentum Equation:} \quad \frac{D\vec{v}}{Dt} = -\frac{1}{\rho} \nabla P \quad (2.6)$$

$$\text{Energy Equation:} \quad \frac{De}{Dt} = -\frac{P}{\rho^2} (\nabla \cdot \vec{v}) \quad (2.7)$$

$$\text{Particle Motion Equation:} \quad \frac{Dx}{Dt} = v . \quad (2.8)$$

Note that the particle motion equation was added, where x is the position of the material point. To complete the system, an equation of state is added to the set of equations. The equation of state, often written as $P = P(\rho, e)$, is discussed later in this chapter.

2.1.3 Conservation Laws. Conservation Laws are the fundamental equations to solve; therefore the basic concepts are discussed here. The derivations below are taken primarily from LeVeque (32), Lax (30), and Quinn (50). Other good sources include Weinacht (67) and Smoller (57).

Although conservation laws are often shown as differential equations, they are in fact integral relationships that equate the rate of change of the integral with the flux across the boundary (ref (32:16))

$$\frac{d}{dt} \int_a^b u(x, t) dx = f(u(a, t)) - f(u(b, t)). \quad (2.9)$$

Integrate this equation in time to obtain

$$\int_a^b u(x, t_2) dx = \int_a^b u(x, t_1) dx + \int_{t_1}^{t_2} f(u(a, t)) dt - \int_{t_1}^{t_2} f(u(b, t)) dt. \quad (2.10)$$

If u and f are differentiable, then

$$u(x, t_2) - u(x, t_1) = \int_{t_1}^{t_2} \frac{\partial}{\partial t} u(x, t) dt \quad (2.11)$$

$$f(u(b, t)) - f(u(a, t)) = \int_a^b \frac{\partial}{\partial x} f(u(x, t)) dx. \quad (2.12)$$

Substituting (2.11) and (2.12) into equation (2.10) yields

$$\int_{t_1}^{t_2} \int_a^b \left\{ \frac{\partial}{\partial t} u(x, t) + \frac{\partial}{\partial x} f(u(x, t)) \right\} dx dt = 0. \quad (2.13)$$

Since this must hold for any region $\{[a, b] \times [t_1, t_2]\}$ it can be concluded that

$$\frac{\partial}{\partial t} u(x, t) + \frac{\partial}{\partial x} f(u(x, t)) = 0. \quad (2.14)$$

This is often referred to as the general form of the conservation law. It is usually given with $t_1 = 0$ and an initial condition such as

$$u(x, 0) = u_o(x) \quad x \in [a, b]. \quad (2.15)$$

Differential equations written as initial value problems, such as (2.14)–(2.15), are often used as the model to solve (such as the Euler equations given earlier) and the desired solutions are known as *classical solutions*. Lax has shown (in (30)) that a solution for this initial value problem exists and is unique (under certain restrictions discussed later).

Definition 1 (Continuous Function Spaces)

- $C^n(\Omega)$ denotes a space of n times continuously differentiable functions on Ω .
- $C_o^n(\Omega)$ denotes a $C^n(\Omega)$ space where all functions have compact support.

Definition 2 (Classical Solution) $u(x, t)$ is a classical solution of the conservation law (2.14), (2.15) if the following holds

1. $u \in C^1([a, b] \times (0, t_2])$
2. $u_t(x, t) + [f(u(x, t))]_x = 0 \quad (x, t) \in \{[a, b] \times (0, t_2]\}$
3. $u \in C([a, b] \times [0, t_2])$
4. $u(x, 0) = u_o(x) \quad x \in [a, b].$

The assumptions above, that u and f be differentiable (or even continuous) over the entire domain, do not always hold. In the equations to be solve, this most often

occurs at a shock. At those times a classical solution of (2.14) fails to exist and other solutions must be sought out. The most common approach is to consider the so called *weak solution*. The name *weak* as used here indicates less continuity in the solution.

Definition 3 $C_0^1(\mathcal{R} \times \mathcal{R}^+)$ denotes the space of continuously differentiable functions $f(x, t)$ defined on $\{(-\infty, \infty) \times (0, \infty)\}$ and for each function there exists real constants r_1, r_2 , and τ such that $f(x, t) = 0$ for $x < r_1, x > r_2$, or $t > \tau$.

Definition 4 (Weak Solution) $u(x, t)$ is a weak solution of the conservation law (2.14) if the following holds for all test functions $\phi(x, t) \in C_0^1(\mathcal{R} \times \mathcal{R}^+)$

$$\int_0^\infty \int_{-\infty}^\infty [\phi_t u + \phi_x f(u)] dx dt = - \int_{-\infty}^\infty \phi(x, 0) u(x, 0) dx. \quad (2.16)$$

It is relatively straightforward to see that a classical solution of (2.14) will satisfy (2.16). Simply multiply (2.14) by $\phi(x, t)$, integrate over all time and space, and then integrate by parts. Due to the compact support of ϕ , most of the boundary terms vanish and equation (2.16) is obtained.

The disadvantage of weak solutions is that they are not necessarily unique. So an additional requirement must be levied in order to obtain the desired solution. This is often an entropy condition, which relies on using the Rankine-Hugoniot jump relationship to ensure entropy does not decrease across the shock. One form of the entropy condition (sometimes referred to as Condition E) is as follows. If u^- and u^+ are the limits of u from the left and right respectively at a given time, and if v is between u^- and u^+ then

$$S[v, u^-] \geq S[u^+, u^-] \quad (2.17)$$

$$\text{where} \quad S[a, b] = \frac{f(a) - f(b)}{a - b}. \quad (2.18)$$

This condition can be explained by stating that the flux, f , must lie above the chord $[u^-, u^+]$ when $u^- < u^+$ and below the chord $[u^+, u^-]$ when $u^+ < u^-$. Quinn (50) proved that a piecewise continuously differentiable solution to the initial value problem for the conservation law which satisfies condition E is unique. That proof is not repeated here. Other entropy conditions are given in the literature, but they are all essentially the same since the Rankine-Hugoniot relationship is the foundation of all the forms.

2.1.4 Additional Equations and Models. In addition to the conservation equations just discussed (particularly the Euler equations), the equation of state and constitutive equations must be considered. First, the equation of state (EOS) which "accounts for compressibility effects (changes in density) and irreversible thermodynamic processes such as shock heating." (1:34) Put simply, the relationship among pressure, density (or specific volume), and internal energy (or temperature) can be obtained. This is often represented as $P = P(\rho, e)$. This relationship is derived mostly from statistical mechanics and also often involves the Hugoniot. The Hugoniot curve comes from the locus of points produced by shock compression and can be considered a material property analogous to a stress-strain curve. Most EOSs are only valid over a limited range of its parameters. So several different EOSs need to be available for use with any numerical algorithm. Some of the more common EOSs for HVI are identified by Zukas (72:600) or Holian and Holian (21, 22).

Holian and Holian (21, 22) state that the Tillotson EOS has traditionally been the favorite for HVI problems; however, from personal experience the Mie - Grüneisen is also frequently used. Asay and Kerley state "the Tillotson EOS is an improvement to the Mie-Grüneisen formula that has been useful for hypervelocity impact calculations. However, it is oversimplified and does not give a good description of many of the phenomena In order to construct an EOS that is accurate over a wide range of densities and temperatures, it is necessary to develop a theoretical model that includes a treatment of many physical phenomena, as are illustrated in Figure 4

[Figure 2.1 here].” (2:75) This figure points out the difficulty of accurately modeling the EOS and is an area on the physics side of the problem in which work could be done. Holian and Holian (21, 22) compared the Tillotson, Osborne (an analytical polynomial EOS), and the SESAME library (a tabular EOS). From their work it appears that the SESAME library EOS may currently be best for HVI type problems, but more work should be done to verify this (especially for SPH). However, that is a subject of future work and will not be pursued in this dissertation.

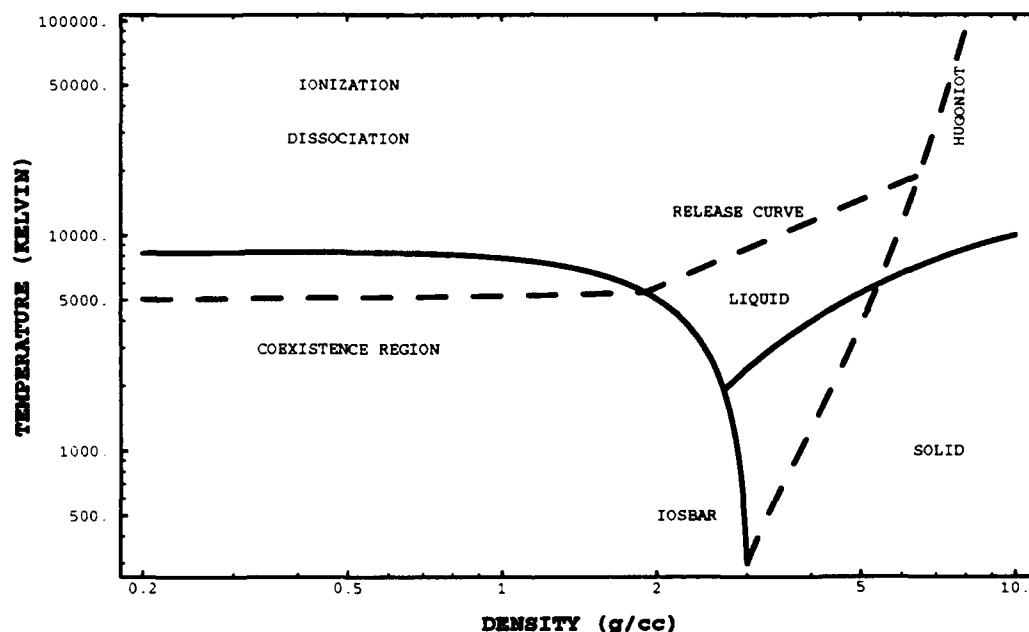


Figure 2.1 Equations of State Phenomena (2:77)

The last set of equations discussed here are the constitutive equations. These are employed to calculate stress, for the most part as a function of strain, strain rate, internal energy, and damage. As noted earlier, constitutive equations are not going to be included in the analysis for this dissertation, but a few words are included here for completeness. The modeler has a great number of choices as to exactly what

to include and how to implement these effects. The exact implementation of the material strength is performed by what is usually referred to as a strength model; while failure mechanisms are usually referred to as fracture models and/or fragmentation models. For HVI problems, simple elastic-perfectly plastic representations are usually sufficient, especially for early-time initial impacts, as the material strength plays only a small role in the results. However, if the problem is carried out for longer periods of time, other strength models may be better. Also for this problem, the secondary, tertiary, etc. impacts occur at lower velocities and may require the use of more accurate strength models. Failure models are not always used, but in all cases should provide more accurate results, especially when calculating the debris cloud after an impact event.

2.2 *Standard Numerical Techniques*

"Analytical modeling of hypervelocity events is relatively straightforward. In numerical simulations, the accuracy achievable and the problems addressable are limited mainly by the speed and memory of the computer. The compressible fluid analogy serves well for many practical engineering applications." (72:595) From this quote, it is apparent that Zukas has an optimistic view of the modeling process, but compared to many other types of problems he may be correct. In this section, numerical methods used to solve HVI problems are discussed. "Computer programs which handle the propagation of shock waves and compute velocities, strains, stresses, etc., as a function of time and position are called *hydrocodes*. Early formulations did not include strength effects. Thus, metals were treated as a fluid, with no viscosity, and the expression, *hydrodynamic computer code* came into being; with time, this was shortened to hydrocodes." (1:34) Of course, from the previous section it is obvious that strength can be included in these codes, but the name hydrocode has stuck. Two methods that have been in use for many years and can be considered standard techniques are finite difference methods and finite element methods. A

popular quote credited to Gordon Johnson that provides a general feeling of the difference between these is "finite difference techniques are an approximate solution to an exact problem, and finite element techniques are an exact solution of an approximate problem." (1:43) The standard techniques can also be classified based on the type of grid they employ. These are the Eulerian grid (often associated with finite differences) and the Lagrangian grid (often associated with finite elements). Both of these methods have been used with varying degrees of success for several years to study HVI problems. However, both methods have difficulties solving these problems. This section highlights some of the advantages and disadvantages of each method and concludes with a discussion of why a particle method might be able to combine the advantages of each to provide better results.

In the Lagrangian grid method, the grid is fixed to the material and moves with it. An example of this is seen in Figure 2.2. This seems to have several advantages, especially for the HVI problem. Some of these are: the code is conceptually simpler and should be faster because of no convective terms, time histories are easily obtainable, material interfaces and geometric boundaries are sharply defined, the opening and closing of voids at interfaces can be computed, material models (constitutive equations) are well integrated into the method, and irregular geometries are easily treated. The disadvantages center around two areas: a sliding interface and mesh distortion. Elaborate sliding interfaces are required to model impact (as well as other) problems, reducing or eliminating the computational simplicity and cost advantage. In addition, these sliding interfaces have little theoretical basis to guarantee convergence to a physical result. The very large distortions (which occur in HVI) can have even worse effects. The time step (based on the smallest element size) can become too small to be efficient. Quadrilateral elements can become turned inside out (or bow-tied) causing negative volumes, which causes conservation to be lost. Triangular elements can also have problems where one element might have very large positive pressure and its neighbor have very large negative pressure. Finally, highly

distorted elements can cause errors in constitutive equation evaluation. The option to rezone is available in Lagrangian codes. However, with each rezone some material diffusion occurs and material histories are lost. Also, as the frequency of rezones goes up, the code starts to resemble an Eulerian code (in an overall sense). So even though there are some very good advantages to Lagrangian codes, the disadvantages often lead modelers to Eulerian representations.

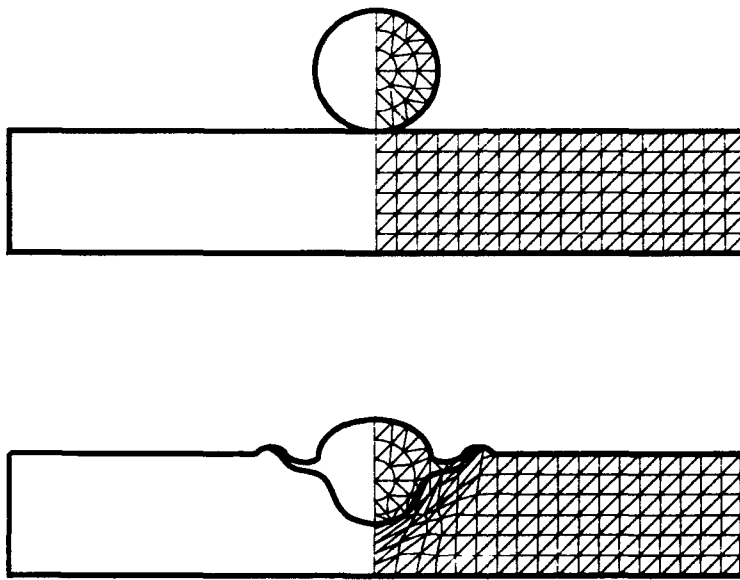


Figure 2.2 Lagrangian Example (72:602)

An overall preference for Eulerian methods is indicated by the large percentage of papers in the proceedings of the last two Hypervelocity Impact Symposia (23, 24). The Eulerian method has a fixed grid in which material is placed in this grid and is allowed to flow through it. An example of this is seen in Figure 2.3 (although the material interfaces in the partially filled cells are not as distinct as shown). The advantages and disadvantages seem to center around the same item: the mixing of material in each mesh cell. For problems that physically have materials that mix this

is advantageous, albeit a numerical mixing process rather than physical. Also, large distortions do not cause the numerical problems of the Lagrangian method. However, material interfaces can quickly become lost in this method. Although many new techniques to reduce this problem and handle mixed-cells are being derived, there are still inaccuracies as well as a limit on the number of materials in a cell (often 2). In addition, any unusual geometric shape is distorted and often has details lost using an Eulerian grid. The last disadvantage of Eulerian methods is their requirement to grid and model the entire problem space. In a problem that has a large amount of void, such as a satellite impact, this void becomes part of the computational process. This usually requires the modeler to use a larger grid spacing for computational efficiency at the expense of resolution and accuracy.

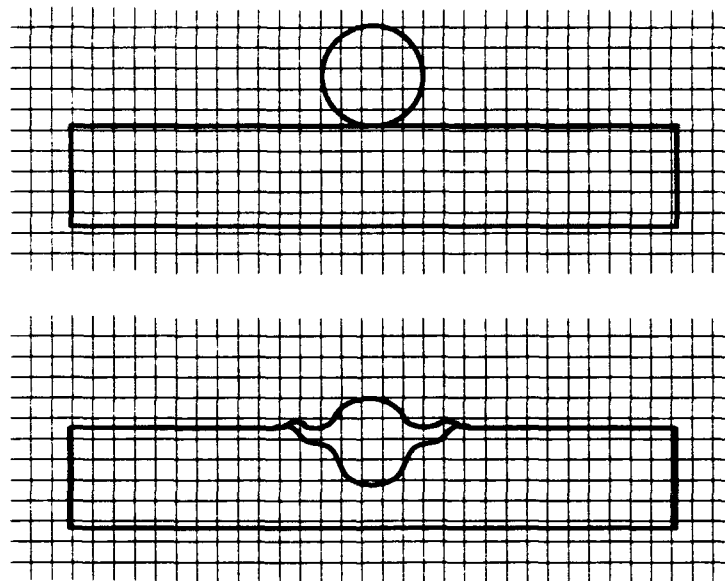


Figure 2.3 Eulerian Example (72:603)

From the discussion in this section, it may appear that the existing, standard techniques have no merit. This, of course, is untrue. Many of the problems in these

methods come from the combination of factors that make up an HVI problem. Also, for small-scale, single-impact analyses some of the disadvantages do not cause major difficulties and results from these techniques may be used. However, when analyzing a large-scale situation, impact modelers looked elsewhere for numerical techniques to more accurately model the HVI problem. This search lead them to consider particle methods. Although there are several different approaches to particle methods (7, 20, 61, 12, 33), as discussed in the introduction, the focus in this work is on Smoothed Particle Hydrodynamics (SPH). The general notion in SPH is to represent the material at discrete points (or particles). These points can be considered analogous to grid points (from finite differences) or even elements (from finite elements). But, it is best to consider them as interpolation points. Provided a sufficient number of particles are used, material interfaces should be modeled quite well like a Lagrangian code. But since there is no grid in SPH, it should not have the problems of distortion and tangling caused by HVI. The particles must be *smoothed* out to represent a fluid continuum flow and not just a discrete molecular interaction (such as on an atomic level). Then, if the method can be made computationally efficient it would combine the best of both worlds. Of course, like any numerical technique SPH has its disadvantages as well. However, it seems to have great promise and needs further study. Hence, the remainder of this dissertation reports the results of that additional study on the method known as smoothed particle hydrodynamics.

2.3 *Smoothed Particle Hydrodynamics*

As described at the end of the previous section, Smoothed Particle Hydrodynamics (SPH) is of interest as a possible alternative to the more standard finite difference and finite element techniques in solving hypervelocity impact type problems. In this section, the basics of SPH and some of the enhancements are described.

2.3.1 Introduction. SPH is a gridless, pure Lagrangian method for solving the Euler equations of gas dynamics. Within particle methods, SPH fits into

a Particle-Particle category as described by Hockney and Eastwood (20). That is, the state of a system is determined by a collection of particle positions and velocities while forces are calculated through interparticle interactions. Particle-particle methods should be quite efficient provided long range forces are not calculated. SPH was originated by Lucy (35) and Gingold and Monaghan (12) in 1977. It has been used to study several different types of problems, including: astrophysics, gas dynamics, plasma (MHD), relativity, and impact. A large amount of literature on SPH was studied and assimilated into this section. Some of the better sources used here include: Gingold and Monaghan (12, 13), Monaghan and Gingold (37), Monaghan (36, 38, 39, 42, 44), Benz (5), Bicknell (6), Libersky (34), and the two SPH workshops (9, 69).

2.3.2 Kernel Approximation. SPH is often derived in a two step approach. First is the kernel approximation described here. Second is the particle approximation described in the next subsection. The name used in the SPH literature is *kernel estimate*. However, it is somewhat misleading, especially in the presentation in this dissertation. More appropriate names would be kernel approximation, kernel average, or smoothed average. Hence, the term kernel approximation is used in this dissertation.

The kernel approximation can be thought of in two ways. First, using ideas from distribution theory, an approximation to a delta distribution representation of a function can be obtained. This is only mentioned in passing in a few papers so I will concentrate on the second, more popular notion. First, select a continuous function with other appropriate requirements described later and label this function as the kernel. Then multiply an equation by the kernel and integrate to obtain the same results as the distribution idea. These ideas lead to the kernel approximation of f shown in equation (2.19)

$$\langle f(\vec{r}_o) \rangle = f_k(\vec{r}_o) = \int_{\Omega} f(\vec{r}) W(\vec{r}_o - \vec{r}, h) d\vec{r} \quad (2.19)$$

where

$$\int_{\Omega} W(\vec{r}_o - \vec{r}, h) d\vec{r} = 1, \quad (2.20)$$

h (the smoothing length) is a measure of the width of the kernel function W , and Ω is the spatial domain. In equation (2.19) the notation of the angle brackets ($\langle f(\vec{r}_o) \rangle$) and the subscript k ($f_k(\vec{r}_o)$) are found frequently in the literature to identify the kernel approximation (estimate) of a function, so they are used here.

In the SPH literature, the kernel approximation (estimate) is often referred to as an order h^2 or second order method. The error analysis appears to some degree in Monaghan (36), but not to the extent that I would like to see it. Therefore, the derivation of the error bound is omitted here and derived fully in the next chapter. However, simply note, that if the kernel W is normalized, is an even function, and has compact support then

$$f_k(\vec{r}_o) = f(\vec{r}_o) + E_k(f, \vec{r}_o) \quad (2.21)$$

$$\text{where} \quad E_k(f, \vec{r}_o) = \frac{1}{2} \int_{\Omega} [\vec{u} \cdot \nabla]^2 f(\vec{\xi}_o) W(-\vec{u}, h) d\vec{u} \quad (2.22)$$

for $\vec{\xi}_o = \vec{\xi}_o(\vec{u}) \in \Omega$.

The bound on the error term is

$$|E_k(f, \vec{r}_o)| \leq e_k h^2, \quad (2.23)$$

for a small, bounded constant e_k (see equation (3.5) in the next chapter).

2.3.3 Particle Approximation. If a set of N points is given, distributed randomly (or quasi-randomly) according to number density, $n(\vec{r})$, a Monte Carlo approximation (2.24) of equation (2.19) known as the particle approximation may be obtained. See Hammersley and Handscomb (14) and Niederreiter (46) for more

information. The approximation is

$$f_n(\vec{r}_o) = \sum_{j=1}^N \frac{f(\vec{r}_j)}{n(\vec{r}_j)} W(\vec{r}_o - \vec{r}_j, h), \quad (2.24)$$

where $n(\vec{r}_j)$ is the number density. This particle approximation was shown by Monaghan (36) to be similar to orthogonal function interpolation. However, they differ in the type of kernel being used and in the error. Also interpolation often uses a fixed set of points usually determined by the method, but in SPH the points move and are determined by the problem itself. Regardless of how to get to the particle approximation, it may be easily believed that as $N \rightarrow \infty$, if $\frac{1}{n(\vec{r}_j)} \rightarrow 0 \forall j \in \mathcal{N}$, then $f_n(\vec{r}_o) \rightarrow f_k(\vec{r}_o)$. Of course, there are errors in the particle approximation, but they are more difficult to develop than the errors in the kernel approximation. But it would still be desirable to show the relationship

$$f_n(x_o) = f_k(x_o) + E_n(f, x_o). \quad (2.25)$$

Unfortunately at this time it would require a great deal of background in probability and Monte Carlo theory, so just a few general comments are made. The older SPH journal articles used a Monte Carlo argument, stating the error would be proportional to $\frac{1}{\sqrt{N}}$. An error such as this could easily dominate the problem or require extremely large numbers of particles to be used. However, this was found to be not very close to the actual errors seen in numerical experiments (too pessimistic). Monaghan (36) hypothesized this was because disorder was initially low (and so were fluctuations) and when the problem became more disordered large fluctuations were prevented because they required too much energy. Basically the physics of the problem kept the numerical errors from getting out of hand. So then, looking at the problem even when an instability arises, the error is more likely to be based on disordered quasi-randomly distributed numbers which has error $O(\frac{(\ln N)^d}{N})$ where d is the dimension. See Niederreiter (46) for more information on this argument.

2.3.4 *Procedure.* For any particle i , there exists a mass, $m_i = m(\vec{r}_i)$ and mass density, $\rho_i = \rho(\vec{r}_i)$ such that the number density equals the mass density divided by the mass, $n(\vec{r}_i) = \frac{\rho_i}{m_i}$. So the general SPH approximation for a function can be obtained from equation (2.24) as shown in equation (2.26).

$$f_n(\vec{r}_o) = \sum_{j=1}^N \frac{m_j}{\rho_j} f(\vec{r}_j) W(\vec{r}_o - \vec{r}_j, h). \quad (2.26)$$

In the next chapter the relationship $f_n(\vec{r}) = f(\vec{r}) + O(h^2, h\Delta x)$ is derived fully with the value of $f_n(\vec{r})$ given in equation (2.26). However, at this time, note that the bounds given in the literature are

$$\begin{aligned} f(\vec{r}) &= f_n(\vec{r}) - E_k(f, \vec{r}) - E_n(f, \vec{r}) \\ &= \sum_{j=1}^N \frac{m_j}{\rho_j} f(\vec{r}_j) W(\vec{r} - \vec{r}_j, h) + O(h^2, \frac{(\ln N)^d}{N}). \end{aligned} \quad (2.27)$$

In addition to the equation above, there are two other formulations that would be useful to generalize in SPH for later use: the gradient and the divergence. These are given below.

The Gradient. Given a general partial differential equation: $\frac{d\vec{A}}{dt} = \nabla B$ for functions \vec{A} and B , the particle approximation may be systematically derived as follows. First, multiply by the kernel (W), integrate, and then use Gauss's Theorem. Consider only the ∇B term

$$\begin{aligned} \langle \nabla B \rangle &= \int_{\Omega} [\nabla_{\vec{r}} B(\vec{r})] W(\vec{r}_o - \vec{r}, h) d\vec{r} \\ &= \int_{\partial\Omega} B(\vec{r}) W(\vec{r}_o - \vec{r}, h) \vec{n} dS - \int_{\Omega} B(\vec{r}) \nabla_{\vec{r}} W(\vec{r}_o - \vec{r}, h) d\vec{r}, \end{aligned}$$

where $\nabla_{\vec{r}}$ is the gradient with respect to \vec{r} . W is defined to have compact support and often B has only short range effects (so in some sense B has compact support

as well), therefore the surface term is taken to be zero. The result is then

$$\begin{aligned} \langle \nabla B \rangle &= - \int_{\Omega} B(\vec{r}) \nabla_{\vec{r}} W(\vec{r}_o - \vec{r}, h) d\vec{r} = \int_{\Omega} B(\vec{r}) \nabla_o W(\vec{r}_o - \vec{r}, h) d\vec{r} \\ &= \nabla_o \int_{\Omega} B(\vec{r}) W(\vec{r}_o - \vec{r}, h) d\vec{r} = \nabla \langle B \rangle, \end{aligned}$$

where ∇_o is the gradient with respect to \vec{r}_o . Therefore, for problems with boundaries at infinity or when B is sufficiently far from the boundary, the surface terms are zero. Hence this results in $\langle \nabla B \rangle = \nabla \langle B \rangle$. Note: for boundary value problems, the surface terms do not necessarily vanish and can cause large difficulties and confusing formulas. See Chapter III, VIII, and Campbell (8) for a discussion of these types of problems. Now consider the entire equation $\frac{d\vec{A}}{dt} = \nabla B$. Then

$$\left\langle \frac{d\vec{A}}{dt} \right\rangle = \langle \nabla B \rangle.$$

Using equation (2.21) and the work above to obtain

$$\frac{d\vec{A}}{dt} + E_k \left(\frac{d\vec{A}}{dt}, r \right) = \nabla \langle B \rangle.$$

From equation (2.25) the particle approximation of B , B_n , is used for the $\langle B \rangle$ term with the results

$$\begin{aligned} \frac{d\vec{A}}{dt} &= \nabla B_n - E_n(B, r) - E_k \left(\frac{d\vec{A}}{dt}, r \right) \\ &= \nabla \left[\sum_{j=1}^N \frac{m_j}{\rho_j} B(\vec{r}_j) W(\vec{r} - \vec{r}_j, h) \right] - E_n(B, r) - E_k \left(\frac{d\vec{A}}{dt}, r \right) \\ &= \sum_{j=1}^N \frac{m_j}{\rho_j} B(\vec{r}_j) \nabla W(\vec{r} - \vec{r}_j, h) - E_n(B, r) - E_k \left(\frac{d\vec{A}}{dt}, r \right), \end{aligned}$$

or for particle i

$$\left(\frac{d\vec{A}}{dt}\right)_i = (\nabla B)_i = \sum_{j=1}^N \frac{m_j}{\rho_j} B(\vec{r}_j) \nabla_i W(\vec{r}_i - \vec{r}_j, h) + O(h^2, \frac{(\ln N)^d}{N}), \quad (2.28)$$

where ∇_i is the gradient with respect to \vec{r}_i .

The Divergence. Given a general partial differential equation: $\frac{dA}{dt} = \nabla \cdot \vec{B}$ for functions A and \vec{B} , the particle approximation may be systematically derived similarly as before. Multiply by the kernel, W , integrate, and use the divergence theorem to obtain a surface integral. Considering only the $\nabla \cdot \vec{B}$ term

$$\begin{aligned} \langle \nabla \cdot \vec{B} \rangle &= \int_{\Omega} [\nabla_r \cdot \vec{B}(\vec{r})] W(\vec{r}_o - \vec{r}, h) d\vec{r} \\ &= \int_{\Omega} \left\{ \nabla_r \cdot [\vec{B}(\vec{r}) W(\vec{r}_o - \vec{r}, h)] - [\vec{B}(\vec{r}) \cdot \nabla_r W(\vec{r}_o - \vec{r}, h)] \right\} d\vec{r} \\ &= \int_{\partial\Omega} \vec{B}(\vec{r}) W(\vec{r}_o - \vec{r}, h) \cdot \vec{n} dA - \int_{\Omega} \vec{B}(\vec{r}) \cdot \nabla_r W(\vec{r}_o - \vec{r}, h) d\vec{r} \\ &= \int_{\Omega} \vec{B}(\vec{r}) \cdot \nabla_o W(\vec{r}_o - \vec{r}, h) d\vec{r}, \end{aligned}$$

where ∇_r is the gradient with respect to \vec{r} and ∇_o is the gradient with respect to \vec{r}_o . The last step uses the compact support of the kernel as before, making the term on the surface zero. Also, since W is assumed to be even, the gradient of the kernel can be interchanged from ∇_r to ∇_o with a negative sign cancelling the existing one. The result is then

$$\begin{aligned} \langle \nabla \cdot \vec{B} \rangle &= \int_{\Omega} \vec{B}(\vec{r}) \cdot \nabla_o W(\vec{r}_o - \vec{r}, h) d\vec{r} \\ &= \nabla_o \cdot \int_{\Omega} \vec{B}(\vec{r}) W(\vec{r}_o - \vec{r}, h) d\vec{r} = \nabla \cdot \langle \vec{B} \rangle. \end{aligned}$$

Therefore, for problems with boundaries at infinity or when B is sufficiently far from the boundary, the surface terms are zero. Hence this results in $\langle \nabla \cdot \vec{B} \rangle = \nabla \cdot \langle \vec{B} \rangle$. Now consider the equation multiplied by ρ , $\rho \frac{dA}{dt} = \rho(\nabla \cdot \vec{B})$. Expand

the product to obtain

$$\rho \frac{dA}{dt} = \rho (\nabla \cdot \vec{B}) = \nabla \cdot (\rho \vec{B}) - \vec{B} \cdot \nabla \rho.$$

Apply the results from the gradient and the divergence above and equations (2.21) and (2.25) to obtain

$$\rho \frac{dA}{dt} = \nabla \cdot (\rho \vec{B})_n - \vec{B} \cdot \nabla \rho_n - E_k(\rho \frac{dA}{dt}, x) - E_n(\rho \vec{B}, x) + \vec{B} \cdot E_n(\rho, x).$$

Use equations (2.26) and (2.28) above to obtain

$$\begin{aligned} \rho_i \left(\frac{dA}{dt} \right)_i &= \left[\nabla_i \cdot \sum_{j=1}^N m_j \vec{B}(\vec{r}_j) W(\vec{r}_i - \vec{r}_j, h) \right] \\ &\quad - \left[\vec{B}(\vec{r}_i) \cdot \sum_{j=1}^N m_j \nabla_i W(\vec{r}_i - \vec{r}_j, h) \right] + O(h^2, \frac{(\ln N)^d}{N}) \\ &= \sum_{j=1}^N m_j \vec{B}(\vec{r}_j) \cdot \nabla_i W(\vec{r}_i - \vec{r}_j, h) - \sum_{j=1}^N m_j \vec{B}(\vec{r}_i) \cdot \nabla_i W(\vec{r}_i - \vec{r}_j, h) \\ &\quad + O(h^2, \frac{(\ln N)^d}{N}). \end{aligned}$$

So for particle i

$$\begin{aligned} \left(\frac{dA}{dt} \right)_i &= (\nabla \cdot \vec{B})_i = \frac{1}{\rho_i} \sum_{j=1}^N m_j (\vec{B}(\vec{r}_j) - \vec{B}(\vec{r}_i)) \cdot \nabla_i W(\vec{r}_i - \vec{r}_j, h) \\ &\quad + O(h^2, \frac{(\ln N)^d}{N}). \end{aligned} \tag{2.29}$$

Using these procedures the mass, momentum, and energy conservation equations may be derived in SPH format. Note: it is possible to derive other equations as well using this general procedure. In subsequent equations, the error terms are often dropped and ' \approx ' is used for the estimates and approximations.

Product Rule. A product rule for the SPH approximations is needed in the work that follows. So for functions A and B

$$\begin{aligned}
 \langle A \rangle \langle B \rangle &= [A + E_k(A, x)] [B + E_k(B, x)] \\
 &= AB + B E_k(A, x) + A E_k(B, x) + E_k(A, x) E_k(B, x) \\
 &= \langle AB \rangle - E_k(AB, x) + B E_k(A, x) + A E_k(B, x) \\
 &\quad + E_k(A, x) E_k(B, x) .
 \end{aligned}$$

Hence, to within the order of the method, the approximation of a product equals the product of the approximations.

2.3.5 Density. Since the distribution of the particles is based on number density, the mass density (ρ) should play a significant role in this method. There are two ways in which to calculate the density, both of which are frequently used. The most common, especially in the older SPH literature, is to calculate the density directly from the particle approximation given earlier in equation (2.26). If the function, $f(\vec{r})$ is taken to be $\rho(\vec{r})$, and therefore $f(\vec{r}_j) = \rho_j$, the result is shown in equation (2.30):

$$\rho(\vec{r}) \approx \rho_n(\vec{r}) = \sum_{j=1}^N m_j W(\vec{r} - \vec{r}_j, h) . \quad (2.30)$$

Several of the early papers had $m_j = m$ constant for each particle. So for $M = \text{Total Mass}$, $\frac{M}{N} = m$ and $\rho(\vec{r}) \approx m \sum_{j=1}^N W(\vec{r} - \vec{r}_j, h) = \frac{M}{N} \sum_{j=1}^N W(\vec{r} - \vec{r}_j, h)$. However, the more general form (2.30) is used throughout this dissertation.

Some general notes on conservation of mass. In the following integrals, W has compact support so the domain Ω can be taken as finite. This justifies the interchange in the order of integration.

$$\begin{aligned}
(i) \quad \int_{\Omega} \rho_k(\vec{r}) d\vec{r} &= \int_{\Omega} \int_{\Omega} \rho(\vec{x}) W(\vec{r} - \vec{x}, h) d\vec{x} d\vec{r} \\
&= \int_{\Omega} \rho(\vec{x}) \int_{\Omega} W(\vec{r} - \vec{x}, h) d\vec{r} d\vec{x} = \int_{\Omega} \rho(\vec{x}) d\vec{x} = M
\end{aligned}$$

So ρ_k conserves mass exactly.

$$\begin{aligned}
(ii) \quad \int_{\Omega} \rho_n(\vec{r}) d\vec{r} &= \int_{\Omega} \sum_{j=1}^N m_j W(\vec{r} - \vec{r}_j, h) d\vec{r} \\
&= \sum_{j=1}^N m_j \int_{\Omega} W(\vec{r} - \vec{r}_j, h) d\vec{r} = \sum_{j=1}^N m_j = M
\end{aligned}$$

So ρ_n also conserves mass exactly. Hence, using the SPH density-by-summation form (2.30) conserves mass exactly.

The second method to calculate density is to solve the continuity or conservation of mass equation (2.31) directly in addition to the momentum and energy equations:

$$\frac{D\rho_i}{Dt} = -(\rho \nabla \cdot \vec{v})_i. \quad (2.31)$$

where $\frac{D}{Dt}$ is the Stokesian derivative. The continuity equation form is discussed very little in the literature except to say that there may be some computational efficiencies to be gained by using this form. However, from recent symposia it appears that for HVI problems this approach is receiving more attention because of its ability to handle material boundaries better. It does, however, take away the natural notion of the density obtained in SPH, but that is not a major problem. One SPH form for equation (2.31) is

$$\frac{D\rho_i}{Dt} = -\rho_i \sum_{j=1}^N \frac{m_j}{\rho_j} \vec{v}_j \cdot \nabla_i W(\vec{r}_i - \vec{r}_j, h), \quad (2.32)$$

where \vec{v} is the velocity and the subscripts i and j are values at \vec{r}_i and \vec{r}_j respectively. This is not a very popular form; but noting (let $B = 1$ from the gradient work earlier)

$$0 = (\rho \vec{v} \cdot \nabla 1)_i \approx \rho_i \vec{v}_i \cdot \sum_{j=1}^N \frac{m_j}{\rho_j} \nabla_i W(\vec{r}_i - \vec{r}_j, h). \quad (2.33)$$

So adding zero in the form of equation (2.33) to equation (2.32) yields

$$\frac{D\rho_i}{Dt} = \rho_i \sum_{j=1}^N \frac{m_j}{\rho_j} (\vec{v}_i - \vec{v}_j) \cdot \nabla_i W(\vec{r}_i - \vec{r}_j, h). \quad (2.34)$$

Although equation (2.34) is somewhat popular, the most popular form is obtained by applying the identity

$$\rho (\nabla \cdot \vec{v}) = \nabla \cdot (\rho \vec{v}) - \vec{v} \cdot \nabla \rho,$$

and using the general procedures given previously in equation (2.29) to obtain the SPH formulation shown in equation (2.35):

$$\frac{D\rho_i}{Dt} = \sum_{j=1}^N m_j (\vec{v}_i - \vec{v}_j) \cdot \nabla_i W(\vec{r}_i - \vec{r}_j, h). \quad (2.35)$$

where \vec{v}_i and \vec{v}_j are velocities at particles i and j respectively. This points out a use of what Monaghan calls the "second golden rule of SPH which is to rewrite formulae with the density placed inside operators." (44:545)

2.3.6 Momentum Equation. The general form of the momentum equation is: $\frac{D\vec{v}}{Dt} = -\frac{1}{\rho} \nabla P - \nabla \Phi + F_{visc}$. Where P is the pressure, Φ is an external force and F_{visc} is a viscosity term. However, only the simplified (inviscid) momentum equation is considered in this paper: $\frac{D\vec{v}}{Dt} = -\frac{1}{\rho} \nabla P$. So then using the product rule $\langle \frac{D\vec{v}}{Dt} \rangle \approx -\langle \frac{1}{\rho} \rangle \nabla \langle P \rangle$, and using P_n for $\langle P \rangle$, SPH equations may be obtained. However, this form can lead to conservation quandaries (both energy and momentum) because conservation can only be guaranteed to within the order of the

scheme. Hence, some momentum could be lost (or gained) at each time step. So consider a few different identities

$$(i) \quad \frac{\nabla P}{\rho} = \nabla \left(\frac{P}{\rho} \right) + \frac{P}{\rho^2} \nabla \rho. \quad (2.36)$$

Then derive the following using the gradient work earlier, where the i and j subscripts imply evaluation at the points \vec{r}_i and \vec{r}_j

$$\begin{aligned} \nabla \left(\frac{P}{\rho} \right) &\approx \nabla \left(\frac{P}{\rho} \right)_n = \sum_{j=1}^N \frac{m_j P_j}{\rho_j^2} \nabla W(\vec{r} - \vec{r}_j, h) \\ \nabla(\rho) &\approx \sum_{j=1}^N m_j \nabla W(\vec{r} - \vec{r}_j, h). \end{aligned}$$

Hence for particle i

$$\begin{aligned} \left(\frac{D\vec{v}}{Dt} \right)_i &= -\nabla \left(\frac{P}{\rho} \right)_i - \frac{P_i}{\rho_i^2} (\nabla \rho)_i \\ &\approx -\sum_{j=1}^N \frac{m_j P_j}{\rho_j^2} \nabla_i W(\vec{r}_i - \vec{r}_j, h) - \frac{P_i}{\rho_i^2} \sum_{j=1}^N m_j \nabla_i W(\vec{r}_i - \vec{r}_j, h) \\ &= -\sum_{j=1}^N m_j \left(\frac{P_j}{\rho_j^2} + \frac{P_i}{\rho_i^2} \right) \nabla_i W(\vec{r}_i - \vec{r}_j, h). \end{aligned} \quad (2.37)$$

With W even and m constant in time, this conserves momentum exactly since

$$\frac{D}{Dt} \sum_{i=1}^N m_i \vec{v}_i = \sum_{i=1}^N m_i \frac{D\vec{v}_i}{Dt} = -\sum_{i=1}^N \sum_{j=1}^N m_i m_j \left(\frac{P_j}{\rho_j^2} + \frac{P_i}{\rho_i^2} \right) \nabla_i W(\vec{r}_i - \vec{r}_j, h) = 0.$$

(ii)

$$\begin{aligned} \frac{\nabla P}{\rho} &= \frac{2\sqrt{P}}{\rho} \nabla(\sqrt{P}) \\ \left(\frac{D\vec{v}}{Dt} \right)_i &= -\frac{2\sqrt{P_i}}{\rho_i} \nabla(\sqrt{P})_i \end{aligned} \quad (2.38)$$

$$\approx \sum_{j=1}^N 2 m_j \frac{\sqrt{P_i P_j}}{\rho_i \rho_j} \nabla_i W(\vec{r}_i - \vec{r}_j, h) \quad (2.39)$$

Derivations using the identity (2.38) can be found in some of the references. Momentum is also conserved exactly with this, but it does not work if P is negative. Version (i) is much more common in the literature. There are additional forms, some of which are addressed later. Finally, an artificial viscosity term is frequently added to any of these forms and is discussed more later in this section.

2.3.7 Energy Equation. The general form of the internal energy equation (without sources or sinks) is: $\frac{De}{Dt} = -\frac{P}{\rho} \nabla \cdot \vec{v}$. There are several ways to develop the SPH equations for this, but the identity used in the momentum equation and the artificial viscosity must be compatible with whatever method is used, or else conservation could be lost. One possibility is to use the total energy equation

$$\sum_{i=1}^N (m_i e_i + \frac{1}{2} m_i \vec{v}_i^2) = \text{constant}.$$

Then taking the derivative to find

$$\begin{aligned} \frac{D}{Dt} \left[\sum_{i=1}^N (m_i e_i + \frac{1}{2} m_i \vec{v}_i^2) \right] &= \sum_{i=1}^N (m_i \frac{De_i}{Dt} + m_i \vec{v}_i \cdot \frac{D\vec{v}_i}{Dt}) = 0. \\ \text{So,} \quad \sum_{i=1}^N m_i \left(\frac{De_i}{Dt} \right) &= \sum_{i=1}^N m_i \left(-\vec{v}_i \cdot \frac{D\vec{v}_i}{Dt} \right). \end{aligned}$$

The SPH form for De/Dt is then obtained by using the SPH momentum equation for $D\vec{v}/Dt$. A more common technique is to use identities similar to what was done for the momentum equation, such as

$$\begin{aligned} \left(\frac{De}{Dt} \right)_i &= -\frac{P_i}{\rho_i} (\nabla \cdot \vec{v})_i \\ &= -\frac{P_i}{\rho_i^2} [\nabla \cdot (\rho \vec{v}) - \vec{v} \cdot \nabla \rho]_i \end{aligned} \quad (2.40)$$

$$\approx \frac{P_i}{\rho_i^2} \sum_{j=1}^N m_j (\vec{v}_i - \vec{v}_j) \cdot \nabla_i W(\vec{r}_i - \vec{r}_j, h) . \quad (2.41)$$

The version of the SPH energy equation found in equation (2.41) is one of the more common found in the literature; however several others are found. For example, by taking

$$\frac{De}{Dt} = - \nabla \cdot \left(\frac{P\vec{v}}{\rho} \right) + \vec{v} \cdot \nabla \left(\frac{P}{\rho} \right) ,$$

equation (2.42) may be obtained:

$$\left(\frac{De}{Dt} \right)_i \approx \sum_{j=1}^N m_j \frac{P_j}{\rho_j^2} (\vec{v}_i - \vec{v}_j) \cdot \nabla_i W(\vec{r}_i - \vec{r}_j, h) . \quad (2.42)$$

Another popular form is found by taking the average of equations (2.41) and (2.42) to obtain the symmetric form found in equation (2.43):

$$\left(\frac{De}{Dt} \right)_i \approx \frac{1}{2} \sum_{j=1}^N m_j \left(\frac{P_j}{\rho_j^2} + \frac{P_i}{\rho_i^2} \right) (\vec{v}_i - \vec{v}_j) \cdot \nabla_i W(\vec{r}_i - \vec{r}_j, h) . \quad (2.43)$$

2.3.8 Conservation. An interesting difficulty with the SPH formulations given previously is that frequently a form is derived that represents the given equation, but conservation is lost. Monaghan points this out even more by: "it has been found that if the thermal energy equation is integrated using any of the SPH forms given above, and if the density is calculated using equation 3.8 [equation (2.30) here], the total entropy is not conserved as accurately as the energy. If an entropy equation is integrated then the total energy is not conserved as accurately as the entropy. However, if the gas is ideal, the total entropy is conserved exactly if the density is calculated using equation 3.9 [equation (2.35) here] and the thermal energy is calculated using any of the forms given above. In this case the mass is not conserved exactly. It seems one cannot have everything!" (44:549)

2.3.9 Particle Placement. Very little information appears in the literature regarding initial particle placement. For the most part, the impression is that particles are just poured into the object being modeled until its full and then the problem is actually solved. This, of course, is far from the truth. For rectangular objects in Cartesian coordinates, placing particles on a regular rectangular mesh seems to be reasonable and is a common practice. When problems involve objects with more irregular shapes or other geometries are being studied, other placement schemes may be in order.

Monaghan (41) experimented with placing particles on a rectangular mesh where the rows in an impactor lined up with a target and compared that to when the rows were offset by half a row with each other. His results indicated that with just an artificial viscosity term some non-physical penetration (known as streaming) is seen under certain conditions. He proposed a method to move the particles with a different velocity than the fluid which eliminated the penetration. This is discussed more later in this section. However, it does point out that initial particle placement is important and must be considered.

A more unusual example given by Fulk (11) involved a smaller projectile impacting a thinner target than Monaghan used. When the particles were placed on a rectangular mesh, a non-physical peeling of the layers was observed on the front of the target. That is, lines of particles separated as a whole). Some backsplash is expected, but it was too extreme. A second calculation was performed where the particles were placed on a rectangular mesh and then randomly perturbed by a small amount around the mesh point. The output from this was much more realistic and almost all of the non-physical peeling was eliminated.

A third example is for the Riemann Shock Tube problem in one dimension. In this problem there is a pressure shock. However, numerical techniques in general do not model a shock, but a steep pressure gradient of the form: $\frac{\Delta P}{\Delta x}$. In performing this test case, the velocity is not nearly reaching the peak value it should from the

analytic solution. But by changing the particle spacing in a very small region around the initial shock, the results were much more accurate. However, if the particles on either side of the shock were placed too close initially, they tended to cause a crossing of two particles and erroneous results.

From these three examples it seems that for even a geometrically simple problem, the initial particle placement must be considered. This is a topic for future study and will not be addressed further in this dissertation.

2.3.10 Neighbor Searches. With all the simplicity that comes with SPH, there are some difficulties. One of the biggest is the need to find the *neighbors* of any given particle at each time step. To calculate the sums given previously for a given particle i , all other particles may be used. Unfortunately, this would make the method scale as $O(N^2)$ which could be cost prohibitive in computation time. However, if the compactness of the kernel is taken into consideration, only a small subset of the total number of particles need be considered for any given particle. The question of how to efficiently find the particles that are within a small range is known in computer terms as range searching. In SPH it is more commonly referred to as nearest neighbor searching (although nearer or near neighbor would be more appropriate). Currently two methods are popular in the literature (although this issue is not often addressed): linked-lists and tree search.

The grid generated linked list method is the older of the two and most popular if h is constant in space. In this method a temporary grid is overlaid on the problem domain. The grid spacing is carefully selected to match the kernel being used. For example, if B-Splines are being used as the kernel, they have $2h$ compact support, so the mesh spacing should be set to $2h$. Then for a given particle, its nearest neighbors are going to be in the same grid cell or the immediately adjoining cells. So this search is only over 3, 9, or 27 cells for 1, 2, or 3 dimensions respectively. The linked lists method allows for each particle to be assigned to a cell and for all the particles in a

cell to be chained together for easy access. Creation of the linked list is only about $3N$ operations. When actually calculating the equations of motion, the outer loop should be over all the mesh cells. This allows the forces between any two particles to be calculated only once instead of twice. This method scales as $N_c N$ where N_c is the average number of particles per cell. Provided N_c is sufficiently small in comparison with N , this method is quite efficient and considered $O(N)$. The biggest difficulty with this method is when variable smoothing length is used. The grid spacing cannot be optimum for every particle and therefore, could be much less efficient. Linked lists are discussed in more detail by Hockney and Eastwood (20:277).

Tree searches became popular when authors started working with variable smoothing lengths. They involve creating ordered trees based on the particle position. Once formed, the trees can be efficiently searched to find the nearest neighbors. Several different tree algorithms have been proposed, but the most popular seems to be the oct-tree. This method recursively splits the region into octants that contain the particles. Eventually the leaves on the tree are the individual particles. Tree methods, in general, scale as $O(N \ln(N))$. This makes them not quite as efficient as the linked lists for fixed h , but they may be more efficient for variable h . References for the tree algorithms include: Sedgewick (52), Hernquist and Katz (19), and Stellingwerf and Campbell (59).

2.3.11 Artificial Viscosity. Because of the smoothing nature of the SPH method, it might not be able to handle shocks very accurately. But, in fact, if an appropriate artificial viscosity term is used, SPH can handle shocks as well as any standard technique. The original thought was to use bulk $(-\alpha h \rho c \nabla \cdot \vec{v})$ and/or von Neumann-Richtmyer $(\alpha \rho h^2 (\nabla \cdot \vec{v})^2)$ viscosity terms from finite difference techniques. This proved to be disappointing in shock tube calculations. So modified versions of those were needed. A good summary of the work may be found in Lattanzio, et al. (28). They first add the term shown in equation (2.44) to the conservation

equations:

$$\omega_{ij} = \begin{cases} \frac{h \vec{v}_{ij} \cdot \vec{r}_{ij}}{c_i(\vec{r}_{ij}^2 + \eta^2)} & \text{if } \vec{v}_{ij} \cdot \vec{r}_{ij} \leq 0 \\ 0 & \text{otherwise,} \end{cases} \quad (2.44)$$

where $\vec{v}_{ij} = \vec{v}_i - \vec{v}_j$, $\vec{r}_{ij} = \vec{r}_i - \vec{r}_j$, c_i is the sound speed, and $\eta \approx 0.1h$. This term handles bulk and shear viscosities and is similar to the bulk viscosity given earlier. However, in high Mach number shocks, this does not stop streaming (the non-physical particle interpenetration). So a second term, quadratic in ω is also added. This term is similar to the von Neumann-Richtmyer term from earlier. The final result is shown in equation (2.45):

$$\Pi_{ij} = \begin{cases} \frac{\alpha \bar{c}_{ij} \omega_{ij} + \beta \omega_{ij}^2}{\bar{\rho}_{ij}} & \text{if } \vec{v}_{ij} \cdot \vec{r}_{ij} \leq 0 \\ 0 & \text{otherwise,} \end{cases} \quad (2.45)$$

where α and β are free constants, $\bar{c}_{ij} = \frac{1}{2}(c_i + c_j)$, and $\bar{\rho}_{ij} = \frac{1}{2}(\rho_i + \rho_j)$. This Π_{ij} term is added to the $\frac{P}{\rho_i^2}$ term in the momentum and energy equations. Note: most authors use μ instead of ω for this second term. More information on artificial viscosity and controlling penetration may be found in Lattanzio, et al. (28), Monaghan and Poinracic (40), and Monaghan (43).

2.3.12 Artificial Heat Conduction. The artificial viscosity term discussed previously often provides good results when modeling shocks; however, under some severe conditions excess heating can result. This term is usually referred to as wall heating from the classic example of a stream of gas being brought to rest against a rigid wall. The excess heating problem was fixed by Noh (47) by adding an artificial heat conduction term to the energy equation. An SPH version of the wall heating term was derived by Monaghan and is given in equation (2.46):

$$H_i = 2 \sum_{j=1}^N \frac{\bar{\zeta}_{ij}}{\bar{\rho}_{ij}} \frac{e_i - e_j}{|\vec{r}_i - \vec{r}_j|^2} (\vec{r}_i - \vec{r}_j) \cdot \nabla_i W(\vec{r}_i - \vec{r}_j, h) \quad (2.46)$$

$$\zeta = g_1 h c + g_2 h^2 (|\nabla \cdot \vec{v}| - \nabla \cdot \vec{v}), \quad (2.47)$$

where $\bar{A}_{ij} = \frac{1}{2}(A_i + A_j)$ and g_1 and g_2 are user supplied constants. The H_i term above is added to the end of the energy equation when necessary.

2.3.13 Penetration Avoidance. One of the difficulties of particle methods applied to impact problems is that lines of particles can penetrate or stream through one another. This results in a non-physical mixing of the materials. It occurs in SPH because field variables (in particular, the velocity field) do not have to be single-valued. The lack of single-valued fields can allow two different particles with different velocities to occupy the same position. Of course, a judicious choice of initial particle placement can reduce this, but that is not solving the difficulty, just masking it. Most, or all, of this can be eliminated by using an appropriate artificial viscosity term (there are several examples in the published literature). However, in certain problems, such as subsonic flows, this is not sufficient. Monaghan (41, 43) suggested an alternative: move the particles at a velocity approximately equal to the average velocity in its neighborhood instead of the velocity of the particle itself. Equation (2.48) is the standard formula for moving the particles.

$$\frac{D\vec{r}_i}{Dt} = \vec{v}_i. \quad (2.48)$$

The velocity is replaced with \vec{v}_i as follows

$$\frac{D\vec{r}_i}{Dt} = \vec{v}_i = \vec{v}_i - \epsilon \sum_{j=1}^N m_j \left(\frac{\vec{v}_i - \vec{v}_j}{\bar{\rho}_{ij}} \right) W(\vec{r}_i - \vec{r}_j, h), \quad (2.49)$$

where $\bar{\rho}_{ij} = \frac{1}{2}(\rho_i + \rho_j)$ and ϵ is a small constant. This concept can introduce extra dispersion, but no dissipation.

2.3.14 Equations of State. The equation of state (EOS) has received very little attention in SPH papers so far. The main reason is that the EOS is more related to the problem being studied, than to the method itself. For the HVI problem discussed in the previous section, an EOS that handles metals and high pressures

must be used, such as the Mie - Grüneisen EOS. From the literature, Tillotson, Mie - Grüneisen, and SESAME library have all been used. As long as care is taken in the implementation, the choice of EOS should not cause too many new difficulties. Forms for both the Mie - Grüneisen and Tillotson EOS are given below.

As described by Libersky, et al. (34) the Mie - Grüneisen is quite simple. Pressure is a function of both density and internal energy as follows

$$P(\rho, e) = P'_h(\rho) \rho_o c_o^2 \left(1 - \frac{\Gamma}{2} \mu\right) + \Gamma \rho (e - e_o) \quad (2.50)$$

$$P'_h(\rho) = \begin{cases} \mu + (S_o - 1)\mu^2 + (S_o - 1)(3S_o - 1)\mu^3 & \text{if } \mu > 0 \text{ (Compression)} \\ \mu & \text{if } \mu < 0 \text{ (Tension)} \end{cases} \quad (2.51)$$

$$\mu = \frac{\rho}{\rho_o} - 1 \quad (2.52)$$

$$\Gamma = \frac{\rho_o}{\rho} \Gamma_o, \quad (2.53)$$

where Γ_o , S_o , c_o , and ρ_o are material constants and e_o is the initial energy. Also see Anderson (1) or Segletes (53) for more information.

As described by Benz, et al. (4) the Tillotson EOS is also relatively simple to implement. The Pressure, P , is a function of both density and internal energy and takes on one of three different values as shown in equations (2.54) - (2.56):

$$P_c = a \rho e + \frac{b \rho e}{1 + \frac{e \rho_o^2}{e_o \rho^2}} + A \left(\frac{\rho}{\rho_o} - 1\right) + B \left(\frac{\rho}{\rho_o} - 1\right)^2 \quad (2.54)$$

$$P_e = a \rho e + \left(\frac{b \rho e}{1 + \frac{e \rho_o^2}{e_o \rho^2}} + A \left(\frac{\rho}{\rho_o} - 1\right) e^{-\nu \left(\frac{e_o}{\rho} - 1\right)} \right) e^{-\xi \left(\frac{e_o}{\rho} - 1\right)^2} \quad (2.55)$$

$$P_t = \frac{P_e(e - e_s) + P_c(e'_s - e)}{e'_s - e_s}, \quad (2.56)$$

where $a, b, e_o, \rho_o, A, B, e_s, e'_s, \nu$, and ξ are constants that must be supplied by the user. The P_c function is used for condensed states, the P_e function for expanded hot states, and P_t for the transition between the two. The exact determination for

which function to use for P is given in equation (2.57):

$$P(\rho, e) = \begin{cases} P_c & \text{if } \rho > \rho_o \text{ or } e < e_s, \\ P_e & \text{if } \rho < \rho_o \text{ and } e > e'_s, \\ P_t & \text{if } \rho < \rho_o \text{ and } e_s < e < e'_s. \end{cases} \quad (2.57)$$

2.3.15 Strength Models. As discussed earlier in this chapter, material models such as strength, fracture, and fragmentation can be important in modeling impacts (especially for metals and at lower speeds). The references to material models in the literature are mostly from Libersky, et al. (33, 34). These papers are also the first ones in which extensive use of the continuity equation is used to find density instead of just the SPH approximation. However, the main additions in these papers are that of an elastic-perfectly plastic strength model to SPH. Key to adding the strength model (constitutive relation) is replacing the pressure (P) in the previous formulas with the viscous stress tensor (σ). The stress tensor is defined in equation (2.58):

$$\begin{aligned} \sigma &= P\delta - S \\ \text{or } \sigma^{\alpha\beta} &= P\delta^{\alpha\beta} - S^{\alpha\beta}, \end{aligned} \quad (2.58)$$

where P is the pressure, δ is a Kronecker delta tensor, and S is the traceless symmetric deviatoric stress tensor. The Greek superscripts are used to denote the space direction with summation on repeated indices. Note: if the deviatoric stress is zero (as in the case of purely hydrodynamic flow) this just reduces to the pressure as before. There are several different formulations for the Stress rates, but according to Libersky the most common is the Jaumann rate. This is given in equation (2.59):

$$\begin{aligned} \dot{S}^{\alpha\beta} &= \mu(\dot{\epsilon}^{\alpha\beta} - \frac{1}{3}\delta^{\alpha\beta}\dot{\epsilon}^{\gamma\gamma}) + S^{\alpha\gamma}\dot{R}^{\beta\gamma} + \dot{S}^{\gamma\beta}R^{\alpha\gamma} \\ &= \mu\dot{\bar{\epsilon}}^{\alpha\beta} + S^{\alpha\gamma}\dot{R}^{\beta\gamma} + \dot{S}^{\gamma\beta}R^{\alpha\gamma}, \end{aligned} \quad (2.59)$$

where μ is the shear modulus, $\dot{\epsilon}$ is the strain rate tensor, $\bar{\epsilon}$ is its traceless part, and \dot{R} is the rotation rate tensor. Formulas for $\dot{\epsilon}$ and \dot{R} are given in equations (2.60) – (2.61):

$$\dot{\epsilon}^{\alpha\beta} = \frac{1}{2} \left(\frac{\partial v^\alpha}{\partial x^\beta} + \frac{\partial v^\beta}{\partial x^\alpha} \right) \quad (2.60)$$

$$\dot{R}^{\alpha\beta} = \frac{1}{2} \left(\frac{\partial v^\alpha}{\partial x^\beta} - \frac{\partial v^\beta}{\partial x^\alpha} \right). \quad (2.61)$$

SPH formulations for the above equations can be derived in several variations as with everything else in SPH, but the forms given by Libersky, et al. are shown in equations (2.62) – (2.63):

$$\begin{aligned} \mu \bar{\epsilon}_i^{\alpha\beta} = & \frac{\mu}{2} \sum_{j=1}^N \frac{m_j}{\rho_j} \left[(v_j^\alpha - v_i^\alpha) \nabla_i^\beta W(\vec{r}_i - \vec{r}_j, h) + (v_j^\beta - v_i^\beta) \nabla_i^\alpha W(\vec{r}_i - \vec{r}_j, h) \right. \\ & \left. - \frac{1}{3} D_i \delta^{\alpha\beta} \right] \end{aligned} \quad (2.62)$$

$$\dot{R}_i^{\alpha\beta} = \sum_{j=1}^N \frac{m_j}{\rho_j} \left[(v_j^\alpha - v_i^\alpha) \nabla_i^\beta W(\vec{r}_i - \vec{r}_j, h) + (v_j^\beta - v_i^\beta) \nabla_i^\alpha W(\vec{r}_i - \vec{r}_j, h) \right]. \quad (2.63)$$

To model the plastic flow, a von Mises criterion is used. When the second stress invariant, $J^2 = S^{\alpha\beta} S^{\alpha\beta}$, exceeds the flow stress (Y_o) the deviators are brought back to the flow surface shown in equation (2.64):

$$S^{\alpha\beta} = S^{\alpha\beta} \sqrt{\frac{Y_o}{3J^2}}. \quad (2.64)$$

The above equations may be added to the others in order to solve for the stress tensor and then the momentum and energy equations. As mentioned earlier, the momentum equation is changed by using the stress tensor instead of the pressure term; the energy equation is also modified by adding a term that has the deviatoric

stress times strain. This new equation is given in (2.65):

$$\frac{De_i}{Dt} = -\frac{1}{\rho_i} (P_i D_i - S_i^{\alpha\beta} \bar{\epsilon}_i^{\alpha\beta}) . \quad (2.65)$$

2.4 Summary

Throughout this chapter, several equations and various forms of these were shown. Although the set of SPH equations should be determined by the problem being studied, the following is a fairly standard set and offers a good starting point:

Continuity:

$$\frac{D\rho_i}{Dt} = \sum_{j=1}^N m_j (\vec{v}_i - \vec{v}_j) \cdot \nabla_i W_{ij}$$

Momentum:

$$\frac{D\vec{v}_i}{Dt} = - \sum_{j=1}^N m_j \left(\frac{P_j}{\rho_j^2} + \frac{P_i}{\rho_i^2} + \Pi_{ij} \right) \nabla_i W_{ij}$$

Energy:

$$\frac{De_i}{Dt} = \frac{1}{2} \sum_{j=1}^N m_j \left(\frac{P_j}{\rho_j^2} + \frac{P_i}{\rho_i^2} + \Pi_{ij} \right) (\vec{v}_i - \vec{v}_j) \cdot \nabla_i W_{ij} + H_i$$

Particle Motion:

$$\frac{D\vec{r}_i}{Dt} = \vec{v}_i$$

Equation of State:

$$P_i = P(\rho_i, e_i)$$

where $W_{ij} = W(\vec{r}_i - \vec{r}_j, h)$ is the SPH kernel, Π_{ij} is the artificial viscosity term, and H_i is the wall heating term.

At this point, the fundamentals of smoothed particle hydrodynamics and the background application (hypervelocity impact), are complete. Based on this understanding of the method, and a fundamental knowledge of numerical analysis, the reader can now progress to the new contributions for SPH presented in the rest of this dissertation. Note: additional background material is scattered throughout the next six chapters when more appropriate for clarity of understanding. The new contributions are split into two major categories: the numerical properties (Chapters III-VI) and the implementation (Chapters VI- VIII). From this point the reader may move on to any of the six chapters, but I recommend that the reader start with either Chapter III or VII, depending on their background and interest.

III. CONSISTENCY

This chapter addresses the mathematical concept known as consistency with regards to SPH. The basic concept of consistency is related to how well the numerical equations (SPH) approximate the physical equations. That is, consistency is analysis of truncation error. SPH has two parts, a function approximation and derivative approximation; so the truncation error of both of these is discussed.

The consistency is approached first by analyzing the method under the assumptions of sufficiently smooth data. This is done by assuming the numerical function is smooth between the SPH particles. Since information on the function is not available on a micro-particle scale, this is usually acceptable. This analysis is performed by taking a two step process. The first is known as the kernel approximation and the second is known as the particle approximation. In this second step, consistency results are obtained by taking the volume elements based on the particle spacing to be equivalent to those based on the mass and density. This approach ends by proving both the SPH function approximation and derivative approximation are consistent and of order $O(h^2, h\Delta x)$.

A second approach to consistency is then taken by considering what happens when a function is not smooth enough to apply the first approach. In the process, a new version of SPH is developed that is consistent even if the function has a discontinuity in it.

The work in this chapter, as with much of this dissertation, is performed in one space dimension. However, the two approaches described above are both shown to still hold in higher dimensions. Also as an aside to the chapter, SPH forms of artificial viscosity and artificial heat conduction are introduced for later use and shown to be consistent. That is, they vanish as h and Δx approach zero.

To start, a formal definition is given. The following general operators are defined to use in the analysis in this chapter: P is the spatial partial differential

operator and S is the approximation operator to P . For example, if the spatial partial differential operator is the first order wave equation then P is $\frac{\partial}{\partial x}$. However, in general P is taken as a non-linear first order operator. The following hyperbolic equations may be defined for any dimension d as

$$\begin{aligned}\frac{D\vec{v}(\vec{X})}{Dt} &= P\vec{v}(\vec{X}) & \vec{X} \in \mathcal{D} \\ \frac{D\vec{u}(\vec{X})}{Dt} &= S\vec{u}(\vec{X}) & \vec{X} \in \tilde{\mathcal{D}} \\ \text{where } \vec{X} &= (t, x_1, \dots, x_d) \\ \mathcal{D} &= ([0, T] \times \Omega) \\ &\text{and } \tilde{\mathcal{D}} \text{ are the mesh points (particles) in } \mathcal{D} .\end{aligned}$$

The system is hyperbolic if $P\vec{v}(\vec{X}) = A(\vec{v}, \vec{X})\vec{v}_x$ where the eigenvalues of the matrix A are real and distinct (see Lax (30)).

Definition 5 (Consistency) *Given any function $f(\vec{X})$ that is sufficiently smooth in \mathcal{D} (and $\partial\mathcal{D}$); let $\tau(f(\vec{X})) \equiv P f(\vec{X}) - S f(\vec{X})$ for each $\vec{X} \in \tilde{\mathcal{D}}$. Then the semi-discrete approximation method is consistent (with the partial differential equation) iff*

$$\|\tau(f)\| \rightarrow 0 \quad \text{as } \Delta t, \Delta x_i \rightarrow 0 .$$

Reference: Isaacson and Keller (25) or Strikwerda (60).

In summary, consistency deals with the local truncation error. It is a measure of how closely the approximation operator resembles the differential operator. The error estimates needed to prove consistency for SPH will now be built.

3.1 Kernel Approximation

As mentioned in the Chapter II, the kernel approximation can be viewed from the point of view of distribution theory. That is, the delta distribution $\delta(\vec{r}_o - \vec{r})$ applied to $f(\vec{r})$ results in $f(\vec{r}_o)$. This property is what is approximated using the

SPH methodology. However, instead of using the delta distribution, apply a kernel function W to $f(\vec{r})$ and examine how the integral of this relates to $f(\vec{r}_o)$. See Stakgold (58) or Keener (26) for more information on distribution theory. The SPH kernel approximation as used in this dissertation is shown in equation (3.1)

$$\langle f(\vec{r}_o) \rangle = f_k(\vec{r}_o) = \int_{\Omega} f(\vec{r}) W(\vec{r}_o - \vec{r}, h) d\vec{r} \quad (3.1)$$

where

$$\int_{\Omega} W(\vec{r}_o - \vec{r}, h) d\vec{r} = 1, \quad (3.2)$$

h (the smoothing length) is a measure of the width of the kernel function W , and Ω is a spatial domain. Note, for the time being equation (3.2) needs to hold only in the limit as $h \rightarrow 0$. However, it is useful later on for this to be true for all h . It may then be hypothesized: if $W \rightarrow \delta$ distributionally as $h \rightarrow 0$, then $f_k \rightarrow f$ as $h \rightarrow 0$. There is obviously some numerical error in this approximation when h is not in the limit; this needs to be made more exact.

Errors in the kernel approximation may best be seen by using a Taylor series expansion with remainder. This is shown here for the one dimensional case only (see the section 3.6 later for additional work). Assume f is sufficiently smooth (to be defined more exactly later) so that it can be expanded about $x = x_o$ and let $u = x - x_o$. Also assume the kernel W satisfies equation (3.2), is an even function, and has compact support. Note at this time, under these assumptions on W , if $u \in \text{supp}(W)$ (the support of W) then $|u| \leq \kappa h$, where κ is the constant that specifies the support of the kernel. That is, $W(u) = 0$ for $|u| > \kappa h$. Equation (3.1) now results in

$$\begin{aligned} f_k(x_o) &= \int_{\Omega} f(x) W(x_o - x, h) dx = \int_{\Omega} f(u + x_o) W(-u, h) du \\ &= \int_{\Omega} W(-u, h) \left[f(x_o) + u f'(x_o) + \frac{u^2}{2!} f''(\xi_o) \right] du \end{aligned}$$

$$\begin{aligned}
&= f(x_o) \int_{\Omega} W(-u, h) du \\
&\quad + f'(x_o) \int_{\Omega} u W(-u, h) du \\
&\quad + \frac{1}{2} \int_{\Omega} u^2 W(-u, h) f''(\xi_o) du,
\end{aligned}$$

where $\xi_o = \xi_o(u)$. Since W is normalized, the integral in the first term of the sum is 1. Also, since W is an even function, the integral in the second term of the sum is 0. Therefore, the result is

$$f_k(x_o) = f(x_o) + E_k(f, x_o) \quad (3.3)$$

$$\begin{aligned}
\text{where} \quad E_k(f, x_o) &= \frac{1}{2} \int_{\Omega} u^2 W(-u, h) f''(\xi_o) du \\
&\text{for } \xi_o \in \Omega.
\end{aligned} \quad (3.4)$$

To obtain a bound on the error term, $E_k(f, x_o)$, define

$$e_k = \frac{\kappa^2}{2} \sup_{\xi \in \Omega} |f''(\xi)|. \quad (3.5)$$

Note: for the kernels considered in this dissertation $\kappa \leq 9$ (and is most often taken as 2). By the compact support and normalization of the kernel noted earlier, the bound is

$$\begin{aligned}
|E_k(f, x_o)| &= \frac{1}{2} \left| \int_{\Omega} u^2 W(-u, h) f''(\xi_o) du \right| \leq \frac{1}{2} \int_{\Omega} |u^2| |W(-u, h)| |f''(\xi_o)| du \\
&\leq \int_{\Omega} \frac{1}{2} \kappa^2 h^2 W(-u, h) \frac{2e_k}{\kappa^2} du = e_k h^2 \int_{\Omega} W(-u, h) du \\
&= e_k h^2.
\end{aligned} \quad (3.6)$$

It is also easily seen that if $f(x) = g'(x)$ then equation (3.6) still holds (Note: in e_k the f'' term now equals g'''). Also a higher order error bound is possible, but a new kernel would need to be obtained that has successively higher order even moments equal zero (see Chapter VI for a discussion of this).

3.2 Particle Approximation/Rectangle Rule

As noted in the previous chapter from the published literature, a Monte Carlo approximation (3.7) of equation (3.1) known as the particle approximation may be obtained:

$$f_n(\vec{r}_o) = \sum_{j=1}^N \frac{f(\vec{r}_j)}{n(\vec{r}_j)} W(\vec{r}_o - \vec{r}_j, h) = \sum_{j=1}^N \frac{m_j}{\rho_j} f(\vec{r}_j) W(\vec{r}_o - \vec{r}_j, h). \quad (3.7)$$

It was further noted

$$f_n(\vec{r}_o) = f_k(\vec{r}_o) + E_n(f, \vec{r}_o), \quad (3.8)$$

and the error term, $E_n(f, \vec{r}_o)$, is proportional to $O(\frac{(\ln N)^d}{N})$. This implies that as $N \rightarrow \infty$, if $\frac{1}{n(\vec{r}_j)} \rightarrow 0 \forall j \in \mathcal{N}$, then $f_n(\vec{r}_o) \rightarrow f_k(\vec{r}_o)$. This discussion from the literature appears to be valid, but lacks most of the details I would like to see. Instead of trying to fill in the many holes, alternative quadrature rules are investigated here. Through this, it was discovered that by applying the most basic of the rules, the rectangle rule, a reasonable error bound and results similar to Monte Carlo can be obtained. That analysis is shown here.

Start with the general forward rectangle rule for one dimension (reference Young and Gregory (70))

$$\int_{x_i}^{x_{i+1}} f(x) dx = (x_{i+1} - x_i) f(x_i) + E(f, x_i, x_{i+1}) \quad (3.9)$$

where $E(f, x_i, x_{i+1}) = \frac{1}{2} (x_{i+1} - x_i)^2 f'(\xi_i) \quad \xi_i \in (x_i, x_{i+1}).$

Note that in one dimension, the domain Ω is an interval. Further, because the kernel has compact support, the supported interval around \tilde{x} is just $[\tilde{x} - \kappa h, \tilde{x} + \kappa h]$; $[a, b]$ is used for simplicity. Assume this interval contains N_k particles. Number them x_1, \dots, x_{N_k} and label the point immediately to the left of a , as x_o and to the right of b as x_{N_k+1} . This may be seen in Figure 3.1.

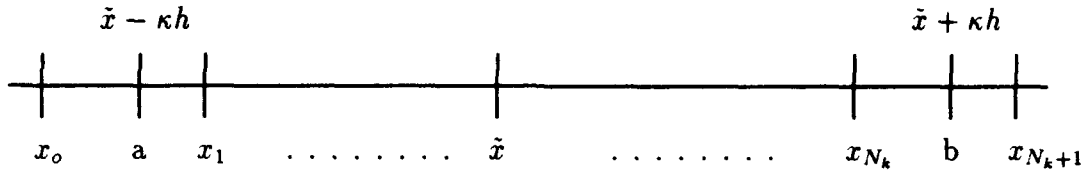


Figure 3.1 Partition for Rectangle Rule

The composite rule is then

$$\begin{aligned}
 \int_{\Omega} f(x) W(\tilde{x} - x, h) dx &= \int_a^b f(x) W(\tilde{x} - x, h) dx \\
 &= \int_{x_0}^{x_{N_k+1}} f(x) W(\tilde{x} - x, h) dx \\
 &= \sum_{j=0}^{N_k} \int_{x_j}^{x_{j+1}} f(x) W(\tilde{x} - x, h) dx \\
 &= \sum_{j=0}^{N_k} [(x_{j+1} - x_j) f(x_j) W(\tilde{x} - x_j, h)] + E_r(f, \tilde{x}). \quad (3.10)
 \end{aligned}$$

By compact support $W(\tilde{x} - x_0, h) = 0$, so the $j = 0$ term in the sum in equation (3.10) is zero. The equation is then

$$\int_{\Omega} f(x) W(\tilde{x} - x, h) dx = \sum_{j=1}^{N_k} [(x_{j+1} - x_j) f(x_j) W(\tilde{x} - x_j, h)] + E_r(f, \tilde{x}) \quad (3.11)$$

$$\text{where} \quad E_r(f, \tilde{x}) = \sum_{j=1}^{N_k} \frac{1}{2} (x_{j+1} - x_j)^2 [f(\xi_j) W(\tilde{x} - \xi_j, h)]', \quad (3.12)$$

and $\xi_j \in [x_j, x_{j+1}]$. To obtain a bound on the error term found in equation (3.12) define

$$\begin{aligned}
 M_x &= \sup_j |x_{j+1} - x_j| \\
 e_r &= \frac{\kappa c_1}{2} \sup_{\xi \in \Omega} |[f(\xi) W(\tilde{x} - \xi, h)]'|. \quad (3.13)
 \end{aligned}$$

To determine c_1 , note that the particles are chosen initially so that $2\kappa - 2M_x \leq N_k M_x / h \leq 2\kappa + 2M_x$. During a calculation, the particles should be tracked to determine c_1 such that $N_k M_x / h \leq c_1 \kappa$, where c_1 is a constant defined as $2 \leq c_1 < \infty$. If c_1 becomes too large (e.g. 10) restart with a new distribution of particles. The error bound is now

$$\begin{aligned} |E_r(f, \tilde{x})| &= \left| \sum_{j=1}^{N_k} \frac{1}{2} (x_{j+1} - x_j)^2 [f(\xi_j) W(\tilde{x} - \xi_j, h)]' \right| \\ &\leq \sum_{j=1}^{N_k} \frac{1}{2} |x_{j+1} - x_j|^2 |[f(\xi_j) W(\tilde{x} - \xi_j, h)]'| \\ &\leq \sum_{j=1}^{N_k} M_x^2 \frac{e_r}{\kappa c_1} = \frac{M_x^2 N_k e_r}{\kappa c_1}. \end{aligned}$$

Note that, c_1 is a gauge that is used in the above equations to verify that Δx becomes dense everywhere, and somewhat uniformly. Provided that happens, c_1 will be close to 2. So the error bound is

$$|E_r(f, \tilde{x})| \leq e_r h M_x. \quad (3.14)$$

A backward rectangle rule,

$$\int_{\tilde{x}}^{x_{i+1}} f(x) dx = (x_{i+1} - \tilde{x}) f(x_{i+1}) + E(f, \tilde{x}, x_{i+1}),$$

can be used instead of a forward rectangle rule. The analysis follows exactly as above so many of the steps are removed:

$$\begin{aligned} \int_{\Omega} f(x) W(\tilde{x} - x, h) dx &= \sum_{j=0}^{N_k} [(x_{j+1} - x_j) f(x_{j+1}) W(\tilde{x} - x_{j+1}, h)] \\ &\quad + E_r(f, \tilde{x}) \\ &= \sum_{j=1}^{N_k} [(x_j - x_{j-1}) f(x_j) W(\tilde{x} - x_j, h)] \\ &\quad + E_r(f, \tilde{x}) \end{aligned} \quad (3.15)$$

$$\text{where} \quad |E_r(f, \tilde{x})| \leq e_r h M_x . \quad (3.16)$$

Hence, the formula (3.15) is very similar to formula (3.11) and has the same error bound. Finally, averaging the forward and backward methods obtains

$$\int_{\Omega} f(x) W(\tilde{x}-x, h) dx = \sum_{j=1}^{N_k} \left(\frac{x_{j+1} - x_{j-1}}{2} \right) f(x_j) W(\tilde{x}-x_j, h) + E_r(f, \tilde{x}) , \quad (3.17)$$

with the same error bound as the other two methods.

3.3 Volume Element Calculation

In the previous section, a volume element (Δx) was calculated by using the particle position. However, in SPH a volume element is usually (if not always) calculated using mass and density (m/ρ). In this section, two ideas are discussed to show that these two concepts are similar to each other. First, the two volume elements are moved forward in time to examine how they differ after one time step. Second, the two are equated with each other and some of the ramifications of this choice are noted.

- Consider how the two volume elements change with time. Assume that the relationship

$$\Delta x \approx \frac{m}{\rho} \quad (3.18)$$

holds exactly at a given point in time, then it should still be close after the next time step as will now be shown. This idea is developed in one dimension as follows. At time 0, the equivalence is exact, since mass is assigned based on initial density and initial particle spacing. Writing Δx in a general fashion as $\Delta x = (x_+ - x_-)/c_x$ (for an appropriate constant c_x) yields

$$\frac{D}{Dt}(\Delta x) = \frac{v_+ - v_-}{c_x} ;$$

and it can also be seen that

$$\frac{D}{Dt} \left(\frac{m}{\rho} \right) = m \frac{D}{Dt} \left(\frac{1}{\rho} \right) = -\frac{m}{\rho^2} \frac{D\rho}{Dt} = \frac{m}{\rho} v',$$

where v' is solved for using the SPH derivative. Now assume the relationship holds exactly at time n and apply a time scheme. For example, use the basic forward Euler method to find

$$\begin{aligned} \Delta x^{n+1} &= \Delta x^n + \Delta t \left(\frac{v_+ - v_-}{c_x} \right) \\ \left(\frac{m}{\rho} \right)^{n+1} &= \left(\frac{m}{\rho} \right)^n + \Delta t \left(\frac{m}{\rho} \right)^n (v')^n. \end{aligned}$$

But since $\Delta x^n = \left(\frac{m}{\rho} \right)^n$ then

$$\begin{aligned} \Delta x^{n+1} - \left(\frac{m}{\rho} \right)^{n+1} &= \Delta t \left[\Delta x^n \left(\frac{v_+ - v_-}{c_x \Delta x^n} \right) - \left(\frac{m}{\rho} \right)^n (v')^n \right] \\ &= \Delta t \Delta x^n \left[\frac{v_+ - v_-}{c_x \Delta x^n} - (v')^n \right] \end{aligned}$$

This shows that the difference between Δx and m/ρ after one time step is equal to the difference between two methods of calculating the velocity divergence. When using the central space, $c_x = 2$. So the first term in the brackets would be a central difference form of the velocity divergence. This is second order for uniform spacing, first order otherwise. So the term in brackets is the difference between two derivative approximations, both at least first order. Hence, the two volume elements differ after one time step by a term that is only $O(\Delta x^2)$ (higher order under some assumptions).

- Consider if the relationship (equation (3.18)) is taken to be exactly equal for all time. That is,

$$\Delta x \equiv \frac{m}{\rho}. \quad (3.19)$$

To ensure this is maintained, the computer program must either calculate mass or density using this formula. If calculating mass using the formula, the density is solved using either SPH density-by-summation or SPH continuity equation. This is a relatively small change from standard SPH, but conservation of mass is no longer guaranteed. If calculating density using the formula, mass is taken as constant in time (as usual) and equation (3.19) is used to arrive at density. In one dimension this is a minor change, but in higher dimensions the cost to find $\Delta \vec{x}$ may be extremely expensive from a computational standpoint. This is because, as shown later in this chapter, Delaunay triangulation is used in proving consistency in higher dimensions. This is a expensive process to implement, but required in some circumstances to ensure consistency.

Hence, using either of these two ideas, the equivalence of volume elements calculated by the particle position or the field variables should be attainable.

3.4 Consistency Result

Consistency for the SPH approximation of a function and its derivative may now be proved in general. First, define the following operators

$$\text{Identity Operator} : I u = u$$

$$\text{Derivative Operator} : P u = \frac{\partial u}{\partial x}$$

$$\text{Kernel Operator} : K u(x_o) = \int_{\Omega} u(x) W(x_o - x, h) dx$$

$$\text{SPH Operator} : S u(x_o) = \sum_{j=1}^N \frac{m_j}{\rho_j} u_j W(x_o - x_j, h)$$

$$\text{SPH Derivative Operator} : S' u(x_o) = \sum_{j=1}^N \frac{m_j}{\rho_j} u_j W'(x_o - x_j, h)$$

$$\text{where } W' = \frac{\partial W}{\partial x_o} .$$

Lemma 1 (Consistency for the SPH Approximation) *Given any function $u(\vec{X}) \in C^2(\Omega)$; and given a kernel function, W , that is even, positive, normalized, and has compact support, then the SPH function approximation is consistent with the identity operator under the sup norm provided Δx is equivalent to m/ρ .*

Proof.

$$\|Iu - Su\|_{\infty} = \|Iu - Ku + Ku - Su\|_{\infty} \leq \|Iu - Ku\|_{\infty} + \|Ku - Su\|_{\infty}. \quad (3.20)$$

Based on equations (3.3) and (3.4) obtain

$$\begin{aligned} |Iu(x) - Ku(x)| &= |u(x) - [u(x) + E_k(u, x)]| = |E_k(u, x)| \\ &= \left| \frac{1}{2} \int_{\Omega} z^2 W(-z, h) u''(\xi_0) dz \right|, \end{aligned}$$

and from equation (3.6) obtain

$$\|Iu - Ku\|_{\infty} = \sup_{x \in \Omega} |Iu(x) - Ku(x)| = \sup_{x \in \Omega} |E_k(u, x)| \leq e_k h^2. \quad (3.21)$$

The last term in equation (3.20) becomes

$$\begin{aligned} Ku(x) - Su(x) &= \int_{\Omega} u(\xi) W(x - \xi) d\xi - \sum_{j=1}^{N_k} \frac{m_j}{\rho_j} u_j W(x - x_j) \\ &= \int_{\Omega} u(\xi) W(x - \xi) d\xi - \sum_{j=1}^{N_k} \left(\frac{x_{j+1} - x_{j-1}}{2} \right) u_j W(x - x_j) \\ &\quad + \sum_{j=1}^{N_k} \left[\left(\frac{x_{j+1} - x_{j-1}}{2} \right) - \frac{m_j}{\rho_j} \right] u_j W(x - x_j). \end{aligned}$$

But $\frac{m_j}{\rho_j}$ is the one dimensional volume (ie. distance) and can be taken to equal $(x_{j+1} - x_{j-1})/2$. It is taken as exactly equal in this proof, but can be bounded as well based on results in the previous section. Therefore, the last sum is exactly equal

to zero. From equation (3.17), $Ku(x) - Su(x) = E_r(u, x)$ and from equation (3.14),

$$\|Ku - Su\|_\infty = \sup_{x \in \Omega} |E_r(u, x)| \leq e_r h M_x. \quad (3.22)$$

Thus combining equation (3.20) with equations (3.21) and (3.22) results in

$$\|Iu - Su\|_\infty \leq e_k h^2 + e_r h M_x.$$

Noting from equations (3.5) and (3.13) that e_k and e_r are independent of h and M_x yields

$$\|Iu - Su\|_\infty \rightarrow 0 \quad \text{as } h, M_x \rightarrow 0.$$

□

Note: In the lemma u was required to be $C^2(\Omega)$; however, it is sufficient to be $C^1(\Omega)$ provided u'' exists and is bounded. This is because existence and boundedness was all that was required in the proof and in equations (3.3) and (3.6).

Lemma 2 (Consistency of the SPH Derivative) *Given any function $u(\vec{X})$ and its derivative $u'(\vec{X})$ where $u(\vec{X}) \in C^3(\Omega)$; and given a kernel function, W , that is even, positive, normalized, C^1 , and has compact support, then the SPH Derivative Operator is consistent with the derivative operator under the sup norm provided Δx is equivalent to m/ρ .*

Proof.

$$\|Pu - S'u\|_\infty = \|Pu - Ku' + Ku' - S'u\|_\infty \leq \|Pu - Ku'\|_\infty + \|Ku' - S'u\|_\infty. \quad (3.23)$$

Based on equations (3.3) and (3.4) obtain

$$\begin{aligned} |Pu(x) - Ku'(x)| &= |u'(x) - [u'(x) + E_k(u', x)]| = |E_k(u', x)| \\ &= \left| \frac{1}{2} \int_{\Omega} z^2 W(-z, h) u'''(\xi_o) dz \right|, \end{aligned}$$

and from equation (3.6), and the sentence following, obtain

$$\|Pu - Ku'\|_\infty = \sup_{x \in \Omega} |Pu(x) - Ku'(x)| = \sup_{x \in \Omega} |E_k(u', x)| \leq e'_k h^2 \quad (3.24)$$

$$\text{where } e'_k = \frac{\kappa^2}{2} \sup_{\xi \in \Omega} |u'''(\xi)|. \quad (3.25)$$

The last term in equation (3.23) becomes (using the compact support of W)

$$\begin{aligned} Ku'(x) - S'u(x) &= \int_{\Omega} u'(\xi) W(x - \xi) d\xi - \sum_{j=1}^{N_k} \frac{m_j}{\rho_j} u_j W'(x - x_j) \\ &= u(\xi) W(x - \xi)|_{\partial\Omega} - \int_{\Omega} u(\xi) \frac{\partial}{\partial \xi} W(x - \xi) d\xi \\ &\quad - \sum_{j=1}^{N_k} \frac{m_j}{\rho_j} u_j W'(x - x_j) \\ &= \int_{\Omega} u(\xi) W'(x - \xi) d\xi - \sum_{j=1}^{N_k} \frac{m_j}{\rho_j} u_j W'(x - x_j) \\ &= \int_{\Omega} u(\xi) W'(x - \xi) d\xi - \sum_{j=1}^{N_k} \left(\frac{x_{j+1} - x_{j-1}}{2} \right) u_j W'(x - x_j) \\ &\quad + \sum_{j=1}^{N_k} \left[\left(\frac{x_{j+1} - x_{j-1}}{2} \right) - \frac{m_j}{\rho_j} \right] u_j W'(x - x_j). \end{aligned}$$

Once again, $\frac{m_j}{\rho_j}$ is the one dimensional volume (ie. distance) and is taken to equal $(x_{j+1} - x_{j-1})/2$. As in the previous lemma, this term could also be bounded based on results in the previous section. Therefore, the last sum is exactly equal to zero.

From equation (3.17), $Ku'(x) - S'u(x) = E_r(u', x)$ and from equation (3.14),

$$\|Ku' - S'u\|_\infty = \sup_{x \in \Omega} |E_r(u', x)| \leq e'_r h M_x \quad (3.26)$$

$$\text{where } e'_r = \frac{\kappa c_1}{2} \sup_{\xi \in \Omega} |[u(\xi) W'(x - \xi)]'|. \quad (3.27)$$

Thus combining equation (3.23) with equations (3.24) and (3.26) results in

$$\|Pu - S'u\|_\infty \leq e'_k h^2 + e'_r h M_x.$$

Noting from equations (3.25) and (3.27) that e'_k and e'_r are independent of h and M_x yields

$$\|Pu - S'u\|_\infty \longrightarrow 0 \quad \text{as } h, M_x \rightarrow 0.$$

□

Note: In the lemma u was required to be $C^3(\Omega)$; however, it is sufficient to be $C^2(\Omega)$ provided u'' exists and is bounded. This is because existence and boundedness was all that was required in the proof and in equations (3.3) and (3.6).

3.5 Applying SPH/Linearizing

The primary equations used in hypervelocity impact are the Euler equations of gas dynamics. These and the SPH semi-discrete forms for these (or at least one version) are shown in Chapter II. Methods as to how SPH forms for these or any other equations may be derived in a consistent manner are discussed. There are two primary methods that should give comparable, yet slightly different, error terms. These are the full equation method and the spatial derivative method.

1. Full Equation Method. This approach was introduced by Monaghan (36). It involves taking a given equation, multiplying by the kernel, and then integrating both sides over all space. This equates to stating that if a and b satisfy

$$\begin{aligned} \frac{Da}{Dt} &= -\frac{\partial b}{\partial x}, \\ \text{then } \left\langle \frac{Da}{Dt} \right\rangle &= -\left\langle \frac{\partial b}{\partial x} \right\rangle. \end{aligned}$$

Applying the kernel approximation and corresponding error analysis on the left side of the equation yields $\frac{Da}{Dt}$ back plus an error term. Similarly, applying the particle approximation (including the integration-by-parts) and corresponding error analysis to the right side of the equation yields the SPH semi-discrete

form of the problem. This can be summarized as

$$\frac{Da}{Dt} = - \sum_{j=1}^N \frac{m_j}{\rho_j} b_j W'_{ij} - E_k \left(\frac{Da}{Dt}, x_i \right) - E_r(b, x_i). \quad (3.28)$$

The notation W'_{ij} means $W'(x_i - x_j)$, is standard in SPH, and is used throughout the rest of this paper. The difficulty of this method comes when the right side of the equation cannot be written as the derivative of some function. For example,

$$\frac{Da}{Dt} = -c \frac{\partial b}{\partial x}. \quad (3.29)$$

In this form, the integration-by-parts step cannot be used directly to move the derivative from the function onto the kernel. A linearization step is usually included to eliminate this difficulty. So for variables a , b , c and linearization error, E_l , which is defined by

$$E_l = c \left\langle \frac{\partial b}{\partial x} \right\rangle - \left\langle c \frac{\partial b}{\partial x} \right\rangle,$$

So, if

$$\begin{aligned} \frac{Da}{Dt} &= -c \frac{\partial b}{\partial x}, \\ \text{then } \left\langle \frac{Da}{Dt} \right\rangle &= - \left\langle c \frac{\partial b}{\partial x} \right\rangle = -c \left\langle \frac{\partial b}{\partial x} \right\rangle + E_l. \end{aligned}$$

Now use integration-by-parts on the right side and apply the particle approximation. This situation is summarized as

$$\frac{Da}{Dt} = -c_i \sum_{j=1}^N \frac{m_j}{\rho_j} b_j W'_{ij} - E_k \left(\frac{Da}{Dt}, x_i \right) + E_l - c E_r(b, x_i). \quad (3.30)$$

Concern over the size of this linearization term led to the derivation of a second method.

2. Spatial Derivative Method. This approach does not deal with the entire equation, just the spatial derivatives. In the earlier parts of this chapter, the partial derivative was shown to be equivalent to the SPH derivative plus some errors. This relationship may be used and substituted directly into an equation. This equates to stating that if a and b satisfy

$$\frac{Da}{Dt} = -\frac{\partial b}{\partial x}, \quad (3.31)$$

$$\text{then } \frac{Da}{Dt} = -\sum_{j=1}^N \frac{m_j}{\rho_j} b_j W'_{ij} + E_k \left(\frac{\partial b}{\partial x}, x_i \right) - E_r(b, x_i). \quad (3.32)$$

This result compares quite similarly with the full equation method found in equation (3.28). In addition, with this method, if the right side of the equation involves non-linear terms (such as (3.29)), no linearization step is done. Just substitute into an equation the proper terms from the consistency analysis. So for variables a, b, c , if

$$\frac{Da}{Dt} = -c \frac{\partial b}{\partial x}, \quad (3.33)$$

$$\text{then } \frac{Da}{Dt} = -c_i \sum_{j=1}^N \frac{m_j}{\rho_j} b_j W'_{ij} + c E_k \left(\frac{\partial b}{\partial x}, x_i \right) - c E_r(b, x_i). \quad (3.34)$$

Taking the difference between the two methods, eqn (3.30) - eqn (3.34) results in

$$E_l = E_k \left(\frac{Da}{Dt}, x_i \right) + c E_k \left(\frac{\partial b}{\partial x}, x_i \right) = -E_k \left(c \frac{\partial b}{\partial x}, x_i \right) + c E_k \left(\frac{\partial b}{\partial x}, x_i \right).$$

This shows that E_l equals the difference between two $O(h^2, h\Delta x)$ terms. So it is of the same order as the error already in the method. This allows for the conclusion that either method of developing the SPH form for the Euler equations is acceptable and consistent. It can also be concluded that the concern over linearization error is unfounded.

One final note, consistency analysis is based on the assumptions of smooth data. Applying a method in an area where there is a discontinuity could result in E_l being larger; showing a larger difference between the methods. The integration-by-parts step that is performed in both methods introduces boundary errors in this case and causes these differences. This comment is meant to emphasize the difference between the mathematical construct known as consistency and a real world application. It also leads us to the next section on non-smooth functions and points to one of the primary methods of controlling the errors near a discontinuity, artificial viscosity (discussed at the end of this chapter).

3.6 *Non-Smooth Functions*

The lemmas given earlier in this chapter only applied when functions are sufficiently smooth; which is the traditional definition of consistency. But it is not always the case in actual calculations. There are at least two ways to resolve the question of how to prove consistency when functions are not sufficiently smooth.

First, proceed as if the functions actually were smooth. Since nothing (or little) is known about the function between particles, it is acceptable to simply assume the function is smooth there. This has the effect of numerically solving a differential equation for a slightly different problem: one with large gradients instead of shocks. However, the consistency analysis of section 3.3 would directly apply and this is the concept that is often taken. Also, in the limit as $\Delta x \rightarrow 0$ this smooth problem will approach the discontinuous problem.

Second, derive an SPH form that allows for shocks while still being consistent. The remainder of this section does just that.

3.6.1 *Scalar Equations.* The goal here is to develop a kernel approximation and corresponding SPH particle approximation for $u'(x_o)$. This is a rather long and tedious process, so the details are left out here and placed in Appendix A. Consider

the interval shown in Figure 3.2. Let $a \leq x_o - \kappa h$ and $b \geq x_o + \kappa h$. Assume there exists an integrable discontinuity in the function, $f(x)$, at d . For now assume $x_o < d \leq b$.

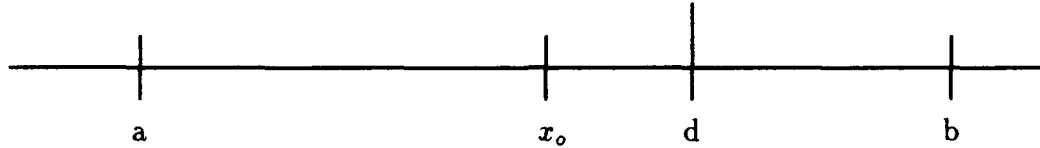


Figure 3.2 Non-Smooth Data Consistency part 1

In section 3.1 a Taylor series expansion technique was used to develop the kernel approximation. However, an expansion cannot be performed across a discontinuity, so the interval $[a, b]$ must be split into $[a, d)$ and $[d, b]$. Let x_1 be a point in $[d, b]$ and perform expansions about x_o and x_1 in their respective intervals to obtain

$$\int_a^b f(x) W(x_o - x) dx = f(x_o) + [f(x_1) - f(x_o)] \int_d^b W(x_o - x) dx + O(h) . \quad (3.35)$$

Note that the second integral is only over part of the interval and therefore is not equal to one. This implies for non-smooth data when $x_o \rightarrow d$

$$\int_a^b f(x) W(x_o - x) dx \nrightarrow f(x_o) \quad \text{as } h \rightarrow 0 .$$

However, retaining the second term on the right-hand-side of equation (3.35) ($\sim \Delta f$) allows for the method to be consistent (in the context of this section) and of order $O(h)$.

Now consider $f(x) = u'(x)$, where u' , u'' , and u''' exist everywhere except at d and are bounded on $[a, d) \cup (d, b]$. Substitute into equation (3.35) and then integrate by parts. Unlike earlier in section 3.3, the boundary terms (in this case across the discontinuity) do not vanish. The results are

$$u'(x_o) = -[u'(x_1) - u'(x_o)] \int_d^b W(x_o - x) dx + [u(d^-) - u(d^+)]W(x_o - d) + \int_a^b u(x) W'(x_o - x) dx + O(h), \quad (3.36)$$

where d^- and d^+ are the limits of d from the left and right respectively. Since x_1 previously was chosen arbitrarily in $[d, b]$, now let $x_1 = d$. Expressions for $u'(d)$ and $u(d^-)$ must now be found. The expression for $u'(d)$ is obtained in a similar process to what was done so far while the expression for $u(d^-)$ is taken from a Taylor series expansion around x_o . The results are

$$u'(x_o) = \left[\frac{1}{\theta - (d - x_o)[W(x_o - d) - (1 - \theta)W(0)]} \right] \left\{ \int_a^b u(x) [\theta W'(x_o - x) - (1 - \theta)(d - x_o)W''(x_o - x)] dx + [u(x_o) - u(d)][W(x_o - d) - (1 - \theta)W(0)] \right\} + O(h), \quad (3.37)$$

where θ is a measure of how close x_o is to d defined by $\theta = 2 \int_{x_o}^d W(x_o - x) dx$

In Appendix A, further simplifications are made to obtain a particle approximation form of this equation; but that work is omitted here. Also consider the shock on the other side of x_o as shown in Figure 3.3 in the Appendix. This follows exactly as in the first case, so all the steps are left out in this case and the reader is referred to Appendix A.

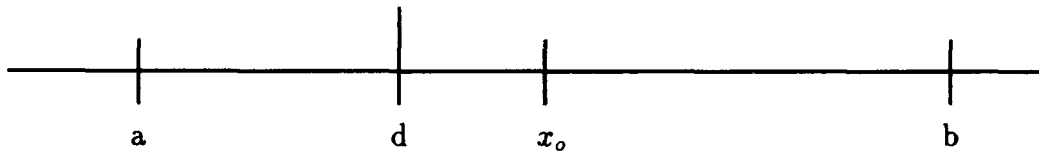


Figure 3.3 Non-Smooth Data Consistency part 2

Now combine the results contained in equations (A.1) - (A.21) and surrounding work in the Appendix for a particle x_i on either side of the discontinuity as follows: Given x_i , let d be the location of a discontinuity, x_d be the nearest particle on the

opposite side of the discontinuity from x_i , and use the usual format for the kernel ($W(x, h) = \frac{1}{h} K(\frac{x}{h})$). Provided x_d is quite close to d the results are

$$\theta = 2 \int_0^{\frac{|x_i - d|}{h}} K(v) dv \quad (3.38)$$

$$B = [W_{id} - (1 - \theta)W_o](x_d - x_i) \operatorname{sgn}(x_i - x_d) \quad (3.39)$$

$$u'(x_i) = \sum_{j=1}^N \frac{m_j}{\rho_j} u_j W'_{ij} - \left(\frac{1}{\theta + B} \right) \left\{ \sum_{j=1}^N \frac{m_j}{\rho_j} u_j [B W'_{ij} - (1 - \theta)(x_d - x_i) W''_{ij}] - B \left(\frac{u_i - u_d}{x_i - x_d} \right) \right\} \quad (3.40)$$

Note that $0 \leq \theta \leq 1$ and to ensure θ is well defined at the ends investigate equation (3.40) near 0 and 1.

(i) As $|x_i - d|$ increases, ie. x_i moves away from the shock, θ increases until $|x_i - d| = \kappa h$ where θ equals 1. At that point θ stays at 1 no matter how far x_i gets from d . From equation (3.40) if $\theta \rightarrow 1$ then

$$u'(x_i) \rightarrow \sum_{j=1}^N \frac{m_j}{\rho_j} u_j \left(\frac{1}{1 + B} \right) W'_{ij} + \left(\frac{B}{1 + B} \right) \left(\frac{u_i - u_d}{x_i - x_d} \right).$$

But B also goes to 0 in this case since W has compact support. Therefore when $|x_i - d| = \kappa h$, the correction term drops completely out and yields the smooth data result

$$u'(x_i) = \sum_{j=1}^N \frac{m_j}{\rho_j} u_j W'_{ij}.$$

(ii) As $x_i \rightarrow d$, ie. x_i moves towards the shock, θ decreases to 0. θ never actually reaches 0 since x_i cannot equal d under the assumptions, but it can get very close. Therefore consider some of the terms as $\theta \rightarrow 0$. Using equation (3.40), let $d = x_d = x_i + \epsilon h$, $h \gg \epsilon > 0$ and substituting to obtain

$$\begin{aligned}
u'(x_i) &= \left(\frac{\theta}{\theta + B} \right) \left\{ \sum_{j=1}^N \frac{m_j}{\rho_j} u_j \left[W'(x_i - x_j) + \left(\frac{1-\theta}{\theta} \right) (x_i + \varepsilon h - x_i) W''(x_i - x_j) \right] \right. \\
&\quad \left. + \frac{B}{\theta} \left[\frac{u(x_i) - u(x_i + \varepsilon h)}{x_i - (x_i + \varepsilon h)} \right] \right\} \\
B &= [W(x_i - x_i - \varepsilon h) - (1 - \theta)W(0)] (x_i + \varepsilon h - x_i) \operatorname{sgn}(x_i - x_i - \varepsilon h) \\
&= -\varepsilon h [W(-\varepsilon h) - (1 - \theta)W(0)] .
\end{aligned} \tag{3.41}$$

Substituting B into equation (3.41) yields

$$\begin{aligned}
u'(x_i) &= \left[\frac{1}{1 - \frac{\varepsilon h}{\theta} [W(-\varepsilon h) - (1 - \theta)W(0)]} \right] \left\{ \sum_{j=1}^N \frac{m_j}{\rho_j} u_j \left[W'_{ij} + \left(\frac{1-\theta}{\theta} \right) \varepsilon h W''_{ij} \right] \right. \\
&\quad \left. + \frac{1}{\theta} [u(x_i) - u(x_i + \varepsilon h)] [W(-\varepsilon h) - (1 - \theta)W(0)] \right\} .
\end{aligned}$$

Expand the kernel in a Taylor series. This assumes the kernel has a Taylor series expansion. Note: even if the kernel does not have a series expansion the analysis after this will still follow, but it is just more confusing

$$W(-\varepsilon h) = W(0) - \varepsilon h W'(0) + \frac{1}{2} \varepsilon^2 h^2 W''(0) + \dots$$

Substitute to find

$$\begin{aligned}
u'(x_i) &= \left[\frac{1}{1 - \varepsilon h [W(0) - (\frac{\varepsilon h}{\theta}) W'(0)]} \right] \left\{ \sum_{j=1}^N \frac{m_j}{\rho_j} u_j [W'_{ij} + (1 - \theta) \left(\frac{\varepsilon h}{\theta} \right) W''_{ij}] \right. \\
&\quad \left. + [u(x_i) - u(x_i + \varepsilon h)] [W(0) - \frac{\varepsilon h}{\theta} W'(0)] \right\} + O(\varepsilon^2) .
\end{aligned}$$

From equation (3.38) and $d = x_i + \varepsilon h$, θ becomes

$$\theta = 2 \int_0^\varepsilon K(v) dv . \tag{3.42}$$

Then $\theta \rightarrow 0$ as $\varepsilon \rightarrow 0$, $\frac{\varepsilon h}{\theta} \rightarrow \frac{0}{0}$ as $\varepsilon \rightarrow 0$. It is necessary to know if $\frac{\varepsilon h}{\theta}$ is bounded as

$\varepsilon \rightarrow 0$. Use L'Hôpital's Rule to find $\frac{\varepsilon h}{\theta} \rightarrow \frac{h}{\frac{d\theta}{d\varepsilon}}$ and by the Fundamental Theorem of Calculus from equation (3.42), $\frac{d\theta}{d\varepsilon} = 2K(\varepsilon)$. Therefore

$$\frac{\varepsilon h}{\theta} \rightarrow \frac{h}{2K(\varepsilon)} = \frac{1}{2W(\varepsilon)}.$$

Then add the requirement that $K(u) \rightarrow 0$ as $u \rightarrow 0$. For example if $K(u)$ is a polynomial it must include a constant term. So in conclusion, $\frac{\varepsilon h}{\theta} \rightarrow \frac{1}{2W(0)}$ as $\varepsilon \rightarrow 0$. Hence

$$u'(x_i) \rightarrow \sum_{j=1}^N \frac{m_j}{\rho_j} u_j \left[W'_{ij} + \frac{W''_{ij}}{2W(0)} \right] + \frac{\Delta u_d [2W^2(0) - W'(0)]}{2W(0)} \quad (3.43)$$

as $x_i \rightarrow d$ where $\Delta u_d = u(d^+) - u(d^-)$.

Therefore, equations (3.38) - (3.40) are well defined at the limits of θ .

3.6.2 Euler Equations. Using the consistent form of u' just derived, new SPH forms of the Euler equations for one dimension may be derived. As with all SPH equations these are not unique, but simply one possibility. Note: in the equations to follow, the notation u_d implies the value of some field variable u at the closest point of the opposite side of the shock from x_i .

Continuity Equation:

$$\begin{aligned} \dot{\rho} &= -(\rho \nabla \cdot \vec{v}) = \vec{v} \cdot \nabla \rho - \nabla \cdot (\rho \vec{v}) = v \rho' - (\rho v)' \\ \dot{\rho}_i &= v_i \left\{ \sum_{j=1}^N \frac{m_j}{\rho_j} \rho_j W'_{ij} - \left(\frac{1}{\theta + B} \right) \left[\sum_{j=1}^N \frac{m_j}{\rho_j} \rho_j (B W'_{ij} + (1 - \theta) x_{di} W''_{ij}) \right. \right. \\ &\quad \left. \left. - B \frac{(\rho_i - \rho_d)}{(x_i - x_d)} \right] \right\} \\ &\quad - \left\{ \sum_{j=1}^N \frac{m_j}{\rho_j} \rho_j v_j W'_{ij} - \left(\frac{1}{\theta + B} \right) \left[\sum_{j=1}^N \frac{m_j}{\rho_j} \rho_j v_j (B W'_{ij} + (1 - \theta) x_{di} W''_{ij}) \right. \right. \\ &\quad \left. \left. - B \frac{(\rho_i v_i - \rho_d v_d)}{(x_i - x_d)} \right] \right\} \end{aligned}$$

$$\dot{\rho}_i = \sum_{j=1}^N m_j (v_i - v_j) W'_{ij} - \left(\frac{1}{\theta + B} \right) \left\{ \sum_{j=1}^N m_j (v_i - v_j) [B W'_{ij} + (1 - \theta) x_{di} W''_{ij}] + B \rho_d \frac{(v_i - v_d)}{(x_i - x_d)} \right\} . \quad (3.44)$$

Note: if using the SPH density-by-summation form instead of the continuity equation, a correction is still required because

$$\begin{aligned} \int_a^b f(x) W(x_o - x) dx &= f(x_o) + [f(x_d) - f(x_o)] \frac{1}{2} (1 - \theta) . \\ \Rightarrow f(x_o) &= \left(\frac{2}{1 + \theta} \right) \int_a^b f(x) W(x_o - x) dx - \left(\frac{1 - \theta}{1 + \theta} \right) f(x_d) \\ \text{so } f(x_i) &= \sum_{j=1}^N \frac{m_j}{\rho_j} f_j W_{ij} + \left(\frac{1 - \theta}{1 + \theta} \right) \left[\sum_{j=1}^N \frac{m_j}{\rho_j} f_j W_{ij} - f(x_d) \right] \end{aligned} \quad (3.45)$$

$$\text{Hence } \rho_i = \sum_{j=1}^N m_j W_{ij} + \left(\frac{1 - \theta}{1 + \theta} \right) \left[\sum_{j=1}^N m_j W_{ij} - \rho_d \right] \quad (3.46)$$

An alternative to using $f(x_d)$ explicitly, is obtained by using equation (A.6):

$$\frac{f(x_o) + f(x_d)}{2} = \int_a^b f(x) W(x_d - x) dx .$$

Substitute this into equation (3.45) and simplify to find

$$f(x_i) = \sum_{j=1}^N \frac{m_j}{\rho_j} f_j W_{ij} + \left(\frac{1 - \theta}{\theta} \right) \sum_{j=1}^N \frac{m_j}{\rho_j} f_j (W_{ij} - W_{dj}) . \quad (3.47)$$

$$\text{Hence } \rho_i = \sum_{j=1}^N m_j W_{ij} - \left(\frac{1 - \theta}{\theta} \right) \sum_{j=1}^N m_j (x_{di}) W'_{ij} \quad (3.48)$$

Momentum Equation:

$$\vec{v} = - \frac{\nabla P}{\rho} = - \frac{P}{\rho^2} \nabla \rho - \nabla \left(\frac{P}{\rho} \right) = - \frac{P}{\rho^2} \rho' - \left(\frac{P}{\rho} \right)'$$

$$\begin{aligned}
\dot{v}_i &= -\frac{P_i}{\rho_i^2} \left\{ \sum_{j=1}^N \frac{m_j}{\rho_j} \rho_j W'_{ij} - \left(\frac{1}{\theta + B} \right) \left[\sum_{j=1}^N \frac{m_j}{\rho_j} \rho_j (BW'_{ij} - (1 - \theta)x_{di}W''_{ij}) \right. \right. \\
&\quad \left. \left. - B \frac{(\rho_i - \rho_d)}{(x_i - x_d)} \right] \right\} \\
&\quad - \left\{ \sum_{j=1}^N \frac{m_j}{\rho_j} \frac{P_j}{\rho_j} W'_{ij} - \left(\frac{1}{\theta + B} \right) \left[\sum_{j=1}^N \frac{m_j}{\rho_j} \frac{P_j}{\rho_j} (BW'_{ij} + (1 - \theta)x_{di}W''_{ij}) \right. \right. \\
&\quad \left. \left. - \frac{B}{(x_i - x_d)} \left(\frac{P_i}{\rho_i} - \frac{P_d}{\rho_d} \right) \right] \right\} \\
\dot{v}_i &= -\sum_{j=1}^N m_j \left(\frac{P_i}{\rho_i^2} + \frac{P_j}{\rho_j^2} \right) W'_{ij} - \left(\frac{1}{\theta + B} \right) \left\{ -\sum_{j=1}^N m_j \left(\frac{P_i}{\rho_i^2} + \frac{P_j}{\rho_j^2} \right) [BW'_{ij} \right. \\
&\quad \left. + (1 - \theta)x_{di}W''_{ij}] + \frac{B}{(x_i - x_d)} \left(\frac{2P_i}{\rho_i} - \frac{P_i\rho_d}{\rho_i^2} - \frac{P_d}{\rho_d} \right) \right\}. \quad (3.49)
\end{aligned}$$

Energy Equation:

$$\begin{aligned}
\dot{e} &= -\frac{P}{\rho} \nabla \cdot \vec{v} = -\frac{P}{\rho^2} (\nabla \cdot (\rho \vec{v}) - \vec{v} \cdot \nabla \rho) = \frac{P}{\rho^2} (-(\rho v)' + v \rho') \\
\dot{e}_i &= \frac{P_i}{\rho_i^2} \left[\sum_{j=1}^N m_j (v_i - v_j) W'_{ij} - \left(\frac{1}{\theta + B} \right) \left\{ \sum_{j=1}^N m_j (v_i - v_j) [BW'_{ij} + (1 - \theta)x_{di}W''_{ij}] \right. \right. \\
&\quad \left. \left. + \frac{B}{(x_i - x_d)} \rho_d (v_i - v_d) \right\} \right]. \quad (3.50)
\end{aligned}$$

Also,

$$\begin{aligned}
\dot{e} &= -\frac{P}{\rho} \nabla \cdot \vec{v} = \vec{v} \cdot \nabla \left(\frac{P}{\rho} \right) - \nabla \cdot \left(\frac{P \vec{v}}{\rho} \right) = v \left(\frac{P}{\rho} \right)' - \left(\frac{P v}{\rho} \right)' \\
\dot{e}_i &= v_i \left\{ \sum_{j=1}^N \frac{m_j}{\rho_j} \frac{P_j}{\rho_j} W'_{ij} - \left(\frac{1}{\theta + B} \right) \left[\sum_{j=1}^N \frac{m_j}{\rho_j} \frac{P_j}{\rho_j} (BW'_{ij} + (1 - \theta)x_{di}W''_{ij}) \right. \right. \\
&\quad \left. \left. - \frac{B}{(x_i - x_d)} \left(\frac{P_i}{\rho_i} - \frac{P_d}{\rho_d} \right) \right] \right\} \\
&\quad - \left\{ \sum_{j=1}^N \frac{m_j}{\rho_j} \frac{P_j}{\rho_j} v_j W'_{ij} - \left(\frac{1}{\theta + B} \right) \left[\sum_{j=1}^N \frac{m_j}{\rho_j} \frac{P_j}{\rho_j} v_j (BW'_{ij} + (1 - \theta)x_{di}W''_{ij}) \right. \right. \\
&\quad \left. \left. - \frac{B}{(x_i - x_d)} \left(\frac{P_i v_i}{\rho_i} - \frac{P_d v_d}{\rho_d} \right) \right] \right\}
\end{aligned}$$

$$\dot{e}_i = \sum_{j=1}^N m_j \frac{P_j}{\rho_j^2} (v_i - v_j) W'_{ij} - \left(\frac{1}{\theta + B} \right) \left\{ \sum_{j=1}^N m_j \frac{P_j}{\rho_j^2} (v_i - v_j) [B W'_{ij} + (1 - \theta) x_{di} W''_{ij}] + \frac{B}{(x_i - x_d)} \frac{P_d}{\rho_d} (v_i - v_d) \right\}. \quad (3.51)$$

Average equations (3.50) and 3.51) to obtain

$$\dot{e}_i = \frac{1}{2} \sum_{j=1}^N m_j \left(\frac{P_i}{\rho_i^2} + \frac{P_j}{\rho_j^2} \right) (v_i - v_j) W'_{ij} - \left(\frac{1}{\theta + B} \right) \left\{ \frac{1}{2} \sum_{j=1}^N m_j \left(\frac{P_i}{\rho_i^2} + \frac{P_j}{\rho_j^2} \right) \times (v_i - v_j) [B W'_{ij} + (1 - \theta) x_{di} W''_{ij}] + \frac{B}{2} \frac{(v_i - v_d)}{(x_i - x_d)} \left(\frac{P_i \rho_d}{\rho_i^2} + \frac{P_d}{\rho_d} \right) \right\}. \quad (3.52)$$

To actually apply these new SPH Euler equations, a shock capturing or detection algorithm is required. In this way, θ can be calculated for each particle at each time step without having to track the shock, which is usually very expensive. See Chapter VIII for more information on shock capturing techniques.

3.7 Higher Dimensions

So far in this dissertation, most of the consistency analysis has been performed in one dimension. However, it can be extended to higher dimensions. Since the work here is similar to that already done, many of the details will be omitted.

The analysis from section 3.1 on the Kernel Approximation is done in a straightforward manner following exactly the same process. However, it involves using Taylor series expansions for functions of more than one variable, which is a more complicated process. It can be simplified by using the following notation (note: for two dimensions terms involving z will not appear)

$$\begin{aligned} \vec{u} &= \vec{r} - \vec{r}_o = (x - x_o, y - y_o, z - z_o) \\ \vec{u} \cdot \nabla &= (x - x_o) \frac{\partial}{\partial x} + (y - y_o) \frac{\partial}{\partial y} + (z - z_o) \frac{\partial}{\partial z} \\ [\vec{u} \cdot \nabla]^2 &= (x - x_o)^2 \frac{\partial^2}{\partial x^2} + 2(x - x_o)(y - y_o) \frac{\partial^2}{\partial x \partial y} + \cdots + (z - z_o)^2 \frac{\partial^2}{\partial z^2}. \end{aligned}$$

Then obtain

$$\begin{aligned}
f_k(\vec{r}_o) &= \int_{\Omega} f(\vec{r}) W(\vec{r}_o - \vec{r}, h) d\vec{r} = \int_{\Omega} f(\vec{r}_o + \vec{u}) W(-\vec{u}, h) d\vec{u} \\
&= \int_{\Omega} W(-\vec{u}, h) \left[f(\vec{r}_o) + [\vec{u} \cdot \nabla] f(\vec{r}_o) + \frac{1}{2} [\vec{u} \cdot \nabla]^2 f(\vec{r}_o) \right] d\vec{u} \\
&= f(\vec{r}_o) \int_{\Omega} W(-\vec{u}, h) d\vec{u} \\
&\quad + \nabla f(\vec{r}_o) \cdot \int_{\Omega} \vec{u} W(-\vec{u}, h) d\vec{u} \\
&\quad + \frac{1}{2} \int_{\Omega} [\vec{u} \cdot \nabla]^2 f(\vec{r}_o) W(-\vec{u}, h) d\vec{u}.
\end{aligned}$$

If W is normalized, as shown in equation (3.2), then the integral in the first term of the sum is 1. As in the one dimensional case, if W is a symmetric function, the integral in the second term of the sum is 0, as is now shown. Let $W(\vec{u}, h) = \frac{1}{h^2} K\left(\frac{|\vec{u}|}{h}\right)$ and then in two dimensions

$$\begin{aligned}
\int_{\Omega} \vec{u} W(-\vec{u}, h) d\vec{u} &= \frac{1}{h^2} \int \int_{\Omega} \vec{u} K\left(\frac{|\vec{u}|}{h}\right) dx dy \\
&= \frac{1}{h^2} \int_0^{\kappa h} \int_0^{2\pi} (r \cos \theta, r \sin \theta) K\left(\frac{r}{h}\right) r d\theta dr \\
&= \frac{1}{h^2} \int_0^{\kappa h} \left[(\sin \theta, -\cos \theta) \Big|_0^{2\pi} \right] r^2 K\left(\frac{r}{h}\right) dr = (0, 0),
\end{aligned}$$

where κ is defined as before from the support of the kernel. That is, $W(\vec{u}) = 0$ for $|\vec{u}| > \kappa h$. Similarly in three dimensions

$$\begin{aligned}
\int_{\Omega} \vec{u} W(-\vec{u}, h) d\vec{u} &= \frac{1}{h^3} \int \int \int_{\Omega} \vec{u} K\left(\frac{|\vec{u}|}{h}\right) dx dy dz \\
&= \frac{1}{h^3} \int_0^{\kappa h} \int_0^{2\pi} \int_0^{\pi} (r \cos \theta \sin \phi, r \sin \theta \sin \phi, r \cos \theta) K\left(\frac{r}{h}\right) r^2 \sin \phi d\phi d\theta dr \\
&= \frac{1}{h^3} \int_0^{\kappa h} \int_0^{\pi} \left[(\sin \theta \sin \phi, -\cos \theta \sin \phi, \theta \cos \phi) \Big|_{\theta=0}^{2\pi} \right] r^3 \sin \phi K\left(\frac{r}{h}\right) d\phi dr \\
&= \frac{1}{h^3} \int_0^{\kappa h} \int_0^{\pi} (0, 0, 2\pi \cos \phi) r^3 \sin \phi K\left(\frac{r}{h}\right) d\phi dr
\end{aligned}$$

$$= \frac{1}{h^3} \int_0^{\kappa h} \left[(0, 0, \pi \sin^2 \phi) \right]_0^\pi r^3 K\left(\frac{r}{h}\right) dr = (0, 0, 0).$$

Therefore, the result is

$$f_k(\vec{r}_o) = f(\vec{r}_o) + E_k(f, \vec{r}_o) \quad (3.53)$$

$$\text{where} \quad E_k(f, \vec{r}_o) = \frac{1}{2} \int_{\Omega} [\vec{u} \cdot \nabla]^2 f(\vec{\xi}_o) W(-\vec{u}, h) d\vec{u} \quad (3.54)$$

for $\xi_o \in \Omega$.

To find a bound on the error term $E_k(f, \vec{r}_o)$, define

$$e_k = \frac{\kappa^2 d^2}{2} \sup_{\xi \in \Omega} |D^2 f(\vec{\xi})|,$$

where d is the dimension (2 or 3) and D^2 means any second partial derivative (pure and mixed):

$$\begin{aligned} |E_k(f, \vec{r}_o)| &= \frac{1}{2} \left| \int_{\Omega} [\vec{u} \cdot \nabla]^2 f(\vec{\xi}_o) W(-\vec{u}, h) d\vec{u} \right| \leq \frac{1}{2} \int_{\Omega} |[\vec{u} \cdot \nabla]^2 f(\vec{\xi}_o)| |W(-\vec{u}, h)| d\vec{u} \\ &\leq \frac{1}{2} \int_{\Omega} h^2 d^2 |D^2 f(\vec{\xi}_o)| |W(-\vec{u}, h)| d\vec{u} \leq \int_{\Omega} \frac{1}{2} \kappa^2 h^2 W(-\vec{u}, h) \frac{2e_k}{\kappa^2} d\vec{u} \\ &= e_k h^2 \int_{\Omega} W(-\vec{u}, h) d\vec{u} = e_k h^2. \end{aligned} \quad (3.55)$$

The work in section 3.2 on the rectangular rule is also applicable to higher dimensions, but it may not be as obvious. The following procedure is given for two dimensions but easily generalizes to three dimensions. Given a set of particles, triangulate the particles using a procedure known as Delaunay triangulation, ie. create a triangular mesh with the particles as the vertices. Then create a Voronoi polygon by placing a point at the centroid of each triangle. Connecting these points around a given particle creates a convex polygon containing exactly one particle. Further, this unique polygon has the property that any point inside it is closer to the particle contained in it than to any other particle. If this procedure is carried

out for all particles in a given region, the region will be completely covered with non-overlapping convex polygons (CP). Note: for more details regarding this construction see papers on Delaunay Triangulation and Voronoi Polygons, such as Baker (3), Kennon (27), and Sloan (56). Figure 3.4 contains a diagram of this procedure.

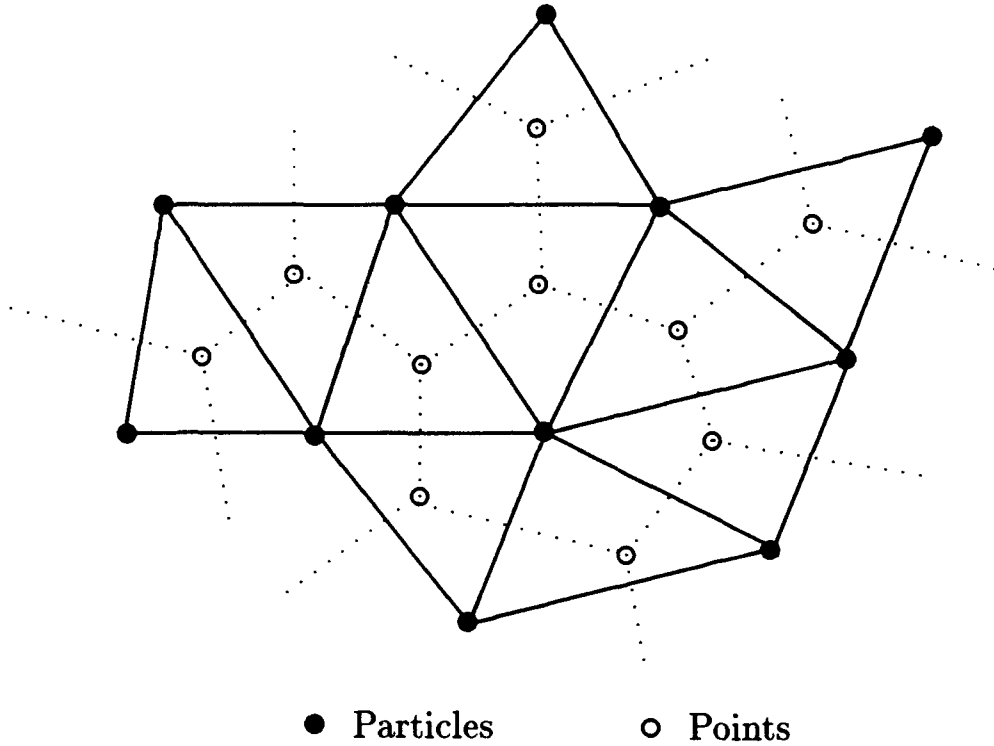


Figure 3.4 2-D Particle Triangulation

To integrate over any of these convex polygons, create triangles with one vertex at the particle of interest and the others at consecutive vertices along the boundary of the convex polygon. Then use a composite rule integrating over each triangle. Finally to integrate over the triangle map it to a right triangle and apply the one dimensional Rectangle Rule twice (once in each direction). See Figure 3.5 for a picture of this procedure. So for some domain Ω_k there are N_k convex polygons covering this domain and

$$\iint_{\Omega_k} f(x, y) dx dy = \sum_{j=1}^{N_k} \iint_{CP_j} f(x, y) dx dy .$$

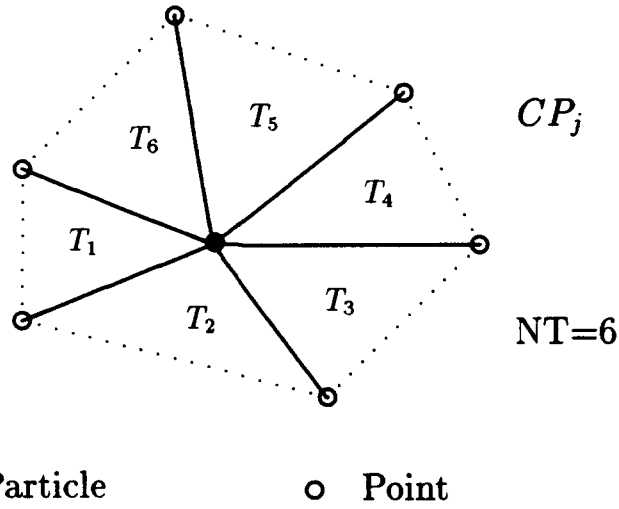


Figure 3.5 2-D Particle Convex Polygon

Then for any convex polygon, CP_j , there are NT_j triangles, T , within CP_j , and

$$\begin{aligned} \iint_{CP_j} f(x, y) dx dy &= \sum_{l=1}^{NT_j} \iint_{T_l} f(x, y) dx dy = \sum_{l=1}^{NT_j} [a_l f(x_j, y_j) + e_l] \\ &= A_j f(x_j, y_j) + E_j, \end{aligned}$$

where a_l is the area of triangle T_l and $A_j = \sum_{l=1}^{NT_j} a_l$ is the area of the polygon around the particle at (x_j, y_j) .

Hence

$$\sum_{j=1}^{N_k} \iint_{CP_j} f(x, y) dx dy = \sum_{j=1}^{N_k} [A_j f(x_j, y_j) + E_j] = \sum_{j=1}^{N_k} A_j f(x_j, y_j) + E.$$

As in the one dimensional rule, A_j (Δx in one dimension) can be taken to equal $\frac{m_j}{\rho_j}$.

The error bound is

$$|E| \leq N_k \max_j |E_j| \leq N_k \max_j |NT_j \max_l |e_l|| \leq N_k \max_j |NT_j M_a M_x e_a|,$$

where M_a is the area of the largest triangle and e_a is a small constant. Allowing for $\Delta T N_k M_a \sim \pi h^2 \kappa^2$ and for some small constant e_d

$$|E| \lesssim e_d h^2 M_x .$$

3.8 Artificial Viscosity/Wall Heating

In many numerical methods, artificial viscosity and artificial heat conduction (wall heating) are used to handle physical problems, especially near discontinuities. This dissertation only address three forms of artificial viscosity and one form of wall heating found in the published literature for SPH. In this section the techniques are introduced for later use and while simply commenting that they are consistent. That is, they vanish as $h \rightarrow 0$. The details of the consistency analysis may be found in Appendix A.

Starting with artificial viscosity, the three forms are attributed to: Monaghan, et al. (37), Hernquist and Katz (19), and Lattanzio, et al. (28).

1. Monaghan. For the SPH form, in the momentum and energy equations replace the $\frac{P}{\rho^2}$ term with $\frac{P}{\rho^2} + \frac{1}{2}\Pi$ where the function $\Pi_{ij} = \Pi(x_i, x_j)$ is defined by

$$\Pi_{ij} = \frac{-\alpha 0.5(c_i + c_j)\mu_{ij} + \beta \mu_{ij}^2}{0.5(\rho_i + \rho_j)} \quad (3.56)$$

$$\mu_{ij} = \begin{cases} \frac{h(v_i - v_j) \cdot (x_i - x_j)}{(x_i - x_j)^2 + \eta h^2} & (v_i - v_j) \cdot (x_i - x_j) < 0 \\ 0 & \text{otherwise} . \end{cases} \quad (3.57)$$

In these equations c is the material speed of sound, η is a small constant (often .01), and α and β are user specified parameters. These last two are sometimes referred to as the artificial viscosity coefficients and are usually in the range [0.5, 3.0]. In Appendix A, the artificial viscosity term is shown to be consistent with (when

$$\frac{\partial v}{\partial x} < 0)$$

$$\frac{\alpha h}{2\rho} \frac{\partial}{\partial x} \left[c\rho \frac{\partial v}{\partial x} \right] - \frac{\beta h^2}{2\rho} \frac{\partial}{\partial x} \left[\rho \left(\frac{\partial v}{\partial x} \right)^2 \right] . \quad (3.58)$$

With the h factors present, this form will vanish as $h \rightarrow 0$, maintaining the consistency of the overall method.

2. Hernquist and Katz. For the SPH form, in the momentum and energy equations replace the $\frac{P}{\rho^2}$ term with $\frac{P}{\rho^2} + \frac{1}{2}\Pi$ where the function $\Pi_{ij} = \Pi(x_i, x_j)$ is defined by

$$\Pi_{ij} = \frac{q_i}{\rho_i^2} + \frac{q_j}{\rho_j^2} \quad (3.59)$$

$$q_i = \begin{cases} \alpha h_i \rho_i c_i |\nabla \cdot v|_i + \beta h_i^2 \rho_i (\nabla \cdot v)_i^2 & (v_i - v_j) \cdot (x_i - x_j) < 0 \\ 0 & \text{otherwise} \end{cases} \quad (3.60)$$

$$\text{note : } (\nabla \cdot v)_i = -\frac{1}{\rho_i} \sum_j m_j (v_i - v_j) W'_{ij} .$$

In these equations c is the material speed of sound and α and β are user specified parameters. These last two are sometimes referred to as the artificial viscosity coefficients and are usually in the range $[0.5, 3.0]$. In Appendix A the artificial viscosity term is shown to be consistent with (when $\frac{\partial v}{\partial x} < 0$)

$$-\frac{\alpha h c}{\rho} \left| \frac{\partial v}{\partial x} \right| - \frac{\beta h^2}{\rho} \left(\frac{\partial v}{\partial x} \right)^2 . \quad (3.61)$$

With the h factors present, this form will vanish as $h \rightarrow 0$, maintaining the consistency of the overall method.

3. Lattanzio. This form is very similar to the Monaghan version. Therefore, the derivation should follow exactly as in the Monaghan case. In the SPH momentum and energy equations replace the $\frac{P}{\rho^2}$ term with $\frac{P}{\rho^2}(1 + \Pi)$ where the function $\Pi_{ij} =$

$\Pi(x_i, x_j)$ is defined by

$$\Pi_{ij} = -\alpha\mu_{ij} + \beta\mu_{ij}^2 \quad (3.62)$$

$$\mu_{ij} = \begin{cases} \frac{h(v_i - v_j) \cdot (x_i - x_j)}{c((x_i - x_j)^2 + \eta h^2)} & (v_i - v_j) \cdot (x_i - x_j) < 0 \\ 0 & \text{otherwise} . \end{cases} \quad (3.63)$$

In these equations c is the material speed of sound, η is a small constant (often .01), and α and β are user specified parameters. These last two are sometimes referred to as the artificial viscosity coefficients and are usually in the range [0.5, 3.0]. In Appendix A the artificial viscosity term is shown to be consistent with (when $\frac{\partial v}{\partial x} < 0$)

$$\frac{\alpha h}{c\rho} \frac{\partial}{\partial x} \left[P \frac{\partial v}{\partial x} \right] - \frac{\beta h^2}{c^2 \rho} \frac{\partial}{\partial x} \left[P \left(\frac{\partial v}{\partial x} \right)^2 \right] . \quad (3.64)$$

With the h factors present, this form will vanish as $h \rightarrow 0$, maintaining the consistency of the overall method.

4. Wall Heating. There is currently only one form in use, attributed to Monaghan (41). To implement it, add an additional term H in the SPH energy, where

$$H_i = - \sum_{j=1}^N m_j \frac{(q_i + q_j)(e_i - e_j)(x_i - x_j)}{0.5(\rho_i + \rho_j)((x_i - x_j)^2 + \eta h^2)} W'_{ij} \quad (3.65)$$

$$q_s = g_1 h_s c_s |\nabla \cdot v|_s + g_2 h_s^2 (\nabla \cdot v)_s^2 \quad (3.66)$$

$$(\nabla \cdot v)_s = -\frac{1}{\rho_s} \sum_j m_j (v_s - v_j) W'_{sj} .$$

In these equations c is the material speed of sound, η is a small constant (often .01), and g_1 and g_2 are user specified parameters. These last two are sometimes referred to as the wall heating coefficients and are usually in the range [0.25, 1.5]. In Appendix A the wall heating term is shown to be consistent with

$$\frac{1}{\rho} \nabla \cdot (Q \nabla e) . \quad (3.67)$$

The Q term contains factors proportional to h , so this term will vanish as $h \rightarrow 0$, maintaining the consistency of the overall method.

3.9 Summary

In this chapter, consistency of the SPH method was analyzed. The key results were the derivation of truncation error terms and the identification of bounds for those terms. For SPH, as usually implemented, those bounds are of order $O(h^2, h\Delta x)$. This implies the numerical method will be close to the differential equation for sufficiently small h and Δx . There are two basic assumptions that went into these results. First, that the function being approximated is smooth. Second, that volume elements calculated by the particle position equal those calculated by mass and density. This second assumption departs somewhat from standard SPH and comments on how to control this assumption are included in the chapter.

In addition to the work just described, a second approach of proving consistency was taken when the function being approximated has a discontinuity in it. This results in the derivation of a first order SPH approximation that is consistent even near a shock. Also in this chapter, the consistency of artificial viscosity and wall heating terms were analyzed for later use.

IV. STABILITY

This chapter addresses the mathematical concept known as stability as it applies to SPH. Stability is essentially the study of error propagation in numerical methods. As such, this is a natural continuation of the error analysis begun in the previous chapter. Two different approaches are taken in this chapter to investigate the stability of the semi-discrete (spatial) approximation. A semi-discrete approximation is obtained by discretizing the conservation equation $\frac{Du}{Dt} = -[f(u)]_x$ only in space to obtain $\frac{Du}{Dt} = -S(f(u))$. The result is a system of ordinary differential equations in time.

First, a linearized approach is taken in which an instability is indicated. This approach develops an *amplification matrix* from the Euler equations by representing the field variables as perturbations around equilibrium points. The system is linearized in the perturbations allowing Fourier analysis to be performed. Assumptions are made that the data is from a uniformly spaced, smooth data problem. From this work, the resulting matrix equation is analyzed to determine if there are any amplifications (or growths) in the perturbations. To keep the system well defined, the eigenvalues of the amplification matrix must have non-positive real parts. This form of stability analysis is closer to what Strikwerda (60:51) calls dynamic stability than to numerical stability, but is just as important.

Second, a total variation approach is taken in which a new SPH formulation is developed. The total variation approach is better than the linearized approach for non-linear equations, but is much more difficult to apply. In fact, neither the stability nor instability of common SPH forms can be determined with this. So, the approach taken here is to develop a total variation stable version of SPH starting from the basic one dimensional wave equation. This concept is then generalized for use with the Euler equations.

Although the two approaches differ in how to obtain stability, the goal of both is the same: to analyze and comment on the stability (growth or errors) in SPH and propose other forms that can alleviate any difficulties found by the research.

4.1 Linear Stability Analysis

This analysis is performed by taking a set of one dimensional SPH equations, linearizing them, and investigating the properties of the eigenvalues from the resulting matrix equation. This work is performed in detail for one set of SPH equations and then indicated how similar results are obtained for many other forms. All the forms arrive at a similar unstable condition, indicating it is fairly fundamental problem in SPH. A note is made that another group of analysts first found this instability and the work here extends and expands upon those findings. Finally in this section, artificial viscosity and wall heating terms are reviewed as possible stabilizing effects and found that they do not remove the fundamental instability. The results from this section are used in the next section to propose stabilizing techniques.

4.1.1 Analysis Details. The following are the one-dimensional set of SPH equations used in this analysis (for a particle s)

$$\begin{aligned}
 \dot{\rho}_s &= \sum_{j=1}^N m_j (v_s - v_j) W'_{sj} \\
 \dot{v}_s &= - \sum_{j=1}^N m_j \left(\frac{P_j}{\rho_j^2} + \frac{P_s}{\rho_s^2} \right) W'_{sj} \\
 \dot{e}_s &= \frac{1}{2} \sum_{j=1}^N m_j \left(\frac{P_j}{\rho_j^2} + \frac{P_s}{\rho_s^2} \right) (v_s - v_j) W'_{sj} \\
 \dot{x}_s &= v_s .
 \end{aligned} \tag{4.1}$$

Assume the field values may be accurately represented by perturbations $(\phi, \nu, \varepsilon, \chi)$ around equilibrium points $(\bar{\rho}, \bar{v}, \bar{e}, \bar{x})$ as follows

$$\begin{aligned}\rho_s &= \bar{\rho}_s + \phi_s \\ v_s &= \bar{v}_s + \nu_s \\ e_s &= \bar{e}_s + \varepsilon_s \\ x_s &= \bar{x}_s + \chi_s.\end{aligned}\tag{4.2}$$

Then

$$\begin{aligned}\dot{\bar{\rho}}_s + \dot{\phi}_s &= \sum_{j=1}^N m_j (\bar{v}_s - \bar{v}_j + \nu_s - \nu_j) W'_{sj} \\ \dot{\bar{v}}_s + \dot{\nu}_s &= - \sum_{j=1}^N m_j \left(\frac{P_j}{(\bar{\rho}_j + \phi_j)^2} + \frac{P_s}{(\bar{\rho}_s + \phi_s)^2} \right) W'_{sj} \\ \dot{\bar{e}}_s + \dot{\varepsilon}_s &= \frac{1}{2} \sum_{j=1}^N m_j \left(\frac{P_j}{(\bar{\rho}_j + \phi_j)^2} + \frac{P_s}{(\bar{\rho}_s + \phi_s)^2} \right) (\bar{v}_s - \bar{v}_j + \nu_s - \nu_j) W'_{sj} \\ \dot{\bar{x}}_s + \dot{\chi}_s &= \bar{v}_s + \nu_s.\end{aligned}\tag{4.3}$$

Values for the kernel, W , and the pressure, P , at the perturbed points need to be found. First, expand the kernel in a Taylor series as follows

$$\begin{aligned}W'_{sj} &= W'(x_s - x_j) = W'((\bar{x}_s - \bar{x}_j) + (\chi_s - \chi_j)) \\ &= W'(\bar{x}_s - \bar{x}_j) + (\chi_s - \chi_j) W''(\bar{x}_s - \bar{x}_j) + O(\chi^2) \\ &= W'_{sj} + (\chi_s - \chi_j) W''_{sj} + O(\chi^2).\end{aligned}\tag{4.4}$$

For the pressure, consider, $P = P(\rho, e)$, then pressure has the algebraic form: $P \approx \tilde{A} + \tilde{B}\phi + \tilde{C}\varepsilon$ where $\tilde{A} = P(\bar{\rho}, \bar{e})$ and $\tilde{B}, \tilde{C} > 0$. Further,

$$\frac{1}{(\bar{\rho} + \phi)^2} = \frac{1}{\bar{\rho}^2} - \frac{2\phi}{\bar{\rho}^3} + O(\phi^2).$$

This gives the algebraic form

$$\frac{P}{\rho^2} = \frac{\tilde{A} + \tilde{B}\phi + \tilde{C}\varepsilon}{(\bar{\rho} + \phi)^2} \approx A + B\phi + C\varepsilon + O(\phi^2, \varepsilon^2)$$

where

$$\begin{aligned} A &= \frac{\tilde{A}}{\bar{\rho}^2} \\ B &= \frac{\tilde{B}}{\bar{\rho}^2} - \frac{2\tilde{A}}{\bar{\rho}^3} \\ C &= \frac{\tilde{C}}{\bar{\rho}^2}. \end{aligned} \quad (4.5)$$

Substitute equations (4.4) and (4.5) into equation (4.3), dropping 2nd and higher order perturbation terms. This results in the following equations

$$\begin{aligned} \dot{\bar{\rho}}_s + \dot{\phi}_s &= \sum_{j=1}^N m_j (\bar{v}_s - \bar{v}_j + \nu_s - \nu_j) (W'_{sj} + (\chi_s - \chi_j) W''_{sj}) \\ &= \sum_{j=1}^N m_j (\bar{v}_s - \bar{v}_j) W'_{sj} + \sum_{j=1}^N m_j [(\nu_s - \nu_j) W'_{sj} \\ &\quad + (\bar{v}_s - \bar{v}_j) (\chi_s - \chi_j) W''_{sj}], \\ \dot{\bar{v}}_s + \dot{\nu}_s &= - \sum_{j=1}^N m_j (A_j + B_j \phi_j + C_j \varepsilon_j + A_s + B_s \phi_s + C_s \varepsilon_s) (W'_{sj} + (\chi_s - \chi_j) W''_{sj}) \\ &= - \sum_{j=1}^N m_j (A_j + A_s) W'_{sj} - \sum_{j=1}^N m_j [(B_j \phi_j + B_s \phi_s) W'_{sj} \\ &\quad + (C_j \varepsilon_j + C_s \varepsilon_s) W'_{sj} + (A_j + A_s) (\chi_s - \chi_j) W''_{sj}], \\ \dot{\bar{e}}_s + \dot{\varepsilon}_s &= \frac{1}{2} \sum_{j=1}^N m_j (A_j + B_j \phi_j + C_j \varepsilon_j + A_s + B_s \phi_s + C_s \varepsilon_s) (\bar{v}_s - \bar{v}_j + \nu_s - \nu_j) \\ &\quad \times (W'_{sj} + (\chi_s - \chi_j) W''_{sj}) \\ &= \frac{1}{2} \sum_{j=1}^N m_j (A_j + A_s) (\bar{v}_s - \bar{v}_j) W'_{sj} + \frac{1}{2} \sum_{j=1}^N m_j [(B_j \phi_j + B_s \phi_s) \\ &\quad \times (\bar{v}_s - \bar{v}_j) W'_{sj} + (C_j \varepsilon_j + C_s \varepsilon_s) (\bar{v}_s - \bar{v}_j) W'_{sj} \\ &\quad + (A_j + A_s) (\nu_s - \nu_j) W'_{sj} + (A_j + A_s) (\bar{v}_s - \bar{v}_j) (\chi_s - \chi_j) W''_{sj}], \\ \dot{\bar{x}}_s + \dot{\chi}_s &= \bar{v}_s + \nu_s. \end{aligned} \quad (4.6)$$

Now allow the equilibrium points $(\bar{\rho}, \bar{v}, \bar{\epsilon}, \bar{\chi})$ to satisfy the original set of equations (4.1). Therefore, parts of the equations in (4.6) may be removed to obtain

$$\begin{aligned}
 \dot{\phi}_s &= \sum_{j=1}^N m_j [(\nu_s - \nu_j) W'_{sj} + (\bar{v}_s - \bar{v}_j)(\chi_s - \chi_j) W''_{sj}] \\
 \dot{\nu}_s &= - \sum_{j=1}^N m_j [(B_j \phi_j + B_s \phi_s) W'_{sj} + (C_j \epsilon_j + C_s \epsilon_s) W'_{sj} + (A_j + A_s)(\chi_s - \chi_j) W''_{sj}] \\
 \dot{\epsilon}_s &= \frac{1}{2} \sum_{j=1}^N m_j [(B_j \phi_j + B_s \phi_s)(\bar{v}_s - \bar{v}_j) W'_{sj} + (C_j \epsilon_j + C_s \epsilon_s)(\bar{v}_s - \bar{v}_j) W'_{sj} \\
 &\quad + (A_j + A_s)(\nu_s - \nu_j) W'_{sj} + (A_j + A_s)(\bar{v}_s - \bar{v}_j)(\chi_s - \chi_j) W''_{sj}] \\
 \dot{\chi}_s &= \nu_s.
 \end{aligned} \tag{4.7}$$

This system is now linear in the perturbations so a Fourier analysis may be applied. For this, let

$$\phi_s = \phi e^{isk}, \quad \nu_s = \nu e^{isk}, \quad \epsilon_s = \epsilon e^{isk}, \quad \chi_s = \chi e^{isk},$$

where $k = 2\pi\Delta x/\mu$, μ is the wavelength, and $i = \sqrt{-1}$. Uniform spacing is being required at this point. Imposing this requirement could be delayed until later, but the notation would become quite ugly. Further, in the next subsection this assumption is made anyway, so imposing it now does not change the analysis being performing. So, substitute the above values into the previous equations and divide both sides of the resulting equations by e^{isk} to obtain

$$\begin{aligned}
 \dot{\phi} &= \sum_{j=1}^N m_j [(1 - e^{i(j-s)k}) \nu W'_{sj} + (\bar{v}_s - \bar{v}_j)(1 - e^{i(j-s)k}) \chi W''_{sj}] \\
 \dot{\nu} &= - \sum_{j=1}^N m_j [(B_s + B_j e^{i(j-s)k}) \phi W'_{sj} + (C_s + C_j e^{i(j-s)k}) \epsilon W'_{sj} \\
 &\quad + (A_j + A_s)(1 - e^{i(j-s)k}) \chi W''_{sj}]
 \end{aligned}$$

$$\begin{aligned}
\dot{\varepsilon} &= \frac{1}{2} \sum_{j=1}^N m_j [(B_s + B_j e^{i(j-s)k})(\bar{v}_s - \bar{v}_j) \phi W'_{sj} + (C_s + C_j e^{i(j-s)k})(\bar{v}_s - \bar{v}_j) \varepsilon W'_{sj} \\
&\quad + (A_j + A_s)(1 - e^{i(j-s)k}) \nu W'_{sj} + (A_j + A_s)(\bar{v}_s - \bar{v}_j)(1 - e^{i(j-s)k}) \chi W''_{sj}] \\
\dot{\chi} &= \nu.
\end{aligned} \tag{4.8}$$

These equations can be evaluated as is, but it is easier if some notational simplifications are made. These take advantage of the kernel having compact support and require the kernel to be even. Let $l = j - s$, then the sums in equation (4.8) change from $j = 1, N$ to $l = -\infty, \infty$. Also $W'_{sj} = -W'_{js} = -W'_l$ and $W''_{sj} = W''_{js} = W''_l$. Also assume the mass is constant and can be factored out of the sums. Note: this assumption is not necessary and is justified later on. Substituting into equation (4.8) yields

$$\begin{aligned}
\dot{\phi} &= \left[-m \sum_{l=-\infty}^{\infty} (1 - e^{ilk}) W'_l \right] \nu + \left[m \sum_{l=-\infty}^{\infty} (\bar{v}_s - \bar{v}_{s+l}) (1 - e^{ilk}) W''_l \right] \chi \\
\dot{\nu} &= \left[m \sum_{l=-\infty}^{\infty} (B_s + B_{s+l} e^{ilk}) W'_l \right] \phi + \left[m \sum_{l=-\infty}^{\infty} (C_s + C_{s+l} e^{ilk}) W'_l \right] \varepsilon \\
&\quad + \left[-m \sum_{l=-\infty}^{\infty} (A_s + A_{s+l}) (1 - e^{ilk}) W''_l \right] \chi \\
\dot{\varepsilon} &= \left[\frac{-m}{2} \sum_{l=-\infty}^{\infty} (B_s + B_{s+l} e^{ilk}) (\bar{v}_s - \bar{v}_{s+l}) W'_l \right] \phi \\
&\quad + \left[\frac{-m}{2} \sum_{l=-\infty}^{\infty} (C_s + C_{s+l} e^{ilk}) (\bar{v}_s - \bar{v}_{s+l}) W'_l \right] \varepsilon \\
&\quad + \left[\frac{-m}{2} \sum_{l=-\infty}^{\infty} (A_s + A_{s+l}) (1 - e^{ilk}) W'_l \right] \nu \\
&\quad + \left[\frac{m}{2} \sum_{l=-\infty}^{\infty} (A_s + A_{s+l}) (\bar{v}_s - \bar{v}_{s+l}) (1 - e^{ilk}) W''_l \right] \chi \\
\dot{\chi} &= \nu.
\end{aligned} \tag{4.9}$$

The following matrix equation can be obtained from the equations above: $\dot{\vec{U}} = R\vec{U}$ where $\vec{U} = [\phi \ \nu \ \varepsilon \ \chi]^T$ and the matrix R contains the terms in the brackets from equation (4.9). This matrix is similar to the amplification matrix used in numerical stability. Like numerical stability the eigenvalues of this matrix in dynamic stability will provide the stability results; therefore, R is referred to as the amplification matrix in subsequent work.

4.1.2 Smooth Data Analysis. Two important assumptions are made at this time that are necessary to continue the analysis for smooth data. First, the data is quite smooth. As long as the support of the kernel (h) is small enough, this is a valid assumption for a limited period of time. To represent this, the equilibrium points are taken to be constant inside the support of the kernel plus a small perturbation. Since each particle already has a perturbation associated with it (ϕ , ν , ε , and χ) the definition of the perturbations is extended to include the spatial perturbations as well as the temporal perturbations. The equilibrium points can then be taken as constant inside the support of the kernel giving $\bar{\rho}_j = \bar{\rho}$, $\bar{v}_j = \bar{v}$, $\bar{e}_j = \bar{e}$ for any j within the support of W_{sj} . Based on the algebraic notation defined earlier in equation (4.5), $A_j = A$, $B_j = B$, and $C_j = C$. This assumption is valid if h is small enough, no shocks are present, and the data is very smooth. Equation (4.9) is then simplified to

$$\begin{aligned}\dot{\phi} &= \left[-m \sum_{l=-\infty}^{\infty} (1 - e^{ilk}) W'_l \right] \nu \\ \dot{\nu} &= \left[m B \sum_{l=-\infty}^{\infty} (1 + e^{ilk}) W'_l \right] \phi + \left[m C \sum_{l=-\infty}^{\infty} (1 + e^{ilk}) W'_l \right] \varepsilon \\ &\quad + \left[-2m A \sum_{l=-\infty}^{\infty} (1 - e^{ilk}) W''_l \right] \chi \\ \dot{\varepsilon} &= \left[-m A \sum_{l=-\infty}^{\infty} (1 - e^{ilk}) W'_l \right] \nu \\ \dot{\chi} &= \nu.\end{aligned}\tag{4.10}$$

In order to simplify the analysis, some further algebraic substitutions are made. Let

$$\begin{aligned} G_1 &= m \sum_{l=-\infty}^{\infty} (1 - e^{ilk}) W'_l \\ G_2 &= m \sum_{l=-\infty}^{\infty} (1 + e^{ilk}) W'_l \\ G_3 &= m \sum_{l=-\infty}^{\infty} (1 - e^{ilk}) W''_l . \end{aligned}$$

The amplification matrix, R , is now

$$R = \begin{bmatrix} 0 & 0 & 0 & 0 \\ BG_2 & 0 & CG_2 & -2AG_3 \\ 0 & -AG_1 & 0 & 0 \\ 0 & 1 & 0 & 0 \end{bmatrix} . \quad (4.11)$$

The eigenvalues of R are determined by solving the characteristic equation, $\det(R - \lambda I) = 0$. For R as given in equation (4.11) the following must be solved

$$\lambda^2 \left[\lambda^2 + AC G_1 G_2 + B G_1 G_2 + 2 A G_3 \right] = 0 ,$$

which has solutions: $\lambda = 0, 0, \pm \sqrt{-(AC + B) G_1 G_2 - 2 A G_3}$.

The second assumption under this subsection is uniform spacing. This turns out to be not only useful in simplifying the equations, but based on the assumptions up to this point, it is necessary. Previously the mass was assumed to be constant and the field values were locally constant; in particular, $\bar{\rho}$ is locally constant. SPH uses $\Delta x \approx \frac{m}{\rho}$, so Δx_j must be constant for all j . Using uniform spacing together with an even kernel, G_1, G_2, G_3 may be simplified as

$$G_1 = -im \sum_{l=-\infty}^{\infty} \sin(lk) W'_l = -2im \sum_{l=1}^{\infty} \sin(lk) W'_l$$

$$\begin{aligned}
G_2 &= im \sum_{l=-\infty}^{\infty} \sin(lk) W'_l = 2im \sum_{l=1}^{\infty} \sin(lk) W'_l \\
G_1 G_2 &= m^2 \left(\sum_{l=-\infty}^{\infty} \sin(lk) W'_l \right)^2 = 4m^2 \left(\sum_{l=1}^{\infty} \sin(lk) W'_l \right)^2 \\
G_3 &= m \sum_{l=-\infty}^{\infty} (1 - \cos(lk)) W''_l = 2m \sum_{l=1}^{\infty} (1 - \cos(lk)) W''_l.
\end{aligned}$$

The eigenvalues of R are now

$$\lambda = 0, 0, \pm\sqrt{-D} \quad (4.12)$$

$$\text{where } D = D_1 + D_2 \quad (4.13)$$

$$D_1 = \frac{4m^2}{\bar{\rho}^4} (\tilde{A}\tilde{C} + \bar{\rho}^2\tilde{B} - 2\bar{\rho}\tilde{A}) \left(\sum_{l=1}^{\infty} \sin(lk) W'_l \right)^2 \quad (4.14)$$

$$D_2 = \frac{4m}{\bar{\rho}^2} \tilde{A} \sum_{l=1}^{\infty} (1 - \cos(lk)) W''_l. \quad (4.15)$$

For the analysis to be complete all values of $k \in [0, \pi]$ must be considered. However, the k equal to π case is going to be concentrated on at this time. There are two reasons for this. First, for non-linear equations, linearized stability is only a necessary condition for global stability, not a sufficient condition. In other words, an instability found in the linearized analysis is sufficient for the actual method to be unstable. Second, the $k = \pi$ case corresponds to the minimum wavelength (or highest frequency) case. This is often where problems in numerical methods arise. So, letting k equal π , equations (4.14) and (4.15) reduce to

$$D_1 = 0 \quad (4.16)$$

$$D_2 = \frac{4m}{\bar{\rho}^2} \tilde{A} \sum_{l=1}^{\infty} (1 - (-1)^l) W''_l = \frac{8m}{\bar{\rho}^2} \tilde{A} \sum_{l=1, \text{odd}}^{\infty} W''_l. \quad (4.17)$$

Based on equation (4.12), R will have a positive real eigenvalue if D is real and $D < 0$. In this case, $D = D_2$. Also recall from earlier, $\tilde{A} = \bar{P}$, the pressure at the equilibrium points. Because m and ρ are always positive, the sign of D is controlled by PW'' .

For most of the popular kernels (bell shaped), W'' has both positive and negative parts. Hence, the method could be unstable in either tension or compression. Note: from conversations with other analysts the problems are more pronounced in tension ($\bar{P} < 0$).

Also note, Appendix B looks into the D_1 term shown in equation (4.14) above in more detail. In particular, this equation is studied for two equations of state: the Ideal Gas Law and the Mie-Grüneisen. From that analysis the D_1 term is found to usually be non-negative for any wavelength. Hence, this term can help to stabilize the method for some wavelengths and for others does not help nor hinder stability. Therefore, efforts concentrated on the D_2 term are most important, as it is the primary source of the numerical instability in the method.

4.1.3 Reconciliation with Other Analyses. Although the work in this chapter was performed independently, two other groups that performed stability analyses on SPH (neither is currently available in the published literature). In this subsection, the results just found in this dissertation are shown to correspond to each of the other groups results under appropriate simplifications.

1. Petschek and Libersky (PL). See reference (49) for more information. They assumed $P = P(\rho)$ only, allowing them to uncouple and discard the energy equation from the analysis. From equation (4.11) remove the third row and column from R to obtain

$$R_{PL} = \begin{bmatrix} 0 & -G_1 & 0 \\ BG_2 & 0 & -2AG_3 \\ 0 & 1 & 0 \end{bmatrix}. \quad (4.18)$$

Note: PL start with slightly different forms of the SPH equations, but they reduce to the same as the one presented earlier under the assumptions in the analysis. The

eigenvalues of R_{PL} are: $\lambda = 0, \pm\sqrt{-D}$, where $D = D_1 + D_2$ and

$$D_1 = 4m^2 B \left(\sum_{l=1}^{\infty} \sin(lk) W_l' \right)^2 = 4m^2 B S^2 \quad (4.19)$$

$$D_2 = 2mA \left(\sum_{l=1}^{\infty} 2W_l'' - \sum_{l=1}^{\infty} 2\cos(lk) W_l'' \right) = 2mA(2\Omega - 2C) . \quad (4.20)$$

The notation at the end of equations (4.19) and (4.20) is from the PL paper, showing that their form and the one in this dissertation match under appropriate assumptions.

2. Swegle, Hicks, and Attaway (SHA). See references (64, 65) for more information. As with Petschek and Libersky, Swegle, Hicks and Attaway also assumed $P = P(\rho)$ only, allowing them to uncouple and discard the energy equation from the analysis. Further, they assumed early on in their analysis that density was constant, allowing them to discard the continuity equation as well. This may sound like they performed a weak analysis, however, the opposite is true. The analysis is quite thorough and bears reading for those interested in more information on the linearized stability analysis. From equation (4.11) remove the first and third rows and columns from R to obtain

$$R_{SHA} = \begin{bmatrix} 0 & -2AG_3 \\ 1 & 0 \end{bmatrix} . \quad (4.21)$$

The eigenvalues of R_{SHA} are: $\lambda = \pm\sqrt{-D_2}$, where

$$D_2 = m \frac{4\tilde{A}}{\rho^2} \sum_{l=1}^{\infty} (1 - \cos(lk)) W_l'' = -m \frac{2T}{\rho^2} \sum_{l=1}^{\infty} (1 - \cos(lk)) W_l'' .$$

The notation at the end of the equation is from the SHA paper, showing that the their form and the one from this dissertation match under appropriate assumptions. Note: their paper uses $T \approx -\bar{P}$, the stress tensor positive in tension where this paper uses negative. This explains the sign differences. Their form will also not match this one exactly, since SHA performed their analysis on a fully discretized problem (using central time) and this one only does a semi-discrete problem.

4.1.4 *Other Equations.* In the previous subsection, the analysis performed in this dissertation was shown to appear like that performed by other analysts under appropriate simplifications. In this subsection, the analysis from earlier in the chapter is extended to many different forms of the SPH equations, not just the popular ones. The forms considered are shown in equations (4.22) - (4.34):

$$\dot{\rho}_s = \sum_{j=1}^N m_j (v_s - v_j) W'_{sj} \quad (4.22)$$

$$\dot{\rho}_s = \rho_s \sum_{j=1}^N \frac{m_j}{\rho_j} (v_s - v_j) W'_{sj} \quad (4.23)$$

$$\dot{v}_s = - \sum_{j=1}^N m_j \left(\frac{P_j}{\rho_j^2} + \frac{P_s}{\rho_s^2} \right) W'_{sj} \quad (4.24)$$

$$\dot{v}_s = -2 \sum_{j=1}^N m_j \frac{\sqrt{P_j P_s}}{\rho_j \rho_s} W'_{sj} \quad (4.25)$$

$$\dot{v}_s = - \sum_{j=1}^N m_j \left(\frac{P_j}{\rho_j \rho_s} \right) W'_{sj} \quad (4.26)$$

$$\dot{v}_s = - \sum_{j=1}^N m_j \left(\frac{P_j + P_s}{\rho_j \rho_s} \right) W'_{sj} \quad (4.27)$$

$$\dot{e}_s = \sum_{j=1}^N m_j \left(\frac{P_s}{\rho_s^2} \right) (v_s - v_j) W'_{sj} \quad (4.28)$$

$$\dot{e}_s = \sum_{j=1}^N m_j \left(\frac{P_s}{\rho_s \rho_j} \right) (v_s - v_j) W'_{sj} \quad (4.29)$$

$$\dot{e}_s = \sum_{j=1}^N m_j \left(\frac{P_j}{\rho_j^2} \right) (v_s - v_j) W'_{sj} \quad (4.30)$$

$$\dot{e}_s = \frac{1}{2} \sum_{j=1}^N m_j \left(\frac{P_j}{\rho_j^2} + \frac{P_s}{\rho_s^2} \right) (v_s - v_j) W'_{sj} \quad (4.31)$$

$$\dot{e}_s = \sum_{j=1}^N m_j \frac{\sqrt{P_j P_s}}{\rho_j \rho_s} (v_s - v_j) W'_{sj} \quad (4.32)$$

$$\dot{x}_s = v_s \quad (4.33)$$

$$\dot{x}_s = v_s + \epsilon \sum_{j=1}^N m_j \left(\frac{v_j - v_s}{0.5(\rho_s + \rho_j)} \right) W_{sj} \quad (4.34)$$

Equations (4.22), (4.24), (4.31), and (4.33) make up the system already studied. For the remainder of the equations the detailed analysis is found in Appendix B. It may be easily summarized by stating: under the assumptions for smooth data analysis, all the forms of the SPH equations above reduce to those found in the earlier analysis (except for form (4.34)). Therefore, the instabilities found in those earlier forms also are instabilities for these other forms. Hence, it is reasonable to expect that techniques to resolve the instabilities in one form also are just as universal. More on form (4.34) in the Techniques for Obtaining Linearized Stability Section (Section 4.2).

4.1.5 Artificial Viscosity/Wall Heating. In many numerical methods, artificial viscosity and artificial heat conduction (wall heating) are used to handle physical problems, especially near discontinuities. However, they are also used to control or assist in stabilizing a method. As discussed earlier, the SPH forms used for the Euler equations can be unstable regardless of the values of Δt , h , or Δx . So it is reasonable to question whether these techniques can stabilize SPH; which is done here. All of these techniques were first introduced in Chapter III showing that they vanish as $h \rightarrow 0$.

Starting with artificial viscosity, only those forms found in the published literature for SPH are considered. The three forms are attributed to: Monaghan, et al. (37), Hernquist and Katz (19), and Lattanzio, et al. (28).

1. Monaghan, et al. See equations (3.56)–(3.58). In the SPH momentum and energy equations replace the $\frac{P}{\rho^2}$ term with $\frac{P}{\rho^2} + \frac{1}{2}\Pi$ where

$$\Pi_{sj} = \frac{-\alpha 0.5(c_s + c_j)\mu_{sj} + \beta \mu_{sj}^2}{0.5(\rho_s + \rho_j)} \quad (4.35)$$

$$\mu_{sj} = \begin{cases} \frac{h(v_s - v_j) \cdot (x_s - x_j)}{(x_s - x_j)^2 + \eta h^2} & (v_s - v_j) \cdot (x_s - x_j) < 0 \\ 0 & \text{otherwise} \end{cases} \quad (4.36)$$

For stability, the previous analysis (labeled old below) is valid as is with just the correction terms $-\sum_j m_j \bar{\Pi}_{sj} W'_{sj}$ in the momentum equation and $\frac{1}{2} \sum_j m_j \bar{\Pi}_{sj} (\bar{v}_s - \bar{v}_j) W'_{sj}$ in the energy equation. If $\Pi_{sj} = \bar{\Pi}_{sj} + \pi_{sj}$ then for the momentum equation, the linearized correction term is

$$\begin{aligned}
-\sum_{j=1}^N m_j \Pi_{sj} W'_{sj} &= -\sum_{j=1}^N m_j (\bar{\Pi}_{sj} + \pi_{sj}) (W'_{sj} + (\chi_s - \chi_j) W''_{sj}) \\
&= -\sum_{j=1}^N m_j [\bar{\Pi}_{sj} W'_{sj} + \pi_{sj} W'_{sj} + \bar{\Pi}_{sj} (\chi_s - \chi_j) W''_{sj}] \\
\Rightarrow \dot{v}_s(new) &= \dot{v}_s(old) - \sum_{j=1}^N m_j [\pi_{sj} W'_{sj} + \bar{\Pi}_{sj} (\chi_s - \chi_j) W''_{sj}] . \quad (4.37)
\end{aligned}$$

For the energy equation, the linearized correction term is

$$\begin{aligned}
\frac{1}{2} \sum_{j=1}^N m_j \Pi_{sj} (\bar{v}_s - \bar{v}_j) W'_{sj} &= \frac{1}{2} \sum_{j=1}^N m_j (\bar{\Pi}_{sj} + \pi_{sj}) (\bar{v}_s - \bar{v}_j) W'_{sj} \\
&\quad \times (W'_{sj} + (\chi_s - \chi_j) W''_{sj}) \\
&= \frac{1}{2} \sum_{j=1}^N m_j [\bar{\Pi}_{sj} (\bar{v}_s - \bar{v}_j) W'_{sj} + \pi_{sj} (\bar{v}_s - \bar{v}_j) W'_{sj} \\
&\quad + \bar{\Pi}_{sj} (\bar{v}_s - \bar{v}_j) W'_{sj} + \bar{\Pi}_{sj} (\chi_s - \chi_j) W''_{sj}] \\
\Rightarrow \dot{e}_s(new) &= \dot{e}_s(old) + \frac{1}{2} \sum_{j=1}^N m_j [\pi_{sj} (\bar{v}_s - \bar{v}_j) W'_{sj} + \bar{\Pi}_{sj} (\bar{v}_s - \bar{v}_j) W'_{sj} \\
&\quad + \bar{\Pi}_{sj} (\chi_s - \chi_j) W''_{sj}] . \quad (4.38)
\end{aligned}$$

So the $\bar{\Pi}_{sj}$ and π_{sj} terms need to now be studied. The intermediate steps in deriving these are left out as they just follow the previous stability analyses. Using μ_{sj} as μ at the equilibrium points, then

$$\bar{\Pi}_{sj} = \frac{-\alpha 0.5(c_s + c_j) \mu_{sj} + \beta \mu_{sj}^2}{0.5(\bar{\rho}_s + \bar{\rho}_j)}$$

$$\begin{aligned}
\pi_{sj} = & \left[\frac{\alpha 0.5(c_s + c_j)\mu_{sj} - \beta\mu_{sj}^2}{0.5(\bar{\rho}_s + \bar{\rho}_j)^2} \right] (\phi_s + \phi_j) \\
& + \left[\frac{-\alpha 0.5(c_s + c_j) + \beta\mu_{sj}}{0.5(\bar{\rho}_s + \bar{\rho}_j)} \right] \left[\frac{h(\bar{x}_s - \bar{x}_j)}{(\bar{x}_s - \bar{x}_j)^2 + \eta h^2} \right] (\nu_s - \nu_j) \\
& + \left[\frac{-\alpha 0.5(c_s + c_j) + \beta\mu_{sj}}{0.5(\bar{\rho}_s + \bar{\rho}_j)} \right] \left[\frac{h(\bar{v}_s - \bar{v}_j)}{(\bar{x}_s - \bar{x}_j)^2 + \eta h^2} \right. \\
& \quad \left. - \frac{2h(\bar{v}_s - \bar{v}_j)(\bar{x}_s - \bar{x}_j)^2}{((\bar{x}_s - \bar{x}_j)^2 + \eta h^2)^2} \right] (\chi_s - \chi_j) .
\end{aligned}$$

Under the smooth data analysis, $\mu_{sj} = 0$. This causes most of these new terms to vanish leaving

$$\begin{aligned}
\bar{\Pi}_{sj} &= 0 \\
\pi_{sj} &= \left[\frac{-\alpha ch(\bar{x}_s - \bar{x}_j)}{\bar{\rho}((\bar{x}_s - \bar{x}_j)^2 + \eta h^2)} \right] (\nu_s - \nu_j) .
\end{aligned}$$

Therefore, with the smooth data assumptions,

$$\begin{aligned}
\dot{\nu}_s(new) &= \dot{\nu}_s(old) - \sum_{j=1}^N m_j \left[\frac{-\alpha ch(\bar{x}_s - \bar{x}_j)}{\bar{\rho}((\bar{x}_s - \bar{x}_j)^2 + \eta h^2)} \right] (\nu_s - \nu_j) W'_{sj} \quad (4.39) \\
\dot{\epsilon}_s(new) &= \dot{\epsilon}_s(old) + 0 .
\end{aligned}$$

2. Hernquist and Katz. See equations (3.59)–(3.61). In the SPH momentum and energy equations replace the $\frac{P}{\rho^2}$ term with $\frac{P}{\rho^2} + \frac{1}{2}\Pi$ where

$$\Pi_{sj} = \frac{q_s}{\rho_s^2} + \frac{q_j}{\rho_j^2} \quad (4.40)$$

$$q_s = \begin{cases} \alpha h_s \rho_s c_s |\nabla \cdot v|_s + \beta h_s^2 \rho_s (\nabla \cdot v)_s^2 & \text{if } (v_s - v_j) \cdot (x_s - x_j) < 0 \\ 0 & \text{otherwise} \end{cases} \quad (4.41)$$

$$\mu_s = \rho_s (\nabla \cdot v)_s = - \sum_{j=1}^N m_j (v_s - v_j) W'_{sj} . \quad (4.42)$$

For stability, the work for this method is the same as for the first few steps of the Monaghan method leading to equations (4.37) and (4.38). Hence, $\bar{\Pi}_{sj}$ and π_{sj} must also be found for this method. Once again, several of the intermediate steps are left out as they just follow the previous analyses:

$$\begin{aligned}\bar{\Pi}_{sj} &= \frac{\alpha c_s h \mu_{\bar{s}} + 3h \mu_{\bar{s}}^2}{\bar{\rho}_s} + \frac{\alpha c_j h \mu_j + 3h \mu_j^2}{\bar{\rho}_j} \\ \pi_{sj} &= - \left[\frac{\alpha c_s h \mu_{\bar{s}} + 3h \mu_{\bar{s}}^2}{\bar{\rho}_s} \right] \phi_s - \left[\frac{\alpha c_j h \mu_j + 3h \mu_j^2}{\bar{\rho}_j} \right] \phi_j + \left[\frac{\alpha c_s h + 2\beta h \mu_{\bar{s}}}{\bar{\rho}_s} \right] \\ &\quad \sum_{k=1}^N m_k \left[\frac{\bar{v}_s - \bar{v}_k}{\bar{\rho}_s^2} W'_{sk} \phi_s - \frac{\nu_s - \nu_k}{\bar{\rho}_s} W'_{sk} - \frac{\bar{v}_s - \bar{v}_k}{\bar{\rho}_s} (\chi_s - \chi_k) W''_{sk} \right] \\ &\quad + \left[\frac{\alpha c_j h + 2\beta h \mu_j}{\bar{\rho}_j} \right] \sum_{k=1}^N m_k \left[\frac{\bar{v}_j - \bar{v}_k}{\bar{\rho}_j^2} W'_{jk} \phi_j - \frac{\nu_j - \nu_k}{\bar{\rho}_j} W'_{jk} \right. \\ &\quad \left. - \frac{\bar{v}_j - \bar{v}_k}{\bar{\rho}_j} (\chi_j - \chi_k) W''_{jk} \right] .\end{aligned}$$

With the smooth data assumptions, $\mu_{\bar{s}} = 0$. This causes most of these new terms once again to vanish leaving

$$\begin{aligned}\bar{\Pi}_{sj} &= 0 \\ \pi_{sj} &= \frac{-\alpha c h}{\bar{\rho}^2} \sum_{k=1}^N m_k \left[(\nu_s - \nu_k) W'_{sk} + (\nu_j - \nu_k) W'_{jk} \right] .\end{aligned}$$

Therefore, with the smooth data assumptions,

$$\begin{aligned}\dot{\nu}_s(new) &= \dot{\nu}_s(old) - \sum_{j=1}^N m_j \left(\frac{-\alpha c h}{\bar{\rho}^2} \right) \sum_{k=1}^N m_k \left[(\nu_s - \nu_k) W'_{sk} \right. \\ &\quad \left. + (\nu_j - \nu_k) W'_{jk} \right] W'_{sj} \\ \dot{\varepsilon}_s(new) &= \dot{\varepsilon}_s(old) + 0 .\end{aligned} \tag{4.43}$$

3. Lattanzio, et al. See equations (3.62)-(3.64). In the SPH momentum and energy equations replace the $\frac{P_s}{\rho_s^2}$ term with $\frac{P_s}{\rho_s^2}(1 + \Pi)$ where

$$\Pi_{sj} = -\alpha\mu_{sj} + \beta\mu_{sj}^2 \quad (4.44)$$

$$\mu_{sj} = \begin{cases} \frac{h(v_s - v_j) \cdot (x_s - x_j)}{c((x_s - x_j)^2 + \eta h^2)} & \text{if } (v_s - v_j) \cdot (x_s - x_j) < 0 \\ 0 & \text{otherwise} \end{cases} \quad (4.45)$$

For stability, the previous analysis is valid as is with correction terms: $-\sum_j m_j \left(\frac{P_s}{\rho_s^2} + \frac{P_j}{\rho_j^2} \right) \Pi_{sj} W'_{sj}$ in the momentum equation and: $\frac{1}{2} \sum_j m_j \left(\frac{P_s}{\rho_s^2} + \frac{P_j}{\rho_j^2} \right) \Pi_{sj} (v_s - v_j) W'_{sj}$ in the energy equation. If $\Pi_{sj} = \bar{\Pi}_{sj} + \pi_{sj}$ then for the momentum equation, the linearized correction term is

$$\begin{aligned} -\sum_{j=1}^N m_j \left(\frac{P_s}{\rho_s^2} + \frac{P_j}{\rho_j^2} \right) \Pi_{sj} W'_{sj} &= -\sum_{j=1}^N m_j (A_s + B_s \phi_s + C_s \varepsilon_s + A_j + B_j \phi_j + C_j \varepsilon_j) \\ &\quad \times (\bar{\Pi}_{sj} + \pi_{sj}) (W'_{sj} + (\chi_s - \chi_j) W''_{sj}) \\ \Rightarrow \dot{v}_s(\text{new}) &= \dot{v}_s(\text{old}) [1 + \bar{\Pi}_{sj}] - \sum_{j=1}^N m_j (A_j + A_s) \pi_{sj} W'_{sj} \end{aligned} \quad (4.46)$$

For the energy equation, the correction term is

$$\begin{aligned} \frac{1}{2} \sum_{j=1}^N m_j \Pi_{sj} \left(\frac{P_s}{\rho_s^2} + \frac{P_j}{\rho_j^2} \right) (v_s - v_j) W'_{sj} &= \frac{1}{2} \sum_{j=1}^N m_j (A_s + B_s \phi_s + C_s \varepsilon_s + A_j \\ &\quad + B_j \phi_j + C_j \varepsilon_j) (\bar{\Pi}_{sj} + \pi_{sj}) (\bar{v}_s - \bar{v}_j \nu_s - \nu_j) (W'_{sj} + (\chi_s - \chi_j) W''_{sj}) \\ \Rightarrow \dot{\varepsilon}_s(\text{new}) &= \dot{\varepsilon}_s(\text{old}) [1 + \bar{\Pi}_{sj}] + \frac{1}{2} \sum_{j=1}^N m_j (A_j + A_s) \pi_{sj} (\bar{v}_s - \bar{v}_j) W'_{sj} \end{aligned} \quad (4.47)$$

So the $\bar{\Pi}_{sj}$ and π_{sj} terms need to now be studied. The intermediate steps are left out again as they just follow the previous stability analyses. Using μ_{sj} as μ at the equilibrium points, then

$$\bar{\Pi}_{sj} = -\alpha\mu_{sj} + \beta\mu_{sj}^2$$

$$\pi_{sj} = \left[\frac{(-\alpha + 2\beta\mu_{sj})(\bar{x}_s - \bar{x}_j)h}{c((\bar{x}_s - \bar{x}_j)^2 + \eta h^2)} \right] (\nu_s - \nu_j) + \left[\frac{(-\alpha + 2\beta\mu_{sj})(\bar{v}_s - \bar{v}_j)h}{c((\bar{x}_s - \bar{x}_j)^2 + \eta h^2)} \right] \\ \times \left[1 - \frac{2(\bar{x}_s - \bar{x}_j)^2}{((\bar{x}_s - \bar{x}_j)^2 + \eta h^2)} \right] (\chi_s - \chi_j).$$

With the smooth data assumptions, $\mu_{sj} = 0$. This causes most of these new terms to cancel leaving

$$\bar{\Pi}_{sj} = 0 \\ \pi_{sj} = \left[\frac{-\alpha h(\bar{x}_s - \bar{x}_j)}{c((\bar{x}_s - \bar{x}_j)^2 + \eta h^2)} \right] (\nu_s - \nu_j).$$

Therefore, with the smooth data assumptions,

$$\dot{\nu}_s(new) = \dot{\nu}_s(old) - 2A \sum_{j=1}^N m_j \left[\frac{-\alpha h(\bar{x}_s - \bar{x}_j)}{c((\bar{x}_s - \bar{x}_j)^2 + \eta h^2)} \right] (\nu_s - \nu_j) W'_{sj} \quad (4.48) \\ \dot{\varepsilon}_s(new) = \dot{\varepsilon}_s(old) + 0.$$

4. Summary of artificial viscosity techniques. All three forms studied here reduce to similar forms under smooth data analysis assumptions. Namely, a term is added in the momentum equation in the ν position which is labeled R_ν . This gives a new amplification matrix R

$$R = \begin{bmatrix} 0 & -G_1 & 0 & 0 \\ BG_2 & R_\nu & CG_2 & -2AG_3 \\ 0 & -AG_1 & 0 & 0 \\ 0 & 1 & 0 & 0 \end{bmatrix}. \quad (4.49)$$

The eigenvalues of the new R are: $\lambda = 0, 0, \frac{R_\nu}{2} \pm \sqrt{\frac{R_\nu^2}{4} - (AC + B)G_1G_2 - 2AG_3}$. Without any more study of R_ν for each of the methods, some general comments can be made, remembering that $(AC + B)G_1G_2 + 2AG_3 < 0$. If R_ν is real, this does not stabilize the method. If R_ν is positive an eigenvalue with a positive real part

is obtained. If R_v is negative it could make the positive real part of the eigenvalue caused by the $2AG_3$ term (instability) smaller, but does not remove it. Alternatively, if R_v is imaginary or complex with a negative real part it could stabilize the method. However, the only way to get an imaginary part is from the term e^{ilk} . But, at the minimum wavelength, k equals π which removes the imaginary part. This implies that none of these methods help at (or near) the minimum wavelength.

For completeness, the Monaghan and Lattanzio methods result in real R_v terms, which should be negative. The Hernquist and Katz method should result in R_v being complex. However, it is a very complicated form and appears that the real part can have both positive and negative parts depending on particle position and kernel. These are shown below

$$\text{Monaghan: } R_v = -\frac{\alpha chm}{\bar{\rho}} \sum_{l=-\infty}^{\infty} \frac{(\bar{x}_s - \bar{x}_j)}{(\bar{x}_s - \bar{x}_j)^2 + \eta h^2} (1 - e^{ilk}) W'_l$$

$$\text{Hernquist: } R_v = -\frac{\alpha chm}{\bar{\rho}^2} \sum_{l=-\infty}^{\infty} \left[\sum_{n=1}^N \left[(1 - e^{i(n-s)k}) W'_{sn} + (e^{ilk} - e^{i(n-s)k}) W'_{jn} \right] \right] W'_l$$

$$\text{Lattanzio: } R_v = -\frac{\alpha h 2Am}{c} \sum_{l=-\infty}^{\infty} \frac{(\bar{x}_s - \bar{x}_j)}{((\bar{x}_s - \bar{x}_j)^2 + \eta h^2)} (1 - e^{ilk}) W'_l .$$

5. Wall Heating. As described in Chapter III, the wall heating term, H is added to the energy equation outside the sums. See equations (3.65)–(3.67). So the stability terms have the form

$$\dot{\epsilon}_s(\text{new}) = \dot{\epsilon}_s(\text{old}) + H_s ,$$

where

$$H_s = \sum_{j=1}^N m_j \hat{H}_j \quad (4.50)$$

$$\hat{H}_j = \frac{(q_s + q_j)(e_s - e_j)(x_s - x_j)}{0.5(\rho_s + \rho_j)((x_s - x_j)^2 + \eta h^2)} W'_{sj} \quad (4.51)$$

$$q_i = hg_1 c + h^2 g_2 (|\nabla \cdot v|_i - \nabla \cdot v_i) . \quad (4.52)$$

$$\begin{aligned}\frac{1}{x_{sj}^2} &= \frac{1}{(\bar{x}_s - \bar{x}_j + \chi_s - \chi_j)^2} = \frac{1}{(\bar{x}_s - \bar{x}_j)^2} - \frac{2(\bar{x}_s - \bar{x}_j)(\chi_s - \chi_j)}{(\bar{x}_s - \bar{x}_j)^4} \\ \frac{1}{\rho_s + \rho_j} &= \frac{1}{(\bar{\rho}_s - \bar{\rho}_j + \phi_s - \phi_j)} = \frac{1}{\bar{\rho}_s - \bar{\rho}_j} - \frac{(\phi_s + \phi_j)}{(\bar{\rho}_s - \bar{\rho}_j)^2}.\end{aligned}$$

So for \hat{H}_j obtain

$$\begin{aligned}\hat{H}_j &= 2(q_s + q_j) \left(\frac{1}{\bar{\rho}_s - \bar{\rho}_j} - \frac{(\phi_s + \phi_j)}{(\bar{\rho}_s - \bar{\rho}_j)^2} \right) (\bar{e}_s - \bar{e}_j + \varepsilon_s - \varepsilon_j) \left(\frac{1}{(\bar{x}_s - \bar{x}_j)^2} \right. \\ &\quad \left. - \frac{2(\chi_s - \chi_j)}{(\bar{x}_s - \bar{x}_j)^3} \right) (\bar{x}_s - \bar{x}_j + \chi_s - \chi_j) (W'_{sj} + (\chi_s - \chi_j)W''_{sj}) \\ &= 2(q_s + q_j) \left[\frac{(\bar{e}_s - \bar{e}_j)(\bar{x}_s - \bar{x}_j)}{(\bar{\rho}_s - \bar{\rho}_j)(\bar{x}_s - \bar{x}_j)^2} W'_{sj} - \frac{(\bar{e}_s - \bar{e}_j)(\bar{x}_s - \bar{x}_j)}{(\bar{\rho}_s - \bar{\rho}_j)^2(\bar{x}_s - \bar{x}_j)^2} (\phi_s + \phi_j) W'_{sj} \right. \\ &\quad \left. + \frac{(\bar{x}_s - \bar{x}_j)}{(\bar{\rho}_s + \bar{\rho}_j)(\bar{x}_s - \bar{x}_j)^2} (\varepsilon_s - \varepsilon_j) W'_{sj} - \frac{2(\bar{e}_s - \bar{e}_j)(\bar{x}_s - \bar{x}_j)}{(\bar{\rho}_s + \bar{\rho}_j)(\bar{x}_s - \bar{x}_j)^3} (\chi_s - \chi_j) W'_{sj} \right. \\ &\quad \left. + \frac{(\bar{e}_s - \bar{e}_j)}{(\bar{\rho}_s + \bar{\rho}_j)(\bar{x}_s - \bar{x}_j)^2} (\chi_s - \chi_j) W'_{sj} + \frac{(\bar{e}_s - \bar{e}_j)(\bar{x}_s - \bar{x}_j)}{(\bar{\rho}_s + \bar{\rho}_j)(\bar{x}_s - \bar{x}_j)^2} (\chi_s - \chi_j) W''_{sj} \right] \\ &= 2(q_s + q_j) \left[\frac{(\bar{e}_s - \bar{e}_j)}{(\bar{\rho}_s - \bar{\rho}_j)(\bar{x}_s - \bar{x}_j)} W'_{sj} - \frac{(\bar{e}_s - \bar{e}_j)}{(\bar{\rho}_s - \bar{\rho}_j)^2(\bar{x}_s - \bar{x}_j)} (\phi_s + \phi_j) W'_{sj} \right. \\ &\quad \left. + \frac{1}{(\bar{\rho}_s + \bar{\rho}_j)(\bar{x}_s - \bar{x}_j)} (\varepsilon_s - \varepsilon_j) W'_{sj} - \frac{(\bar{e}_s - \bar{e}_j)}{(\bar{\rho}_s + \bar{\rho}_j)(\bar{x}_s - \bar{x}_j)^2} (\chi_s - \chi_j) W'_{sj} \right. \\ &\quad \left. + \frac{(\bar{e}_s - \bar{e}_j)}{(\bar{\rho}_s + \bar{\rho}_j)(\bar{x}_s - \bar{x}_j)} (\chi_s - \chi_j) W''_{sj} \right]. \quad (4.53)\end{aligned}$$

The following is needed for the q terms:

$$\begin{aligned}(\nabla \cdot v)_s &= -\frac{1}{\rho_s} \sum_{j=1}^N m_j (v_s - v_j) W'_{sj} \\ &= -\left(\frac{1}{\bar{\rho}_s + \phi_s} \right) \sum_{j=1}^N m_j (\bar{v}_s - \bar{v}_j + \nu_s - \nu_j) (W'_{sj} + (\chi_s - \chi_j) W''_{sj}) \\ &= \left(-\frac{1}{\bar{\rho}_s} + \frac{\phi_s}{\bar{\rho}_s^2} \right) \sum_{j=1}^N m_j [(\bar{v}_s - \bar{v}_j) W'_{sj} + (\nu_s - \nu_j) W'_{sj} \\ &\quad + (\bar{v}_s - \bar{v}_j)(\chi_s - \chi_j) W''_{sj}]\end{aligned}$$

$$\begin{aligned}
= & -\frac{1}{\bar{\rho}_s} \sum_{j=1}^N m_j (\bar{v}_s - \bar{v}_j) W'_{sj} + \sum_{j=1}^N m_j \left[\frac{(\bar{v}_s - \bar{v}_j)}{\bar{\rho}_s^2} \phi_s W'_{sj} - \frac{1}{\bar{\rho}_s} (\nu_s - \nu_j) W'_{sj} \right. \\
& \left. - \frac{(\bar{v}_s - \bar{v}_j)}{\bar{\rho}_s} (\chi_s - \chi_j) W''_{sj} \right]. \quad (4.54)
\end{aligned}$$

Substitute equation (4.54) in equation (4.53) for q , then update the \hat{H} analysis to obtain

$$\begin{aligned}
\hat{H}_j = & 2 \left[2hc g_1 + \left(\frac{2h^2 g_2}{\bar{\rho}_s} \right) \sum_{n=1}^N m_n (\bar{v}_s - \bar{v}_n) W'_{sn} + \left(\frac{2h^2 g_2}{\bar{\rho}_j} \right) \sum_{n=1}^N m_n (\bar{v}_j - \bar{v}_n) W'_{jn} \right] \\
& \times \left[\frac{1}{(\bar{\rho}_s + \bar{\rho}_j)(\bar{x}_s - \bar{x}_j)} \right] \left[(\bar{e}_s - \bar{e}_j) W'_{sj} - \frac{(\bar{e}_s - \bar{e}_j)}{(\bar{\rho}_s - \bar{\rho}_j)} (\phi_s + \phi_j) W'_{sj} \right. \\
& \left. + (\epsilon_s - \epsilon_j) W'_{sj} - \frac{(\bar{e}_s - \bar{e}_j)}{(\bar{x}_s - \bar{x}_j)} (\chi_s - \chi_j) W'_{sj} + (\bar{e}_s - \bar{e}_j) (\chi_s - \chi_j) W'_{sj} \right] \\
& + \left[\frac{2(\bar{e}_s - \bar{e}_j)}{(\bar{\rho}_s + \bar{\rho}_j)(\bar{x}_s - \bar{x}_j)} W'_{sj} \right] \sum_{n=1}^N m_j \left[\frac{(\bar{v}_s - \bar{v}_n)}{\bar{\rho}_s^2} \phi_s W'_{sn} - \frac{1}{\bar{\rho}_s} (\nu_s - \nu_n) W'_{sn} \right. \\
& \left. - \frac{(\bar{v}_s - \bar{v}_n)}{\bar{\rho}_s} (\chi_s - \chi_n) W''_{sn} \right].
\end{aligned}$$

Applying the smooth data assumptions, most terms drop out, leaving

$$\begin{aligned}
\hat{H}_j &= 2(2hg_1c) \left(\frac{1}{(\bar{\rho}_s + \bar{\rho}_j)(\bar{x}_s - \bar{x}_j)} \right) (\epsilon_s - \epsilon_j) W'_{sj} \\
\text{so } H_s &= \sum_{j=1}^N 2hg_1c \left(\frac{\epsilon_s - \epsilon_j}{\bar{\rho}(\bar{x}_s - \bar{x}_j)} \right) W'_{sj} \\
&= \left[\frac{-2hg_1cm}{\bar{\rho}} \sum_{l=-\infty}^{\infty} \left(\frac{1 - e^{ilk}}{(\bar{x}_s - \bar{x}_j)} \right) W'_l \right] \epsilon.
\end{aligned}$$

Apply uniform spacing and label the result R_H to use in the amplification matrix

$$R_H = \left[4hg_1c \sum_{l=1}^{\infty} \left(\frac{1 - \cos(lk)}{x_l} \right) W'_l \right]. \quad (4.55)$$

The R_H term is added in the energy equation in the ϵ position giving a new amplification matrix R

$$R = \begin{bmatrix} 0 & -G_1 & 0 & 0 \\ BG_2 & 0 & CG_2 & -2AG_3 \\ 0 & -AG_1 & R_H & 0 \\ 0 & 1 & 0 & 0 \end{bmatrix}. \quad (4.56)$$

To find the eigenvalues of the new R , a 4th degree polynomial equation must be solved. The characteristic equation is

$$\lambda \left[\lambda^3 + \lambda^2(-R_H) + \lambda((AC + B)G_1G_2 + 2AG_3) - (BR_HG_1G_2 + 2AR_HG_3) \right] = 0.$$

This requires finding the roots of a cubic equation. Using Mathematica the roots were found to be extremely complicated. However, upon investigating this equation further, for the minimum wavelength case, the PW'' condition is still sufficient to cause an instability. However, due to the complicated nature of the eigenvalues, no additional general statements can be made about the wall heating term.

4.2 Techniques for Obtaining Linear Stability

In the previous section several commonly used implementations of SPH for the Euler equations were shown to have an instability arise. The key element is a term whose sign is controlled by PW'' . This term needs to be always non-negative or else the amplification matrix cannot be guaranteed to have a non-positive real eigenvalue. In this section, four methods are introduced that can be applied to control the stability. They consist of (1) using concave up or concave down kernels, (2) adding a constant to the pressure (two variations), (3) using a pressure difference form (two variations), (4) making a particle motion correction.

4.2.1 Technique 1 - Concave Up/Down Kernels. From earlier, the eigenvalues of the amplification matrix, R , were: $\lambda = 0, 0, \pm\sqrt{-D}$, where $D = D_1 + D_2$

and

$$D_1 = \frac{4m^2}{\bar{\rho}^4} (\tilde{A}\tilde{C} + \bar{\rho}^2 \tilde{B} - 2\bar{\rho} \tilde{A}) \left(\sum_{l=1}^{\infty} \sin(lk) W_l' \right)^2 \quad (4.57)$$

$$D_2 = \frac{4m}{\bar{\rho}^2} \tilde{A} \sum_{l=1}^{\infty} (1 - \cos(lk)) W_l'' . \quad (4.58)$$

At minimum wavelength, k equals π , $D_1 = 0$ and $D_2 \propto \tilde{A}W''$. Recall that $\tilde{A} = P(\bar{\rho}, \bar{\epsilon})$. Therefore

$$\begin{array}{ll} \text{if } P_s \leq 0 \quad \forall s & \text{then choose } W \text{ such that } W'' \leq 0 \\ \text{if } P_s \geq 0 \quad \forall s & \text{then choose } W \text{ such that } W'' \geq 0 . \end{array}$$

These requirements will ensure stability, at least at minimum wavelengths. For the second derivative of the kernel to be of one sign, use either concave down kernels (referred to in Chapter VI as parabolic shaped) for $W'' \leq 0$ or concave up kernels (referred to in Chapter VI as hyperbolic shaped) for $W'' \geq 0$. It is possible to use other shaped kernels (such as bell shaped), but only if supported particles are not too extreme (too close or too far away) and particle motion is small. If this later case is used, a check in the solution algorithm should be included to stop when unstable conditions arise.

In Chapter VI, bell shaped kernels are shown to give better results and these other shapes poorer. So although this technique works for problems with constant signed pressure, it trades stability for accuracy. If a large number of particles are used (small h and small Δx), this is a reasonable trade. Since, the stability should allow the algorithm to run longer and probably converge to an actual solution; and accuracy is improved with more particles. However, if particles are sparsely spaced, the inaccuracies of the kernel used in this technique probably outweigh the stabilizing effects and other techniques should be sought.

Hence the advantages of this method are that it requires no change to the equations, maintains conservation, and stabilizes the method. The disadvantages are that it can only be applied for problems with constant signed pressure and a new (possibly less accurate) kernel must be used.

4.2.2 Technique 2 - Add a Constant to the Pressure in the Momentum Equation. In the momentum equation, if a constant is added to the pressure term, the effect is to add a zero term plus $O(h^2)$ to the final SPH momentum equations as shown below:

$$\frac{Dv}{Dt} = -\frac{1}{\rho} \nabla P = -\nabla \left(\frac{P}{\rho} \right) - \left(\frac{P}{\rho^2} \right) \nabla \rho \quad (4.59)$$

$$P \rightarrow P + P_o \quad (4.60)$$

$$\frac{Dv}{Dt} = -\frac{1}{\rho} \nabla (P + P_o) = -\frac{1}{\rho} \nabla P - \frac{1}{\rho} \nabla P_o = -\frac{1}{\rho} \nabla P. \quad (4.61)$$

So adding a constant, P_o , results in no change to the actual differential equation. Note: P_o can also be a function of time only and not change these results; this might be more advantageous in actual implementations. As with equation (4.59), the chain rule may be applied to the P_o term to obtain

$$\frac{Dv}{Dt} = \left[-\nabla \left(\frac{P}{\rho} \right) - \left(\frac{P}{\rho^2} \right) \nabla \rho \right] + \left[-\nabla \left(\frac{P_o}{\rho} \right) - \left(\frac{P_o}{\rho^2} \right) \nabla \rho \right].$$

Label the additional term in the momentum equation as F , and obtain

$$F = -\nabla \left(\frac{P_o}{\rho} \right) - \left(\frac{P_o}{\rho^2} \right) \nabla \rho = 0$$

$$F_s \approx -\sum_{j=1}^N m_j \left(\frac{(P_o)_j}{\rho_j^2} + \frac{(P_o)_s}{\rho_s^2} \right) \nabla_s W_{sj} = -P_o \sum_{j=1}^N m_j \left(\frac{1}{\rho_j^2} + \frac{1}{\rho_s^2} \right) \nabla_s W_{sj}. \quad (4.62)$$

So adding F_s to the SPH momentum equation is equivalent to adding $0 + O(h^2, h\Delta x)$.

Further for symmetric kernels

$$\sum_{s=1}^N m_s F_s = -P_o \sum_{s=1}^N \sum_{j=1}^N m_s m_j \left(\frac{1}{\rho_j^2} + \frac{1}{\rho_s^2} \right) \nabla_s W_{sj} = 0.$$

Hence, for symmetric kernels, F_s does not change the momentum conservation. From earlier in stability, use equation (4.10) for the momentum equation

$$\begin{aligned} \dot{\nu} = & \left[m B \sum_{l=-\infty}^{\infty} (1 + e^{ilk}) W'_l \right] \phi + \left[m C \sum_{l=-\infty}^{\infty} (1 + e^{ilk}) W'_l \right] \varepsilon \\ & + \left[-2 m A \sum_{l=-\infty}^{\infty} (1 - e^{ilk}) W''_l \right] \chi. \end{aligned} \quad (4.63)$$

Consider F_s perturbed, removing the constant term

$$\begin{aligned} F_s &= -P_o \sum_{j=1}^N m_j \left(\frac{1}{(\bar{\rho}_j + \phi_j)^2} + \frac{1}{(\bar{\rho}_s + \phi_s)^2} \right) (W'_{sj} + (\chi_s - \chi_j) W''_{sj}) \\ &= 2P_o \sum_{j=1}^N m_j \left(\frac{\phi_j}{\bar{\rho}_j^3} + \frac{\phi_s}{\bar{\rho}_s^3} \right) W'_{sj} - P_o \sum_{j=1}^N m_j \left(\frac{1}{\bar{\rho}_j^2} + \frac{1}{\bar{\rho}_s^2} \right) (\chi_s - \chi_j) W''_{sj} \\ F_s &= \left[2P_o \sum_{j=1}^N m_j \left(\frac{1}{\bar{\rho}_s^3} + \frac{1}{\bar{\rho}_j^3} e^{i(j-s)k} \right) W'_{sj} \right] \phi \\ &+ \left[-P_o \sum_{j=1}^N m_j \left(\frac{1}{\bar{\rho}_s^2} + \frac{1}{\bar{\rho}_j^2} \right) (1 - e^{i(j-s)k}) W''_{sj} \right] \chi. \end{aligned}$$

Under locally smooth assumptions, the following terms are added to the momentum equation in the amplification matrix (4.63)

$$\left[\frac{-2P_o}{\bar{\rho}^3} m \sum_{l=-\infty}^{\infty} (1 + e^{ilk}) W'_l \right] \phi + \left[\frac{-2P_o}{\bar{\rho}^2} m \sum_{l=-\infty}^{\infty} (1 - e^{ilk}) W''_l \right] \chi.$$

Earlier in equations (4.12)-(4.13) the eigenvalues of the amplification matrix, R , were shown as

$$\lambda(old) = 0, 0, \pm \sqrt{-D_1 - D_2},$$

where D_1 and D_2 are given in equations (4.14) and (4.15). Now using this stabilizing technique, the eigenvalues of R have the same form as before, but with D_1 and D_2

defined as

$$D_1 = \frac{4m^2}{\bar{\rho}^4} (\tilde{A}\tilde{C} + \bar{\rho}^2\tilde{B} - 2\bar{\rho}(\tilde{A} + P_o)) \left(\sum_{l=1}^{\infty} \sin(lk) W'_l \right)^2 \quad (4.64)$$

$$D_2 = \frac{4m}{\bar{\rho}^2} (\tilde{A} + P_o) \sum_{l=1}^{\infty} (1 - \cos(lk)) W''_l. \quad (4.65)$$

The key change is the $\tilde{A} + P_o$ term in D_2 where only \tilde{A} was before. This allows for two choices:

1. $P_o \geq 0$. Choose $P_o \geq -\min_s(\tilde{A}_s, 0)$ in order to keep the pressure term always positive. However, this then requires the use of a concave up kernel (hyperbolic shaped) so that $W'' \geq 0$. This ensures that $D_2 \geq 0$. One side effect is that D_1 is made more negative (more unstable). This should not be a problem, but might deserve monitoring.
2. $P_o \leq 0$. Choose $P_o \leq -\max_s(\tilde{A}_s, 0)$ in order to keep the pressure term always negative. However, this then requires the use of a concave down kernel (parabolic shaped) so that $W'' \leq 0$. This ensures that $D_2 \geq 0$. In addition a good side effect is that D_1 is made more positive (more stable).

So the advantages of this method are that it allows continued use of symmetric equations, maintains conservation, can be applied for problems with pressure of either sign, and stabilizes the method. The disadvantage is that a new (possibly less accurate) kernel must be used.

4.2.3 Technique 2a - Add a Constant to the Pressure in the Energy Equation.

In Technique 2, a constant is added to the pressure term in the momentum equation. A similar change can be made to the energy equation. The reasons to do this are to keep the momentum and energy equations in agreement with one another and to help the D_1 term if needed. However, it is more difficult to see that this is consistent since the pressure term does not occur inside a derivative in the differential equation. So instead of deriving the SPH energy equation directly from the internal energy

differential equation, derive the SPH form from the total energy equation and the SPH momentum equation. Define

$$\begin{aligned}\sigma_{sj} &= \frac{P_s}{\rho_s^2} + \frac{P_j}{\rho_j^2} \\ \tilde{\sigma}_{sj} &= \sigma_{sj} + \frac{P_o}{\rho_s^2 + \rho_j^2} \\ \frac{Dv_s}{Dt} &= - \sum_{j=1}^N m_j \tilde{\sigma}_{sj} \nabla_s W_{sj} .\end{aligned}$$

Starting with the total energy conservation form

$$\begin{aligned}\sum_{s=1}^N (m_s e_s + \frac{1}{2} m_s \vec{v}_s^2) &= \text{constant} . \\ \frac{D}{Dt} \left[\sum_{s=1}^N (m_s e_s + \frac{1}{2} m_s \vec{v}_s^2) \right] &= \sum_{s=1}^N (m_s \frac{De_s}{Dt} + m_s \vec{v}_s \cdot \frac{D\vec{v}_s}{Dt}) = 0 \\ \sum_{s=1}^N m_s \frac{De_s}{Dt} &= - \sum_{s=1}^N m_s \vec{v}_s \cdot \left[- \sum_{j=1}^N m_j \tilde{\sigma}_{sj} \nabla_s W_{sj} \right] \\ &= \sum_{s=1}^N \sum_{j=1}^N m_s m_j \tilde{\sigma}_{sj} \vec{v}_s \cdot \nabla_s W_{sj} \quad (4.66)\end{aligned}$$

$$\begin{aligned}&= \sum_{j=1}^N \sum_{s=1}^N m_j m_s \tilde{\sigma}_{js} \vec{v}_j \cdot \nabla_j W_{js} \\ &= \sum_{s=1}^N \sum_{j=1}^N m_s m_j \tilde{\sigma}_{sj} \vec{v}_s \cdot (-\nabla_s W_{sj}) . \quad (4.67)\end{aligned}$$

This last step assumes an even kernel. Now average equations (4.66) and (4.67) to obtain

$$\sum_{s=1}^N m_s \frac{De_s}{Dt} = \frac{1}{2} \sum_{s=1}^N m_s \sum_{j=1}^N m_j \tilde{\sigma}_{sj} (\vec{v}_s - \vec{v}_j) \cdot \nabla_s W_{sj} . \quad (4.68)$$

So now define

$$\frac{De_s}{Dt} = \frac{1}{2} \sum_{j=1}^N m_j \tilde{\sigma}_{sj} (\vec{v}_s - \vec{v}_j) \cdot \nabla_s W_{sj} . \quad (4.69)$$

For stability, the D_2 term is the same as in Technique 2; but the D_1 term is different.

In Technique 2, a term with $-2\bar{\rho}P_o$ is added. In this addition to Technique 2, a term

with $\tilde{C}P_o$ is added. So putting Technique 2 and Technique 2a together, the D_1 term is redefined as

$$D_1(\text{new}) = D_1(\text{old}) + \frac{P_o}{\bar{\rho}^4} (\tilde{C} - 2\bar{\rho}) G_1 G_2 .$$

This new term is usually negative for the two EOS studied, making D_1 more stable. So the advantages of this method are that it allows continued use of symmetric equations, maintains conservation, can be applied for problems with pressure of either sign, keeps the energy and momentum equations in agreement, and stabilizes the method. The disadvantage is that a new (possibly less accurate) kernel must be used.

4.2.4 Technique 3 - A Pressure Difference Form in the Momentum Equation.

In the momentum equation, add a term that has pressure times the gradient of a constant. This results in adding zero plus $O(h^2)$ to the final SPH momentum equations as shown below

$$\frac{Dv}{Dt} = -\frac{1}{\rho} \nabla P = -\nabla \left(\frac{P}{\rho} \right) - \left(\frac{P}{\rho_2} \right) \nabla \rho \quad (4.70)$$

$$\frac{Dv}{Dt} = -\nabla \left(\frac{P}{\rho} \right) - \left(\frac{P}{\rho_2} \right) \nabla \rho + \frac{2P}{\rho} \nabla 1 . \quad (4.71)$$

Label this additional term in the momentum equation as F , and obtain

$$F = \frac{2P}{\rho} \nabla 1 = 0$$

$$F_s \approx - \sum_{j=1}^N m_j \left(\frac{-2P_s}{\rho_s \rho_j} \right) \nabla_s W_{sj} . \quad (4.72)$$

So adding F_s to the SPH momentum equation is equivalent to adding $0 + O(h^2, h\Delta x)$. This form cannot be guaranteed to exactly conserve momentum. However, the stability analysis is performed under smooth data assumptions. In particular, if the

pressure varies only slightly within the support of the kernel, the loss of conservation should be on the same order as the method itself. From earlier for stability, using equation (4.10) for the momentum equation

$$\begin{aligned} \dot{\nu} = & \left[m B \sum_{l=-\infty}^{\infty} (1 + e^{ilk}) W'_l \right] \phi + \left[m C \sum_{l=-\infty}^{\infty} (1 + e^{ilk}) W'_l \right] \varepsilon \\ & + \left[-2 m A \sum_{l=-\infty}^{\infty} (1 - e^{ilk}) W''_l \right] \chi. \end{aligned} \quad (4.73)$$

Consider F_s perturbed, removing the constant term

$$\begin{aligned} F_s &= - \sum_{j=1}^N m_j \left[\frac{-2(\tilde{A}_s + \tilde{B}_s \phi_s + \tilde{C}_s \varepsilon_s)}{(\bar{\rho}_j + \phi_j)(\bar{\rho}_s + \phi_s)} \right] (W'_{sj} + (\chi_s - \chi_j) W''_{sj}) \\ F_s &= - \sum_{j=1}^N m_j \left[\left(\frac{2\tilde{A}_s}{\bar{\rho}_s^2 \bar{\rho}_j} \phi_s + \frac{2\tilde{A}_s}{\bar{\rho}_s \bar{\rho}_j^2} \phi_j - \frac{2\tilde{B}_s}{\bar{\rho}_s \bar{\rho}_j} \phi_s \right) W'_{sj} \right. \\ &\quad \left. - \frac{2\tilde{C}}{\bar{\rho}_s \bar{\rho}_j} \varepsilon_s W'_{sj} - \frac{2\tilde{A}_s}{\bar{\rho}_s \bar{\rho}_j} (\chi_s - \chi_j) W''_{sj} \right] \\ &= \left[- \sum_{j=1}^N m_j \left(\frac{2\tilde{A}_s}{\bar{\rho}_s^2 \bar{\rho}_j} - \frac{2\tilde{B}_s}{\bar{\rho}_s \bar{\rho}_j} + \frac{2\tilde{A}_s}{\bar{\rho}_s \bar{\rho}_j^2} e^{i(j-s)k} \right) W'_{sj} \right] \phi \\ &\quad \left[- \sum_{j=1}^N m_j \frac{-2\tilde{C}}{\bar{\rho}_s \bar{\rho}_j} W'_{sj} \right] \varepsilon + \left[- \sum_{j=1}^N m_j \frac{-2\tilde{A}_s}{\bar{\rho}_s \bar{\rho}_j} (1 - e^{i(j-s)k}) W''_{sj} \right] \chi. \end{aligned}$$

Under locally smooth assumptions, the following terms are added to the momentum equation in the amplification matrix (4.73)

$$\begin{aligned} & \left[\frac{2\tilde{A}}{\bar{\rho}^3} m \sum_{l=-\infty}^{\infty} (1 + e^{ilk}) W'_l + \frac{-2\tilde{B}}{\bar{\rho}^2} m \sum_{l=-\infty}^{\infty} W'_l \right] \phi + \left[\frac{-2\tilde{C}}{\bar{\rho}^2} m \sum_{l=-\infty}^{\infty} W'_l \right] \varepsilon \\ & + \left[\frac{2\tilde{A}}{\bar{\rho}^2} m \sum_{l=-\infty}^{\infty} (1 - e^{ilk}) W''_l \right] \chi. \end{aligned}$$

From section 4.1, in which a stabilizing technique was not used, the eigenvalues of the amplification matrix, R , were

$$\lambda(old) = 0, 0, \pm \sqrt{-D_1 - D_2},$$

where D_1 and D_2 are given in equations (4.14) and (4.15). Now using this stabilizing technique, the eigenvalues of R have the same form as before, but with D_1 and D_2 defined as

$$D_1 = \frac{4m^2}{\bar{\rho}^4} (\tilde{A} \tilde{C} + \bar{\rho}^2 \tilde{B}) \left(\sum_{l=1}^{\infty} \sin(lk) W'_l \right)^2 \quad (4.74)$$

$$D_2 = 0. \quad (4.75)$$

The key change is that the troublesome D_2 term is removed completely. The D_1 term also changed, but should still not be a problem. See Appendix B.2 for a further discussion of the D_1 term.

So the advantages of this method are that it allows continued use of symmetric equations, continued use of the same kernel, can be applied for problems with pressure of either sign (easily), and stabilizes the method. The disadvantage is that momentum conservation may be lost.

4.2.5 Technique 3a - A Pressure Difference Form in the Energy Equation.

As was done with Technique 2, a change similar to Technique 3 can be added to the energy equation. The reasons to do this are to keep the momentum and energy equations in agreement with one another and to help the D_1 term if needed. However, it is more difficult to see that this is consistent since the pressure term does not occur inside a derivative in the differential equation. So instead of deriving the SPH energy equation from the internal energy differential equation, derive the SPH form from the total energy equation and the SPH momentum equation as was done in Technique 2a. Define

$$\sigma_{sj} = \frac{P_s}{\rho_s^2} + \frac{P_j}{\rho_j^2}$$

$$\begin{aligned}\tilde{\sigma}_{sj} &= \sigma_{sj} - \frac{2P_s}{\rho_s \rho_j} \\ \frac{Dv_s}{Dt} &= - \sum_{j=1}^N m_j \tilde{\sigma}_{sj} \nabla_s W_{sj} .\end{aligned}$$

Starting with the total energy conservation form

$$\begin{aligned}\sum_{s=1}^N (m_s e_s + \frac{1}{2} m_s \vec{v}_s^2) &= \text{constant} . \\ \frac{D}{Dt} \left[\sum_{s=1}^N (m_s e_s + \frac{1}{2} m_s \vec{v}_s^2) \right] &= \sum_{s=1}^N (m_s \frac{De_s}{Dt} + m_s \vec{v}_s \cdot \frac{D\vec{v}_s}{Dt}) = 0 \\ \sum_{s=1}^N m_s \frac{De_s}{Dt} &= - \sum_{s=1}^N m_s \vec{v}_s \cdot \left[- \sum_{j=1}^N m_j \tilde{\sigma}_{sj} \nabla_s W_{sj} \right] \\ &= \sum_{s=1}^N \sum_{j=1}^N m_s m_j \tilde{\sigma}_{sj} \vec{v}_s \cdot \nabla_s W_{sj} \quad (4.76)\end{aligned}$$

$$\begin{aligned}&= \sum_{j=1}^N \sum_{s=1}^N m_j m_s \tilde{\sigma}_{js} \vec{v}_j \cdot \nabla_j W_{js} \\ &= \sum_{s=1}^N \sum_{j=1}^N m_s m_j \tilde{\sigma}_{js} \vec{v}_j \cdot (-\nabla_s W_{sj}) . \quad (4.77)\end{aligned}$$

Therefore, average equations (4.76) and (4.77) to obtain

$$\begin{aligned}\sum_{s=1}^N m_s \frac{De_s}{Dt} &= \frac{1}{2} \sum_{s=1}^N m_s \sum_{j=1}^N m_j (\tilde{\sigma}_{sj} \vec{v}_s - \tilde{\sigma}_{js} \vec{v}_j) \cdot \nabla_s W_{sj} \\ &= \sum_{s=1}^N m_s \left[\frac{1}{2} \sum_{j=1}^N m_j \sigma_{sj} (\vec{v}_s - \vec{v}_j) \cdot \nabla_s W_{sj} \right. \\ &\quad \left. - \frac{1}{2} \sum_{j=1}^N m_j \frac{P_s \vec{v}_s - P_j \vec{v}_j}{\rho_s \rho_j} \cdot \nabla_s W_{sj} \right] . \quad (4.78)\end{aligned}$$

So define

$$\frac{De_s}{Dt} = \frac{1}{2} \sum_{j=1}^N m_j \sigma_{sj} (\vec{v}_s - \vec{v}_j) \cdot \nabla_s W_{sj} - \sum_{j=1}^N m_j \left(\frac{P_s \vec{v}_s - P_j \vec{v}_j}{\rho_s \rho_j} \right) \cdot \nabla_s W_{sj} . \quad (4.79)$$

This implies the additional term, F , for the energy equation is

$$F_s = - \sum_{j=1}^N m_j \left(\frac{P_s \vec{v}_s - P_j \vec{v}_j}{\rho_s \rho_j} \right) \cdot \nabla_s W_{sj} . \quad (4.80)$$

For stability of this method, consider F_s perturbed, with the constant term removed

$$\begin{aligned} F_s &= - \sum_{j=1}^N m_j \left[\frac{(\tilde{A}_s + \tilde{B}_s \phi_s + \tilde{C}_s \epsilon_s)(\bar{v}_s + \nu_s) - (\tilde{A}_j + \tilde{B}_j \phi_j + \tilde{C}_j \epsilon_j)(\bar{v}_j + \nu_j)}{(\bar{\rho}_j + \phi_j)(\bar{\rho}_s + \phi_s)} \right] \\ &\quad \times (W'_{sj} + (\chi_s - \chi_j)W''_{sj}) \\ &= - \sum_{j=1}^N m_j \left\{ \left[- \left(\frac{\tilde{A}_s \bar{v}_s - \tilde{A}_j \bar{v}_j}{\bar{\rho}_s \bar{\rho}_j^2} \right) \phi_j - \left(\frac{\tilde{A}_s \bar{v}_s - \tilde{A}_j \bar{v}_j}{\bar{\rho}_s^2 \bar{\rho}_j} \right) \phi_s \right. \right. \\ &\quad + \left(\frac{\tilde{B}_s \bar{v}_s \phi_s - \tilde{B}_j \bar{v}_j \phi_j}{\bar{\rho}_s \bar{\rho}_j} \right) + \left(\frac{\tilde{A}_s \nu_s - \tilde{A}_j \nu_j}{\bar{\rho}_s \bar{\rho}_j} \right) + \left. \left(\frac{\tilde{C}_s \bar{v}_s \epsilon_s - \tilde{C}_j \bar{v}_j \epsilon_j}{\bar{\rho}_s \bar{\rho}_j} \right) \right] W'_{sj} \\ &\quad + \left. \left[\left(\frac{\tilde{A}_s \bar{v}_s - \tilde{A}_j \bar{v}_j}{\bar{\rho}_s \bar{\rho}_j} \right) (\chi_s - \chi_j) W''_{sj} \right] \right\} \\ &= \sum_{j=1}^N m_j \left\{ \left[\frac{\tilde{A}_s \bar{v}_s - \tilde{A}_j \bar{v}_j + \bar{\rho}_j \tilde{B}_j \bar{v}_j}{\bar{\rho}_s \bar{\rho}_j^2} \right] \phi_j + \left[\frac{\tilde{A}_s \bar{v}_s - \tilde{A}_j \bar{v}_j - \bar{\rho}_s \tilde{B}_s \bar{v}_s}{\bar{\rho}_s^2 \bar{\rho}_j} \right] \phi_s \right\} W'_{sj} \\ &\quad - \sum_{j=1}^N m_j \left(\frac{\tilde{A}_s \nu_s - \tilde{A}_j \nu_j}{\bar{\rho}_s \bar{\rho}_j} \right) W'_{sj} - \sum_{j=1}^N m_j \left(\frac{\tilde{C}_s \bar{v}_s \epsilon_s - \tilde{C}_j \bar{v}_j \epsilon_j}{\bar{\rho}_s \bar{\rho}_j} \right) W'_{sj} \\ &\quad - \sum_{j=1}^N m_j \left(\frac{\tilde{A}_s \bar{v}_s - \tilde{A}_j \bar{v}_j}{\bar{\rho}_s \bar{\rho}_j} \right) (\chi_s - \chi_j) W''_{sj} . \end{aligned}$$

Under locally smooth assumptions, most of the terms vanish and only the following term needs to be added to the energy equation in the amplification matrix

$$\left[\frac{\tilde{B} \bar{v}}{\bar{\rho}^2} m \sum_{l=-\infty}^{\infty} (1 - e^{ilk}) W'_l \right] \phi .$$

With the addition of this term, the characteristic equation becomes

$$\lambda \left[\lambda^3 - \lambda \left(\frac{G_1^2}{\bar{\rho}^4} \right) (\tilde{A} \tilde{C} + \bar{\rho}^2 \tilde{B}) - \left(\frac{G_1^3}{\bar{\rho}^4} \right) (\tilde{B} \tilde{C} \bar{v}) \right] = 0 .$$

As with the wall heating term this equation does not yield simple eigenvalues. But, at minimum wavelength $G_1 = 0$ so the eigenvalues are all zero. For other than the minimum wavelength case, this form of the equations does not permit any general comments.

So the advantages of this method are that it allows continued use of symmetric equations, keeps energy and momentum equations in agreement, and can be applied for problems with pressure of either sign. The disadvantages are that conservation may be lost and with the complicated eigenvalues stability is difficult to determine for certain. In fact, since the technique can only guarantee non-positive real parts of the eigenvalues for the minimum wavelength, it would be more appropriate to refer to this as less unstable or conditionally stable.

4.2.6 Technique 4 - Particle Motion Correction. As noted earlier in this chapter, and detailed in Appendix B, the following form of the particle motion equation can have a stabilizing effect

$$\dot{x}_s = v_s + \epsilon \sum_{j=1}^N m_j \left(\frac{v_j - v_s}{0.5(\rho_s + \rho_j)} \right) W_{sj} = v_s - \epsilon \Delta v. \quad (4.81)$$

This equation was originally proposed by Monaghan (41, 43) to solve a problem with streaming; where particles from one material unphysically penetrate into another in a collision. Although artificial viscosity helped the situation, it did not remove it in all cases. Similarly, artificial viscosity can make the eigenvalues of the amplification matrix smaller, but cannot stabilize the method. Further, this form was proposed for streaming because the velocity field may not be single-valued in SPH and using the usual $\dot{x} = v$ equation can result in incorrect particle movement. This last notion also applies in the stability case. The velocity is not properly calculated (in a stability sense) causing the particle movement to be incorrect unless a correction term is added.

From the material in Appendix B leading up to equations (B.15) and (B.16), the eigenvalues of amplification matrix using this technique are $\lambda = 0, 0, \pm\sqrt{-D}$, where $D = D_1 + D_2$ and

$$D_1 = \frac{4m^2}{\bar{\rho}^4} (\tilde{A}\tilde{C} + \bar{\rho}^2\tilde{B} - 2\bar{\rho}\tilde{A}) \left(\sum_{l=1}^{\infty} \sin(lk) W_l' \right)^2 \quad (4.82)$$

$$D_2 = \tilde{A} \left[\frac{4m}{\bar{\rho}^2} \sum_{l=1}^{\infty} (1 - \cos(lk)) W_l'' \right] \left[1 - \epsilon \frac{m}{\bar{\rho}} \sum_{l=1}^{\infty} (1 - \cos(lk)) W_l \right]. \quad (4.83)$$

At minimum wavelength, k equals π , so $D_1 = 0$ and $D_2 \propto \tilde{A}W''(1 - 2\epsilon)$. The stability analysis was already performed in Appendix B, but three questions remain: Is this correction consistent, conservative, and how big does ϵ have to be to ensure stability?

1. Consistency. Use the following:

$$\begin{aligned} v_s - v_j &= v_s - (v_s - x_{sj}v_s' + \frac{x_{sj}^2}{2}v_s'' + \dots) = x_{sj}v_s' - \frac{x_{sj}^2}{2}v_s'' + O(h^2) \\ \frac{2}{\rho_s + \rho_j} &= \frac{2}{\rho_s + (\rho_s - x_{sj}\rho_s' + \dots)} = \frac{2}{2\rho_s - x_{sj}\rho_s' + \dots} = \frac{1}{\rho_s} + \frac{x_{sj}}{2} \left(\frac{\rho_s'}{\rho_s^2} \right) + O(h^2), \end{aligned}$$

to obtain

$$\left(\frac{v_s - v_j}{0.5(\rho_s + \rho_j)} \right) = \left(\frac{v_s'}{\rho_s} \right) x_{sj} + \left(\frac{v_s'\rho_s'}{\rho_s^2} - \frac{v_s''}{\rho_s} \right) \frac{x_{sj}^2}{2} + O(h^2).$$

Using the information above, the additional term becomes

$$\begin{aligned} \Delta v &= \sum_{j=1}^N m_j \left(\frac{v_s - v_j}{0.5(\rho_s + \rho_j)} \right) W_{sj} = \sum_{j=1}^N m_j \left(\frac{v_s'}{\rho_s} \right) x_{sj} W_{sj} \\ &\quad + \sum_{j=1}^N m_j \left(\frac{v_s'\rho_s'}{\rho_s^2} - \frac{v_s''}{\rho_s} \right) \frac{x_{sj}^2}{2} W_{sj} \\ &= \left(\frac{v_s'}{\rho_s} \right) \sum_{j=1}^N m_j x_{sj} W_{sj} + \left(\frac{v_s'\rho_s'}{2\rho_s^2} - \frac{v_s''}{2\rho_s} \right) \sum_{j=1}^N m_j x_{sj}^2 W_{sj}. \end{aligned}$$

Investigating the sums in the above equation yields

$$\begin{aligned}\sum_{j=1}^N m_j x_{sj} W_{sj} &= x_s \sum_{j=1}^N m_j W_{sj} - \sum_{j=1}^N m_j x_j W_{sj} \approx x_s \langle \rho_s \rangle - \langle x_s \rho_s \rangle \approx 0 \\ \sum_{j=1}^N m_j x_{sj}^2 W_{sj} &= x_s^2 \sum_{j=1}^N m_j W_{sj} - 2x_s \sum_{j=1}^N m_j x_j W_{sj} + \sum_{j=1}^N m_j x_j^2 W_{sj} \\ &\approx x_s^2 \langle \rho_s \rangle - 2x_s \langle x_s \rho_s \rangle + \langle x_s^2 \rho_s \rangle \approx 0.\end{aligned}$$

Therefore, the Δv (additional term) term is equal to zero within the order of the method. This implies it is a consistent technique.

2. Conservation. For conservation of momentum note

$$\begin{aligned}\sum_{s=1}^N m_s \dot{x}_s &= \sum_{s=1}^N m_s (v_s - \epsilon \Delta v) = \sum_{s=1}^N m_s v_s \\ &\quad - \epsilon \sum_{s=1}^N \sum_{j=1}^N m_s m_j \left(\frac{v_s - v_j}{0.5(\rho_s + \rho_j)} \right) W_{sj} = \sum_{s=1}^N m_s v_s + 0.\end{aligned}$$

So adding the $\epsilon \Delta v$ term to the SPH particle motion equation is equivalent to adding $0 + O(h^2, h\Delta x)$ and for symmetric kernels maintains momentum conservation.

3. Magnitude of the ϵ Factor. Concentrating on the troublesome D_2 term, ϵ needs to be large enough so that $2AG_3(1 - \epsilon \frac{G_5}{\bar{\rho}}) \geq 0$. By definition, ρ and G_5 are non-negative. So, consider two cases:

a. $PW'' \geq 0$. This implies $2AG_3 \geq 0$. Then ϵ needs to be small, in order that $1 - \epsilon \frac{G_5}{\bar{\rho}} \geq 0$. Although more analysis can be performed, the easiest solution is just to let ϵ be zero in this case.

b. $PW'' \leq 0$. This implies $2AG_3 \leq 0$. Then ϵ needs to be large enough for $1 - \epsilon \frac{G_5}{\bar{\rho}} \leq 0$ to hold. For the $\frac{G_5}{\bar{\rho}}$ factor note that

$$\frac{G_5}{\bar{\rho}} = \frac{2m}{\bar{\rho}} \sum_{l=1}^{\infty} (1 - \cos(lk)) W_l.$$

At minimum wavelength that term approaches 2 as $\Delta x \rightarrow 0$ and at $k = \frac{\pi}{2}$, it approaches 1 as $\Delta x \rightarrow 0$. This implies for the lower wavelengths, ϵ can be quite reasonable, around 1 as long as Δx is sufficiently small. In fact, based on some tests for the popular B-Spline kernel, for $\Delta x \leq 1.4h$ (rather large), a value for ϵ of 5 stabilizes the minimum wavelengths. If the particles are guaranteed to be more tightly spaced, the value for ϵ can decrease, approaching 0.5 in the limit. To be able to stabilize wavelengths up to $k = \frac{\pi}{2}$, double the value selected for ϵ . Considering the small values often used for h , these values for ϵ are still reasonable. A problem with this technique is that as particle spacing becomes more sparse, ϵ needs to be increased. However, for spacing much larger than $\Delta x = h$, the accuracy becomes quite poor as shown in Chapter VI. Hence, it seems reasonable not to worry about stabilizing the method when it is highly inaccurate.

A more significant concern with this method is that it does not work for all wavelengths. This is because as $k \rightarrow 0$, $G_5 \rightarrow 0$. And although it is not a problem when k is exactly zero (since G_3 is also zero), it is for all other small values of k .

So the advantages of this method are that it allows continued use of symmetric equations, keeps energy and momentum equations in agreement, can be applied for problems with pressure of either sign, and maintains conservation. The disadvantage is that it only works for lower wavelengths. Since this removes the instability from higher frequencies (lower wavelengths), this might be more appropriately referred to as a high frequency filter. However, that does not indicate the stability process. So using the terms less unstable or conditionally stable from the previous technique might be more appropriate.

4.2.7 Some Computational Results. Based on the work in this section and Chapter VI, I feel that Technique 3a - A Pressure Difference Form and Technique 4 - Particle Motion Correction are the best possibilities. The first few techniques are still valid, but in Chapter VI the concave up kernels (hyperbolic shaped) and

concave down kernels (parabolic shaped) are shown to be not nearly as accurate as bell shaped kernels, so those will not be considered at this time.

In this subsection a one dimensional stability test is performed, similar to one proposed by Swegle (63) (the concept is the same as Swegle's, but some of the parameter settings are different). The initial setup is a line of 2300 particles contained in the interval $[-90, 140]$ with $h = 0.15$ and $\Delta x = 2h/3$. The material chosen is Aluminum that has an ambient density of 2.71 gm/cc. All particles are given the following initial settings: $\rho_o = 2.57$, $e_o = 1 \times 10^{-8}$, $v_o = 0.0$. The initial density is about 95% of the ambient density, implying the material is in tension. Using the Mie - Grüneisen equation of state the initial pressure is -.0425 everywhere. Then one particle in the middle of the line is perturbed by giving it an initial velocity of 10^{-5} ; all other values of the perturbed particle are unchanged. Other important settings include using the W-4 B-Spline kernel, using central time, a CFL factor (c_{CFL}) of 0.3, and time step calculated by

$$\Delta t = c_{CFL} \sqrt{h^2/v^2 + c_s^2}$$

where c_s is the speed of sound.

Without any artificial damping terms, the perturbation should cause a wave to travel in both directions while the velocity of the perturbed particle to decrease (in absolute value) with time. A baseline test case is performed using the settings above and a standard SPH formulation. The calculation is then repeated using Techniques 3a and 4. Plots of the pressure and velocity for each of the calculations at 25 μ sec are shown below in Figures 4.1-4.3.

In the baseline, the velocity perturbation obviously is seen not to decrease with time, but grown tremendously. Further, the perturbation has also caused a growth in pressure. Upon applying either of the two stability enhancements the growth is removed. In both, the growth is completely eliminated (at least to plotting accuracy)

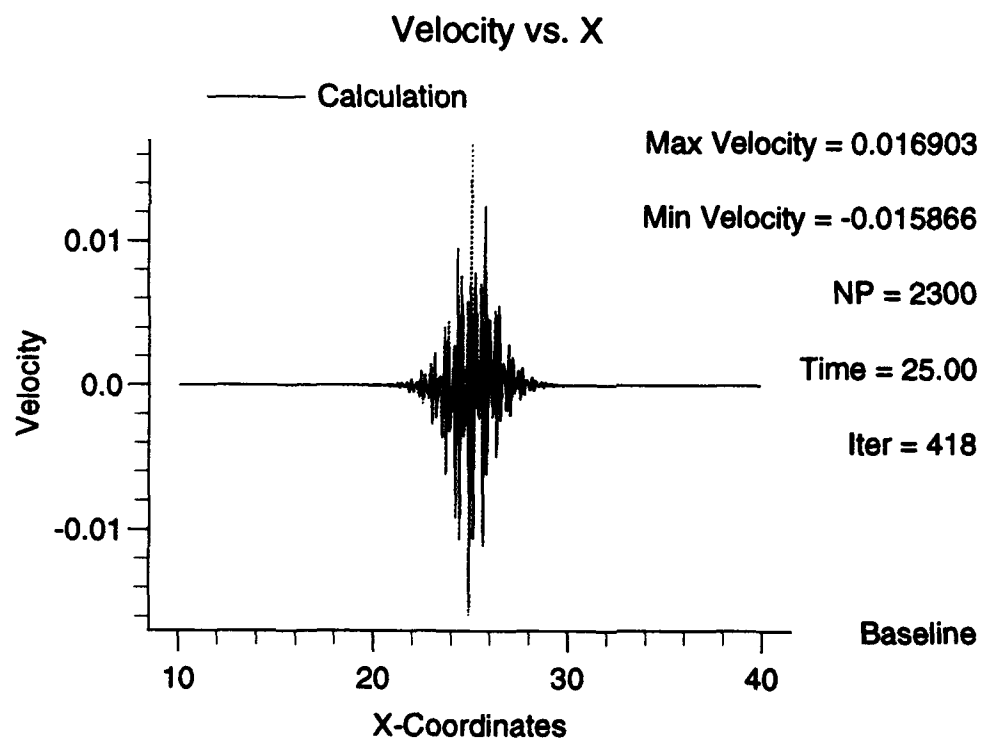
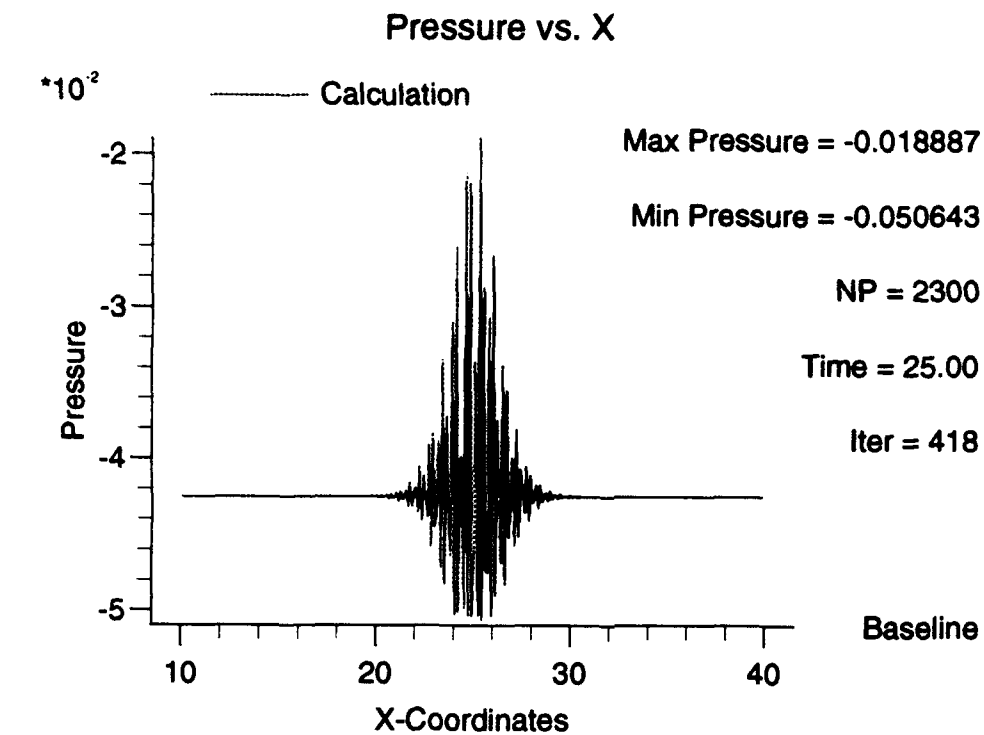


Figure 4.1 Baseline Stability Results

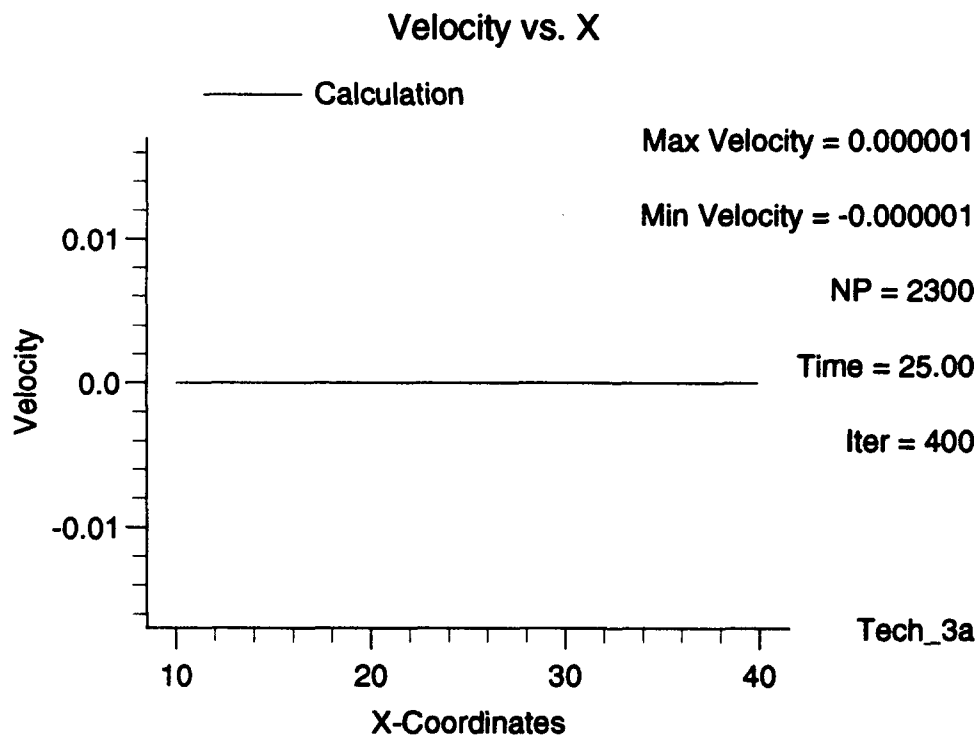
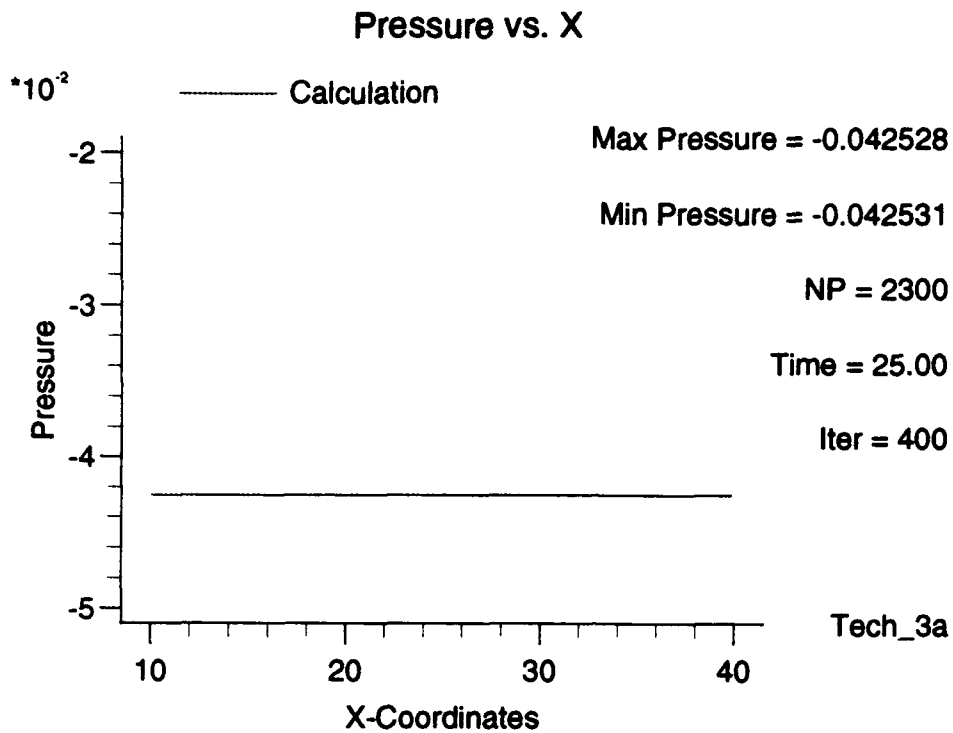


Figure 4.2 Technique 3a Stability Results

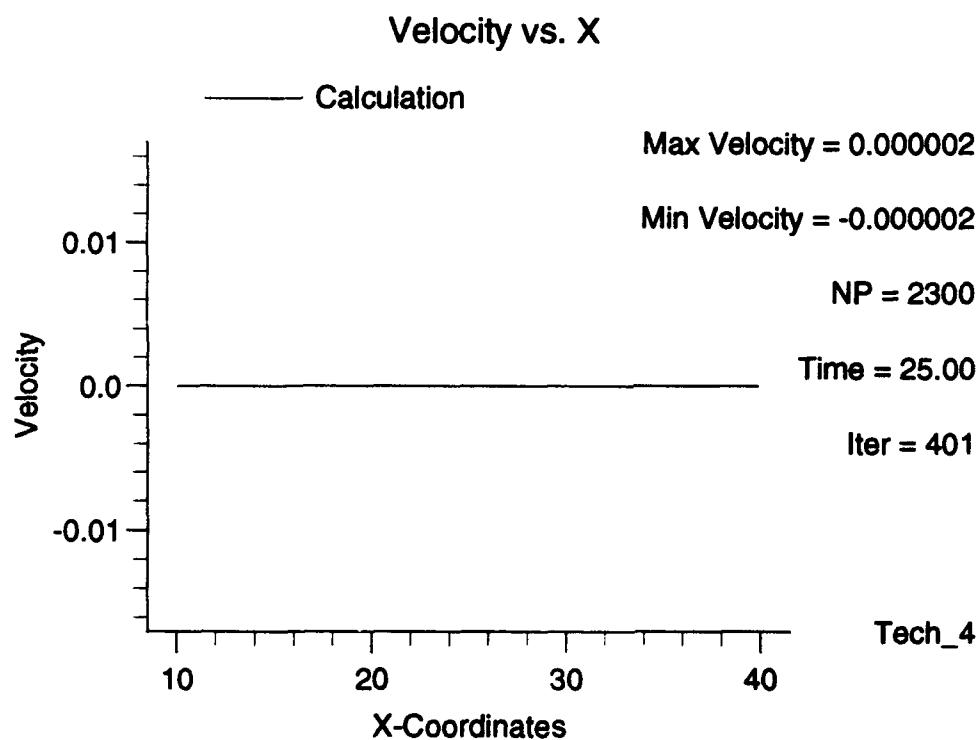
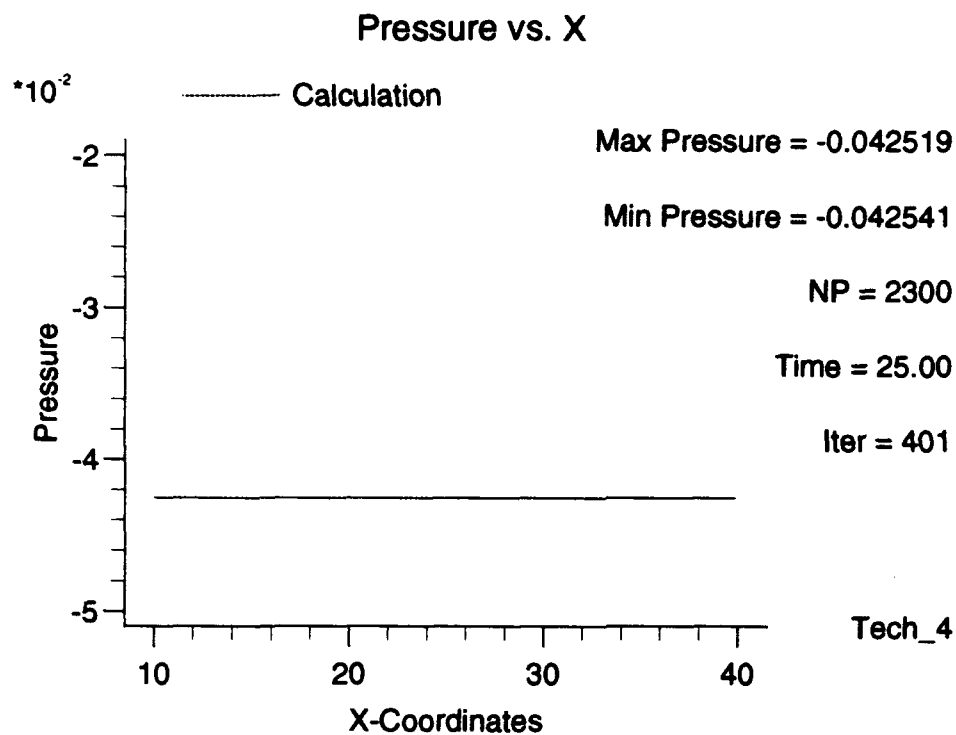


Figure 4.3 Technique 4 Stability Results

for velocity. In Technique 4, there is a little more noise (especially in pressure), but it is not even to the accuracy of the plot. A comparison of the velocities over time is shown in Figure 4.4

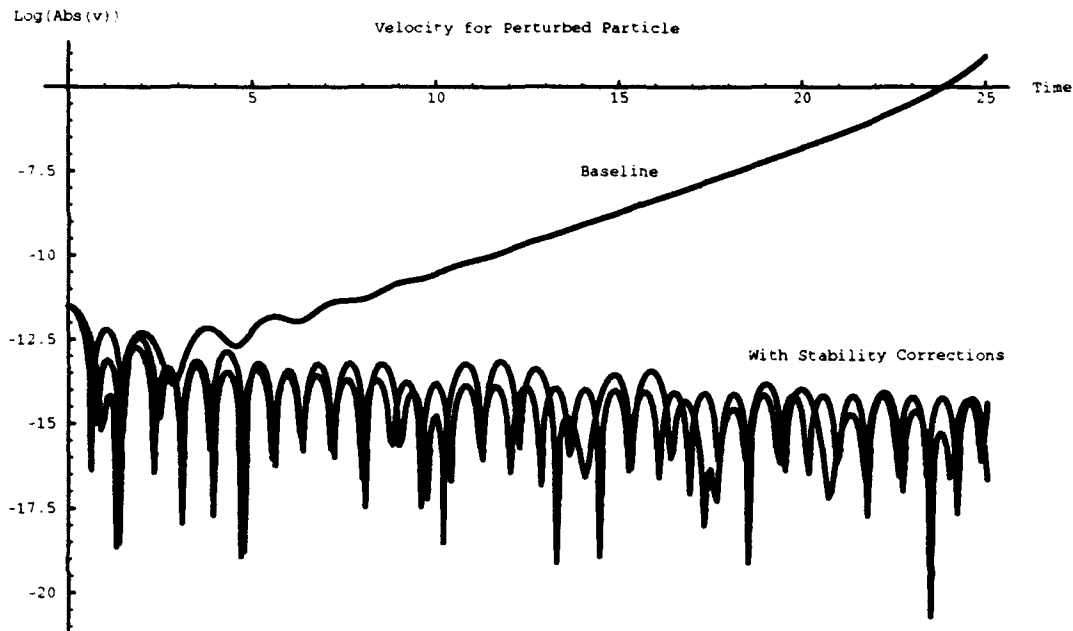


Figure 4.4 Velocity Stability Comparisons

The baseline has an exponential growth of velocity (plotting is on a log scale), while the others slowly decrease over time. This shows the unstable nature of the baseline and stabilizing nature of the techniques 3a and 4. Also note that both techniques maintained conservation of volume, momentum, and energy exactly. This should help to alleviate some of the concerns over Technique 3a maintaining conservation.

In addition to the tests shown here, tests were performed with spacing of $\Delta x = h$ and initial perturbation velocities of 10^{-3} and 10^{-8} . The results for all the runs were similar. The amount of growth and the time scales were somewhat different, but the bottom line is the baseline grows exponentially while the stabilizing techniques do not.

4.3 Total Variation Analysis

In this section the concept of total variation stability is introduced. Much of the analysis in this chapter so far is based on concepts dealing with linear equations. This allows many simplifications and makes the analysis easier. However, the linear approximation is valid for non-linear problems locally. That is, as long as perturbations are generally small in a given space and time domain around any point, the analysis holds. If these assumptions do not hold, or that is too restrictive, other definitions of stability must be found. One such definition is total variation stability. A good summary for this as applied in finite differences may be found in LeVeque (32).

The approach taken in this section is to develop two total variation stable versions of SPH starting from the basic one dimensional wave equation. In particular, the versions developed here are monotone schemes. A comment is then made as to how this concept can be generalized for use a general conservation equation. However, first a few notes on this relatively new concept.

The basic idea in total variation stability is to bound the total variation of the numerical solution. Conceptually, that means to bound the amount that errors can grow, a basic tenet of stability. For this reason, total variation stability and total variation bounded (TVB) are used interchangeably. There are two equivalent definitions of total variation (at least)

$$TV(u) = \sum_{i=1}^N |u(x_{i+1}) - u(x_i)| \quad (4.84)$$

$$TV(u) = \int_{-\infty}^{\infty} |u'(x)| dx . \quad (4.85)$$

The first definition is for discrete functions and the second for continuous functions. These ideas can also be extended to functions of both space and time as

$$TV_T(u) = \limsup_{\epsilon \rightarrow 0} \frac{1}{\epsilon} \int_0^T \int_{-\infty}^{\infty} |u(x + \epsilon, t) - u(x, t)| dx dt \\ + \limsup_{\epsilon \rightarrow 0} \frac{1}{\epsilon} \int_0^T \int_{-\infty}^{\infty} |u(x, t + \epsilon) - u(x, t)| dx dt . \quad (4.86)$$

A subset of TVB methods known as total variation diminishing (TVD) methods were actually developed first. They are also more prevalent in the literature. TVD methods were introduced about 12 years ago by Harten (17). A numerical scheme, $u_i^{n+1} = \mathcal{H}(u_i^n)$, is known as TVD if

$$TV(u^{n+1}) \leq TV(u^n) .$$

Other good sources on TVD methods are: Harten (18), LeVeque and Goodman (31), Osher and Chakravarthy (48), and Shu (54). In addition to TVD there are several other categories of TVB methods, each one a subset of the previous ending with monotone methods. Monotone methods are quite smooth and stable, but as shown by Harten, et al. (16) they are only first order accurate. So there is a stability versus accuracy concern for monotone methods.

As a way of introducing the total variation ideas to SPH, two monotone methods are developed in this dissertation. In the hierarchy given by LeVeque, these methods will also be l_1 contracting, TVD, and TVB. The two SPH monotone methods being proposed are: the Lax-Friedrichs and a General monotone SPH.

4.3.1 Lax-Friedrichs. This notion is derived fully in Chapter VII, so only the formula will be given at this time. For the one dimensional wave equation $u_t + au_x = 0$,

$$u_i^{n+1} = \sum_{j=1}^N \Delta x_j u_j^n \bar{W}_{ij} - a \Delta t \sum_{j=1}^N \Delta x_j u_j^n W'_{ij} . \quad (4.87)$$

Note: \bar{W} and W do not have to be the same kernel. To show this method is monotone, let $\mathcal{H}(u_i)$ be the right hand side of equation (4.87) and then show

$$\frac{\partial \mathcal{H}(u_i)}{\partial u_k^n} \geq 0 \quad \forall k, i, u^n.$$

For this method

$$\frac{\partial \mathcal{H}}{\partial u_k^n} = \Delta x_k \bar{W}_{ik} - a \Delta t \Delta x_k W'_{ij}.$$

When $k = i$, the results are

$$\frac{\partial \mathcal{H}}{\partial u_i^n} = \Delta x_i \bar{W}_o - a \Delta t \Delta x_i W'_o \geq 0,$$

since W'_o is taken as 0 (at least in all the kernels in Chapter VI) and \bar{W}_o is positive.

Also for $k = j \neq i$ and $\bar{W} \geq 0$,

$$\begin{aligned} \frac{\partial \mathcal{H}}{\partial u_j^n} &= \Delta x_j (\bar{W}_{ij} - a \Delta t W'_{ij}) = \Delta x_j \bar{W}_{ij} \left(1 - a \Delta t \frac{W'_{ij}}{\bar{W}_{ij}} \right). \\ \text{If } \left| \frac{W'_{ij}}{\bar{W}_{ij}} \right| &\leq \frac{B}{h} \quad \text{then } \left| a \Delta t \frac{W'_{ij}}{\bar{W}_{ij}} \right| \leq \left| \frac{a \Delta t}{h} B \right|, \end{aligned}$$

where B is a constant to be discussed at the end of this section. So, choose $\Delta t \leq \frac{h}{aB}$ to obtain

$$\frac{\partial \mathcal{H}}{\partial u_j^n} \geq 0.$$

Hence, the SPH Lax-Friedrichs method (4.87) is monotone for the wave equation. The restriction on Δt is similar to the famous Courant-Friedrichs-Lewy (CFL) condition. It specifies the values Δt can take not only to be monotone, but to ensure non-physical particle movement does not occur (such as particles crossing in one dimension). This result can be extended to the general conservation equation $u_t + [f(u)]_x = 0$ by letting $a(u) = f'(u)$ and rewriting the equation as $u_t + a(u) u_x = 0$. In this case, Δt must be chosen such that $\frac{a(u) \Delta t}{h} \leq \frac{1}{B}$ to obtain the monotone results.

Although the SPH Lax-Friedrichs method given above was shown to be monotone, in SPH a difference form of the SPH derivative is often used. So now a similar Lax-Friedrichs form can be derived for these methods. Let u be the function to be solved for and v be some other differentiable function then

$$\begin{aligned} (vu)' &= v u' + v' u \\ \text{so} \quad u' &= -\frac{1}{v} [u v' - (vu)'] \\ \text{then} \quad u'(x_i) &\approx -\sum_{j=1}^N \Delta x_j \frac{v_j}{v_i} (u_i - u_j) W'_{ij} . \end{aligned}$$

Note that v can be a constant function, in which case this reduces to simply adding zero to u' , to within the order of the method. For the field term use

$$\begin{aligned} u(x_i) &\approx \frac{1}{v_i} \langle vu \rangle_i \approx \sum_{j=1}^N \Delta x_j \frac{v_j}{v_i} u_j \bar{W}_{ij} \\ u(x_i) &\approx \frac{u_i}{v_i} \langle v \rangle_i \approx \sum_{j=1}^N \Delta x_j \frac{v_j}{v_i} u_i \bar{W}_{ij} \\ \text{so} \quad u(x_i) &\approx \sum_{j=1}^N \Delta x_j \frac{v_j}{v_i} \left(\frac{u_i + u_j}{2} \right) \bar{W}_{ij} . \end{aligned}$$

Then the Lax-Friedrichs type form for this SPH formulation is

$$u_i^{n+1} = \sum_{j=1}^N \Delta x_j \frac{v_j}{v_i} \left(\frac{u_i^n + u_j^n}{2} \right) \bar{W}_{ij} + a \Delta t \sum_{j=1}^N \Delta x_j \frac{v_j}{v_i} (u_i^n - u_j^n) W'_{ij} . \quad (4.88)$$

Let $\mathcal{H}(u_i)$ be the right hand side of equation (4.88) and investigate its monotonicity:

$$\begin{aligned} \frac{\partial \mathcal{H}}{\partial u_i^n} &= \frac{\Delta x_i}{2} \bar{W}_o + \sum_{j=1}^N \Delta x_j \frac{v_j}{v_i} \left(\frac{\bar{W}_{ij}}{2} + a \Delta t W'_{ij} \right) \\ \frac{\partial \mathcal{H}}{\partial u_j^n} &= \frac{\Delta x_j v_j}{2 v_i} (\bar{W}_{ij} - 2 a \Delta t W'_{ij}) . \end{aligned}$$

$W'_0 = 0$ is assumed to obtain the above equations. For this case choose $\Delta t \leq \frac{h}{2aB}$ to obtain

$$\frac{\partial \mathcal{H}}{\partial u_j^n} \geq 0.$$

This new requirement on Δt is half the original requirement (CFL number). Other Lax-Friedrichs type formulations are possible in SPH, but they are not developed in this dissertation. Instead, attention will now be given to the next type of monotone method.

4.3.2 General Monotone SPH Scheme. In this scheme zero is added, to within the order of the method, to an SPH formula to obtain a monotone method. Start with the one dimensional wave equation again, $u_t + au_x = 0$. Use the following forward time, SPH (in difference form) space

$$u_i^{n+1} = u_i^n + a \Delta t \sum_{j=1}^N \Delta x_j (u_i^n - u_j^n) W'_{ij}. \quad (4.89)$$

Also use the following approximations

$$\begin{aligned} u(x_i) &\approx \langle u \rangle_i \approx \sum_{j=1}^N \Delta x_j u_j \bar{W}_{ij} \\ u(x_i) &\approx u_i \langle 1 \rangle_i \approx \sum_{j=1}^N \Delta x_j u_i \bar{W}_{ij} \\ \text{so} \quad 0 &\approx - \sum_{j=1}^N \Delta x_j (u_i - u_j) \bar{W}_{ij}. \end{aligned} \quad (4.90)$$

Add equation (4.90) to equation (4.89), noting that \bar{W} and W do not have to be the same kernel, to obtain the new scheme

$$u_i^{n+1} = u_i^n - \sum_{j=1}^N \Delta x_j (u_i^n - u_j^n) \bar{W}_{ij} + a \Delta t \sum_{j=1}^N \Delta x_j (u_i^n - u_j^n) W'_{ij}. \quad (4.91)$$

Let $\mathcal{H}(u_i)$ be the right hand side of equation (4.91) and show that it is monotone

$$\frac{\partial \mathcal{H}}{\partial u_i^n} = 1 - \sum_{j=1}^N \Delta x_j \bar{W}_{ij} + a \Delta t \sum_{j=1}^N \Delta x_j W'_{ij} + \Delta x_i \bar{W}_o.$$

The first sum is approximately 1 and is exactly 1 as $h, \Delta x \rightarrow 0$. So 1 minus this sum is an $O(h^2, h\Delta x)$ term. The second sum is approximately 0 and is exactly zero as $h, \Delta x \rightarrow 0$ or if the particles are uniformly spaced and the kernel is even. This leaves the \bar{W}_o term which is positive and should be larger than the $O(h^2, h\Delta x)$ terms. The second partial derivative term (for $j \neq i$) is the same as for the original Lax-Friedrichs method

$$\frac{\partial \mathcal{H}}{\partial u_j^n} = \Delta x_j (\bar{W}_{ij} - a \Delta t W'_{ij}).$$

So this term will be positive under the same CFL condition given earlier, namely

$$\frac{a \Delta t}{h} \leq \frac{1}{B}$$

4.3.3 Kernels Ratio. A bound (B) on the ratio of the two kernels was used several times in this section and is now addressed in more detail here. Writing the kernel as $W(x, h) = \frac{1}{h} K(\frac{x}{h})$, the desired bound is

$$\frac{K'(u)}{K(u)} \leq B. \quad (4.92)$$

A natural question to ask is what happens if the two kernels are taken to be the same. For the most part the ratio provides a good bound, but as $u \rightarrow \kappa h$, the denominator will approach zero since the kernel is compactly supported. Even if the derivative also has compact support, using L'Hôpital's Rule shows that that $B \rightarrow \infty$. This will cause $\Delta t \rightarrow 0$ to ensure monotonicity. However, from an implementation point of view, if particle separation can be ensured not to cause a particle to be close to the edge of the support, the same kernel can be used.

A better idea is to use two different kernels. In Chapter VI, 18 kernels are studied, several of which are quite good and should give similar results. Since the denominator approaches zero near the support of \bar{K} , K' needs to have compact support. In addition, \bar{K}' should not be zero near κh . This can be generalized by requiring K to have compact support one derivative level higher than \bar{K} . To demonstrate this idea, use the B-Spline and Quartic-1 kernels for K and the Q-Gaussian and T-Gaussian kernels for \bar{K} . The definition of each of these kernels is found in Table 6.2 in Chapter VI. Define $\mathcal{B}(u) = -K'(u)/\bar{K}(u)$ and consider only $u \in [0, 2]$. The results are shown in Table 4.1.

K	\bar{K}	$\mathcal{B}(2)$	$B = \max \mathcal{B}$	u at max	$1/B$
Quartic-1	Q-Gaussian	0.0	7.272706	1.735403	0.1375
Quartic-1	T-Gaussian	0.0	3.449569	1.567588	0.289891
B-Spline	Q-Gaussian	0.0	4.541915	1.675131	0.220171
B-Spline	T-Gaussian	0.0	2.493523	1.325998	0.401039

Table 4.1 Examples of Kernels Ratio

As shown in the table, the ratio of two different kernels is well defined at all values. The last column ($1/B$) gives the CFL number. Note that for these examples $1/B$ is less than 1; but this number is not too low, especially for the last example.

4.4 Summary

The material in this chapter addressed the stability question from two sides. First, the linearized analysis addressed the question of the stability of current SPH schemes. Upon finding an unstable condition, four techniques were proposed to resolve that difficulty. Actually, techniques 1, 2, 2a, and 3 are all stabilizing without any restriction on the wavelength while techniques 3a and 4 are only conditionally stable. Second, the total variation analysis addressed the question of what is a highly stable SPH scheme. The *best* SPH scheme probably lies somewhere between the two.

The linearized analysis does not take the non-linearities of the equations into account and tries to minimize the changes necessary to obtain stability. This is because stability is often viewed as the opposite of accuracy, which is frequently not true. Also, because the current versions of SPH apparently do not have serious difficulties due to stability, only minor changes might be needed. This approach should assist the SPH users immediately. The cost of this approach is not considering major changes that might allow for better stability while maintaining accuracy (and conservation).

The total variation approach provides the opposite extreme. New schemes were developed, and these traded accuracy for significantly improved stability. Although these new schemes will probably not be used by themselves they are useful in hybrid schemes (see Chapter VIII), provide a stability baseline, introduce total variation notions to SPH, and provide the ability to "window-in" on the best methods.

V. CONVERGENCE

In this chapter, the consistency and stability results of the previous two chapters are used to obtain convergence results for SPH. Convergence is probably the most important concept in numerical analysis since it addresses how close a numerical solution is to the actual solution. Usually convergence theorems are proven using consistency and stability results; and that is the approach taken here.

In this chapter, a convergence theorem, taken from finite differences, is extended to SPH through the statement and proof of three new lemmas. The first lemma is used when only considering the kernel approximation. The second lemma is used for the entire SPH method, but assumes the function is at least piecewise continuous. The third lemma is an extension of the second when the function is only piecewise constant. Since these lemmas use the consistency results from Chapter III, they have the same restrictions as noted there. However, the most restrictive assumption, that Δx is equal to m/ρ is actually not important in the first two lemmas. Most of the work described here is based on the work of Lax and Wendroff (29). A good summary of convergence results for finite differences may be found in LeVeque (32).

The first section of this chapter details the convergence results from finite differences in a rather general fashion. The second section then states and proves the three lemmas allowing the finite difference work to be extended to SPH. To start, consider the initial value problem for the general conservation equation:

$$u_t + f(u)_x = 0 \quad (5.1)$$

$$u(x, 0) = u_o(x). \quad (5.2)$$

5.1 Finite Difference Approach

Consider the finite difference method written in conservation form

$$V_j^{n+1} = V_j^n - \frac{\Delta t}{\Delta x} [F(V^n; j) - F(V^n; j-1)], \quad (5.3)$$

where $F(V^n; j)$ is the numerical flux function more completely written $F(V_{j-p}^n, V_{j-p+1}^n, \dots, V_{j+q}^n)$ for some $p \geq 0$ and $q \geq 1$.

Definition 6 (Weak Solution) $u(x, t)$ is a weak solution of the conservation law (5.1) if the following holds for all test functions $\phi(x, t) \in C_0^1(\mathcal{R} \times \mathcal{R}^+)$

$$\int_0^\infty \int_{-\infty}^\infty [\phi_t u + \phi_x f(u)] dx dt = - \int_{-\infty}^\infty \phi(x, 0) u(x, 0) dx. \quad (5.4)$$

A discussion of weak and classical solutions to the general conservation equation is included in Chapter II; see that section for more information and references. The main theorem of this chapter is the Lax-Wendroff Theorem. The proof is not included here, but the three lemmas derived from this theorem later in this chapter are proved in a similar manner. See Lax (29) for the original proof.

Theorem 1 (Lax-Wendroff) Let $V_{\Delta x, \Delta t}(x, t)$ be a solution of (5.3), consistent with (5.1). Assume $V_{\Delta x, \Delta t}(x, t) \rightarrow V(x, t)$ as $\Delta x, \Delta t \rightarrow 0$, where the convergence is in a bounded a.e. sense. Then $V(x, t)$ is a weak solution of (5.1)–(5.2).

Although Lax and Wendroff are not specific about what they mean by “convergence in a bounded a.e. sense,” it is defined in this dissertation as follows:

Definition 7 A sequence of Lebesgue measurable functions, $\{f_i\}$, defined on a space \mathcal{L} , converges in a bounded almost everywhere (a.e.) sense to f if $|f_i(x)| < M(x)$ a.e. and $\lim_{i \rightarrow \infty} f_i = f$ a.e. using (the norm for \mathcal{L}).

(Reference Naylor and Sell (45))

The following theorem, definitions, and other ideas are needed from functional and real analysis. See Royden (51) or Naylor and Sell (45) for more information and proofs.

Theorem 2 (Compactness) *Let (X, d) be a metric space. Then the following statements are equivalent:*

- (X, d) is compact
- (X, d) is sequentially compact
- (X, d) is complete and totally bounded

Definition 8 (Sequentially Compact) *A metric space (X, d) is said to be sequentially compact if every sequence in (X, d) contains a convergent subsequence.*

Definition 9 *The space $L_{1,T}$ is an extension on the Lebesgue space, L_1 , for functions of both time and space where*

$$L_{1,T} = \{u : \|u\|_{1,T} < \infty\} \quad (5.5)$$

$$\|u\|_{1,T} = \int_0^T \int_{-\infty}^{\infty} |u(x, t)| dx dt . \quad (5.6)$$

Definition 10 $TV_T(u)$ is an extension of the total variation function, $TV(u)$, for functions u of both time and space. It is defined as

$$\begin{aligned} TV_T(u) = & \limsup_{\epsilon \rightarrow 0} \frac{1}{\epsilon} \int_0^T \int_{-\infty}^{\infty} |u(x + \epsilon, t) - u(x, t)| dx dt \\ & + \limsup_{\epsilon \rightarrow 0} \frac{1}{\epsilon} \int_0^T \int_{-\infty}^{\infty} |u(x, t + \epsilon) - u(x, t)| dx dt . \end{aligned}$$

Definition 11 *The notation, $\text{supp}_x(u)$, is used to identify the support of the function $u(x, t)$ with respect to the x variable.*

With these theorems, definitions and the material in the Chapter II, a convergence result (Theorem 3) is obtained. Consider the following domain where B , R , and T are positive constants

$$\mathcal{D} = \{u \in L_{1,T} : TV_T(u) \leq B \text{ and } \text{supp}_x(u) \subset [-R, R] \forall t \in [0, T]\} .$$

It can be shown that \mathcal{D} is a compact set. Now for the convergence definition, theorem and outline of the proof. These ideas are taken from LeVeque (32).

Definition 12 (Convergence) *Let \mathcal{W} be the set of all weak solutions to the conservation law and let $\text{dist}(V, \mathcal{W})$, the distance from a function V to the set, be defined as*

$$\text{dist}(V, \mathcal{W}) = \inf_{w \in \mathcal{W}} \|V - w\|_{1,T}.$$

Then by convergence we mean

$$\text{dist}(V_\kappa, \mathcal{W}) \rightarrow 0 \quad \text{as } \kappa \rightarrow 0.$$

LeVeque makes the following comment in regards to the convergence definition. "There is no guarantee that $\|V_\kappa - w\|_{1,T} \rightarrow 0$ as $\kappa \rightarrow 0$ for any fixed weak solution $w(x, t)$. The computed V_κ might be close to one weak solution for one value of κ and close to a completely different weak solution for a slightly smaller value of the time step κ ." (32:159) He states further that "what the convergence tells us is by taking a fine enough grid, we can be guaranteed of being arbitrarily close to some weak solution." (32:159) Under this definition, uniqueness can be a concern as is addressed in the note after the proof of Theorem 3.

Theorem 3 (Convergence) *If $V_\kappa(x, t)$ is a solution to (5.3), consistent with (5.1), in conservation form, has a Lipschitz continuous numerical flux, and is contained in the domain \mathcal{D} then $V_\kappa(x, t)$ converges to a weak solution of (5.1). (Reference LeVeque (32))*

An outline of the convergence proof is as follows. Define \mathcal{W} as the set of all weak solutions to the conservation law. Assume V_κ does not converge to any $w \in \mathcal{W}$. Then there is some $\epsilon > 0$ and some sequence of approximations $\{V_{\kappa_1}, V_{\kappa_2}, \dots\}$ such

that $\kappa_j \rightarrow 0$ as $j \rightarrow \infty$ while

$$\text{dist}(V_{\kappa_j}, \mathcal{W}) = \inf_{w \in \mathcal{W}} \|V_{\kappa_j} - w\|_{1,T} > \epsilon \quad \text{for all } j. \quad (5.7)$$

That is, let ϵ be as chosen previous to equation (5.7). Then there exists $0 < k_1$ such that $\text{dist}(V_{k_1}, \mathcal{W}) > \epsilon$. Next choose $0 < k_2 < k_1$ such that $\text{dist}(V_{k_2}, \mathcal{W}) > \epsilon$. Finally choose $0 < k_{l+1} < k_l$ such that $\text{dist}(V_{k_{l+1}}, \mathcal{W}) > \epsilon$. Therefore the distance of $\hat{V}_l = V_{k_l}$ from \mathcal{W} is larger than ϵ for all l . Because $\hat{V}_l \in \mathcal{D}$, a compact metric space, by the compactness theorem this sequence must have a convergent subsequence, $\{\hat{V}_{l_m}\}$, converging to some function $V \in \mathcal{D}$. Then, far enough out in the subsequence

$$\|\hat{V}_{l_m} - V\|_{1,T} < \epsilon \quad \text{for sufficiently large } m. \quad (5.8)$$

Further, by applying the Lax-Wendroff Theorem on this subsequence, the result that V must be a weak solution of the conservation law is obtained, ie. $V \in \mathcal{W}$. But each \hat{V}_{l_m} is one of the V_{k_l} 's. This implies for large enough m , $\text{dist}(\hat{V}_{l_m}, \mathcal{W}) > \epsilon$ and $\text{dist}(\hat{V}_{l_m}, w) < \epsilon$. This is a contradiction, so the original assumption that the arbitrary sequence V_{κ} does not converge to a weak solution is false; and the proof is complete.

Note: the above work only guarantees convergence to some weak solution, not a unique weak solution. For uniqueness an additional requirement, such as consistency with an entropy condition, must be imposed. See equations (2.17)–(2.18) and surrounding material in the Chapter II regarding the entropy condition.

5.2 SPH Extensions

The convergence ideas just discussed are now extended to SPH. This is done by stating and proving three lemmas, derived from the Lax-Wendroff Theorem. Start

with the kernel approximation form

$$\dot{u} = -Rf(u) \quad \text{for } u(x, t) \in C_*(\Omega \times [0, T]) \quad (5.9)$$

$$\text{where} \quad Rf(u(x, t)) = \int_{\Omega} f(u(x_o, t)) W'(x - x_o) dx_o.$$

C_* is the space of piecewise continuous functions and Ω is the spatial domain of u . Since only one dimensional problems are considered here, Ω is simply an interval on the real line.

Lemma 3 (Kernel Approximation) *Let $u_h(x, t)$ be a solution of (5.9), consistent with (5.1). Assume $\exists u(x, t)$ such that $u_h(x, t) \rightarrow u(x, t)$ as $h \rightarrow 0$ in a bounded a.e. sense. Then $u(x, t)$ is a weak solution of (5.1)–(5.2).*

Proof. Let $\phi(x, t) \in C_0^1(\mathcal{R} \times \mathcal{R}^+)$ and $u_h(x, t)$ be a solution of (5.9). Multiply equation (5.9) by $\phi(x, t)$ and integrate over all time and space

$$\begin{aligned} \int_0^\infty \int_{-\infty}^\infty \phi(x, t) \frac{\partial}{\partial t} u_h(x, t) dx dt \\ = - \int_0^\infty \int_{-\infty}^\infty \phi(x, t) \int_{\Omega} f(u_h(x_o, t)) \frac{\partial}{\partial x} W(x - x_o) dx_o dx dt. \end{aligned} \quad (5.10)$$

Since ϕ has compact support, there exist positive constants τ and r such that

$$\phi(x, t) = 0 \quad \forall x \in \mathcal{R} \text{ when } t \geq \tau \quad (5.11)$$

$$\phi(x, t) = 0 \quad \forall t \in \mathcal{R}^+ \text{ when } |x| \geq r, \quad (5.12)$$

ie. ϕ is only non-zero in the box $\{[-r, r] \times [0, \tau]\}$. Therefore in the integrals to follow, the integrals are actually not taken over an infinite domain, but a finite domain.

First, consider the left hand side of equation (5.10). Change the order of integration, integrate by parts, simplify using the compact support of ϕ , and change the order of integration back again. Changing the order of integration is justified

considering the compact support of ϕ and the Fubini Theorem:

$$\begin{aligned}
\int_0^\infty \int_{-\infty}^\infty \phi(x, t) \frac{\partial}{\partial t} u_h(x, t) dx dt &= \int_{-\infty}^\infty \int_0^\infty \phi(x, t) \frac{\partial}{\partial t} u_h(x, t) dt dx \\
&= \int_{-\infty}^\infty \left\{ \phi(x, t) u_h(x, t) \Big|_{t=0}^\infty - \int_0^\infty \frac{\partial}{\partial t} \phi(x, t) u_h(x, t) dt \right\} dx \\
&= - \int_{-\infty}^\infty \phi(x, 0) u_h(x, 0) dx - \int_{-\infty}^\infty \int_0^\infty \phi_t(x, t) u_h(x, t) dt dx \\
&= - \int_{-\infty}^\infty \phi(x, 0) u_h(x, 0) dx - \int_0^\infty \int_{-\infty}^\infty \phi_t(x, t) u_h(x, t) dx dt . \quad (5.13)
\end{aligned}$$

Second, consider the right hand side of equation (5.10). Change the order of the inner integration, integrate by parts, simplify using the compact support of ϕ , and change the order of integration back again. Once again, changing the order of integration is allowed based on note regarding the compact support of ϕ earlier and the Fubini Theorem:

$$\begin{aligned}
- \int_0^\infty \int_{-\infty}^\infty \phi(x, t) \int_\Omega f(u_h(x_o, t)) \frac{\partial}{\partial x} W(x - x_o) dx_o dx dt \\
&= - \int_0^\infty \int_\Omega f(u_h(x_o, t)) \int_{-\infty}^\infty \phi(x, t) \frac{\partial}{\partial x} W(x - x_o) dx dx_o dt \\
&= - \int_0^\infty \int_\Omega f(u_h(x_o, t)) \left\{ \phi(x, t) W(x - x_o) \Big|_{x=-\infty}^\infty \right. \\
&\quad \left. - \int_{-\infty}^\infty \frac{\partial}{\partial x} \phi(x, t) W(x - x_o) dx \right\} dx_o dt \\
&= \int_0^\infty \int_\Omega f(u_h(x_o, t)) \int_{-\infty}^\infty \phi_x(x, t) W(x - x_o) dx dx_o dt \\
&= \int_0^\infty \int_{-\infty}^\infty \phi_x(x, t) \int_\Omega f(u_h(x_o, t)) W(x - x_o) dx_o dx dt . \quad (5.14)
\end{aligned}$$

Put the two sides of equation (5.10) back together (from equations (5.13) and (5.14)) to obtain

$$\begin{aligned}
- \int_{-\infty}^\infty \phi(x, 0) u_h(x, 0) dx &= \int_0^\infty \int_{-\infty}^\infty \left\{ \phi_t(x, t) u_h(x, t) \right. \\
&\quad \left. + \phi_x(x, t) \int_\Omega f(u_h(x_o, t)) W(x - x_o) dx_o \right\} dx dt . \quad (5.15)
\end{aligned}$$

For the first term in equation (5.15) the following is developed. By the assumption that u_h converges in bounded a.e. sense, $u_h(x) < M(x)$ a.e. Then there exist Lebesgue integrable functions $g = M|\phi|$, $f_h = \phi u_h$, and $f = \phi u$. Further since ϕ is continuous, f_h converges to f a.e. Then apply the Lebesgue Dominated Convergence Theorem ($\lim_{h \rightarrow 0} \int f_h = \int \lim_{h \rightarrow 0} f_h = \int f$) to obtain

$$\begin{aligned} \lim_{h \rightarrow 0} \left[- \int_{-\infty}^{\infty} \phi(x, 0) u_h(x, 0) dx \right] &= - \int_{-\infty}^{\infty} \lim_{h \rightarrow 0} [(\phi(x, 0) u_h(x, 0))] dx \\ &= - \int_{-\infty}^{\infty} \phi(x, 0) u(x, 0) dx . \end{aligned}$$

The second term in equation (5.15) is handled similarly

$$\int_0^{\infty} \int_{-\infty}^{\infty} \phi_t(x, t) u_h(x, t) dx dt \longrightarrow \int_0^{\infty} \int_{-\infty}^{\infty} \phi_t(x, t) u(x, t) dx dt \quad \text{as } h \rightarrow 0 .$$

From consistency

$$\int_{\Omega} f(u_h(x_o, t)) W(x - x_o) dx_o = f(u_h(x, t)) + h^2 e_k ,$$

where $e_k = \frac{\kappa^2}{2} \sup_{\xi \in \Omega} |f''(\xi)|$. If f is Lipschitz continuous, and since $u_h \rightarrow u$ in a bounded a.e. sense, then $f(u_h)$ is bounded and $f(u_h) \rightarrow f(u)$ a.e. Then apply the Lebesgue Dominated Convergence Theorem on the last term

$$\begin{aligned} \lim_{h \rightarrow 0} \int_0^{\infty} \int_{-\infty}^{\infty} \phi_x(x, t) \int_{\Omega} f(u_h(x_o, t)) W(x - x_o) dx_o dx dt \\ = \lim_{h \rightarrow 0} \int_0^{\infty} \int_{-\infty}^{\infty} \phi_x(x, t) [f(u_h(x, t)) + h^2 e_k] dx dt \\ = \int_0^{\infty} \int_{-\infty}^{\infty} \phi_x(x, t) f(u(x, t)) dx dt . \end{aligned}$$

Therefore, conclude from equation (5.15) that

$$\int_0^{\infty} \int_{-\infty}^{\infty} [\phi_t(x, t) u(x, t) + \phi_x(x, t) f(u)] dx dt = - \int_{-\infty}^{\infty} \phi(x, 0) u(x, 0) dx . \quad (5.16)$$

Since equation (5.16) holds for any test function ϕ , u is a weak solution of (5.1).

□

The second extension of the Lax-Wendroff ideas to SPH addresses the particle approximation form

$$\dot{u} = -S'f(u) \quad \text{where } S'f(u(x_i, t)) = \sum_{j=1}^N \Delta x_j f(u(x_j, t)) W'(x_i - x_j). \quad (5.17)$$

Lemma 4 (Continuous Particle Approximation) *Let $u_h(x, t) \in C_*(\Omega \times [0, T])$ be piecewise continuous and a solution of (5.17), consistent with (5.1). Assume $\exists u(x, t)$ such that $u_h(x, t) \rightarrow u(x, t)$ as $h \rightarrow 0, \Delta x \rightarrow 0$ in a bounded a.e. sense. Then $u(x, t)$ is a weak solution of (5.1)–(5.2).*

Proof. Let $\phi(x, t) \in C_0^1(\mathcal{R} \times \mathcal{R}^+)$ and $u_h(x, t)$ be a solution of (5.17). Multiply equation (5.17) by $\phi(x, t)$ and integrate over all time and space

$$\begin{aligned} \int_0^\infty \int_{-\infty}^\infty \phi(x, t) \frac{\partial}{\partial t} u_h(x, t) dx dt \\ = - \int_0^\infty \int_{-\infty}^\infty \phi(x, t) \sum_{j=1}^N \Delta x_j f(u_h(x_j, t)) \frac{\partial}{\partial x} W(x - x_j) dx dt. \end{aligned} \quad (5.18)$$

As in the proof of the previous lemma, take note of the compact support of ϕ and will use equations (5.11) and (5.12) in this proof.

First, consider the left hand side of equation (5.18). Note this is exactly the same as in the proof for the last lemma. Therefore, the same steps will be done and not shown here. Namely, change the order of integration, integrate by parts, simplify using the compact support of ϕ , and change the order of integration back again

$$\begin{aligned} \int_0^\infty \int_{-\infty}^\infty \phi(x, t) \frac{\partial}{\partial t} u_h(x, t) dx dt \\ = - \int_{-\infty}^\infty \phi(x, 0) u_h(x, 0) dx - \int_0^\infty \int_{-\infty}^\infty \phi_t(x, t) u_h(x, t) dx dt. \end{aligned} \quad (5.19)$$

Second, consider the right hand side of equation (5.18). Change the order of the inner integration and summation, integrate by parts, simplify using the compact support of ϕ , and change the order back again. As in the previous proof, use equations (5.11) and (5.12) to justify changing the order of integration and summation:

$$\begin{aligned}
& - \int_0^\infty \int_{-\infty}^\infty \phi(x, t) \sum_{j=1}^N \Delta x_j f(u_h(x_j, t)) \frac{\partial}{\partial x} W(x - x_j) dx dt \\
&= - \int_0^\infty \sum_{j=1}^N \Delta x_j f(u_h(x_j, t)) \int_{-\infty}^\infty \phi(x, t) \frac{\partial}{\partial x} W(x - x_j) dx dt \\
&= - \int_0^\infty \sum_{j=1}^N \Delta x_j f(u_h(x_j, t)) \left\{ \phi(x, t) W(x - x_j) \Big|_{x=-\infty}^\infty \right. \\
&\quad \left. - \int_{-\infty}^\infty \frac{\partial}{\partial x} \phi(x, t) W(x - x_j) dx \right\} dt \\
&= \int_0^\infty \sum_{j=1}^N \Delta x_j f(u_h(x_j, t)) \int_{-\infty}^\infty \phi_x(x, t) W(x - x_j) dx dt \\
&= \int_0^\infty \int_{-\infty}^\infty \phi_x(x, t) \left[\sum_{j=1}^N \Delta x_j f(u_h(x_j, t)) W(x - x_j) \right] dx dt. \quad (5.20)
\end{aligned}$$

Put the two sides of equation (5.18) back together (from equations (5.19) and (5.20)) to obtain

$$\begin{aligned}
- \int_{-\infty}^\infty \phi(x, 0) u_h(x, 0) dx &= \int_0^\infty \int_{-\infty}^\infty \left\{ \phi_t(x, t) u_h(x, t) + \phi_x(x, t) \right. \\
&\quad \left. \times \left[\sum_{j=1}^N \Delta x_j f(u_h(x_j, t)) W(x - x_j) \right] \right\} dx dt. \quad (5.21)
\end{aligned}$$

As in the proof of the previous lemma, by the assumption that $u_h \rightarrow u$ in a bounded a.e. sense, use the Lebesgue Dominated Convergence Theorem on the first and second terms in equation (5.21) to obtain

$$- \int_{-\infty}^\infty \phi(x, 0) u(x, 0) dx$$

and

$$\int_0^\infty \int_{-\infty}^\infty \phi_t(x, t) u(x, t) dx dt$$

respectively as $h \rightarrow 0$. From consistency

$$\begin{aligned} \sum_{j=1}^N \Delta x_j f(u_h(x_j, t)) W(x - x_j) &= \int_{\Omega} f(u_h(x_o, t)) W(x - x_o) dx_o + h \Delta x e_r \\ &= f(u_h(x, t)) + h^2 e_k + h \Delta x e_r, \end{aligned}$$

where $e_k = \frac{\kappa^2}{2} \sup_{\xi \in \Omega} |f''(\xi)|$ and $e_r = \frac{\kappa_0}{2} \sup_{\xi \in \Omega} |[f(\xi)W(x - \xi)]'|$. Since $u_h \rightarrow u$ in a bounded a.e. sense and f is Lipschitz continuous, as in the proof of the last lemma as $h \rightarrow 0$ and $\Delta x \rightarrow 0$ the last term becomes

$$\begin{aligned} \lim_{h \rightarrow 0} \lim_{\Delta x \rightarrow 0} \int_0^\infty \int_{-\infty}^\infty \phi_x(x, t) \left[\sum_{j=1}^N \Delta x_j f(u_h(x_j, t)) W(x - x_j) \right] dx dt \\ = \lim_{h \rightarrow 0} \lim_{\Delta x \rightarrow 0} \int_0^\infty \int_{-\infty}^\infty \phi_x(x, t) [f(u_h(x, t)) + h^2 e_k + h \Delta x e_r] dx dt \\ = \int_0^\infty \int_{-\infty}^\infty \phi_x(x, t) f(u(x, t)) dx dt. \end{aligned}$$

Therefore conclude from equation (5.21) that

$$\int_0^\infty \int_{-\infty}^\infty [\phi_t(x, t) u(x, t) + \phi_x(x, t) f(u)] dx dt = - \int_{-\infty}^\infty \phi(x, 0) u(x, 0) dx. \quad (5.22)$$

Since equation (5.22) holds for any test function ϕ , u is a weak solution of (5.1).

□

The third extension of the Lax-Wendroff ideas to SPH also addresses the particle approximation form (5.17). However, at this time instead of assuming that $u_h(x, t)$ is continuous (piecewise), assume it is only grid function in x .

Definition 13 (Grid Function) $u_h(x, t)$ is a grid function in x if it is a piecewise constant function defined at the grid points and constant in a region around each grid point.

Sometimes a grid function is defined as a linear interpolation between the grid points instead of simply constant. In that case, the previous lemma would apply. However, the piecewise constant notion of a grid function is maintained here.

Lemma 5 (Discrete Particle Approximation) *Let $u_h(x, t)$, a grid function in x , be a solution of (5.17), consistent with (5.1). Assume $\exists u(x, t)$ such that $u_h(x, t) \rightarrow u(x, t)$ as $h \rightarrow 0, \Delta x \rightarrow 0$ in a bounded a.e. sense, using the $L_{1,T}$ norm given in equation (5.6) (ie. $\int_0^T \int_{-\infty}^{\infty} |u_h(x, t) - u(x, t)| dx dt \rightarrow 0$). Then $u(x, t)$ is a weak solution of (5.1)-(5.2).*

Proof. Let $\phi(x, t) \in C_0^1(\mathcal{R} \times \mathcal{R}^+)$ and $u_h(x_i, t)$ be a solution of (5.17). Multiply equation (5.17) by $\Delta x_i \phi(x_i, t)$, sum over all space, and integrate over time:

$$\begin{aligned} \int_0^\infty \sum_{i=-\infty}^{\infty} \Delta x_i \phi(x_i, t) \frac{\partial}{\partial t} u_h(x_i, t) dt &= - \int_0^\infty \sum_{i=-\infty}^{\infty} \Delta x_i \phi(x_i, t) \\ &\quad \times \sum_{j=1}^N \Delta x_j f(u_h(x_j, t)) W'(x_i - x_j) dt. \end{aligned} \quad (5.23)$$

As with the last two lemmas, use the compact support of ϕ and the relationships shown in equations (5.11) and (5.12) in this proof to deal with only finite domains.

First, consider the left hand side of equation (5.23). Change the order of integration and summation, integrate by parts, simplify using the compact support of ϕ , and change the order back again. As in the previous two proofs, use equations (5.11) and (5.12) to justify changing the order of integration:

$$\begin{aligned} \int_0^\infty \sum_{i=-\infty}^{\infty} \Delta x_i \phi(x_i, t) \frac{\partial}{\partial t} u_h(x_i, t) dt &= \sum_{i=-\infty}^{\infty} \Delta x_i \int_0^\infty \phi(x_i, t) \frac{\partial}{\partial t} u_h(x_i, t) dt \\ &= \sum_{i=-\infty}^{\infty} \Delta x_i \left\{ \phi(x_i, t) u_h(x_i, t) \Big|_{t=0}^\infty - \int_0^\infty \frac{\partial}{\partial t} \phi(x_i, t) u_h(x_i, t) dt \right\} \\ &= - \sum_{i=-\infty}^{\infty} \Delta x_i \phi(x_i, 0) u_h(x_i, 0) - \sum_{i=-\infty}^{\infty} \Delta x_i \int_0^\infty \phi_t(x_i, t) u_h(x_i, t) dt \end{aligned}$$

$$= - \sum_{i=-\infty}^{\infty} \Delta x_i \phi(x_i, 0) u_h(x_i, 0) - \int_0^{\infty} \sum_{i=-\infty}^{\infty} \Delta x_i \phi_t(x_i, t) u_h(x_i, t) dt. \quad (5.24)$$

A process known as summation-by-parts is needed in the next step. It is the discrete analogue to integration-by-parts. Since it is not widely used, a demonstration how it works is provided. For sequences $\{a_i\}$ and $\{b_i\}$ and positive constant R

$$\begin{aligned} \sum_{i=-R}^R a_i (b_{i+1} - b_{i-1}) &= \sum_{i=-R}^R a_i b_{i+1} - \sum_{i=-R}^R a_i b_{i-1} = \sum_{i=-R+1}^{R+1} a_{i-1} b_i - \sum_{i=-R-1}^{R-1} a_{i+1} b_i \\ &= - \sum_{i=-R}^R (a_{i+1} - a_{i-1}) b_i \\ &\quad + a_R b_{R+1} - a_{-R-1} b_{-R} - a_{-R} b_{-R-1} + a_{R+1} b_R. \end{aligned}$$

Now, consider the right hand side of equation (5.23). Change the order of the inner summation, use the definition of the derivative, sum by parts, simplify using the compact support of ϕ , and change the order back again. As before, use equations (5.11) and (5.12) to justify changing the order of summation. Also note: assume that $\Delta x_i = (\Delta x_{i+1} - \Delta x_{i-1})/2$ (see equation (3.17) for consistency). This is used before and after the summation-by-parts to allow that process to work as demonstrated above:

$$\begin{aligned} & - \int_0^{\infty} \sum_{i=-\infty}^{\infty} \Delta x_i \phi(x_i, t) \sum_{j=1}^N \Delta x_j f(u_h(x_j, t)) W'(x_i - x_j) dt \\ &= - \int_0^{\infty} \sum_{j=1}^N \Delta x_j f(u_h(x_j, t)) \left[\sum_{i=-\infty}^{\infty} \Delta x_i \phi(x_i, t) W'(x_i - x_j) \right] dt \\ &= - \int_0^{\infty} \sum_{j=1}^N \Delta x_j f(u_h(x_j, t)) \left\{ \sum_{i=-\infty}^{\infty} \Delta x_i \phi(x_i, t) \right. \\ &\quad \times \left[\frac{W(x_{i+1} - x_j) - W(x_{i-1} - x_j)}{x_{i+1} - x_{i-1}} + O(\Delta x^2) \right] \left. \right\} dt \end{aligned}$$

$$\begin{aligned}
&= \int_0^\infty \sum_{j=1}^N \Delta x_j f(u_h(x_j, t)) \left\{ \sum_{i=-\infty}^\infty \Delta x_i \left[\frac{\phi(x_{i+1}, t) - \phi(x_{i-1}, t)}{x_{i+1} - x_{i-1}} \right. \right. \\
&\quad \left. \left. + O(\Delta x^2) \right] W(x_i - x_j) \right\} dt \\
&= \int_0^\infty \sum_{i=-\infty}^\infty \Delta x_i \left[\frac{\phi(x_{i+1}, t) - \phi(x_{i-1}, t)}{x_{i+1} - x_{i-1}} + O(\Delta x^2) \right] \\
&\quad \times \left[\sum_{j=1}^N \Delta x_j f(u_h(x_j, t)) W(x_i - x_j) \right] dt . \tag{5.25}
\end{aligned}$$

Put the two sides of equation (5.23) back together (from equations (5.24) and (5.25)) to obtain

$$\begin{aligned}
-\sum_{i=-\infty}^\infty \Delta x_i \phi(x_i, 0) u_h(x_i, 0) &= \int_0^\infty \sum_{i=-\infty}^\infty \Delta x_i \left\{ \phi_t(x_i, t) u_h(x_i, t) \right. \\
&\quad \left. + \left[\frac{\phi(x_{i+1}, t) - \phi(x_{i-1}, t)}{x_{i+1} - x_{i-1}} + O(\Delta x^2) \right] \left[\sum_{j=1}^N \Delta x_j f(u_h(x_j, t)) W(x_i - x_j) \right] \right\} dt . \tag{5.26}
\end{aligned}$$

Note by definition of the Riemann integral that the sums in the first two terms in equation (5.26) can be replaced by integrals as $\Delta x \rightarrow 0$. Also as in the proof of the previous two lemmas, by the assumption that $u_h \rightarrow u$ in a bounded a.e. sense, the first and second terms in equation (5.26) become respectively

$$\begin{aligned}
\lim_{h \rightarrow 0} \lim_{\Delta x \rightarrow 0} \left[- \sum_{i=-\infty}^\infty \Delta x_i \phi(x_i, 0) u_h(x_i, 0) \right] &= \lim_{h \rightarrow 0} \left[- \int_{-\infty}^\infty \phi(x, 0) u_h(x, 0) dx \right] \\
&= - \int_{-\infty}^\infty \phi(x, 0) u(x, 0) dx
\end{aligned}$$

and

$$\begin{aligned}
\lim_{h \rightarrow 0} \lim_{\Delta x \rightarrow 0} \int_0^\infty \sum_{i=-\infty}^\infty \Delta x_i \phi_t(x_i, t) u_h(x_i, t) dt &= \lim_{h \rightarrow 0} \int_0^\infty \int_{-\infty}^\infty \phi_t(x, t) u_h(x, t) dx dt \\
&= \int_0^\infty \int_{-\infty}^\infty \phi_t(x, t) u(x, t) dx dt .
\end{aligned}$$

From the definition of the derivative

$$\frac{\phi(x_{i+1}, t) - \phi(x_{i-1}, t)}{x_{i+1} - x_{i-1}} = \phi_x(x, t) + O(\Delta x^2),$$

and from the Consistency Chapter (III)

$$\begin{aligned} \sum_{j=1}^N \Delta x_j f(u_h(x_j, t)) W(x - x_j) &= \int_{\Omega} f(u_h(x_o, t)) W(x - x_o) dx_o + h \Delta x e_r \\ &= f(u_h(x, t)) + h^2 e_k + h \Delta x e_r, \end{aligned}$$

where $e_k = \frac{\kappa^2}{2} \sup_{\xi \in \Omega} |f''(\xi)|$ and $e_r = \frac{\kappa_1}{2} \sup_{\xi \in \Omega} | [f(\xi)W(x - \xi)]' |$. So the third term in equation (5.26) becomes

$$\begin{aligned} \int_0^\infty \sum_{i=-\infty}^\infty \Delta x_i \left[\frac{\phi(x_{i+1}, t) - \phi(x_{i-1}, t)}{x_{i+1} - x_{i-1}} + O(\Delta x^2) \right] \\ \times \left[\sum_{j=1}^N \Delta x_j f(u_h(x_j, t)) W(x_i - x_j) \right] dt \\ = \int_0^\infty \sum_{i=-\infty}^\infty \Delta x_i \phi_x(x_i, t) f(u_h(x_i, t)) dt \\ + \int_0^\infty \sum_{i=-\infty}^\infty \Delta x_i \left[\phi_x(x_i, t) O(h \Delta x, h^2) + f(u_h(x_i, t)) O(\Delta x^2) \right] dt. \end{aligned}$$

Then obtain

$$\begin{aligned} \lim_{\Delta x \rightarrow 0} \left\{ \int_0^\infty \sum_{i=-\infty}^\infty \Delta x_i \phi_x(x_i, t) f(u_h(x_i, t)) dt \right. \\ \left. + \int_0^\infty \sum_{i=-\infty}^\infty \Delta x_i \left[\phi_x(x_i, t) O(h \Delta x, h^2) + f(u_h(x_i, t)) O(\Delta x^2) \right] dt \right\} \\ = \int_0^\infty \int_{-\infty}^\infty \phi_x(x, t) f(u_h(x, t)) dx dt + \int_0^\infty \int_{-\infty}^\infty \phi_x(x, t) O(h^2) dx dt. \end{aligned}$$

Then using $u_h \rightarrow u$ in a bounded a.e. sense and f is Lipshitz continuous, this last term becomes

$$\begin{aligned} \lim_{h \rightarrow 0} \left[\int_0^\infty \int_{i=-\infty}^\infty \phi_x(x, t) f(u_h(x, t)) dx dt + \int_0^\infty \int_{i=-\infty}^\infty \phi_x(x, t) O(h^2) dx dt \right] \\ = \int_0^\infty \int_{i=-\infty}^\infty \phi_x(x, t) f(u(x, t)) dx dt . \end{aligned}$$

Therefore conclude from equation (5.26) as $h \rightarrow 0, \Delta x \rightarrow 0$

$$\int_0^\infty \int_{-\infty}^\infty [\phi_t(x, t) u(x, t) + \phi_x(x, t) f(u)] dx dt = - \int_{-\infty}^\infty \phi(x, 0) u(x, 0) dx . \quad (5.27)$$

Since equation (5.27) holds for any test function ϕ , u is a weak solution of (5.1).

□

5.3 Summary

The proof of the convergence theorem (Theorem 3) given earlier in this chapter from LeVeque relied on set theory and the Lax-Wendroff theorem and not the numerical technique (other than consistency). Hence, the convergence theorem is applicable to SPH as long as a suitable replacement for the Lax-Wendroff theorem is available, since it relies on the specific method (finite differences). The three lemmas that were stated and proved in the last section are such replacements in SPH for the Lax-Wendroff theorem. Therefore under the assumptions of the convergence theorem and the applicable lemma, SPH will converge to a weak solution of the general conservation equation.

VI. KERNELS

In this chapter the key element of the SPH method, the kernel function, is discussed. The kernel plays major roles in consistency (the kernel approximation) and stability (the *PW''* instability and several stabilizing techniques). Hence, it is key to the convergence as well based on the previous chapter. In addition to these more mathematical properties, the kernel affects accuracy; a primary concern of all those using SPH. Although the method is $O(h^2, h\Delta x)$, when h , or Δx are not very small the coefficients of these error terms can become quite important. Those coefficients are controlled by the function being approximated and the kernel. Since the function is, to some extent, a uncontrollable factor and the kernel is easily changed, the kernel becomes a primary factor in accuracy.

The material covered in this chapter involves two areas. First, is the properties of the kernel, which include discussions on the kernel requirement, higher order kernels, and the smoothing length. Second, is a comparison of several kernels. It is this second area that the major contributions are found. This includes the development of measures of merit for kernels and both qualitative and quantitative comparisons of kernels. The results lend insight into the kernel under given assumptions while the measures of merit are general enough so that they can be used under many different assumptions.

6.1 Kernel Properties

In this section some of the basic properties are discussed. These include a list of requirements for a function to be considered an SPH kernel, making kernels higher order, and the smoothing length. Much of this work takes the form of literature review mixed with filling in the details that are lacking.

6.1.1 Kernel Requirements. Many different kernels have been used in SPH as shown in various journal articles. To some extent it should not matter which kernel is used. However, Monaghan's first golden rule of SPH is "if you want to find a physical interpretation of an SPH equation it is always best to assume the kernel is a Gaussian." (44:545) Throughout this dissertation various rules and requirements are applied to the kernel. These are summarized below

- The kernel should be normalized: $\int_{\Omega} W(u) du = 1$
- The kernel should be even (symmetric). This is required to obtain a second order method.
- The kernel should have compact support. In general the support is defined in terms of h and κ . h is a measure of the width of the kernel and provides a standard distance and unit to use. It may be changed from particle to particle. κ is a constant for each kernel that determines the spread of a particular kernel in terms of h . So, define $W(u, h) = 0$ for $|u| \geq \kappa h$.
- The kernel should be sufficiently smooth. For the function approximation it needs to be continuous. For the derivative approximation it also needs to be continuous, but better results will be obtained if it has a continuous first derivative. For linear stability analysis it is necessary to have one order of smoothness higher than listed here.
- The kernel should be of the form $W(x, h) = \frac{1}{h^d} K(\frac{|x|}{h})$ where d is the dimension (1, 2, or 3). Although there does not appear to be a pressing need for this form, it simplifies the choice of kernels and allows the application of distribution theory. Note: the normalization constant is sometimes pulled outside of $K(u)$ so that only the coefficients of K change from one dimension to another. To accommodate this, the notation $K(u) = c_n \tilde{K}(u)$ is used here.
- The kernel should be positive. This is only required if the kernel is being treated as from a Delta Family in distribution theory (see Stakgold (58)). However,

it is also desirable in many cases, especially when performing the function approximation to ensure non-physical results do not occur.

Any function that meets the rules above can be used as an SPH kernel. Note: later in this chapter the requirement that $K'(0) = 0$ is employed. Although not required it appears that this is a good choice for accuracy concerns.

6.1.2 Higher Order Kernels. For the most part, SPH is considered an $O(h^2)$ method. However, it is possible to obtain higher order estimates, just as in finite differences. First, the kernel approximation can be made of order $O(h^4)$ by requiring equation (6.1) to hold:

$$\int_{\Omega} u^2 W(u, h) du = 0. \quad (6.1)$$

When errors were discussed in Chapter III earlier, the terms involving u and u^3 vanished when W was even. So when equation (6.1) holds, the lowest order term has a u^4 factor, which makes the method $O(h^4)$. The trouble is, this makes only the kernel approximation more accurate, not the particle approximation to it. The particle approximation is not effected by changing W , only by increasing the number of particles. The number of particles and corresponding h must be such that the particle approximation is also of higher order or else changing the kernel gains nothing.

Another possible problem is that fourth order kernels must be negative for part of the region over which they are defined in order for equation (6.1) to hold. This can cause density to become negative for some particles (if using density-by-summation form), violating the last rule in the previous subsection. Although these local problems seem significant, the published literature to date implies they do not cause any global problems.

Monaghan (38) gives a procedure for making kernels higher order from their lower order forms (at least for three dimensional kernels). Two of the more popular

examples are the Super-Gaussian and Enhanced W_4 B Spline (both bell shaped). Since the work in this chapter mostly concentrates on one dimensional kernels, those forms of the higher order kernels are listed in Table 6.1. Note: $\tilde{K}(u) = c_n K(u)$ and $W(x, h) = \frac{1}{h} K(\frac{x}{h})$.

Name	$\tilde{K}(u)$	κ	1-D c_n
Super-Gaussian	$(\frac{3}{2} - u^2)e^{-u^2}$	3	$\frac{1}{\pi^{1/2}}$
Enhanced B-Splines	$\begin{cases} 17 - \frac{147}{4}u^2 + \frac{18}{4} u ^3 & \text{if } 0 \leq u \leq 1 \\ \frac{1}{4}(2 - u)^2(49 - 47 u) & \text{if } 1 \leq u \leq 2 \end{cases}$	2	$\frac{1}{18}$
Super-Gaussian 2	$(1.49624 - u^2)e^{-u^2}$	3	0.566214

Table 6.1 One-Dimensional Higher Order kernels

For the Super-Gaussian some of the values are not correct. To six digits, the $\frac{3}{2}$ should be approximately 1.49624 and c_n should be approximately 0.566214 (the actual values involve the error function). However, it is common in SPH to develop the Gaussian on $(-\infty, \infty)$, but then use it on only $(-3h, 3h)$. Although for many problems, the results using the two versions are virtually identical, it is probably best to be consistent in how a kernel is developed and used, especially for the higher order kernels.

6.1.3 Smoothing Length. The smoothing length h is very important in SPH for efficiency, accuracy, and physical processes. The efficiency is obtained when summing over the neighbors for a particular particle, since only neighbor particles within a distance of κh need be included. A smaller h means the sum is over a smaller number of particles. The accuracy comes from having a sufficient number of particles in the κh range. Also, from earlier, it was stated that the kernel approximation was $O(h^2)$. The physical process comes from h controlling the range over which the forces are felt.

The smoothing length has varied quite a bit through the literature. The basic form is for h to be selected at the beginning of the problem and to remain constant thereafter. This fits in well with the Eulerian picture of a fixed mesh. Unfortunately

this is not always as accurate as desired. So two forms of a varying h are discussed. First, h can vary for each time step. This is similar to the basic form and does not require much modification. The second is to allow h to vary for each particle. This is a large departure from the basic form and is discussed later. In general, the analysis performed in this dissertation uses the most basic form of the smoothing length. The remainder of this information is for completeness.

The primary question is how to select the value for h , whether once initially or for each time step. If h is too small (with respect to a given particle spacing), large fluctuations could occur because of not smoothing enough and the algorithm could just be modeling particle motion instead of fluid flow. If h is too large, details are smoothed out losing accuracy. If h is to remain fixed, a simple rule of $h \propto \frac{1}{N^{1/d}}$ is purported to work well in the literature. Also note the relationship in (6.2) holds fairly well, as the errors from the kernel approximation and particle approximation are roughly balanced:

$$O(e_r h M_x) \approx O(e_k h^2) . \quad (6.2)$$

However, if h is to vary in time, Gingold and Monaghan (13) suggested using an average density and later Monaghan (38) recommended using an average number density. The latter is shown in equations (6.3) and (6.4):

$$h \propto \frac{1}{\bar{n}^{1/d}} \quad (6.3)$$

where

$$\bar{n} = \frac{1}{N} \sum_{j=1}^N \frac{\rho_j}{m_j} . \quad (6.4)$$

These formula allow h to decrease when \bar{n} (or $\bar{\rho}$) increases and vice versa keeping the resolution roughly constant throughout the calculation. It should be noted that $\frac{1}{\bar{n}}$ should be approximately equal to the average particle spacing in one dimension. Otherwise the particle approximation is of a disproportionate order to that of the kernel approximation. Note: these relationships (6.2, 6.3) are purported to work

well in three dimensions and fairly well in two dimensions, but not very well in one dimension.

In some problems, having h constant for all particles does not provide the accuracy and resolution required. In areas where particles are highly concentrated, h may be too large, while in other areas it may be too small. So several authors have proposed methods to allow h to vary for each particle, giving h_i for particle i . There are three main concerns with using this scheme: how to choose h_i , how to maintain conservation, and how to account properly for h_i in the derivation of the equations.

To choose h_i at each step, Evrard (10) suggested h_i should scale with local interparticle separation. This leads to the most common method of calculating h_i as shown in equation (6.5):

$$\frac{Dh_i}{Dt} = - \left(\frac{h_i}{\rho_i d} \right) \frac{D\rho_i}{Dt} . \quad (6.5)$$

where d is a constant usually taken to be the number of dimensions. The derivation for this equation was not given by Evrard, so it is done here. First, the desired relationship is

$$\frac{\Delta x}{h} = c , \quad (6.6)$$

where c is a constant. In one-dimension, $\Delta x \approx \frac{m}{\rho}$. But that does not hold in higher dimensions. Assume $\frac{m}{\rho}$ is a square about a particle in two dimensions or a cube in three dimensions, then let Δx be the diagonal of that region. Note: it is also possible to assume $\frac{m}{\rho}$ is a circle (or sphere) with Δx as the diameter and obtain the same form (6.5). In fact, many other choices are possible as long as they lead to $\Delta x = c_h \sqrt[d]{(m/\rho)}$ for dimension d (1,2,or 3) and constant c_h .

$$\begin{aligned} \text{Side of Square} &= s = \sqrt{\text{Area}} = \sqrt{\frac{m}{\rho}} \\ \Delta x &\approx \sqrt{2} s = \sqrt{2} \sqrt{\frac{m}{\rho}} \end{aligned}$$

$$\text{Side of Cube} = s = \sqrt[3]{\text{Volume}} = \sqrt[3]{\frac{m}{\rho}}$$

$$\Delta x \approx \sqrt{3} s = \sqrt{3} \sqrt[3]{\frac{m}{\rho}}.$$

This leads to $\Delta x \approx \sqrt{d}(\frac{m}{\rho})^{\frac{1}{d}}$, for $d = 1, 2$, or 3 or more generally $\Delta x \approx c_h(\frac{m}{\rho})^{\frac{1}{d}}$.

Putting this together with equation (6.6) yields

$$\begin{aligned} ch &= \Delta x \\ c \frac{Dh}{Dt} &= \frac{D(\Delta x)}{Dt} = c_h \sqrt[3]{m} \frac{D(\sqrt[3]{\frac{1}{\rho}})}{Dt} = -\frac{c_h}{d} \sqrt[3]{\frac{m}{\rho}} \frac{1}{\rho} \frac{D\rho}{Dt} \\ &= -\frac{\Delta x}{\rho d} \frac{D\rho}{Dt} = -\frac{ch}{\rho d} \frac{D\rho}{Dt} \\ \Rightarrow \frac{Dh}{Dt} &= -\left(\frac{h}{\rho d}\right) \frac{D\rho}{Dt}. \end{aligned}$$

This equation for h seems to make sense in expanding and contracting gas clouds. However, for problems with material strength it may not be sufficient since fracture and fragmentation are not being properly represented. Also, although this differential equation for h works well overall, for some particles, the $\frac{\Delta x}{h}$ ratio may still be too large. However, by selecting a constant M_{xh} , the maximum value allowed for the ratio, then

$$\frac{\Delta x}{h} = \frac{\sqrt{d}}{h} \left(\frac{m}{\rho}\right)^{\frac{1}{d}} \leq M_{xh} \quad (6.7)$$

$$\Rightarrow h \geq \frac{\sqrt{d}}{M_{xh}} \left(\frac{m}{\rho}\right)^{\frac{1}{d}}. \quad (6.8)$$

In an algorithm, to calculate h use the maximum of h calculated by equations (6.5) and (6.8).

The most common means of maintaining conservation involve replacing h in the standard SPH formulas developed so far with some form of a symmetric combination of h_i 's. For example a simple arithmetic mean seems to work quite well (ie.

$W(u, \frac{h_i+h_j}{2})$). Another method is to replace the entire kernel function with some sort of symmetric combination of two kernel functions (ie. $[W(u, h_i)+W(u, h_j)]/2$). Both methods seem to work well, with neither having a distinct advantage.

The last item is a little more complex. When replacing h with h_i , it must be considered when the gradient or any other derivative of the kernel is taken. By the chain rule an extra term that resembles $\frac{\partial}{\partial h} W \nabla_i h_i$ is obtained. One thought is that h_i does not vary too much from particle to particle and, therefore, the gradient of h is quite small. At least smaller than the error in the particle method itself. This is probably a reasonable assumption, and is the one most often used. However, it does raise the question (as yet unanswered) what if this term is not negligible?

6.2 Kernel Comparisons

As stated earlier in the chapter, to some extent it should not matter what kernel is used. That is true, especially in the limit as h and Δx become small. But when they are not small, as is common in practice, the choice of kernel can drastically change the results. Hence, an analysis to determine what are better kernels and poorer kernels is performed in this section. Although it is done in several stages there are three primary parts to this work. First, measures of merit are developed for kernels under smooth and non-data circumstances. These can be used as given or easily modified to analyze kernels under other assumptions. Second, using the basic equation behind the measure of merit, 18 kernels are analyzed qualitatively. Third, using the measure of merit the 18 kernels are analyzed quantitatively. The overall results are that bell shaped kernels are better to use than either concave up (hyperbolic shaped) or concave down (parabolic shaped).

To start this analysis, consider the eighteen kernels shown in Table 6.2. Plots of these kernels and their derivatives are found in Figures C.1 - C.10 in Appendix C. They are all even, positive, and of the form $W(x, h) = \frac{1}{h} K(\frac{x}{h}) = \frac{c_n}{h} \tilde{K}(\frac{x}{h})$, where c_n is the normalization constant. So the functions K and \tilde{K} are the same except that

K is normalized, and \tilde{K} is not. Note: \tilde{K} is shown in Table 6.2. They are also all defined to be zero outside of κh . In the table, the Type column is either: B - Bell Shaped, P - Parabolic Shaped (concave down), or H - Hyperbolic Shaped (concave up). The parabolic shaped kernels are so named because they resemble a downward opening parabola (# 11 actually is a parabola). Similarly, the hyperbolic shaped kernels are so named because they resemble the negative exponential function which is a hyperbolic function (# 4 actually is a hyperbolic function). Also in the table, c_n is the normalization constant for one dimension (1-D).

#	Name	Type	$\tilde{K}(u)$	κ	1-D c_n
1	Gaussian	B	e^{-u^2}	3	$\frac{1}{\sqrt{\pi}}$
2	W_4 B-Spline	B	$\begin{cases} 1 - \frac{3}{2}u^2 + \frac{3}{4} u ^3 & \text{if } 0 \leq u \leq 1 \\ \frac{1}{4}(2 - u)^3 & \text{if } 1 \leq u \leq 2 \end{cases}$	2	$\frac{2}{3}$
3	Cosine	B	$(1 - \frac{u^2}{4})(1 + \cos(\frac{\pi u}{2}))$	2	$\frac{3\pi^2}{8(\pi^2+3)}$
4	Exponential	H	$e^{- u } - e^{-9}$	9	0.500618
5	$\kappa - 2$ Exponential	H	$e^{-4.5 u } - e^{-9}$	2	2.250555
6	1/X,2	H	$\frac{1}{2+ u } + \frac{ u -6}{16}$	2	7.337061
7	1/X,4	H	$\frac{1}{4+ u } + \frac{ u -8}{36}$	2	30.163694
8	1/X,10	H	$\frac{1}{10+ u } + \frac{ u -14}{144}$	2	283.125508
9	$-X^2$	H	$\frac{1}{2}(u - 2)^2$	2	0.375
10	$-x - e^{-x}$	P	$2 - u - e^{- u } + e^{-2}$	2	0.355617
11	$4 - X^2$	P	$4 - u^2$	2	0.09375
12	$8 - X^3$	P	$8 - u ^3$	2	0.041667
13	$\kappa - 2$ Gaussian	B	$e^{-2.25u^2} - e^{-9}$	2	0.846657
14	L Gaussian	B	$(2 - u)e^{-u^2}$	2	0.392674
15	Q Gaussian	B	$(1 - \frac{u^2}{4})e^{-u^2}$	2	0.643998
16	T Gaussian	B	$e^{-u^2} - e^{-4}$	2	0.591401
17	Quartic-1	B	$(2 + 3 u)(2 - u)^3$	2	0.0390625
18	Quartic-2	B	$16 - 8 u ^3 + 3u^4$	2	0.0260417

Table 6.2 One Dimensional Kernels Analyzed

6.2.1 Accuracy From Consistency Analysis. The first thought is to consider the bound from the consistency analysis in Chapter III. From equation (3.4), for a

sufficiently smooth function, $f(x)$, and for a kernel defined as above, the bound on the kernel approximation in one dimension is

$$\max_{\xi} |f''(\xi)|/2 \int_0^{\kappa} u^2 K(u) du . \quad (6.9)$$

In comparing different kernels, the function f is a constant, so just use the integral. For any given function, a lower value from the integral should indicate a better kernel approximation. It would be desirable that the final SPH approximation is also better for lower values of the integral. Unfortunately, this is not always true. The values for the integral for the 18 kernels are found in Table 6.3.

#	Name	Type	$\int_0^{\kappa} u^2 K(u) du$
1	Gaussian	B	0.24989
2	W_4 B-Splines	B	0.16667
3	Cosine	B	0.206123
4	Exponential	H	0.979983
5	$\kappa - 2$ Exponential	H	0.0483464
6	$1/X, 2$	H	0.165735
7	$1/X, 4$	H	0.179783
8	$1/X, 10$	H	0.190883
9	$-X^2$	H	0.2
10	$-x - e^{-x}$	P	0.372537
11	$4 - X^2$	P	0.4
12	$8 - X^3$	P	0.44444
13	$\kappa - 2$ Gaussian	B	0.110833
14	L Gaussian	B	0.153629
15	Q Gaussian	B	0.181942
16	T Gaussian	B	0.221115
17	Quartic-1	B	0.190476
18	Quartic-2	B	0.31746

Table 6.3 Kernel Integral Analysis

The data in this table indicates that the concave up (H) and bell shaped (B) kernels are, for the most part, the better ones and the concave down (P) are poorer. However, there are several exceptions. Based on work done later in this chapter, this holds

only very broadly. The reason this indicator does not work as well as desired is because it is evaluating only part of the SPH process, the kernel approximation. It says nothing about the particle approximation. It is also a measure of the central peakiness of the kernel. That is, the smaller the value, the larger the peak is at 0. If the error from the particle approximation is quite small, then this indicator would appear more correct. In other words, as $\frac{\Delta x}{h} \rightarrow 0$, the integral results would determine the better kernels to use. But for more sparsely spaced particles, which occurs in practice, a smaller value of the integral could quite easily indicate that not enough smoothing is being done because the kernel is too peaked. So at best, the integral results are only one overall indicator of the goodness of a kernel.

6.2.2 Uniform Space, Smooth Data Analysis. In this section, functions that are fairly smooth (ie. no shocks present) are considered and the particles are required to be uniformly spaced. Also the analysis is performed in one dimension only. The result is an equation that will form the foundation of the measure of merit. Start by defining the following

$$\begin{aligned} f'_i &\approx \sum_{j=1}^N \Delta x_j f_j W'_{ij} \\ x_i &= a + i\Delta x_i \quad \Delta x_i = \Delta x \\ x_{ij} &= x_i - x_j = a + i\Delta x - a - j\Delta x = (i-j)\Delta x \\ W'_{ij} &= \frac{1}{h^2} K' \left(\frac{x_{ij}}{h} \right) = \frac{1}{h^2} K' \left((i-j) \frac{\Delta x}{h} \right) = \frac{1}{h^2} K'_{ij} . \end{aligned}$$

Consider particle $i \in (1, N)$ such that $x_i - x_1 > \kappa h$ and $x_N - x_i > \kappa h$. Then examine functions that are constant, linear, and quadratic under the assumptions here to find a basic relationship.

(1) Assume f is constant. $f = c \Rightarrow f' = 0$. Since K is symmetric (even), then K' is odd. This then yields

$$0 \approx \sum_{j=1}^N \Delta x_j f_j W'_{ij} = \frac{c \Delta x}{h^2} \sum_{j=1}^N K' \left((i-j) \frac{\Delta x}{h} \right) = \frac{c \Delta x}{h^2} K'(0). \quad (6.10)$$

Therefore, $K'(0)$ must equal zero to model the derivative of a constant function exactly (under the above assumptions on K).

(2) Assume f is linear. $f = cx + d \Rightarrow f' = c$. Also assume that $K'(0)$ is zero, so that a constant function is exact and $\sum_{j=1}^N K'_{ij} = 0$. This then yields

$$\begin{aligned} c &\approx \sum_{j=1}^N \Delta x_j f_j W'_{ij} = \frac{\Delta x}{h^2} \sum_{j=1}^N (cx_j + d) K' \left((i-j) \frac{\Delta x}{h} \right) \\ &= \frac{c \Delta x}{h^2} \sum_{j=1}^N x_j K'_{ij} + \frac{d \Delta x}{h^2} \sum_j K'_{ij} \\ &\quad - \frac{c \Delta x}{h^2} x_i \sum_{j=1}^N K'_{ij} \quad \text{(subtract 0)} \\ &= c \left[\frac{\Delta x}{h^2} \sum_{j=1}^N (x_j - x_i) K'_{ij} \right] = c \left[\frac{\Delta x}{h^2} \sum_{j=1}^N (j-i) \Delta x K'_{ij} \right] \\ \Rightarrow \quad 1 &\approx -2 \sum_{l=1}^{\infty} l \left(\frac{\Delta x}{h} \right)^2 K' \left(l \frac{\Delta x}{h} \right). \end{aligned} \quad (6.11)$$

It is fairly easy to see that no function satisfies equation (6.11) for all values of $\frac{\Delta x}{h}$.

(3) Assume f is quadratic. $f = cx^2 + dx + e \Rightarrow f' = 2cx + d$. Also assume that $K'(0)$ is zero again. This then yields

$$\begin{aligned} 2cx_i + d &\approx \sum_{j=1}^N \Delta x_j (cx_j^2 + dx_j + e) W'_{ij} \\ &= \frac{c \Delta x}{h^2} \sum_{j=1}^N x_j^2 K'_{ij} + \frac{d \Delta x}{h^2} \sum_{j=1}^N x_j K'_{ij} + \frac{e \Delta x}{h^2} \sum_{j=1}^N K'_{ij} \\ &\quad \frac{c \Delta x}{h^2} x_i^2 \sum_{j=1}^N K'_{ij} \pm \frac{c \Delta x}{h^2} \sum_{j=1}^N (2x_i x_j) K'_{ij} - \frac{d \Delta x}{h^2} x_i \sum_{j=1}^N K'_{ij} \quad \text{(add 0)} \end{aligned}$$

$$\begin{aligned}
&= c \frac{\Delta x}{h^2} \sum_{j=1}^N x_{ij}^2 K'_{ij} + c \frac{\Delta x}{h^2} \sum_{j=1}^N (2 x_i x_j) K'_{ij} - d \frac{\Delta x}{h^2} \sum_{j=1}^N x_{ij} K'_{ij} \\
&\quad - \frac{c \Delta x}{h^2} 2 x_i^2 \sum_{j=1}^N K'_{ij} \quad \text{(subtract 0)} \\
&= -(2 c x_i + d) \frac{\Delta x}{h^2} \sum_{j=1}^N (x_i - x_j) K'_{ij} \\
\Rightarrow \quad 1 &\approx -2 \sum_{l=1}^{\infty} l \left(\frac{\Delta x}{h} \right)^2 K' \left(l \frac{\Delta x}{h} \right).
\end{aligned}$$

This then shows that the same equation for linear functions works for quadratic functions. However, this relationship does not seem to keep working for even higher order polynomials.

Therefore, a kernel must be selected that that won't satisfy equation (6.11) for some values of $\frac{\Delta x}{h}$. By choosing a particular $\frac{\Delta x}{h}$, it is possible to find which kernels satisfy the equation. This is very useful in selecting the initial particle separation for a given kernel, but does nothing towards indicating what happens when particles move. For unless the volume is held constant during a calculation, even the total average $\frac{\Delta x}{h}$ changes from time step to time step. But consider an interval of values over which $\frac{\Delta x}{h}$ varies. This is not exactly the same as in an actual calculation, but should be close enough to determine what is a good kernel. Now consider three tests based on this notion.

6.2.3 Test 1: Plots of Results. The first test is simply a plot from which qualitative results may be obtained. For each kernel, plot $-2 \sum_{l=1}^{\infty} l \left(\frac{\Delta x}{h} \right)^2 K' \left(l \frac{\Delta x}{h} \right)$ and 1 for $\left(\frac{\Delta x}{h} \right) \in [0.1, 2.0]$. These plots may be found in Appendix C (Figures C.11 – C.28). From these plots three observations may be made. First, an overall opinion as to which kernels are better than others. Second, a list of approximate values where each kernel gives exact results. These are good initial separation values and can be found precisely using a program such as Mathematica or MathCAD. Third, a better understanding as to what happens when the particle separation becomes too large.

For almost every kernel, the results start becoming quite poor when $\Delta x = h$. Of course, for most of the kernels, the results are completely wrong when the separation approaches κh since nothing is being averaged there. In Chapter IV, it was noted that there were problems in tension. Tension, of course, tends to force particles apart. So the tension instability is worsened by the fact that the SPH approximation becomes very poor when particles are too sparsely spaced. This result points out that the instability and inaccuracy are intermixed so that it may be difficult to determine which is the root of a particular problem.

6.2.4 Test 2: Error Norms. Although the results of Test 1 provide good qualitative results, it is desirable to obtain quantitative results as well. To do this, perform relative error norms based on equation (6.11). In this subsection both l_1 and l_2 relative error norms are calculated for 100 values of $(\frac{\Delta x}{h}) \in [0.2, 1.2]$. The formulas for these are shown in equations (6.12) and (6.13):

$$l_1 = \left(\frac{1}{100} \right) \sum_{n=1}^{100} \left| -2 \sum_{l=1}^{\infty} l \left(0.2 + \frac{n}{100} \right)^2 K'(l(0.2 + \frac{n}{100})) - 1 \right| \quad (6.12)$$

$$l_2 = \sqrt{\left(\frac{1}{100} \right) \sum_{n=1}^{100} \left[-2 \sum_{l=1}^{\infty} l \left(0.2 + \frac{n}{100} \right)^2 K'(l(0.2 + \frac{n}{100})) - 1 \right]^2} \quad (6.13)$$

l_{∞} norms could also be calculated, but were not since they can be easily inferred from the previous plots. The interval $[0.2, 1.2]$ can be argued as being too arbitrary. However, it was chosen as follows: all of the kernels are very accurate for values small enough, but seldom does one have the luxury (or computer time) to compute with that many particles. Also, all of the kernels perform poorly when the values become too large, and that might improperly skew the results. So a reasonable range was set. Further, the range was centered on 0.7 (a popular value) and was chosen large enough to apply to fixed h problems. $\Delta x/h$ is more likely to vary over a wider range in a calculation using fixed h than one using variable h . If for a particular problem more information is available on the ranges of Δx , h , or the ratio of the

two other more appropriate intervals could be used. Other information can come from the physical process being modeled. The results for the eighteen kernels may be found in Table 6.4.

#	Name	Type	l_1	l_2
1	Gaussian	B	0.00279564	0.00621844
2	W_4 B-Splines	B	0.0128797	0.0201059
3	Cosine	B	0.0284004	0.0451499
4	Exponential	H	0.0463731	0.0565237
5	$\kappa - 2$ Exponential	H	0.512015	0.569665
6	$1/X, 2$	H	0.12708	0.156575
7	$1/X, 4$	H	0.103547	0.130743
8	$1/X, 10$	H	0.0893328	0.115851
9	$-X^2$	H	0.0802408	0.107258
10	$-x - e^{-x}$	P	0.24071	0.293757
11	$4 - X^2$	P	0.291355	0.356247
12	$8 - X^3$	P	0.383839	0.471477
13	$\kappa - 2$ Gaussian	B	0.0901453	0.16566
14	L Gaussian	B	0.0604716	0.0843238
15	Q Gaussian	B	0.0119989	0.0192021
16	T Gaussian	B	0.0320381	0.0405489
17	Quartic-1	B	0.0196585	0.0305967
18	Quartic-2	B	0.0887839	0.125373

Table 6.4 Relative Error Norms for Kernel Test 2

A few general conclusions can be drawn from the data in Table 6.4. First, the Gaussian is the best of these kernels. However, like the Exponential it has a support (κ) larger than the others; which implies it uses more particles to obtain the average. Therefore, it should be expected to have somewhat better results. Note: the wider support will cost more in computation time since it requires a sum over more particles. So this is an accuracy versus efficiency concern. Second, the top six kernels are all bell shaped (B), the next eight are either bell (B) or hyperbolic (H) shaped, and the last four are parabolic (P) or hyperbolic (H). This clearly shows that bell shaped

kernels should be the kernels of choice; however, the kernel must still be picked with due care.

6.2.5 Test 3: Test Functions. Although the results of Test 1 and Test 2 have theoretical basis, they only show a kernel's worth for polynomial functions up to quadratic. Therefore, three test functions are used to demonstrate if the previous results still hold for higher order functions and validate Test 2 as a measure of merit:

- Third Order Polynomial
- Sine Function
- Linear Step Function.

Plots of these three functions and their corresponding derivatives are shown in Figure 6.1.

l_1 and l_2 relative error norms are calculated for a given $\frac{\Delta x}{h}$ as follows: if f is the function to be evaluated and S is the SPH approximation to f'

$$l_1\left(\frac{\Delta x}{h}\right) = \frac{\sum_{i=0}^N |f'(x_i) - S(x_i)|}{\sum_{i=0}^N |f'(x_i)|}$$

$$l_2\left(\frac{\Delta x}{h}\right) = \frac{\sqrt{\sum_{i=0}^N (f'(x_i) - S(x_i))^2}}{\sqrt{\sum_{i=0}^N (f'(x_i))^2}},$$

where $N = (x_{max} - x_o)/\Delta x$ and $x_i = x_o + i\Delta x$. The values for x_o and x_{max} for each function can be taken from Figure 6.1 as the left and right most points plotted. Note: in order to avoid edge problems, extra particles are used at the ends to calculate $S(x_i)$ when x_i is close to x_o or x_{max} . To obtain a single number for each kernel, 100 values of $\frac{\Delta x}{h}$ are used to calculate an average (absolute or square) of the l_1 and l_2 errors described above. The ranges chosen are, $h \in [0.1, 0.2]$ and $\Delta x \in [0.02, 0.24]$ implying $\frac{\Delta x}{h} \in [0.2, 1.2]$. The formulas for these are

$$\langle l_1 \rangle = \sum_{n=0}^{100} \left(\frac{1}{101} \right) \left| l_1 \left(0.2 + \frac{n}{100} \right) \right|$$

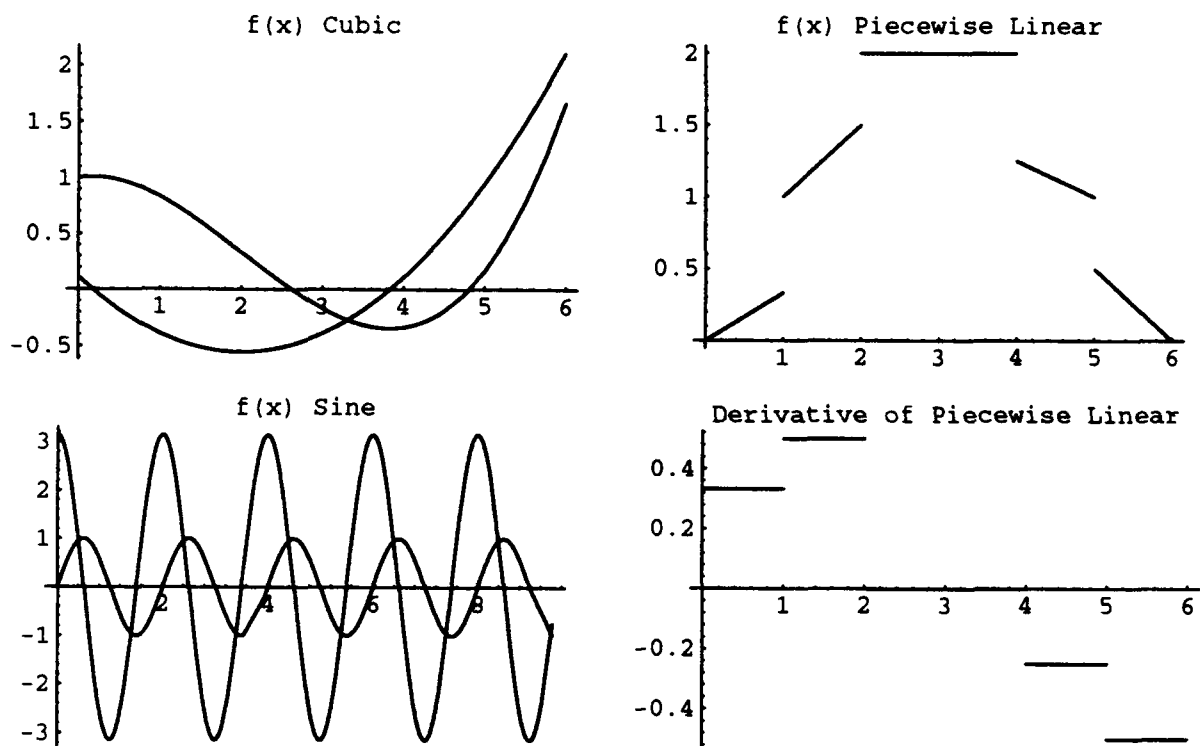


Figure 6.1 Test 3: Test Functions

$$\langle l_2 \rangle = \sqrt{\sum_{n=0}^{100} \left(\frac{1}{101} \right) \left[l_2 \left(0.2 + \frac{n}{100} \right) \right]^2}.$$

The results are found in Tables C.5 and C.6 in Appendix C. In addition to the tables, part of the results may be seen in the bar charts shown in Figures 6.2 and 6.3. In these figures, the line with small boxes is the predicted goodness from Test 2 and the bars are for the function results from Test 3. Only the smooth functions are shown on these figures (Sine and Polynomial) since the properties are quite different for the non-smooth results.

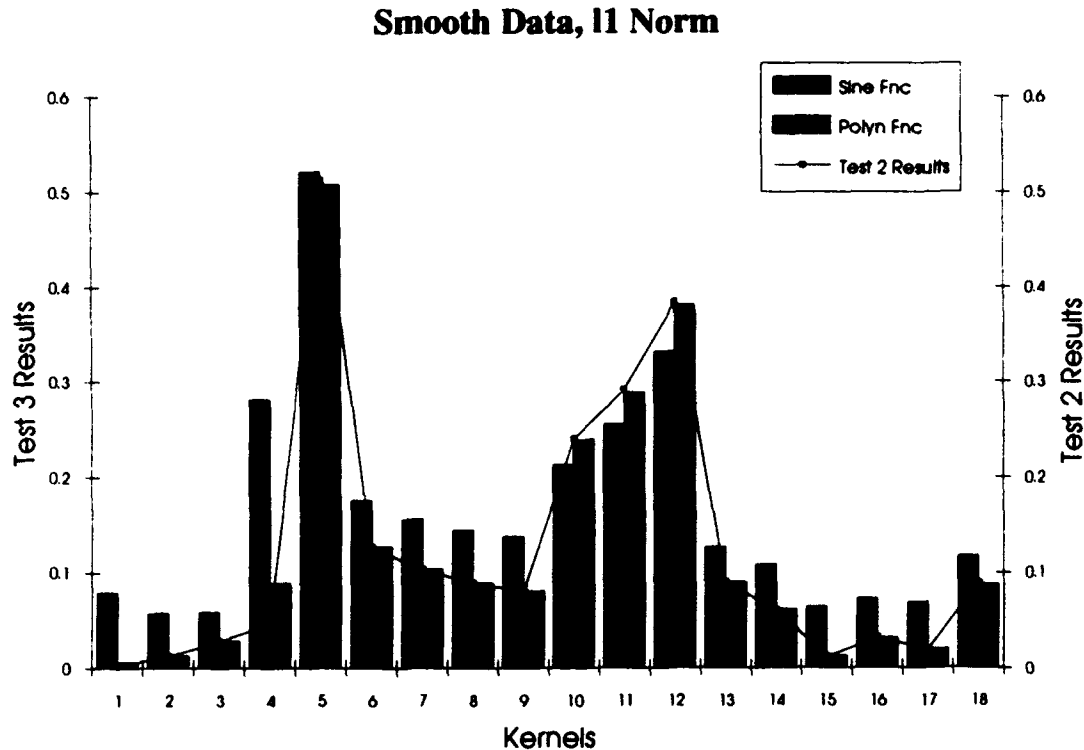


Figure 6.2 Bar Chart for Test 3, l_1 , Smooth Data

Some general conclusions can be drawn from these figures for smooth data. First, the Test 2 results (norms given in Table 6.4) very closely match the norms from the test functions. This implies that the error norm from Test 2 is a good measure of merit of a kernel (at least globally) for smooth data. Second, since the data matches

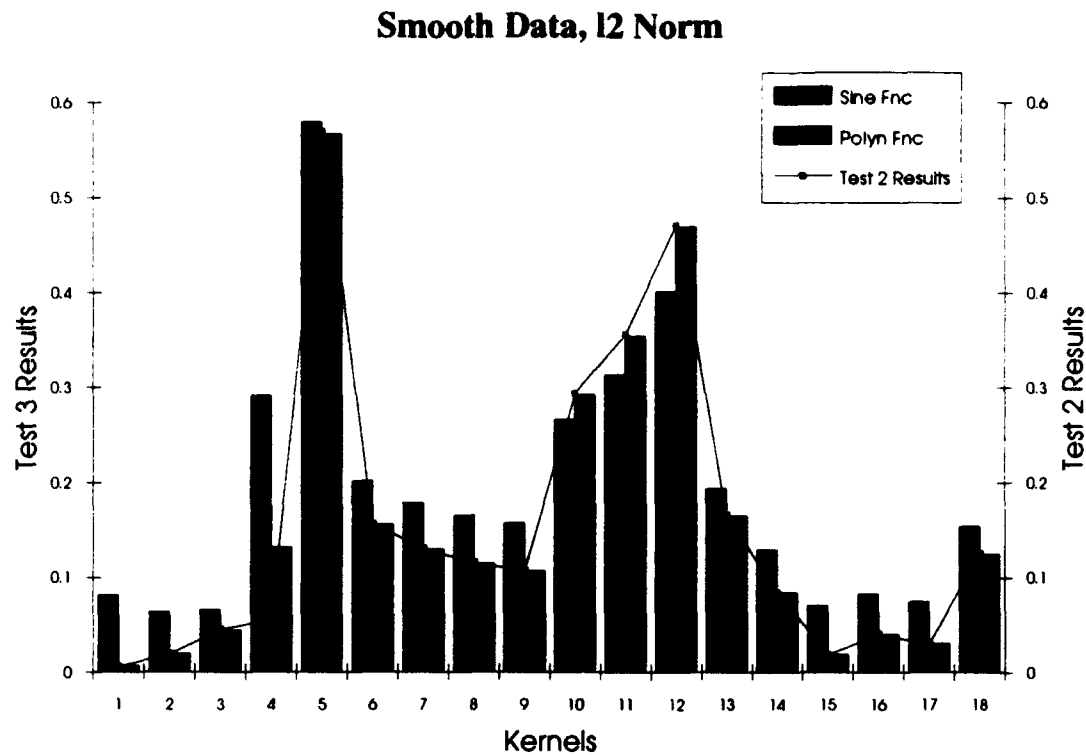


Figure 6.3 Bar Chart for Test3, l_2 , Smooth Data

Test 2 so well, the same conclusion can be made that bell shaped kernels are better. Third, although the Gaussian (kernel # 1) is the best in Test 2 and the polynomial test function, it is fifth best for the sine function. It still performs quite well, but since it costs more in computer time to use it with only mixed results, the other bell shaped kernels are more highly recommended for smooth data.

6.2.6 Higher Order Kernel Comparisons. Up until now, this section has evaluated and compared only *standard* second order SPH kernels. However, in subsection 6.1.2 it was noted that higher order kernels were also possible (in that subsection they were fourth order). Since the analysis in this section does not rely on the order of the kernel, comparisons between the different order kernels is easily accomplished. This will be done using the fourth order kernels listed in Table 6.1.

First, the integral test from subsection 6.2.1 will result in 0, since that is the definition of being higher order. This implies, when compared with the results in Table 6.3, the higher order kernels should perform better. However, as previously noted, the integral test is only valid when $\Delta x/h$ is sufficiently small. Note: the Super-Gaussian actually has a value of about 0.0018799 when integrated over the proper domain; see the note in section 6.1.2 for more information regarding this.

Second, the plots corresponding to Test 1 are found in Appendix C (Figures C.31 – C.33). From these, it appears that the Super-Gaussian (either form) performs quite well while the Enhanced B-Spline is only fair. For all three, the results significantly decrease (even more than standard kernels) when $\Delta x/h$ becomes greater than 1.

Third, the Test 2 results, corresponding to the norms described in subsection 6.2.4, are given in Table 6.5. As compared with standard kernels found in Table 6.4,

Name	Type	l_1	l_2
Super-Gaussian	B	0.0191325	0.0429511
Enhanced B-Spline	B	0.0882854	0.129977
Super-Gaussian 2	B	0.0191335	0.0431463

Table 6.5 Rel Error Norms for Higher Order Kernel Test 2

these results are initially somewhat surprising. The Super-Gaussian would be fourth best (3rd for l_1 and 5th for l_2). The Enhanced B-Spline would be placed in with the poorer bell shapes and better hyperbolic shapes. Although these results do not make these overly bad kernels to use, they do not have any advantages over more standard, lower order kernels. There are two reasons for this. First, since only the kernel approximation is made better by a higher order kernel, the number of particles must be significantly increased before the errors in the particle approximation are of the same order as the kernel approximation (Δx must approach h^3). Second, the

higher order kernels have more elaborate shapes than standard kernels. But unless enough particles are used to take advantage of that shape, it is just more noisy.

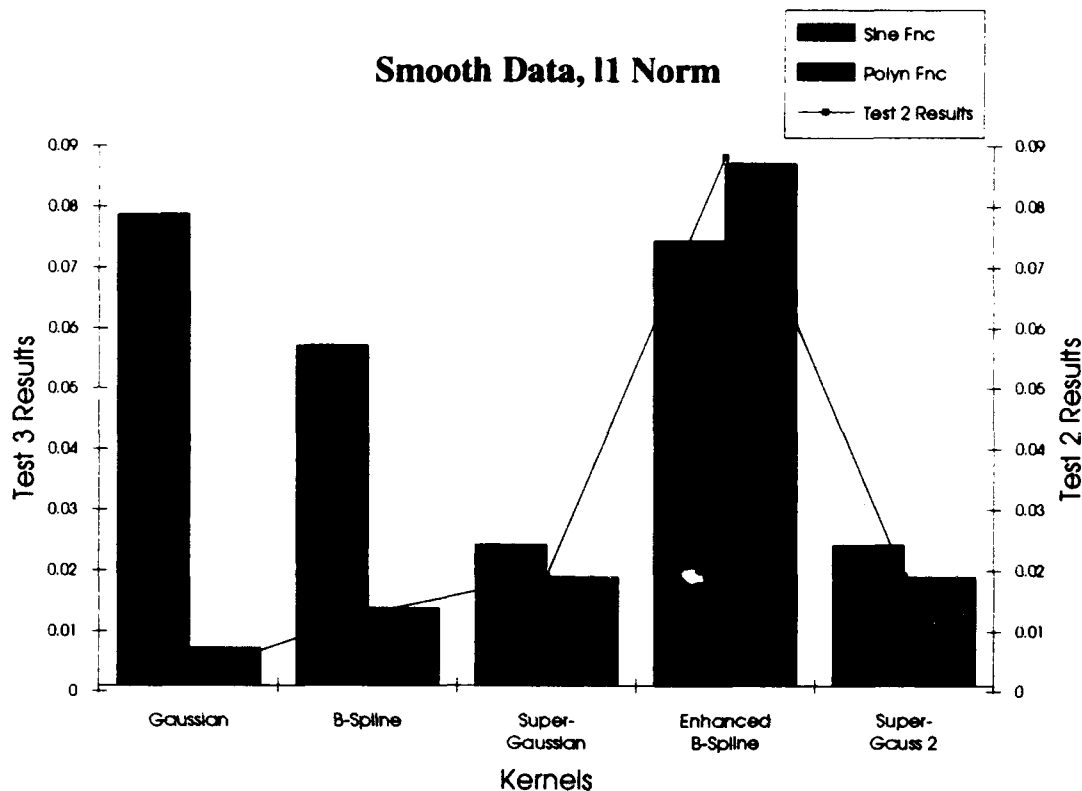


Figure 6.4 Bar Chart for Test 3, l_1 , Smooth Data, Higher Order

Last, the Test 3 results, corresponding to the test functions described in subsection 6.2.5, are given in Tables C.3 and C.4 in Appendix C. The data from these is summarized in the bar charts shown in Figures 6.4 and 6.5. The Gaussian and $W - 4$ B-Spline kernels are included for comparison with standard kernels.

Since the Test 2 results represents the Test 3 results fairly well, the conclusions are same. Overall, the higher order kernels do not gain very much, if anything. They have regions where they are negative and drop off fast when sparsely spaced. The primary gain would be realized if the number of particles per h was quite large ($\Delta x/h$ quite small).

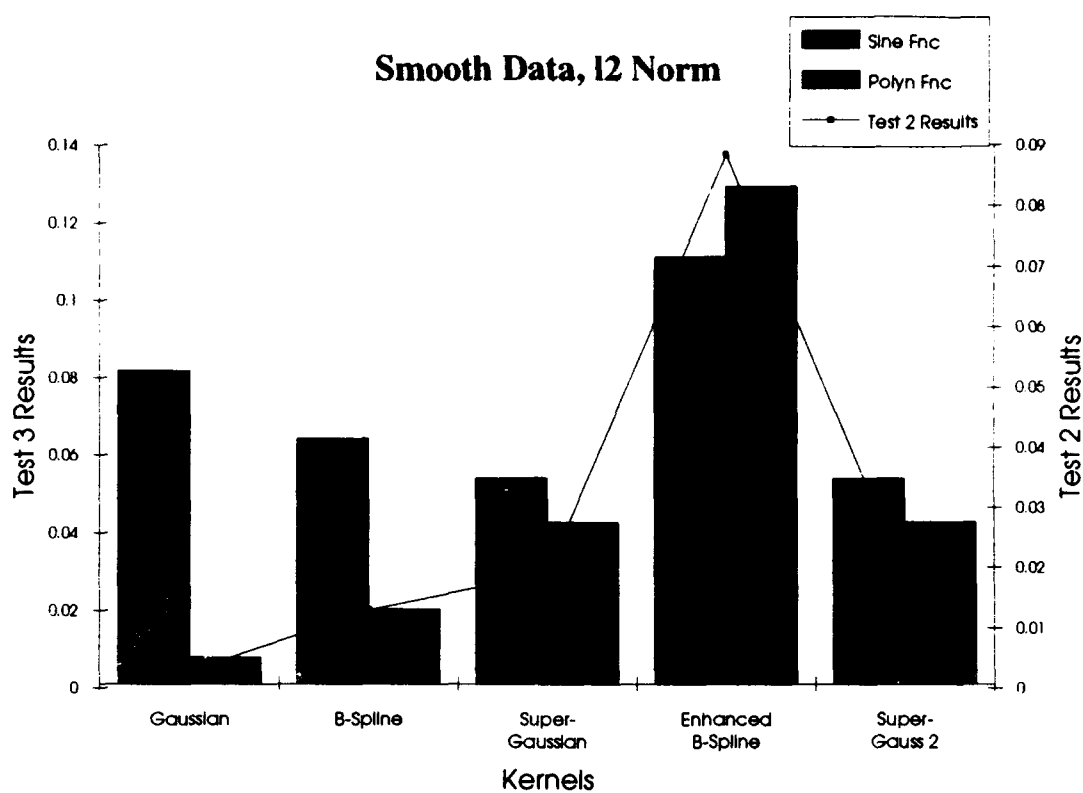


Figure 6.5 Bar Chart for Test3, l_2 , Smooth Data, Higher Order

6.2.7 Non-Smooth Data. In this subsection, the previous work is extended to areas near a shock. However, the uniform spacing assumptions still remain. Consider Figure 6.6 and equation (6.14)

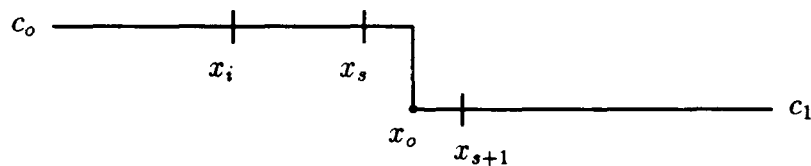


Figure 6.6 Non-Smooth Data Example

$$f = \begin{cases} c_0 & \text{if } x < x_o \\ c_1 & \text{if } x > x_o \end{cases} \quad (6.14)$$

Near the shock

$$f'_i = \sum_{j=1}^N \Delta x_j f_j W'_{ij} = \Delta x c_o \sum_{j=1}^s W'_{ij} + \Delta x c_1 \sum_{j=s+1}^N W'_{ij}.$$

Let $i < s$. Because W'_{ij} is odd, terms from $i+1, \dots, s$ cancel with terms from $i-1, \dots, 2i-s$ leaving

$$f'_i = \Delta x c_o \sum_{j=1}^{2i-s-1} W'_{ij} + \Delta x c_1 \sum_{j=s+1}^N W'_{ij} = (c_o - c_1) \sum_{j=1}^{2i-s-1} \Delta x W'_{ij}.$$

The sum approximates the left tail area of the W' curve. As $i \rightarrow s$ the sum approximates more of the tail, approaching the area under the entire left half of the W' curve. Note: $i \geq s$ just results in the opposite side of the curve. So then f'_i approximately equals

$$f'_i \approx (c_o - c_1) \int_{-\kappa h}^{x_i - x_s} W'(u) du = (c_o - c_1) [W(x_i - x_s) - W(-\kappa h)].$$

By the continuity and compact support properties of the kernel, f'_i is approximately equal to $(c_o - c_1)W_{is}$. Since the actual value of f'_i is 0, an estimate of the l_1 error norm is

$$\sum_{i=1}^N \Delta x_i |f'_i| = |c_o - c_1| \sum_{i \neq s} \Delta x_i W_{is} = |c_o - c_1| \left[\sum_{i=1}^N \Delta x_i W_{is} - \Delta x W_o \right].$$

The summation term at the end of the last equation is an approximation of the integral of W , which is just 1. Since c_o and c_1 are arbitrary and independent of the choice of the kernel, the following is proposed as a measure of merit for kernels under the l_1 norm

$$\min(1 - \Delta x W_o) = \min\left(1 - \frac{\Delta x}{h} K_o\right). \quad (6.15)$$

The same steps can be performed to arrive at the following as a measure of merit for kernels under the l_2 norm

$$\min[W_o(1 - \Delta x W_o)] = \min\left[\frac{1}{h}K_o\left(1 - \frac{\Delta x}{h}K_o\right)\right]. \quad (6.16)$$

The values of $K(0)$, $1 - 0.7 * K(0)$, and $K(0) * (1 - 0.7 * K(0))$ for the 18 kernels are shown in Table 6.6. Note: 0.7 is used since it is an average value for $\Delta x/h$ in this study.

#	Name	Type	$K(0)$	$1 - 0.7K(0)$	$K(0)(1 - 0.7K(0))$
1	Gaussian	B	0.56419	0.605067	0.341373
2	W_4 B-Splines	B	0.666667	0.533333	0.355556
3	Cosine	B	0.575169	0.597382	0.343595
4	Exponential	H	0.500556	0.64961	0.325167
5	$\kappa - 2$ Exponential	H	2.250277	-0.575194	-1.294346
6	$1/X, 2$	H	0.917133	0.358007	0.328340
7	$1/X, 4$	H	0.837880	0.413484	0.346450
8	$1/X, 10$	H	0.78646	0.449478	0.353496
9	$-X^2$	H	0.75	0.475	0.35625
10	$-x - e^{-x}$	P	0.403745	0.717379	0.289638
11	$4 - X^2$	P	0.375	0.7375	0.276563
12	$8 - X^3$	P	0.33333	0.766667	0.255556
13	$\kappa - 2$ Gaussian	B	0.846553	0.407413	0.344897
14	L Gaussian	B	0.785348	0.450256	0.353608
15	Q Gaussian	B	0.643998	0.549201	0.353685
16	T Gaussian	B	0.580569	0.593602	0.344627
17	Quartic-1	B	0.625	0.5625	0.351563
18	Quartic-2	B	0.416667	0.708333	0.295139

Table 6.6 Kernel Value at 0

The data in Table 6.6 shows that the results are different under an l_1 norm than an l_2 norm. For the l_1 norm, based on the column $1 - .7 * K(0)$, the hyperbolics (H) perform the best while the parabolics (P) perform the worst. It should be noted that many of the numbers are quite close, but not as close as for the l_2 norm. From the last column, almost all kernels delivered similar results for the l_2 norm. The

parabolics are slightly better (with one exception for kernel 5), but the rest are then roughly the same. These ideas will now be verified against the step function from Test 3. The results are found in Tables C.5 and C.6 in Appendix C and are summarized in the bar charts shown in Figures 6.7 and 6.8. The lines with small boxes represent the information above and the bars are from test 3 (step function).

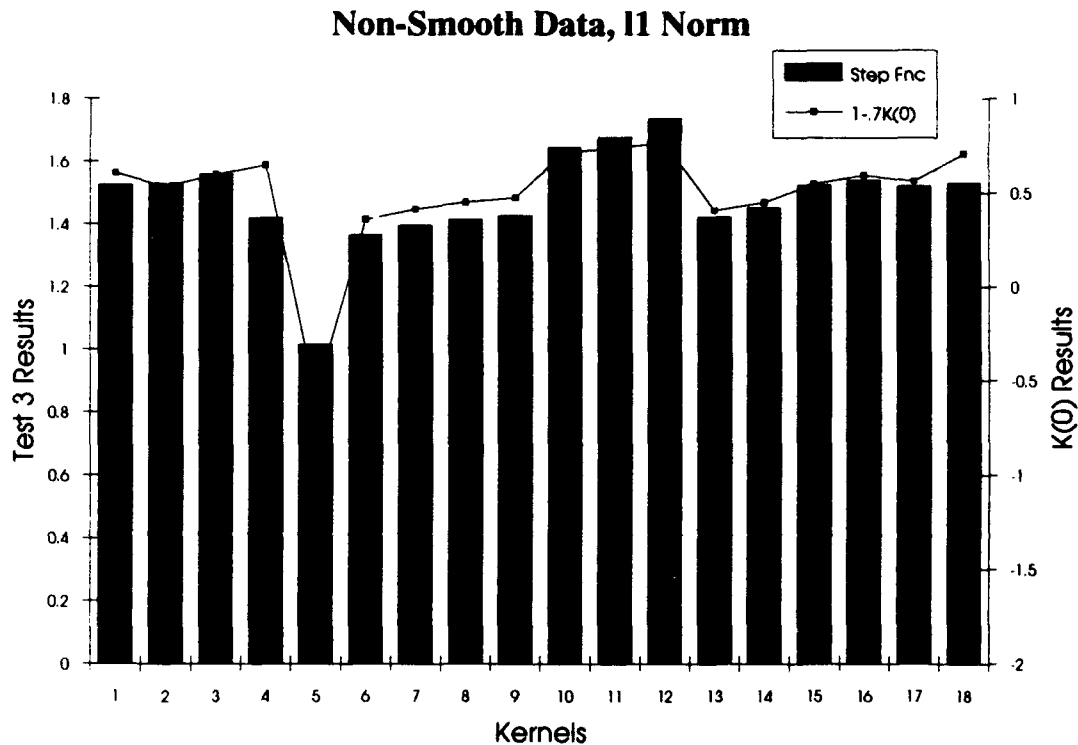


Figure 6.7 Bar Chart for Test 3, l_1 , Non-Smooth Data

Some general conclusions may be drawn from these figures. First, the $K(0)$ results (data given in Table 6.6) match very closely the norms from the test functions, especially l_1 . This implies that the norm predictors from the $K(0)$ work are good measures of merit of a kernel (at least globally) for non-smooth data. Second, based on the measure of merit and data in the figures there does not appear to be any class of kernels that are significantly better than the others under both norms for non-smooth data. The $\kappa - 2$ Exponential has the least error. However, due to the shape of this kernel (very sharply peaked) it is probably not a very good choice.

Non-Smooth Data, l_2 Norm

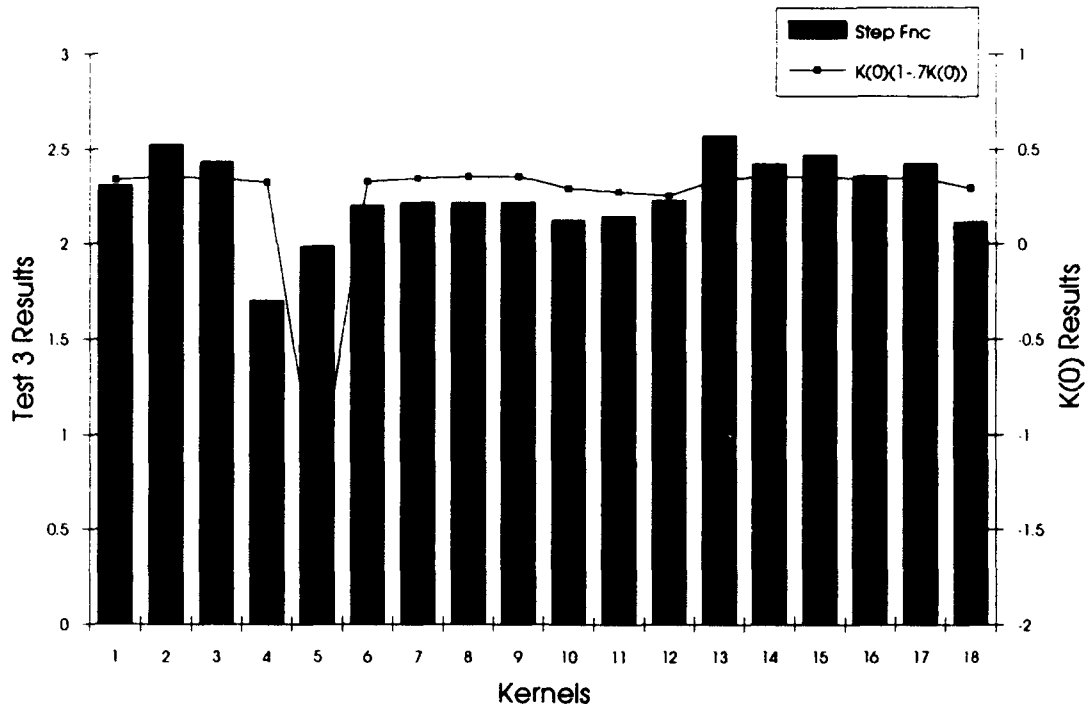


Figure 6.8 Bar Chart for Test3, l_2 , Non-Smooth Data

Third, since the two kernels with κ larger than 2 do not perform significantly better than the others, it is recommended to use a kernel with κ equal to 2.

6.2.8 One-Sided Kernels. Up until now only kernels that were even or symmetric were considered, however there are other possibilities such as asymmetric functions. Although there are an unlimited number of possible shapes, only truncated and condensed one-sided kernels are considered here. The term *truncated*, is used to indicate the same kernels from Table 6.2 given earlier, but with only one side. The other side is taken to be 0. Of course, this makes the kernel discontinuous at zero and must, therefore, have the derivative defined at zero (done later). The term *condensed*, is used to indicate the kernels given earlier are shrunk down to half their width and then shifted to one half plane or the other. The opposite half plane

is zero. Also note, that the normalization constant for these one dimensional kernels is exactly twice that given previously.

Following the procedure from the uniform space, smooth data analysis earlier for these new kernels yields

$$\begin{aligned} f'_i &\approx \sum_{j=1}^N \Delta x_j f_j W'_{ij} \\ x_i &= a + i\Delta x_i \quad \Delta x_i = \Delta x . \end{aligned}$$

Assume, without loss of generality, $K'(u)$ is a backward difference kernel so that $K'(u) = 0, u < 0$.

(1) Assume f is constant. $f = c \Rightarrow f' = 0$.

$$0 \approx \sum_{j=1}^N \Delta x_j f_j W'_{ij} = \frac{c\Delta x}{h^2} \sum_{j=1}^N K' \left((i-j) \frac{\Delta x}{h} \right) . \quad (6.17)$$

Therefore, $K'(0) = -\sum_{l=1}^{\infty} K'(l \frac{\Delta x}{h})$ to exactly model the derivative of a constant function. This should be zero for the condensed kernels.

(2) Assume f is linear. $f = cx + d \Rightarrow f' = c$. Also assume that $K'(0)$ is taken to be the sum above. This then yields

$$\begin{aligned} c &\approx \sum_{j=1}^N \Delta x_j f_j W'_{ij} = \frac{\Delta x}{h^2} \sum_{j=1}^N (cx_j + d) K' \left((i-j) \frac{\Delta x}{h} \right) \\ &= \frac{c\Delta x}{h^2} \sum_{j=1}^N x_j K'_{ij} + \frac{d\Delta x}{h^2} \sum_{j=1}^N K'_{ij} \\ &\quad - \frac{c\Delta x}{h^2} x_i \sum_{j=1}^N K'_{ij} \quad \text{(subtract 0)} \\ &= c \left[\frac{\Delta x}{h^2} \sum_{j=1}^N (x_j - x_i) K'_{ij} \right] \\ \Rightarrow 1 &\approx -\sum_{l=1}^{\infty} l \left(\frac{\Delta x}{h} \right)^2 K' \left(l \frac{\Delta x}{h} \right) . \quad (6.18) \end{aligned}$$

This check is exactly the same as the earlier measure equation, with a coefficient of 2 missing. However, since the normalization constant (hidden in K) is twice that given earlier, the previous measures of merit from Tests 1 and 2 should work for one-sided kernels.

Although one-sided kernels are a little cheaper to compute with, they only give results of order h instead of h^2 . This was reflected in Test 3 type results being worse for one-sided kernels on smooth data. However, near shocks they should be better since a one-sided kernel is analogous to backward or forward differences (ie. upwind schemes). Consider the problem from Figure 6.6 and equation (6.14) again. Near the shock

$$f'_i = \sum_{j=1}^N \Delta x_j f_j W'_{ij} = \Delta x c_0 \sum_{j=1}^s W'_{ij} + \Delta x c_1 \sum_{j=s+1}^N W'_{ij}.$$

Let $i \leq s$. Because W'_{ij} is backward, the second term is just 0. The first term equals zero then if $K'(0) = -\sum_{l=1}^{\infty} K'(l \frac{\Delta x}{h})$

Now let $i \geq s + 1$, then

$$0 \approx \Delta x c_0 \sum_{j=1}^s W'_{ij} + \Delta x c_1 \sum_{j=s+1}^N W'_{ij} = (c_0 - c_1) \sum_{j=1}^s \Delta x W'_{ij}.$$

This is essentially the same as the two-sided kernel check in the area of a shock. So a one-sided kernel should give the same results as a two-sided, error-wise, on one side of the shock, but should be better than the two-sided on the other. Note: a truncated one-sided kernel in the other direction is exactly opposite to the one studied above.

The conclusion is that for non-smooth data, one-sided kernels should be better near a shock. These results may be seen in the bar charts shown in Figures 6.9 - 6.12. The lines represent the information above and the bars are from Test 3 (step function).

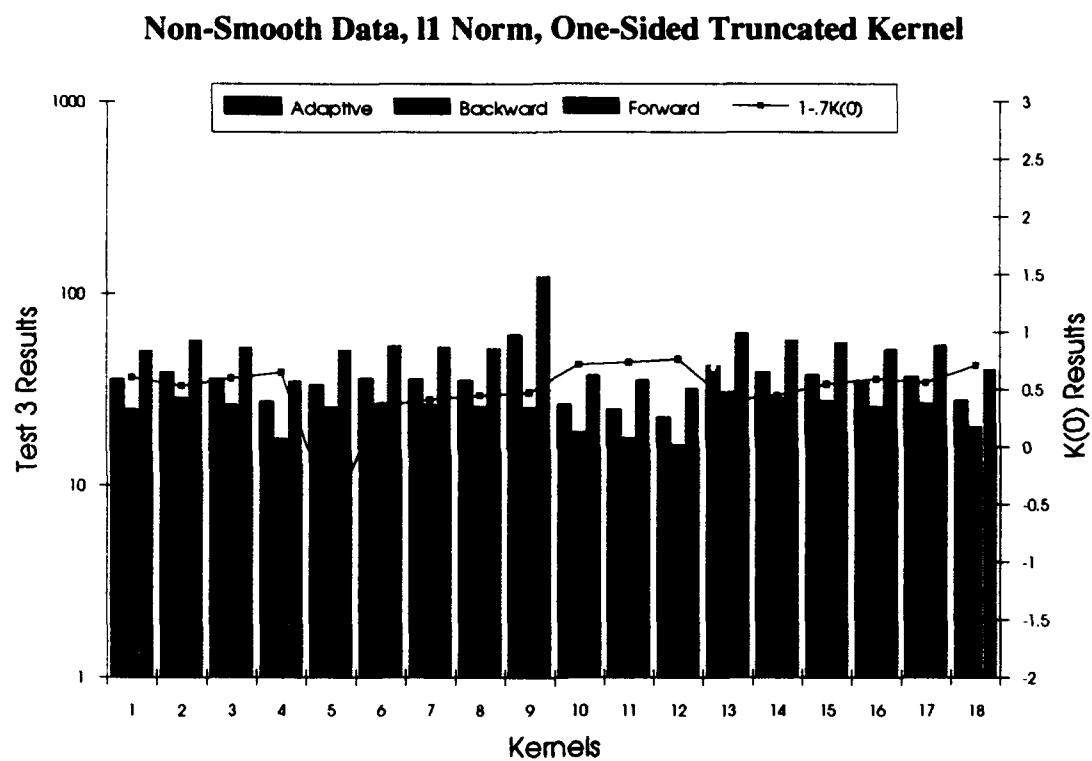


Figure 6.9 Bar Chart for Truncated 1-Sided Kernels, l_1 , Non-Smooth Data

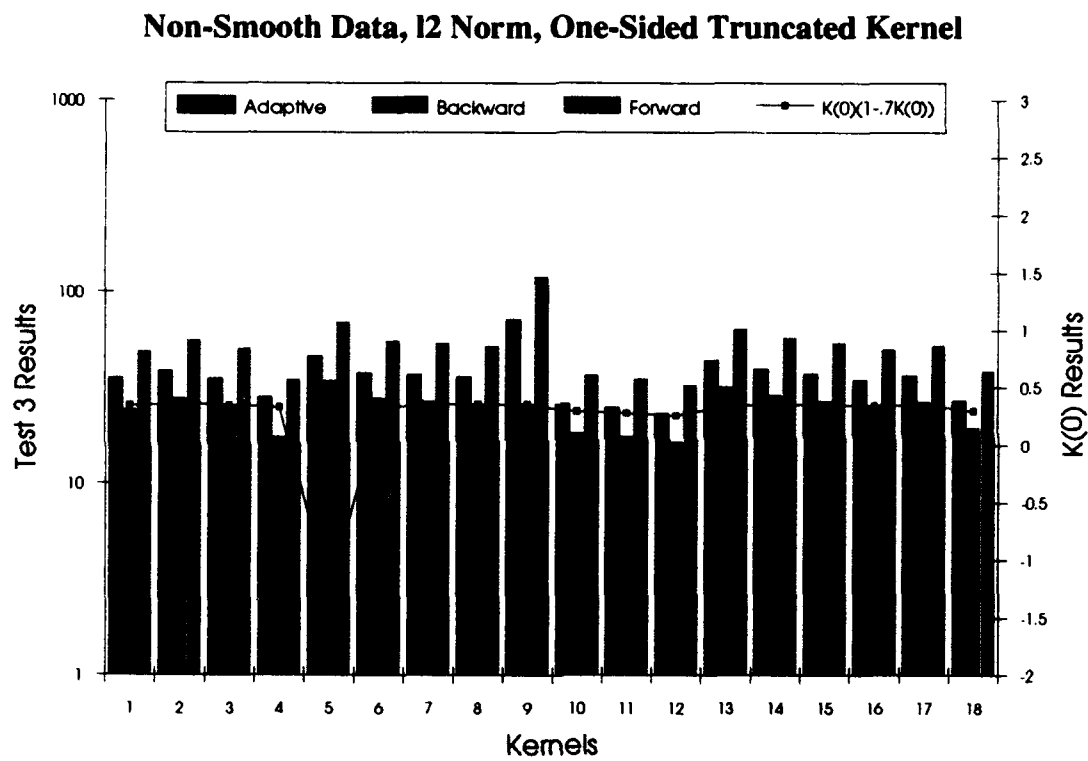


Figure 6.10 Bar Chart for Truncated 1-Sided Kernels, l_2 , Non-Smooth Data

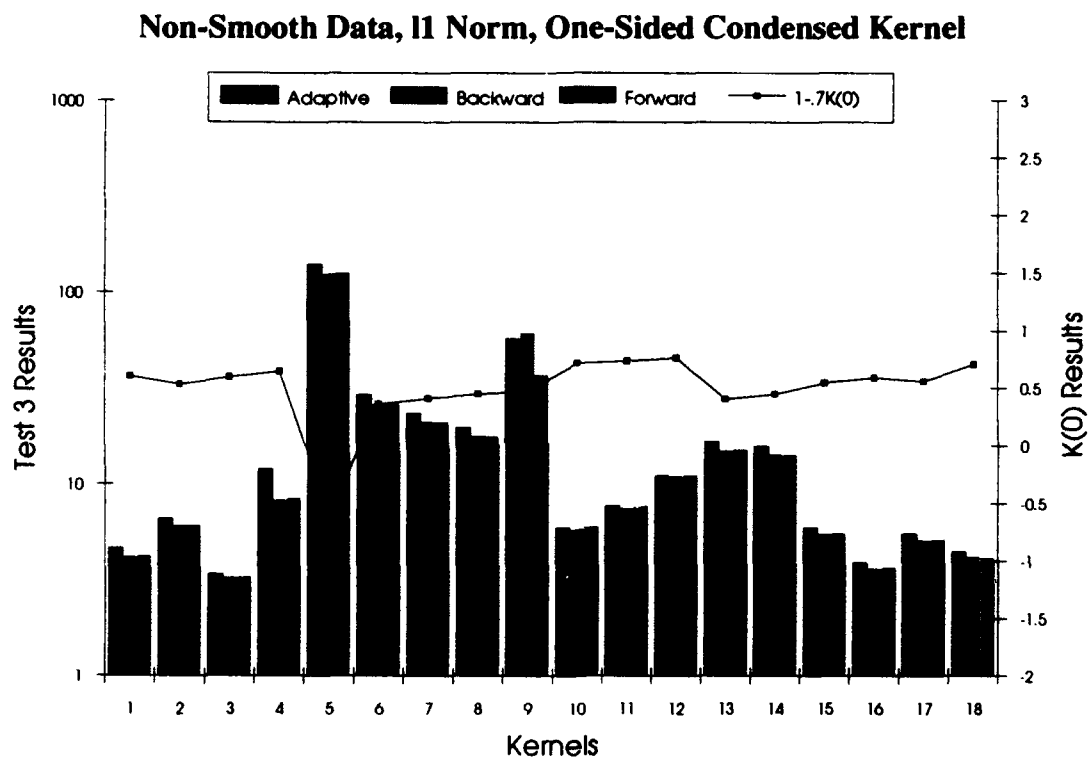


Figure 6.11 Bar Chart for Condensed 1-Sided Kernels, l_1 , Non-Smooth Data

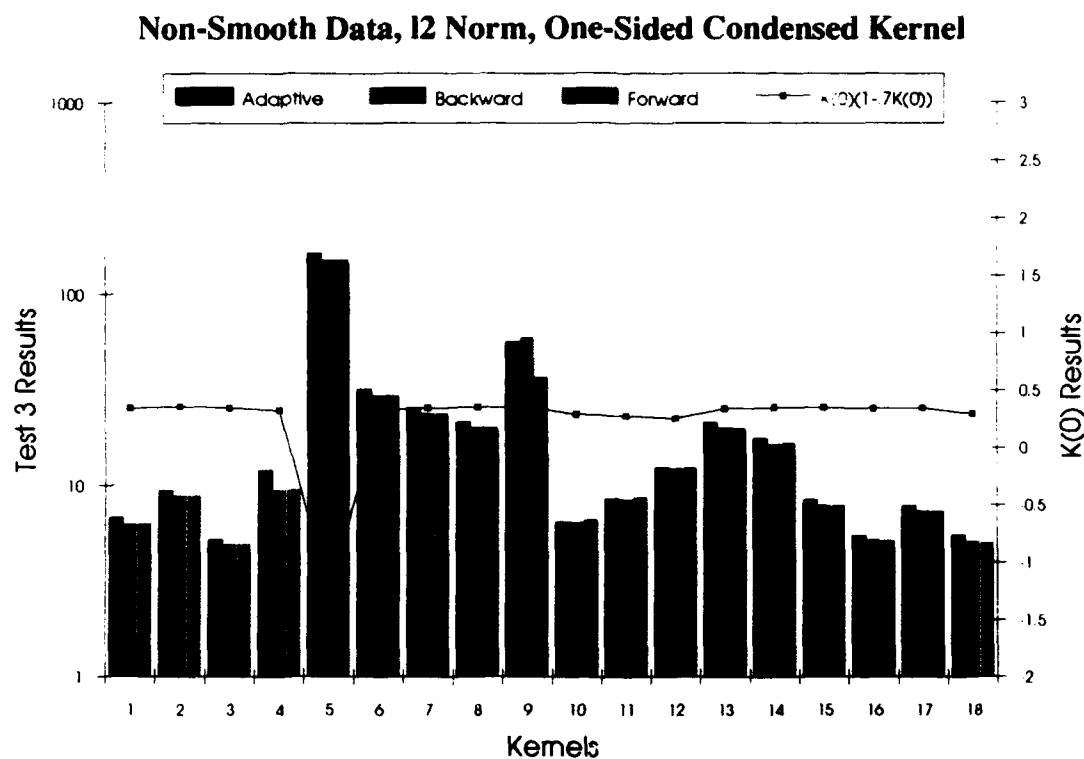


Figure 6.12 Bar Chart for Condensed 1-Sided Kernels, l_2 , Non-Smooth Data

The figures indicate that the one-sided kernels are all about the same and comparing with earlier results do not perform better than symmetric kernels. Further, the measure of merit does not appear to work as well for these kernels (especially condensed). One thought on this is that many more particles are needed with a one-sided kernel than a two-sided to obtain good results. Since additional particles were not added, the results are all quite poor.

6.2.9 Riemann Shock Tube Problem. The Riemann shock tube problem is well known, and not described here (see LeVeque (32) or Smoller (57)). Because it is such a good test for shock problems, it is used both here and again in Chapter VIII. The test case in one dimension uses a line of equally spaced particles on $[0, 1]$ with a discontinuity at 0.5 and the values for all the particles on either side of the

discontinuity are: (u_l - left, u_r - right)

$\rho_l = 1.0$	$\rho_r = 0.125$
$v_l = 0.0$	$v_r = 0.0$
$e_l = 2.5$	$e_r = 2.0$
$P_l = 1.0$	$P_r = 0.1$

Also the gas constant, $\Gamma = 1.4$ is used. From earlier in this chapter, and the corresponding plots in Appendix C, as $\frac{\Delta x}{h}$ varied, the Test 1 results fluctuated around the desired value (1) for most of the kernels. Using MathCAD, an initial ratio was selected for each kernel near 0.7 that was best for each kernel individually. The reason for selecting 0.7 is there will be two neighbors on each side of any particle and this is a fairly popular value in the literature. The initial values are found in Table 6.7.

The column labeled $1.1*\Delta x/h$ in Table 6.7 is used for determining $M_{xh} = \max(\Delta x/h)$ as described in the smoothing length section earlier (equation (6.7)). Although a variable h formulation was used in the tests, this ensures that h is not allowed to become too small. The values for the coefficients of artificial viscosity are (2.5, 2.5) and for the coefficients of wall heating (0.5,0.5). These are fairly standard values.

This test was performed on half of the kernels. Based on the analysis so far, it was predicted that the bell shaped kernels would perform adequately while the others would be questionable. Hence, only one hyperbolic, two parabolics, and six bell shaped kernels were chosen to test. Most of the bell shaped kernels performed admirably, while most of the rest aborted early in the calculation. The reason is this is a very sensitive problem, especially when using SPH. Extra noise added by poorer kernels can easily add to growths in shock spikes causing negative density, negative energy, or particles to cross. The results at 1 microsecond for one of the better calculations is shown in Figures 6.13 and 6.14.

#	Name	Type	$\Delta x/h$	nph	$1.1 * \Delta x/h$
1	Gaussian	B	1.00316	.996849	1.103476
2	W_4 B-Splines	B	0.689898	1.44949	0.758888
3	Cosine	B	0.673815	1.484087	0.741197
4	Exponential	H	3.0	0.333333	3.3
5	$\kappa - 2$ Exponential	H	0.666667	1.5	0.733333
6	$1/X, 2$	H	0.757363	1.320144	0.833099
7	$1/X, 4$	H	0.777197	1.286486	0.854917
8	$1/X, 10$	H	0.791098	1.264131	0.870208
9	$-X^2$	H	0.799783	1.250274	0.879761
10	$-x - e^{-x}$	P	0.807503	1.238386	0.888253
11	$4 - X^2$	P	0.81096	1.233106	0.892056
12	$8 - X^3$	P	0.816495	1.224747	0.898145
13	$\kappa - 2$ Gaussian	B	0.666667	1.5	0.733333
14	L Gaussian	B	0.666667	1.5	0.733333
15	Q Gaussian	B	0.739626	1.352035	0.813589
16	T Gaussian	B	0.769779	1.299073	0.846757
17	Quartic-1	B	0.685996	1.457735	0.754596
18	Quartic-2	B	0.733263	1.363767	0.806589

Table 6.7 Initial Particle Spacing for Shock Tube

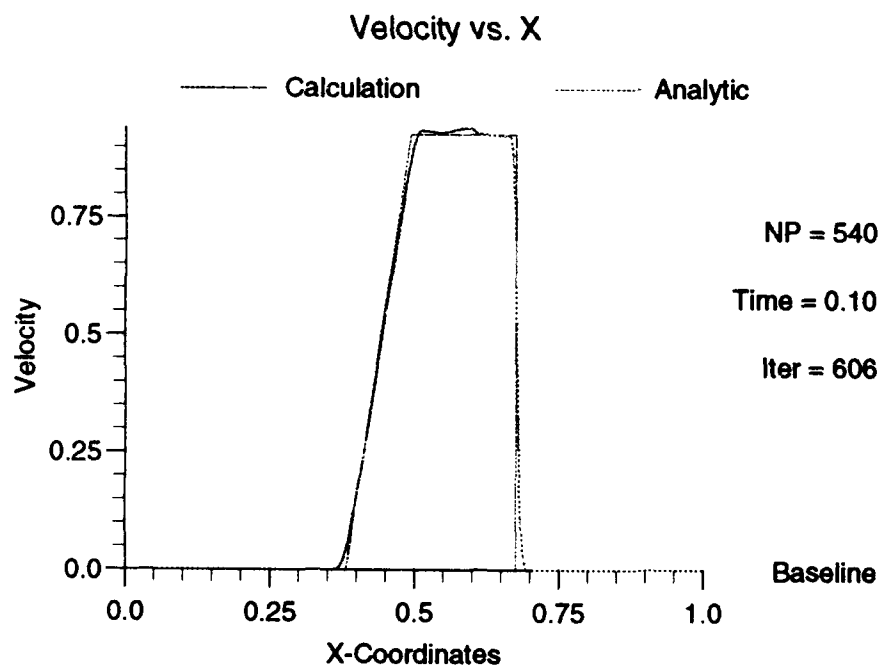
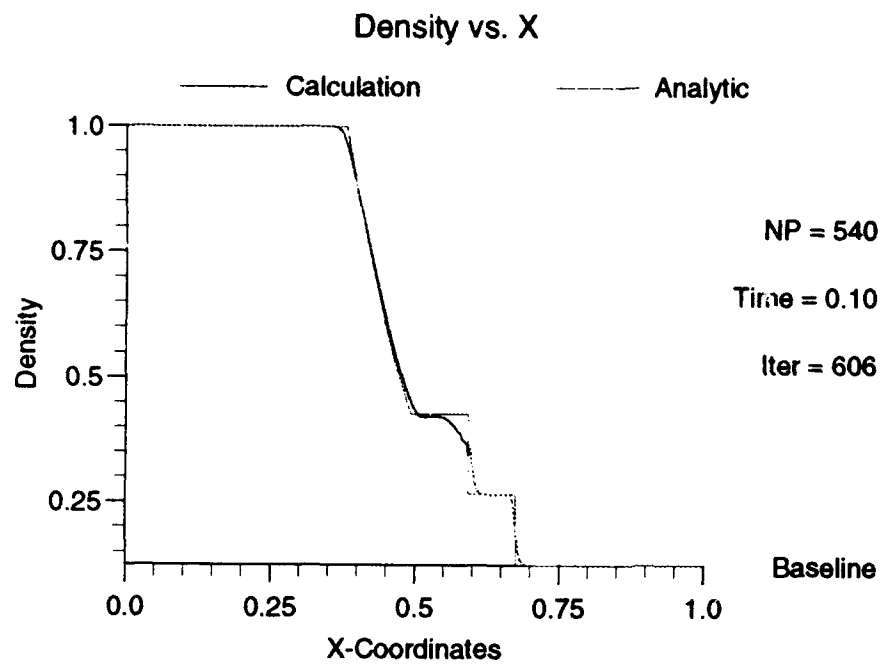


Figure 6.13 Shock Tube Results, Selected Kernel

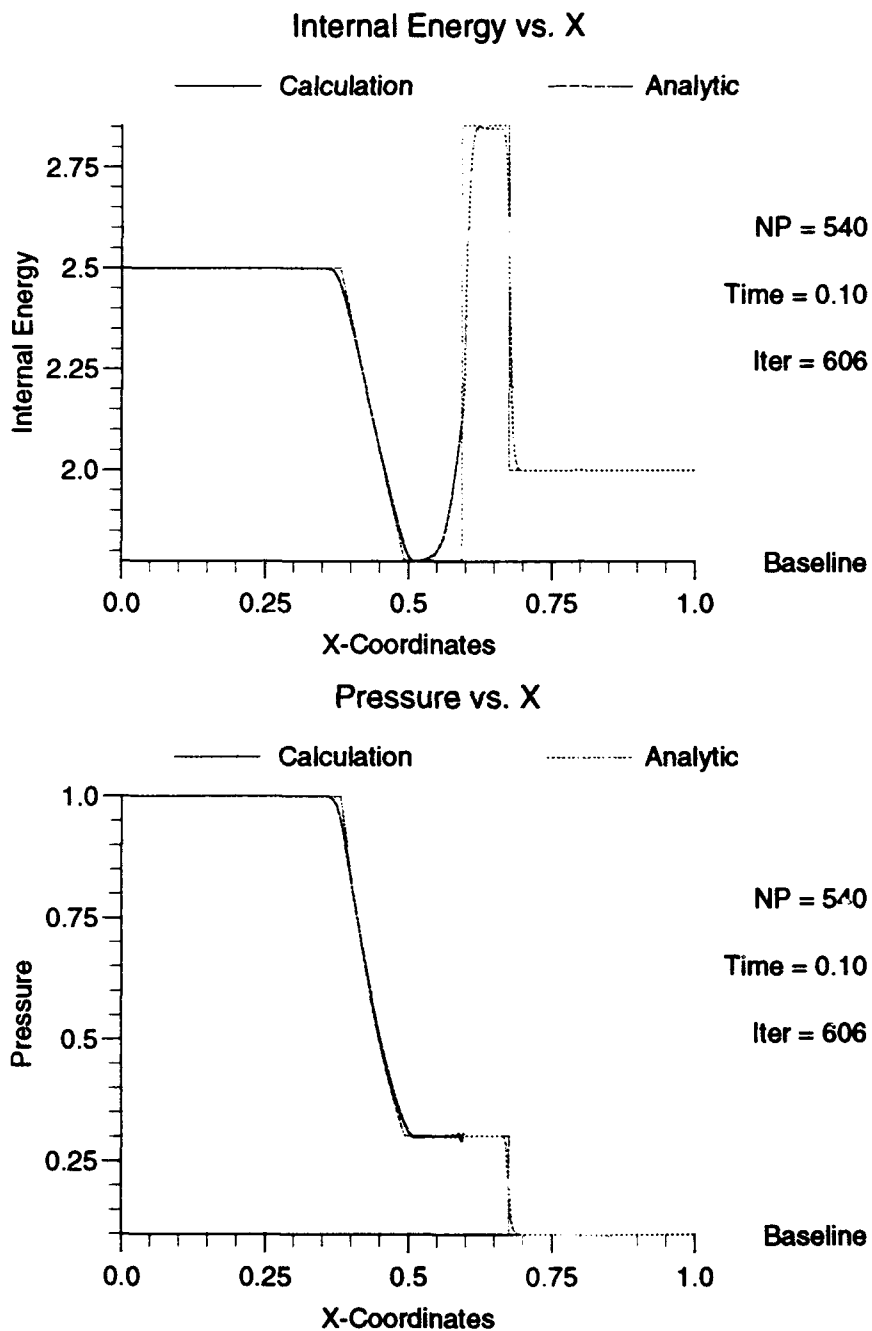


Figure 6.14 Shock Tube Results, Selected Kernel

Error norm results for the selected kernels are shown in Table C.11 in Appendix C. For more details on the calculation of the errors see equations (8.10) and (8.11) and the surrounding material in Chapter VIII. The data in this table is more easily seen in Figures 6.15 and 6.17.

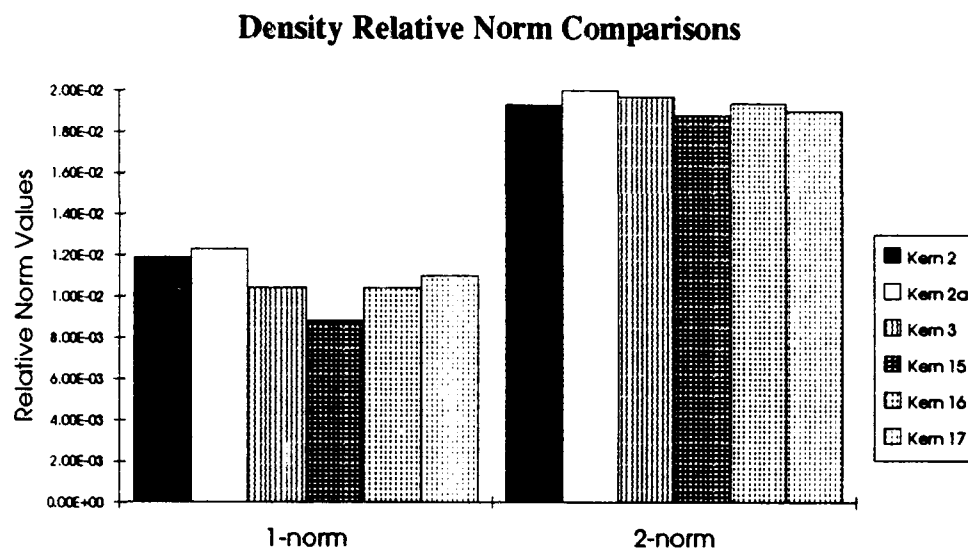
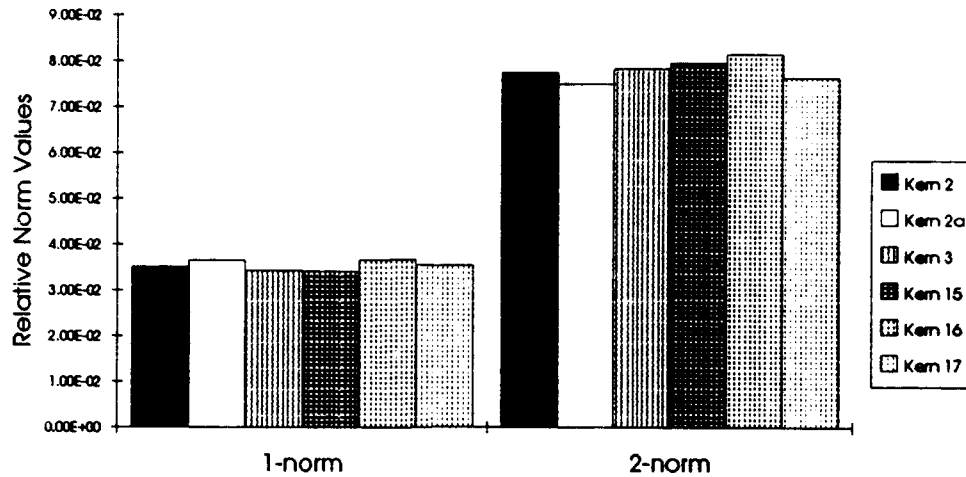


Figure 6.15 Shock Tube Results, Density Comparisons

Some general conclusions may be drawn from Figures 6.15 and 6.17. First, when using kernel 2 (the B-Spline), the results are slightly better when using the recommended starting ratio of 0.6899 instead of 0.6667 (kernel 2a). Note: a starting value of $2/3$ is common in the literature. Second, the Q-Gaussian (kernel 15) performed the best, but the results for these five kernels are so close that all should be considered equally good. Third, using hyperbolic or parabolic shaped kernels is quite risky, the problem may abort, and they are not recommended.

Velocity Relative Norm Comparisons



Energy Relative Norm Comparisons

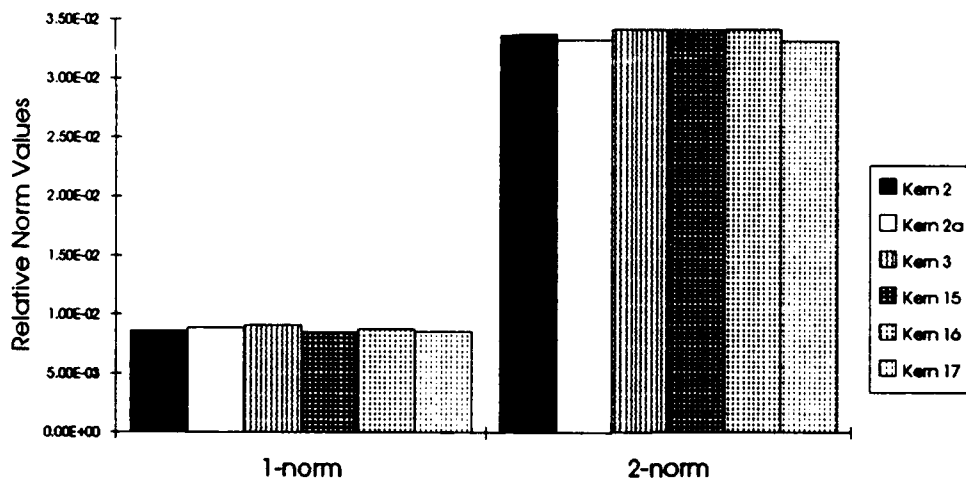


Figure 6.16 Shock Tube Results, Velocity and Energy Comparisons

Pressure Relative Norm Comparisons

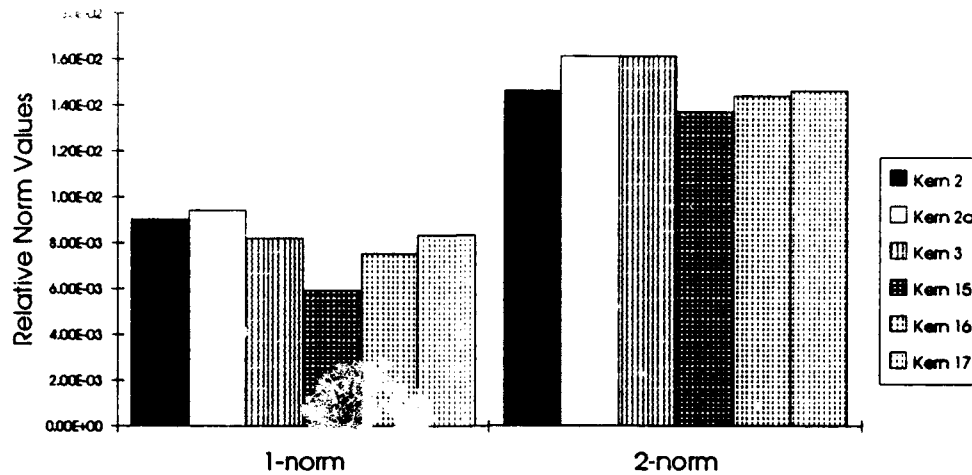


Figure 6.17 Shock Tube Results, Pressure Comparisons

6.3 Conclusions

Much of the data and information in this chapter speaks for itself. However, in this last section some comments are made regarding the data and, in particular, the better and poorer kernels.

- $\kappa - 2$ kernels. Taking a kernel with a wider κ , such as the Gaussian, and modifying it to make κ smaller seems reasonable. However, the process used in the $\kappa - 2$ Exponential and $\kappa - 2$ Gaussian is not very good and should be avoided because the resulting kernel is too highly peaked.
- For smooth data almost any bell shaped kernel provides good results. Of the nine studied, the $\kappa - 2$ Gaussian was the poorest. Although the Q Gaussian performed the best, most of the others are so close as to be considered tied for best.

- Overall the Test 2 equation appears to be a quite good measure of merit for smooth data kernels. It matched the test data well and is easy to calculate using some math package such as Mathematica.
- For non-smooth data almost any kernel provides acceptable results. The parabolics performed slightly worse, but it is not clear if it is a significant difference.
- The $K(0)$ checks for non-smooth data appear to be a fair measures of merit for symmetric kernels on non-smooth data. Since most kernels perform roughly the same for non-smooth data, it is difficult to determine the exact quality of this measure.
- One-sided kernels in general perform poorer than two-sided in non-smooth areas and much worse in smooth areas. This is not obvious as those kernels lead to schemes analogous to upwind schemes. which are usually quite good in finite differences. However, for now, based on this research, using one-sided kernels is not recommend.

VII. TIME SCHEMES

This chapter addresses temporal discretizations that can be applied with the SPH spatial discretization for the complete implementation of the method. It relies on some of the analysis performed in Chapters III, IV, and VI in developing these schemes. The discussion in the previous chapters has only involved the spatial derivatives and function approximation aspects of SPH. These are the parts that primarily make up SPH, but they leave a system of ordinary differential equations (in time) to solve. Therefore, a time scheme must be added to the previous analysis to discretize the Euler equations completely.

In this chapter both higher and lower order schemes are developed. The higher order schemes are Lax-Wendroff, Central, and Shu; all of which are second order in time. The lower order schemes are Upwind and Lax-Friedrichs; which are first order in time. The main purpose of this chapter is to simply introduce these ideas to SPH and show that several times schemes are available. The Lax-Wendroff is probably not going to be very useful for production type SPH computer codes, but should prove quite useful in algorithm development. The Central and Shu schemes are both good choices for the larger problems. By themselves, the lower order schemes are probably not of much interest; however, they are an integral part of the hybrid schemes developed in Chapter VIII.

There are several variations to the Euler equations that may be used in HVI problems; for the analysis in this chapter a one dimensional form given by Anderson (1) or Zukas (72) is used:

$$\text{Continuity Equation : } \frac{D\rho}{Dt} = -\rho \frac{\partial v}{\partial x} \quad (7.1)$$

$$\text{Momentum Equation : } \frac{Dv}{Dt} = -\frac{1}{\rho} \frac{\partial P}{\partial x} \quad (7.2)$$

$$\text{Energy Equation : } \frac{De}{Dt} = -\frac{P}{\rho} \frac{\partial v}{\partial x} \quad (7.3)$$

$$\text{Particle Motion Equation : } \frac{Dx}{Dt} = v . \quad (7.4)$$

The discussion to follow also refers to the general conservation equation and the one dimensional, first order wave equation; they are respectively

$$u_t + [f(u)]_x = 0 \quad (7.5)$$

$$u_t + au_x = 0 . \quad (7.6)$$

The work in this chapter concentrates on three explicit methods. However, implicit, predictor-corrector, or additional explicit (such as Runge-Kutta) type schemes could also be applied. The cost for the implicit methods probably make them unusable for many of the large scale problems associated with HVI. This is because in SPH each particle has a variable number of non-zero contributing neighbors. Thus the use of banded solvers is eliminated and full matrix solvers are often quite expensive. Some preliminary experimentation was done with a Heun second order predictor-corrector, but the initial work showed no significant improvement over a central time scheme (described below). Hence, further development of this method was not done at this time. Lower order explicit Runge-Kutta methods are essentially what is being considering. The forward Euler method is not used because it is first order in time and forward time/central space is often treated as unstable in finite differences (although it is actually conditionally stable). So forward time/symmetric kernel space would probably not be a good choice in SPH. Higher order Runge-Kutta methods could be used, they just require additional function evaluations and storage. This might be a problem for large scale problems.

So the effort is concentrated on the three main schemes: Lax-Wendroff, Central, and Shu. All three are used in finite differences, often with good results. Central time has been in use with SPH since its inception while the other methods are being used here for the first time with SPH.

7.1 Lax-Wendroff

This scheme was first developed by Lax and Wendroff (29) in 1960 and it uses a Taylor series expansion approach. In the finite difference literature it is one of the most prominent second order schemes. The scheme is introduced here using the first order wave equation and then derived using the SPH form for the Euler equations.

7.1.1 First Order Wave Equation. The Lax-Wendroff finite difference form for the first order wave equation is

$$u_i^{n+1} = u_i^n - \frac{a \Delta t}{2 \Delta x} (u_{i+1}^n - u_{i-1}^n) + \frac{a^2 \Delta t^2}{2 \Delta x^2} (u_{i+1}^n - 2u_i^n + u_{i-1}^n). \quad (7.7)$$

This method is second order in both time and space, can be written in conservation form, and is conditionally stable. As seen above, the first order space derivative uses a central space form. The same flavor may be obtained in SPH by using a standard symmetric kernel. The second order space derivative is also a central difference form. This too is analogous in SPH to using a symmetric kernel, but requires W' to be smooth and have compact support. Most of the bell shaped kernels discussed in the previous chapter fit these requirements quite well. The SPH form of Lax-Wendroff for the wave equation is defined as

$$u_i^{n+1} = u_i^n - a \Delta t \sum_{j=1}^N \Delta x_j u_j^n W'_{ij} + \frac{a^2 \Delta t^2}{2} \sum_{j=1}^N \Delta x_j u_j^n \tilde{W}''_{ij}. \quad (7.8)$$

Note that W and \tilde{W} can be the same kernel, but do not have to be. An intriguing variation is obtained if the SPH function approximation is used for u_i^n in equation (7.8) and just one kernel is used. Collect terms to obtain

$$u_i^{n+1} = \sum_{j=1}^N \Delta x_j u_j^n \left[W_{ij} - a \Delta t W'_{ij} + \frac{a^2 \Delta t^2}{2} W''_{ij} \right]. \quad (7.9)$$

The formula in brackets in equation (7.9) is simply a Taylor series expansion of $W(x_i - x_j - a\Delta t)$ to three terms. This makes the right hand side of equation (7.9) equivalent to the SPH function approximation for u_i using u_j at time t_n and x at time t_{n+1} in the kernel.

In order to extend this work to SPH one needs to look beyond the formula for Lax-Wendroff given earlier to the idea behind the method and how it was derived. Quite simply, u_i^{n+1} is expanded in a Taylor series around u_i^n . The first order time derivative is replaced by a spatial derivative according to the PDE. For the second order time derivative, take the derivative with respect to time of the PDE and rearrange terms until a form with only the function and spatial derivatives is obtained. Of course, this is rather simple for a linear PDE, but for a non-linear system it is much more complicated.

7.1.2 Euler Equations. Following the expansion and reorganization ideas described above for each of the conservation equations, SPH Lax-Wendroff forms the Euler equations may be developed.

Continuity Equation

$$\begin{aligned}
 \rho_i^{n+1} &= \rho_i^n + \Delta t \frac{D\rho_i^n}{Dt} + \frac{\Delta t^2}{2} \frac{D^2\rho_i^n}{Dt^2} + O(\Delta t^3) \\
 \frac{D\rho}{Dt} &= -\rho \frac{\partial v}{\partial x} \\
 \frac{D^2\rho}{Dt^2} &= \frac{D}{Dt} \left(\frac{D\rho}{Dt} \right) = \frac{D}{Dt} \left(-\rho \frac{\partial v}{\partial x} \right) = -\frac{D\rho}{Dt} \frac{\partial v}{\partial x} - \rho \frac{D}{Dt} \left(\frac{\partial v}{\partial x} \right) \\
 &= \rho \left(\frac{\partial v}{\partial x} \right)^2 - \rho \frac{\partial}{\partial t} \left(\frac{\partial v}{\partial x} \right) - \rho v \frac{\partial}{\partial x} \left(\frac{\partial v}{\partial x} \right) \\
 &= \rho \left(\frac{\partial v}{\partial x} \right)^2 - \rho \frac{\partial}{\partial x} \left(\frac{\partial v}{\partial t} \right) - \rho v \frac{\partial}{\partial x} \left(\frac{\partial v}{\partial x} \right) \pm \rho \frac{\partial}{\partial x} \left(v \frac{\partial v}{\partial x} \right) \\
 &= \rho \left(\frac{\partial v}{\partial x} \right)^2 - \rho \frac{\partial}{\partial x} \left(\frac{\partial v}{\partial t} + v \frac{\partial v}{\partial x} \right) + \rho \frac{\partial}{\partial x} \left(v \frac{\partial v}{\partial x} \right) - \rho v \frac{\partial}{\partial x} \left(\frac{\partial v}{\partial x} \right) \\
 &= \rho \left(\frac{\partial v}{\partial x} \right)^2 - \rho \frac{\partial}{\partial x} \left(\frac{Dv}{Dt} \right) + \rho \left(\frac{\partial v}{\partial x} \right)^2
 \end{aligned}$$

$$= 2\rho \left(\frac{\partial v}{\partial x} \right)^2 - \rho \frac{\partial}{\partial x} \left(-\frac{1}{\rho} \frac{\partial P}{\partial x} \right) = \rho \left[2 \left(\frac{\partial v}{\partial x} \right)^2 + \frac{\partial}{\partial x} \left(\frac{1}{\rho} \frac{\partial P}{\partial x} \right) \right]$$

Use the forms derived above to obtain for the continuity equation

$$\rho_i^{n+1} = \rho_i^n + \Delta t \left(-\rho \frac{\partial v}{\partial x} \right)_i^n + \frac{\Delta t^2}{2} \rho_i^n \left[2 \left(\frac{\partial v}{\partial x} \right)^2 + \frac{\partial}{\partial x} \left(\frac{1}{\rho} \frac{\partial P}{\partial x} \right) \right]_i^n + O(\Delta t^3). \quad (7.10)$$

Momentum Equation

$$v_i^{n+1} = v_i^n + \Delta t \frac{Dv_i^n}{Dt} + \frac{\Delta t^2}{2} \frac{D^2 v_i^n}{Dt^2} + O(\Delta t^3)$$

$$\frac{Dv}{Dt} = -\frac{1}{\rho} \frac{\partial P}{\partial x}$$

$$\begin{aligned} \frac{D^2 v}{Dt^2} &= \frac{D}{Dt} \left(\frac{Dv}{Dt} \right) = \frac{D}{Dt} \left(-\frac{1}{\rho} \frac{\partial P}{\partial x} \right) = -\frac{D \left(\frac{1}{\rho} \right)}{Dt} \frac{\partial P}{\partial x} - \frac{1}{\rho} \frac{D}{Dt} \left(\frac{\partial P}{\partial x} \right) \\ &= \frac{1}{\rho^2} \left(\frac{\partial P}{\partial x} \right) \frac{D\rho}{Dt} - \frac{1}{\rho} \frac{\partial}{\partial t} \left(\frac{\partial P}{\partial x} \right) - \frac{v}{\rho} \frac{\partial}{\partial x} \left(\frac{\partial P}{\partial x} \right) \\ &= -\frac{1}{\rho} \left(\frac{\partial P}{\partial x} \right) \left(\frac{\partial v}{\partial x} \right) - \frac{1}{\rho} \frac{\partial}{\partial x} \left(\frac{\partial P}{\partial t} \right) - \frac{v}{\rho} \left(\frac{\partial^2 P}{\partial x^2} \right) \end{aligned} \quad (7.11)$$

$$\begin{aligned} \frac{\partial P}{\partial t} &= \frac{\partial P}{\partial \rho} \frac{\partial \rho}{\partial t} + \frac{\partial P}{\partial e} \frac{\partial e}{\partial t} = \left(\frac{\partial P}{\partial \rho} \right) \left(-\rho \frac{\partial v}{\partial x} - v \frac{\partial \rho}{\partial x} \right) \\ &\quad + \left(\frac{\partial P}{\partial e} \right) \left(-\frac{P}{\rho} \frac{\partial v}{\partial x} - v \frac{\partial e}{\partial x} \right) \\ \frac{\partial}{\partial x} \left(\frac{\partial P}{\partial t} \right) &= \left(\frac{\partial^2 P}{\partial x \partial \rho} \right) \left(-\rho \frac{\partial v}{\partial x} - v \frac{\partial \rho}{\partial x} \right) + \left(\frac{\partial P}{\partial \rho} \right) \left(-2 \frac{\partial \rho}{\partial x} \frac{\partial v}{\partial x} - \rho \frac{\partial^2 v}{\partial x^2} - v \frac{\partial^2 \rho}{\partial x^2} \right) \\ &\quad + \left(\frac{\partial^2 P}{\partial x \partial e} \right) \left(-\frac{P}{\rho} \frac{\partial v}{\partial x} - v \frac{\partial e}{\partial x} \right) \\ &\quad + \left(\frac{\partial P}{\partial e} \right) \left(-\frac{\partial}{\partial x} \left(\frac{P}{\rho} \right) \frac{\partial v}{\partial x} - \frac{P}{\rho} \frac{\partial^2 v}{\partial x^2} - v \frac{\partial^2 e}{\partial x^2} - \frac{\partial v}{\partial x} \frac{\partial e}{\partial x} \right) \end{aligned} \quad (7.12)$$

Use equation (7.12) in (7.11) to obtain

$$\begin{aligned}
\frac{D^2 v}{Dt} = & \left[-\frac{v}{\rho} \left(\frac{\partial^2 P}{\partial x^2} \right) + \frac{v}{\rho} \left(\frac{\partial P}{\partial \rho} \right) \left(\frac{\partial^2 \rho}{\partial x^2} \right) + \left(\frac{\partial P}{\partial \rho} \right) \left(\frac{\partial^2 v}{\partial x^2} \right) + \frac{P}{\rho^2} \left(\frac{\partial P}{\partial \epsilon} \right) \left(\frac{\partial^2 v}{\partial x^2} \right) \right. \\
& + \left. \frac{v}{\rho} \left(\frac{\partial P}{\partial \epsilon} \right) \left(\frac{\partial^2 \epsilon}{\partial x^2} \right) \right] + \left[-\frac{1}{\rho} \left(\frac{\partial P}{\partial x} \right) \left(\frac{\partial v}{\partial x} \right) + \frac{v}{\rho} \left(\frac{\partial^2 P}{\partial x \partial \rho} \right) \left(\frac{\partial \rho}{\partial x} \right) \right. \\
& + \left(\frac{\partial^2 P}{\partial x \partial \rho} \right) \left(\frac{\partial v}{\partial x} \right) + \frac{2}{\rho} \left(\frac{\partial P}{\partial \rho} \right) \left(\frac{\partial \rho}{\partial x} \right) \left(\frac{\partial v}{\partial x} \right) + \frac{P}{\rho^2} \left(\frac{\partial v}{\partial x} \right) \left(\frac{\partial^2 P}{\partial x \partial \epsilon} \right) \\
& + \frac{v}{\rho} \left(\frac{\partial^2 P}{\partial x \partial \epsilon} \right) \left(\frac{\partial \epsilon}{\partial x} \right) + \frac{1}{\rho} \left(\frac{\partial P}{\partial \epsilon} \right) \left(\frac{\partial v}{\partial x} \right) \frac{\partial}{\partial x} \left(\frac{P}{\rho} \right) \\
& \left. + \frac{1}{\rho} \left(\frac{\partial P}{\partial \epsilon} \right) \left(\frac{\partial v}{\partial x} \right) \left(\frac{\partial \epsilon}{\partial x} \right) \right] \quad (7.13)
\end{aligned}$$

$$\begin{aligned}
\frac{\partial P}{\partial x} &= \frac{\partial P}{\partial \rho} \frac{\partial \rho}{\partial x} + \frac{\partial P}{\partial \epsilon} \frac{\partial \epsilon}{\partial x} \\
\frac{\partial}{\partial x} \left(\frac{\partial P}{\partial x} \right) &= \left(\frac{\partial^2 P}{\partial x \partial \rho} \right) \left(\frac{\partial \rho}{\partial x} \right) + \left(\frac{\partial P}{\partial \rho} \right) \left(\frac{\partial^2 \rho}{\partial x^2} \right) \\
&+ \left(\frac{\partial^2 P}{\partial x \partial \epsilon} \right) \left(\frac{\partial \epsilon}{\partial x} \right) + \left(\frac{\partial P}{\partial \epsilon} \right) \left(\frac{\partial^2 \epsilon}{\partial x^2} \right) \quad (7.14)
\end{aligned}$$

Now use equation (7.14) in equation (7.13) and simplify to find

$$\frac{D^2 v}{Dt} = \frac{1}{\rho} \left(\frac{\partial^2 v}{\partial x^2} \right) \left(\rho \frac{\partial P}{\partial \rho} + \frac{P}{\rho} \frac{\partial P}{\partial \epsilon} \right) + \frac{1}{\rho} \left(\frac{\partial v}{\partial x} \right) \frac{\partial}{\partial x} \left(\rho \frac{\partial P}{\partial \rho} + \frac{P}{\rho} \frac{\partial P}{\partial \epsilon} \right).$$

Use the forms derived above to obtain for the momentum equation

$$\begin{aligned}
v_i^{n+1} = & v_i^n + \Delta t \left(-\frac{1}{\rho} \frac{\partial P}{\partial x} \right)_i^n + \frac{\Delta t^2}{2} \frac{1}{\rho_i^n} \left[\left(\frac{\partial^2 v}{\partial x^2} \right) \left(\rho \frac{\partial P}{\partial \rho} + \frac{P}{\rho} \frac{\partial P}{\partial \epsilon} \right) \right. \\
& \left. + \left(\frac{\partial v}{\partial x} \right) \frac{\partial}{\partial x} \left(\rho \frac{\partial P}{\partial \rho} + \frac{P}{\rho} \frac{\partial P}{\partial \epsilon} \right) \right]_i^n + O(\Delta t^3). \quad (7.15)
\end{aligned}$$

Energy Equation

$$\begin{aligned}
e_i^{n+1} &= e_i^n + \Delta t \frac{De_i^n}{Dt} + \frac{\Delta t^2}{2} \frac{D^2 e_i^n}{Dt^2} + O(\Delta t^3) \\
\frac{De}{Dt} &= -\frac{P}{\rho} \frac{\partial v}{\partial x}
\end{aligned}$$

$$\begin{aligned}
\frac{D^2 \epsilon}{Dt^2} &= \frac{D}{Dt} \left(\frac{D\epsilon}{Dt} \right) = \frac{D}{Dt} \left(-\frac{P}{\rho} \frac{\partial v}{\partial x} \right) = -\frac{D \left(\frac{P}{\rho} \right)}{Dt} \frac{\partial v}{\partial x} - \frac{P}{\rho} \frac{D}{Dt} \left(\frac{\partial v}{\partial x} \right) \\
&= -\frac{1}{\rho} \left(\frac{DP}{Dt} \right) \left(\frac{\partial v}{\partial x} \right) + \frac{P}{\rho^2} \left(\frac{D\rho}{Dt} \right) \left(\frac{\partial v}{\partial x} \right) - \frac{P}{\rho} \frac{\partial}{\partial t} \left(\frac{\partial v}{\partial x} \right) - \frac{Pv}{\rho} \left(\frac{\partial^2 v}{\partial x^2} \right) \\
&= -\frac{1}{\rho} \left(\frac{DP}{Dt} \right) \left(\frac{\partial v}{\partial x} \right) - \frac{P}{\rho} \left(\frac{\partial v}{\partial x} \right)^2 - \frac{P}{\rho} \frac{\partial}{\partial x} \left(\frac{\partial v}{\partial t} + v \frac{\partial v}{\partial x} \right) \\
&\quad + \frac{P}{\rho} \frac{\partial}{\partial x} \left(v \frac{\partial v}{\partial x} \right) - \frac{Pv}{\rho} \left(\frac{\partial^2 v}{\partial x^2} \right) \\
&= -\frac{1}{\rho} \left(\frac{DP}{Dt} \right) \left(\frac{\partial v}{\partial x} \right) - \frac{P}{\rho} \left(\frac{\partial v}{\partial x} \right)^2 - \frac{P}{\rho} \frac{\partial}{\partial x} \left(\frac{Dv}{Dt} \right) + \frac{P}{\rho} \left(\frac{\partial v}{\partial x} \right)^2 \\
&= -\frac{1}{\rho} \left(\frac{\partial v}{\partial x} \right) \left(\frac{DP}{Dt} \right) + \frac{P}{\rho} \frac{\partial}{\partial x} \left(\frac{1}{\rho} \frac{\partial P}{\partial x} \right) \tag{7.16}
\end{aligned}$$

$$\begin{aligned}
\frac{DP}{Dt} &= \frac{\partial P}{\partial t} + v \frac{\partial P}{\partial x} = \left(\frac{\partial P}{\partial \rho} \right) \left(\frac{\partial \rho}{\partial t} + v \frac{\partial \rho}{\partial x} \right) + \left(\frac{\partial P}{\partial \epsilon} \right) \left(\frac{\partial \epsilon}{\partial t} + v \frac{\partial \epsilon}{\partial x} \right) \\
&= \left(\frac{\partial P}{\partial \rho} \right) \left(\frac{D\rho}{Dt} \right) + \left(\frac{\partial P}{\partial \epsilon} \right) \left(\frac{D\epsilon}{Dt} \right) \tag{7.17}
\end{aligned}$$

Use equation (7.17) in equation (7.16) to obtain

$$\begin{aligned}
\frac{D^2 \epsilon}{Dt^2} &= -\frac{1}{\rho} \left(\frac{\partial v}{\partial x} \right) \left(\frac{\partial P}{\partial \rho} \right) \left(-\rho \frac{\partial v}{\partial x} \right) - \frac{1}{\rho} \left(\frac{\partial v}{\partial x} \right) \left(\frac{\partial P}{\partial \epsilon} \right) \left(-\frac{P}{\rho} \frac{\partial v}{\partial x} \right) + \frac{P}{\rho} \frac{\partial}{\partial x} \left(\frac{1}{\rho} \frac{\partial P}{\partial x} \right) \\
&= \left(\frac{\partial v}{\partial x} \right)^2 \left[\left(\frac{\partial P}{\partial \rho} \right) + \frac{P}{\rho^2} \left(\frac{\partial P}{\partial \epsilon} \right) \right] + \frac{P}{\rho} \frac{\partial}{\partial x} \left(\frac{1}{\rho} \frac{\partial P}{\partial x} \right) .
\end{aligned}$$

Use the forms derived above to obtain for the energy equation

$$\begin{aligned}
e_i^{n+1} &= e_i^n + \Delta t \left(-\frac{P}{\rho} \frac{\partial v}{\partial x} \right)_i + \frac{\Delta t^2}{2} \left[\left(\frac{\partial v}{\partial x} \right)^2 \left(\frac{\partial P}{\partial \rho} + \frac{P}{\rho^2} \left(\frac{\partial P}{\partial \epsilon} \right) \right) \right. \\
&\quad \left. + \left(\frac{P}{\rho} \right) \frac{\partial}{\partial x} \left(\frac{1}{\rho} \frac{\partial P}{\partial x} \right) \right]_i + O(\Delta t^3) . \tag{7.18}
\end{aligned}$$

One SPH Form. Based on the three equations developed above, (7.10), (7.15), and (7.18) the SPH equations may now be derived for these. Since for any derivative there are many SPH forms, there cannot be just one Lax-Wendroff SPH form. The one included here uses symmetric forms of the equations where possible to help

maintain conservation.

$$S1_i^n = \frac{\partial v_i^n}{\partial x} = -\frac{1}{\rho_i^n} \left[\frac{\partial}{\partial x} (\rho v)_i^n - v_i^n \frac{\partial \rho_i^n}{\partial x} \right] \approx -\frac{1}{\rho_i^n} \sum_{j=1}^N m_j (v_i^n - v_j^n) W'_{ij} \quad (7.19)$$

$$\begin{aligned} S2_i^n &= \rho_i^n \frac{\partial}{\partial x} \left(\frac{1}{\rho_i^n} \frac{\partial P_i^n}{\partial x} \right) = \frac{1}{\rho_i^n} \left[\frac{\partial^2 (P\rho)}{\partial x^2} - P \frac{\partial^2 \rho}{\partial x^2} \right]_i^n + \left(-3 \frac{\partial \rho_i^n}{\partial x} \right) \left(\frac{1}{\rho_i^n} \frac{\partial P_i^n}{\partial x} \right) \\ &\approx \sum_{j=1}^N \frac{m_j}{\rho_i^n} (P_j^n - P_i^n) W''_{ij} + 3 \left[\sum_{j=1}^N \frac{m_j}{\rho_j^n} (\rho_i^n - \rho_j^n) W'_{ij} \right] \\ &\quad \times \left[\sum_{j=1}^N m_j \left(\frac{P_j^n}{\rho_j^2} + \frac{P_i^n}{\rho_i^2} \right) W'_{ij} \right] \end{aligned} \quad (7.20)$$

$$S3_i^n = \frac{1}{\rho_i^n} \frac{\partial P_i^n}{\partial x} \approx \sum_{j=1}^N m_j \left(\frac{P_j^n}{\rho_j^2} + \frac{P_i^n}{\rho_i^2} \right) W'_{ij} \quad (7.21)$$

$$\begin{aligned} S4_i^n &= \frac{\partial^2 v}{\partial x^2} = \frac{1}{\rho_i^n} \left[\frac{\partial^2 (v\rho)}{\partial x^2} - v \frac{\partial^2 \rho}{\partial x^2} \right]_i^n - \frac{2}{\rho_i^n} \frac{\partial v_i^n}{\partial x} \frac{\partial \rho_i^n}{\partial x} \approx -\sum_{j=1}^N \frac{m_j}{\rho_i^n} (v_i^n - v_j^n) W''_{ij} \\ &\quad - \frac{2}{\rho_i^n} \left[\frac{1}{\rho_i^n} \sum_{j=1}^N m_j (v_i^n - v_j^n) W'_{ij} \right] \left[\sum_{j=1}^N \frac{m_j}{\rho_j^n} (\rho_i^n - \rho_j^n) W'_{ij} \right] \end{aligned} \quad (7.22)$$

$$S5_i^n = \frac{\partial}{\partial x} \left(\rho_i^n \frac{\partial P_i^n}{\partial \rho} + \frac{P_i^n}{\rho_i^n} \frac{\partial P_i^n}{\partial e} \right) \approx \sum_{j=1}^N m_j \left[\left(\frac{\partial P}{\partial \rho} \right)_i^n + \frac{P_j^n}{(\rho_j^n)^2} \left(\frac{\partial P}{\partial e} \right)_i^n \right] W'_{ij} \quad (7.23)$$

$$S6_i^n = -\frac{P_i^n}{\rho_i^n} \frac{\partial v_i^n}{\partial x} \approx \frac{1}{2} \sum_{j=1}^N m_j \left(\frac{P_j^n}{\rho_j^2} + \frac{P_i^n}{\rho_i^2} \right) (v_i^n - v_j^n) W'_{ij} \quad (7.24)$$

$$\rho_i^{n+1} = \rho_i^n \left[1 - \Delta t S1_i^n + \frac{\Delta t^2}{2} (S1_i^n)^2 \right] + \frac{\Delta t^2}{2} [(S1_i^n)^2 \rho_i^n + S2_i^n] \quad (7.25)$$

$$\begin{aligned} v_i^{n+1} &= v_i^n - \Delta t S3_i^n + \frac{\Delta t^2}{2} \left\{ \left[\left(\frac{\partial P}{\partial \rho} \right)_i^n + \frac{P_i^n}{\rho_i^2} \left(\frac{\partial P}{\partial e} \right)_i^n \right] S4_i^n \right. \\ &\quad \left. + \frac{1}{\rho_i^n} S1_i^n S5_i^n \right\} \end{aligned} \quad (7.26)$$

$$\begin{aligned} e_i^{n+1} &= e_i^n + \Delta t S6_i^n + \frac{\Delta t^2}{2} \left\{ (S1_i^n)^2 \left[\left(\frac{\partial P}{\partial \rho} \right)_i^n + \frac{P_i^n}{\rho_i^2} \left(\frac{\partial P}{\partial e} \right)_i^n \right] \right. \\ &\quad \left. + \frac{P_i^n}{(\rho_i^n)^2} S2_i^n \right\} \end{aligned} \quad (7.27)$$

$$x_i^{n+1} = x_i^n + \Delta t v_i^n - \frac{\Delta t^2}{2} S3_i^n \quad (7.28)$$

7.2 Central Time

The second time scheme considered is much simpler: using the central time approach. This is a rather easy to apply and a relatively old technique in SPH. It can be derived using either Taylor series expansions or the midpoint quadrature rule. The scheme is introduced using the general conservation equation and then derived using an SPH form for the Euler equations.

7.2.1 General Conservation Equation. The central time finite difference form for the general conservation equation is

$$u^{n+1} = u^{n-1} - 2\Delta t f(u^n)_x + O(\Delta t^3). \quad (7.29)$$

This method is second order in time, can be written in conservation form, and is conditionally stable. The method is derived below using a Taylor series form. Using the two Taylor series expansions

$$u^{n+1} = u^n + \Delta t (u^n)_t + \frac{\Delta t^2}{2} (u^n)_{tt} + \frac{\Delta t^3}{6} (u^n)_{ttt} + \dots \quad (7.30)$$

$$u^{n-1} = u^n - \Delta t (u^n)_t + \frac{\Delta t^2}{2} (u^n)_{tt} - \frac{\Delta t^3}{6} (u^n)_{ttt} + \dots \quad (7.31)$$

Subtract equation (7.31) from (7.30) to obtain the central time form

$$u^{n+1} = u^{n-1} + 2\Delta t (u^n)_t + \frac{2\Delta t^3}{6} (u^n)_{ttt} + \dots \quad (7.32)$$

Substituting the general conservation equation (7.5) into equation (7.32) for the temporal derivative term results in the form given earlier in equation (7.29).

7.2.2 Euler Equations. The final form of this method has just a first order time derivative which is replaced with a spatial derivative using the general conservation equation. So there is nothing special to applying this technique to the

Euler equations or in SPH. Hence, any SPH formulation for the spatial derivatives will work by directly substituting it into the general form (7.29). As with other time schemes, maintaining conservation is important, so symmetric forms of the SPH equations are usually best.

It was discovered that a common practice in SPH is to not use a true central time for all field variables as it is more costly, especially in memory requirements. Two variations are investigated which will be called approximate central time and near central time as well as a full central time approach. For full central time, two levels of some of the field variables are needed (at least ρ , v , e , and x). This should be the only additional cost of using a full central time approach; still it is sometimes not used. The other two forms use only one level of storage, but two passes through the particles. The first for velocity updates, the later for the remaining updates. This does not add any cost, just some additional code. This method is known as the approximate central time. The near central is the same as the approximate central except it does a correction for particle position between the two passes and recalculates the kernel for the second pass through the particles (\tilde{x}). It was also found that some people use an even simpler form with only one storage level and one pass (which is called faux central time here). However, this method is not recommended as it is essentially a forward time/central space type method (which is only first order and unstable for the usual time restriction, $\Delta t/h < \text{constant}$). These forms may be more easily understood symbolically

$$\begin{aligned}
 \text{Full Central Time:} \quad & v^{n+1} = v^{n-1} + F_1(\rho^n, e^n, x^n) \\
 & \rho^{n+1} = \rho^{n-1} + F_2(v^n, x^n) \\
 & e^{n+1} = e^{n-1} + F_3(\rho^n, e^n, v^n, x^n) \\
 & x^{n+1} = x^{n-1} + F_4(v^n) \\
 \text{Near Central Time:} \quad & v^n = v^{n-2} + F_1(\rho^{n-1}, e^{n-1}, x^{n-1}) \\
 & \rho^{n+1} = \rho^{n-1} + F_2(v^n, \tilde{x}^n)
 \end{aligned}$$

$$e^{n+1} = e^{n-1} + F_3(\rho^{n-1}, e^{n-1}, v^n, \dot{x}^n)$$

$$x^{n+1} = x^{n-1} + F_4(v^n)$$

Approximate Central Time: $v^n = v^{n-2} + F_1(\rho^{n-1}, e^{n-1}, x^{n-1})$

$$\rho^{n+1} = \rho^{n-1} + F_2(v^n, x^{n-1})$$

$$e^{n+1} = e^{n-1} + F_3(\rho^{n-1}, e^{n-1}, v^n, x^{n-1})$$

$$x^{n+1} = x^{n-1} + F_4(v^n)$$

Faux Central Time: $v^n = v^{n-2} + F_1(\rho^{n-1}, e^{n-1}, x^{n-1})$

$$\rho^{n+1} = \rho^{n-1} + F_2(v^{n-2}, x^{n-1})$$

$$e^{n+1} = e^{n-1} + F_3(\rho^{n-1}, e^{n-1}, v^{n-2}, x^{n-1})$$

$$x^{n+1} = x^{n-1} + F_4(v^{n-2})$$

The following is proposed as the complete discretization for full central time

$$\rho_i^{n+1} = \rho_i^{n-1} + 2 \Delta t \sum_{j=1}^N m_j (v_i^n - v_j^n) W'(x_i^n - x_j^n) \quad (7.33)$$

$$v_i^{n+1} = v_i^{n-1} - 2 \Delta t \sum_{j=1}^N m_j \left(\frac{P_j^n}{(\rho_j^n)^2} + \frac{P_i^n}{(\rho_i^n)^2} \right) W'(x_i^n - x_j^n) \quad (7.34)$$

$$e_i^{n+1} = e_i^{n-1} + \Delta t \sum_{j=1}^N m_j \left(\frac{P_j^n}{(\rho_j^n)^2} + \frac{P_i^n}{(\rho_i^n)^2} \right) (v_i^n - v_j^n) W'(x_i^n - x_j^n) \quad (7.35)$$

$$x_i^{n+1} = x_i^{n-1} + 2 \Delta t v_i^n. \quad (7.36)$$

7.3 Shu

The third scheme considered here was first developed by Shu (55) in 1988 and designed to be used with Total Variation Diminishing (TVD) finite difference schemes. Actually, the version presented here is just part of an entire class of TVD multilevel schemes proposed by Shu. This particular form was chosen out of that class because it was only 2-level and second order. Although this form rarely appears in the literature for finite differences, it seems to have some good potential. To my

knowledge this is the first time this scheme has been applied in SPH. This scheme is introduced using the general conservation equation and then derived using an SPH form for the Euler equations.

7.3.1 General Conservation Equation. The Shu finite difference form used here for the general conservation equation is

$$u^{n+1} = \frac{4}{5}u^n + \frac{1}{5}u^{n-1} - \frac{8}{5}\Delta t f(u^n)_x + \frac{2}{5}\Delta t f(u^{n-1})_x. \quad (7.37)$$

This method is second order in time, can be written in conservation form, and is conditionally stable. However, it is not readily apparent that the method is second order or that it is even consistent. Hence, the method is derived below. Note: the scheme is derived differently from Shu who derived the entire class as a whole. Start with the following three Taylor series expansions

$$u^{n+1} = u^n + \Delta t(u^n)_t + \frac{\Delta t^2}{2}(u^n)_{tt} + \frac{\Delta t^3}{6}(u^n)_{ttt} + \dots \quad (7.38)$$

$$u^{n+1} = u^{n-1} + 2\Delta t(u^{n-1})_t + \frac{(2\Delta t)^2}{2}(u^{n-1})_{tt} + \frac{(2\Delta t)^3}{6}(u^{n-1})_{ttt} + \dots \quad (7.39)$$

$$u^{n-1} = u^n - \Delta t(u^n)_t + \frac{\Delta t^2}{2}(u^n)_{tt} - \frac{\Delta t^3}{6}(u^n)_{ttt} + \dots \quad (7.40)$$

Subtract equation (7.40) from (7.38) to obtain the central time form

$$u^{n+1} = u^{n-1} + 2\Delta t(u^n)_t + \frac{2\Delta t^3}{6}(u^n)_{ttt} + \dots \quad (7.41)$$

Form the following weighted sum: $\frac{4}{5} * \text{Eqn (7.38)} - \frac{1}{5} * \text{Eqn (7.39)} + \frac{2}{5} * \text{Eqn (7.41)}$ to obtain

$$u^{n+1} = \frac{4}{5}u^n + \frac{1}{5}u^{n-1} + \frac{8}{5}\Delta t(u^n)_t - \frac{2}{5}\Delta t(u^{n-1})_t + E, \quad (7.42)$$

$$\text{where } E = \frac{2}{5}\Delta t^2[(u^n)_{tt} - (u^{n-1})_{tt}] + \frac{4}{15}\Delta t^3[(u^n)_{ttt} - (u^{n-1})_{ttt}] + O(\Delta t^4).$$

$$\text{But, } (u^n)_{tt} - (u^{n-1})_{tt} = \Delta t(u^n)_{ttt} + O(\Delta t^2)$$

$$\begin{aligned}
& \text{and} \quad (u^n)_{ttt} - (u^{n-1})_{ttt} = \Delta t (u^n)_{tttt} + O(\Delta t^2), \\
\text{so } E &= \frac{2}{5} \Delta t^3 [(u^n)_{ttt} + O(\Delta t)] + \frac{4}{15} \Delta t^4 [(u^n)_{tttt} + O(\Delta t)] + O(\Delta t^4) \\
&= \frac{2}{5} \Delta t^3 (u^n)_{ttt} + O(\Delta t^4). \tag{7.43}
\end{aligned}$$

Substituting the general conservation equation (7.5) into equation (7.42) yields the form given earlier in equation (7.37). Also, as seen in equation (7.43), the method is consistent and second order.

7.3.2 Euler Equations. As with central time, this method ends up with just a first order time derivative which is replaced with a spatial derivative using the general conservation equation. So there is nothing special to applying this technique to the Euler equations or in SPH. Hence, any SPH formulation may be chosen and directly substituted it into this form. As with other time schemes, maintaining conservation is important, so symmetric forms of the SPH equations is usually best. With that in mind, the following is proposed for the complete discretization

$$\begin{aligned}
\rho_i^{n+1} &= \frac{4}{5} \rho_i^n + \frac{1}{5} \rho_i^{n-1} + \Delta t \sum_{j=1}^N m_j \left[\frac{8}{5} (v_i^n - v_j^n) W'(x_i^n - x_j^n) \right. \\
&\quad \left. - \frac{2}{5} (v_i^{n-1} - v_j^{n-1}) W'(x_i^{n-1} - x_j^{n-1}) \right] \tag{7.44}
\end{aligned}$$

$$\begin{aligned}
v_i^{n+1} &= \frac{4}{5} v_i^n + \frac{1}{5} v_i^{n-1} - \Delta t \sum_{j=1}^N m_j \left[\frac{8}{5} \left(\frac{P_j^n}{(\rho_j^n)^2} + \frac{P_i^n}{(\rho_i^n)^2} \right) W'(x_i^n - x_j^n) \right. \\
&\quad \left. - \frac{2}{5} \left(\frac{P_j^{n-1}}{(\rho_j^{n-1})^2} + \frac{P_i^{n-1}}{(\rho_i^{n-1})^2} \right) W'(x_i^{n-1} - x_j^{n-1}) \right] \tag{7.45}
\end{aligned}$$

$$\begin{aligned}
e_i^{n+1} &= \frac{4}{5} e_i^n + \frac{1}{5} e_i^{n-1} + \frac{1}{2} \Delta t \sum_{j=1}^N m_j \left[\frac{8}{5} \left(\frac{P_j^n}{(\rho_j^n)^2} + \frac{P_i^n}{(\rho_i^n)^2} \right) (v_i^n - v_j^n) W'(x_i^n - x_j^n) \right. \\
&\quad \left. - \frac{2}{5} \left(\frac{P_j^{n-1}}{(\rho_j^{n-1})^2} + \frac{P_i^{n-1}}{(\rho_i^{n-1})^2} \right) (v_i^{n-1} - v_j^{n-1}) W'(x_i^{n-1} - x_j^{n-1}) \right] \tag{7.46}
\end{aligned}$$

$$x_i^{n+1} = \frac{4}{5} x_i^n + \frac{1}{5} x_i^{n-1} + \Delta t \left[\frac{8}{5} v_i^n - \frac{2}{5} v_i^{n-1} \right]. \tag{7.47}$$

7.4 Lower Order Methods

Since three second order time schemes were just developed, and SPH is usually second order in space, to develop a lower order scheme now seems to be going backwards. However, the hybrid methods discussed in the next chapter make use of both higher and lower order schemes, so the basic information will be provided here on two lower order ideas. Since SPH was developed as a higher order method, lower order forms were not already available. So two methods were chosen from finite differences, a Lax-Friedrichs type scheme and an upwind scheme.

7.4.1 Lax-Friedrichs. The first lower order scheme comes from the idea of the Lax-Friedrichs method. The general idea is to use a forward Euler time scheme (first order) with a central difference space scheme (second order). However, since that scheme by itself can be unstable under many time restrictions, a correction is made. The variable evaluated at the previous time step is replaced by a central average (second order in space). This correction makes the method not only conditionally stable, but monotone as well. This idea was introduced earlier in the Total Variation section in Chapter IV. Written for the first order wave equation (7.6), the finite difference form is

$$u_i^{n+1} = \frac{u_{i+1}^n + u_{i-1}^n}{2} + \Delta t \left(\frac{u_{i+1}^n - u_{i-1}^n}{2\Delta x} \right). \quad (7.48)$$

As seen above, the spatial derivative is a central difference form. This is more or less analogous in SPH to a symmetric kernel. Also in Lax-Friedrichs the previous time step is replaced with a central average. The SPH function approximation with a symmetric kernel can be used for this version. The resulting form for SPH is

$$u_i^{n+1} = \sum_{j=1}^N \Delta x_j u_j^n \bar{W}_{ij} + \Delta t \sum_{j=1}^N \Delta x_j u_j^n W'_{ij}. \quad (7.49)$$

To see that this method is consistent, use a Taylor expansion in time

$$u_i^{n+1} = u_i^n + \Delta t (u_i^n)_t + \frac{\Delta t^2}{2} (u_i^n)_{tt} + \dots \quad (7.50)$$

Noting from equation (7.6), $u_t = -au_x$ and using the errors obtained in Chapter III for the SPH function approximation and derivative yields

$$\begin{aligned} u_i^n &= \sum_{j=1}^N \Delta x_j u_j^n \bar{W}_{ij} + O(h^2, h \Delta x) \\ (u_i^n)_t &= -a (u_i^n)_x = -a \sum_{j=1}^N \Delta x_j u_j^n W'_{ij} + O(h^2, h \Delta x). \end{aligned}$$

Substitute these into equation (7.50) to obtain

$$\begin{aligned} u_i^{n+1} &= \left[\sum_{j=1}^N \Delta x_j u_j^n \bar{W}_{ij} + O(h^2, h \Delta x) \right] + \Delta t \left[-a \sum_{j=1}^N \Delta x_j u_j^n W'_{ij} + O(h^2, h \Delta x) \right] \\ &\quad + O(\Delta t^2) \\ u_i^{n+1} &= \sum_{j=1}^N \Delta x_j u_j^n \bar{W}_{ij} - a \Delta t \sum_{j=1}^N \Delta x_j u_j^n W'_{ij} + O(\Delta t^2, h^2 \Delta t, \Delta t h \Delta x, h^2, h \Delta x). \end{aligned}$$

Note: this shows the order of the local truncation error; and one order in time is lost for the global error. So, the SPH Lax-Friedrichs form is consistent for the first order wave equation and is first order in time and first order in space (if $\Delta t \approx \Delta x$).

As discussed in the Total Variation Section in Chapter IV, the Lax-Friedrichs method is in a category of very smooth techniques known as monotone methods. These methods are all total variation diminishing (and stable). To show that this method is monotone, let $\mathcal{H}(u_i)$ be the right hand side of equation (7.49). Following LeVeque (32) it is sufficient to show

$$\frac{\partial \mathcal{H}(u_i)}{\partial u_k^n} \geq 0 \quad \forall k, i, u^n,$$

to prove a scheme is monotone. Consider two cases: $k = i$, and $k \neq i$.

$$\underline{k = i.}$$

$$\begin{aligned}\frac{\partial \mathcal{H}}{\partial u_i^n} &= \Delta x_i (\bar{W}(0) - a\Delta t W'(0)) \\ \bar{W}(0) &\geq 0 \quad \text{usually, and assumed here} \\ W'(0) &= 0 \quad \text{usually, and assumed here} \\ \Rightarrow \frac{\partial \mathcal{H}}{\partial u_i^n} &= \Delta x_i \bar{W}(0) \geq 0\end{aligned}$$

$$\underline{k \neq i}$$

$$\begin{aligned}\frac{\partial \mathcal{H}}{\partial u_j^n} &= \Delta x_j (\bar{W}_{ij} - a\Delta t W'_{ij}) \\ \bar{W}_{ij} &\geq 0 \quad \text{usually, and assumed here}\end{aligned}$$

If the kernels are chosen such that K'/\bar{K} is bounded above by a positive constant, say B , then for 'a' positive and Δt chosen sufficiently small

$$\begin{aligned}\frac{K'}{\bar{K}} &\leq B \\ a\Delta t \left(\frac{W'}{\bar{W}} \right) &= \frac{a\Delta t}{h} \left(\frac{K'}{\bar{K}} \right) \leq \frac{a\Delta t}{h} B \leq 1 \\ \bar{W}_{ij} - a\Delta t W'_{ij} &\geq 0 \\ \Rightarrow \frac{\partial \mathcal{H}}{\partial u_i^n} &\geq 0.\end{aligned}$$

Hence for $\frac{K'}{\bar{K}} \leq B$ and $\frac{a\Delta t}{h} \leq \frac{1}{B}$ the SPH Lax-Friedrichs method is consistent and monotone (conditionally). Note if 'a' is negative K'/\bar{K} needs to be bounded below by a negative constant. As shown in Chapter VI, there are several kernels that work quite well and are similar to each other. For example, a combination such as the T-Gaussian for \bar{W} and the B-Spline for W will result in $B = 2.5$ creating a CFL number for this scheme of 0.4.

This scheme can be extended in two very useful ways. First, using the general conservation equation (7.5) instead of the first order wave equation yields

$$u_i^{n+1} = \sum_{j=1}^N \Delta x_j u_j^n \bar{W}_{ij} + \Delta t \sum_{j=1}^N \Delta x_j f(u_j^n) W'_{ij}. \quad (7.51)$$

Second, by applying the key step, averaging the variable at the previous time step, this notion can be extended to any time scheme; not just the forward Euler. This second generalization can help other time schemes become more monotone, but does not guarantee that they will be truly monotone. However, this powerful generalization has much promise and to avoid confusion with a true Lax-Friedrichs form, the process of averaging the field variable at previous time step is referred to simply as Field Averaging.

One possible application of these ideas to the Euler equations is

$$\begin{aligned} \rho_i^{n+1} &= \rho_i^n + \Delta t \left(-\rho \frac{\partial v}{\partial x} \right)_i^n = \rho_i^n + \Delta t \left(v \frac{\partial \rho}{\partial x} - \frac{\partial(\rho v)}{\partial x} \right)_i^n \\ &\approx \sum_{j=1}^N m_j \left[\bar{W}_{ij} + \Delta t (v_i^n - v_j^n) W'_{ij} \right] \end{aligned} \quad (7.52)$$

$$\begin{aligned} v_i^{n+1} &= v_i^n + \Delta t \left(-\frac{1}{\rho} \frac{\partial P}{\partial x} \right)_i^n = v_i^n - \Delta t \left(\frac{\partial(P/\rho)}{\partial x} + \frac{P}{\rho^2} \frac{\partial \rho}{\partial x} \right)_i^n \\ &\approx \sum_{j=1}^N m_j \left[\frac{v_j^n}{\rho_j^n} \bar{W}_{ij} - \Delta t \left(\frac{P_i^n}{(\rho_i^n)^2} + \frac{P_j^n}{(\rho_j^n)^2} \right) W'_{ij} \right] \end{aligned} \quad (7.53)$$

$$\begin{aligned} e_i^{n+1} &= e_i^n + \Delta t \left(-\frac{P}{\rho} \frac{\partial v}{\partial x} \right)_i^n = e_i^n + \frac{\Delta t}{2} \left[\frac{P}{\rho^2} \left(v \frac{\partial \rho}{\partial x} - \frac{\partial(\rho v)}{\partial x} \right) \right. \\ &\quad \left. + \left(v \frac{\partial(P/\rho)}{\partial x} - \frac{\partial(Pv/\rho)}{\partial x} \right) \right]_i^n \\ &\approx \sum_{j=1}^N m_j \left[\frac{e_j^n}{\rho_j^n} \bar{W}_{ij} + \frac{\Delta t}{2} \left(\frac{P_i^n}{(\rho_i^n)^2} + \frac{P_j^n}{(\rho_j^n)^2} \right) (v_i^n - v_j^n) W'_{ij} \right] \end{aligned} \quad (7.54)$$

$$x_i^{n+1} = x_i^n + \Delta t v_i^n. \quad (7.55)$$

7.4.2 *Upwind.* The second lower order scheme considered is motivated by upwind finite difference schemes; in particular, forward time/forward (backward) space. Shown for the general conservation equation

$$u_i^{n+1} = u_i^n - \Delta t \left[\frac{f(u_{i+1}^n) - f(u_i^n)}{\Delta x} \right]. \quad (7.56)$$

The upwind scheme is relatively easy to apply since the spatial derivative is analogous to a one-sided kernel function in SPH. Two types of one-sided kernels were discussed in the previous chapter: truncated forms and condensed forms of a symmetric kernel. A truncated kernel is where a symmetric kernel is used for $x_i - x_j$ positive (or negative) and the kernel is 0 otherwise. A condensed kernel is where a symmetric kernel shrunk down to half its width and then shifted to one half plane or the other. The other half plane is 0. So the SPH upwind scheme for the general conservation equation is

$$u_i^{n+1} = u_i^n - \Delta t \left[\varsigma f(u_i^n) \hat{W}(0) + \sum_{j=1}^N \Delta x_j f(u_j^n) \hat{W}'_{ij} \right]. \quad (7.57)$$

The extra term in the spatial derivative (involving ς) will be discussed and derived below. Following the work done in Chapter III, this is now shown to be a first order approximation. Let

$$\langle f'(u_o) \rangle = f'_k(u_o) = \int_{\Omega} f'(u) \hat{W}(u_o - u, h) du.$$

Expand $f'(u)$ about $u = u_o$, let $x = (u - u_o)$, and use the normalization of \hat{W} to obtain

$$\begin{aligned} f'_k(u_o) &= \int_{\Omega} f'(u) \hat{W}(u_o - u, h) du = \int_{\Omega} f'(x + u_o) \hat{W}(-x, h) dx \\ &= \int_{\Omega} \hat{W}(-x, h) [f'(u_o) + x f''(u_o) + \frac{x^2}{2!} f'''(\xi_o)] dx \end{aligned}$$

$$\begin{aligned}
&= f'(u_o) \int_{\Omega} \hat{W}(-x, h) dx \\
&+ f''(u_o) \int_{\Omega} x \hat{W}(-x, h) dx \\
&+ \frac{1}{2} \int_{\Omega} x^2 \hat{W}(-x, h) f'''(\xi_o) dx \\
&= f'(u_o) + E_o,
\end{aligned} \tag{7.58}$$

where

$$E_o = f''(u_o) \int_{\Omega} x \hat{W}(-x, h) dx + \frac{1}{2} \int_{\Omega} x^2 \hat{W}(-x, h) f'''(\xi_o) dx.$$

It is possible for the first integral in E_o to be zero, as in the symmetric kernel case, but only if \hat{W} is allowed to be negative over part of its support. This is not usually done, and would make a distribution theory analysis much more difficult. Hence, that case will not be allowed at this time. So dropping the second term shown in E_o (as the error will go as the first term) yields

$$E_o = \int_{\Omega} x \hat{W}(-x, h) f''(\xi_o) dx, \tag{7.59}$$

for $\xi_o \in \Omega$. To obtain a bound on the error term E_o , define

$$e_o = \kappa \sup_{\xi \in \Omega_{\kappa}} |f''(\xi)|,$$

where Ω_{κ} is the κh wide region around u_o . Then noting that the kernel is non-zero only when $|x| \leq \kappa h$, the bound is

$$\begin{aligned}
|E_o| &= \left| \int_{\Omega} x W(-x, h) f''(\xi_o) dx \right| \leq \int_{\Omega} |x| |W(-x, h)| |f''(\xi_o)| dx \\
&\leq \int_{\Omega} \kappa h W(-x, h) \frac{e_o}{\kappa} dx = e_o h \int_{\Omega} W(-x, h) dx = e_o h.
\end{aligned} \tag{7.60}$$

Therefore,

$$f'(u_o) = f'_k(u_o) + O(h) = \int_{\Omega} f'(u) \hat{W}(u_o - u, h) du + O(h). \quad (7.61)$$

Following procedures similar to Chapter III, integrate by parts and then replace the integral by a sum. For the condensed kernels these steps will be the same as the symmetric kernel case. But for the truncated kernels, the integration-by-parts step creates an extra boundary term. For the forward kernel that is $-f(u_o)\hat{W}(0)$ (the backward will be positive). Since for the condensed kernels $\hat{W}(0) = 0$, the results can be generalized for either type of kernel as

$$f'(u_i) = \varsigma f(u_i)\hat{W}(0) + \sum_{j=1}^N \Delta x_j f(u_j^n) \hat{W}'_{ij} + O(h, \Delta x), \quad (7.62)$$

where $\varsigma = \begin{cases} +1 & \text{if } \hat{W}(u) = 0 \text{ for } u < 0 \text{ (backward)} \\ -1 & \text{if } \hat{W}(u) = 0 \text{ for } u > 0 \text{ (forward)} \end{cases}$.

Note, from Chapter VI for these one-sided kernels,

$$\hat{W}(0) = -\sum_{j=1}^N \Delta x_j \hat{W}'_{ij}. \quad (7.63)$$

But note

$$-\sum_{j=1}^N \Delta x_j \hat{W}'_{ij} \approx \int_{\Omega} \hat{W}'(x_i - x) dx = \varsigma [\hat{W}(0) - \hat{W}(\kappa h)] = \varsigma \hat{W}(0).$$

So the extra term developed here and that derived in Chapter VI are equivalent to within the order of the method. Thus either one may be used; but from the work in Chapter VI, equation (7.63) might give a better result at a higher cost. However, at this time $\varsigma \hat{W}(0)$ form will continue to be used.

One possible application of these ideas to the Euler equations is

$$\begin{aligned}
 \rho_i^{n+1} &= \rho_i^n + \Delta t \left(-\rho \frac{\partial v}{\partial x} \right)_i^n = \rho_i^n + \Delta t \left(v \frac{\partial \rho}{\partial x} - \frac{\partial(\rho v)}{\partial x} \right)_i^n \\
 &\approx \rho_i^n + \Delta t \left\{ v_i^n \left[\varsigma \rho_i^n \hat{W}(0) + \sum_{j=1}^N m_j \hat{W}'_{ij} \right] - \left[\varsigma \rho_i^n v_i^n \hat{W}(0) + \sum_{j=1}^N m_j v_j^n \hat{W}'_{ij} \right] \right\} \\
 &= \rho_i^n + \Delta t \sum_{j=1}^N m_j (v_i^n - v_j^n) \hat{W}'_{ij} \quad (7.64)
 \end{aligned}$$

$$\begin{aligned}
 v_i^{n+1} &= v_i^n + \Delta t \left(-\frac{1}{\rho} \frac{\partial P}{\partial x} \right)_i^n = v_i^n - \Delta t \left(\frac{\partial(\frac{P}{\rho})}{\partial x} + \frac{P}{\rho^2} \frac{\partial \rho}{\partial x} \right)_i^n \\
 &\approx v_i^n - \Delta t \left\{ \left[\varsigma \frac{P_i^n}{\rho_i^n} \hat{W}(0) + \sum_{j=1}^N m_j \left(\frac{P_j^n}{(\rho_j^n)^2} \right) \hat{W}'_{ij} \right] \right. \\
 &\quad \left. + \left[\varsigma \frac{P_i^n}{\rho_i^n} \hat{W}(0) + \sum_{j=1}^N m_j \left(\frac{P_i^n}{(\rho_i^n)^2} \right) \hat{W}'_{ij} \right] \right\} \\
 &= v_i^n - \Delta t \left[\varsigma \frac{2P_i^n}{\rho_i^n} \hat{W}(0) + \sum_{j=1}^N m_j \left(\frac{P_j^n}{(\rho_j^n)^2} + \frac{P_i^n}{(\rho_i^n)^2} \right) \hat{W}'_{ij} \right] \quad (7.65)
 \end{aligned}$$

$$\begin{aligned}
 e_i^{n+1} &= e_i^n + \Delta t \left(-\frac{P}{\rho} \frac{\partial v}{\partial x} \right)_i^n = e_i^n + \frac{\Delta t}{2} \left[\frac{P}{\rho^2} \left(v \frac{\partial \rho}{\partial x} - \frac{\partial(\rho v)}{\partial x} \right) \right. \\
 &\quad \left. + \left(v \frac{\partial(\frac{P}{\rho})}{\partial x} - \frac{\partial(\frac{Pv}{\rho})}{\partial x} \right) \right]_i^n \\
 &\approx e_i^n + \frac{\Delta t}{2} \left\{ \frac{P_i^n}{(\rho_i^n)^2} \left[v_i^n \varsigma \rho_i^n \hat{W}(0) + v_i^n \sum_{j=1}^N m_j \hat{W}'_{ij} - \varsigma v_i^n \rho_i^n \hat{W}(0) \right. \right. \\
 &\quad \left. \left. + \sum_{j=1}^N m_j v_j^n \hat{W}'_{ij} \right] + \left[v_i^n \varsigma \frac{P_i^n}{\rho_i^n} \hat{W}(0) + v_i^n \sum_{j=1}^N m_j \frac{P_j^n}{(\rho_j^n)^2} \hat{W}'_{ij} \right. \right. \\
 &\quad \left. \left. - \varsigma v_i^n \frac{P_i^n}{\rho_i^n} \hat{W}(0) - \sum_{j=1}^N m_j v_j^n \frac{P_j^n}{(\rho_j^n)^2} \hat{W}'_{ij} \right] \right\} \\
 &= e_i^n + \frac{\Delta t}{2} \sum_{j=1}^N m_j \left(\frac{P_j^n}{(\rho_j^n)^2} + \frac{P_i^n}{(\rho_i^n)^2} \right) (v_i^n - v_j^n) \hat{W}'_{ij} \quad (7.66)
 \end{aligned}$$

$$x_i^{n+1} = x_i^n + \Delta t v_i^n. \quad (7.67)$$

7.5 *Summary*

In this chapter, several time schemes were proposed for use with SPH. The second order schemes are more likely to be used for most problems, because of their higher order accuracy. However, the Lax-Wendroff form is more suitable for small scale problems due to the cost of calculating the second derivative terms. The Central and Shu schemes should work well for a vast majority of problems of all sizes. Since quantitative comparisons between them were not made, the choice of which to use is up to the individual user. The lower order schemes are of limited use by themselves, but will be of importance in the next chapter.

VIII. HYBRID METHODS

This chapter introduces the concept of flux-limited hybrid schemes from finite differences to SPH as a way to handle shocks. Problems of hypervelocity impact, among others, are often characterized by large areas of relatively smooth data with intermittent areas of discontinuous data. When modeling problems such as these, the largest concern often is how to handle the discontinuities or shocks properly. This is also a concern in the consistency of a method, and as such was discussed in Chapter III. Flux-limited hybrid schemes are much newer than the more traditional artificial viscosity notion in finite differences, but in some case seems to perform better. The schemes weight average lower and higher order methods based on the closeness to a sensed shock. Therefore, the difference order time schemes discussed in the previous chapter will be quite important here. In this chapter, the hybrid notion is more fully described and the six SPH hybrid schemes are proposed and tested against a baseline case. Under basic assumptions (no-frills implementation) the hybrid schemes perform roughly the same as the baseline. This concept is not ready for production SPH codes, but the basic foundation for the work is laid here.

8.1 Introduction

A category of techniques that handle discontinuities quite well is known as high resolution methods. One of the main ideas found in these techniques is to use a high order method away from the shock, while near the shock use a method that has more dissipation. The reason for the greater dissipation is to control the oscillations and stability while accurately resolving the shock.

Decades ago these notions gave rise to artificial viscous techniques applied to finite difference methods. Some of the earlier work was performed by Von Neumann and Richtmyer (66) and Lax and Wendroff (29). These were designed to control fluctuations near a shock by mimicking higher order spatial derivatives (viscous

terms) in a controlled manner. Through the years since then, several variations were derived for finite difference techniques and more recently for SPH. However, it was felt by some authors that it was too difficult to control this "artificial viscosity". Just enough is needed to smooth the oscillations, but not too much so that the shock is overly smeared.

So, in the early 1970s, a new approach for finite differences was proposed known now as the flux-limiter technique. These ideas were first popularized in finite differences by Harten and Zwas (15). Quite simply, they involve using two different techniques and a weight function (or limiter) to select which method to use. In this way, a high order method (or flux) can be used in areas of smooth data while a low order flux can be used near a discontinuity. A weight function, or limiter, is used to determine which flux or what proportion of each to use. Hence, a hybrid flux is developed. Using F_H for the high order flux and F_L for the low order flux, the hybrid flux can be represented as

$$F(U) = \theta F_L(U) + (1 - \theta) F_H(U) . \quad (8.1)$$

In this example, θ is the flux limiter that would usually be contained in $[0,1]$. Equation (8.1) can also be rewritten as

$$F(U) = F_H(U) + \theta [F_L(U) - F_H(U)] . \quad (8.2)$$

The second term (involving θ) can be thought of as an artificial viscosity term added to the higher order method. This points out these two ideas may not be quite as distinct as they originally may appear. For an introduction to these ideas (for finite differences) see LeVeque (32) or Woodward and Colella (68).

As noted earlier, the artificial viscosity technique has been used in SPH for several years now with some success. However, there are some concerns that it is not adequate in all cases. For example, when modeling the Riemann shock tube problem

(a classic test case described later), artificial viscosity is not enough to allow the SPH continuity equation to be used. Instead, the less favorable density-by-summation form must be used. It is concerns with test cases such as this, together with the success of flux-limiter techniques in finite differences that influenced the choice to propose hybrid methods for SPH.

Two general ways of obtaining a hybrid method are proposed in this chapter: using a consistency argument and using two different methods. These are addressed in the next two sections.

8.2 Consistency Approach

This notion is introduced in Chapter III, Non-Smooth Functions section (3.5). The basic idea is to develop an SPH method that is consistent in areas near discontinuities. Since the work for this was already done, it will not be repeated here. The results of that work can be written as the sum of the *standard* SPH method plus a correction term. Although this is not quite the same as a flux-limited hybrid method, at least not as it appears in the finite difference literature, it has the same basic tenets. That is, in areas of smooth data one equation is used and near a shock another. The limiter function is built into the derivation performed in Chapter III and Appendix A.

Currently this approach is strictly an academic exercise. There has been very little success in obtaining computational results on known test problems. There could be several reasons both computationally and algorithmically. Some of the more likely reasons are: poor time scheme, poor choice of time stepping, poor choice of kernel, poor shock sensing algorithm, or poor choice of test problems. It is, of course, conceivable that the algorithm, time scheme, etc. are not implemented correctly. However, this was reviewed and it is less likely than the other reasons. Hence, this approach will not be addressed any further here.

8.3 Two Method Approach

This approach follows the ideas of flux-limited hybrid methods from the finite difference literature and uses equations (8.1) or (8.2) above. In this approach, the high order flux is not of prime concern to us; since from earlier in this dissertation, SPH was shown, in general, to be a second order method. So any of the second order time schemes discussed in the last chapter should work well. The bigger concerns are what low order scheme to use, do the two schemes match, and what to use for the flux-limiter.

Low order schemes. Because SPH is usually considered second order, little attention has been given to lower order SPH approximations. The most obvious lower order SPH method is to use non-symmetric kernels. Although it is possible to have a second order method with non-symmetric kernels, it is much more difficult. A good example of a non-symmetric kernel is a one-sided kernel. This corresponds to the notion of forward/backward differences, or more generally upwind schemes. So a forward time with one-sided kernel SPH would be analogous to the most basic finite difference upwind method. Another possibility is the field averaged time (either central or forward) with SPH symmetric kernel. These also would be first order time, first order space. They may smooth more, but are more easily applied in higher dimensions. Both of these ideas were introduced in the previous chapter.

A good match. The best matches are when the two methods have several terms in common so that they appear to converge to each other as a particle moves closer or further from the discontinuity. In this way the combination is much smoother and should not be effected as much if particles are more sparsely spaced. When selecting the two methods to combine, more thought needs to be used than to simply attempt every possible combination. Methods should be selected that by themselves are reasonable (either high or low order) and that fit well together. These are sometimes at odds with one another. For example, the central time/SPH space is a good high order method that would match well with central time/upwind SPH. However, from

finite differences it can be shown that central time/forward (or backward) space is unstable (under usual time restrictions). Other examples of bad hybrid schemes are available, but this chapter will concentrate on those that show promise.

Limiter Function In order to perform calculations, a limiter function needs to be developed for SPH. Starting with work found in the published literature for scalar conservation laws (e.g. Sweby (62)) and then expanding upon it for the Euler equations proved useful. It is decided that discontinuities in any of the field variables (ρ, v, e) should be captured. Also it is desirable that the method not be strictly for one dimensional problems. This yields a flexible function that may be used for higher dimension problems, although the exact implementation of this algorithm is done only in one dimension here. Also note that efficiency is not taken into consideration.

The algorithm basically calculates a ratio of the local field difference to the maximum difference $((u_i - u_j)/\Delta u_{max})$. This is then multiplied by a negative exponential function based on how close the particle is to the sensed shock. This picks up only relatively large discontinuities, but is sufficient for this problem.

Algorithm 1 *SPH Flux-Limiter 1*

Given: ϵ_1 and ϵ_2

Find: $\rho_{min}, \rho_{max}, v_{min}, v_{max}, e_{min}, e_{max}$

Define:

$$\hat{\rho} = \rho_{max} - \rho_{min}$$

$$\hat{v} = v_{max} - v_{min}$$

$$\hat{e} = e_{max} - e_{min}$$

end define

Before the SPH sums are calculated do:

$$mxk = mxj = i$$

$$\delta = 0$$

$$\text{while } (|x_i - x_j| < \kappa h) \text{ and } j < i$$

```

    if  $\left(\left|\frac{\rho_1 - \rho_i}{\hat{\rho}}\right| > \epsilon_1\right)$  and  $\left(\left|\frac{\rho_1 - \rho_i}{\hat{\rho}}\right| > \delta\right)$ 
    then
         $\delta = \frac{\rho_1 - \rho_i}{\hat{\rho}}$ 
         $mxj = j$ 
        if  $(|\delta| > \epsilon_2)$  go to loop
    end if
end while
repeat for  $v$  and  $e$ 
repeat for  $\rho$ ,  $v$ , and  $e$  for  $j > i$  to get  $mxk$ 
loop:  $\theta_i = \delta * \exp[0.5 - \max(\kappa h, x_{mxk} - x_{mxj}) / (2\kappa h)]$ 
end  $\theta$  calculation
end

```

Instead of using Δu_{max} ($\hat{\rho}$, \hat{v} , or \hat{e} in Algorithm 1), where the maximum is taken over all particles, one might want to use Δu_{lmax} , where the maximum is taken as the largest local maximum; ie. the maximum difference within the support of the kernel. This would detect more discontinuities than the original form. Since shock detection algorithms are not exact, the implementation is more of an artform than science.

Note for higher dimensions this algorithm can be easily changed to find the ratio (δ) within the support of the kernel, thus extending the hybrid notion to higher dimensions. Also note in some applications it might be advantageous to use a θ_{ij} formulation instead of just θ_i , although it was not done here. Some simple ways to do this are to use an algorithm such as the one above and then use $(\theta_i + \theta_j)/2$, $\theta_i \theta_j$, or $\max(\theta_i, \theta_j)$.

Based on the ideas discussed so far, some possible hybrid methods are now presented. However, first a few notes on notation. The formulas given in the rest of

this section are for the general conservation equation

$$u_t = -[f(u)]_x. \quad (8.3)$$

In the equations to follow, $u_i^{n+1} = F(u_i^n)$ is used as one solution when $F(U)$ is given as in equation (8.1). Also, in the formulas to follow, \hat{W} is used for one-sided kernels, \bar{W} for field averaged kernels, and W and \tilde{W} for just any symmetric kernel. Where they appear in the same equation, the kernels may be the same, but the notation is used to point out that they do not have to be. The methods were numbered 1-20 based on original plans. Methods 2, 4, 6, 8, 12, and 20 are discussed below. Methods 1, 3, 5, 7, and 11 did not converge and are briefly discussed later. The remaining numbers in the sequence (9, 10, and 13-19) were reserved for other methods originally planned for development; but never actually completed. So start with Method 2.

8.3.1 Method 2. High order: SPH Lax-Wendroff/Symmetric SPH. Low Order: Forward Field Average/Symmetric SPH.

This method combines the forward time with field averaging in the area of a shock (8.4) with the SPH version of Lax-Wendroff away from the shock (8.5). The low order method uses a first order time scheme with the second order space scheme. The high order method should be second order everywhere. This is the first time that a Lax-Wendroff type SPH approximation has been attempted.

$$F_L = \sum_{j=1}^N \Delta x_j u_j^n \bar{W}_{ij} - \Delta t \sum_{j=1}^N \Delta x_j f(u_j^n) W'_{ij} \quad (8.4)$$

$$F_H = u_i^n - \Delta t \sum_{j=1}^N \Delta x_j f(u_j^n) W'_{ij} + \frac{\Delta t^2}{2} \sum_{j=1}^N \Delta x_j f(u_j^n) \tilde{W}''_{ij} \quad (8.5)$$

This is similar to a classic finite difference technique. The one dimensional wave equation analogy would be Lax-Wendroff in smooth regions with Lax-Friedrichs near the shock.

8.3.2 *Methods 4, 6, and 8.* High order: Central Time/Symmetric SPH.
Low Order: Central Field Average/Symmetric SPH.

This method combines the central time with field averaging in the area of a shock (8.6) with the central time away from the shock (8.7). Method 4 uses the approximate central time formulation, Method 6 the near central time, and Method 8 the full central time. Each of these ideas was discussed in the previous chapter. More than one form is investigated to see if there is any noticeable advantage to truer central time forms.

$$F_L = \sum_{j=1}^N \Delta x_j u_j^{n-1} \bar{W}_{ij} - 2\Delta t \sum_{j=1}^N \Delta x_j f(u_j^n) W'_{ij} \quad (8.6)$$

$$F_H = u_i^{n-1} - 2\Delta t \sum_{j=1}^N \Delta x_j f(u_j^n) W'_{ij} \quad (8.7)$$

The biggest advantage of this method is its simplicity. The two fluxes are very close, with only the value at the previous time step different. The one dimensional wave equation analogy would be central time-central space in smooth regions with a modified Lax-Friedrichs near the shock. The reason it is a modified Lax-Friedrichs is that the usual version uses forward time with averaging where central time with averaging is used here. A more standard Lax-Friedrichs could be used when the full central time is used.

8.3.3 *Method 12.* High order: Shu Time/Symmetric SPH. Low Order: Forward Field Average/Symmetric SPH.

This method combines the forward time with field averaging in the area of a shock (8.8) with the Shu time (see equation (7.37)) away from the shock (8.9).

$$F_L = \sum_{j=1}^N \Delta x_j u_j^n \bar{W}_{ij} - \Delta t \sum_{j=1}^N \Delta x_j f(u_j^n) W'_{ij} \quad (8.8)$$

$$F_H = \frac{4}{5}u_i^n + \frac{1}{5}u_i^{n-1} + \frac{8}{5}\Delta t \sum_{j=1}^N \Delta x_j f(u_j^n) W'_{ij} - \frac{2}{5}\Delta t \sum_{j=1}^N \Delta x_j f(u_j^{n-1}) W'_{ij} \quad (8.9)$$

The two fluxes are very close, and easy to combine. The Shu time is also useful in stabilizing a method (Shu proposed this to go with Total Variation Stable schemes).

8.3.4 *Method 20.* High order: Approximate Central Time/Symmetric SPH. Low Order: Central Field Average/Symmetric SPH.

This is the same basic form as Method 4 (equations (8.6) and (8.7)). The difference is an option is given to vary the amount of smoothing obtained from the lower order method in each conservation equation separately. This version is derived because in the current SPH methods where there is no smoothing in the continuity equation, artificial viscosity in the momentum equation, artificial viscosity and wall heating in the energy equation, and no smoothing in the particle motion equation. This allow me to hypothesis that the other hybrid methods may have too much smoothing in some equations; this corrects that possible problem.

8.3.5 *Methods that Failed to Converge.* There are several hybrid methods that were attempted because they seemed like good choices at the time, but they would not work when applied to the Riemann shock tube problem. This, of course, is not conclusive evidence that they will not work on other problems. However, it is felt that it is better to use the methods that work for a proven test case.

- Method 1 - High order: SPH Lax-Wendroff. Low Order: Forward Time / One-Sided SPH.
- Method 3 - High order: Approximate Central Time/Symmetric SPH. Low Order: Approximate Central Time/One-Sided SPH.
- Method 5 - High order: Near Central Time/Symmetric SPH. Low Order: Near Central Time/One-Sided SPH.
- Method 7 - High order: Full Central Time/Symmetric SPH. Low Order: Full Central Time/One-Sided SPH.

- Method 11 - High order: Shu Time/Symmetric SPH. Low Order: Forward Time/ One-Sided SPH.
- Method Con1 - High order: Approximate Central Time/Symmetric SPH. Low Order: Approximate Central Time/Shock Consistently Corrected Symmetric SPH.

The one-sided methods did not work very well for this test case. This is possibly due to similar problems with using artificial viscosity in SPH. Namely, some distortions are smoothed out while others, like a spike (both positive and negative), grow uncontrolled until a non-physical result (such as negative density or particles crossing) occurs.

8.4 Sample Calculations

For all the methods in the previous section, the one dimensional Riemann shock tube test problem is performed. This test does not conclusively eliminate the poorer methods, but casts doubt on their use as general techniques. The Riemann shock tube problem is well known, and not described here (see LeVeque (32) or Smoller (57)). For the test case in one dimension, use a line of equally spaced particles on $[0, 1]$ with a discontinuity at 0.5 and the values for all the particles on either side of the discontinuity are: (u_l - left, u_r - right)

$\rho_l = 1.0$	$\rho_r = 0.125$
$v_l = 0.0$	$v_r = 0.0$
$e_l = 2.5$	$e_r = 2.0$
$P_l = 1.0$	$P_r = 0.1$

Also the gas constant, $\Gamma = 1.4$ is used. The solution is described in several places including (32) and is shown on the plots to follow and those in Appendix D.

In addition to performing this test and obtaining qualitative results (plots), error norms are calculated. For every method, three relative norms are calculated for each of density, velocity, energy, and pressure using two different sets of points. This seems like overkill (and may be), but the information is useful and can be easily summarized. The three different norms are l_1 , l_2 , and l_∞ calculated as

$$l_1 = \frac{\sum_{i=1}^N |f(x_i) - S(x_i)|}{\sum_{i=1}^N |f(x_i)|} \quad (8.10)$$

$$l_2 = \sqrt{\frac{\sum_{i=1}^N (f(x_i) - S(x_i))^2}{\sum_{i=1}^N (f(x_i))^2}} \quad (8.11)$$

$$l_\infty = \frac{\max_i |f(x_i) - S(x_i)|}{\max_i |f(x_i)|} \quad (8.12)$$

The two different sets of points are: 1) 1000 uniformly spaced points and 2) using the SPH particles as the points. Note that the two sets of points provide roughly the same results, demonstrating the approximating nature of this method (as opposed to an interpolatory nature). Further note that the l_∞ norm proves not to be very useful as it can be roughly determined by examining at the difference between the calculated and true solutions on the plots to follow and those in Appendix D. Therefore, in the next section only the l_1 and l_2 norms for the 1000 uniformly spaced points are summarized. The entire sets of data may be found in Appendix D.

The initial problem setup uses a fixed h , the B-Spline kernel (kernel # 2 from Chapter VI), CFL number of 0.2, and no wall heating. Although there are better settings for the baseline case, reducing the number of variables and comparing the various methods in as basic a form as possible is more appropriate at this point in the analysis. Therefore, items such as wall heating and variable h are deliberately left out to avoid clouding the comparisons. Two difference computations are made for each method. First, 600 particles are used with $\Delta x = 2h/3$. This is similar to many calculations used by other analysts and in the published literature. The second

set of calculations uses 816 particles. In this case $\Delta x = 0.5h$ everywhere except near the shock where $\Delta x = 0.4h$.

8.4.1 Baseline. In addition to the methods described in the previous section, the following is used as the Baseline: Approximate Central Time with density-by-summation. This form for calculating density in SPH has been used often and results for the Riemann shock tube problem have been published several times (including Monaghan and Gingold (37)). However, using the density-by-summation has some accuracy concerns in certain types of calculations, especially those involving metallic equations of state such as HVI problems (69). However, up until now, obtaining density using the continuity equation was not possible for this simple test case. Also artificial viscosity (with coefficients 2.5 and 2.5) is used for the Baseline.

For the Shock Tube Test, the results at 1 microsecond for the Baseline are shown in Figures 8.1 - 8.4. The data shown in Figures 8.1 and 8.2 uses 600 particles uniformly spaced. The data shown in Figures 8.3 and 8.4 uses 816 particles with higher concentrations of particles near the shock.

The 600 particle case, shown in Figures 8.1 and 8.2, is a fairly good match to the analytic solution, except for the density and energy near the contact surface. These shortfalls cause the shortfall in velocity and the extra step in the pressure contour. The shortfalls are caused by not having enough particles in that area to accurately represent the derivative. This behavior can be expected whenever the interparticle spacing becomes larger than h (Chapter VI). This happens much more often when using a fixed h form of SPH, as was done here. The overshoot in energy (the spike) can often be controlled by using a wall heating term. This was not done for all the examples in this dissertation.

The 816 particle case, shown in Figures 8.3 and 8.4, is an excellent match to the analytic solution (except for the small energy spike). This increase in accuracy is a good indication of the method converging to the proper solution as $\Delta x \rightarrow 0$.

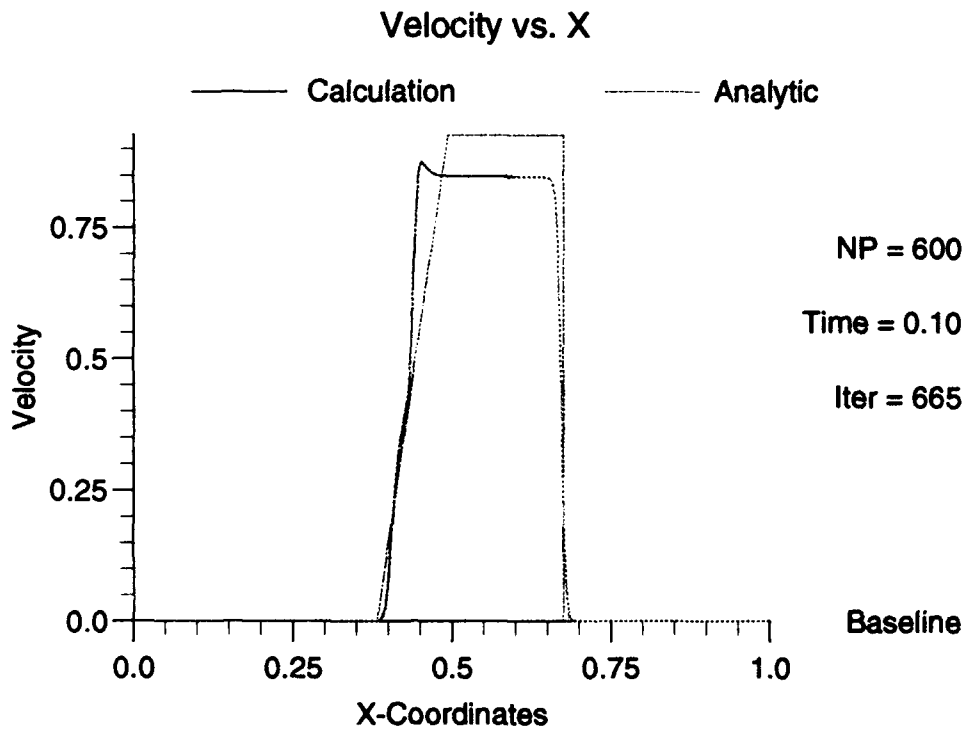
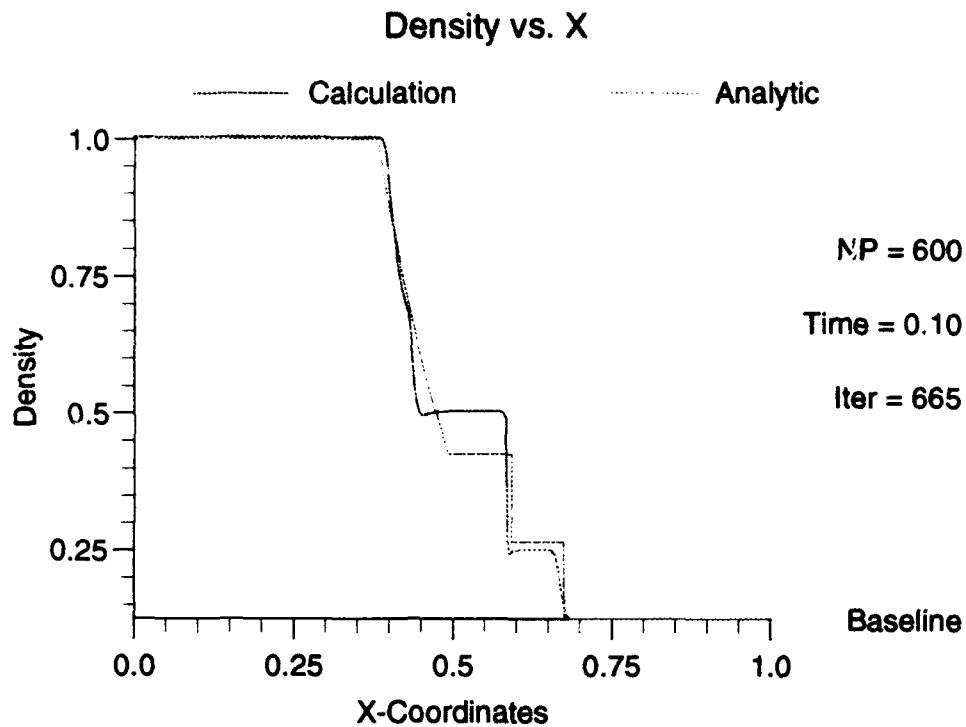


Figure 8.1 Baseline Shock Tube Results

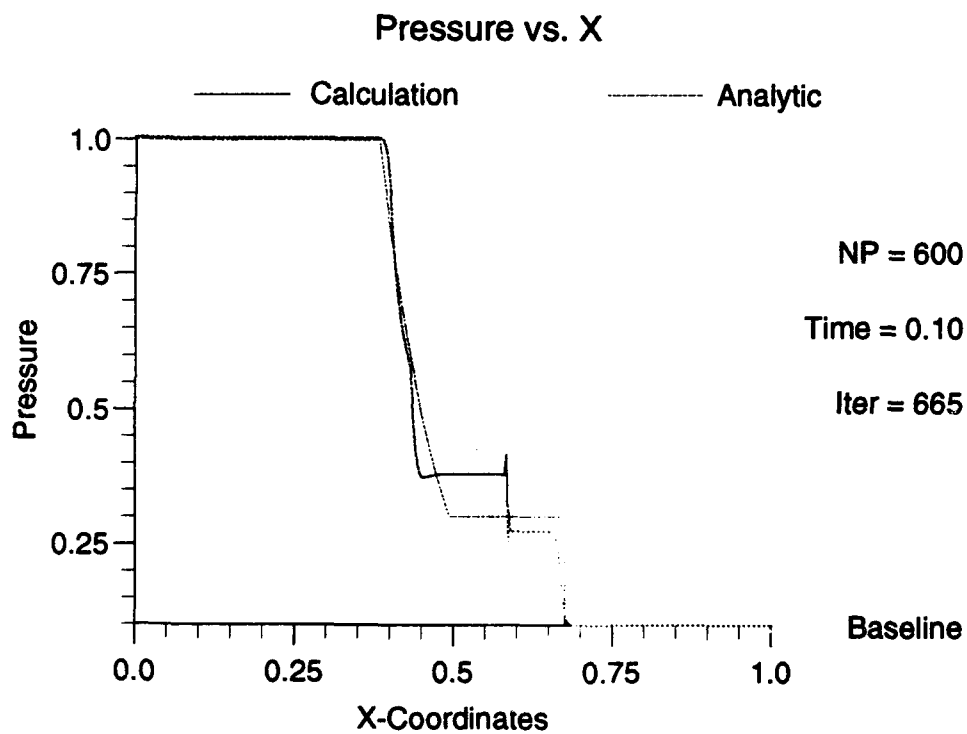
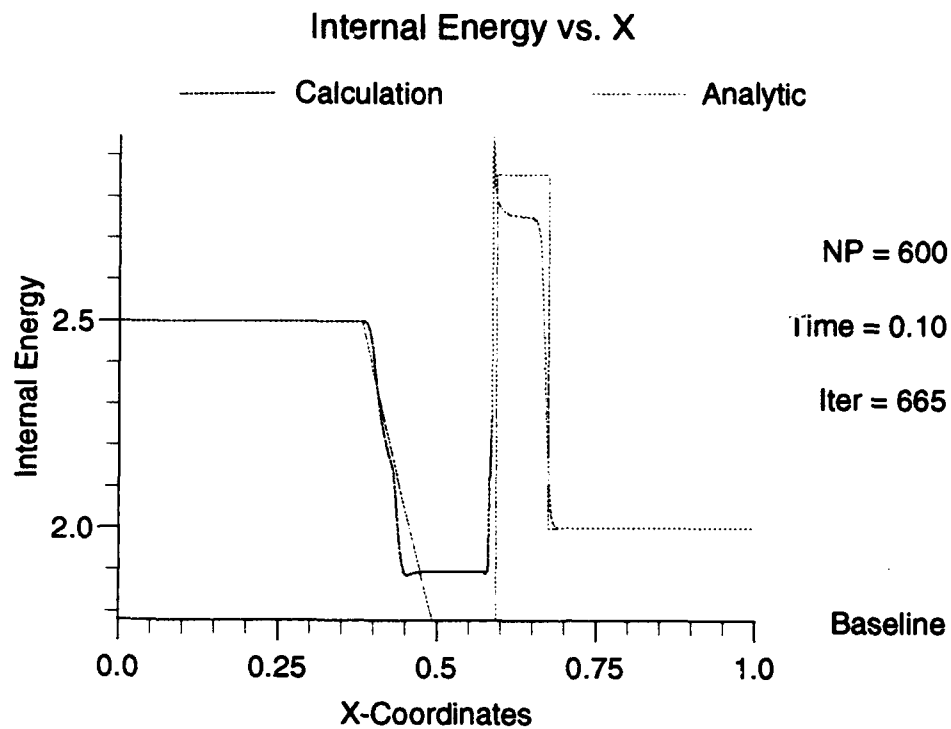


Figure 8.2 Baseline Shock Tube Results

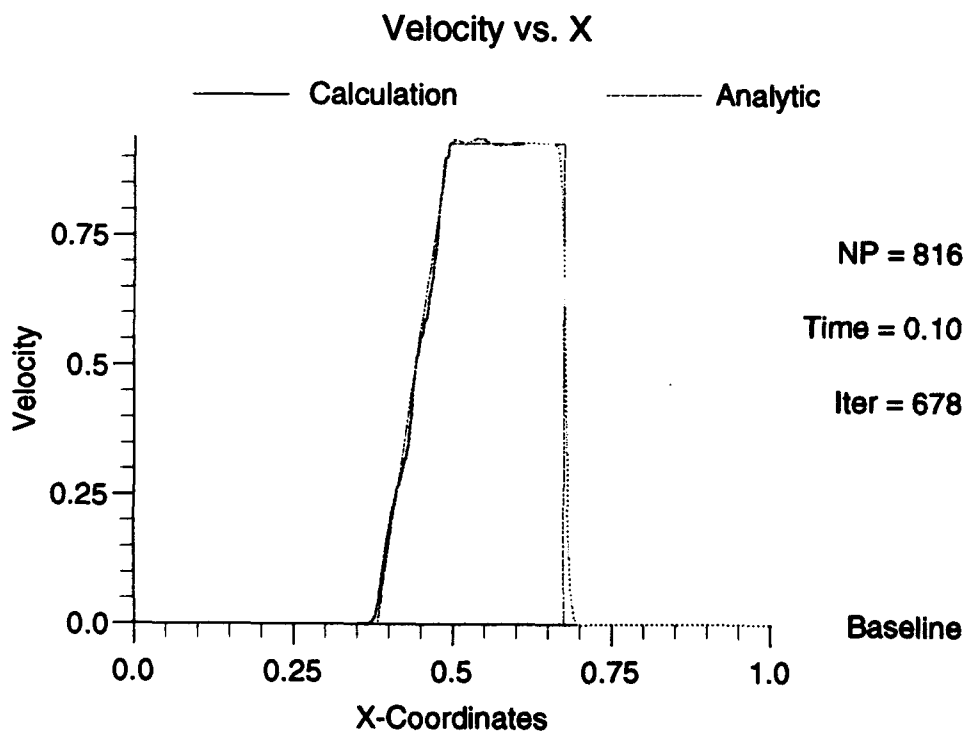
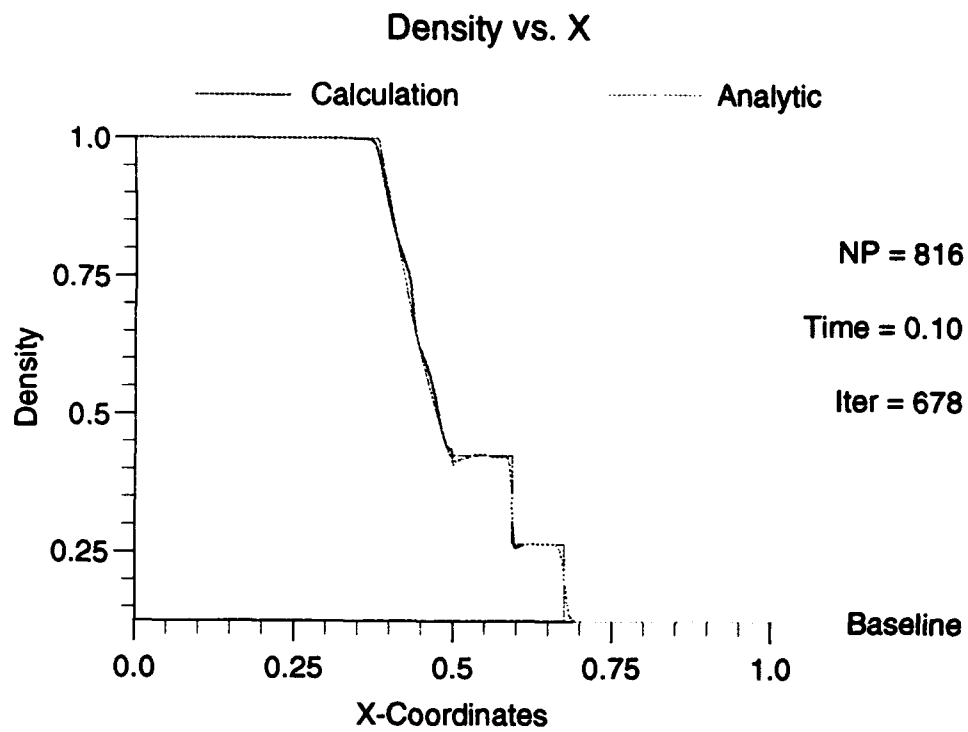


Figure 8.3 Baseline Shock Tube Results - Extra Particles

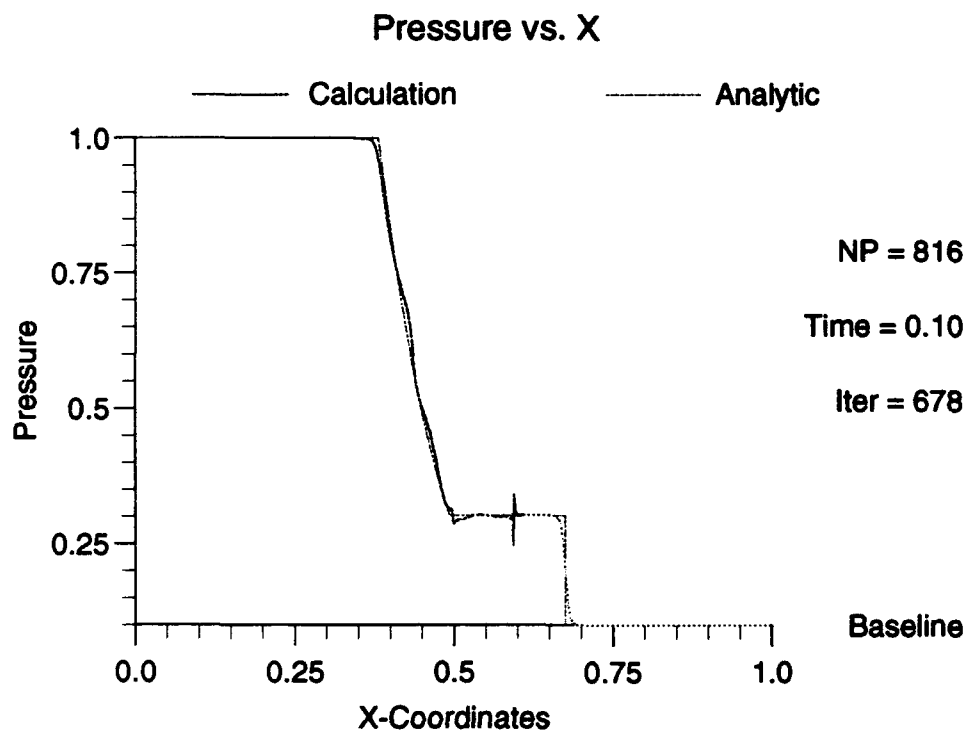
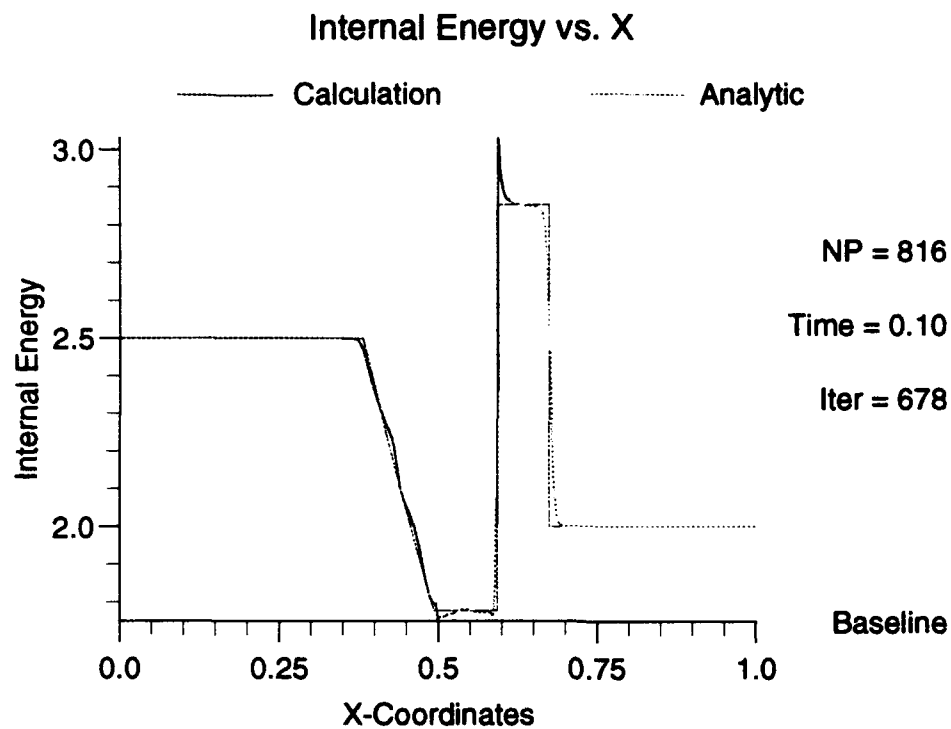


Figure 8.4 Baseline Shock Tube Results - Extra Particles

For the remaining methods, a brief discussion is given on the individual results (which may be found in Appendix D) and then a comparison of all the methods is given in the next section.

8.4.2 Method 2. For the Shock Tube Test, the results at 1 microsecond for Method 2 are shown in Appendix D in Figures D.5 - D.10.

The 600 particle case, shown in Figures D.5 and D.6, matches the true solution relatively well and is similar to the Baseline case. There is a small energy spike, some noise in velocity near the rarefaction wave, and the shortfall in all the variables is still present. However, the biggest problem is that the location of the front of the shock wave is missed. The 816 particle case, shown in Figures D.7 and D.8 is a nice improvement for this method. This seems to indicate that this new method is converging. The results for this case match the true solution quite nicely except for being slightly short in energy. The front of the shock is still a little off, but it is improving.

The results of a variable h case (shown in Figures D.9 and D.10) are included to demonstrate the effectiveness of variable h and demonstrate that it can be used to control most of the fluctuations and the shortfall in the SPH Lax-Wendroff and other forms. The results are not quite as good as the 816 particle case, but better than the 600 particle case.

8.4.3 Methods 4, 6, and 8. For the Shock Tube Test, the results at 1 microsecond for these methods are shown in Appendix D in Figures D.11 - D.22.

The 600 particle case for Method 4, shown in Figures D.11 and D.12, is quite similar to the Baseline case. There is some additional noise (Gibbs phenomena and a larger energy spike), but the biggest difference is the front edge of the shock is lagging. This could imply a lack of conservation and is further addressed in Method 20. The results shown in Figures D.13 and D.14 are for a special form of the 600

particle case. As this is analogous to a Lax-Friedrichs form alone, more smoothing is expected (and seen). This extra smoothing causes the shortfalls to be even more exaggerated than in the hybrid case. The 816 particle case for Method 4, shown in Figures D.15 and D.16, is quite an improvement over the previous two results. It has the advantage over the Baseline of not having an energy spike (and corresponding pressure spike), but it misses the velocity by more than the Baseline and still misses the front edge of the shock.

The 600 particle case for Method 6, shown in Figures D.17 and D.18, is extremely similar to the Method 4 case. This tends to imply the extra cost of performing the near central time (Method 6) over the approximate central time (Method 4) is probably not cost effective.

The 600 particle case for Method 8, shown in Figures D.19 and D.20, is also similar to the Baseline and Method 4 cases. There is a little more noise in velocity and a slightly smaller energy spike over Method 4. This method also misses the front edge of the shock, but by a smaller amount than Method 4. The 816 particle case for Method 8, shown in Figures D.21 and D.22, is also similar to the Baseline and Method 4 cases. The same differences noted for the 600 particle case are still present, only smaller. Overall Method 8 (true central time) is better than Methods 4 or 6 (pseudo central time schemes). So, for small problems the added memory requirements could be easily handled for the better results. For larger problems the trade-off of memory versus accuracy needs to be considered on a case by case basis.

8.4.4 Method 12. For the Shock Tube Test, the results at 1 microsecond for Method 12 are shown in Appendix D in Figures D.23 - D.26.

The 600 particle case, shown in Figures D.23 and D.24, is one of the better of the hybrid schemes. The front edge of the shock is matched correctly and only minor noise is noticed within the results. The shortfall due to not enough particles is still present, but that is a problem with all the 600 particle examples (with fixed

h). The 816 particle case for Method 12, shown in Figures D.25 and D.26, is only a slight improvement over the 600 particle case. Although much of the shortfall is eliminated, the improvements seen in this method are not as good as those seen in other methods.

8.4.5 Method 20. For the Shock Tube Test, the results at 1 microsecond for Method 20 is shown in Appendix D in Figures D.27 - D.30.

The 600 particle case, shown in Figures D.27 and D.28, is actually a special case of Method 4 where the smoothing varies from equation to equation. This has allowed the front edge of the shock to be matched quite nicely. However, the price paid is in additional noise. The 816 particle case for Method 20, shown in Figures D.29 and D.30, shows that this special case of Method 4 converges quite nicely. Although some noise (especially Gibbs type phenomena) is still present, the results are quite acceptable.

8.5 Method Comparisons

The error norms for the tests in the previous section are found in Tables D.1 - D.7 in Appendix D. As discussed earlier, only the data for the l_1 and l_2 norms for the 1000 point analysis is summarized here. The formulas for the norms were given in equations (8.10) and (8.11). The summarized results are given in Figures 8.5 and 8.6. On each chart the l_1 norm appears in the bars on the left and l_2 norm in the bars on the right. The small boxes at the end of the line segment in each plot are the results for the Baseline.

The 600 particle case is probably close to standard since the particle spacing is the very popular $2/3 h$. Comparative results for all the methods can be seen in Figure 8.5. Note that the hybrid schemes perform approximately the same as the Baseline for density, pressure, and energy. Methods 2, 4, 6, and 8 do not perform as

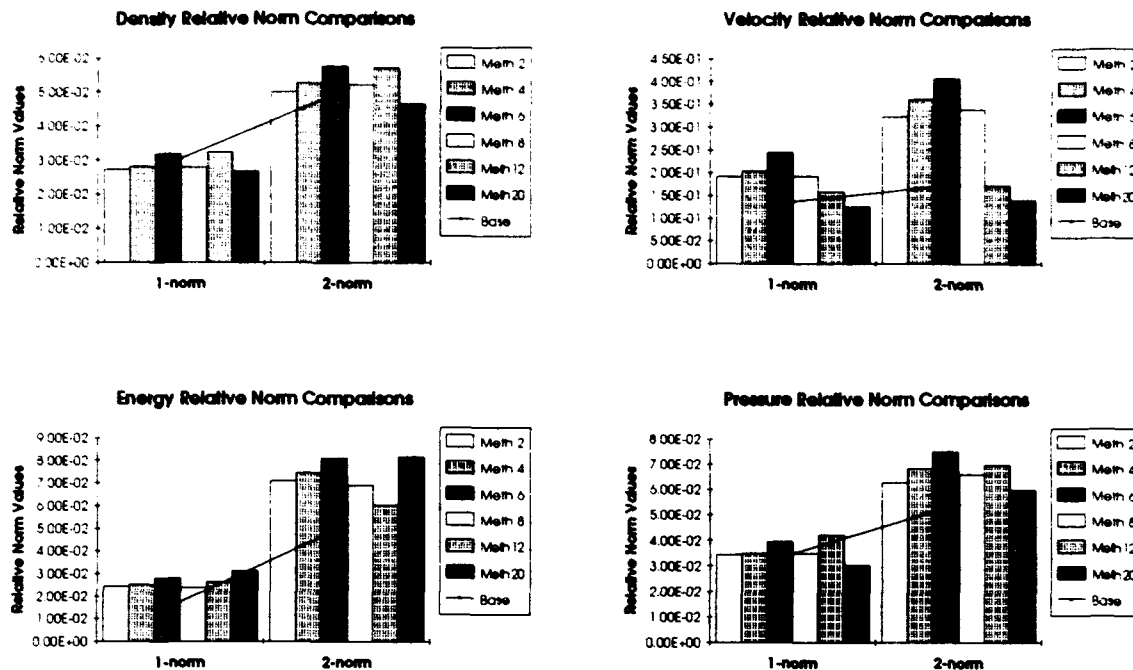


Figure 8.5 Shock Tube Results - 600 particles

well on modeling the front edge of the shock causing the velocity for those methods to be somewhat poorer than the Baseline.

For the 816 particle case comparative results are shown in Figure 8.6. All the methods improve over the 600 particle case, showing their overall tendency to converge as $\Delta x \rightarrow 0$. However, the improvement is somewhat better in the Baseline than for the hybrid methods. This probably indicates the limiter function or the actual way in which the methods are combined may need to be studied further.

8.6 Summary

In this chapter the concept of flux-limited hybrid methods was introduced, developed for SPH, and tested on a set of SPH schemes. The development is quite promising since the concept is well rooted in the finite difference community and the implementation is relatively straightforward in SPH (even in higher dimensions). The

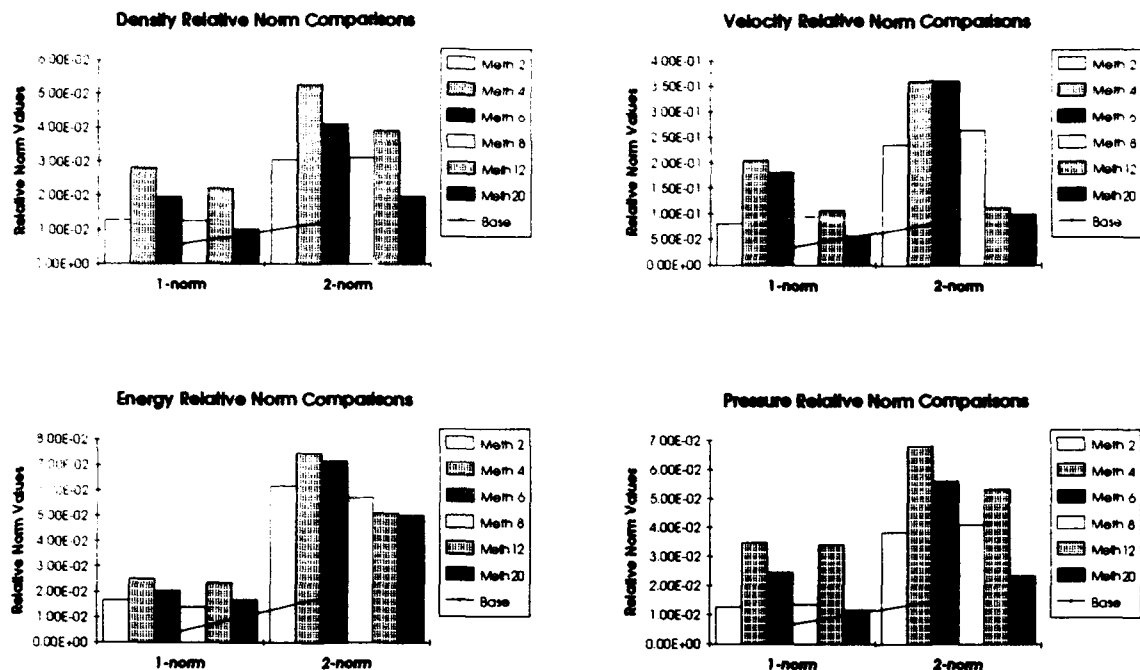


Figure 8.6 Shock Tube Results - 816 particles

tests performed in this chapter verify a hypothesis that flux-limited SPH performs roughly the same as current SPH techniques under basic assumptions. Some of the methods performed better for some of the field variables, while others were poorer.

At this stage in the development, it is difficult to determine if there is a significant advantage to using flux-limited SPH. It has allowed for SPH to use the continuity equation for the first time when performing the Riemann shock tube problem. This is a significant feat, and by itself asserts that the development of this concept should continue. Additional work is obviously needed to take this concept and apply it in production type codes. However, that will not be done in this dissertation.

IX. SUMMARY/CONTRIBUTIONS

Throughout this dissertation results were summarized and commented on as appropriate. The purpose of this chapter is to summarize the work as a whole and to point out the important contributions to the research community. Also, areas of future research are addressed.

The work is broken into two major categories: the numerical properties of SPH and the implementation of SPH. For the most part, material from Chapters III-V (and Appendices A and B) address the numerical properties of SPH while material from Chapters VII and VIII (and Appendix D) address the implementation of SPH. Chapter VI (and Appendix C) can be placed in either category since the subject of kernels is relevant to both. There is, of course, some overlap of these two categories in all chapters, but the categorization mostly holds and makes the summary easier. Also, since numerical analysis often lies between pure (theoretical) mathematics and the application (engineering or physics) each group may be identified with a category. The numerical properties chapters will be of more interest to the mathematics community while the remaining chapters will be of more interest to the engineering community.

Each of the chapters in the dissertation will now be reviewed, grouped according to the discussion above.

9.1 *Numerical Properties*

Summary. Chapter III (and Appendix A) concentrated on consistency. This chapter has important connections with Chapters V, VI, and VIII. It started with a detailed derivation of the kernel approximation and the particle approximation. This allowed for the proof of two consistency lemmas. Then a discussion of how the process may be applied to differential equations, including Euler's equations was performed. Although consistency analysis is traditionally performed under smooth

data assumptions, an alternative SPH form was investigated and derived after relaxing those assumptions. Finally it was shown how the previous material may be applied in higher dimensions. As an aside, the SPH forms of artificial viscosity and wall heating were shown to also be consistent.

Chapter IV (and Appendix B) concentrated on stability. This chapter has important connections with Chapters V, VI, and VII. A detailed linearized stability analysis was performed corroborating the existence and nature of an instability seen by other analysts. Four different solutions were proposed to eliminate the problem. Finally an initial total variation stability analysis was performed, leading to two monotone SPH schemes.

Chapter V concentrated on convergence. This chapter has important connections with Chapters III and IV. This chapter reviewed a convergence result from finite differences and then extended the result to SPH. The primary work was in the statement and proof of three lemmas derived from the Lax-Wendroff theorem.

Contributions. Some of the material found in Chapter III (Consistency) and Chapter IV (Stability) has been addressed in the SPH literature, but never with the rigor given here. There are several individual items of new work in these two chapters that are important, such as the instability and proposed solutions having direct relevance to difficulties SPH has in tension. But, the real gain in these two chapters is a thorough understanding of the process of obtaining consistency and stability in SPH. However, the most significant contribution to the SPH community from the numerical properties category comes from Chapter V (Convergence). It is my understanding that this is the first mathematical proof of convergence of SPH to be obtained. Previously, results from SPH calculations would be compared to analytic or experimental solutions to determine if the method was adequate. This empirical proof of convergence is important and should not be dismissed, but the mathematical proof of convergence will allow provide for a rigorous foundation and provide support that the method is a reliable technique.

9.2 *The Kernel*

Summary. Chapter VI (and Appendix C) concentrated on the SPH kernel. This chapter has important connections with Chapters III, IV, VII, and VIII. This chapter started with a review of the requirements placed on a function to be an SPH kernel. The chapter then quickly reviewed how to create higher order kernels and discussed the smoothing length. This included an investigation into the derivation of a variable h . The primary work in this chapter was the derivation of measures of merit used to compare kernels. Eighteen kernels (many of which were proposed here for the first time) were studied using these measures to determine their usefulness and that of the measure itself. Analytic results were compared with calculations from a test problem to verify the work.

Contributions. The kernel, with only a few exceptions, is not addressed at great lengths in the SPH literature. That is, it is simply treated as a given part of the implementation of SPH. However, since the kernel is such an important aspect of SPH, it deserves more analysis. Chapter VI (Kernels) provided both qualitative and quantitative measures of merit and procedures for determining them. These measures will allow general comparisons of kernels and further development of SPH based on good kernels, ensuring more accurate results. There are additional items of interest in this chapter (such as proposing new kernels and evaluating 18 kernels), but the measures of merit are the key contribution from these sections.

9.3 *The Implementation*

Summary. Chapter VII concentrated on time schemes to use with SPH. This chapter has important connections with Chapters IV, VI and VIII. In this chapter three second order time schemes are proposed: Lax-Wendroff, Central, and Shu to use with SPH. Only Central Time has been used in SPH before. Two lower order schemes were developed primarily to use with the hybrid methods in Chapter VIII.

Chapter VIII (and Appendix D) concentrated on hybrid methods for SPH. This chapter has important connections with Chapters III, VI and VII. This chapter started with a review of a method derived in Chapter III. Although it was not a flux-limited hybrid method, it has many of the same properties and fits in well here. The chapter then discussed and develop the notion of flux-limited hybrid SPH. Six combinations were proposed and compared against a baseline with favorable results.

Contributions. Although the discussion of time schemes found in Chapter VII is important to the user community, the major contribution here comes from the hybrid formulations found in Chapter VIII. Problems at interfaces of dissimilar materials and at shocks within a material have been a primary concern in SPH (and other numerical techniques) for many years. The hybrid form of SPH may not solve all these concerns, but it should be able to solve many. The ease at which hybrid methods can be incorporated into computer programs, even in three dimensions, should make this a popular notion in the near future.

9.4 *Future Direction*

It is, of course, impossible to predict the future direction in the development of SPH. But, based on the work in this dissertation there are some quite reasonable paths. Also, some of the work here was limited based on several factors that could now be further investigated. Hence, a list is provided that centers on future work in six areas that follow directly from the work in this dissertation.

- Reduce the impact of the $\Delta x = m/\rho$ assumption. This assumption was key in developing the consistency of SPH. It also was used several of places. There are two paths for this. First, show in a mathematical way that the two volume elements are close and bounded. Second, find more efficient methods to implement the equivalence.
- Continue the development of total variation stable SPH schemes. Especially, consider developing a TVD SPH scheme (if possible).

- Extend the kernel measures of merit to higher dimensions and other shapes of kernels. For example, one shape that might have promise is a kernel with two relative maxima known as double hump kernels. These measures of merit should be useful in one dimension, but would be invaluable in higher dimensions.
- Continue the development of flux-limited hybrid SPH. Especially, in the areas of the limiter function, higher dimensions, variable h , and efficiency.
- Further investigations into the effects of a variable smoothing length (variable h). This includes the effects on consistency, stability, and convergence.
- Further investigations into difficulties in SPH involving problems in tension. Some effects on consistency, stability, and accuracy were addressed individually in this dissertation. However, a unifying analysis of this problem together with possible fracture models would be useful.

In conclusion, I feel this dissertation has added significantly to the mathematical foundation of the SPH technique while at the same time providing insights into the computational aspects of the method through the SPH kernel and proposing a new method for SPH to handle one of the primary difficulties in applications (shocks).

Appendix A. ADDITIONAL CONSISTENCY NOTES

This appendix includes work related to the Consistency Chapter (Chapter III), but the details were left out earlier.

A.1 Non-Smooth Functions

The lemmas given earlier in Chapter III only applied when the functions were sufficiently smooth. Also introduced in that chapter was the notion of deriving an algorithm that is consistent even when the functions are not smooth. However, the details were omitted from that derivation to this point. So the derivation of how to obtain an SPH approximation for $u'(x_i)$ is now shown.

First, examine the kernel approximation for any function $f(x)$. Consider the interval shown in Figure A.1. Let $a \leq x_o - \kappa h$ and $b \geq x_o + \kappa h$. Assume there exists an integrable discontinuity in the function, $f(x)$, at d . For now assume $x_o < d \leq b$.

$$\int_a^b f(x) W(x_o - x) dx = \int_a^d f(x) W(x_o - x) dx + \int_d^b f(x) W(x_o - x) dx$$

Expand $f(x)$ in the first integral on the right-hand-side above about x_o and about x_1 in the last integral, where $d \leq x_1 \leq b$:

$$\begin{aligned} & \int_a^b f(x) W(x_o - x) dx \\ &= \int_a^d W(x_o - x) [f(x_o) + (x - x_o)f'(x_o) + \frac{1}{2}(x - x_o)^2 f''(\xi_o)] dx \\ & \quad + \int_d^b W(x_o - x) [f(x_1) + (x - x_1)f'(x_1) + \frac{1}{2}(x - x_1)^2 f''(\xi_1)] dx \end{aligned}$$

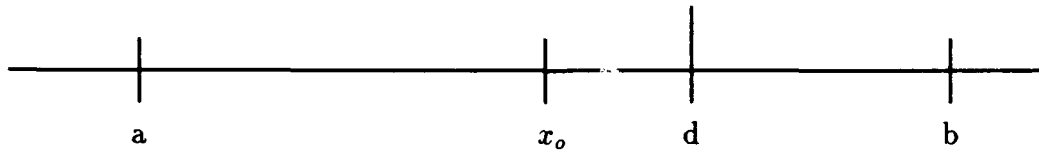


Figure A.1 Non-Smooth Data Consistency part 1

$$\begin{aligned}
&= f(x_o) \int_a^d W(x_o - x) dx + f(x_1) \int_d^b W(x_o - x) dx \\
&\quad + f'(x_o) \int_a^d (x - x_o) W(x_o - x) dx + f'(x_1) \int_d^b (x - x_1) W(x_o - x) dx \\
&\quad + \frac{1}{2} \int_a^d (x - x_o)^2 f''(\xi_o) W(x_o - x) dx \\
&\quad + \frac{1}{2} \int_d^b (x - x_1)^2 f''(\xi_1) W(x_o - x) dx \\
&= f(x_o) \int_a^b W(x_o - x) dx + [f(x_1) - f(x_o)] \int_d^b W(x_o - x) dx \\
&\quad + f'(x_o) \int_a^b (x - x_o) W(x_o - x) dx \\
&\quad + \int_d^b [(x - x_1)f'(x_1) - (x - x_o)f'(x_o)] W(x_o - x) dx \\
&\quad + \frac{1}{2} \int_a^d (x - x_o)^2 f''(\xi_o) W(x_o - x) dx \\
&\quad + \frac{1}{2} \int_d^b (x - x_1)^2 f''(\xi_1) W(x_o - x) dx .
\end{aligned}$$

Now assume the kernel W , is even, is normalized, and has compact support. The previous equation then simplifies to

$$\begin{aligned}
\int_a^b f(x) W(x_o - x) dx &= f(x_o) + [f(x_1) - f(x_o)] \int_d^b W(x_o - x) dx \\
&\quad + \int_d^b [(x - x_1)f'(x_1) - (x - x_o)f'(x_o)] W(x_o - x) dx \\
&\quad + \frac{1}{2} \int_a^d (x - x_o)^2 f''(\xi_o) W(x_o - x) dx \\
&\quad + \frac{1}{2} \int_d^b (x - x_1)^2 f''(\xi_1) W(x_o - x) dx . \tag{A.1}
\end{aligned}$$

Note: by the compact support of W , $|x - x_1| \leq \kappa h$ and $|x - x_o| \leq \kappa h$ in the domains for the integrals above. Therefore the last three lines in equation (A.1) can be bounded by terms of order h , h^2 , and h^2 respectively as long as f' and f'' can be bounded in the following sense: f , f' , and f'' must all exist and be bounded on $[a, d) \cup (d, b]$, $\lim_{x \rightarrow d \pm} |f'| \leq M$, and $\lim_{x \rightarrow d \pm} |f''| \leq M$. Previously in Chapter III,

for smooth data

$$\int_a^b f(x) W(x_o - x) dx = f(x_o) + O(h^2),$$

but now the equation is

$$\int_a^b f(x) W(x_o - x) dx = f(x_o) + [f(x_1) - f(x_o)] \int_d^b W(x_o - x) dx + O(h). \quad (\text{A.2})$$

Note that the second integral is only over part of the interval and therefore is not equal to one. This implies for non-smooth data when $x_o \rightarrow d$

$$\int_a^b f(x) W(x_o - x) dx \nrightarrow f(x_o) \quad \text{as } h \rightarrow 0.$$

Consequently, in the context of this presentation, using the normal SPH approximation to model a shock is inconsistent. However, if the second term in the right-hand-side of equation (A.2) ($\sim \Delta f$) is retained, then the method would be consistent and of order $O(h)$. That is what is done here.

Now consider $f(x) = u'(x)$, where u' , u'' , u''' exist and are bounded on $[a, d] \cup (d, b]$. Then

$$\int_a^b u'(x) W(x_o - x) dx = u'(x_o) + [u'(x_1) - u'(x_o)] \int_d^b W(x_o - x) dx + O(h). \quad (\text{A.3})$$

Use the details above along with integration-by-parts to obtain a new form for $u'(x_o)$.

So integrating by parts yields

$$\begin{aligned} \int_a^b u'(x) W(x_o - x) dx &= \int_a^d u'(x) W(x_o - x) dx + \int_d^b u'(x) W(x_o - x) dx \\ &= u(x) W(x_o - x) \Big|_a^{d^-} + u(x) W(x_o - x) \Big|_d^b \\ &\quad - \int_a^b u(x) \frac{\partial}{\partial x} W(x_o - x) dx. \end{aligned}$$

Use the compact support of the kernel and change the derivative on the kernel from x to x_o to obtain

$$\int_a^b u'(x) W(x_o - x) dx = [u(d^-) - u(d^+)] W(x_o - d) + \int_a^b u(x) W'(x_o - x) dx . \quad (\text{A.4})$$

Put equations (A.3) and (A.4) together to obtain

$$u'(x_o) + [u'(x_1) - u'(x_o)] \int_d^b W(x_o - x) dx + O(h) = [u(d^-) - u(d^+)] W(x_o - d) + \int_a^b u(x) W'(x_o - x) dx .$$

Since x_1 was chosen arbitrarily in $[d, b]$ now let $x_1 = d$ and then note

$$\begin{aligned} \int_d^b W(x_o - x) dx &= \int_{x_o}^b W(x_o - x) dx - \int_{x_o}^d W(x_o - x) dx \\ &= \frac{1}{2} - \frac{1}{2} \left[2 \int_{x_o}^d W(x_o - x) dx \right] ; . \end{aligned}$$

Define $\theta = 2 \int_{x_o}^d W(x_o - x) dx$ to now obtain

$$u'(x_o) + [u'(d) - u'(x_o)] \left[\frac{1}{2} - \frac{\theta}{2} \right] + O(h) = [u(d^-) - u(d^+)] W(x_o - d) + \int_a^b u(x) W'(x_o - x) dx ; .$$

Combine terms and rearrange to obtain

$$u'(x_o) = \left(\frac{2}{1 + \theta} \right) \left\{ \int_a^b u(x) W'(x_o - x) dx + [u(d^-) - u(d^+)] W(x_o - d) - \frac{1}{2}(1 - \theta) u'(d) \right\} + O(h) ; . \quad (\text{A.5})$$

To derive a more usable form, obtain expressions for $u'(d)$ and $u(d^-)$. To find the expression for $u'(d)$, follow the same procedures that were used up to this point (abbreviating the steps):

$$\begin{aligned}
\int_a^b f(x) W(d-x) dx &= \int_a^d f(x) W(d-x) dx + \int_d^b f(x) W(d-x) dx \\
&= f(d) + [f(x_o) - f(d)] \int_a^d W(d-x) dx + O(h) .
\end{aligned}$$

However,

$$\frac{1}{2} = \int_a^d W(d-x) dx .$$

Therefore,

$$\int_a^b f(x) W(d-x) dx = \frac{f(d) + f(x_o)}{2} . \quad (\text{A.6})$$

Now let $f(x) = u'(x)$ and note

$$\begin{aligned}
\int_a^b u'(x) W(d-x) dx &= \int_a^d u'(x) W(d-x) dx + \int_d^b u'(x) W(d-x) dx \\
&= u(x) W(d-x) \Big|_a^{d^-} + u(x) W(d-x) \Big|_d^b + \int_a^b u(x) W'(d-x) dx \\
&= u(d^-) W(d-d^-) - u(d^+) W(d-d^+) + \int_a^b u(x) W'(d-x) dx \\
&= [u(d^-) - u(d^+)] W(0) + \int_a^b u(x) W'(d-x) dx .
\end{aligned}$$

Therefore,

$$\frac{u'(d) + u'(x_o)}{2} = [u(d^-) - u(d^+)] W(0) + \int_a^b u(x) W'(d-x) dx . \quad (\text{A.7})$$

Solve equation (A.7) for $u'(d)$ and substitute into equation (A.5):

$$\begin{aligned}
u'(x_o) &= \left(\frac{2}{1+\theta} \right) \left\{ \int_a^b u(x) W'(x_o - x) dx + [u(d^-) - u(d^+)] W(x_o - d) \right. \\
&\quad \left. - \frac{1}{2}(1-\theta) \left[-u'(x_o) + 2[u(d^-) - u(d^+)] W(0) \right. \right. \\
&\quad \left. \left. + 2 \int_a^b u(x) W'(d-x) dx \right] \right\} + O(h) .
\end{aligned}$$

Combine $u'(x_o)$ terms to obtain

$$u'(x_o) = \frac{1}{\theta} \left\{ \int_a^b u(x) W'(x_o - x) dx + [u(d^-) - u(d^+)] W(x_o - d) \right. \\ \left. - (1 - \theta)[u(d^-) - u(d^+)] W(0) - (1 - \theta) \int_a^b u(x) W'(d - x) dx \right\} + O(h).$$

$$u'(x_o) = \int_a^b u(x) \left[\frac{1}{\theta} W'(x_o - x) - \left(\frac{1 - \theta}{\theta} \right) W'(d - x) \right] dx \\ + \frac{1}{\theta} [u(d^-) - u(d^+)] [W(x_o - d) - (1 - \theta) W(0)] + O(h) \quad (A.8)$$

Now obtain an expression for $u(d^-)$ using a Taylor series expansion

$$u(d^-) = u(x_o) + (d^- - x_o) u'(x_o) + \dots \approx u(x_o) + (d - x_o) u'(x_o).$$

Substitute this into equation (A.8) and solve for $u'(x_o)$ to obtain

$$u'(x_o) = \left[\frac{\theta}{\theta - (d - x_o)[W(x_o - d) - (1 - \theta)W(0)]} \right] \left\{ \int_a^b u(x) \left[\frac{1}{\theta} W'(x_o - x) \right. \right. \\ \left. \left. - \left(\frac{1 - \theta}{\theta} \right) W'(d - x) \right] dx + \frac{1}{\theta} [u(x_o) - u(d^+)] [W(x_o - d) \right. \right. \\ \left. \left. - (1 - \theta)W(0)] + O(h) \right\}. \quad (A.9)$$

It is advantageous in the implementation to replace $W'(d - x)$ in equation (A.9) as follows

$$W'(d - x) = W'(x_o - x) + (d - x_o) W''(x_o - x) + \dots$$

Substituting this into equation (A.9) yields

$$u'(x_o) = \left[\frac{1}{\theta - (d - x_o)[W(x_o - d) - (1 - \theta)W(0)]} \right] \left\{ \int_a^b u(x) [\theta W'(x_o - x) \right. \\ \left. - (1 - \theta)(d - x_o) W''(x_o - x)] dx + [u(x_o) - u(d^+)] [W(x_o - d) \right. \\ \left. - (1 - \theta)W(0)] \right\} + O(h). \quad (A.10)$$

This is now a kernel approximation form that involves only $u(x_o)$, $u(d^+)$, and the associated kernel and integral values for these. To obtain a particle approximation let

$$B_o = (d - x_o)[W(x_o - d) - (1 - \theta)W(0)] ,$$

placing this in the final SPH form (replacing integrals with sums) and writing it for some particle i

$$\begin{aligned} u'(x_i) = & \left(\frac{\theta_i}{\theta_i - B_i} \right) \left\{ \sum_{j=1}^N \frac{m_j}{\rho_j} u_j \left[W'_{ij} - \left(\frac{1 - \theta_i}{\theta_i} \right) (d - x_i) W''_{ij} \right] \right. \\ & \left. + \frac{B_i}{\theta_i} \left[\frac{u(x_i) - u(d^+)}{d - x_i} \right] \right\} + O(h) . \end{aligned} \quad (\text{A.11})$$

Rewrite equation (A.11) as the sum of the consistent form for smooth data plus a correction term by

$$\begin{aligned} u'(x_i) = & \sum_{j=1}^N \frac{m_j}{\rho_j} u_j W'_{ij} + \left(\frac{1}{\theta_i - B_i} \right) \left\{ \sum_{j=1}^N \frac{m_j}{\rho_j} u_j \left[B_i W'_{ij} - (1 - \theta_i)(d - x_i) W''_{ij} \right] \right. \\ & \left. + B_i \left[\frac{u(x_i) - u(d^+)}{d - x_i} \right] \right\} . \end{aligned} \quad (\text{A.12})$$

Taking the usual format for the kernel: $W(x, h) = \frac{1}{h} K(\frac{x}{h})$, the following expression for θ may be found

$$\theta = 2 \int_{\frac{x_i - d}{h}}^0 K(v) dv ; \quad (\text{A.13})$$

Note that $0 \leq \theta \leq 1$ and θ should be investigated at the ends using (A.11) or (A.12) to ensure they are well defined.

(i) As $|x_i - d|$ increases, ie. x_i moves away from the shock, θ increases until $|x_i - d| = \kappa h$ where θ equals 1. At that point θ stays at 1 no matter how far x_i gets from d . Using the form from equation (A.11), as $\theta \rightarrow 1$

$$u'(x_i) \rightarrow \sum_{j=1}^N \frac{m_j}{\rho_j} u_j \left(\frac{1}{1 - B} \right) W'_{ij} + \left(\frac{B}{1 - B} \right) \left[\frac{u(x_i) - u(d^+)}{d - x} \right] .$$

But B also goes to 0 in this case by the compact support of W . Therefore when $|x_i - d| = \kappa h$, the correction term drops completely out and becomes the smooth data result

$$u'(x_i) = \sum_{j=1}^N \frac{m_j}{\rho_j} u_j W'_{ij}.$$

(ii) As $x_i \rightarrow d$, ie. x_i moves towards the shock, θ decreases to 0. θ never actually reaches 0 since x_i cannot equal d under the assumptions, but it can get very close. Therefore, consider some of the terms as $\theta \rightarrow 0$. Using the form in equation (A.11) let $d = x_i + \varepsilon h$, $h \gg \varepsilon > 0$ and substituting to obtain

$$\begin{aligned} u'(x_i) &= \left(\frac{\theta}{\theta - B} \right) \left\{ \sum_{j=1}^N \frac{m_j}{\rho_j} u_j \left[W'(x_i - x_j) - \left(\frac{1 - \theta}{\theta} \right) (x_i + \varepsilon h - x_i) W''(x_i - x_j) \right] \right. \\ &\quad \left. + \frac{B}{\theta} \left[\frac{u(x_i) - u(x_i + \varepsilon h)}{x_i + \varepsilon h - x_i} \right] \right\} \\ B &= (x_i + \varepsilon h - x_i)[W(x_i - x_i - \varepsilon h) - (1 - \theta)W(0)] \\ &= \varepsilon h[W(-\varepsilon h) - (1 - \theta)W(0)]. \end{aligned} \quad (\text{A.14})$$

Substitute B into equation (A.14) to obtain

$$\begin{aligned} u'(x_i) &= \left[\frac{1}{1 - \frac{\varepsilon h}{\theta}[W(-\varepsilon h) - (1 - \theta)W(0)]} \right] \left\{ \sum_{j=1}^N \frac{m_j}{\rho_j} u_j \left[W'_{ij} - \left(\frac{1 - \theta}{\theta} \right) \varepsilon h W''_{ij} \right] \right. \\ &\quad \left. + \frac{1}{\theta} [u(x_i) - u(x_i + \varepsilon h)][W(-\varepsilon h) - (1 - \theta)W(0)] \right\};. \end{aligned}$$

Expand the kernel in a Taylor series

$$W(-\varepsilon h) = W(0) - \varepsilon h W'(0) + \frac{1}{2} \varepsilon^2 h^2 W''(0) + \dots$$

Substitute to find

$$u'(x_i) = \left[\frac{1}{1 - \varepsilon h [W(0) - (\frac{\varepsilon h}{\theta}) W'(0)]} \right] \left\{ \sum_{j=1}^N \frac{m_j}{\rho_j} u_j [W'_{ij} - (1 - \theta) \left(\frac{\varepsilon h}{\theta} \right) W''_{ij}] \right. \\ \left. + [u(x_i) - u(x_i + \varepsilon h)] [W(0) - \frac{\varepsilon h}{\theta} W'(0)] \right\} + O(\varepsilon^2).$$

Use equation (A.13) and $d = x_i + \varepsilon h$ to obtain

$$\theta = 2 \int_{-\varepsilon}^0 K(v) dv = 2 \int_0^{\varepsilon} K(v) dv. \quad (\text{A.15})$$

Then $\theta \rightarrow 0$ as $\varepsilon \rightarrow 0$, $\frac{\varepsilon h}{\theta} \rightarrow \frac{0}{0}$ as $\varepsilon \rightarrow 0$. It is necessary to know if $\frac{\varepsilon h}{\theta}$ bounded as $\varepsilon \rightarrow 0$. Use L'Hôpital's Rule to find $\frac{\varepsilon h}{\theta} \rightarrow \frac{h}{\frac{d\theta}{d\varepsilon}}$ and by the Fundamental Theorem of Calculus from equation (A.15), $\frac{d\theta}{d\varepsilon} = 2K(\varepsilon)$. Therefore

$$\frac{\varepsilon h}{\theta} \rightarrow \frac{h}{2K(\varepsilon)} = \frac{1}{2W(\varepsilon)}.$$

Then add the requirement that $K(u) \rightarrow 0$ as $u \rightarrow 0$, ie. $K(u)$ includes the constant term. So in conclusion, $\frac{\varepsilon h}{\theta} \rightarrow \frac{1}{2W(0)}$ as $\varepsilon \rightarrow 0$. Hence

$$u'(x_i) \rightarrow \sum_{j=1}^N \frac{m_j}{\rho_j} u_j \left[W'_{ij} - \frac{W''_{ij}}{2W(0)} \right] + \frac{\Delta u_d [2W^2(0) - W'(0)]}{2W(0)} \quad (\text{A.16}) \\ \text{as } x_i \rightarrow d \quad \text{where } \Delta u_d = u(d^+) - u(d^-).$$

So this form is well defined at the limits of θ .

Now consider the shock on the other side of x_o as shown in Figure A.2. Next find an expression for $u'(x_o)$ again. This follows exactly as in the first case as contained in equations (A.1) - (A.16) and the surrounding work. Therefore, in the work below many of the intermediate steps are dropped.

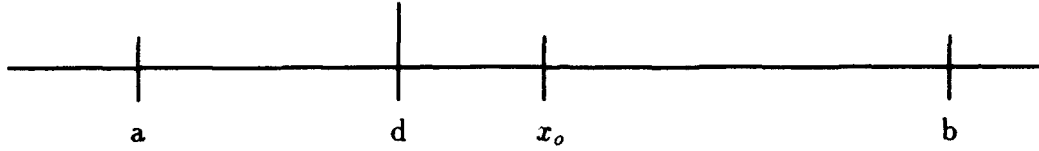


Figure A.2 Non-Smooth Data Consistency part 2

For this case equation (A.3) becomes

$$\int_a^b u'(x) W(x_o - x) dx = u'(x_o) + [u'(x_1) - u'(x_o)] \int_a^d W(x_o - x) dx + O(h).$$

Equation (A.4) remains the same yielding

$$u'(x_o) + [u'(x_1) - u'(x_o)] \int_a^d W(x_o - x) dx + O(h) = [u(d^-) - u(d^+)] W(x_o - d) + \int_a^b u(x) W'(x_o - x) dx; .$$

Now let $x_1 = d$ and then note

$$\begin{aligned} \int_a^d W(x_o - x) dx &= \int_a^{x_o} W(x_o - x) dx - \int_d^{x_o} W(x_o - x) dx \\ &= \frac{1}{2} + \frac{1}{2} \left[2 \int_{x_o}^d W(x_o - x) dx \right] \leq \frac{1}{2}(1 + \theta); , \end{aligned}$$

where θ defined as before. Equation (A.5) becomes

$$\begin{aligned} u'(x_o) &= \left(\frac{2}{1 - \theta} \right) \left\{ \int_a^b u(x) W'(x_o - x) dx + [u(d^-) - u(d^+)] W(x_o - d) \right. \\ &\quad \left. - \frac{1}{2} (1 + \theta) u'(d) \right\} + O(h) . \end{aligned}$$

Once again an expression for $u'(d)$ is needed. Obtaining it as before, equation (A.7) becomes

$$\frac{u'(d) + u'(x_o)}{2} = [u(d^-) - u(d^+)] W(0) + \int_a^b u(x) W'(d - x) dx .$$

Solve for $u'(d)$ and substitute to obtain

$$\begin{aligned} u'(x_o) = & \left(\frac{2}{1-\theta} \right) \left\{ \int_a^b u(x) W'(x_o - x) dx + [u(d^-) - u(d^+)] W(x_o - d) \right. \\ & - \frac{1}{2}(1+\theta) \left[-u'(x_o) + 2[u(d^-) - u(d^+)]W(0) \right. \\ & \left. \left. + 2 \int_a^b u(x) W'(d - x) dx \right] \right\} + O(h). \end{aligned}$$

Combine $u'(x_o)$ terms and equation (A.8) becomes

$$\begin{aligned} u'(x_o) = & \int_a^b u(x) \left[-\frac{1}{\theta} W'(x_o - x) + \left(\frac{1+\theta}{\theta} \right) W'(d - x) \right] dx \\ & - \frac{1}{\theta} [u(d^-) - u(d^+)] [W(x_o - d) - (1+\theta)W(0)] + O(h). \end{aligned}$$

For $u(d^+)$ use

$$u(d^+) = u(x_o) + (d^+ - x_o)u'(x_o) + \dots \approx u(x_o) + (d - x_o)u'(x_o).$$

Also let

$$B_o = (d - x_o)[W(x_o - d) - (1+\theta)W(0)].$$

Substitute to obtain

$$\begin{aligned} u'(x_o) = & \left(\frac{\theta}{\theta - B} \right) \left\{ \int_a^b u(x) \left[-\frac{1}{\theta} W'(x_o - x) + \left(\frac{1+\theta}{\theta} \right) W'(d - x) \right] dx \right. \\ & \left. - \frac{B}{\theta} \left[\frac{u(d^-) - u(x_o)}{d - x_o} \right] + O(h) \right\}. \\ u'(x_o) = & \left(\frac{\theta}{\theta - B} \right) \left\{ \int_a^b u(x) \left[W'(x_o - x) + \left(\frac{1+\theta}{\theta} \right) (d - x_o) W''(x_o - x) \right] dx \right. \\ & \left. - \frac{B}{\theta} \left[\frac{u(d^-) - u(x_o)}{d - x_o} \right] \right\} + O(h) \end{aligned}$$

Placing this in the final SPH form (replacing integrals with sums) and writing it for some particle i

$$u'(x_i) = \left(\frac{\theta_i}{\theta_i - B_i} \right) \left\{ \sum_{j=1}^N \frac{m_j}{\rho_j} u_j \left[W'_{ij} + \left(\frac{1 + \theta}{\theta} \right) (d - x_i) W''_{ij} \right] - \frac{B_i}{\theta_i} \left[\frac{u(d^-) - u(x_i)}{d - x_i} \right] \right\} + O(h). \quad (\text{A.17})$$

As before, rewrite equation (A.17) as the sum of the consistent form for smooth data plus a correction term as

$$u'(x_i) = \sum_{j=1}^N \frac{m_j}{\rho_j} u_j W'_{ij} + \left(\frac{1}{\theta_i - B_i} \right) \left\{ \sum_{j=1}^N \frac{m_j}{\rho_j} u_j [B_i W'_{ij} - (1 + \theta_i)(d - x_i) W''_{ij}] - B_i \left[\frac{u(d^-) - u(x_i)}{d - x_i} \right] \right\}. \quad (\text{A.18})$$

Recall, $\theta = 2 \int_{x_i}^d W(x_i - x) dx$ which in the first case, $\theta \in [0, 1]$ but in the second case $\theta \in [-1, 0]$. Instead if θ is redefined as

$$\theta = 2 \left| \int_{x_i}^d W(x_i - x) dx \right| = 2 \int_0^{\frac{|x_i - d|}{h}} K(v) dv. \quad (\text{A.19})$$

then there are no changes necessary for equations (A.1) - (A.12) from earlier, but in the second case θ needs to be replaced with $-\theta$ everywhere. So the last two equations, (A.17) and (A.18) become

$$u'(x_i) = \left(\frac{\theta_i}{\theta_i + B_i} \right) \left\{ \sum_{j=1}^N \frac{m_j}{\rho_j} u_j \left[W'_{ij} - \left(\frac{1 - \theta_i}{\theta_i} \right) (d - x_i) W''_{ij} \right] + \frac{B_i}{\theta_i} \left[\frac{u(d^-) - u(x_i)}{d - x_i} \right] \right\}. \quad (\text{A.20})$$

$$u'(x_i) = \sum_{j=1}^N \frac{m_j}{\rho_j} u_j W'_{ij} + \left(\frac{1}{\theta_i + B_i} \right) \left\{ \sum_{j=1}^N \frac{m_j}{\rho_j} u_j [-B_i W'_{ij} - (1 - \theta_i) W''_{ij}] + B_i \left[\frac{u(d^-) - u(x_i)}{d - x_i} \right] \right\} \quad (\text{A.21})$$

To generalize the results, combine the results of equations (A.12) and (A.21) as follows: Given x_i , let d be the location of a discontinuity and x_d be the nearest particle on the opposite side of the discontinuity from x_i . Provided x_d is quite close to d the results are

$$\theta = 2 \int_0^{\frac{|x_i-d|}{h}} K(v) dv \quad (\text{A.22})$$

$$B = [W_{id} - (1 - \theta)W_o](x_{di}) \text{sgn}(x_{id}) \quad (\text{A.23})$$

$$u'(x_i) = \sum_{j=1}^N \frac{m_j}{\rho_j} u_j W'_{ij} - \left(\frac{1}{\theta + B} \right) \left\{ \sum_{j=1}^N \frac{m_j}{\rho_j} u_j [B W'_{ij} - (1 - \theta) x_{di} W''_{ij}] - B \left(\frac{u_i - u_d}{x_i - x_d} \right) \right\} \quad (\text{A.24})$$

A.2 Artificial Viscosity/Wall Heating

In Chapter III (Consistency), three forms of artificial viscosity and one form of wall heating found in the published literature for SPH are introduced. At that time, these terms were stated as being consistent without showing the details. Those details are shown here.

Start with artificial viscosity. The three forms are attributed to: Monaghan, et al. (37), Hernquist and Katz (19), and Lattanzio, et al. (28).

1. Monaghan. It will be shown for the momentum equation (when $\frac{\partial v}{\partial x} < 0$), this form of the artificial viscosity corresponds to

$$\frac{\alpha h}{2\rho} \frac{\partial}{\partial x} \left(c\rho \frac{\partial v}{\partial x} \right) - \frac{\beta h^2}{2\rho} \frac{\partial}{\partial x} \left[\rho \left(\frac{\partial v}{\partial x} \right)^2 \right] \quad (\text{A.25})$$

For the SPH form, in the momentum and energy equations replace the $\frac{P}{\rho^2}$ term with $\frac{P}{\rho^2} + \frac{1}{2}\Pi$ where the function $\Pi_{ij} = \Pi(x_i, x_j)$ is defined by

$$\Pi_{ij} = \frac{-\alpha 0.5 (c_i + c_j) \mu_{ij} + \beta \mu_{ij}^2}{0.5 (\rho_i + \rho_j)} \quad (\text{A.26})$$

$$\mu_{ij} = \begin{cases} \frac{h(v_i - v_j) \cdot (x_i - x_j)}{(x_i - x_j)^2 + \eta h^2} & (v_i - v_j) \cdot (x_i - x_j) < 0 \\ 0 & \text{otherwise} \end{cases} \quad (\text{A.27})$$

The Π term has a linear term that is referred to as π_a and a quadratic term that is called π_b . First consider the linear term.

$$\begin{aligned} \pi_a &= \frac{-\alpha 0.5(c_i + c_j)\mu_{ij}}{0.5(\rho_i + \rho_j)} = (-\alpha h) \left(\frac{c_i + c_j}{\rho_i + \rho_j} \right) (v_i - v_j) \left(\frac{x_i - x_j}{(x_i - x_j)^2 + \eta h^2} \right) \\ \frac{c_i + c_j}{\rho_i + \rho_j} &= \frac{c_i + (c_i - x_{ij}c'_i + \dots)}{\rho_i + (\rho_i - x_{ij}\rho'_i + \dots)} = \frac{2c_i - x_{ij}c'_i + \dots}{2\rho_i - x_{ij}\rho'_i + \dots} = \frac{c_i}{\rho_i} - \frac{x_{ij}}{2} \left(\frac{c_i}{\rho_i} \right)' + O(h^2) \\ v_i - v_j &= v_i - (v_i - x_{ij}v'_i + \frac{x_{ij}^2}{2}v''_i + \dots) = x_{ij}v'_i - \frac{x_{ij}^2}{2}v''_i + O(h^2) \\ \text{Hence } \left(\frac{c_i + c_j}{\rho_i + \rho_j} \right) (v_i - v_j) &= \left(\frac{c_i}{\rho_i} v'_i \right) x_{ij} - \left[\left(\frac{c_i}{\rho_i} \right)' v'_i + \left(\frac{c_i}{\rho_i} \right) v''_i \right] \frac{x_{ij}^2}{2} + O(h^2) \end{aligned}$$

So for the term that contains π_a

$$\begin{aligned} \sum_{j=1}^N m_j \pi_a W'_{ij} &= -\alpha h \left\{ \left[\frac{c_i}{\rho_i} v'_i \sum_{j=1}^N m_j \left(\frac{x_{ij}^2}{x_{ij}^2 + \eta h^2} \right) W'_{ij} \right] \right. \\ &\quad \left. - \left[\left(\left(\frac{c_i}{\rho_i} \right)' v'_i + \left(\frac{c_i}{\rho_i} \right) v''_i \right) \frac{1}{2} \sum_{j=1}^N m_j \left(\frac{x_{ij}^3}{x_{ij}^2 + \eta h^2} \right) W'_{ij} \right] \right\} + O(h^3). \end{aligned}$$

Examine the summation terms:

$$\begin{aligned} \sum_{j=1}^N m_j \left(\frac{x_{ij}^2}{x_{ij}^2 + \eta h^2} \right) W'_{ij} &= \sum_{j=1}^N m_j W'_{ij} + O(h^2) = \sum_{j=1}^N \frac{m_j}{\rho_j} \rho_j W'_{ij} + O(h^2) \\ &= \rho'_i + O(h^2) \\ \sum_{j=1}^N m_j \left(\frac{x_{ij}^3}{x_{ij}^2 + \eta h^2} \right) W'_{ij} &= \sum_{j=1}^N m_j x_{ij} W'_{ij} + O(h^2) \\ &= x_i \sum_{j=1}^N m_j W'_{ij} - \sum_{j=1}^N m_j x_j W'_{ij} + O(h^2) \\ &= x_i \sum_{j=1}^N \frac{m_j}{\rho_j} \rho_j W'_{ij} - \sum_{j=1}^N \frac{m_j}{\rho_j} x_j \rho_j W'_{ij} + O(h^2) \\ &= x_i \rho'_i - (x\rho)'_i + O(h^2) = -\rho_i + O(h^2) \end{aligned}$$

Therefore,

$$\begin{aligned}
\sum_{j=1}^N m_j \pi_a W'_{ij} &= -\alpha h \left\{ \frac{c_i}{\rho_i} v'_i \rho'_i + \left[\left(\frac{c_i}{\rho_i} \right)' v'_i + \left(\frac{c_i}{\rho_i} \right) v''_i \right] \frac{\rho_i}{2} \right\} + O(h^3) \\
&= -\alpha h \left(\frac{c_i v'_i \rho'_i}{\rho_i} + \frac{c'_i v'_i}{2} - \frac{c_i v'_i \rho'_i}{2\rho_i} + \frac{c_i v''_i}{2} \right) + O(h^3) \\
&= -\alpha h \left(\frac{c_i v'_i \rho'_i}{2\rho_i} + \frac{c'_i v'_i + c_i v''_i}{2} \right) + O(h^3) \\
&= -\frac{\alpha h}{2} \left(\frac{c_i v'_i \rho'_i}{\rho_i} + (c_i v'_i)' \right) + O(h^3) = -\frac{\alpha h}{2} \frac{1}{\rho_i} (c_i v'_i \rho_i)' + O(h^3)
\end{aligned}$$

$$\text{Thus } \sum_j m_j \pi_a W'_{ij} = -\frac{\alpha h}{2\rho} \frac{\partial}{\partial x} \left(c\rho \frac{\partial v}{\partial x} \right) + O(h^3)$$

Next consider the quadratic term.

$$\begin{aligned}
\pi_b &= \frac{\beta \mu_{ij}^2}{0.5(\rho_i + \rho_j)} = (\beta h^2) \frac{2(v_{ij} x_{ij})^2}{(\rho_i + \rho_j)((x_i - x_j)^2 + \eta h^2)^2} \\
\frac{2}{\rho_i + \rho_j} &= \frac{2}{\rho_i + (\rho_i - x_{ij} \rho'_i + \dots)} = \frac{2}{2\rho_i - x_{ij} \rho'_i + \dots} = \frac{1}{\rho_i} + \frac{x_{ij} \rho'_i}{2\rho_i^2} + O(h^2) \\
v_{ij} &= v_i - v_j = v_i - (v_i - x_{ij} v'_i + \frac{x_{ij}^2}{2} v''_i + \dots) = x_{ij} v'_i - \frac{x_{ij}^2}{2} v''_i + O(h^2) \\
v_{ij} x_{ij} &= x_{ij}^2 v'_i - \frac{x_{ij}^3}{2} v''_i + O(h^2) \\
(v_{ij} x_{ij})^2 &= x_{ij}^4 (v'_i)^2 - x_{ij}^5 v'_i v''_i + O(h^2) \\
\text{Hence } \frac{(v_{ij} x_{ij})^2}{\frac{1}{2}(\rho_i + \rho_j)} &= \frac{x_{ij}^4 (v'_i)^2}{\rho_i} + x_{ij}^5 \left(\frac{\rho'_i (v'_i)^2}{2\rho_i^2} - \frac{v'_i v''_i}{\rho_i} \right) + O(h^4)
\end{aligned}$$

So for the term that contains π_b

$$\begin{aligned}
\sum_j m_j \pi_b W'_{ij} &= \beta h^2 \left\{ \left[\frac{(v'_i)^2}{\rho_i} \sum_{j=1}^N m_j \left(\frac{x_{ij}^4}{(x_{ij}^2 + \eta h^2)^2} \right) W'_{ij} \right] \right. \\
&\quad \left. + \left[\left(\frac{\rho'_i (v'_i)^2}{2\rho_i^2} - \frac{v'_i v''_i}{\rho_i} \right) \sum_{j=1}^N m_j \left(\frac{x_{ij}^5}{(x_{ij}^2 + \eta h^2)^2} \right) W'_{ij} \right] \right\} + O(h^4).
\end{aligned}$$

As before, the first sum is approximately ρ'_i and the second sum is approximately $-\rho_i$. Therefore,

$$\begin{aligned}
\sum_{j=1}^N m_j \pi_b W'_{ij} &= \beta h^2 \left[\frac{(v'_i)^2 \rho'_i}{\rho_i} - \frac{\rho'_i (v'_i)^2 \rho_i}{2\rho_i^2} + \frac{v'_i v''_i \rho_i}{\rho_i} \right] + O(h^4) \\
&= \beta h^2 \left[\frac{\rho'_i (v'_i)^2}{2\rho_i} + v'_i v''_i \right] + O(h^4) \\
&= \frac{\beta h^2}{2\rho_i} [\rho'_i (v'_i)^2 + 2\rho_i v'_i v''_i] + O(h^4) \\
&= \frac{\beta h^2}{2\rho_i} [\rho'_i (v'_i)^2]' + O(h^4)
\end{aligned}$$

$$\text{Thus } \sum_{j=1}^N m_j \pi_b W'_{ij} = \frac{\beta h^2}{2\rho} \frac{\partial}{\partial x} \left[\rho \left(\frac{\partial v}{\partial x} \right)^2 \right] + O(h^4)$$

Finally this results in

$$\begin{aligned}
-\sum_{j=1}^N m_j \Pi_{ij} W'_{ij} &= -\sum_{j=1}^N m_j \pi_a W'_{ij} - \sum_{j=1}^N m_j \pi_b W'_{ij} \\
&= \frac{\alpha h}{2\rho} \frac{\partial}{\partial x} \left(c\rho \frac{\partial v}{\partial x} \right) - \frac{\beta h^2}{2\rho} \frac{\partial}{\partial x} \left[\rho \left(\frac{\partial v}{\partial x} \right)^2 \right] + O(h^3).
\end{aligned}$$

2. Hernquist and Katz. This form does not require any derivation or consistency analysis since it is given below (and in the literature) in differential form

$$-\frac{\alpha h c}{\rho} \left| \frac{\partial v}{\partial x} \right| - \frac{\beta h^2}{\rho} \left(\frac{\partial v}{\partial x} \right)^2. \quad (\text{A.28})$$

For the SPH form, in the momentum and energy equations replace the $\frac{P}{\rho^2}$ term with $\frac{P}{\rho^2} + \frac{1}{2}\Pi$ where the function $\Pi_{ij} = \Pi(x_i, x_j)$ is defined by

$$\Pi_{ij} = \frac{q_i}{\rho_i^2} + \frac{q_j}{\rho_j^2} \quad (\text{A.29})$$

$$q_i = \begin{cases} \alpha h_i \rho_i c_i |\nabla \cdot v|_i + \beta h_i^2 \rho_i (\nabla \cdot v)_i^2 & (v_i - v_j) \cdot (x_i - x_j) < 0 \\ 0 & \text{otherwise} \end{cases} \quad (\text{A.30})$$

$$\text{note : } (\nabla \cdot v)_i = -\frac{1}{\rho_i} \sum_j m_j (v_i - v_j) W'_{ij} .$$

3. Lattanzio. It will be shown for the momentum, this form of the artificial viscosity corresponds to

$$\frac{\alpha h}{c\rho} \frac{\partial}{\partial x} \left(P \frac{\partial v}{\partial x} \right) - \frac{\beta h^2}{c^2 \rho} \frac{\partial}{\partial x} \left[P \left(\frac{\partial v}{\partial x} \right)^2 \right] . \quad (\text{A.31})$$

This form is very similar to the Monaghan version (P instead of ρc and a factor of $\frac{2}{c}$). Therefore, the derivation should follow exactly as in the Monaghan case, and is not done here, other than to give the SPH form: In the momentum and energy equations replace the $\frac{P}{\rho^2}$ term with $\frac{P}{\rho^2}(1 + \Pi)$ where the function $\Pi_{ij} = \Pi(x_i, x_j)$ is defined by

$$\Pi_{ij} = -\alpha \mu_{ij} + \beta \mu_{ij}^2 \quad (\text{A.32})$$

$$\mu_{ij} = \begin{cases} \frac{h(v_i - v_j) \cdot (x_i - x_j)}{c((x_i - x_j)^2 + \eta h^2)} & (v_i - v_j) \cdot (x_i - x_j) < 0 \\ 0 & \text{otherwise} . \end{cases} \quad (\text{A.33})$$

4. Wall Heating. There is currently only one form in use, attributed to Monaghan (41). Although it is given in differential form in the literature, the consistency for this one form will be shown here. The energy equation is modified as

$$\frac{De}{Dt} = -\frac{P}{\rho} \frac{\partial v}{\partial x} + \frac{1}{\rho} \nabla \cdot (Q \nabla e) . \quad (\text{A.34})$$

To implement this in the SPH energy equation, add an additional term, H , where

$$H_i = -\sum_{j=1}^N m_j \frac{(q_i + q_j)(e_i - e_j)(x_i - x_j)}{0.5(\rho_i + \rho_j)((x_i - x_j)^2 + \eta h^2)} W'_{ij} \quad (\text{A.35})$$

$$q_s = \alpha h_s c_s |\nabla \cdot v|_s + \beta h_s^2 (\nabla \cdot v)_s^2 \quad (\text{A.36})$$

$$(\nabla \cdot v)_s = -\frac{1}{\rho_s} \sum_j m_j (v_s - v_j) W'_{sj} .$$

The following procedure follows that for the Monaghan artificial viscosity quite closely.

$$\begin{aligned}\frac{1}{0.5(\rho_i + \rho_j)} &= \frac{2}{\rho_i + (\rho_i - x_{ij}\rho'_i + \dots)} = \frac{2}{2\rho_i - x_{ij}\rho'_i + \dots} = \frac{1}{\rho_i} + \frac{x_{ij}\rho'_i}{2\rho_i^2} + O(h^2) \\ e_i - e_j &= e_i - (e_i - x_{ij}e'_i + \frac{x_{ij}^2}{2}e''_i + \dots) = x_{ij}e'_i - \frac{x_{ij}^2}{2}e''_i + O(h^2) \\ \frac{e_i - e_j}{0.5(\rho_i + \rho_j)} &= \left(\frac{1}{\rho_i} + \frac{x_{ij}\rho'_i}{2\rho_i^2} \right) \left(x_{ij}e'_i - \frac{x_{ij}^2}{2}e''_i \right) = \frac{e'_i}{\rho_i} x_{ij} - \left(\frac{e'_i\rho'_i}{\rho_i^2} - \frac{e''_i}{\rho_i} \right) \frac{x_{ij}^2}{2} + O(h^2)\end{aligned}$$

So the H_i term is now

$$\begin{aligned}H_i &= -\frac{e'_i}{\rho_i} \sum_{j=1}^N m_j (q_i + q_j) \left(\frac{x_{ij}^2}{x_{ij}^2 + \eta h^2} \right) W'_{ij} \\ &\quad - \left(\frac{e'_i\rho'_i}{2\rho_i^2} - \frac{e''_i}{2\rho_i} \right) \sum_{j=1}^N m_j (q_i + q_j) \left(\frac{x_{ij}^3}{x_{ij}^2 + \eta h^2} \right) W'_{ij} + O(h^2) \\ q_i + q_j &= q_i + (q_i - x_{ij}q'_i + \frac{x_{ij}^2}{2}q''_i + \dots) = 2q_i - x_{ij}q'_i + \frac{x_{ij}^2}{2}q''_i + O(h^2)\end{aligned}$$

So the H_i term now becomes

$$\begin{aligned}H_i &= -\frac{2q_i e'_i}{\rho_i} \sum_{j=1}^N m_j \left(\frac{x_{ij}^2}{x_{ij}^2 + \eta h^2} \right) W'_{ij} \\ &\quad - \left(\frac{-q'_i e'_i}{\rho_i} + \frac{2q_i e'_i \rho'_i}{2\rho_i^2} - \frac{2q_i e''_i}{2\rho_i} \right) \sum_{j=1}^N m_j \left(\frac{x_{ij}^3}{x_{ij}^2 + \eta h^2} \right) W'_{ij} + O(h^2)\end{aligned}$$

The summation terms were shown under the Monaghan artificial viscosity to approximate ρ'_i and $-\rho_i$ respectively. Substitute to obtain

$$\begin{aligned}H_i &= -\frac{2q_i e'_i \rho'_i}{\rho_i} - \left(-\frac{q'_i e'_i}{\rho_i} + \frac{q_i e'_i \rho'_i}{\rho_i^2} - \frac{q_i e''_i}{\rho_i} \right) (-\rho_i) + O(h^2) \\ &= -\frac{1}{\rho_i} [e'_i (2q_i \rho'_i + q'_i \rho_i - q_i \rho'_i) + e''_i (q_i \rho_i)] + O(h^2) \\ &= -\frac{1}{\rho_i} [e'_i (q_i \rho_i)' + e''_i (q_i \rho_i)] + O(h^2) \\ &= -\frac{1}{\rho_i} [e'_i (q_i \rho_i)]' + O(h^2)\end{aligned}$$

$$\text{Thus } H = -\frac{1}{\rho} \frac{\partial}{\partial x} \left[(q\rho) \frac{\partial e}{\partial x} \right] + O(h^2)$$

If Q equals $-q\rho$ the differential form is recovered plus terms of order h^2 . Also note that q has terms of order h and h^2 in it, so the Q term goes to zero as h goes to zero. Thus, this wall heating term is consistent.

Appendix B. ADDITIONAL STABILITY NOTES

This appendix includes work related to the Stability Chapter (Chapter IV), but the details were left out earlier.

B.1 Stability for Several Equations

In the Chapter IV, one SPH form (probably the most popular) was shown to have an unconditional instability. Further, this form can be simplified to appear like those used by other analysts in performing stability analysis. In this section, it is shown that the previous analysis applies to many different forms of the SPH equations, not just the popular one. The forms considered are shown in equations (B.1) - (B.13) for particle s

$$\dot{\rho}_s = \sum_{j=1}^N m_j (v_s - v_j) W'_{sj} \quad (\text{B.1})$$

$$\dot{\rho}_s = \rho_s \sum_{j=1}^N \frac{m_j}{\rho_j} (v_s - v_j) W'_{sj} \quad (\text{B.2})$$

$$\dot{v}_s = - \sum_{j=1}^N m_j \left(\frac{P_j}{\rho_j^2} + \frac{P_s}{\rho_s^2} \right) W'_{sj} \quad (\text{B.3})$$

$$\dot{v}_s = -2 \sum_{j=1}^N m_j \frac{\sqrt{P_j P_s}}{\rho_j \rho_s} W'_{sj} \quad (\text{B.4})$$

$$\dot{v}_s = - \sum_{j=1}^N m_j \left(\frac{P_j}{\rho_j \rho_s} \right) W'_{sj} \quad (\text{B.5})$$

$$\dot{v}_s = - \sum_{j=1}^N m_j \left(\frac{P_j + P_s}{\rho_j \rho_s} \right) W'_{sj} \quad (\text{B.6})$$

$$\dot{e}_s = \sum_{j=1}^N m_j \left(\frac{P_s}{\rho_s^2} \right) (v_s - v_j) W'_{sj} \quad (\text{B.7})$$

$$\dot{e}_s = \sum_{j=1}^N m_j \left(\frac{P_s}{\rho_s \rho_j} \right) (v_s - v_j) W'_{sj} \quad (\text{B.8})$$

$$\dot{e}_s = \sum_{j=1}^N m_j \left(\frac{P_j}{\rho_j^2} \right) (v_s - v_j) W'_{sj} \quad (\text{B.9})$$

$$\dot{e}_s = \frac{1}{2} \sum_{j=1}^N m_j \left(\frac{P_j}{\rho_j^2} + \frac{P_s}{\rho_s^2} \right) (v_s - v_j) W'_{sj} \quad (\text{B.10})$$

$$\dot{e}_s = \sum_{j=1}^N m_j \frac{\sqrt{P_j P_s}}{\rho_j \rho_s} (v_s - v_j) W'_{sj} \quad (\text{B.11})$$

$$\dot{x}_s = v_s \quad (\text{B.12})$$

$$\dot{x}_s = v_s + \epsilon \sum_{j=1}^N m_j \left(\frac{v_j - v_s}{0.5(\rho_s + \rho_j)} \right) W_{sj} \quad (\text{B.13})$$

Equations (B.1), (B.3), (B.10), and (B.12) make up the system previously studied.

The remainder are analyzed below:

1. Equation (B.2)

$$\begin{aligned} \dot{\rho}_s &= \rho_s \sum_{j=1}^N \frac{m_j}{\rho_j} (v_s - v_j) W'_{sj} \\ \dot{\bar{\rho}}_s + \dot{\phi}_s &= (\bar{\rho}_s + \phi_s) \sum_{j=1}^N \frac{m_j}{\bar{\rho}_j + \phi_j} (\bar{v}_s - \bar{v}_j + \nu_s - \nu_j) W'_{sj} \\ &= (\bar{\rho}_s + \phi_s) \sum_{j=1}^N \frac{m_j}{\bar{\rho}_j + \phi_j} (\bar{v}_s - \bar{v}_j + \nu_s - \nu_j) [W'_{sj} + (\chi_s - \chi_j) W''_{sj}] \\ &= (\bar{\rho}_s + \phi_s) \sum_{j=1}^N \frac{m_j}{\bar{\rho}_j + \phi_j} \left[(\bar{v}_s - \bar{v}_j) W'_{sj} + (\nu_s - \nu_j) W'_{sj} \right. \\ &\quad \left. + (\bar{v}_s - \bar{v}_j) (\chi_s - \chi_j) W''_{sj} \right] \\ &= \sum_{j=1}^N m_j \left[\frac{\bar{\rho}_s}{\bar{\rho}_j} (\bar{v}_s - \bar{v}_j) W'_{sj} + \frac{\bar{\rho}_s}{\bar{\rho}_j} (\nu_s - \nu_j) W'_{sj} + \frac{\bar{\rho}_s}{\bar{\rho}_j} (\bar{v}_s - \bar{v}_j) (\chi_s - \chi_j) W''_{sj} \right. \\ &\quad \left. - \frac{\bar{\rho}_s}{\bar{\rho}_j^2} (\bar{v}_s - \bar{v}_j) \phi_j W'_{sj} + \frac{(\bar{v}_s - \bar{v}_j)}{\bar{\rho}_j} \phi_s W'_{sj} \right] \end{aligned}$$

Assume

$$\dot{\bar{\rho}}_s = \bar{\rho}_s \sum_{j=1}^N \frac{m_j}{\bar{\rho}_j} (\bar{v}_s - \bar{v}_j) W'_{sj},$$

to obtain

$$\dot{\phi}_s = \sum_{j=1}^N m_j \left[\frac{1}{\bar{\rho}_j^2} (\bar{v}_s - \bar{v}_j) (-\bar{\rho}_s \phi_j + \bar{\rho}_j \phi_s) W'_{sj} + \frac{\bar{\rho}_s}{\bar{\rho}_j} (\nu_s - \nu_j) W'_{sj} + \frac{\bar{\rho}_s}{\bar{\rho}_j} (\bar{v}_s - \bar{v}_j) (\chi_s - \chi_j) W''_{sj} \right].$$

The system is now linear in the perturbations so that Fourier analysis may be applied. Substitute and then divide both sides of the resulting equations by e^{isk} to obtain

$$\dot{\phi} = \sum_{j=1}^N m_j \left[\frac{1}{\bar{\rho}_j^2} (\bar{v}_s - \bar{v}_j) (\bar{\rho}_j - \bar{\rho}_s e^{i(j-s)k}) \phi W'_{sj} + \frac{\bar{\rho}_s}{\bar{\rho}_j} (1 - e^{i(j-s)k}) \nu W'_{sj} + \frac{\bar{\rho}_s}{\bar{\rho}_j} (\bar{v}_s - \bar{v}_j) (1 - e^{i(j-s)k}) \chi W''_{sj} \right].$$

Finally, changing notation and simplifying

$$\dot{\phi} = \left[-m \sum_{l=-\infty}^{\infty} \frac{1}{\bar{\rho}_j^2} (\bar{v}_s - \bar{v}_j) (\bar{\rho}_j - \bar{\rho}_s e^{ilk}) W'_l \right] \phi + \left[-m \sum_{l=-\infty}^{\infty} \frac{\bar{\rho}_s}{\bar{\rho}_j} (1 - e^{ilk}) W'_l \right] \nu + \left[m \sum_{l=-\infty}^{\infty} \frac{\bar{\rho}_s}{\bar{\rho}_j} (\bar{v}_s - \bar{v}_j) (1 - e^{ilk}) W''_l \right] \chi.$$

Compared to Chapter IV, this form of the equation has an additional term (ϕ term) in the amplification matrix. However, under the smooth data assumptions, this term falls out. In fact, under these assumptions, the remaining term is

$$\dot{\phi} = \left[-m \sum_{l=-\infty}^{\infty} (1 - e^{ilk}) W'_l \right] \nu.$$

which is the same as in Chapter IV.

2. Equation (B.4)

$$\dot{v}_s = -2 \sum_{j=1}^N m_j \frac{\sqrt{P_j P_s}}{\rho_j \rho_s} W'_{sj}$$

This form is not a good choice for HVI problems. The square root term could be imaginary. If the pressure field is quite smooth, a smooth transition from real to zero to real again could occur. However, if it is not as smooth, or even worse near a shock, this term would become imaginary. For these reasons, this form was not pursued any further.

3. Equation (B.5)

$$\begin{aligned}
 \dot{v}_s &= - \sum_{j=1}^N m_j \frac{P_j}{\rho_j \rho_s} W'_{sj} \\
 \dot{v}_s + \dot{v}_s &= - \left(\frac{1}{\bar{\rho}_s + \phi_s} \right) \sum_{j=1}^N \frac{m_j P_j}{\bar{\rho}_j + \phi_j} W'_{sj} \\
 &= - \left(\frac{1}{\bar{\rho}_s + \phi_s} \right) \sum_{j=1}^N \frac{m_j}{\bar{\rho}_j + \phi_j} (\tilde{A}_j + \tilde{B}_j \phi_j + \tilde{C}_j \epsilon_j) [W'_{sj} + (\chi_s - \chi_j) W''_{sj}] \\
 &= - \left(\frac{1}{\bar{\rho}_s} - \frac{\phi_s}{\bar{\rho}_s^2} \right) \sum_{j=1}^N m_j \left(\frac{1}{\bar{\rho}_j} - \frac{\phi_j}{\bar{\rho}_j^2} \right) [\tilde{A}_j W'_{sj} + \tilde{B}_j \phi_j W'_{sj} + \tilde{C}_j \epsilon_j W'_{sj} \\
 &\quad + \tilde{A}_j (\chi_s - \chi_j) W''_{sj}] \\
 &= - \sum_{j=1}^N m_j \left(\frac{1}{\bar{\rho}_j \bar{\rho}_s} - \frac{\phi_j}{\bar{\rho}_s \bar{\rho}_j^2} - \frac{\phi_s}{\bar{\rho}_s^2 \bar{\rho}_j} \right) [\tilde{A}_j W'_{sj} + \tilde{B}_j \phi_j W'_{sj} + \tilde{C}_j \epsilon_j W'_{sj} \\
 &\quad + \tilde{A}_j (\chi_s - \chi_j) W''_{sj}] \\
 &= - \sum_{j=1}^N m_j \frac{\tilde{A}_j}{\bar{\rho}_j \bar{\rho}_s} W'_{sj} - \sum_{j=1}^N m_j \left[\left(\frac{\tilde{B}_j}{\bar{\rho}_j \bar{\rho}_s} - \frac{\tilde{A}_j}{\bar{\rho}_j^2 \bar{\rho}_s} \right) \phi_j W'_{sj} - \frac{\tilde{A}_j}{\bar{\rho}_j \bar{\rho}_s^2} \phi_s W'_{sj} \right. \\
 &\quad \left. + \frac{\tilde{C}_j}{\bar{\rho}_j \bar{\rho}_s} \epsilon_j W'_{sj} + \frac{\tilde{A}_j}{\bar{\rho}_j \bar{\rho}_s} (\chi_s - \chi_j) W''_{sj} \right]
 \end{aligned}$$

Then assume

$$\dot{v}_s = - \sum_{j=1}^N m_j \frac{\tilde{A}_j}{\bar{\rho}_j \bar{\rho}_s} W'_{sj},$$

to obtain

$$\dot{\nu}_s = - \sum_{j=1}^N m_j \left[\left(\frac{\tilde{B}_j}{\bar{\rho}_j \bar{\rho}_s} - \frac{\tilde{A}_j}{\bar{\rho}_j^2 \bar{\rho}_s} \right) \phi_j W'_{sj} - \frac{\tilde{A}_j}{\bar{\rho}_j \bar{\rho}_s^2} \phi_s W'_{sj} + \frac{\tilde{C}_j}{\bar{\rho}_j \bar{\rho}_s} \varepsilon_j W'_{sj} + \frac{\tilde{A}_j}{\bar{\rho}_j \bar{\rho}_s} (\chi_s - \chi_j) W''_{sj} \right].$$

The system is now linear in the perturbations so that Fourier analysis may be applied.

Substitute and then divide both sides of the resulting equations by e^{isk} to obtain

$$\dot{\nu} = - \sum_{j=1}^N m_j \left\{ \left[\left(\frac{\tilde{B}_j}{\bar{\rho}_j \bar{\rho}_s} - \frac{\tilde{A}_j}{\bar{\rho}_j^2 \bar{\rho}_s} \right) e^{i(j-s)k} - \frac{\tilde{A}_j}{\bar{\rho}_j \bar{\rho}_s^2} \right] \phi W'_{sj} + \frac{\tilde{C}_j}{\bar{\rho}_j \bar{\rho}_s} e^{i(j-s)k} \varepsilon W'_{sj} + \frac{\tilde{A}_j}{\bar{\rho}_j \bar{\rho}_s} (1 - e^{i(j-s)k}) \chi W''_{sj} \right\}.$$

Finally, changing notation and simplifying

$$\dot{\nu} = \left[m \sum_{l=-\infty}^{\infty} \left(\left(\frac{\tilde{B}_j}{\bar{\rho}_j \bar{\rho}_s} - \frac{\tilde{A}_j}{\bar{\rho}_j^2 \bar{\rho}_s} \right) e^{ilk} - \frac{\tilde{A}_j}{\bar{\rho}_j \bar{\rho}_s^2} \right) W'_l \right] \phi + \left[m \sum_{l=-\infty}^{\infty} \frac{\tilde{C}_j}{\bar{\rho}_j \bar{\rho}_s} e^{ilk} W'_l \right] \varepsilon - \left[m \sum_{l=-\infty}^{\infty} \frac{\tilde{A}_j}{\bar{\rho}_j \bar{\rho}_s} (1 - e^{ilk}) W''_l \right] \chi.$$

Compared to Chapter IV, this form of the equation has the same number of terms under the smooth data assumptions in the amplification matrix; however, they are slightly different. Define G_4 as

$$G_4 = m \sum_{l=-\infty}^{\infty} e^{ilk} W'_l.$$

then the eigenvalues obtained when substituting this equation in for the original forms of the momentum equation are

$$\lambda = 0, 0, \pm \sqrt{- \left(\frac{\tilde{A} \tilde{C}}{\bar{\rho}^4} + \frac{\tilde{B}}{\bar{\rho}^2} \right) G_1 G_4 + \frac{\tilde{A}}{\bar{\rho}^3} G_1 G_2 - \frac{\tilde{A}}{\bar{\rho}^2 G_3}}.$$

This is further simplified with the uniform space assumption to find: $\lambda = 0, 0, \pm\sqrt{-D}$

where $D = D_1 + D_2$ and

$$D_1 = \frac{4m^2}{\bar{\rho}^4} (\dot{\bar{A}}\dot{\bar{C}} + \bar{\rho}^2 \dot{\bar{B}} - \bar{\rho} \dot{\bar{A}}) \left(\sum_{l=1}^{\infty} \sin(lk) W'_l \right)^2$$

$$D_2 = \frac{2m}{\bar{\rho}^2} \dot{\bar{A}} \sum_{l=1}^{\infty} (1 - \cos(lk)) W''_l.$$

This is almost exactly the same as before, and has the same instabilities.

4. Equation (B.6)

$$\begin{aligned} \dot{v}_s &= - \sum_{j=1}^N m_j \left(\frac{P_j + P_s}{\rho_j \rho_s} \right) W'_{sj} \\ \dot{v}_s + \dot{v}_s &= - \sum_{j=1}^N m_j \left[\frac{P_s + P_j}{(\bar{\rho}_j + \phi_j)(\bar{\rho}_s + \phi_s)} \right] W'_{sj} \\ &= - \sum_{j=1}^N m_j \left(\frac{\tilde{A}_s + \tilde{A}_j + \tilde{B}_s \phi_s + \tilde{B}_j \phi_j + \tilde{C}_s \epsilon_s + \tilde{C}_j \epsilon_j}{\bar{\rho}_j \bar{\rho}_s + \bar{\rho}_j \phi_s + \bar{\rho}_s \phi_j} \right) [W'_{sj} + (\chi_s - \chi_j) W''_{sj}] \\ &= - \sum_{j=1}^N m_j \left(\frac{1}{\bar{\rho}_s \bar{\rho}_j} - \frac{\phi_j}{\bar{\rho}_s \bar{\rho}_j^2} - \frac{\phi_s}{\bar{\rho}_s^2 \bar{\rho}_j} \right) [(\tilde{A}_s + \tilde{A}_j) W'_{sj} + (\tilde{B}_s \phi_s + \tilde{B}_j \phi_j) W'_{sj} \\ &\quad + (\tilde{C}_s \epsilon_s + \tilde{C}_j \epsilon_j) W'_{sj} + (\tilde{A}_s + \tilde{A}_j)(\chi_s - \chi_j) W''_{sj}] \\ &= - \sum_{j=1}^N m_j \left(\frac{\tilde{A}_s + \tilde{A}_j}{\bar{\rho}_s \bar{\rho}_j} \right) W'_{sj} - \sum_{j=1}^N m_j \left[\left(\frac{\tilde{B}_j}{\bar{\rho}_j \bar{\rho}_s} - \frac{\tilde{A}_s + \tilde{A}_j}{\bar{\rho}_j^2 \bar{\rho}_s} \right) \phi_j W'_{sj} \right. \\ &\quad \left. - \left(\frac{\tilde{B}_s}{\bar{\rho}_j \bar{\rho}_s} - \frac{\tilde{A}_s + \tilde{A}_j}{\bar{\rho}_j \bar{\rho}_s^2} \right) \phi_s W'_{sj} + \frac{\tilde{C}_j \epsilon_j + \tilde{C}_s \epsilon_s}{\bar{\rho}_j \bar{\rho}_s} W'_{sj} \right. \\ &\quad \left. + \frac{\tilde{A}_s + \tilde{A}_j}{\bar{\rho}_j \bar{\rho}_s} (\chi_s - \chi_j) W''_{sj} \right] \end{aligned}$$

Assume

$$\dot{v}_s = - \sum_{j=1}^N m_j \frac{\tilde{A}_s + \tilde{A}_j}{\bar{\rho}_j \bar{\rho}_s} W'_{sj},$$

to obtain

$$\dot{v}_s = - \sum_{j=1}^N m_j \left[\left(\frac{\tilde{B}_j}{\tilde{\rho}_j \tilde{\rho}_s} - \frac{\tilde{A}_s + \tilde{A}_j}{\tilde{\rho}_j^2 \tilde{\rho}_s} \right) \phi_j W'_{sj} + \left(\frac{\tilde{B}_s}{\tilde{\rho}_j \tilde{\rho}_s} - \frac{\tilde{A}_s + \tilde{A}_j}{\tilde{\rho}_j \tilde{\rho}_s^2} \right) \phi_s W'_{sj} \right. \\ \left. + \frac{\tilde{C}_j \varepsilon_j + \tilde{C}_s \varepsilon_s}{\tilde{\rho}_j \tilde{\rho}_s} W'_{sj} + \frac{\tilde{A}_s + \tilde{A}_j}{\tilde{\rho}_j \tilde{\rho}_s} (\chi_s - \chi_j) W''_{sj} \right].$$

The system is now linear in the perturbations so that Fourier analysis may be applied.

Substitute and then divide both sides of the resulting equations by e^{isk} to obtain

$$\dot{v} = - \sum_{j=1}^N m_j \left\{ \left[\left(\frac{\tilde{B}_j}{\tilde{\rho}_j \tilde{\rho}_s} - \frac{\tilde{A}_s + \tilde{A}_j}{\tilde{\rho}_j^2 \tilde{\rho}_s} \right) e^{i(j-s)k} + \left(\frac{\tilde{B}_s}{\tilde{\rho}_j \tilde{\rho}_s} - \frac{\tilde{A}_s + \tilde{A}_j}{\tilde{\rho}_j \tilde{\rho}_s^2} \right) \right] \phi W'_{sj} \right. \\ \left. + \frac{\tilde{C}_s + \tilde{C}_j e^{i(j-s)k}}{\tilde{\rho}_j \tilde{\rho}_s} \varepsilon W'_{sj} + \frac{\tilde{A}_s + \tilde{A}_j}{\tilde{\rho}_j \tilde{\rho}_s} (1 - e^{i(j-s)k}) \chi W''_{sj} \right\}.$$

Finally, changing notation and simplifying

$$\dot{v} = \left[m \sum_{l=-\infty}^{\infty} (\hat{B}_j e^{ilk} + \hat{B}_s) W'_l \right] \phi + \left[m \sum_{l=-\infty}^{\infty} (\hat{C}_j e^{ilk} + \hat{C}_s) W'_l \right] \varepsilon \\ + \left[-m \sum_{l=-\infty}^{\infty} (\hat{A}_s + \hat{A}_j) (1 - e^{ilk}) W''_l \right] \chi.$$

This form of the equation reduces to exactly the same as the original in Chapter IV under the smooth data assumptions.

5. Equations (B.7), (B.8), (B.9)

These three equations are all very similar and using the letters: α and β appropriately (as seen later) to analyze

$$\dot{e}_s = \sum_{j=1}^N m_j \left(\frac{P_\alpha}{\rho_\alpha \rho_\beta} \right) (v_s - v_j) W'_{sj} \\ \dot{\bar{e}}_s + \dot{\varepsilon}_s = \sum_{j=1}^N m_j \left(\frac{P_\alpha}{\rho_\alpha \rho_\beta} \right) (\bar{v}_s - \bar{v}_j + \nu_s - \nu_j) W'_{sj}$$

$$\begin{aligned}
&= \sum_{j=1}^N m_j \frac{(\tilde{A}_\alpha + \tilde{B}_\alpha \phi_\alpha + \tilde{C}_\alpha \varepsilon_\alpha)}{(\bar{\rho}_\alpha + \phi_\alpha)(\bar{\rho}_\beta + \phi_\beta)} (\bar{v}_s - \bar{v}_j + \nu_s - \nu_j) [W'_{sj} + (\chi_s - \chi_j) W''_{sj}] \\
&= \sum_{j=1}^N m_j (\tilde{A}_\alpha + \tilde{B}_\alpha \phi_\alpha + \tilde{C}_\alpha \varepsilon_\alpha) \left(\frac{1}{\bar{\rho}_\alpha \bar{\rho}_\beta} - \frac{\phi_\beta}{\bar{\rho}_\alpha \bar{\rho}_\beta^2} - \frac{\phi_\alpha}{\bar{\rho}_\alpha^2 \bar{\rho}_\beta} \right) [(\bar{v}_s - \bar{v}_j) W'_{sj} \\
&\quad + (\nu_s - \nu_j) W'_{sj} + (\bar{v}_s - \bar{v}_j)(\chi_s - \chi_j) W''_{sj}] \\
&= \sum_{j=1}^N m_j \left[\frac{\tilde{A}_\alpha}{\bar{\rho}_\alpha \bar{\rho}_\beta} + \left(\frac{\tilde{B}_\alpha}{\bar{\rho}_\alpha \bar{\rho}_\beta} - \frac{\tilde{A}_\alpha}{\bar{\rho}_\alpha^2 \bar{\rho}_\beta} \right) \phi_\alpha - \frac{\tilde{A}_\alpha}{\bar{\rho}_\alpha \bar{\rho}_\beta^2} \phi_\beta + \frac{\tilde{C}_\alpha}{\bar{\rho}_\alpha \bar{\rho}_\beta} \varepsilon_\alpha \right] [(\bar{v}_s - \bar{v}_j) W'_{sj} \\
&\quad + (\nu_s - \nu_j) W'_{sj} + (\bar{v}_s - \bar{v}_j)(\chi_s - \chi_j) W''_{sj}] \\
&= \sum_{j=1}^N m_j \left(\frac{\tilde{A}_\alpha}{\bar{\rho}_\alpha \bar{\rho}_\beta} \right) (\bar{v}_s - \bar{v}_j) W'_{sj} + \sum_{j=1}^N m_j \left[\left(\frac{\tilde{B}_\alpha}{\bar{\rho}_\alpha \bar{\rho}_\beta} - \frac{\tilde{A}_\alpha}{\bar{\rho}_\alpha^2 \bar{\rho}_\beta} \right) (\bar{v}_s - \bar{v}_j) \phi_\alpha W'_{sj} \right. \\
&\quad - \left(\frac{\tilde{A}_\alpha}{\bar{\rho}_\alpha \bar{\rho}_\beta^2} \right) (\bar{v}_s - \bar{v}_j) \phi_\beta W'_{sj} + \left(\frac{\tilde{A}_\alpha}{\bar{\rho}_\alpha \bar{\rho}_\beta} \right) (\nu_s - \nu_j) W'_{sj} \\
&\quad \left. + \left(\frac{\tilde{C}_\alpha}{\bar{\rho}_\alpha \bar{\rho}_\beta} \right) \varepsilon_\alpha W'_{sj} + \left(\frac{\tilde{A}_\alpha}{\bar{\rho}_\alpha \bar{\rho}_\beta} \right) (\bar{v}_s - \bar{v}_j)(\chi_s - \chi_j) W''_{sj} \right]
\end{aligned}$$

Assume

$$\dot{e}_s = \sum_{j=1}^N m_j \frac{\tilde{A}_\alpha}{\bar{\rho}_\alpha \bar{\rho}_\beta} (\bar{v}_s - \bar{v}_j) W'_{sj},$$

to obtain

$$\begin{aligned}
\dot{e}_s = \sum_{j=1}^N m_j &\left[\left(\frac{\tilde{B}_\alpha}{\bar{\rho}_\alpha \bar{\rho}_\beta} - \frac{\tilde{A}_\alpha}{\bar{\rho}_\alpha^2 \bar{\rho}_\beta} \right) (\bar{v}_s - \bar{v}_j) \phi_\alpha W'_{sj} - \frac{\tilde{A}_\alpha}{\bar{\rho}_\alpha \bar{\rho}_\beta^2} (\bar{v}_s - \bar{v}_j) \phi_\beta W'_{sj} \right. \\
&\left. + \frac{\tilde{A}_\alpha}{\bar{\rho}_\alpha \bar{\rho}_\beta} (\nu_s - \nu_j) W'_{sj} + \frac{\tilde{C}_\alpha}{\bar{\rho}_\alpha \bar{\rho}_\beta} \varepsilon_\alpha W'_{sj} + \frac{\tilde{A}_\alpha}{\bar{\rho}_\alpha \bar{\rho}_\beta} (\bar{v}_s - \bar{v}_j)(\chi_s - \chi_j) W''_{sj} \right].
\end{aligned}$$

So under the simplifying assumptions for smooth data and uniform spacing, all the terms drop out except

$$\sum_{j=1}^N m_j \frac{\tilde{A}_\alpha}{\bar{\rho}_\alpha \bar{\rho}_\beta} (\nu_s - \nu_j) W'_{sj}.$$

Now note for each of the equations

equation (B.7) : $\alpha = s, \beta = s$

equation (B.8) : $\alpha = s, \beta = j$

equation (B.9) : $\alpha = j, \beta = j$.

The system is now linear in the perturbations so that Fourier analysis may be applied. Substitute and then divide both sides of the resulting equations by e^{isk} , and simplify the notation to obtain the same result for all three equations

$$\dot{\epsilon} = \left[-mA \sum_{l=-\infty}^{\infty} (1 - e^{ilk}) W'_l \right] \nu.$$

Therefore, these forms of the equations reduce to exactly the same as the original in Chapter IV under the smooth data assumptions.

6. Equation (B.11)

$$\dot{\epsilon}_s = \sum_{j=1}^N m_j \frac{\sqrt{P_j P_s}}{\rho_j \rho_s} (v_s - v_j) W'_{sj}.$$

As with the momentum equation, this form is not a good choice for HVI problems. The square root term could be imaginary. If the pressure field is quite smooth, a smooth transition from real to zero to real again could occur. However, if it is not as smooth, or even worse near a shock, this term would become imaginary. For these reasons, this form was not pursued any further.

7. Equation (B.13)

$$\begin{aligned} \dot{x}_s &= v_s + \epsilon \sum_{j=1}^N m_j \frac{v_j - v_s}{0.5(\rho_s + \rho_j)} W_{sj} \\ \dot{\bar{x}}_s + \dot{\chi}_s &= \bar{v}_s + \nu_s - \epsilon \sum_{j=1}^N m_j \frac{(\bar{v}_s - \bar{v}_j + \nu_s - \nu_j)}{0.5(\bar{\rho}_s + \bar{\rho}_j + \phi_s + \phi_j)} W_{sj} \\ &= \bar{v}_s + \nu_s - 2\epsilon \sum_{j=1}^N m_j (\bar{v}_s - \bar{v}_j + \nu_s - \nu_j) \left[\frac{1}{\bar{\rho}_s + \bar{\rho}_j} - \frac{\phi_s + \phi_j}{(\bar{\rho}_s + \bar{\rho}_j)^2} \right] [W_{sj} \\ &\quad + (\chi_s - \chi_j) W'_{sj}] \\ &= \bar{v}_s + \nu_s - 2\epsilon \sum_{j=1}^N m_j \left[\frac{\bar{v}_s - \bar{v}_j}{\bar{\rho}_s + \bar{\rho}_j} W_{sj} - \frac{\bar{v}_s - \bar{v}_j}{(\bar{\rho}_s + \bar{\rho}_j)^2} (\phi_s + \phi_j) W_{sj} \right. \end{aligned}$$

$$\left. + \frac{\nu_s - \nu_j}{\bar{\rho}_s + \bar{\rho}_j} W_{sj} + \frac{\bar{\nu}_s - \bar{\nu}_j}{\bar{\rho}_s + \bar{\rho}_j} (\chi_s - \chi_j) W'_{sj} \right]$$

Assume

$$\dot{x}_s = \bar{\nu}_s - 2\epsilon \sum_{j=1}^N m_j \left(\frac{\bar{\nu}_s - \bar{\nu}_j}{\bar{\rho}_s + \bar{\rho}_j} \right) W_{sj},$$

to obtain

$$\begin{aligned} \dot{\chi}_s = \nu_s - 2\epsilon \sum_{j=1}^N m_j \left[-\frac{\bar{\nu}_s - \bar{\nu}_j}{(\bar{\rho}_s + \bar{\rho}_j)^2} (\phi_s + \phi_j) W_{sj} + \frac{\nu_s - \nu_j}{\bar{\rho}_s + \bar{\rho}_j} W_{sj} \right. \\ \left. + \frac{\bar{\nu}_s - \bar{\nu}_j}{\bar{\rho}_s + \bar{\rho}_j} (\chi_s - \chi_j) W'_{sj} \right]. \end{aligned}$$

The system is now linear in the perturbations so that Fourier analysis may be applied.

Substitute and then divide both sides of the resulting equations by e^{isk} to obtain

$$\begin{aligned} \dot{\chi} = \nu - 2\epsilon \sum_{j=1}^N m_j \left[-\frac{\bar{\nu}_s - \bar{\nu}_j}{(\bar{\rho}_s + \bar{\rho}_j)^2} (1 + e^{i(j-s)k}) \phi W_{sj} + \frac{1 - e^{i(j-s)k}}{\bar{\rho}_s + \bar{\rho}_j} \nu W_{sj} \right. \\ \left. + \frac{\bar{\nu}_s - \bar{\nu}_j}{\bar{\rho}_s + \bar{\rho}_j} (1 - e^{i(j-s)k}) \chi W'_{sj} \right]. \end{aligned}$$

Finally, changing notation and simplifying

$$\begin{aligned} \dot{\chi} = \left[2\epsilon m \sum_{l=-\infty}^{\infty} \frac{\bar{\nu}_s - \bar{\nu}_j}{(\bar{\rho}_s + \bar{\rho}_j)^2} (1 + e^{ilk}) W_l \right] \phi + \left[1 - 2\epsilon m \sum_{l=-\infty}^{\infty} \frac{1 - e^{ilk}}{\bar{\rho}_s + \bar{\rho}_j} W_l \right] \nu \\ + \left[2\epsilon m \sum_{l=-\infty}^{\infty} \frac{\bar{\nu}_s - \bar{\nu}_j}{\bar{\rho}_s + \bar{\rho}_j} (1 - e^{ilk}) W'_l \right] \chi. \end{aligned}$$

This form of the equation is quite different than the original one found in Chapter IV.

But applying the assumptions under smooth data analysis it reduces to the following

$$\dot{\chi} = \left[1 - \frac{\epsilon m}{\bar{\rho}} \sum_{l=-\infty}^{\infty} (1 - e^{ilk}) W_l \right] \nu \quad (\text{B.14})$$

In calculating the eigenvalues using this new form, the same results are obtained as the original form with one important change. If ϵ in the term above is large enough it can offset the PW'' instability. The eigenvalues are

$$\lambda = 0, 0, \pm \sqrt{-(AC + B)G_1G_2 - 2AG_3(1 - \frac{\epsilon}{\bar{\rho}}G_5)}, \quad (\text{B.15})$$

$$\text{where} \quad G_5 = m \sum_{l=-\infty}^{\infty} (1 - e^{ilk})W_l. \quad (\text{B.16})$$

The $\frac{G_5}{\bar{\rho}}$ term is always positive and under uniform spacing, real. Obviously this form needs to be investigated further. This is done in the Techniques for Obtaining Linearized Stability Section of the Stability Chapter (IV).

B.2 Considerations on Two Equations of State

In the Stability Chapter (IV) it was shown that the instability had two parts, labeled D_1 and D_2 . The D_2 part contained the PW'' instability. The D_1 part vanishes at minimum wavelengths. It is necessary to know if this term is going to be a problem for longer wavelengths. So, in this section a look closer at this D_1 term is done for two specific equations of state: the Ideal Gas Law and the Mie - Grüneisen.

B.2.1 Ideal Gas Law. The form of the Ideal Gas Law Equation of State (EOS) used here is

$$P = (\Gamma - 1)\rho e, \quad (\text{B.17})$$

where Γ is a material constant. From this form for stability

$$\begin{aligned} P(\rho, e) &= P(\bar{\rho} + \phi, \bar{e} + \epsilon) = (\Gamma - 1)(\bar{\rho} + \phi)(\bar{e} + \epsilon) \\ &= (\Gamma - 1)\bar{\rho}\bar{e} + (\Gamma - 1)\bar{e}\phi + (\Gamma - 1)\bar{\rho}\epsilon. \end{aligned}$$

So from our notation in the Stability Chapter ($P = \tilde{A} + \tilde{B}\phi + \tilde{C}\epsilon$)

$$\tilde{A} = (\Gamma - 1) \bar{\rho} \bar{e}$$

$$\tilde{B} = (\Gamma - 1) \bar{e}$$

$$\tilde{C} = (\Gamma - 1) \bar{\rho}.$$

Use the value for D_1 obtained in equation (4.14) to find

$$\begin{aligned} D_1 &= \frac{4m^2}{\bar{\rho}^4} (\tilde{A}\tilde{C} + \bar{\rho}^2\tilde{B} - 2\bar{\rho}\tilde{A}) \left(\sum_{l=1}^{\infty} \sin(lk) W'_l \right)^2 \\ &= \frac{4m^2}{\bar{\rho}^4} \left(\sum_{l=1}^{\infty} \sin(lk) W'_l \right)^2 [(\Gamma - 1)\bar{\rho}\bar{e}(\Gamma - 1)\bar{\rho} + \bar{\rho}^2(\Gamma - 1)\bar{e} - 2\bar{\rho}(\Gamma - 1)\bar{\rho}\bar{e}] \\ &= \frac{4m^2\bar{e}(\Gamma - 1)(\Gamma - 2)}{\bar{\rho}^2} \left(\sum_{l=1}^{\infty} \sin(lk) W'_l \right)^2. \end{aligned}$$

Assume that \bar{e} follows convention and is taken as always positive (otherwise the form of P must change). All the other terms: m , $\bar{\rho}$, and the square term are all real and positive, except possibly the Γ terms. Γ itself is always positive, which implies that D_1 is non-negative for $\Gamma \leq 1$ or $\Gamma \geq 2$; making the D_1 term a stabilizing term for most values of Γ . However, for values of Γ between 1 and 2, the D_1 term is negative and, therefore, could add to the instability at higher wavelengths.

B.2.2 Mie - Grüneisen. The form of the Mie - Grüneisen Equation of State (EOS) used here is

$$P = P'_h \rho_o c_o^2 \left(1 - \frac{\Gamma}{2} \mu \right) + \Gamma \rho (e - e_o) \quad (\text{B.18})$$

$$P'_h = \begin{cases} \mu + (S_o - 1)\mu^2 + (S_o - 1)(3S_o - 1)\mu^3 & \text{if } \mu > 0 \text{ (Compression)} \\ \mu & \text{if } \mu < 0 \text{ (Tension)} \end{cases} \quad (\text{B.19})$$

$$\mu = \frac{\rho}{\rho_o} - 1 \quad (\text{B.20})$$

$$\Gamma = \frac{\rho_o}{\rho} \Gamma_o, \quad (\text{B.21})$$

where Γ_o , S_o , c_o , and ρ_o are material constants and e_o is the initial energy. The following is needed for the stability analysis

$$\begin{aligned}\mu &= \frac{\rho}{\rho_o} - 1 = \frac{\bar{\rho} + \phi - \rho_o}{\rho_o} = \frac{\bar{\rho} - \rho_o}{\rho_o} + \frac{\phi}{\rho_o} = \bar{\mu} + \frac{\phi}{\rho_o} \\ P'_h &= \bar{P}_h + \tilde{P}_h.\end{aligned}$$

Use this form for stability to obtain

$$\begin{aligned}P(\rho, e) &= P(\bar{\rho} + \phi, \bar{e} + \varepsilon) = P'_h \rho_o c_o^2 \left(1 - \frac{\Gamma_o}{2} \left(1 - \frac{\rho_o}{\rho}\right)\right) + \Gamma_o \rho_o (e - e_o) \\ &= \left\{ \bar{P}_h \frac{\rho_o c_o^2}{2} \left[2 - \Gamma_o \left(1 - \frac{\rho_o}{\bar{\rho}}\right)\right] + \Gamma_o \rho_o (\bar{e} - e_o) \right\} \\ &\quad + \left\{ -\bar{P}_h \frac{\rho_o^2 c_o^2 \Gamma_o \phi}{2 \bar{\rho}^2} + \tilde{P}_h \frac{\rho_o c_o^2}{2} \left[2 - \Gamma_o \left(1 - \frac{\rho_o}{\bar{\rho}}\right)\right] \right\} + (\Gamma_o \rho_o \varepsilon) \\ &= \tilde{A} + \tilde{B} \phi + \tilde{C} \varepsilon.\end{aligned}$$

The \tilde{A} term can be easily seen as the first term in braces since it just equates to $P(\bar{\rho}, \bar{e})$. The rest falls in place because P_h is just a function of ρ , not e . This implies that \bar{P}_h is a function of $\bar{\rho}$ and \tilde{P}_h is a function of ϕ . The equation, $\tilde{C} = \Gamma_o \rho_o$, is directly obtained from the above equation. To find an exact value for \tilde{B} a closer look at P_h is needed. Both the tension and compression cases are handled as one, by taking $S_o = 1$ for the tension case.

$$\begin{aligned}\mu^2 &= \bar{\mu}^2 + \frac{2 \bar{\mu} \phi}{\rho_o} \\ \mu^3 &= \bar{\mu}^3 + \frac{3 \bar{\mu}^2 \phi}{\rho_o} \\ P'_h &= \left[\bar{\mu} + (S_o - 1) \bar{\mu}^2 + (S_o - 1)(3S_o - 1) \bar{\mu}^3 \right] \\ &\quad + \frac{1}{\rho_o} \left[1 + 2(S_o - 1) \bar{\mu} + 3(S_o - 1)(3S_o - 1) \bar{\mu}^2 \right] \phi \\ &= \bar{P}_h + \tilde{P}_h\end{aligned}$$

Now obtain an equation for \tilde{B}

$$\begin{aligned}\tilde{B} = & -\frac{\rho_o^2 c_o^2 \Gamma_o}{2 \bar{\rho}^2} \left[\bar{\mu} + (S_o - 1) \bar{\mu}^2 + (S_o - 1)(3S_o - 1) \bar{\mu}^3 \right] \\ & + \frac{c_o^2}{2} \left[2 - \Gamma_o \left(1 - \frac{\rho_o}{\bar{\rho}} \right) \right] \left[1 + 2(S_o - 1) \bar{\mu} + 3(S_o - 1)(3S_o - 1) \bar{\mu}^2 \right].\end{aligned}$$

For the tension case ($\bar{\mu} < 0$ and $S_o = 1$) one can fairly quickly see that \tilde{B} is positive, but it is not as obvious for the compression case. So each of these cases is investigated separately.

1. Tension. Use the value for D_1 obtained in equation (4.14) to obtain

$$\begin{aligned}D_1 = & \frac{4m^2}{\bar{\rho}^4} (\tilde{A}\tilde{C} + \bar{\rho}^2 \tilde{B} - 2\bar{\rho}\tilde{A}) \left(\sum_{l=1}^{\infty} \sin(lk) W'_l \right)^2 \\ = & \frac{4m^2}{\bar{\rho}^4} \left(\sum_{l=1}^{\infty} \sin(lk) W'_l \right)^2 \left[\tilde{A} \Gamma_o \rho_o - \frac{\rho_o^2 c_o^2 \Gamma_o}{2} \left(\frac{\bar{\rho} - \rho_o}{\rho_o} \right) \right. \\ & \left. + \frac{\bar{\rho}^2 c_o^2}{2} \left(2 - \Gamma_o \left(1 - \frac{\rho_o}{\bar{\rho}} \right) \right) - 2\bar{\rho}\tilde{A} \right] \\ = & \frac{4m^2}{\bar{\rho}^4} \left(\sum_{l=1}^{\infty} \sin(lk) W'_l \right)^2 \left[\tilde{A} (\Gamma_o \rho_o - 2\bar{\rho}) + \frac{c_o^2}{2} (2\bar{\rho} + \Gamma_o(\rho_o^2 - \bar{\rho}^2)) \right].\end{aligned}$$

Assume that \bar{e} follows convention and is taken as always positive (otherwise the form of P must change). For some values of ρ and e , the D_1 term is negative. However, considering several different metals (Aluminum, Copper, and Lead) that have various values for the constants leads to the results that for ρ down to about $0.5\rho_o$, D_1 was positive. Results are shown in table B.1. Of course, for density that low the material probably changed phase and may need a different EOS or constants. Hence, for realistic values of ρ in tension, the D_1 term should be non-negative, and therefore does not unstabilize the method.

Metal	Γ_o	ρ_o	c_o	S_o	$D_1 > 0$ for $\rho \gtrsim$
AL	1.68	2.71	0.535	1.34	1.25
CU	2.00	8.92	0.391	1.51	4.50
PB	2.03	11.35	0.203	1.47	6.00

Table B.1 Mie-Gruneisen Tension Results

2. Compression. Once again, use the value for D_1 obtained in equation (4.14) to obtain

$$\begin{aligned}
D_1 &= \frac{4m^2}{\bar{\rho}^4} (\ddot{A}\tilde{C} + \bar{\rho}^2 \ddot{B} - 2\bar{\rho}\ddot{A}) \left(\sum_{l=1}^{\infty} \sin(lk) W'_l \right)^2 \\
&= \frac{4m^2}{\bar{\rho}^4} \left(\sum_{l=1}^{\infty} \sin(lk) W'_l \right)^2 \left\{ \ddot{A}(\Gamma_o \rho_o - 2\bar{\rho}) \right. \\
&\quad \left. - \frac{\rho_o^2 c_o^2 \Gamma_o}{2} [\bar{\mu} + (S_o - 1)\bar{\mu}^2 + (S_o - 1)(3S_o - 1)\bar{\mu}^3] \right. \\
&\quad \left. + \frac{\bar{\rho}^2 c_o^2}{2} \left[2 - \Gamma_o \left(1 - \frac{\rho_o}{\bar{\rho}} \right) \right] [1 + 2(S_o - 1)\bar{\mu} + 3(S_o - 1)(3S_o - 1)\bar{\mu}^2] \right\}.
\end{aligned}$$

Assume that \bar{e} follows convention and is taken as always positive (otherwise the form of P must change). For some values of ρ and e the D_1 term is negative. However, once again several different metals (Aluminum, Copper, and Lead) were considered that had various values for the constants and found that for ρ up to about $2\rho_o$, D_1 was positive. Results may be seen in table B.2. Of course, for density that high the material probably changed phase and may need a different EOS or constants. Hence, for realistic values of ρ in compression the D_1 term should be non-negative, and therefore does not destabilize the method.

Metal	Γ_o	ρ_o	c_o	S_o	$D_1 > 0$ for $\rho \lesssim$
AL	1.68	2.71	0.535	1.34	5.00
CU	2.00	8.92	0.391	1.51	15.00
PB	2.03	11.35	0.203	1.47	16.00

Table B.2 Mie-Gruneisen Compression Results

Appendix C. ADDITIONAL KERNEL NOTES

This appendix includes material related to the Kernels Chapter (Chapter VI).

C.1 Kernels Analyzed

The kernels shown in Table C.1 are used in the analysis found in Chapter VI. All kernels in this table take the form $W(x, h) = \frac{1}{h}K(\frac{x}{h}) = \frac{c_n}{h}\tilde{K}(\frac{x}{h})$. Graphs of all these kernels and their first derivative are shown in Figures C.1–C.10.

#	Name	Type	$\tilde{K}(u)$	κ	1-D c_n
1	Gaussian	B	e^{-u^2}	3	$\frac{1}{\sqrt{\pi}}$
2	W_4 B-Spline	B	$\begin{cases} 1 - \frac{3}{2}u^2 + \frac{3}{4} u ^3 & \text{if } 0 \leq u \leq 1 \\ \frac{1}{4}(2 - u)^3 & \text{if } 1 \leq u \leq 2 \end{cases}$	2	$\frac{2}{3}$
3	Cosine	B	$(1 - \frac{u^2}{4})(1 + \cos(\frac{\pi u}{2}))$	2	$\frac{3\pi^2}{8(\pi^2+3)}$
4	Exponential	H	$e^{- u } - e^{-9}$	9	0.500618
5	$\kappa - 2$ Exponential	H	$e^{-4.5 u } - e^{-9}$	2	2.250555
6	1/X, 2	H	$\frac{1}{2+ u } + \frac{ u -6}{16}$	2	7.337061
7	1/X, 4	H	$\frac{1}{4+ u } + \frac{ u -8}{36}$	2	30.163694
8	1/X, 10	H	$\frac{1}{10+ u } + \frac{ u -14}{144}$	2	283.125508
9	$-X^2$	H	$\frac{1}{2}(u - 2)^2$	2	0.375
10	$-x - e^{-x}$	P	$2 - u - e^{- u } + e^{-2}$	2	0.355617
11	$4 - X^2$	P	$4 - u^2$	2	0.09375
12	$8 - X^3$	P	$8 - u ^3$	2	0.041667
13	$\kappa - 2$ Gaussian	B	$e^{-2.25u^2} - e^{-9}$	2	0.846657
14	L Gaussian	B	$(2 - u)e^{-u^2}$	2	0.392674
15	Q Gaussian	B	$(1 - \frac{u^2}{4})e^{-u^2}$	2	0.643998
16	T Gaussian	B	$e^{-u^2} - e^{-4}$	2	0.591401
17	Quartic-1	B	$(2 + 3 u)(2 - u)^3$	2	0.0390625
18	Quartic-2	B	$16 - 8 u ^3 + 3u^4$	2	0.0260417

Table C.1 Kernels Analyzed

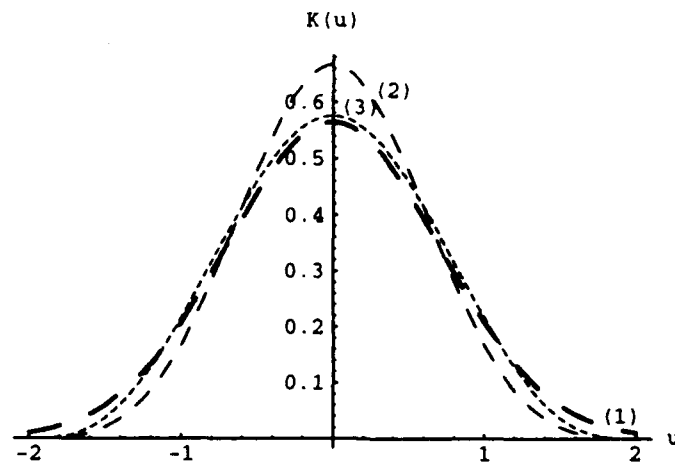


Figure C.1 Bell Shaped Kernels

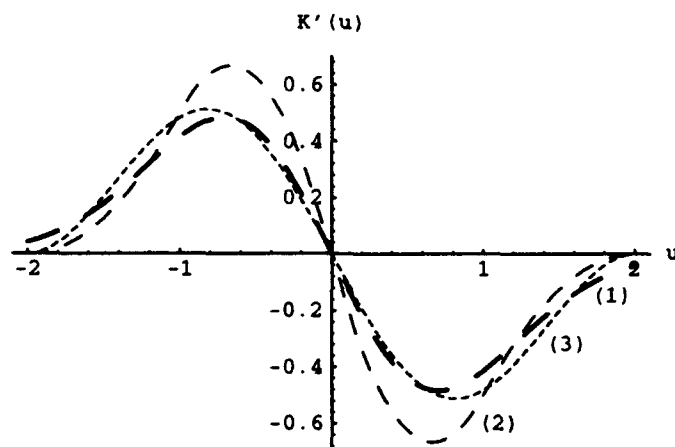


Figure C.2 Derivatives of Bell Shaped Kernels

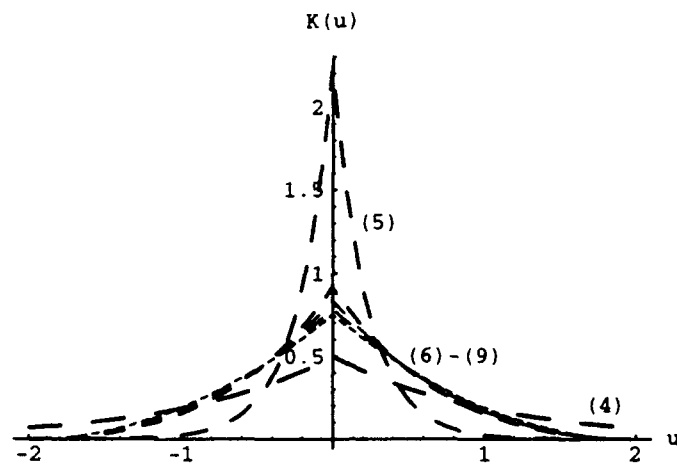


Figure C.3 Hyperbolic Shaped Kernels

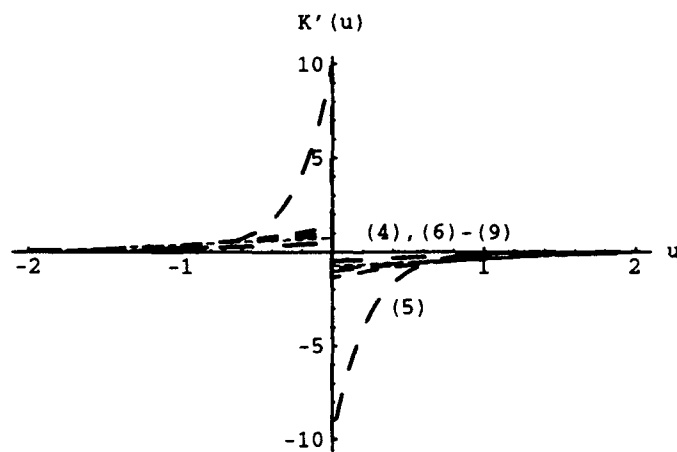


Figure C.4 Derivatives of Hyperbolic Shaped Kernels

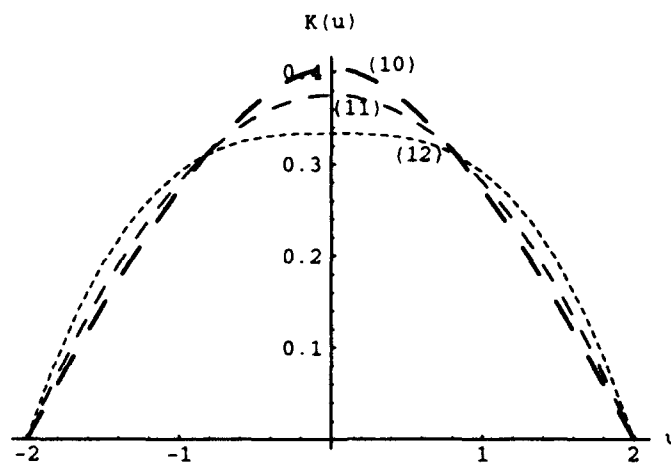


Figure C.5 Parabolic Shaped Kernels

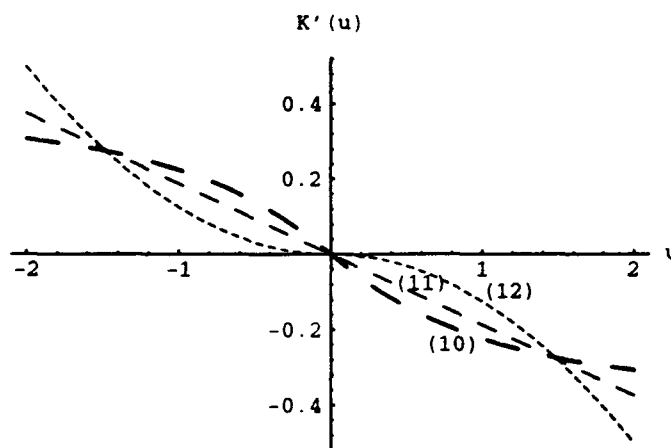


Figure C.6 Derivatives of Parabolic Shaped Kernels

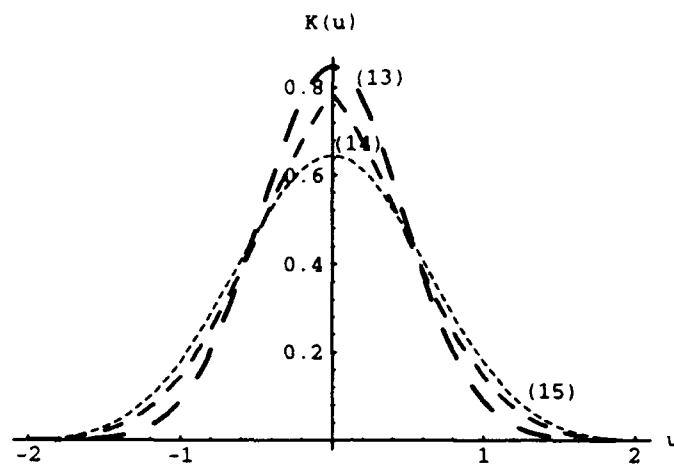


Figure C.7 Additional Bell Shaped Kernels

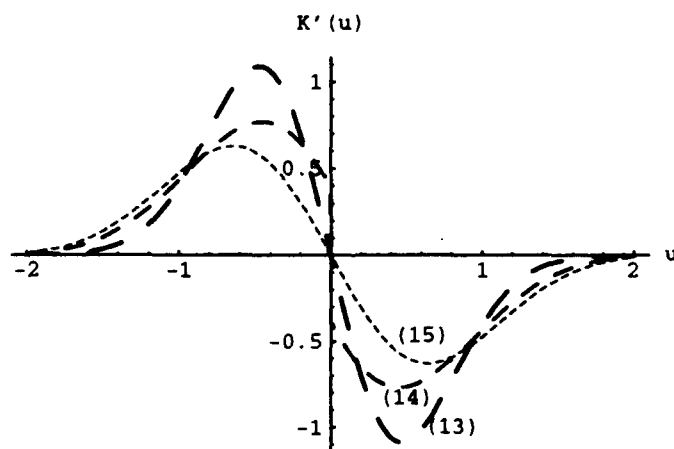


Figure C.8 Derivatives of Additional Bell Shaped Kernels

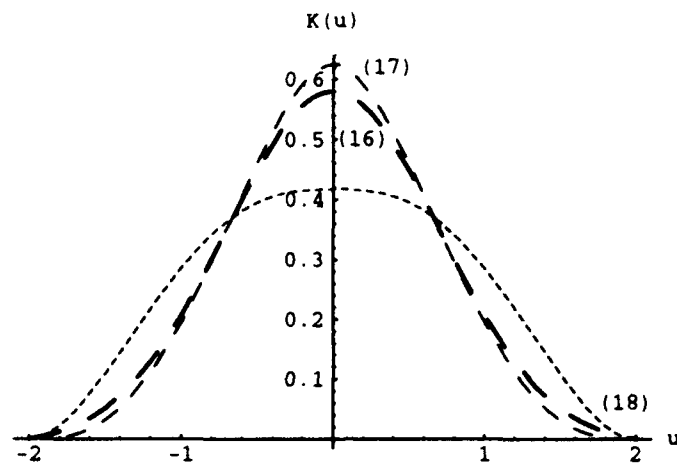


Figure C.9 Additional Bell Shaped Kernels

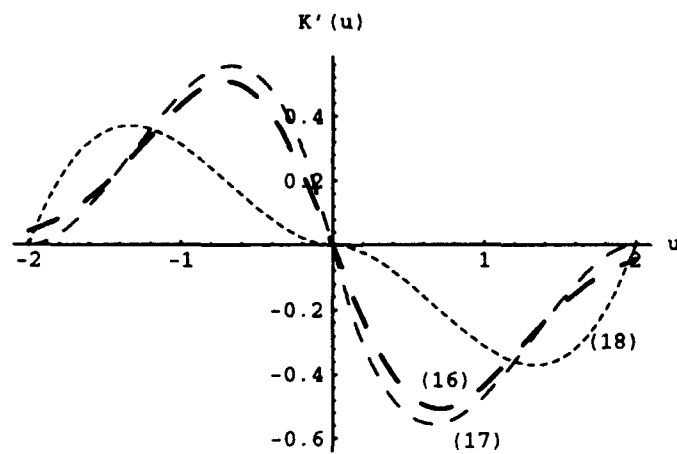


Figure C.10 Derivatives of Additional Bell Shaped Kernels

C.2 Kernel Test 1 Plots

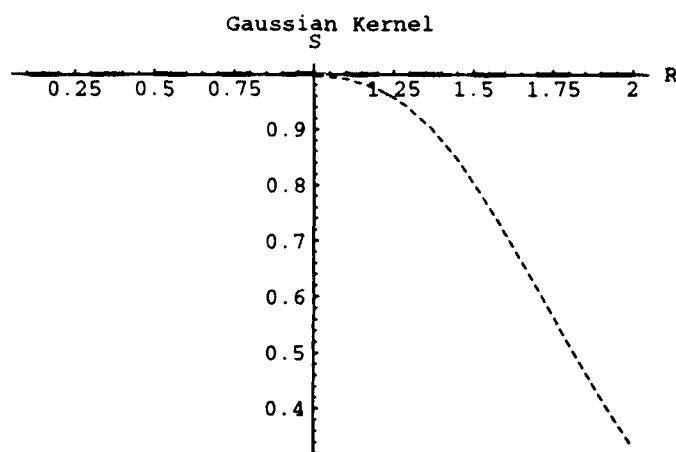


Figure C.11 Gaussian Kernel (1) Test 1, $R = \Delta x/h$

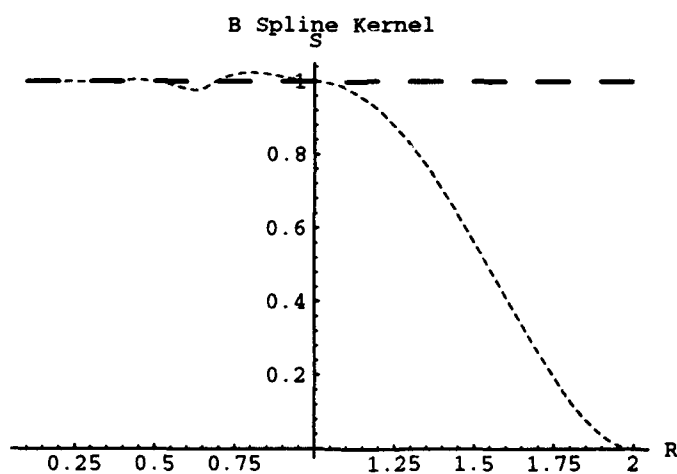


Figure C.12 W4 B-Spline Kernel (2) Test 1, $R = \Delta x/h$

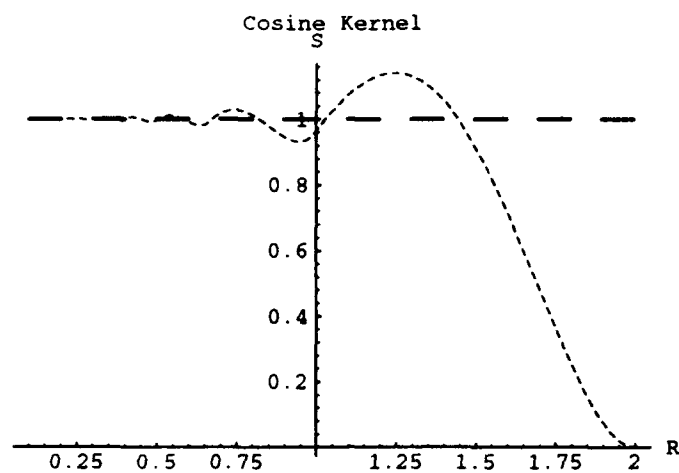


Figure C.13 Cosine Kernel (3) Test 1, $R = \Delta x/h$

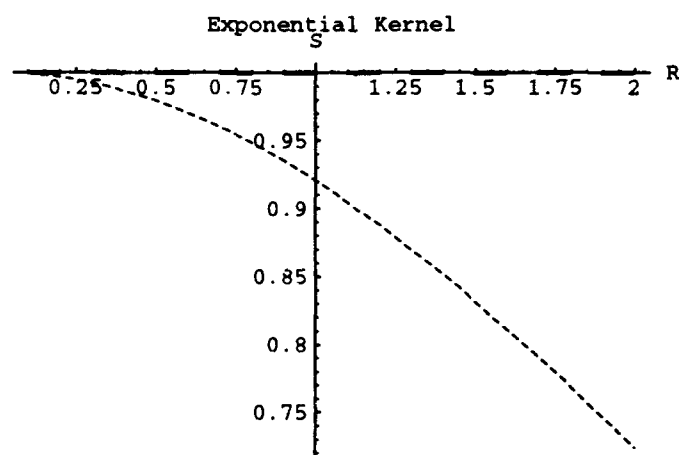


Figure C.14 Exponential Kernel (4) Test 1, $R = \Delta x/h$

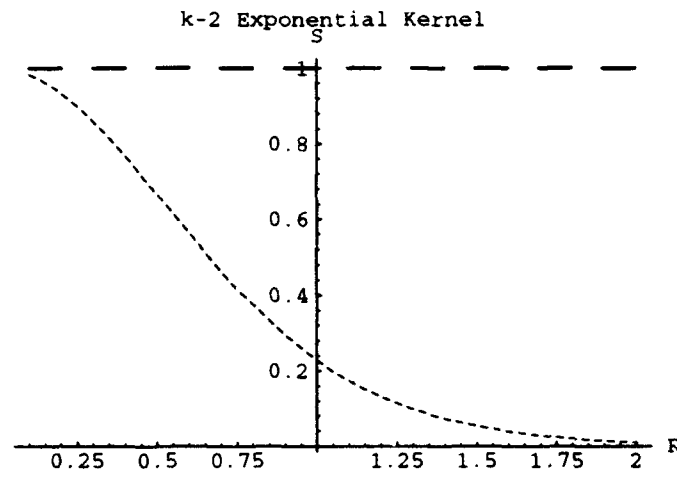


Figure C.15 k-2 Exponential Kernel (5) Test 1, $R = \Delta x/h$

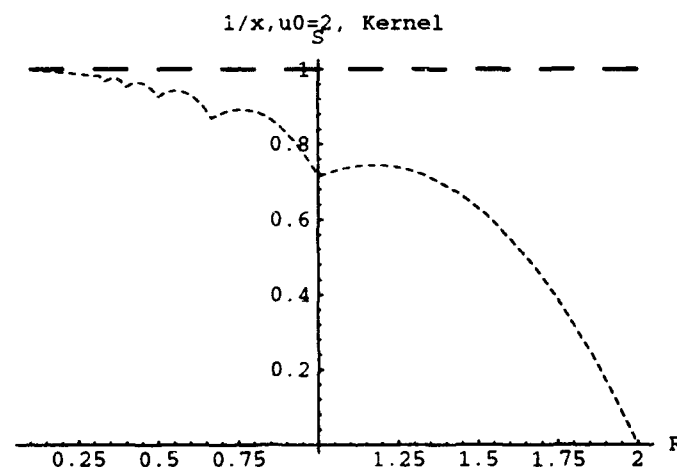


Figure C.16 $1/X, U_0=2$ Kernel (6) Test 1, $R = \Delta x/h$

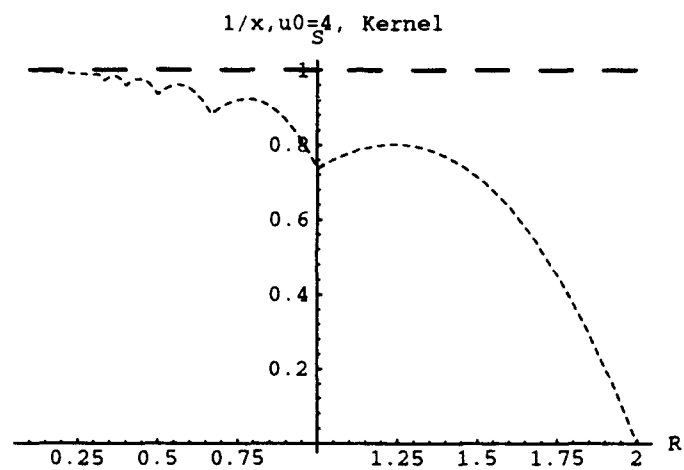


Figure C.17 $1/X, U_0=4$ Kernel (7) Test 1, $R = \Delta x/h$

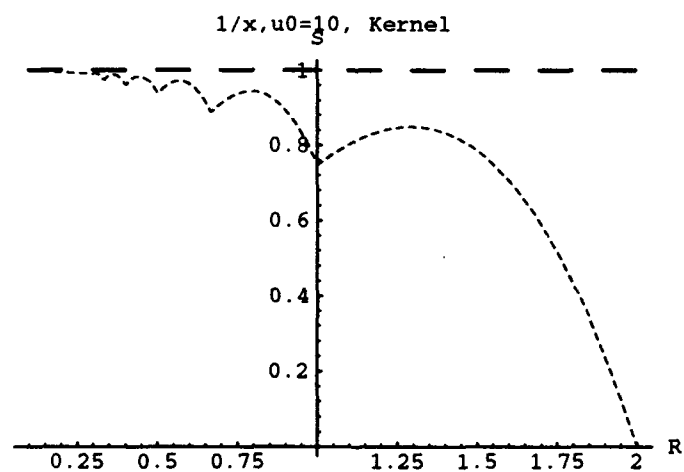


Figure C.18 $1/X, U_0=10$ Kernel (8) Test 1, $R = \Delta x/h$

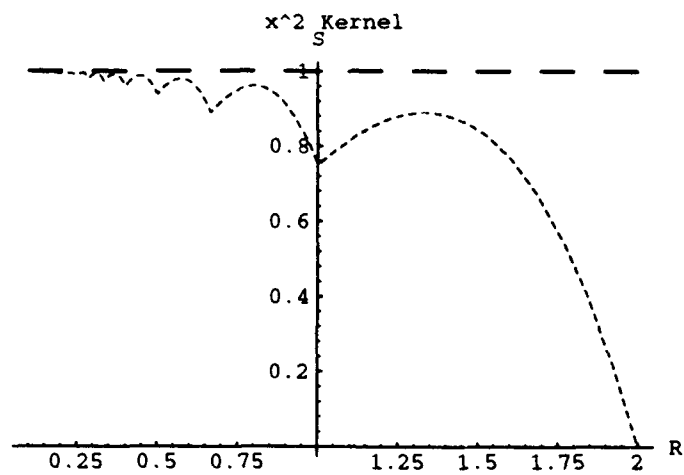


Figure C.19 Kernel (9) Test 1, $R = \Delta x/h$

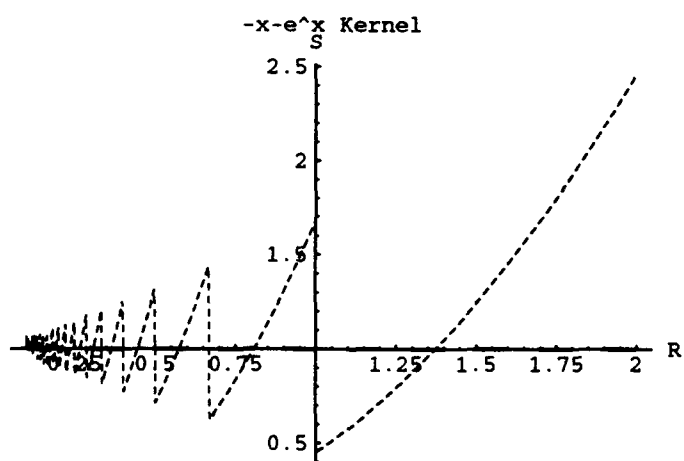


Figure C.20 Kernel (10) Test 1, $R = \Delta x/h$

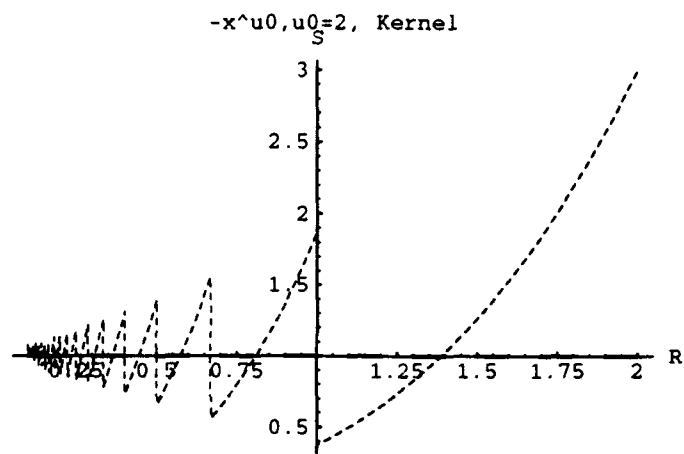


Figure C.21 Kernel (11) Test 1, $R = \Delta x/h$

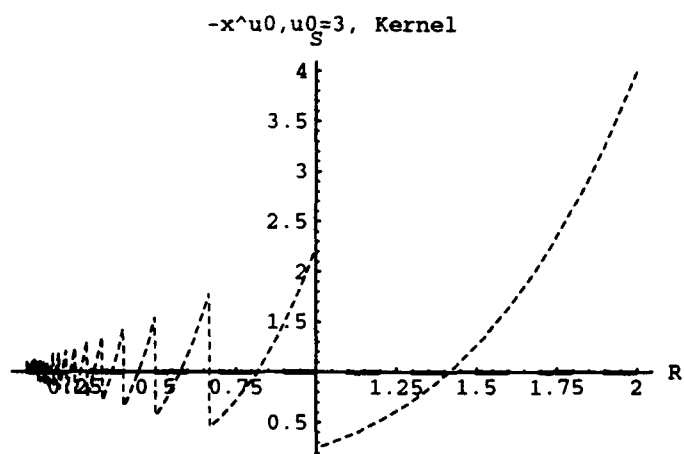


Figure C.22 Kernel (12) Test 1, $R = \Delta x/h$

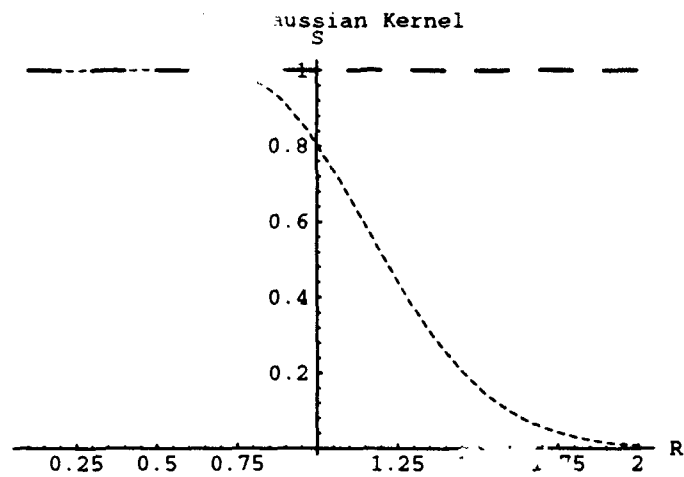


Figure C.23 k-2 Gaussian Kernel (13) Test 1, $R = \Delta x/h$

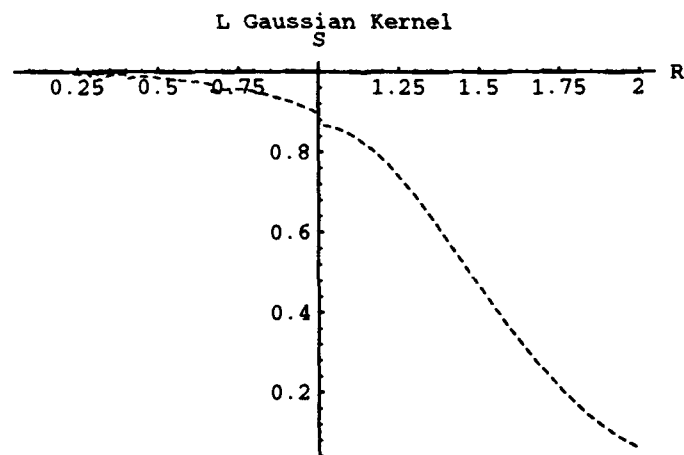


Figure C.24 L Gaussian Kernel (14) Test 1, $R = \Delta x/h$

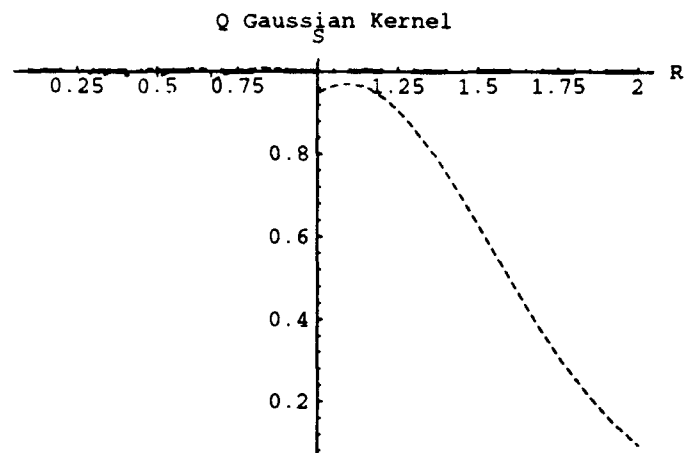


Figure C.25 Q Gaussian Kernel (15) Test 1, $R = \Delta x/h$

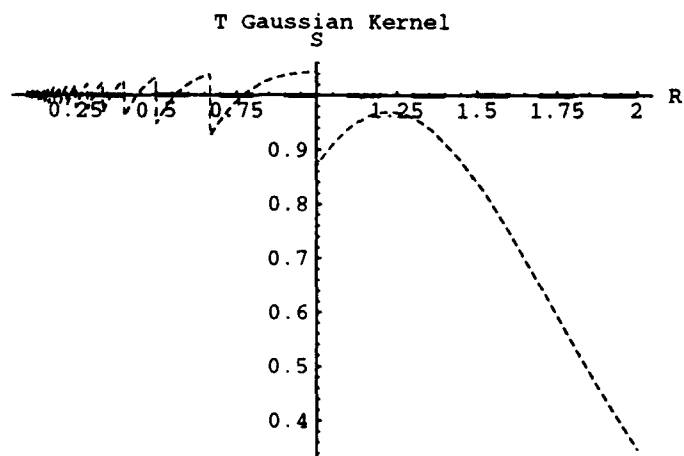


Figure C.26 T Gaussian Kernel (16) Test 1, $R = \Delta x/h$

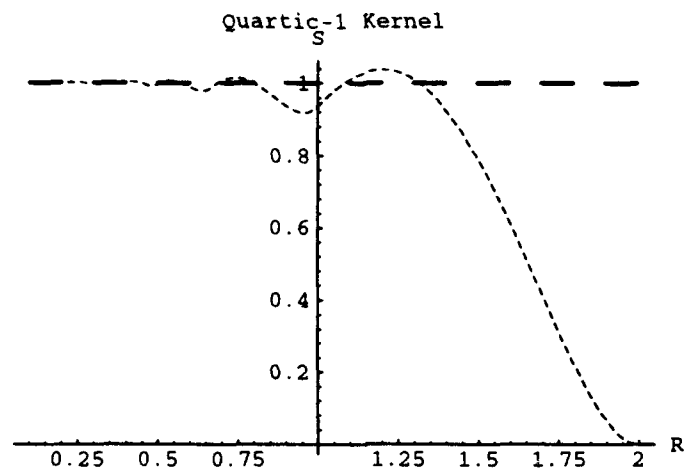


Figure C.27 Quartic-1 Kernel (17) Test 1, $R = \Delta x/h$

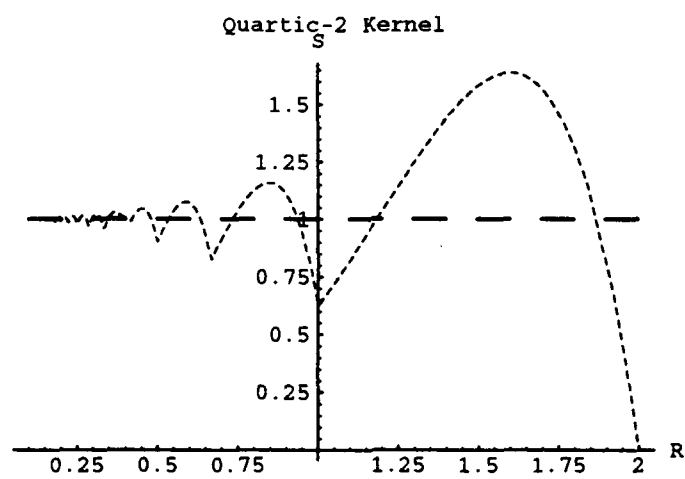


Figure C.28 Quartic-2 Kernel (18) Test 1, $R = \Delta x/h$

C.3 Higher Order Kernel Results

The kernels shown in Table C.2 are used in the analysis found in Chapter VI. All kernels in this table take the form $W(x, h) = \frac{1}{h} K(\frac{x}{h}) = \frac{c_n}{h} \tilde{K}(\frac{x}{h})$. Graphs of all these kernels and their first derivative are shown in Figures C.29–C.30.

Name	$\tilde{K}(u)$	κ	1-D c_n
Super-Gaussian	$(\frac{3}{2} - u^2)e^{-u^2}$	3	$\frac{1}{\pi^{1/2}}$
Enhanced B-Splines	$\begin{cases} 17 - \frac{147}{4}u^2 + \frac{18}{4} u ^3 & \text{if } 0 \leq u \leq 1 \\ \frac{1}{4}(2 - u)^2(49 - 47 u) & \text{if } 1 \leq u \leq 2 \end{cases}$	2	$\frac{1}{18}$
Super-Gaussian 2	$(1.49624 - u^2)e^{-u^2}$	3	0.566214

Table C.2 One-Dimensional Higher Order kernels

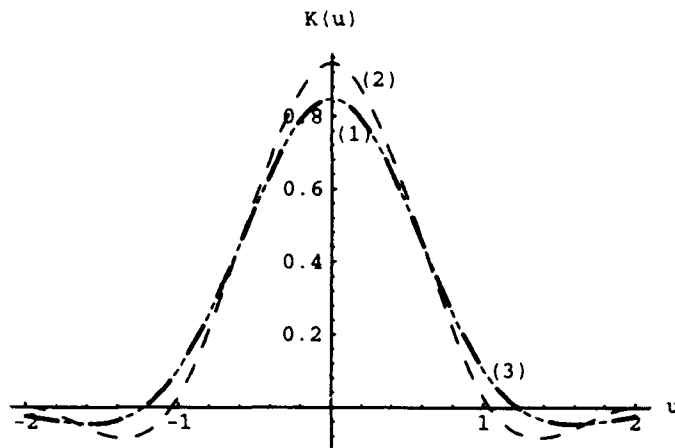


Figure C.29 Higher Order Kernels

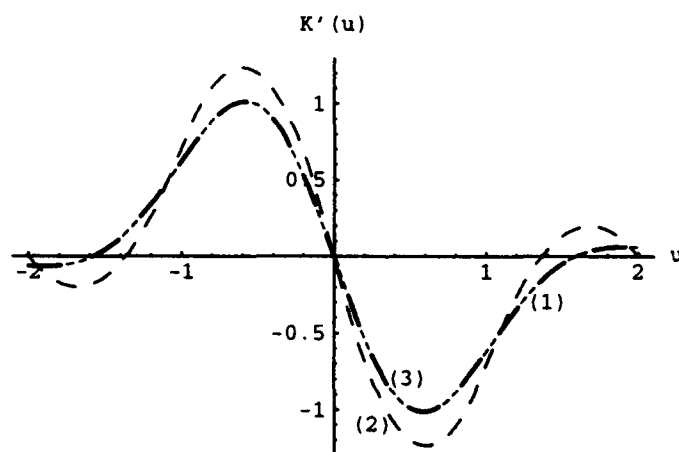


Figure C.30 Derivatives of Higher Order Kernels

Test 1 Plots for Higher Order Kernels

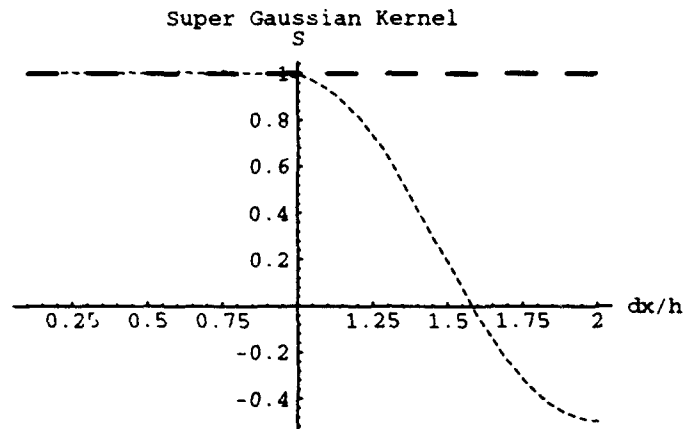


Figure C.31 Super-Gaussian Kernel Test 1, $R = \Delta x/h$

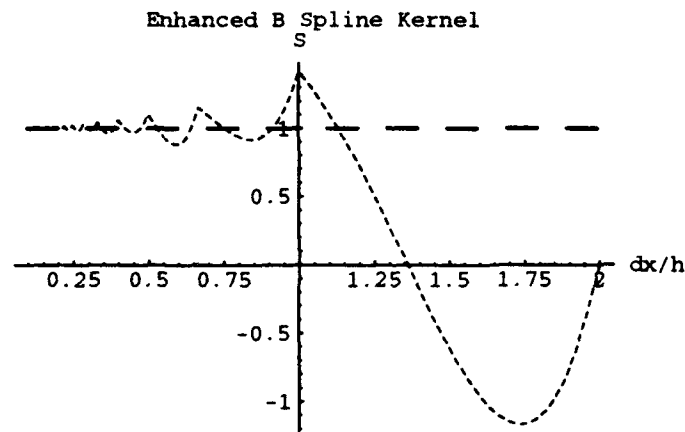


Figure C.32 Enhanced B-Spline Kernel Test 1, $R = \Delta x/h$

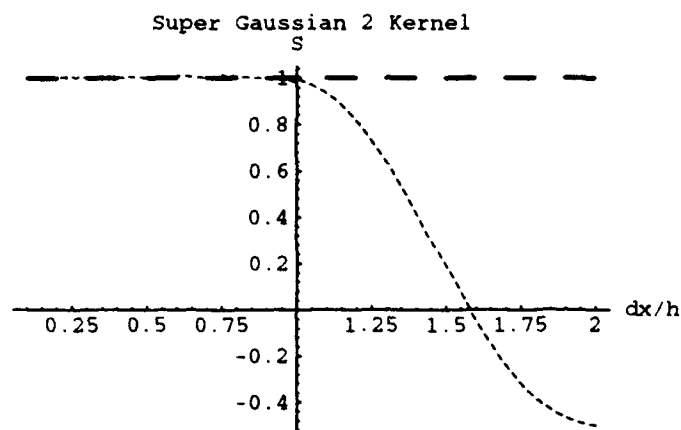


Figure C.33 Super-Gaussian 2 Kernel Test 2, $R = \Delta x/h$

Tables C.3 and C.4 show the l_1 and l_2 results from Test 3 in Chapter VI for the Higher Order Kernels. This data results from using symmetric kernels on the three test functions for all 3 kernels.

Name	Type	Polynomial	Sine	Step
Super-Gaussian	B	0.018911	0.024206	1.785054
Enhanced B-Spline	B	0.087208	0.074404	1.950188
Super-Gaussian 2	B	0.018911	0.024193	1.786731

Table C.3 Avg l_1 Rel Error Norms for Higher Order Kernel Test 3

Name	Type	Polynomial	Sine	Step
Super-Gaussian	B	0.042776	0.054131	2.939078
Enhanced B-Spline	B	0.129249	0.111414	3.231267
Super-Gaussian 2	B	0.042970	0.054224	2.941180

Table C.4 Avg l_2 Rel Error Norms for Higher Order Kernel Test 3

C.4 Kernel Test 3 Results

Tables C.5 and C.6 show the l_1 and l_2 results from Test 3 in Chapter VI. This data results from using symmetric kernels on the three test functions for all 18 kernels.

#	Name	Type	Polynomial	Sine	Step
1	Gaussian	B	0.007119	0.078705	1.525396
2	W_4 B-Splines	B	0.013728	0.057164	1.531404
3	Cosine	B	0.028616	0.058633	1.561539
4	Exponential	H	0.088975	0.281294	1.419907
5	$\kappa - 2$ Exponential	H	0.507906	0.521096	1.015792
6	$1/X, 2$	H	0.127125	0.175582	1.365669
7	$1/X, 4$	H	0.103917	0.156133	1.395861
8	$1/X, 10$	H	0.089925	0.144996	1.414412
9	$-X^2$	H	0.080997	0.138340	1.426459
10	$-x - e^{-x}$	P	0.238686	0.213771	1.644485
11	$4 - X^2$	P	0.288949	0.255279	1.676442
12	$8 - X^3$	P	0.380648	0.331688	1.735950
13	$\kappa - 2$ Gaussian	B	0.090605	0.126439	1.422764
14	L Gaussian	B	0.061084	0.108767	1.451667
15	Q Gaussian	B	0.012795	0.064329	1.524989
16	T Gaussian	B	0.032013	0.073000	1.540140
17	Quartic-1	B	0.020412	0.068948	1.521352
18	Quartic-2	B	0.087969	0.117343	1.532017

Table C.5 Avg l_1 Relative Error Norms for Kernel Test 3

#	Name	Type	Polynomial	Sine	Step
1	Gaussian	B	0.007985	0.081705	2.310485
2	W_4 B-Spline	B	0.020354	0.064281	2.522221
3	Cosine	B	0.045007	0.065928	2.433239
4	Exponential	H	0.132289	0.291637	1.699878
5	$\kappa - 2$ Exponential	H	0.566931	0.579755	1.987313
6	$1/X$, 2	H	0.156022	0.201873	2.203153
7	$1/X$, 4	H	0.130337	0.178867	2.216029
8	$1/X$, 10	H	0.115533	0.165679	2.218148
9	$-X^2$	H	0.106990	0.158004	2.215146
10	$-x - e^{-x}$	P	0.292461	0.266744	2.123883
11	$4 - X^2$	P	0.354653	0.313852	2.144938
12	$8 - X^3$	P	0.469350	0.402054	2.231259
13	$\kappa - 2$ Gaussian	B	0.164966	0.193598	2.569320
14	L Gaussian	B	0.084140	0.129441	2.420860
15	Q Gaussian	B	0.019560	0.070414	2.466266
16	T Gaussian	B	0.040621	0.082925	2.358863
17	Quartic-1	B	0.030735	0.075212	2.425873
18	Quartic-2	B	0.124879	0.154617	2.114397

Table C.6 Avg l_2 Relative Error Norms for Kernel Test 3

Tables C.7 and C.8 show the l_1 and l_2 results from Test 3 Step function only for the truncated 1-sided kernels.

#	Name	Type	Adaptive	Backward	Forward
1	Gaussian	B	35.770172	25.346821	50.589466
2	W_4 B-Spline	B	39.016865	28.821920	57.531830
3	Cosine	B	36.007061	26.473532	52.838074
4	Exponential	H	27.388069	17.761250	35.458717
5	$\kappa - 2$ Exponential	H	33.400810	25.695364	51.122055
6	$1/X$, 2	H	36.192120	26.940407	53.760464
7	$1/X$, 4	H	35.764687	26.554712	52.992195
8	$1/X$, 10	H	35.311211	26.171162	52.227161
9	$-X^2$	H	61.610802	25.816395	123.611145
10	$-x - e^{-x}$	P	26.363857	19.140060	38.176891
11	$4 - X^2$	P	24.932720	18.043724	35.980412
12	$8 - X^3$	P	22.735289	16.362419	32.602768
13	$\kappa - 2$ Gaussian	B	42.133472	31.433580	62.741013
14	L Gaussian	B	38.926849	28.889837	57.663372
15	Q Gaussian	B	37.972710	28.026678	55.942650
16	T Gaussian	B	35.350651	25.005360	51.903835
17	Quartic-1	B	36.938557	27.236271	54.361706
18	Quartic-2	B	27.964264	20.365017	40.628468

Table C.7 Avg l_1 Error Norms for Test 3, Step Function, Truncated Kernels

#	Name	Type	Adaptive	Backward	Forward
1	Gaussian	B	35.266060	24.567732	48.868141
2	W_4 B-Spline	B	38.498535	28.191751	56.090488
3	Cosine	B	35.026104	25.532019	50.773285
4	Exponential	H	27.969044	17.559801	34.975266
5	$\kappa - 2$ Exponential	H	46.150829	34.892223	69.564873
6	$1/X$, 2	H	37.664139	27.824171	55.395535
7	$1/X$, 4	H	36.671600	27.022966	53.790264
8	$1/X$, 10	H	35.873276	26.387548	52.517906
9	$-X^2$	H	71.473541	25.868845	121.344543
10	$-x - e^{-x}$	P	25.929104	18.698484	37.138481
11	$4 - X^2$	P	24.715145	17.764969	35.265335
12	$8 - X^3$	P	23.103941	16.503397	32.725090
13	$\kappa - 2$ Gaussian	B	43.917507	32.446465	64.604774
14	L Gaussian	B	39.424267	29.015673	57.754101
15	Q Gaussian	B	37.427788	27.388683	54.491085
16	T Gaussian	B	34.604794	25.248262	50.220360
17	Quartic-1	B	36.296047	26.537476	52.789551
18	Quartic-2	B	26.995367	19.515217	38.753639

Table C.8 Avg l_2 Error Norms for Test 3, Step Function, Truncated Kernels

Tables C.9 and C.10 show the l_1 and l_2 results from Test 3 Step function only for the condensed 1-sided kernels.

#	Name	Type	Adaptive	Backward	Forward
1	Gaussian	B	4.627463	4.171862	4.224389
2	W_4 B-Spline	B	6.600931	6.091682	6.125278
3	Cosine	B	3.383625	3.269625	3.266023
4	Exponential	H	11.922575	8.278474	8.459723
5	$\kappa - 2$ Exponential	H	138.913773	125.496758	125.621735
6	$1/X, 2$	H	29.136833	26.358891	26.408539
7	$1/X, 4$	H	23.274830	21.076603	21.123383
8	$1/X, 10$	H	19.664471	17.825077	17.871046
9	$-X^2$	H	57.373978	61.558681	37.497616
10	$-x - e^{-x}$	P	5.907393	5.799411	5.962747
11	$4 - X^2$	P	7.691435	7.576866	7.741799
12	$8 - X^3$	P	11.094380	10.981340	11.147852
13	$\kappa - 2$ Gaussian	B	16.707014	15.135881	15.176677
14	L Gaussian	B	15.705833	14.245801	14.293818
15	Q Gaussian	B	5.923904	5.493348	5.530460
16	T Gaussian	B	3.884053	3.635837	3.696250
17	Quartic-1	B	5.542394	5.146575	5.173334
18	Quartic-2	B	4.433723	4.227802	4.134763

Table C.9 Avg l_1 Error Norms for Test 3, Step Function, Condensed Kernels

#	Name	Type	Adaptive	Backward	Forward
1	Gaussian	B	6.777384	6.314503	6.375536
2	W_4 B-Spline	B	9.376309	8.873537	8.860847
3	Cosine	B	5.213538	5.012552	4.963362
4	Exponential	H	12.061853	9.487526	9.572164
5	$\kappa - 2$ Exponential	H	164.067596	153.782288	153.790833
6	$1/X$, 2	H	31.930933	29.944818	29.940264
7	$1/X$, 4	H	25.548899	23.976448	23.968622
8	$1/X$, 10	H	21.664978	20.347097	20.336092
9	$-X^2$	H	56.435982	60.251125	37.391243
10	$-x - e^{-x}$	P	6.452044	6.459867	6.633987
11	$4 - X^2$	P	8.589965	8.557788	8.728765
12	$8 - X^3$	P	12.505659	12.429585	12.599248
13	$\kappa - 2$ Gaussian	B	21.589687	20.246670	20.248573
14	L Gaussian	B	17.908546	16.816137	16.813013
15	Q Gaussian	B	8.417760	7.980781	7.969928
16	T Gaussian	B	5.465341	5.229952	5.226177
17	Quartic-1	B	7.826464	7.436666	7.407992
18	Quartic-2	B	5.515248	5.174659	5.055277

Table C.10 Avg l_2 Error Norms for Test 3, Step Function, Condensed Kernels

C.5 Shock Tube Results for Kernels

The data shown in Table C.11 shows l_1 and l_2 norms for selected kernels applied to the Riemann Shock Tube Problem.

Kernel	Cycle	Norm	Density	Velocity	Energy	Pressure
2	625	1	.119143E-01	.351724E-01	.860845E-02	.901961E-02
2	625	2	.193286E-01	.775102E-01	.336564E-01	.146037E-01
2	617	1	.123399E-01	.366288E-01	.887474E-02	.944356E-02
2	617	2	.199570E-01	.750054E-01	.331870E-01	.160789E-01
3	634	1	.103854E-01	.344368E-01	.912052E-02	.821342E-02
3	634	2	.196988E-01	.784168E-01	.341025E-01	.161296E-01
9	Abort					
10	Abort					
12	Abort					
15	606	1	.879550E-02	.342297E-01	.854017E-02	.593626E-02
15	606	2	.188066E-01	.796244E-01	.341390E-01	.137457E-01
16	646	1	.103807E-01	.365653E-01	.873685E-02	.753665E-02
16	646	2	.194426E-01	.814887E-01	.342294E-01	.144174E-01
17	611	1	.109943E-01	.353594E-01	.856442E-02	.833809E-02
17	611	2	.190161E-01	.763600E-01	.332472E-01	.145838E-01
18	Abort					

Table C.11 Relative Error Norms for Selected Kernels

Appendix D. HYBRID CALCULATIONS

D.1 Introduction

This appendix contains the test results from the hybrid methods discussed in Chapter VIII applied to Riemann Shock Tube Problem. For each method a table of the relative error norms is included. The formulas for these norms are shown in equations (8.10) - (8.12). As described earlier the norms are calculated based on either 1000 evenly spaced points or the particles as the points for a comparison. On each of the plots, the analytic solution is shown. In the tables to follow, the test column key is: N - Normal 600 particles, E - Extra 816 particles, H - Variable h , or A - Always average.

D.2 Baseline

Points	Test	Norm	Density	Velocity	Energy	Pressure
1000	N	1	.306879D-01	.138161D+00	.174816D-01	.349231D-01
1000	N	2	.508795D-01	.174294D+00	.514047D-01	.543121D-01
1000	N	∞	.181351D+00	.768014D+00	.405288D+00	.180250D+00
part	N	1	.302635D-01	.130508D+00	.229058D-01	.326225D-01
part	N	2	.784147D-01	.166399D+00	.791777D-01	.774897D-01
part	N	∞	.100000D+01	.751902D+00	.876105D+00	.100000D+01
1000	E	1	.572092D-02	.358461D-01	.431351D-02	.691356D-02
1000	E	2	.133659D-01	.907235D-01	.200159D-01	.164215D-01
1000	E	∞	.724986D-01	.652194D+00	.290391D+00	.100370D+00
part	E	1	.775876D-02	.361730D-01	.661709D-02	.928497D-02
part	E	2	.542997D-01	.102223D+00	.433878D-01	.561397D-01
part	E	∞	.100000D+01	.680452D+00	.876105D+00	.100000D+01

Table D.1 Relative Error Norms for Baseline

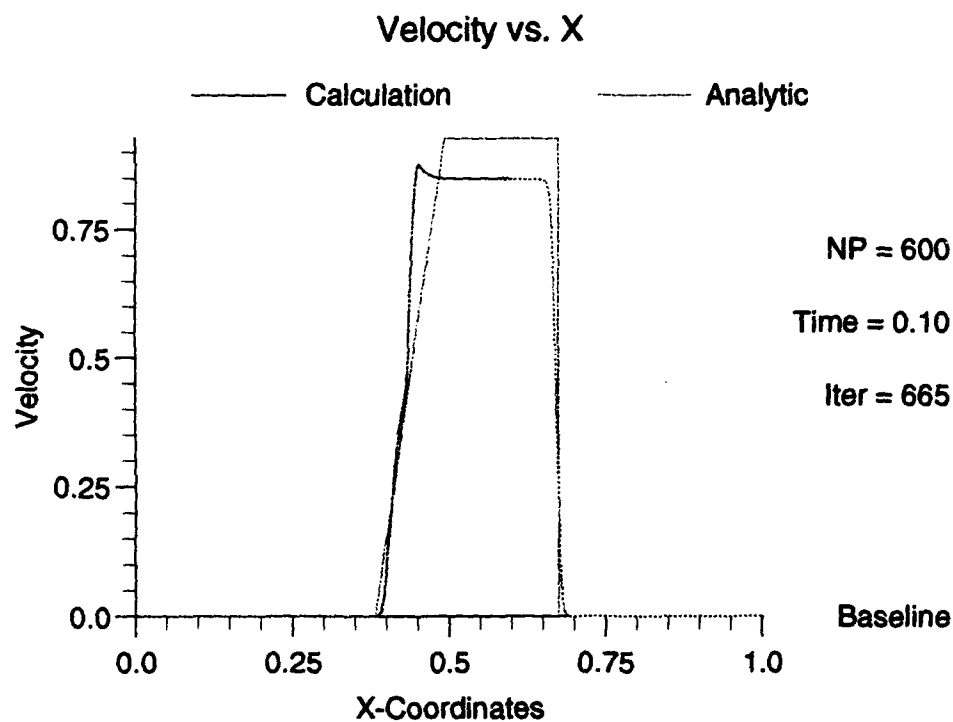
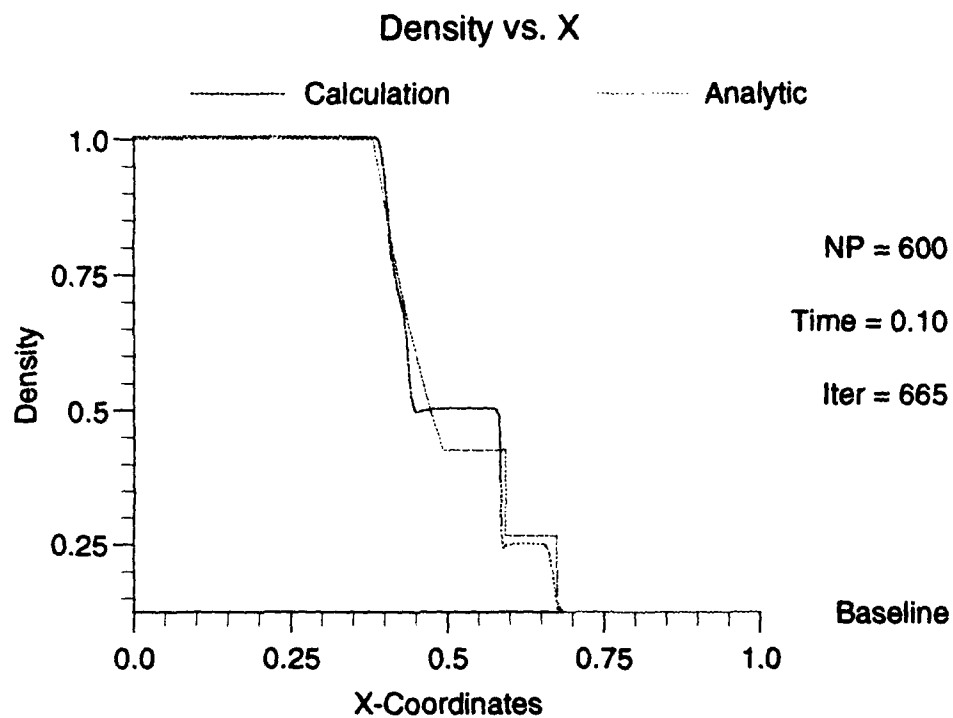


Figure D.1 Baseline Shock Tube Results

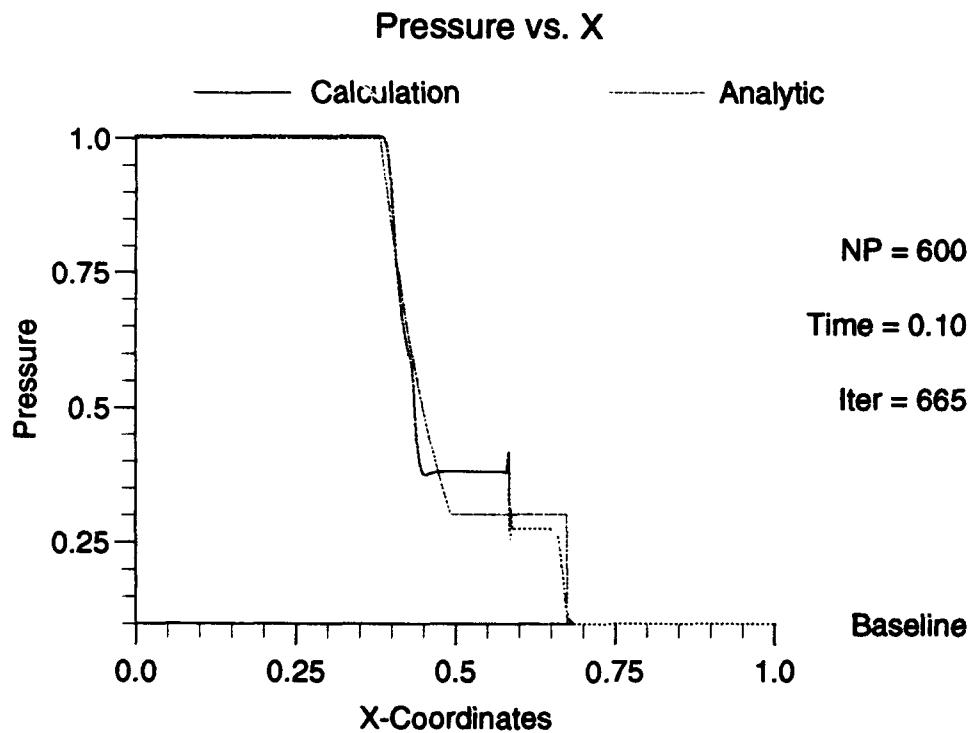
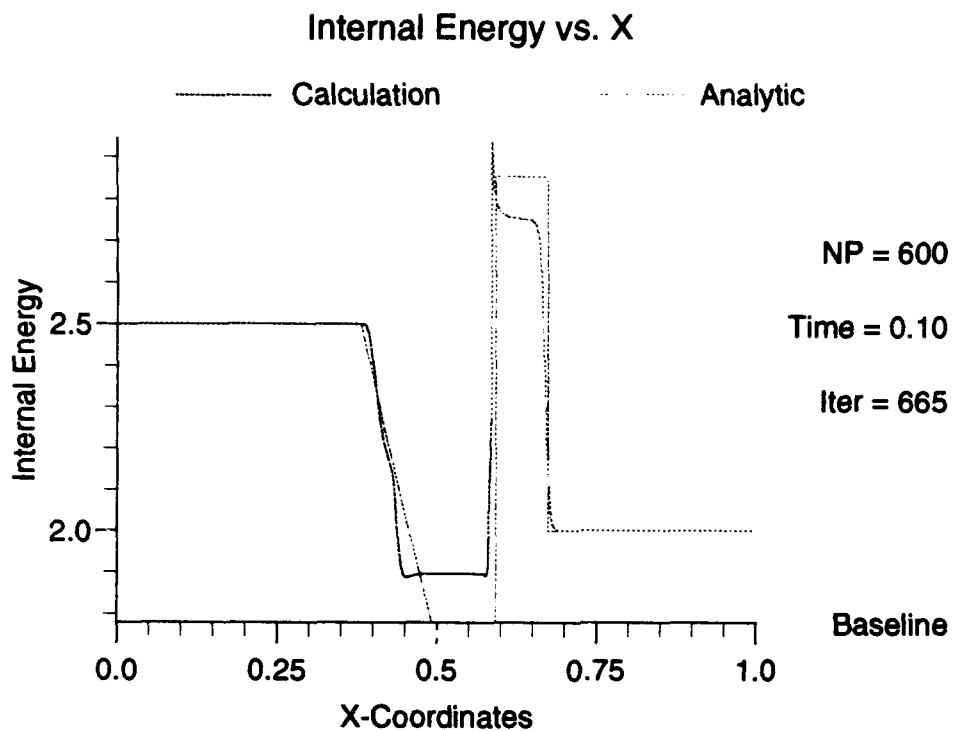


Figure D.2 Baseline Shock Tube Results

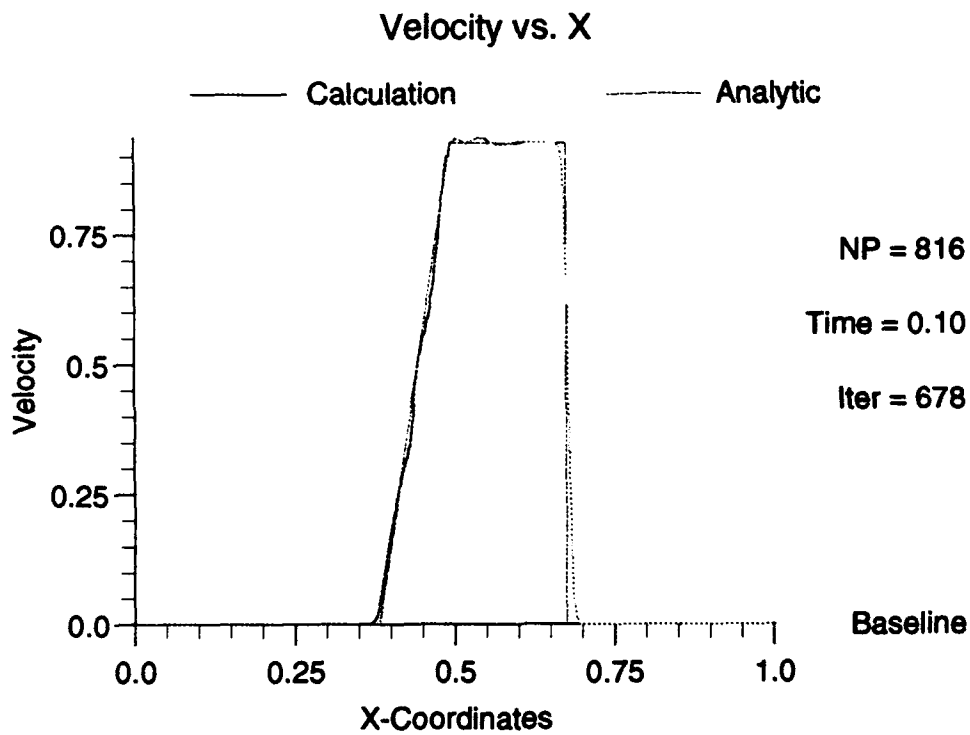
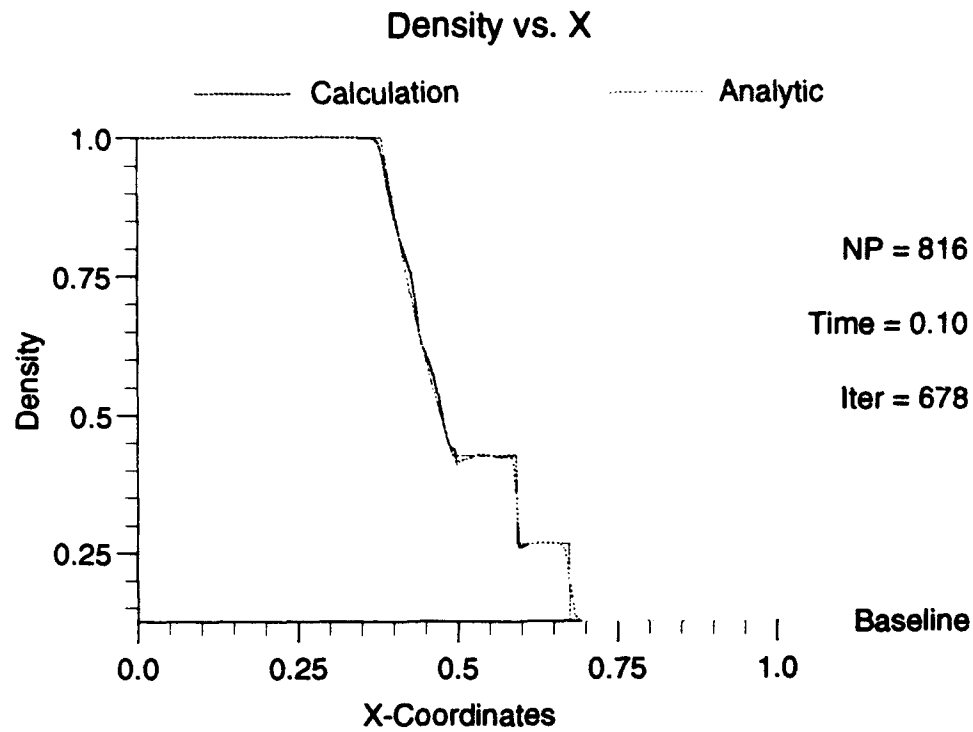


Figure D.3 Baseline Shock Tube Results - Extra Particles

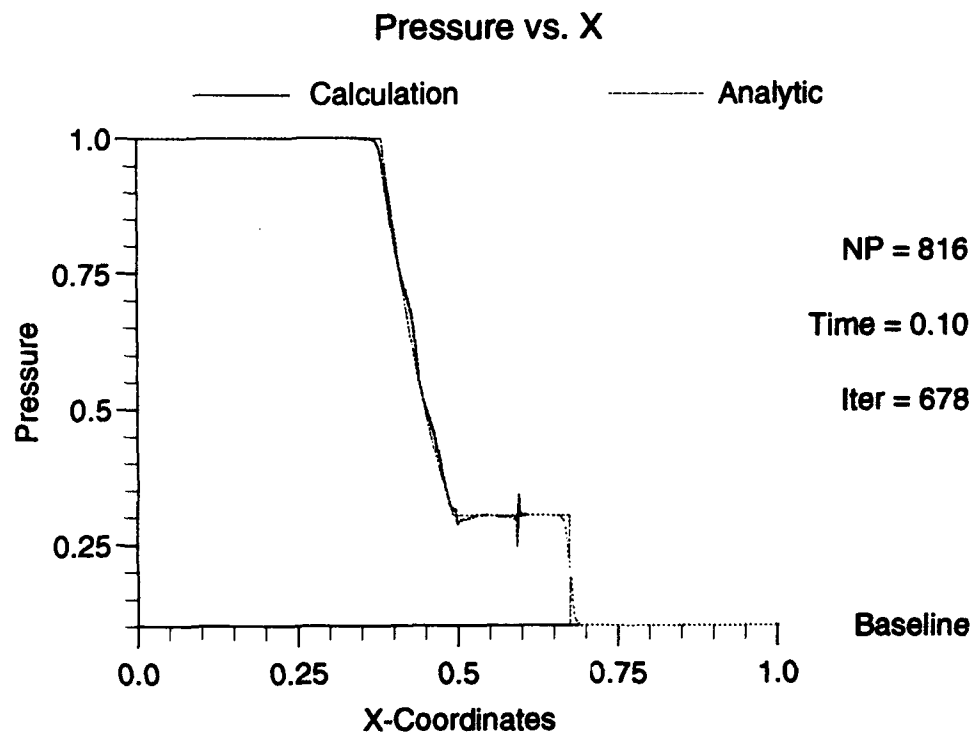
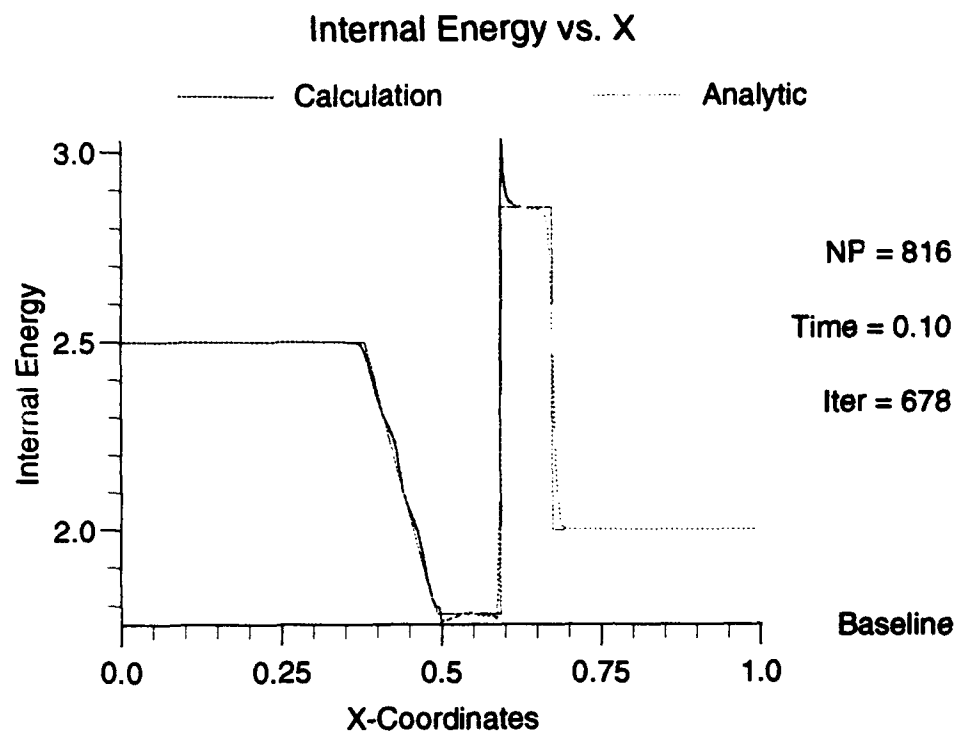


Figure D.4 Baseline Shock Tube Results - Extra Particles

D.3 Method 2

Points	Test	Norm	Density	Velocity	Energy	Pressure
1000	N	1	.272889E-01	.191943E+00	.244260E-01	.342833E-01
1000	N	2	.500100E-01	.322617E+00	.709577E-01	.626991E-01
1000	N	∞	.140617E+00	.100102E+01	.308587E+00	.203194E+00
part	N	1	.264217E-01	.183844E+00	.330583E-01	.332332E-01
part	N	2	.759511E-01	.306687E+00	.918251E-01	.846328E-01
part	N	∞	.100000E+01	.100102E+01	.876105E+00	.100000E+01
1000	E	1	.126022E-01	.811757E-01	.166214E-01	.128609E-01
1000	E	2	.305912E-01	.236765E+00	.616357E-01	.386207E-01
1000	E	∞	.140603E+00	.100101E+01	.313184E+00	.203176E+00
part	E	1	.199853E-01	.670681E-01	.312255E-01	.143112E-01
part	E	2	.650136E-01	.217061E+00	.905540E-01	.657909E-01
part	E	∞	.100000E+01	.100141E+01	.876105E+00	.100000E+01
1000	H	1	.129561E-01	.102615E+00	.219245E-01	.169354E-01
1000	H	2	.334514E-01	.266829E+00	.729890E-01	.431817E-01
1000	H	∞	.141297E+00	.100476E+01	.353619E+00	.205409E+00
part	H	1	.191410E-01	.927628E-01	.359943E-01	.203850E-01
part	H	2	.723576E-01	.254639E+00	.102423E+00	.753285E-01
part	H	∞	.100000E+01	.100485E+01	.876105E+00	.100000E+01

Table D.2 Relative Error Norms for Method 2

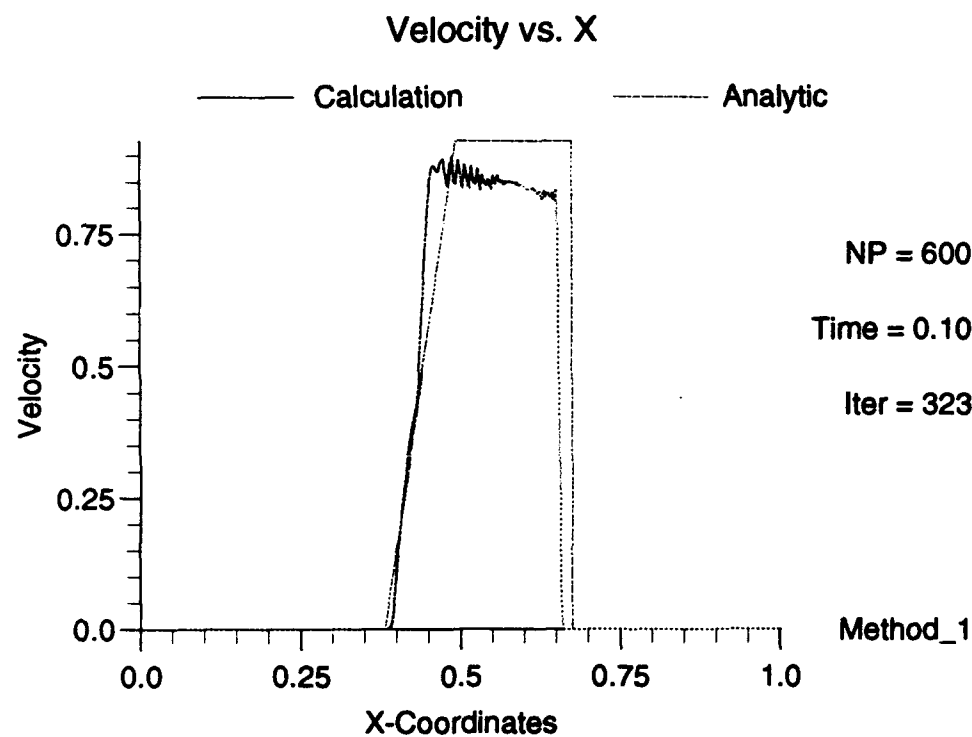
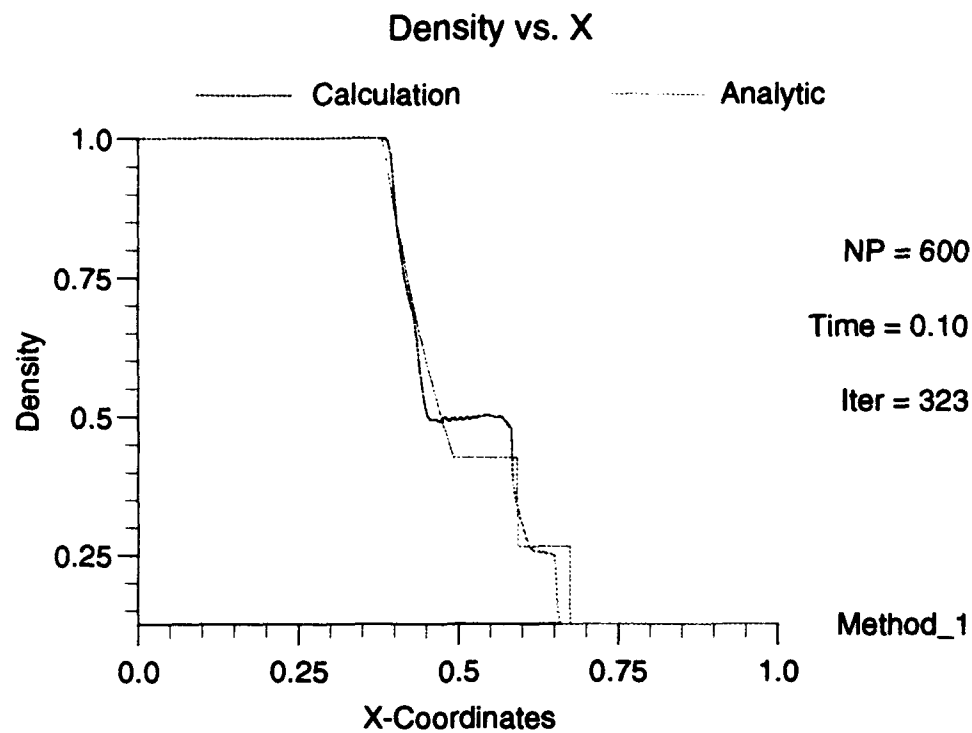


Figure D.5 Shock Tube Results - Method 2

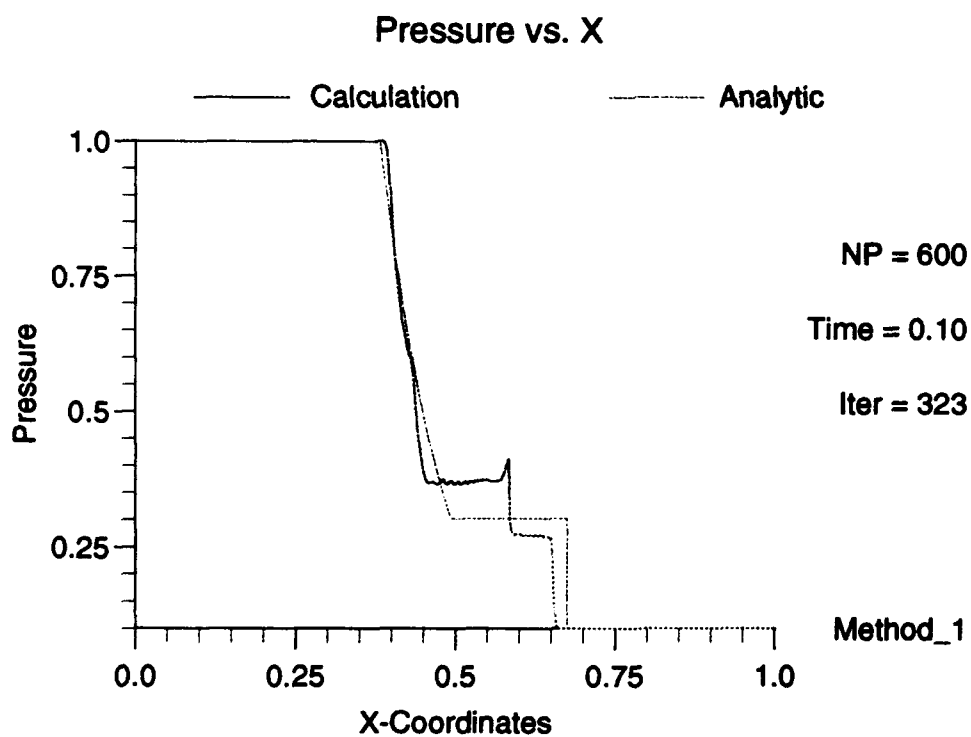
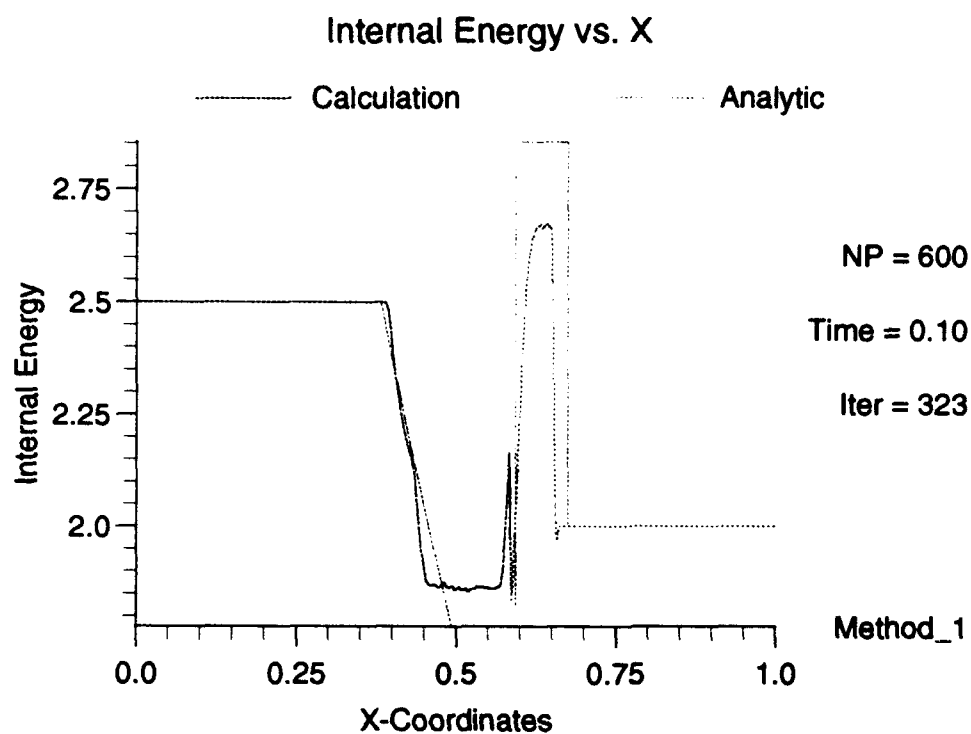


Figure D.6 Shock Tube Results - Method 2

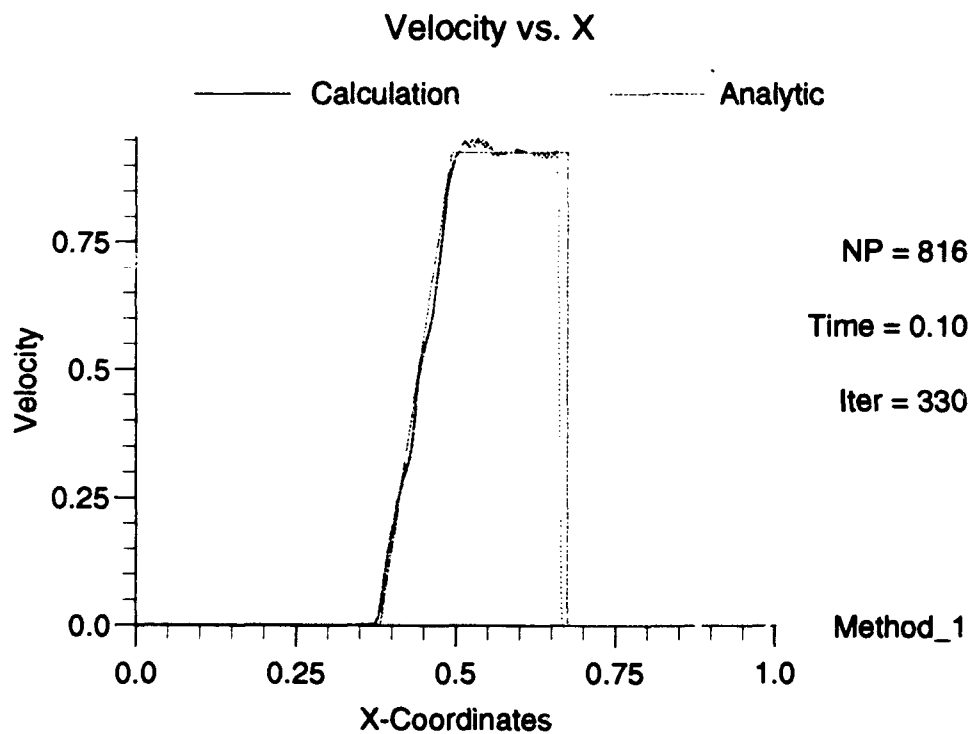
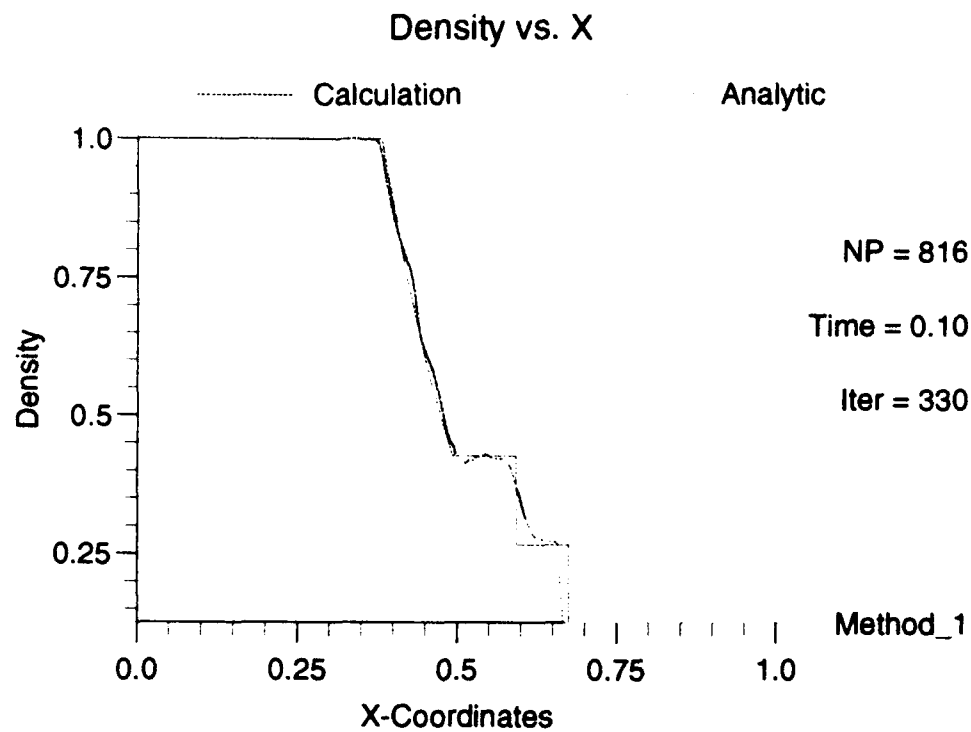


Figure D.7 Shock Tube Results - Method 2 - Extra Particles

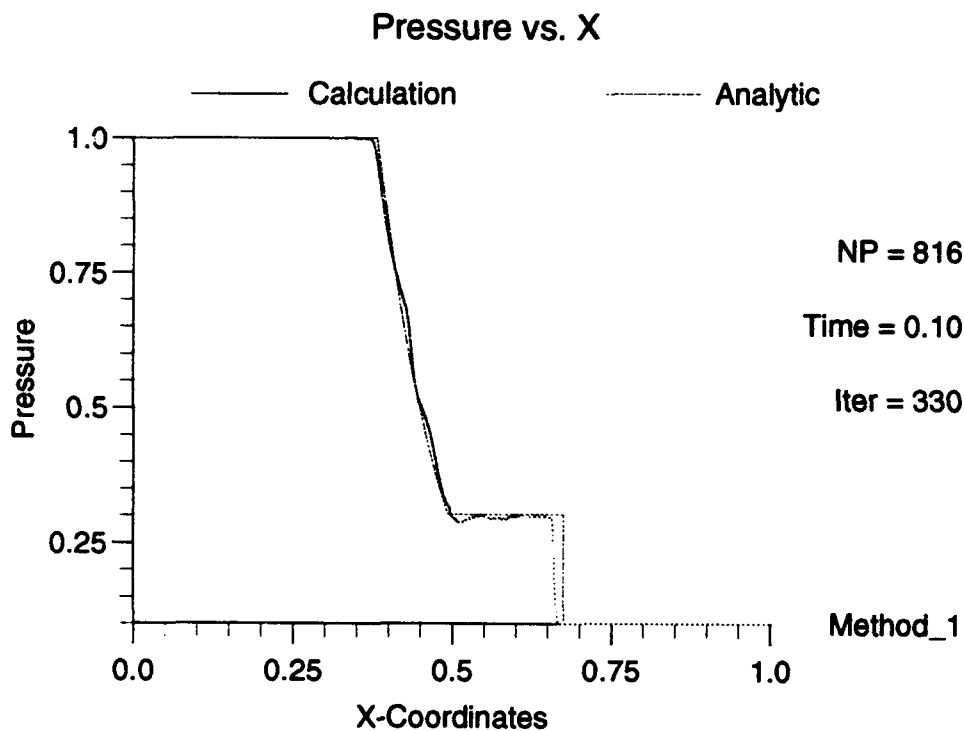
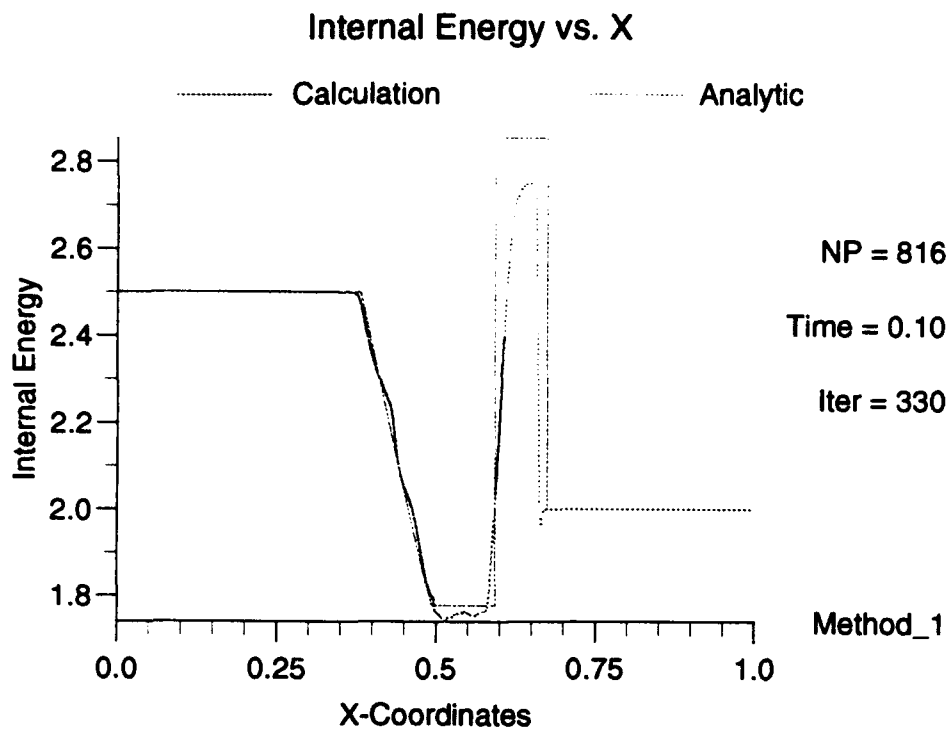


Figure D.8 Shock Tube Results - Method 2 - Extra Particles

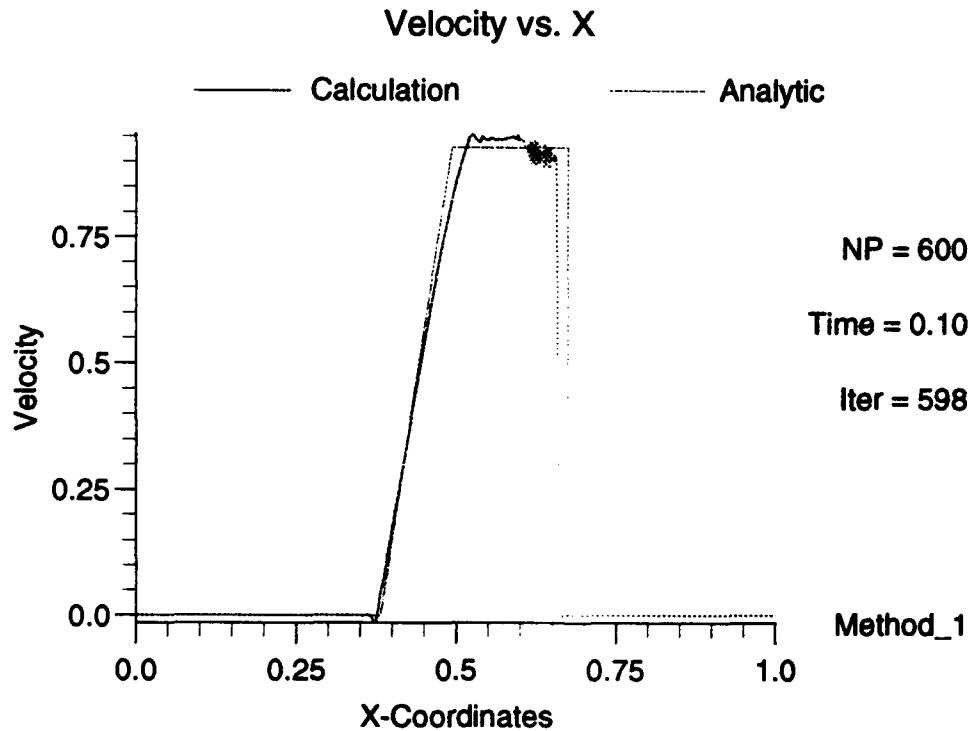
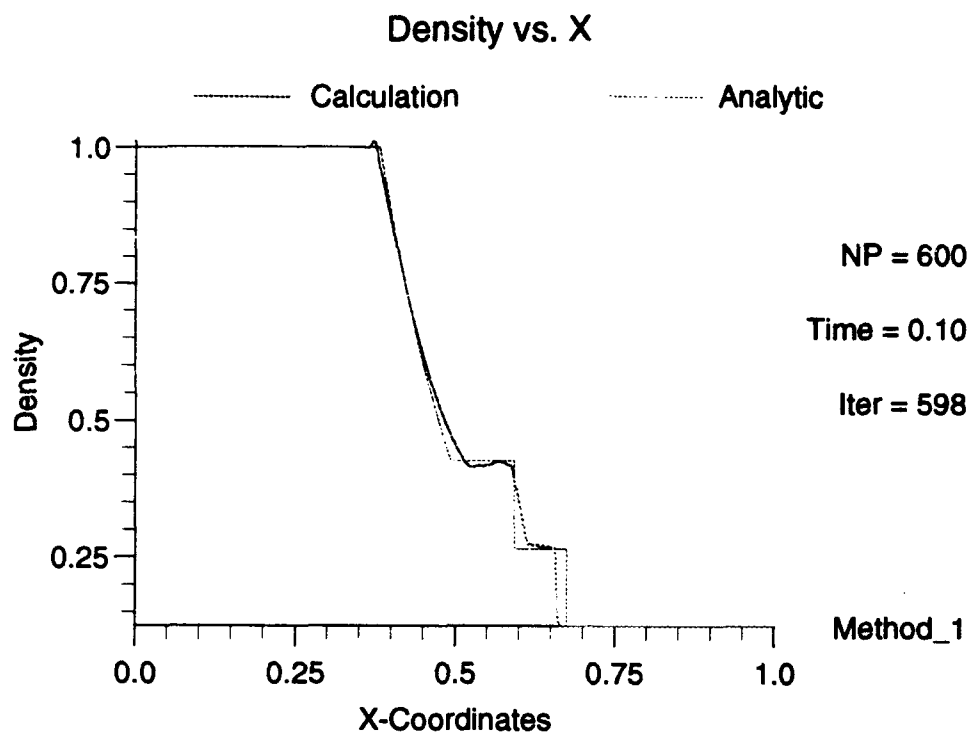


Figure D.9 Shock Tube Results - Method 2 - Variable h

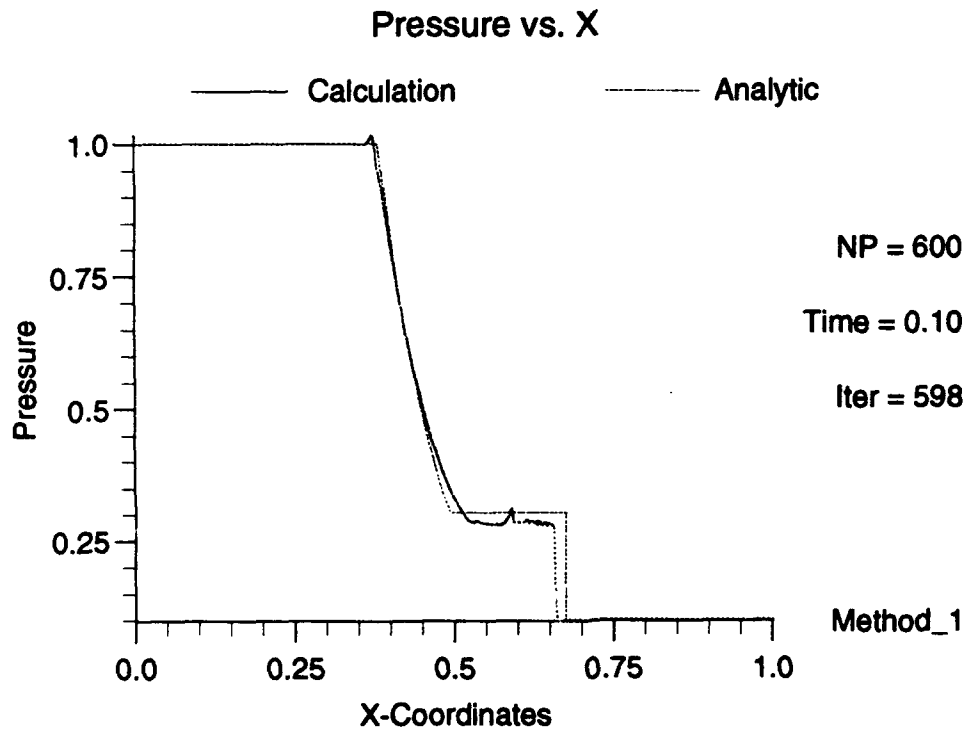
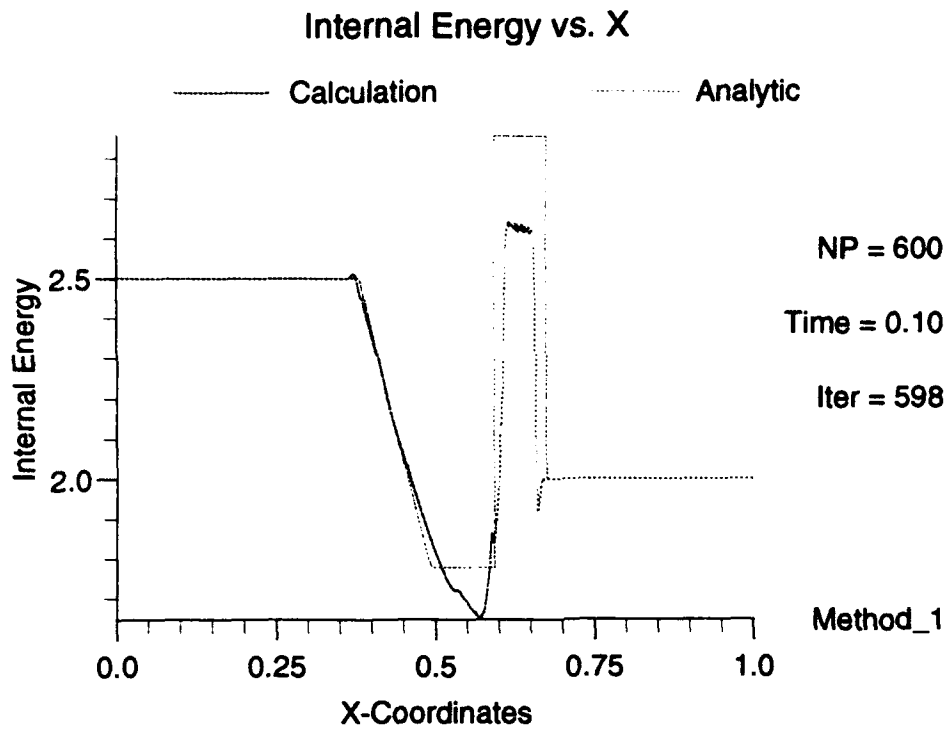


Figure D.10 Shock Tube Results - Method 2 - Variable h

D.4 Methods 4, 6, and 8

Points	Test	Norm	Density	Velocity	Energy	Pressure
1000	N	1	.283069D-01	.205381D+00	.251389D-01	.347989D-01
1000	N	2	.526087D-01	.361139D+00	.745590D-01	.683318D-01
1000	N	∞	.140611D+00	.100102D+01	.310291D+00	.203196D+00
part	N	1	.275758D-01	.195260D+00	.294965D-01	.290924D-01
part	N	2	.780543D-01	.345100D+00	.892641D-01	.869584D-01
part	N	∞	.100000D+01	.100112D+01	.876105D+00	.100000D+01
1000	A	1	.303552D-01	.191807D+00	.370719D-01	.406586D-01
1000	A	2	.502913D-01	.361574D+00	.981243D-01	.691604D-01
1000	A	∞	.141798D+00	.101271D+01	.367483D+00	.207433D+00
part	A	1	.327297D-01	.189121D+00	.530991D-01	.402106D-01
part	A	2	.784696D-01	.347643D+00	.125065D+00	.897604D-01
part	A	∞	.100000D+01	.101320D+01	.876105D+00	.100000D+01
1000	E	1	.162784D-01	.137771D+00	.175494D-01	.194683D-01
1000	E	2	.362037D-01	.309025D+00	.634948D-01	.485241D-01
1000	E	∞	.140609D+00	.100131D+01	.311787D+00	.203172D+00
part	E	1	.221256D-01	.118829D+00	.255566D-01	.217069D-01
part	E	2	.664389D-01	.284307D+00	.806376D-01	.719843D-01
part	E	∞	.100000D+01	.100140D+01	.876105D+00	.100000D+01

Table D.3 Relative Error Norms for Method 4

Points	Test	Norm	Density	Velocity	Energy	Pressure
1000	N	1	.320046D-01	.244760D+00	.280627D-01	.392781D-01
1000	N	2	.576079D-01	.406452D+00	.810759D-01	.749086D-01
1000	N	∞	.140631D+00	.100213D+01	.312249D+00	.203236D+00
part	N	1	.314685D-01	.232772D+00	.326706D-01	.333819D-01
part	N	2	.810679D-01	.388575D+00	.949093D-01	.916139D-01
part	N	∞	.100000D+01	.100259D+01	.876105D+00	.100000D+01

Table D.4 Relative Error Norms for Method 6

Points	Test	Norm	Density	Velocity	Energy	Pressure
1000	N	1	.280756E-01	.193621E+00	.238426E-01	.349017E-01
1000	N	2	.520783E-01	.336727E+00	.690458E-01	.661071E-01
1000	N	∞	.140695E+00	.100210E+01	.313196E+00	.203416E+00
part	N	1	.262176E-01	.181903E+00	.285280E-01	.296929E-01
part	N	2	.769434E-01	.319691E+00	.844894E-01	.850875E-01
part	N	∞	.100000E+01	.100247E+01	.876105E+00	.100000E+01
1000	E	1	.123757E-01	.950932E-01	.139468E-01	.138385E-01
1000	E	2	.312280E-01	.264959E+00	.570272E-01	.411868E-01
1000	E	∞	.140709E+00	.100424E+01	.316054E+00	.203306E+00
part	E	1	.190226E-01	.815595E-01	.220675E-01	.164351E-01
part	E	2	.639188E-01	.242847E+00	.759615E-01	.672266E-01
part	E	∞	.100000E+01	.100534E+01	.876105E+00	.100000E+01

Table D.5 Relative Error Norms for Method 8

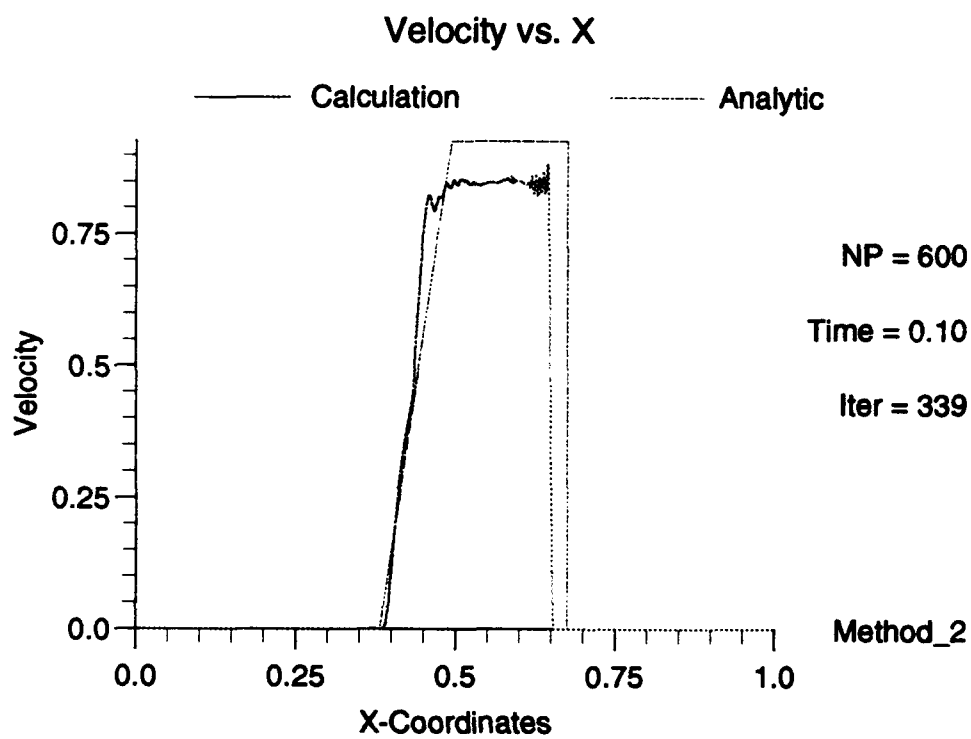
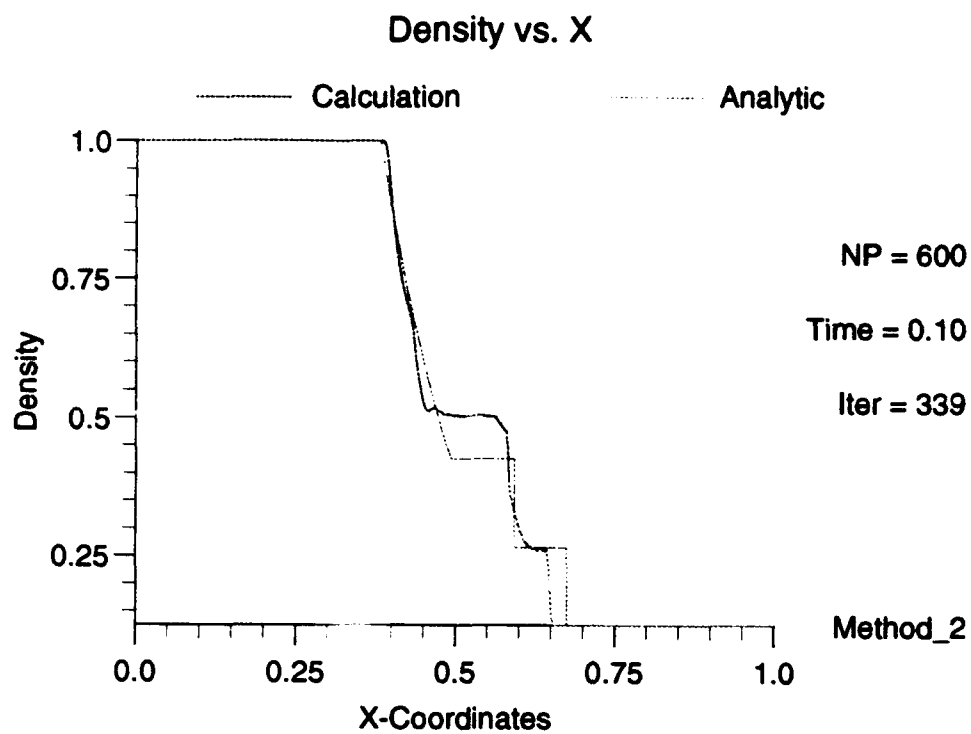


Figure D.11 Shock Tube Results - Method 4

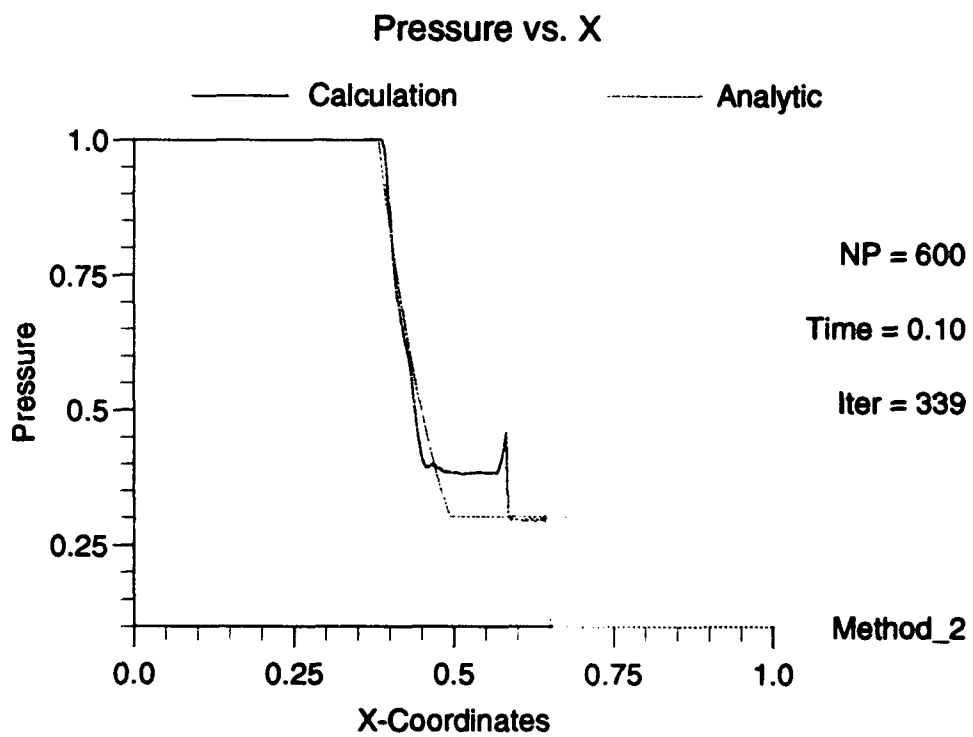
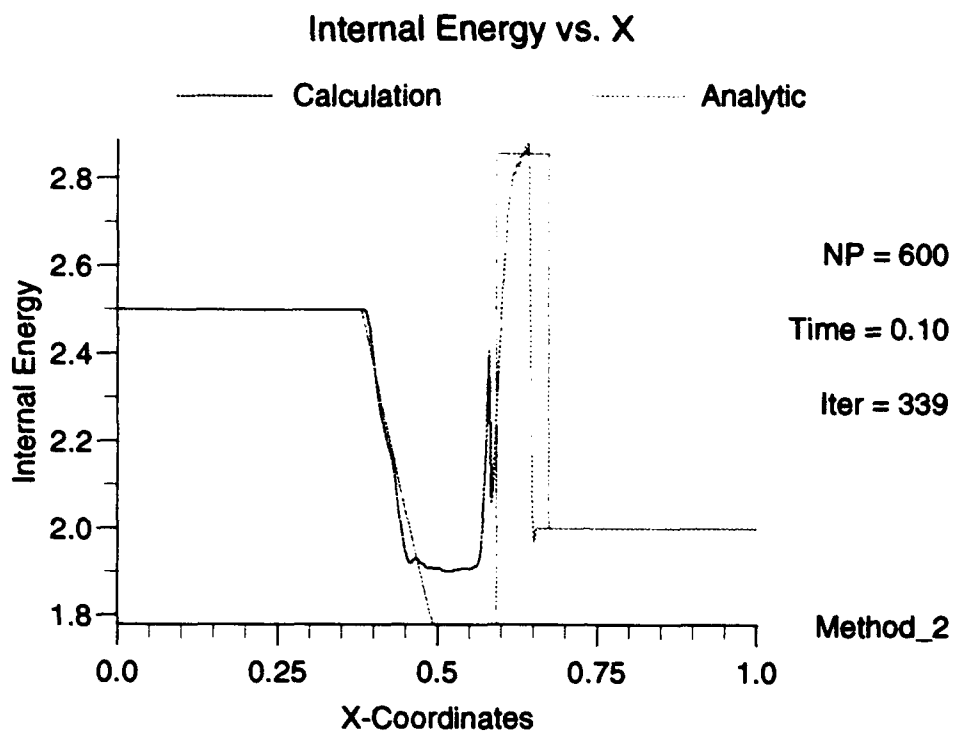


Figure D.12 Shock Tube Results - Method 4

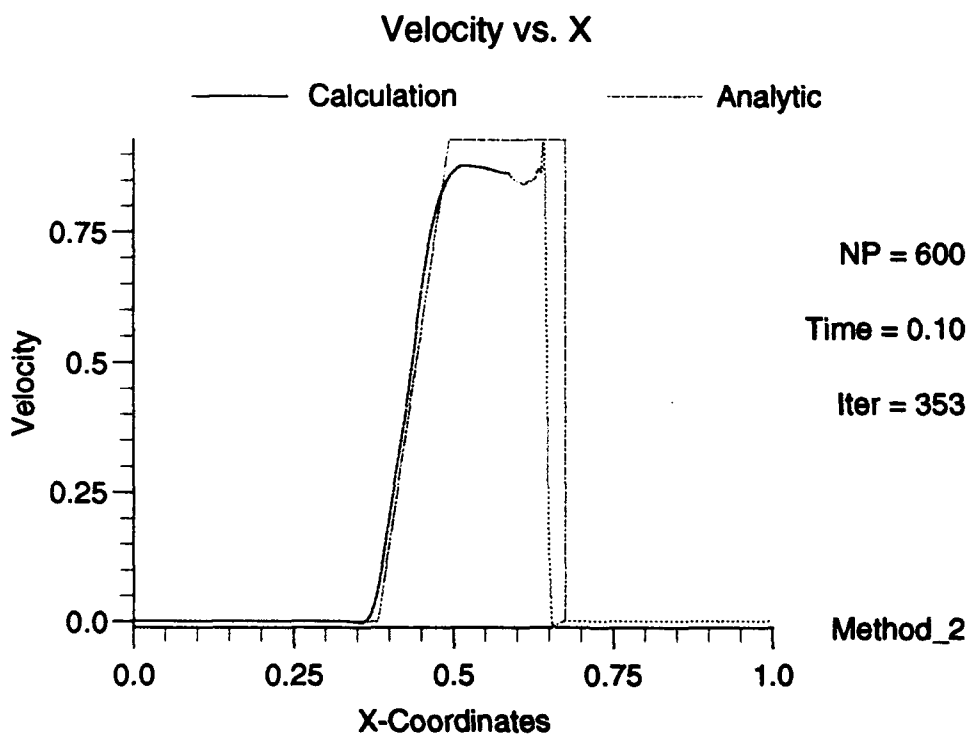
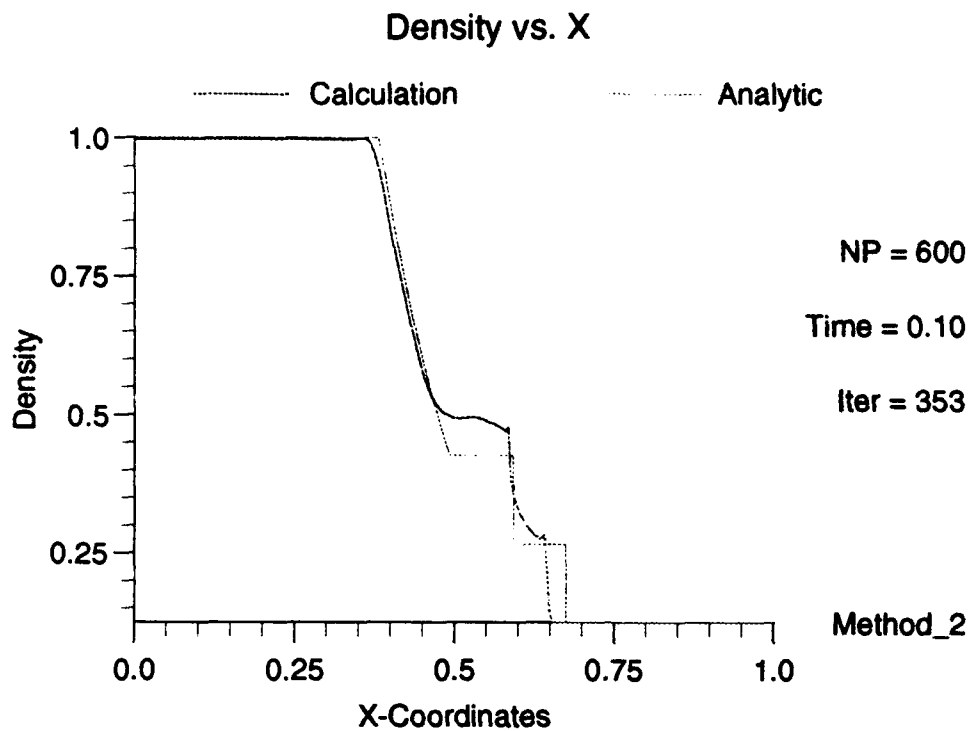


Figure D.13 Shock Tube Results - Method 4 - Always Average

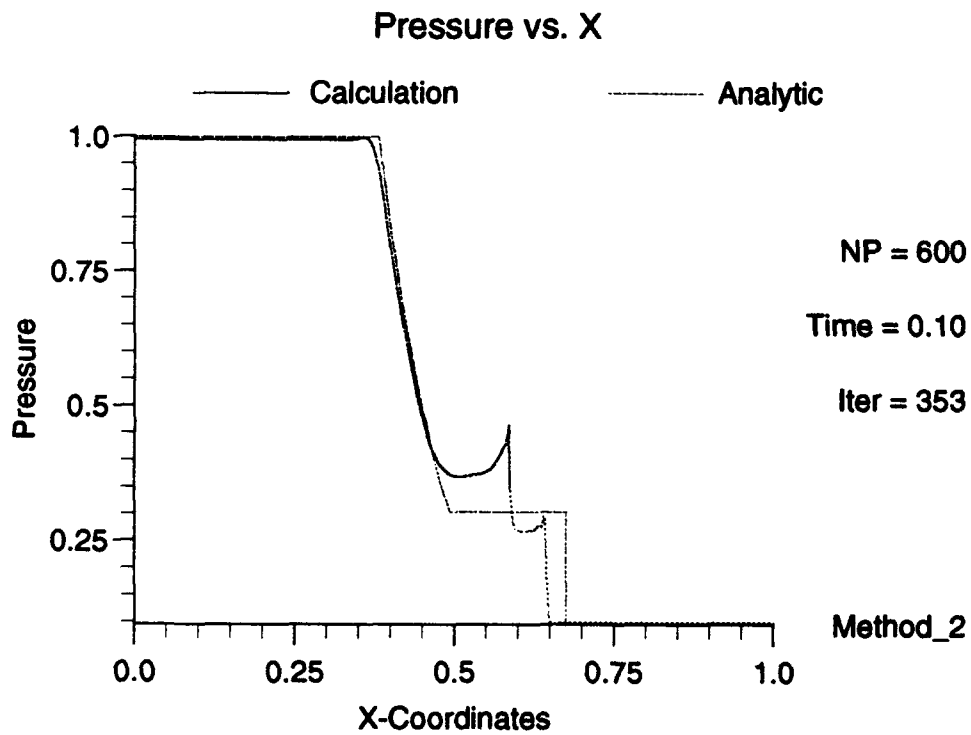
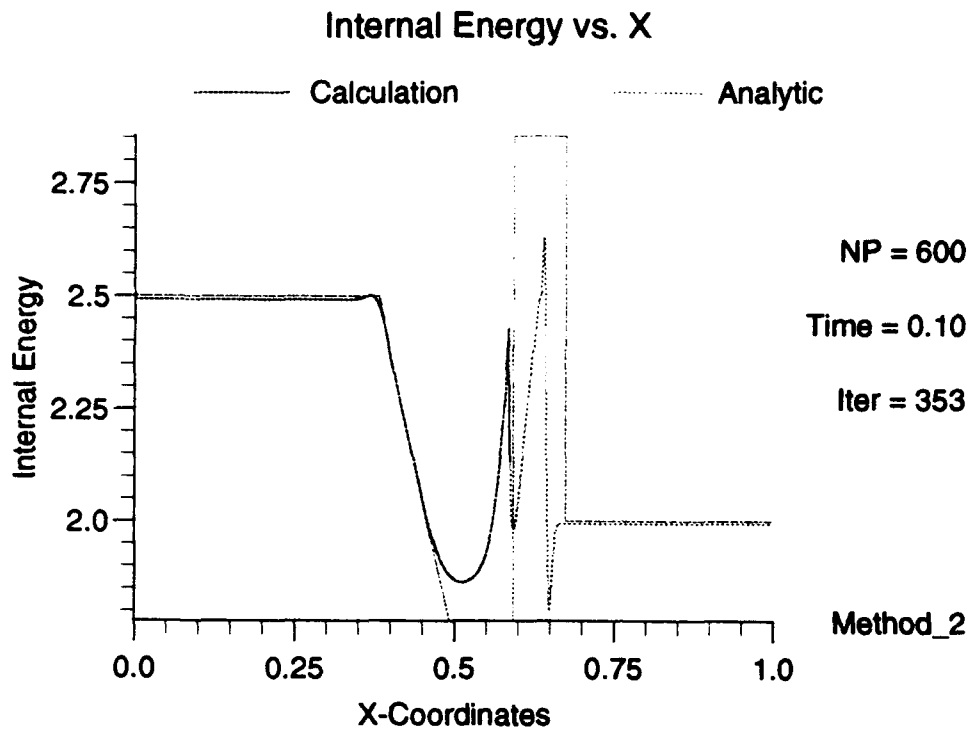


Figure D.14 Shock Tube Results - Method 4 - Always Average

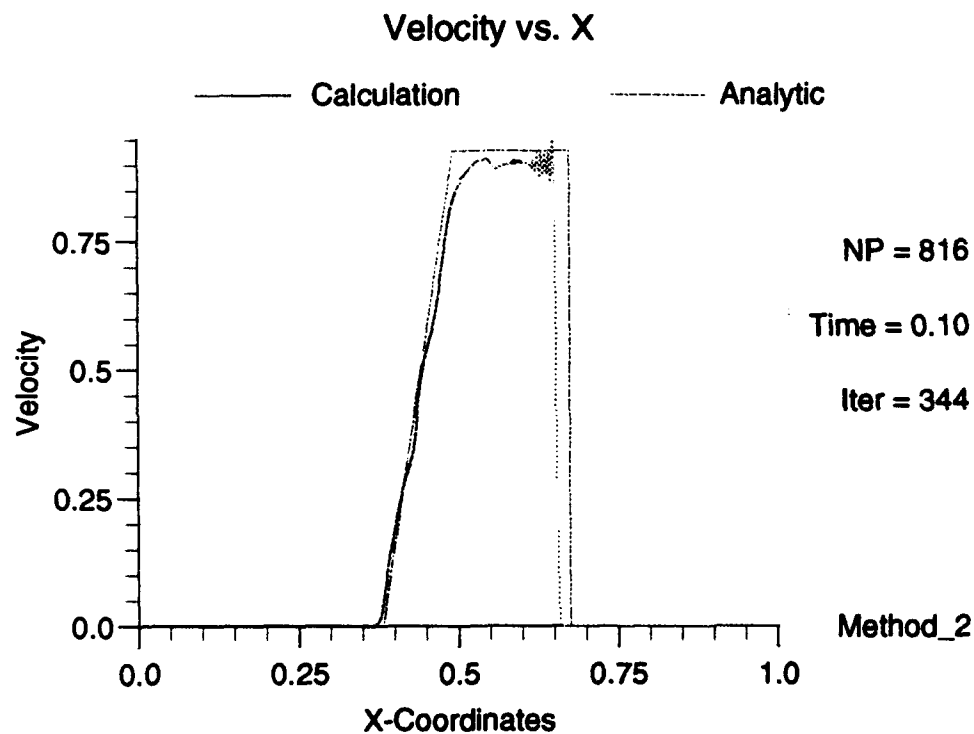
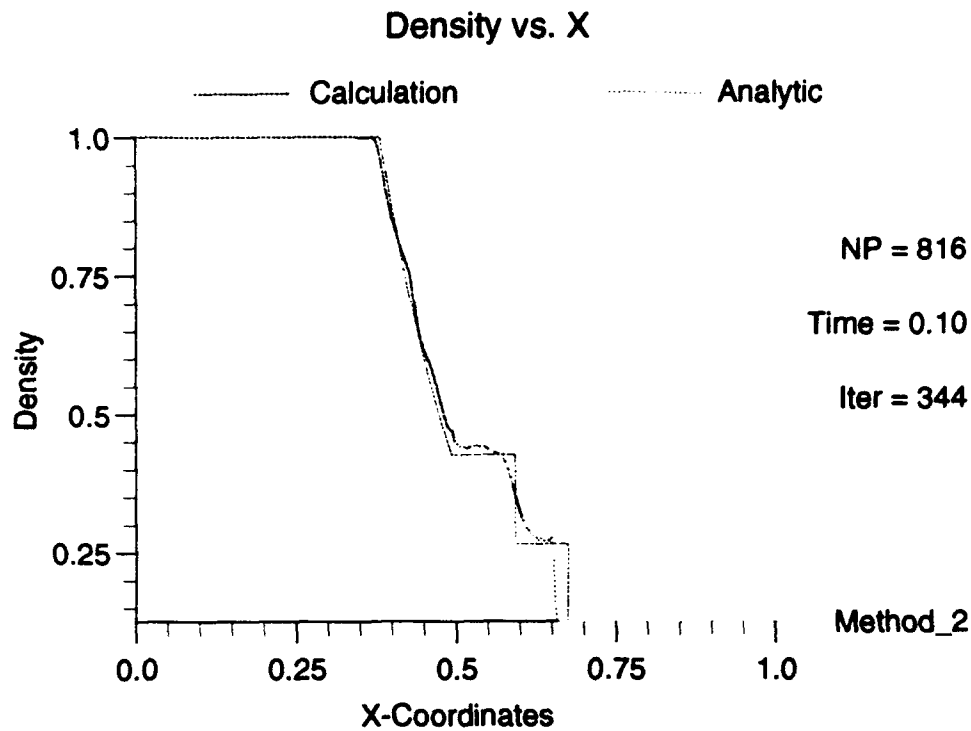


Figure D.15 Shock Tube Results - Method 4 - Extra Particles

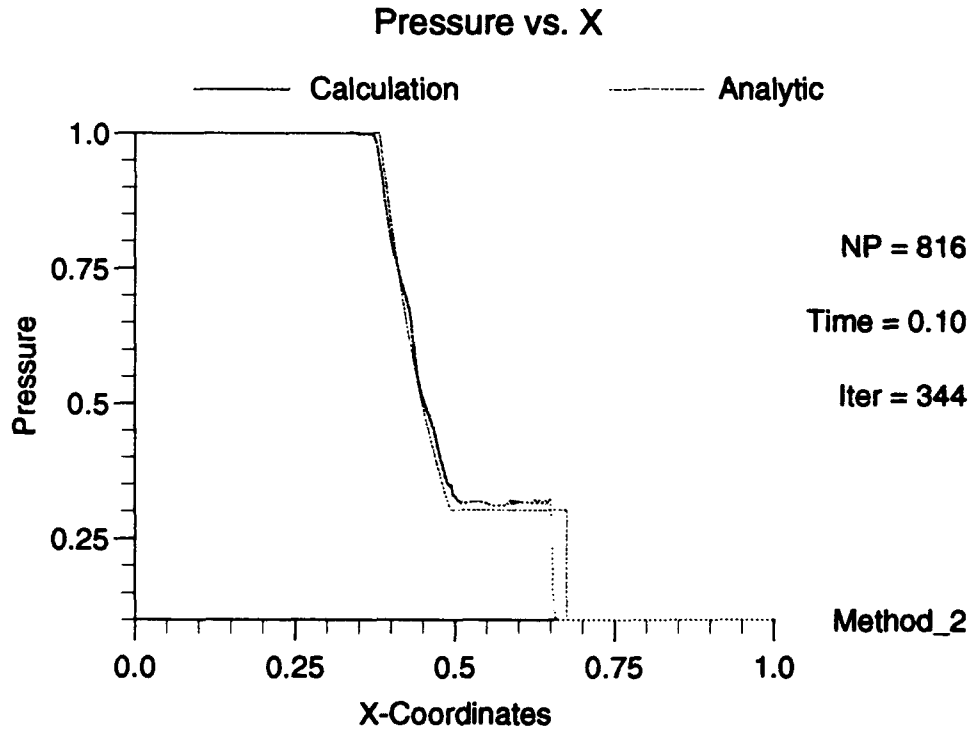
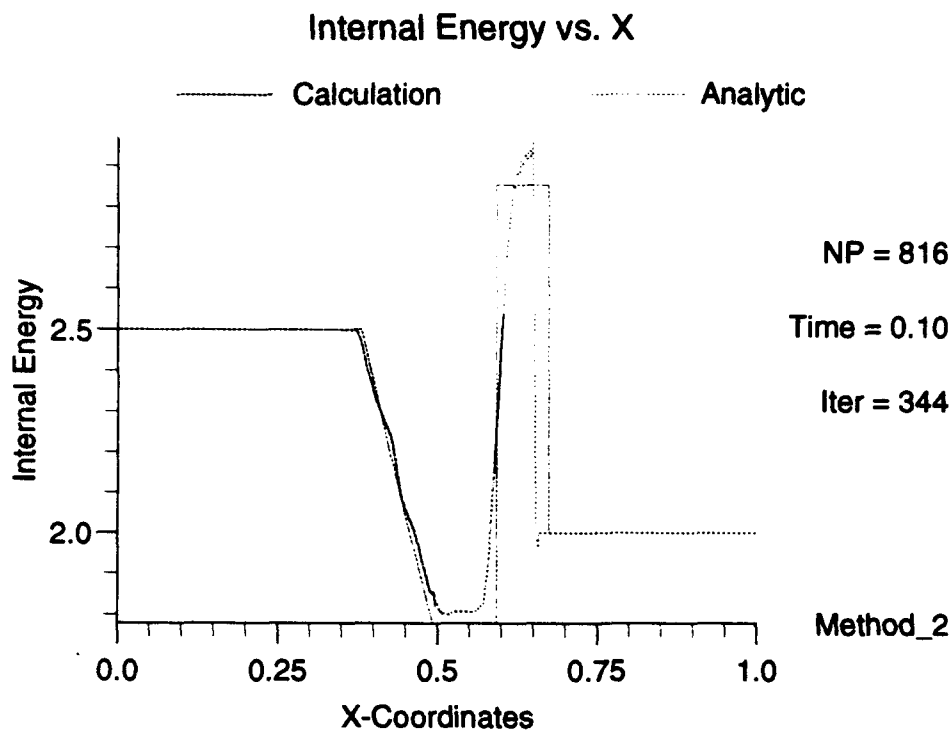


Figure D.16 Shock Tube Results - Method 4 - Extra Particles

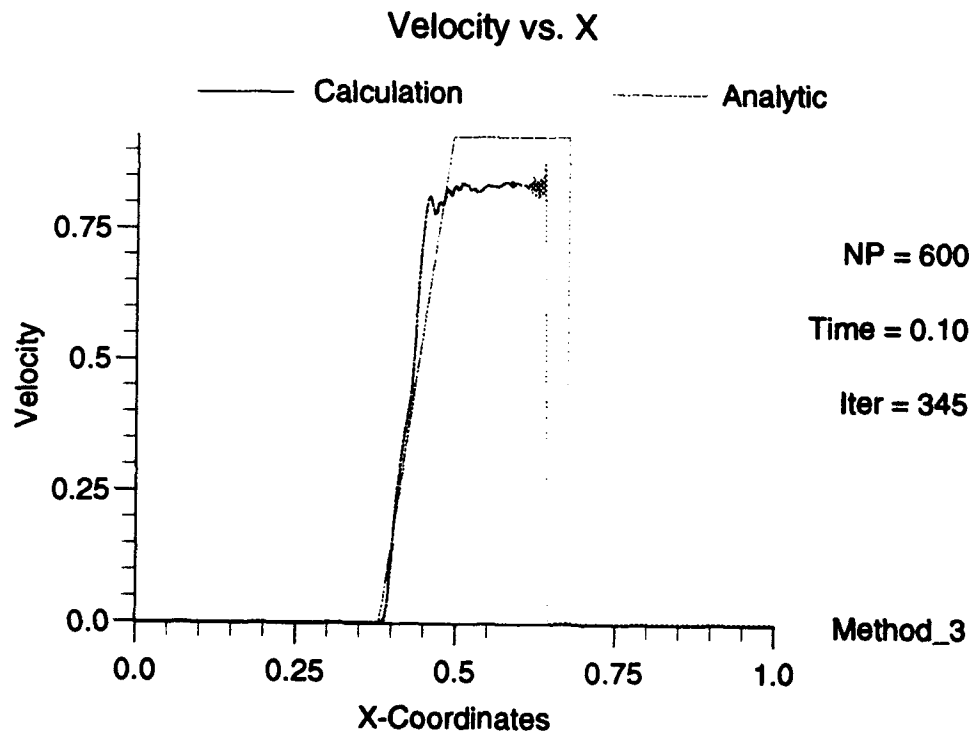
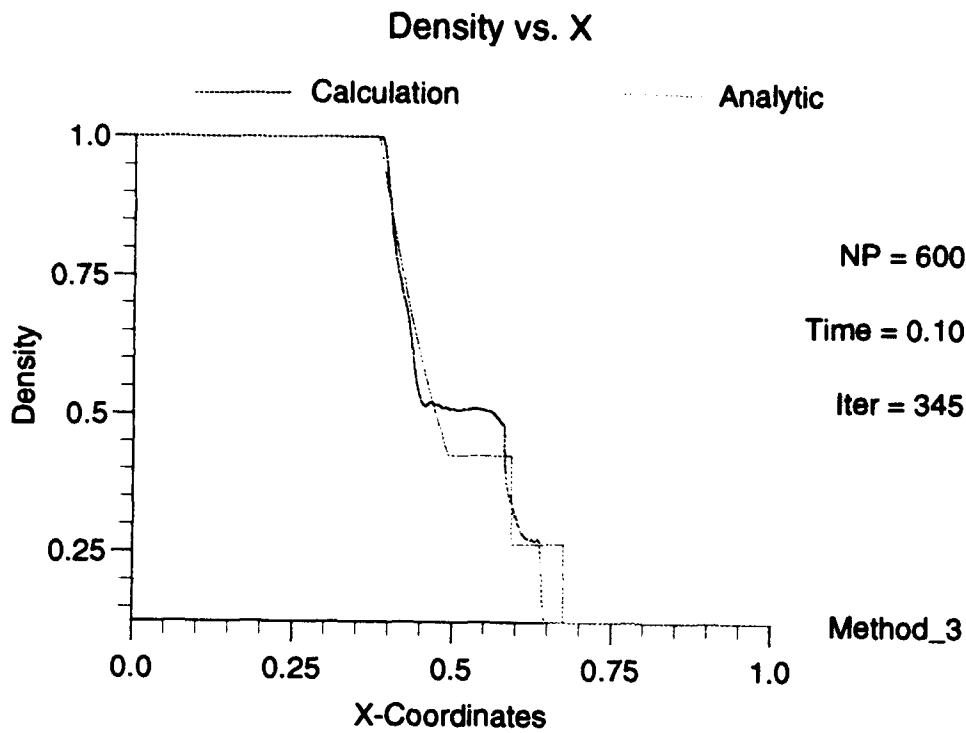


Figure D.17 Shock Tube Results - Method 6

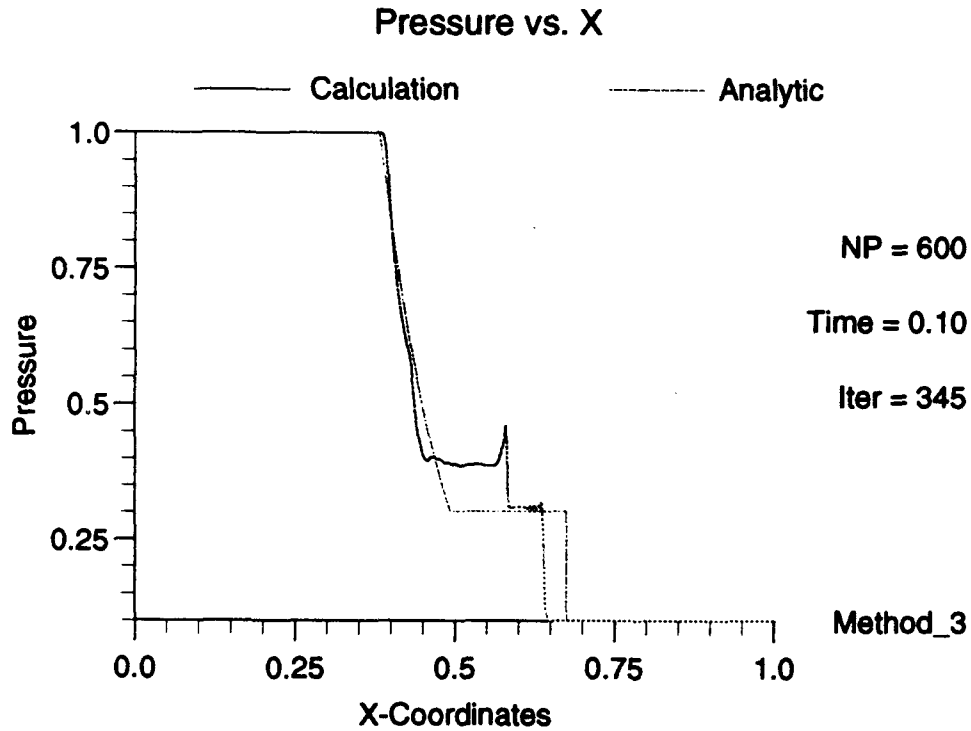
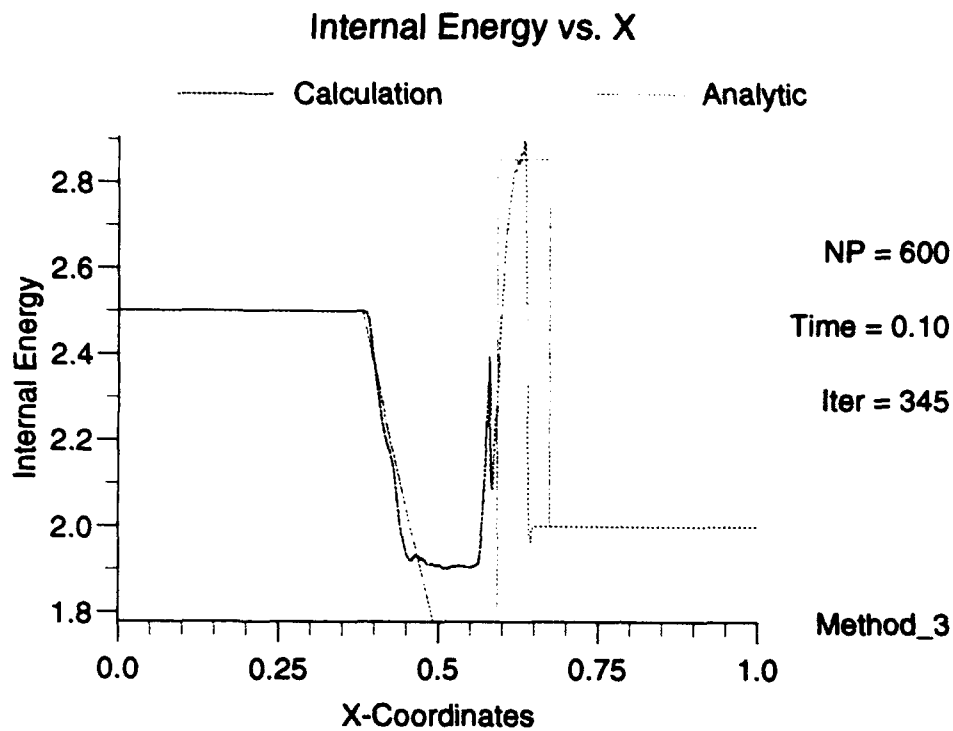


Figure D.18 Shock Tube Results - Method 6

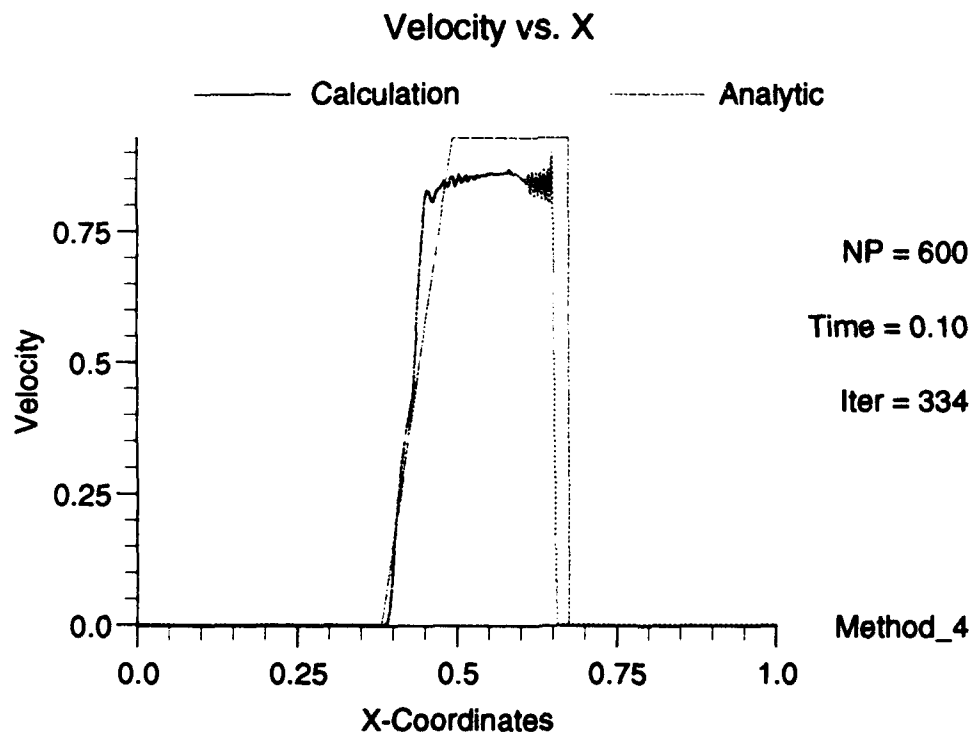
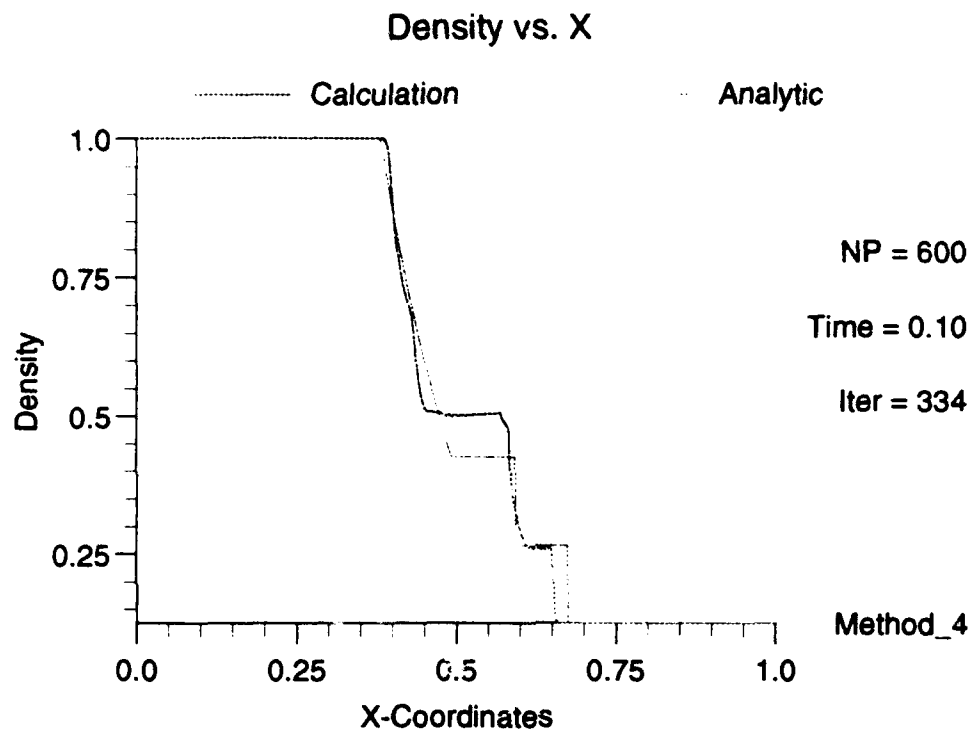


Figure D.19 Shock Tube Results - Method 8

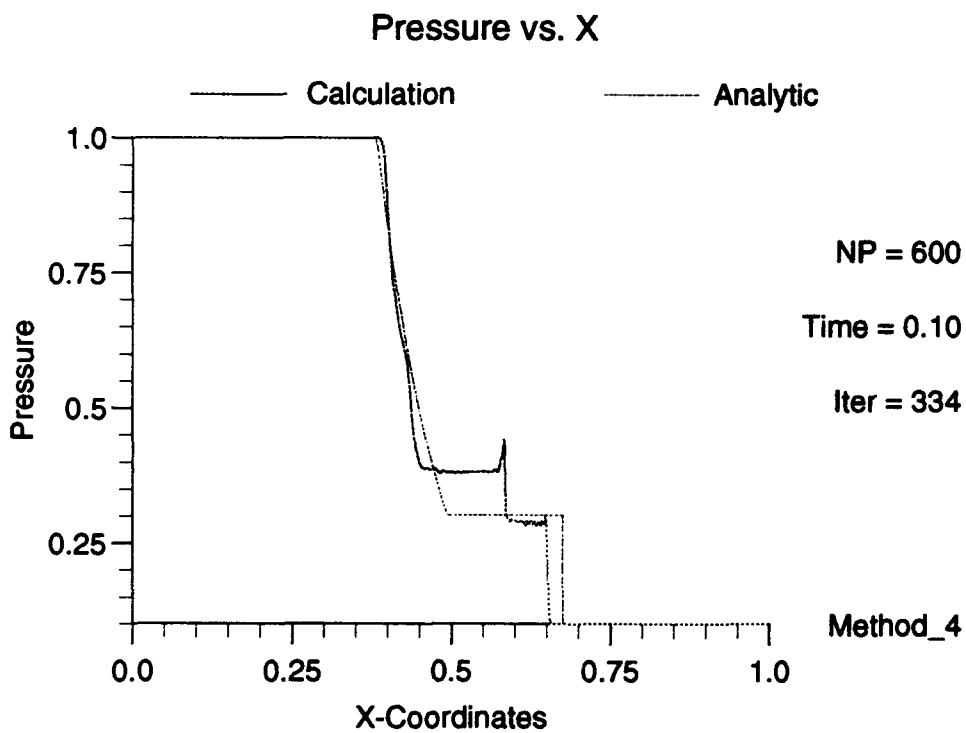
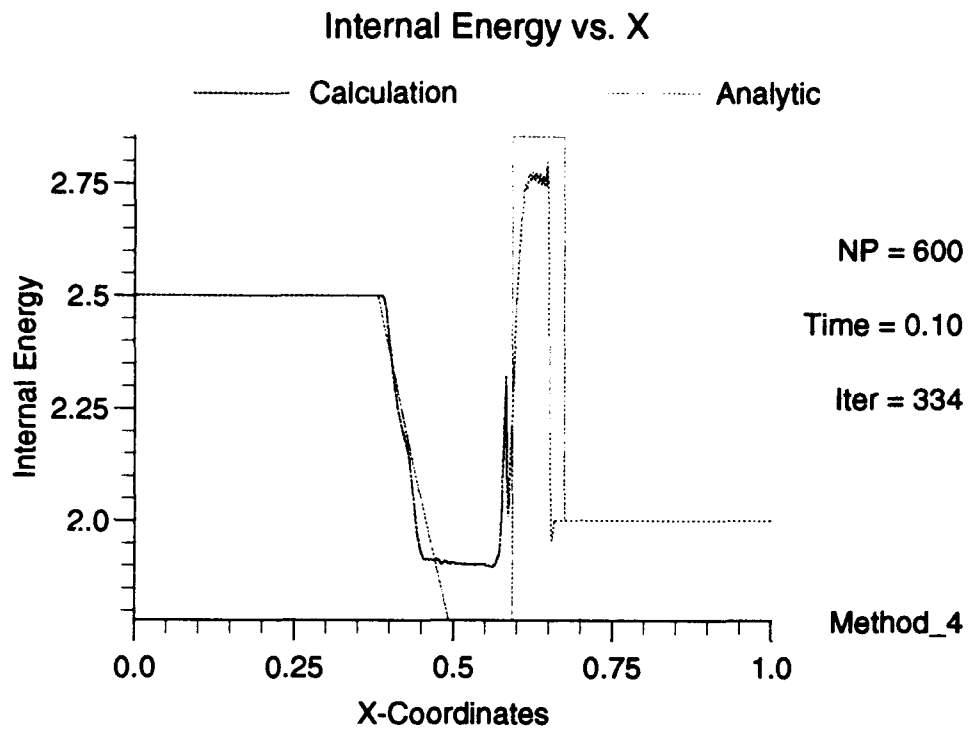


Figure D.20 Shock Tube Results - Method 8

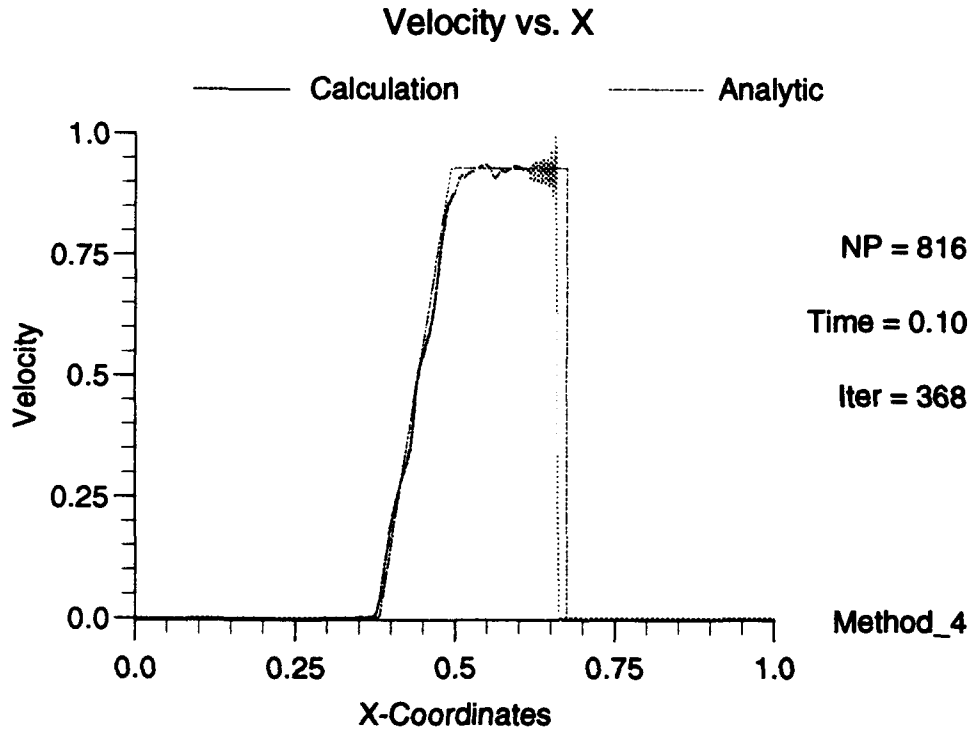
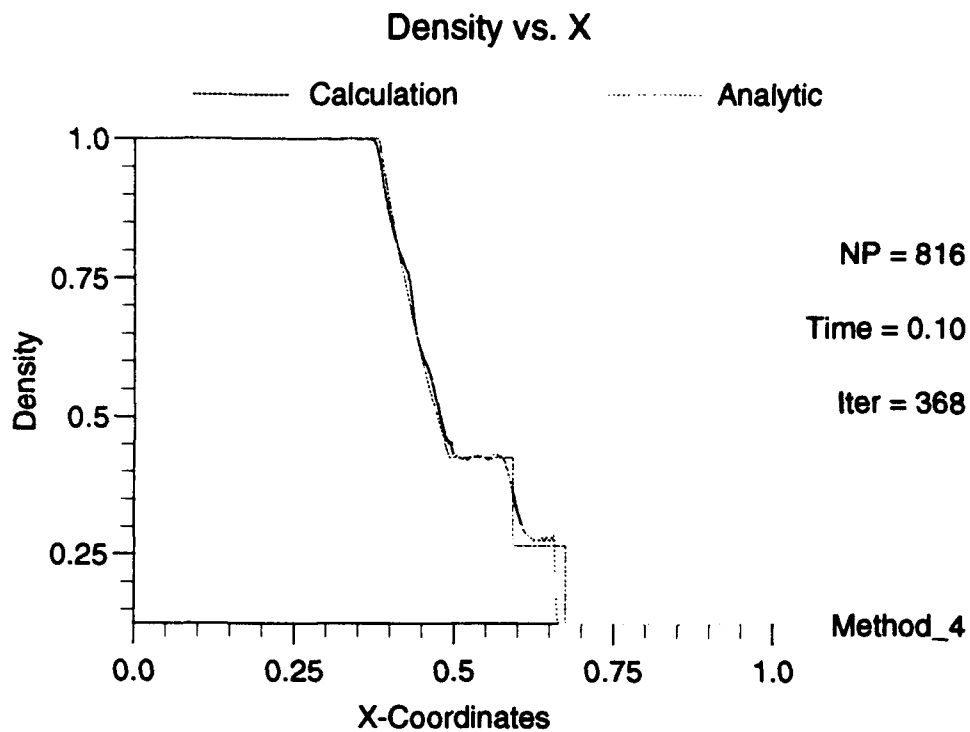


Figure D.21 Shock Tube Results - Method 8 - Extra Particles

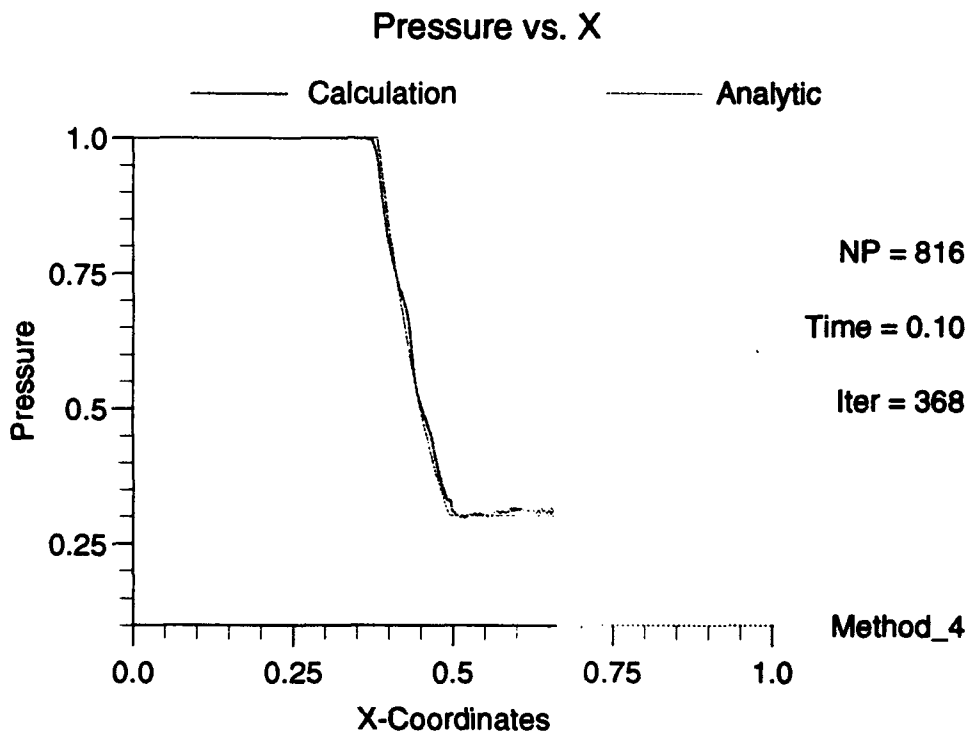
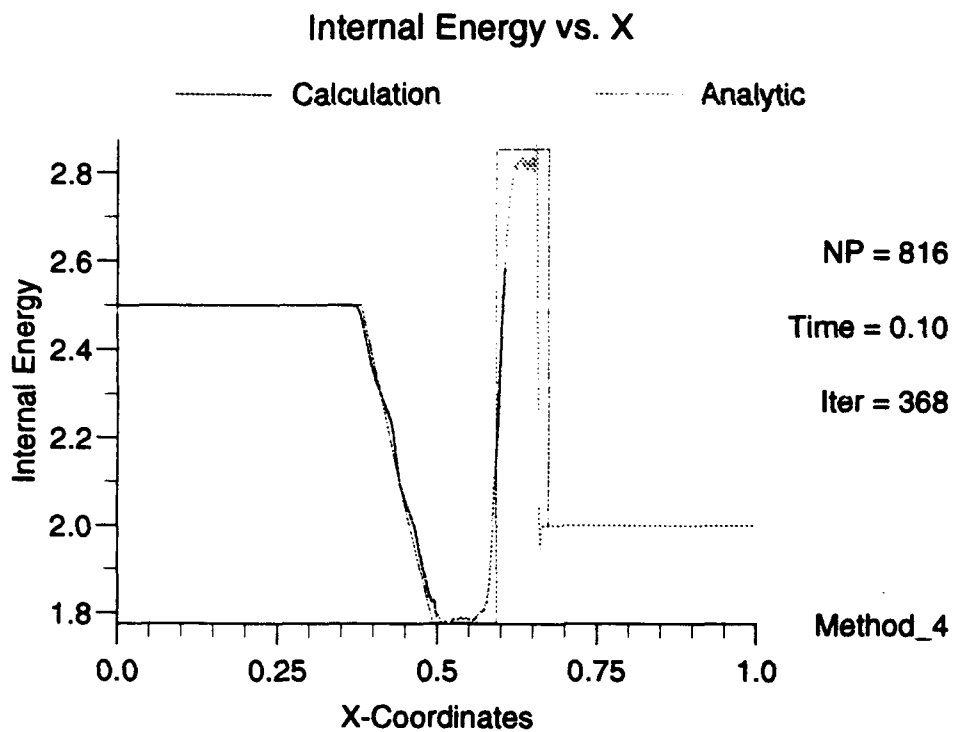


Figure D.22 Shock Tube Results - Method 8 - Extra Particles

D.5 Method 12

Points	Test	Norm	Density	Velocity	Energy	Pressure
1000	N	1	.325480E-01	.158504E+00	.263872E-01	.420911E-01
1000	N	2	.571715E-01	.172209E+00	.601891E-01	.697691E-01
1000	N	∞	.184923E+00	.821038E+00	.276056E+00	.182059E+00
part	N	1	.348307E-01	.159281E+00	.307077E-01	.411532E-01
part	N	2	.839684E-01	.172590E+00	.788086E-01	.870456E-01
part	N	∞	.100000E+01	.775753E+00	.876105E+00	.100000E+01
1000	E	1	.222823E-01	.106705E+00	.236942E-01	.342920E-01
1000	E	2	.392454E-01	.113640E+00	.509963E-01	.533369E-01
1000	E	∞	.165961E+00	.450716E+00	.251182E+00	.129882E+00
part	E	1	.272534E-01	.110921E+00	.278851E-01	.358040E-01
part	E	2	.699270E-01	.118027E+00	.686534E-01	.732711E-01
part	E	∞	.100000E+01	.520853E+00	.876105E+00	.100000E+01

Table D.6 Relative Error Norms for Method 12

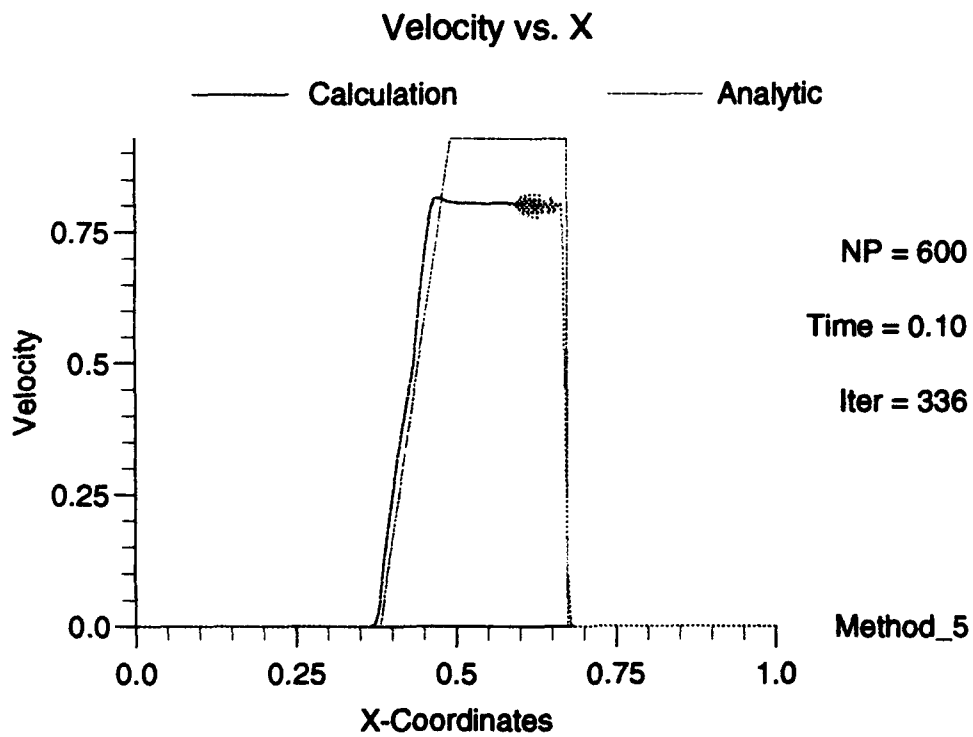
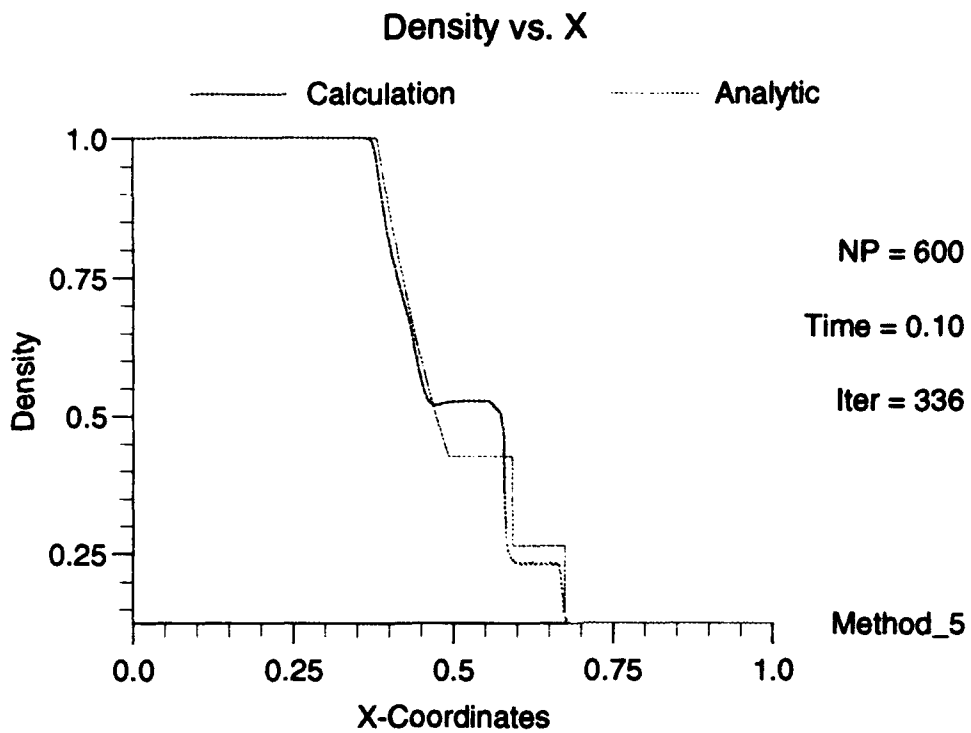


Figure D.23 Shock Tube Results - Method 12

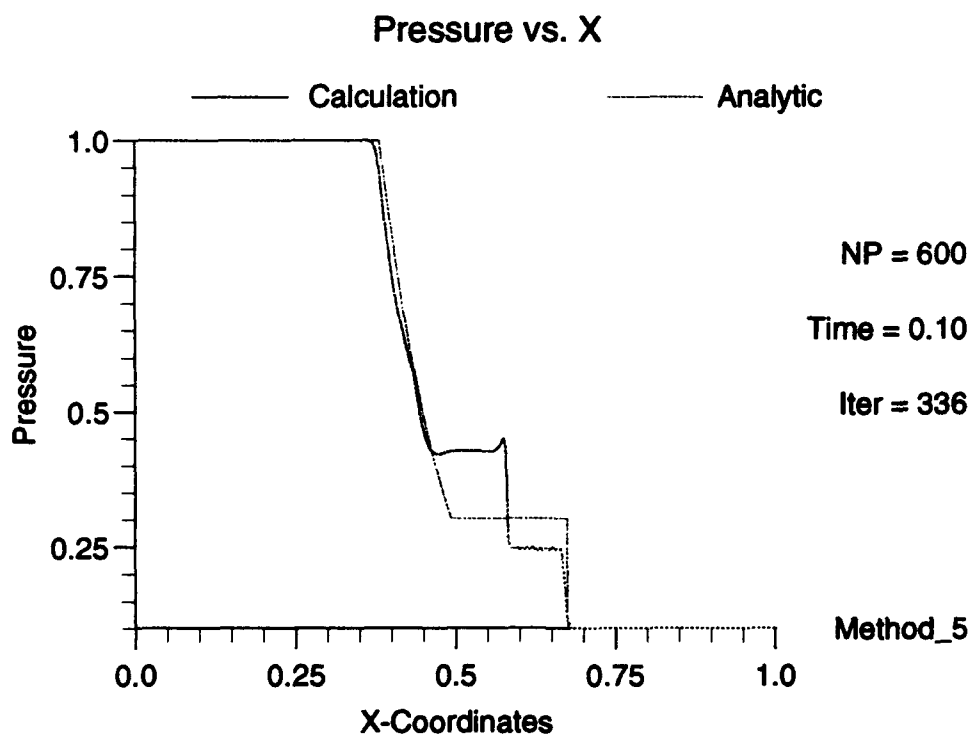
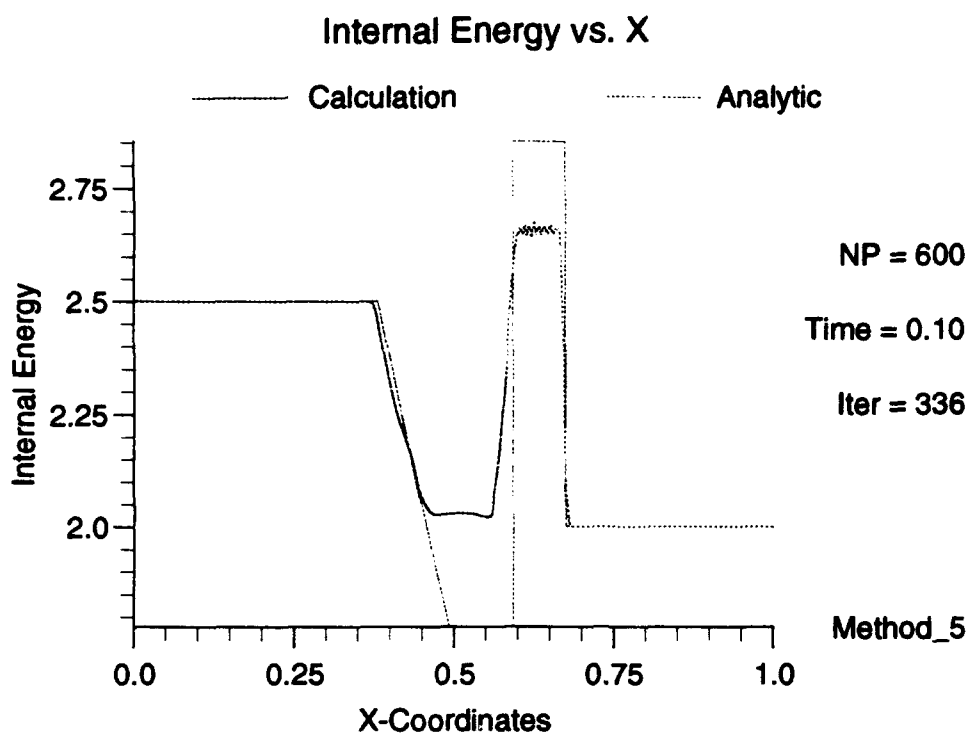


Figure D.24 Shock Tube Results - Method 12

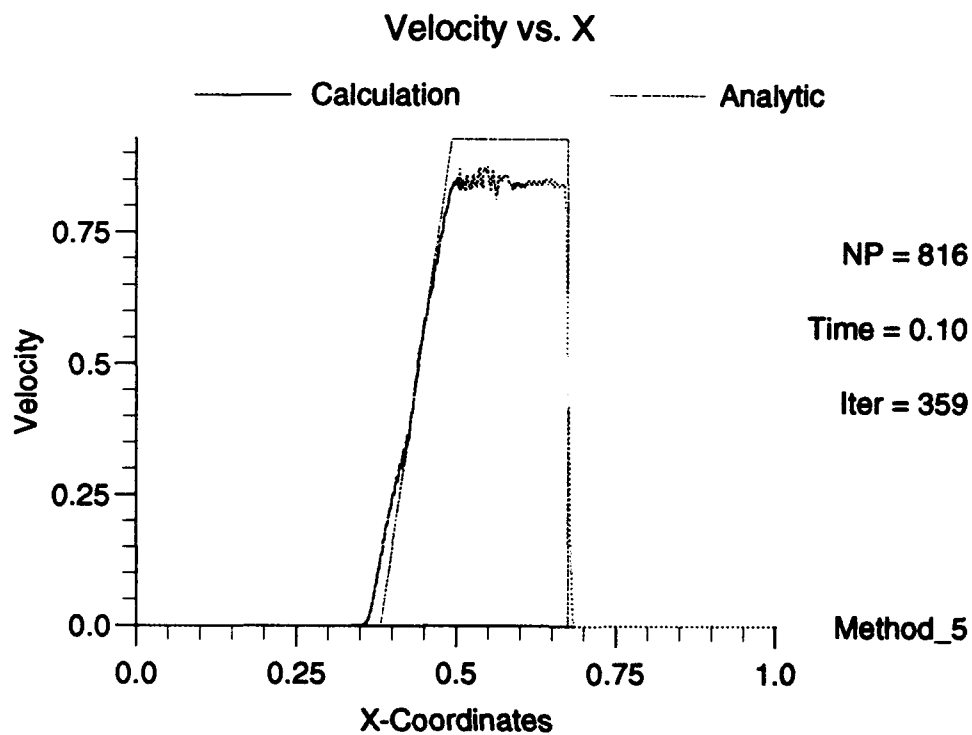
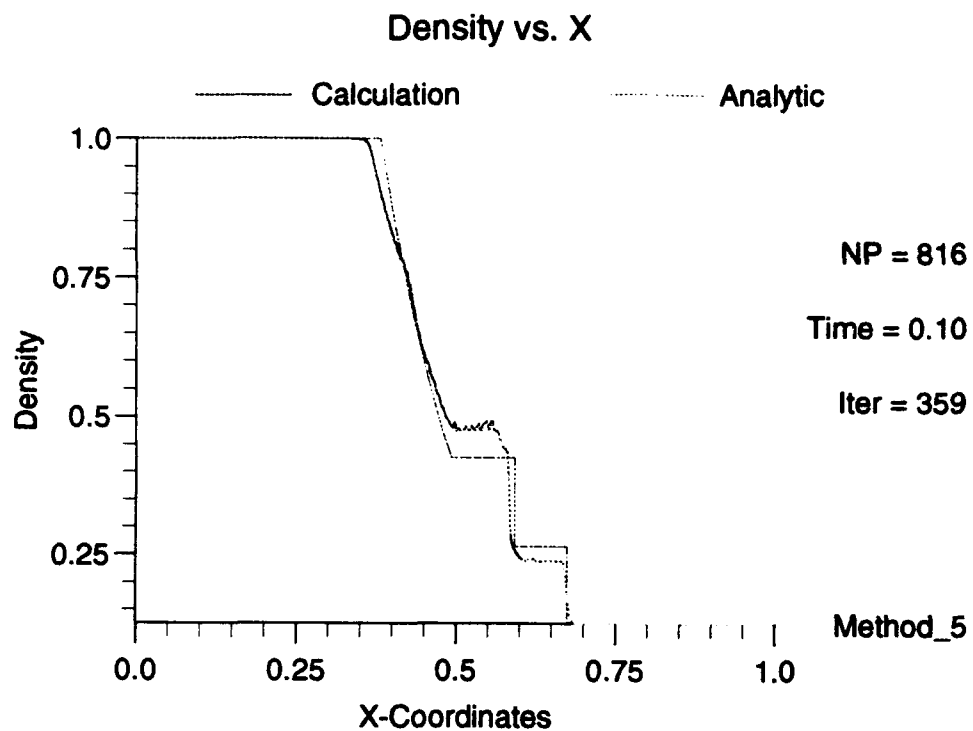


Figure D.25 Shock Tube Results - Method 12 - Extra Particles

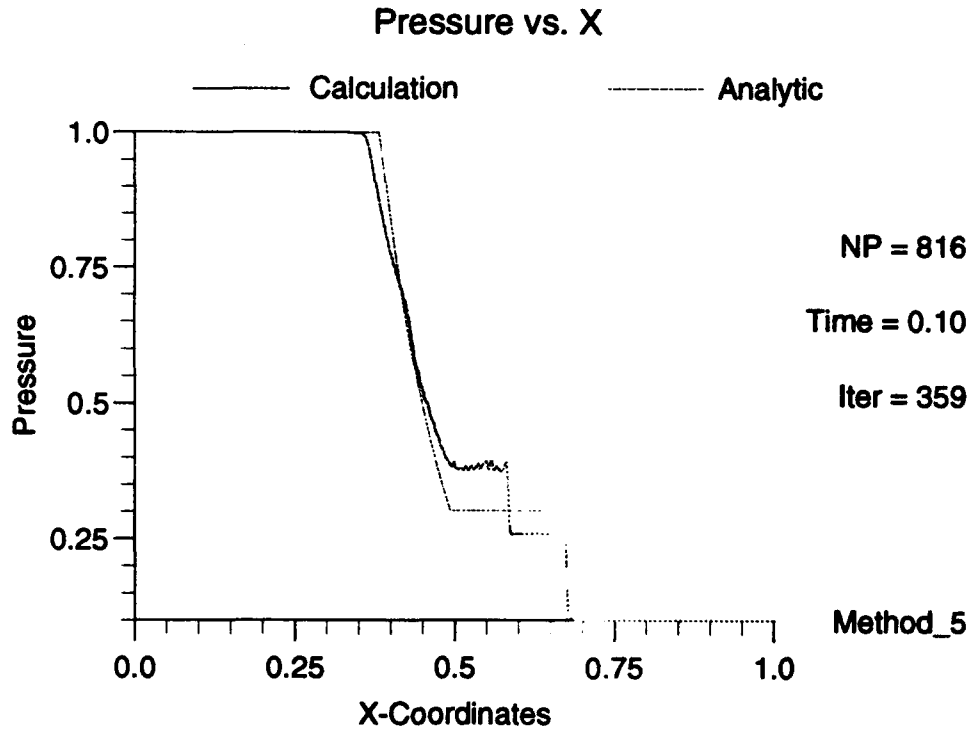
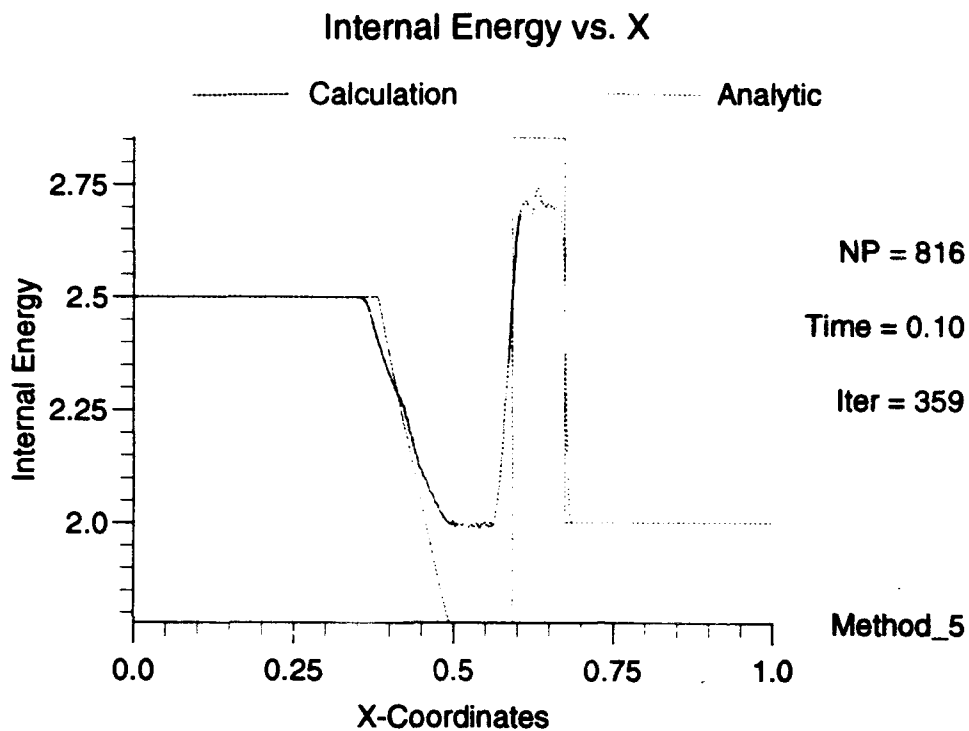


Figure D.26 Shock Tube Results - Method 12 - Extra Particles

D.6 Method 20

Points	Test	Norm	Density	Velocity	Energy	Pressure
1000	N	1	.270497E-01	.124528E+00	.310869E-01	.300437E-01
1000	N	2	.465410E-01	.140433E+00	.816390E-01	.597662E-01
1000	N	∞	.132384E+00	.480361E+00	.494463E+00	.299863E+00
part	N	1	.276355E-01	.110387E+00	.418932E-01	.219570E-01
part	N	2	.748261E-01	.122587E+00	.102776E+00	.760881E-01
part	N	∞	.100000E+01	.409887E+00	.876105E+00	.100000E+01
1000	E	1	.101494E-01	.572613E-01	.167811E-01	.117158E-01
1000	E	2	.198756E-01	.998780E-01	.500583E-01	.233546E-01
1000	E	∞	.119849E+00	.847343E+00	.296220E+00	.186041E+00
part	E	1	.151330E-01	.548147E-01	.288455E-01	.152906E-01
part	E	2	.578502E-01	.956049E-01	.752466E-01	.586174E-01
part	E	∞	.100000E+01	.807053E+00	.876105E+00	.100000E+01

Table D.7 Relative Error Norms for Method 20

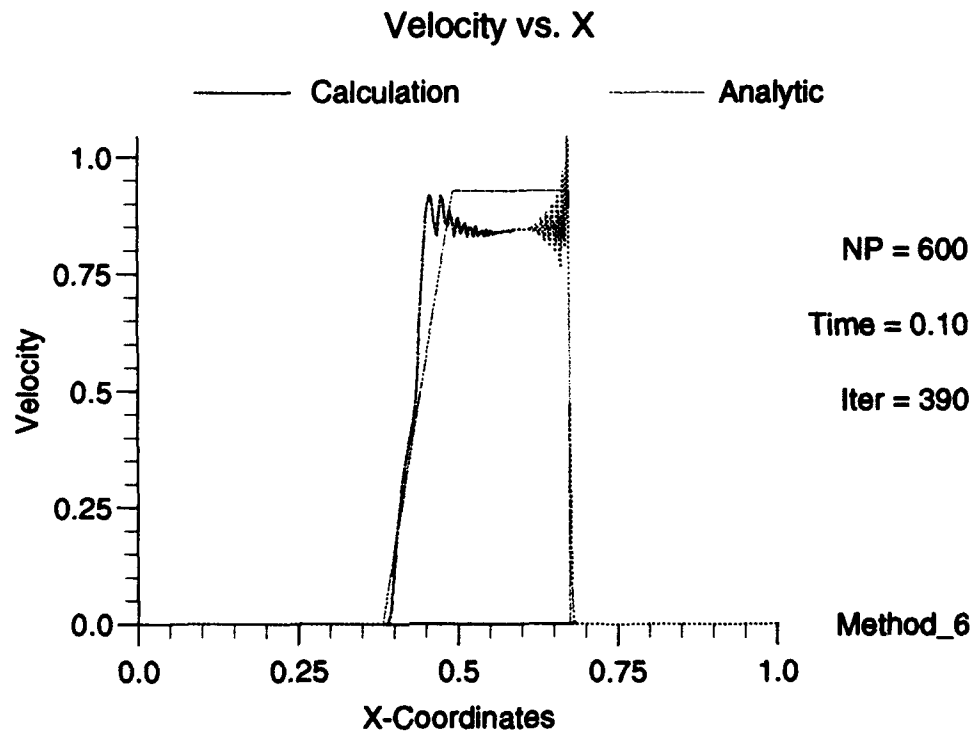
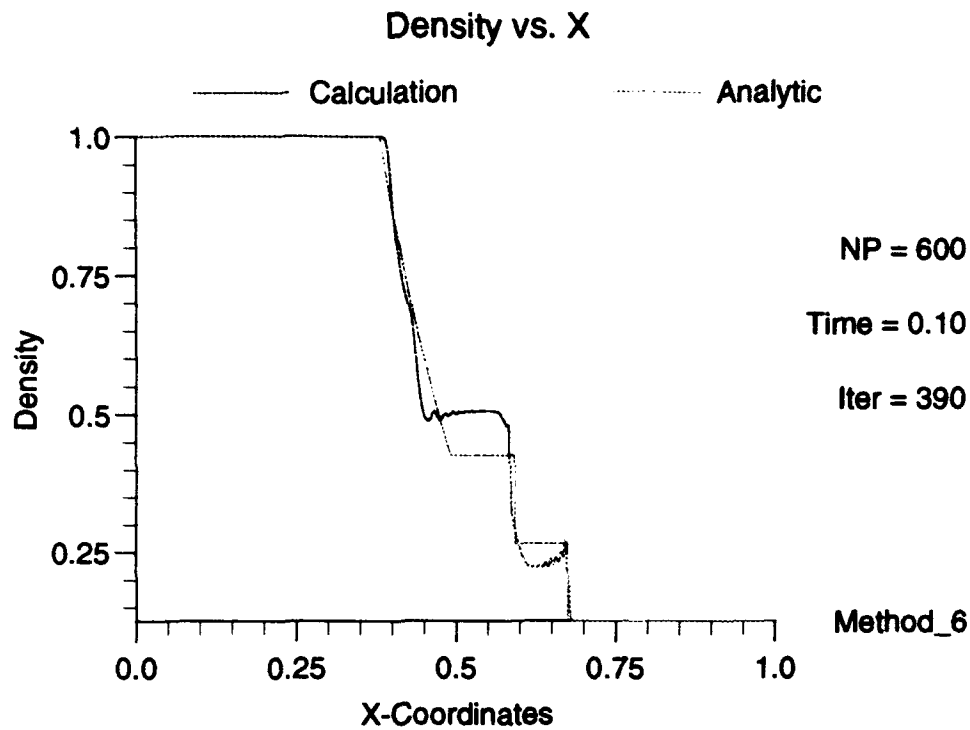


Figure D.27 Shock Tube Results - Method 20

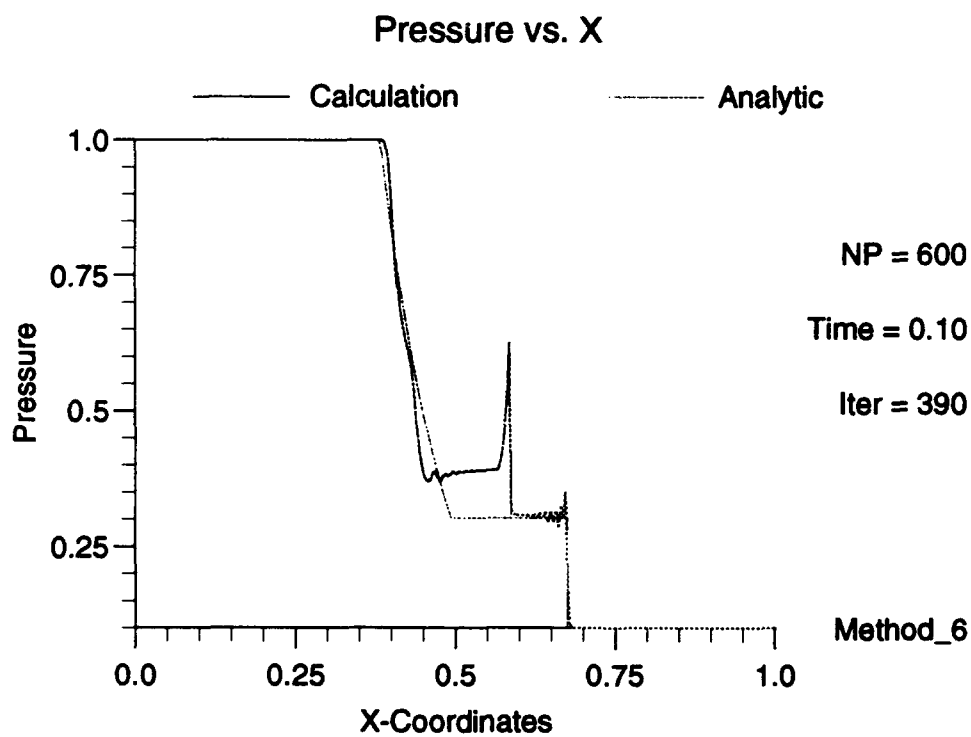
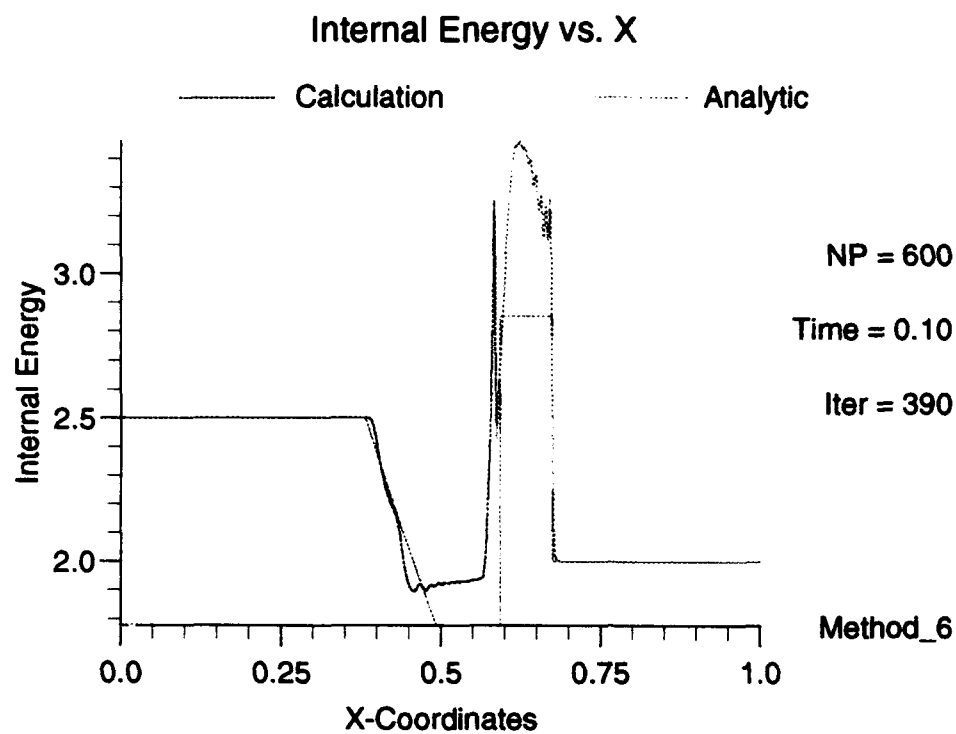


Figure D.28 Shock Tube Results - Method 20

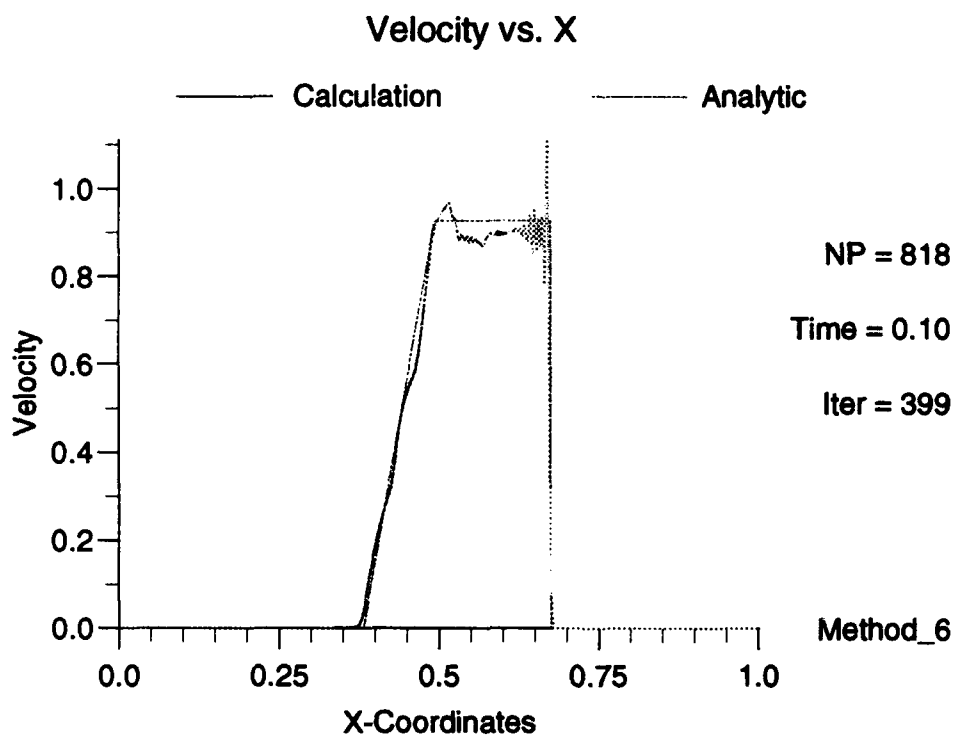
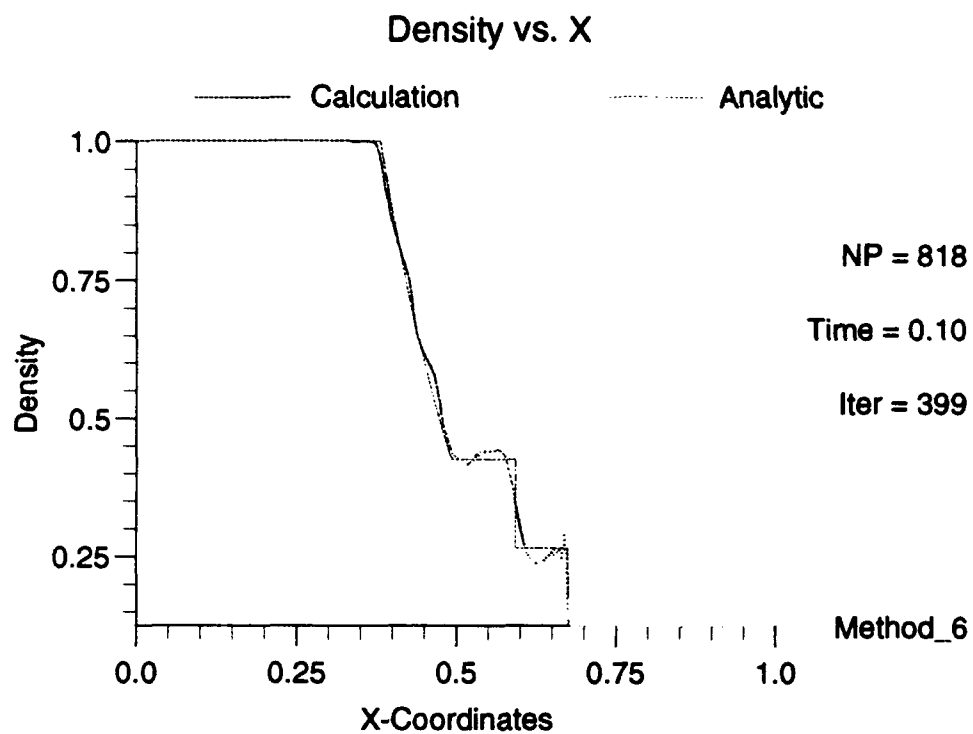


Figure D.29 Shock Tube Results - Method 20 - Extra Particles

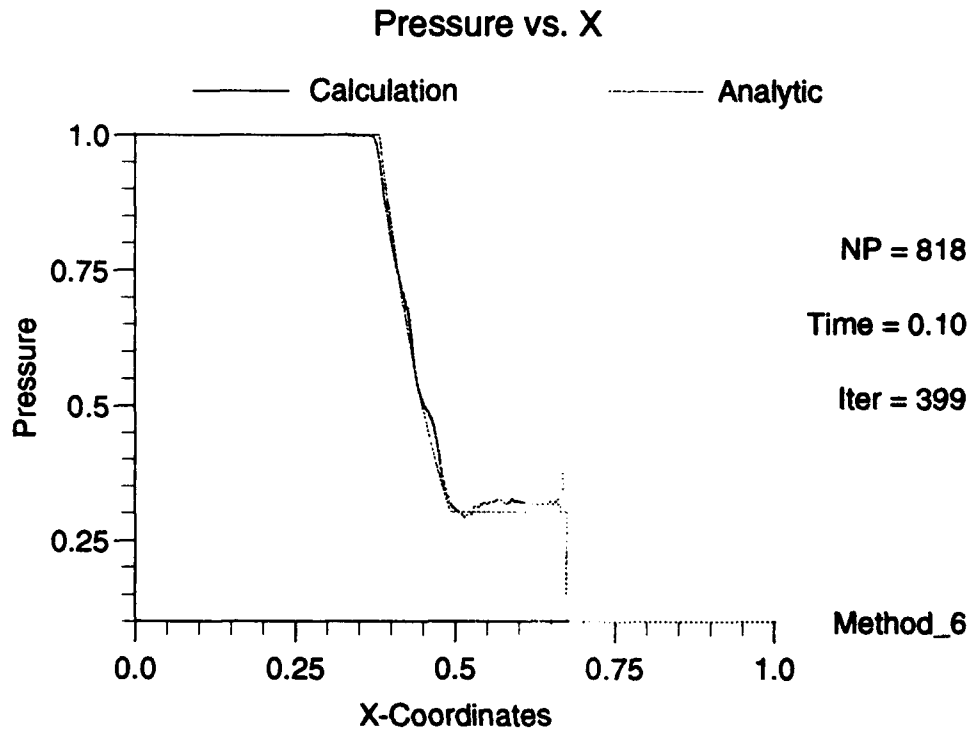
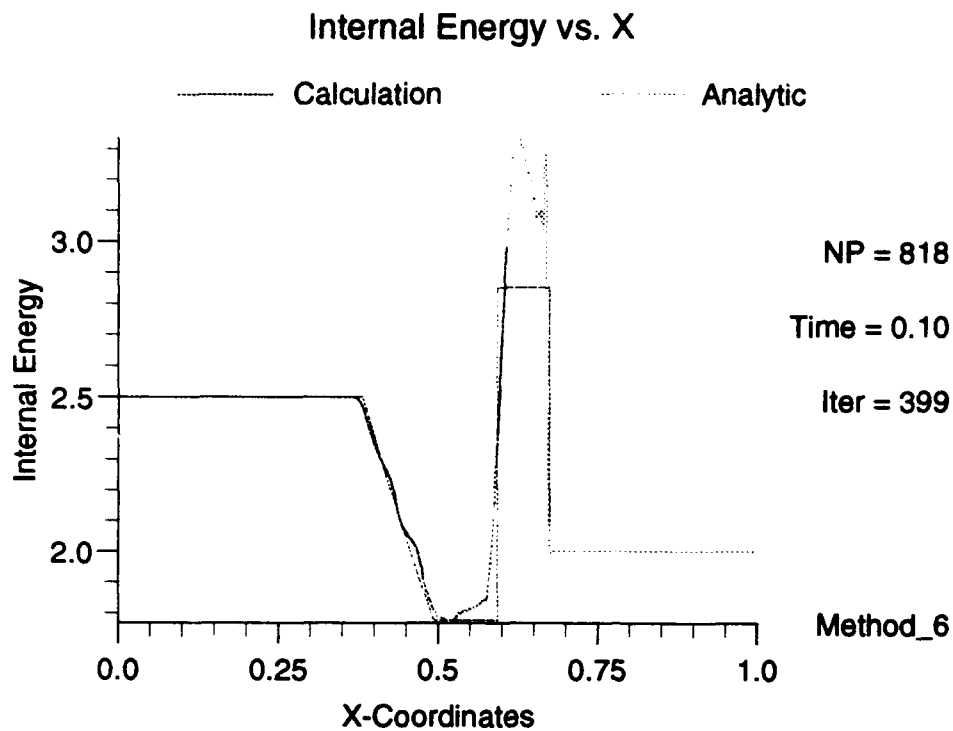


Figure D.30 Shock Tube Results - Method 20 - Extra Particles

Appendix E. SOFTWARE

This appendix briefly describes the software that was use in this dissertation. It is divided into three categories: Kernels, SPH, and Plotting.

Kernels. The computational work in the Kernel Chapter (Chapter VI) and corresponding appendix is performed mostly using the Mathematica package. It is used to normalize the kernels, plot the measures of merit, and obtain the norms. Samples of the code are given in Figures E.1 – E.2. The work on the test problems (called test 3) is done using a Fortran program. That program is not presented here.

SPH. The primary SPH code used was originally developed at the Phillips Laboratory by Captain David Amdahl and is known as DOG. It is based on his own work and that found in the Phillips Laboratory's MAGI SPH code. MAGI has one, two, and three dimensional capabilities and many 'bells and whistles' while the Amdahl DOG code is only one dimensional with a simpler implementation. Both codes are written in Fortran and can run on almost any workstation. Extensive modifications were made to almost all parts of the DOG code (except the neighbor search and list algorithms) for this dissertation. These changes make the code more useful in the research, change the time scheme, make the entire code double precision, and correct problems with the code. Of course, additional modifications were made when testing the different hybrid schemes and stabilizing techniques. To list the code here would take up about 50 pages and not be overly useful to the reader; so it was not done.

In addition to the main Fortran code, a C based graphics post-processor was used that was also originally developed by Capt Amdahl. Some modifications were made including additional options, but all the changes were minor. It is designed as an X-Windows viewing package, but has Postscript output capabilities. Is uses a commercially available graphics package known as UNIRAS. Using graphics primitives from a package makes coding graphics easy, but unfortunately this makes the

```

myabs[x_] := If[x<0,-x,x];

(* Gaussian Kernel *)

k1[u_] := 1/Pi^(1/2)*If[Abs[u]<=3,Exp[-u^2],0];
dk1[u_] := Evaluate[D[k1[u],u]];

(* W-4 B Spline Kernel *)

k2[u_] := 2/3*If[Abs[u]<=1,1-3/2*u^2+3/4*myabs[u]^3,
    If[Abs[u]<=2,1/4*(2-myabs[u])^3,0]];
dk2[u_] := Evaluate[D[k2[u],u]];

(* COS Kernel *)

k3[u_] := If[Abs[u]<=2,1/(8/3+8/(Pi^2))*(1-u^2/4)*(1+Cos[Pi*u/2]), 0];
dk3[u_] := Evaluate[D[k3[u],u]];

(* Mixed Plots *)

plma=Plot[{k1[v],k2[v],k3[v]},{v,-2.0,2.0},PlotRange->All,
    PlotStyle->{{Thickness[.004],Dashing[{0.05,0.05]}},
    {Thickness[.002],Dashing[{0.03,0.03]}},
    {Thickness[.001],Dashing[{0.01,0.01]}}},AxesLabel->{"u","K(u)"}];
plma2=Show[plma,Graphics[Text["(1)",{1.9,.04}],Text["(2)",{.4,.62}],
    Text["(3)",{.18,.59}]]];

plmb=Plot[{dk1[v],dk2[v],dk3[v]},{v,-2.0,2.0},PlotRange->All,
    PlotStyle->{{Thickness[.004],Dashing[{0.05,0.05]}},
    {Thickness[.002],Dashing[{0.03,0.03]}},
    {Thickness[.001],Dashing[{0.01,0.01]}}},AxesLabel->{"u","K'(u)"}];
plmb2=Show[plmb,Graphics[Text["(1)",{1.85,-.15}],
    Text["(2)",{1.1,-.6}],Text["(3)",{1.55,-.32}]]];

plk2a=Plot[{1,-2*dxh*Sum[1*dxh*dk2[1*dxh],{1,1,20}]],{dxh,1/10,2},
    PlotRange->All,PlotStyle->{{Thickness[.004],Dashing[{0.05,0.05]}},
    {Thickness[.001],Dashing[{0.01,0.01]}}},AxesLabel->{"dx/h","S"},
    PlotLabel->"B Spline Kernel"];

```

Figure E.1 Mathematica Code for Kernels Chapter, part 1

(* Error Norms *)

```

11k2=N[Sum[Abs[-2*(.2+n/100)*Sum[1*(.2+n/100)*dk2[1*(.2+n/100)],
{1,1,200/(20+n)}}-1],{n,1,100}]/100];

12k2=Sqrt[N[Sum[(-2*(.2+n/100)*Sum[1*(.2+n/100)*dk2[1*(.2+n/100)],
{1,1,200/(20+n)}}-1)^2,{n,1,100}]/100]];

```

Figure E.2 Mathematica Code for Kernels Chapter, part 2

post-processor not easily portable. In fact, I must still use the product through the internet using the Phillips Laboratory's IBM Risc 6000 workstations. Developing a post-processor that uses X-Windows commands directly should be accomplished. In addition, a graphics capability intertwined with the computational capability would be very useful.

Plotting. In addition to the computational work in the Kernels Chapter and the SPH plots, I used the XFIG package, Mathematica, MathCAD, Excel, Drawing Gallery, and GNUPlot to produce the remaining plots in this work. This was all fairly minor work and no code is included.

Availability. The software discussed above is all available from the author.

Bibliography

1. Anderson, C.E. Jr. "An Overview of the Theory of Hydrocodes," *International Journal of Impact Engineering*, 5: 33-59, 1987.
2. Asay, J.R. and G.I. Kerley. "The Response of Materials to Dynamic Loading," *International Journal of Impact Engineering*, 5: 66-99, 1987.
3. Baker, T.J. "Three Dimensional Mesh Generation by Triangulation of Arbitrary Point Sets," AIAA paper # AIAA-87-1124. AIAA Meeting, Honolulu, June 1987.
4. Benz, W., W.L. Slattery, and A.G.W. Cameron. "The Origin of the Moon and the Single-Impact Hypothesis I," *Icarus*, 66: 515-535, 1986.
5. Benz, W. "Smooth Particle Hydrodynamics: A Review," *Numerical Modeling of Stellar Pulsation: Problems and Prospects*, NATO Workshop, Les Arcs, France, March 1989 (Harvard Smithsonian Center for Astrophysics Preprint No 2884).
6. Bicknell, G.V. "The Equations of Motion of Particles in Smoothed Particle Hydrodynamics," *SIAM Journal on Scientific and Statistical Computing*, 12: 1198-1206, 1991.
7. Brackbill, J.U. and H.M. Ruppel. "FLIP: A Method for Adaptively Zoned, Particle in-Cell Calculations of Fluid Flows in Two Dimensions," *Journal of Computational Physics*, 65: 314-343, 1986.
8. Campbell, P.M. *Some New Algorithms for Boundary Value Problems in Smooth Particle Hydrodynamics*, Defense Nuclear Agency Technical Report # DNA-TR-88-286, 1989.
9. *A Colloquium on Advances in Smoothed Particle Hydrodynamics*, Workshop Proceedings, Phillips Laboratory/Sandia National Laboratory, 21-22 January 1993.
10. Evrard, A. "Beyond N-Body: 3-D Cosmological Gas Dynamics," *Monthly Notices of the Royal Astronomical Society*, 235: 911-934, 1988.
11. Fulk, D.A. "Smooth Particle Hydrodynamics," Preprint of the Appendix to *ESD Quarterly Report*, PL/WSSD, Kirtland AFB NM, 1991.
12. Gingold, R.A. and J.J. Monaghan. "Smoothed Particle Hydrodynamics: Theory and Applications to Non-Spherical Stars," *Monthly Notices of the Royal Astronomical Society*, 181: 375-389, 1977.
13. Gingold, R.A. and J.J. Monaghan. "Kernel Estimates as a Basis for General Particle Methods in Hydrodynamics," *Journal of Computational Physics*, 46: 429-453, 1982.

14. Hammersley, J.M. and D.C. Handscomb. *Monte Carlo Methods*. John Wiley & Sons, New York, 1964.
15. Harten, A. and G. Zwas. "Self-Adjusting Hybrid Schemes for Shock Computations," *Journal of Computational Physics*, 9: 568-583, 1972.
16. Harten, A., J.M. Hyman, and P.D. Lax. "On Finite Difference Approximations and Entropy Conditions for Shocks," *Communications on Pure and Applied Mathematics*, 29: 297-322, 1976.
17. Harten, A. "High Resolution Schemes for Hyperbolic Conservation Laws," *Journal of Computational Physics*, 49: 357-393, 1983.
18. Harten, A. "On a Class of High Resolution Total-Variation-Stable Finite Difference Schemes," *SIAM Journal on Numerical Analysis*, 21: 1-23, 1984.
19. Hernquist, L. and N. Katz. "TREESPH: A Unification of SPH with the Hierarchical Tree Method," *The Astrophysics Journal Supplement Series*, 70: 419-446, 1989.
20. Hockney, and J.W. Eastwood. *Computer Simulations Using Particles*. Adam-Hilger, New York, 1988.
21. Holian, K.S. and B.L. Holian. "Hydrodynamic Simulations of Hypervelocity Impacts," *International Journal of Impact Engineering*, 8: 115-132, 1989.
22. Holian, K.S. "Hydrodynamics Code Calculations of Debris Clouds Produced by Ball Plate Impacts," *International Journal of Impact Engineering*, 10: 231-239, 1990.
23. "Hypervelocity Impact: Proceedings of the 1986 Symposium," *International Journal of Impact Engineering*, 5, 1987.
24. "Hypervelocity Impact: Proceedings of the 1989 Symposium," *International Journal of Impact Engineering*, 10, 1990.
25. Isaacson, E. and H.B. Keller. *Analysis of Numerical Methods*, John Wiley & Sons, New York, 1966.
26. Keener, J.P. *Principles of Applied Mathematics: Transformations and Approximations*. Addison-Wesley Publishing, New York, 1988.
27. Kennon, S.R. "A Vectorized Delaunay Triangulation Scheme for Non-Convex Domains with Automatic Nodal Point Generation," AIAA paper # AIAA-88-0314. AIAA 26th Aerospace Sciences Meeting, Reno, January 1988.
28. Lattanzio, J.C., J.J. Monaghan, H. Pongracic, and M.P. Schwartz. "Controlling Penetration," *SIAM Journal on Scientific and Statistical Computing*, 7: 591-598, 1986.
29. Lax, P. and B. Wendroff. "Systems of Conservation Laws," *Communications on Pure and Applied Mathematics*, 13: 217-237, 1960.

30. Lax, P.D. *Hyperbolic Systems of Conservation Laws and the Mathematical Theory of Shock Waves*, CBMS-NSF Regional Conference Series in Applied Mathematics #11, SIAM, Philadelphia, 1973.
31. LeVeque, R.J. and J.B. Goodman. "TVD Schemes in One and Two Space Dimensions," *Large-Scale Computations in Fluid Mechanics*: 51-63, 1985. (*Lectures in Applied Mathematics, Volume 22, Part 2*, American Mathematical Society, Providence, eds C. Enquist, B.E., S. Osher, and R.C.J. Somerville).
32. LeVeque, R.J. *Numerical Methods for Conservation Laws*, Birkhauser Verlag, Boston, 1992.
33. Libersky, L.D. and A.G. Petschek, "Smooth Particle Hydrodynamics With Strength of Materials," *Advances in the Free-Lagrange Method*, Preprint to the Proceedings of the Next Free-Lagrange Conference, Moran Wy, 3-7 June 1990. Springer-Verlag, New York, 1991.
34. Libersky, L.D., A.G. Petschek, T.C. Carney, J.R. Hipp, and F.A. Allahdadi. "High Strain Lagrangian Hydrodynamics: A Three-Dimensional SPH Code for Dynamic Material Response," PL/WSSD Paper, 1992.
35. Lucy, L.B. "A Numerical Approach to the Testing of the Fission Hypothesis," *Astronomy Journal*, 82: 1013-1024, 1977.
36. Monaghan, J.J. "Why Particle Methods Work," *SIAM Journal on Scientific and Statistical Computing*, 3: 422-433, 1982.
37. Monaghan, J.J. and R.A. Gingold. "Shock Simulation by the Particle Method SPH," *Journal of Computational Physics*, 52: 374-389, 1983.
38. Monaghan, J.J. and J.C. Lattanzio. "A Refined Particle Method for Astrophysical Problems," *Astronomy and Astrophysics*, 149: 135-143, 1985.
39. Monaghan, J.J. "Particle Methods for Hydrodynamics," *Computer Physics Reports*, 3: 71-124, 1985.
40. Monaghan, J.J. and H. Poinracic. "Artificial Viscosity for Particle Methods," *Applied Numerical Mathematics*, 1: 187-194, 1985.
41. Monaghan, J.J. "SPH Meets the Shocks of Noh," Monash University Paper, 1987.
42. Monaghan, J.J. "An Introduction to SPH," *Computer Physics Communications*, 48: 89, 1988.
43. Monaghan, J.J. "On the Problem of Penetration in Particle Methods," *Journal of Computational Physics*, 82: 1-15, 1989.
44. Monaghan, J.J. "Smoothed Particle Hydrodynamics," *Annual Review of Astronomy and Astrophysics*, 30: 543-574, 1992.
45. Naylor, A.W. and G.R. Sell. *Linear Operator Theory in Engineering and Science*, Springer-Verlag, New York, 1982.

46. Niederreiter, H. "Quasi-Monte Carlo Methods and Pseudo-Random Numbers." *The Bulletin of the American Mathematical Society*, 84: 953-1041, 1978.
47. Noh, W.F. "Errors for Calculations of Strong Shocks Using an Artificial Viscosity and an Artificial Heat Flux." *Journal of Computational Physics*, 72: 78-120, 1987.
48. Osher, S. and S. Chakravarthy. "Very High Order Accurate TVD Schemes." *Oscillation Theory, Computation, Computation, and Methods of Compensated Compactness*: 229-274, 1986. (*The IMA Volumes in Mathematics and It's Applications, Volume 2*, Springer-Verlag, New York, eds C. Dafermos, J.L. Ericksen, D. Kinderlehrer, and M. Slemrod).
49. Petschek, A.G. and L.D. Libersky. "A Stability Analysis of SPH: Preliminary Considerations." New Mexico Institute of Mining and Technology paper, 1993.
50. Quinn, B.K. "Solutions with Shocks: An Example of an L_1 -Contractive Semigroup." *Communications on Pure and Applied Mathematics*, 24: 125-132, 1971.
51. Royden, H.L. *Real Analysis*, MacMillan Co, New York, 1963.
52. Sedgewick, R. *Algorithms*. Addison-Wesley Publishing, Reading, Mass., 1983.
53. Segletes, S.B. *An Analysis on the Stability of the Mie-Grüneisen Equation of State for Describing the Behavior of Shock-Loaded Materials*, Ballistic Research Laboratory Technical Report # BRL-TR-3214, 1991.
54. Shu, C. "TVB Uniformly High-Order Schemes for Conservation Laws." *Mathematics of Computation*, 49: 105-121, 1987.
55. Shu, C. "Total-Variation-Diminishing Time Discretizations," *SIAM Journal on Scientific and Statistical Computing*, 9: 1073-1084, 1988.
56. Sloan, S.W. "A Fast Algorithm for Constructing Delaunay Triangulations in the Plane" *Advances in Engineering Software*, 9: 34-55, 1987.
57. Smoller, J. *Shock Waves and Reaction-Diffusion Equations*. Springer-Verlag, New York, 1983.
58. Stakgold, I. *Bessel's Functions and Boundary Value Problems*. Wiley-Interscience, New York, 1979.
59. Stellingwerf, R.F. and P.M. Campbell. "Hypervelocity Impact Modeling Using Smooth Particle Hydrodynamics," Mission Research Corporation Report # MRC/ABQ-N-474. Preprint of paper presented at the WL/AFSTC Hypervelocity Impact Colloquium, 1990.
60. Strikwerda, J.C. *Finite Difference Schemes and Partial Differential Equations*. Wadsworth and Brooks/Cole Advanced Books and Software, Pacific Grove, Ca, 1989.
61. Sulsky, D., Z. Chen, and H.L. Schreyer. "The Application of a Material-Spatial Numerical Method to Penetration," University of New Mexico paper, 1991.

62. Sweby, P.K. "High Resolution Schemes Using Flux Limiters for Hyperbolic Conservation Laws," *SIAM Journal on Numerical Analysis*, 21: 995-1011, 1984.
63. Swegle, J.W. "SPH Behavior in Tension," Sandia National Laboratory memo, 1992.
64. Swegle, J.W., D.L. Hicks, and S.W. Attaway. "Smoothed Particle Hydrodynamics Stability Analysis," Sandia National Laboratory preprint, 1993.
65. Swegle, J.W., S.W. Attaway, M.W. Heinstein, F.j. Mello, and D.L. Hicks *An Analysis of Smoothed Particle Hydrodynamics*, Sandia National Laboratory Technical Report # SAND93-2513, 1994.
66. VonNeumann, J. and R.D. Richtmyer "A Method for the Numerical Calculations of Hydrodynamic Shocks," *Journal of Applied Physics*, 21: 232-237, 1950.
67. Weinacht, R.J. "Weak Solutions of Partial Differential Equations," Informal Paper given at Rensaeller Polytechnic Institute, 1970.
68. Woodward, P. and P. Colella. "The Numerical Simulation of Two-Dimensional Fluid Flow with Strong Shocks," *Journal of Computational Physics*, 54: 115-173, 1984.
69. *Workshop on Advances in Smooth Particle Hydrodynamics*, Workshop Proceedings, Los Alamos National Laboratory, 21-23 September 1993. LANL Technical Report # LA-UR-93-4375, 1993.
70. Young, D.M. and R.T. Gregory. *A Survey of Numerical Mathematics: In Two Volumes*. Dover Publications, New York, 1972.
71. Zukas, J.A., T. Nicholas, H.F. Swift, L.B. Greszczuk, and D.R. Curran. *Impact Dynamics*. John Wiley & Sons, New York, 1982.
72. Zukas, J.A. *High Velocity Impact Dynamics*. John Wiley & Sons, New York, 1990.

Vita

Captain David A. Fulk was born on 29 March 1961 in Syracuse, New York. He grew up in Endicott, New York and graduated from Union-Endicott High School in 1979. He continued his education at Syracuse University, graduating with a Bachelor of Science in Mathematics in May 1983.

Upon graduation, he received a reserve commission in the USAF through the ROTC program and served his first tour of duty at Gunter AFB, Alabama. He began as a computer performance analyst for the Air Force Data Systems Design Center. Later he was chosen as chief of the performance software section for the Standard Systems Center. During this tour he completed squadron officer school by both correspondence and in residence and was awarded a regular commission. He also earned a Master of Business Administration Degree from Auburn University at Montgomery.

From there, Captain Fulk was transferred to the Civil Engineering Research Division at the Air Force Weapons Laboratory, Kirtland AFB New Mexico. He performed several jobs including program task manager and survivability/vulnerability modeler. He was then reassigned to the Space Kinetic Impact and Debris Branch at the Phillips Laboratory where he initiated Air Force research into effects of kinetic impacts on space assets. He also completed a Masters Degree in Applied Mathematics at the University of New Mexico.

Finally he was chosen to attend the School of Engineering, Air Force Institute of Technology, in September 1991.

Permanent address: 18 Badger Ave
Endicott, New York 13760

REPORT DOCUMENTATION PAGE

1. AGENCY USE ONLY (Leave blank) 2. REPORT DATE September 1994 3. REPORT TYPE Doctoral Dissertation

4. TITLE AND SUBTITLE
A NUMERICAL ANALYSIS OF SMOOTHED PARTICLE HYDRODYNAMICS

5. AUTHOR(S)
David A. Fulk, Capt, USAF

6. PERFORMING ORGANIZATION NAME(S) AND ADDRESS(ES)
Air Force Institute of Technology, WPAFB OH 45433-6583
AFIT/DS/ENC/94-1

7. SPONSORING/MONITORING AGENCY NAME(S) AND ADDRESS(ES)
Phillips Laboratory, Dr Allahdadi
PL/WSCD, Kirtland AFB NM 87117

11. SUPPLEMENTARY NOTES

12. DISTRIBUTION STATEMENT (If applicable)
Approved for public release; distribution unlimited

13. ABSTRACT (Maximum length)
This dissertation studies the numerical method of Smoothed Particle Hydrodynamics (SPH) as a technique for solving systems of conservation equations. The research starts with a detailed consistency analysis of the method. Higher dimensions and non-smooth functions are considered in addition to the smooth one dimensional case. A stability analysis is then performed. Using a linear technique, an instability is found. Solutions are proposed to resolve the instability. Also a total variation stability analysis is performed leading to a monotone form of SPH. The concepts of consistency and stability are then used in a convergence proof. This proof uses lemmas derived from the Lax-Wendroff theorem in finite differences. The numerical analysis of the method is concluded with a study of the SPH kernel function. Measures of merit are derived for SPH kernels and these are used to show bell-shaped kernels to be superior over other shaped kernels. Three second-order time schemes are applied to SPH to provide a full discretization of the problem; these are Lax-Wendroff, central, and Shu schemes. In addition a lower-order SPH Lax-Friedrichs type form is developed. This method is used in proposing the use of flux-limited hybrid methods in SPH to resolve shocks.

14. SUBJECT TERMS
Smoothed Particle Hydrodynamics, Numerical Analysis, Error Analysis, Kernel Functions, Hydrodynamic Codes, Particle Codes
15. NUMBER OF PAGES
350

17. SECURITY CLASSIFICATION OF REPORT UNCLASSIFIED	18. SECURITY CLASSIFICATION OF THIS PAGE UNCLASSIFIED	19. SECURITY CLASSIFICATION OF ABSTRACT UNCLASSIFIED	20. LIMITATION OF ABSTRACT UL
---	--	---	----------------------------------

GENERAL INSTRUCTIONS FOR COMPLETING SF 298

The Report Documentation Page (RDP) is used in announcing and cataloging reports. It is important that this information be consistent with the rest of the report, particularly the cover and title page. Instructions for filling in each block of the form follow. It is important to **stay within the lines to meet optical scanning requirements.**

Block 1. Agency Use Only (Leave Blank)

Block 2. Report Date. Full publication date including day, month, and year, if available (e.g. 1 Jan 88). Must cite at least the year.

Block 3. Type of Report and Dates Covered. State whether report is interim, final, etc. If applicable, enter inclusive report dates (e.g. 10 Jun 87 - 30 Jun 88).

Block 4. Title and Subtitle. A title is taken from the part of the report that provides the most meaningful and complete information. When a report is prepared in more than one volume, repeat the primary title, add volume number, and include subtitle for the specific volume. On classified documents enter the title classification in parentheses.

Block 5. Funding Numbers. To include contract and grant numbers; may include program element number(s), project number(s), task number(s), and work unit number(s). Use the following labels:

C - Contract	PR - Project
G - Grant	TA - Task
PE - Program Element	WU - Work Unit Accession No.

Block 6. Author(s). Name(s) of person(s) responsible for writing the report, performing the research, or credited with the content of the report. If editor or compiler, this should follow the name(s).

Block 7. Performing Organization Name(s) and Address(es). Self-explanatory.

Block 8. Performing Organization Report Number. Enter the unique alphanumeric report number(s) assigned by the organization performing the report.

Block 9. Sponsoring/Monitoring Agency Names(s) and Address(es). Self-explanatory.

Block 10. Sponsoring/Monitoring Agency Report Number. (If known)

Block 11. Supplementary Notes. Enter information not included elsewhere such as: Prepared in cooperation with...; Trans. of ..., To be published in When a report is revised, include a statement whether the new report supersedes or supplements the older report.

Block 12a. Distribution/Availability Statement.

Denote public availability or limitation. Cite any availability to the public. Enter additional limitations or special markings in all capitals (e.g. NOFORN, REL, ITAR)

DOD - See DoDD 5230.24, "Distribution Statements on Technical Documents."

DOE - See authorities

NASA - See Handbook NHB 2200.2.

NTIS - Leave blank.

Block 12b. Distribution Code.

DOD - DOD - Leave blank

DOE - DOE - Enter DOE distribution categories from the Standard Distribution for Unclassified Scientific and Technical Reports

NASA - NASA - Leave blank

NTIS - NTIS - Leave blank.

Block 13. Abstract. Include a brief (Maximum 200 words) factual summary of the most significant information contained in the report.

Block 14. Subject Terms. Keywords or phrases identifying major subjects in the report.

Block 15. Number of Pages. Enter the total number of pages.

Block 16. Price Code. Enter appropriate price code (NTIS only).

Blocks 17. - 19. Security Classifications. Self-explanatory. Enter U.S. Security Classification in accordance with U.S. Security Regulations (i.e., UNCLASSIFIED). If form contains classified information, stamp classification on the top and bottom of the page.

Block 20. Limitation of Abstract. This block must be completed to assign a limitation to the abstract. Enter either UL (unlimited) or SAR (same as report). An entry in this block is necessary if the abstract is to be limited. If blank, the abstract is assumed to be unlimited.